THESIS
pt. 1

MICHIGAN STATE UNIVERSITY LIBRARIES
3 1293 00903 2156

This is to certify that the

thesis entitled
Exploratory Synthesis of New Transition Metal Complexes with Polychalcogenide Ligands Using Conventional Solution Reactions and Hydro(solvo)thermal Techniques

presented by

Songping Huang

has been accepted towards fulfillment
of the requirements for

Ph.D. degree in Chemistry

Major professor

Date 3/25/93

O-7639

MSU is an Affirmative Action/Equal Opportunity Institution

LIBRARY
Michigan State
University

PLACE IN RETURN BOX to remove this checkout from your record.
TO AVOID FINES return on or before date due.

DATE DUE	DATE DUE	DATE DUE

MSU Is An Affirmative Action/Equal Opportunity Institution
c:\circ\datedue.pm3-p.1

EXPLORATORY SYNTHESIS OF NEW TRANSITION METAL COMPLEXES WITH POLYCHALCOGENIDE LIGANDS USING CONVENTIONAL SOLUTION REACTIONS AND HYDRO(SOLVO)THERMAL TECHNIQUES

By

Songping Huang

A DISSERTATION

Submitted to
Michigan State University
in partial fulfillment of the requirements
for the degree of

DOCTOR OF PHILOSOPHY

Department of Chemistry

1993

ABSTRACT

EXPLORATORY SYNTHESIS OF NEW TRANSITION METAL COMPLEXES WITH POLYCHALCOGENIDE LIGANDS USING CONVENTIONAL SOLUTION REACTIONS AND HYDRO(SOLVO)THERMAL TECHNIQUES

By

Songping Huang

The coordination chemistry of metal polychalcogenides is fascinating in terms of structural diversity and wealthiness. In the past two decades, the chemistry of metal polysulfides has been extensively studied, while a great deal of attention is currently being paid to metal polyselenides and polytellurides. By using solvent extracted Zintl phases A_2Q_x (A=Na or K; Q=Se or Te; x=2-6) as the starting materials, we have prepared a number of metal heavy polychalcogenide compounds from solution or under hydro(solvo)thermal conditions.

In the Au^{n+}/Q_x^{2-} (Q=Se and Te) system, six new gold polychalcogenide complexes are synthesized from solution. These include $(PPN)_2[Au_2Se_2(Se_4)_2]$, $(Ph_4P)_2[Au_2(Se_2)(Se_3)]$, $(PPN)_2[Au_2(Se_2)(Se_3)]$, $(Ph_4P)_2[Au_2(Se_2)(Se_4)]$, $(Ph_4P)_2[Au_2(Te_2)_2]$ and $(Et_4N)_3[NaAu_{12}Se_8]$. Also isolated from reaction of $AuCl_3$ with Na_2Se_5 is a spiro-cyclic polyselenide compound α-$(Ph_4P)_2[Se(Se_5)_2]$, while β-$(Ph_4P)_2[Se(Se_5)_2]$ and $(Ph_4P)_2[Te(Se_5)_2]$ can be obtained by using I_2 or Na_2Se_5 as oxidant. In the reaction of $Ru_3(CO)_{12}/Fe(CO)_5$ with Na_2Se_5 in solution at ambient temperatures, partial oxidative decarbonylation of the metal center by polyselenide ligands affords CO-containing octahedral complexes $(Et_4N)_{1.5}Na_{0.5}[Ru(CO)_2(Se_4)_2]$, $(Ph_4P)_2[Ru(CO)_2(Se_4)_2$ and $(Ph_4P)_2[Fe(CO)_2(Se_4)_2]$. When such oxidative decarbonylation reactions are carried out under hydro(solvo)thermal conditions, sixteen

novel metal carbonyl chalcogenide clusters are obtained. These include $(Ph_4P)_2[Ru_6(Te_2)_7(CO)_{12}]$, $(Ph_4P)_2[\{Fe_4Te_4(CO)_{10}\}_2(Te_2)]$, $(Ph_4P)_2[\{Fe_2Se(CO)_6\}_2(Se_2)]$, $(Ph_4P)_2[Mn_3(Q_2)_2(QR)(CO)_9]$ (R=H or CH_3 when Q=S; R=CH_3 when Q=Se and Te), $(Ph_4P)_3[Re_4(Te_2)_3(TeCH_3)(CO)_{12}]\cdot CH_3OH$, $(Ph_4P)[Mn_2(QCH_3)_3(CO)_6]$ (Q=S, Se and Te), $(Ph_4P)_2[(CO)_4M(MS_4)]$ (M=Mo and W) and $(Ph_4P)_2[(CO)_4M(MS_4)M(CO)_4]$ (M=Mo and W).

In this dissertation, the synthesis, X-ray crystal structures and the spectroscopic characterization of these newly prepared compounds are reported.

ACKNOWLEGEMENTS

I sincerely wish to thank Prof. Dr. Mercouri G. Kanatzidis for suggesting the studies in this area of chemistry, for his expert guidance, support and patience throughout the course of the experiments and the preparation of this dissertation.

I would like to express special thanks to all members in Kanatzidis group for the friendship and support. Each one of them has taught me many invaluable things.

Appreciation is also extended to the Department of Chemistry, the Center for Fundamental Materials Research (CFMR) at Michigan State University, the Petroleum Research Fund administered by the American Chemical Society and the National Science Foundation for financial support in the forms of chemicals, supplies, teaching and research assistantship.

Finally, I thank my wife and my daughter for their understanding and encouragement during the preparation of this dissertation and the other manuscripts.

TABLE OF CONTENTS

CHAPTER 1 INTRODUCTION 1

I. General Background 1

II. Summary of Synthetic Methods 6

1. Use of polychalcogenide anions generated in situ as reagents 6

2. Use of elemental chalcogens as reagents 7

3. Extraction of transition metal/chalcogen-containing alloys 9

4. Use of other reagents 9

5. Thermolysis 11

6. The molten salt technique 11

7. Use of Zintl phases of alkali metal polychalcogenides as reagents 13

8. Hydro(solvo)thermal reactions 14

III. Spectroscopic Studies of Metal Heavy Polychalcogenides 15

1. The IR and UV/vis Spectroscopy 16

2. NMR Spectroscopy 16

IV. Concluding Remarks 20

REFERENCES 22

CHAPTER 2 POLYSELENIDE AND POLYTELLURIDE CHEMISTRY OF GOLD 34

I. Introduction 34

II. Experimental Section 35

1. Reagents 35

2. Physical Measurements 36

3. Syntheses 38

Preparation of $(PPN)_2[Au_2Se_2(Se_4)_2]$ (2·1) 39

Preparation of $(Ph_4P)_2[Au_2(Se_2)(Se_3)]$ (2·2) 39

Preparation of $(PPN)_2[Au_2(Se_2)(Se_3)]$ (2·3) 40

Preparation of $(Ph_4P)_2[Au_2(Se_2)(Se_4)]$ (2·4) 40

Preparation of $(Et_4N)_3[NaAu_{12}Se_8]$ (2·5) 40

Preparation of $(Ph_4P)_2[Au_2(Te_2)_2]$ (2·6) 41

4. X-ray Diffraction and Crystallographic Studies 41

III. Results 64

1. Description of Crystal and Molecular Structures of the Compounds 64

Structure of $(PPN)_2[Au_2Se_2(Se_4)_2]$ (2·1) 64

Structure of $(Ph_4P)_2[Au_2(Se_2)(Se_3)]$ (2·2) 64

Structure of $(PPN)_2[Au_2(Se_2)(Se_3)]$ (2·3) 70

Structure of $(Ph_4P)_2[Au_2(Se_2)(Se_4)]$ (2·4) 70

Structure of $(Et_4N)_3[NaAu_{12}Se_8]$ (2·5) 74

Structure of $(Ph_4P)_2[Au_2(Te_2)_2]$ (2·6) 75

2. Spectroscopic Studies 82

3. Thermal Decomposition Properties 84

IV. Discussion 93

REFERENCES 100

CHAPTER 3 CHEMISTRY OF HOMO- AND HETEROCHALCOGENIDE COMPOUNDS 105

I. Introduction 105

II. Experimental Section 106

1. Reagents 106

2. Physical Measurements 106

3. Syntheses 107

Preparation of α-$(Ph_4P)_2[Se(Se_5)_2]$ (**4·1**) 107

Preparation of β-$(Ph_4P)_2[Se(Se_5)_2]$ (**4·2**) 107

Preparation of $(Ph_4P)_2[Te(Se_5)_2]$ (**4·3**) 108

4. X-ray Diffraction and Crystallographic Studies 108

III. Results 118

1. Description of Crystal and Molecular Structures of the Compounds 118

Structure of α-$(Ph_4P)_2[Se(Se_5)_2]$ (**4·1**)and β-$(Ph_4P)_2[Se(Se_5)_2]$ (**4·2**) 118

2. Spectroscopic Studies 124

3. Thermal Decomposition 125

IV. Discussion 129

REFERENCES 134

CHAPTER 4 CHEMISTRY OF POLYSELENIDE LIGANDS WITH IRON AND RUTHENIUM CARBONYLS IN SOLUTION 140

I. Introduction 140

II. Experimental Section 141

1. Reagents 141

2. Physical Measurements 141

3. Syntheses 142

Preparation of $(Et_4N)_{1.5}Na_{0.5}[Ru(CO)_2(Se_4)_2]$ (3·1) 142

Preparation of $(Ph_4P)_2[Ru(CO)_2(Se_4)_2]$ (3·2) 142

Preparation of $(Ph_4P)_2[Fe(CO)_2(Se_4)_2]$ (3·3) 143

4. X-ray Diffraction and Crystallographic Studies 143

III. Results 154

1. Description of Crystal and Molecular Structures of the Compounds 154

Structure of $(Et_4N)_{1.5}Na_{0.5}[Ru(CO)_2(Se_4)_2]$ (3·1) 154

Structure of $(Ph_4P)_2[Fe(CO)_2(Se_4)_2]$ (3·3) 159

2. Spectroscopic Studies 163

3. Thermal Decomposition 168

IV. Discussion 171

REFERENCES 174

CHAPTER 5 HYDRO(METHANO)THERMAL SYNTHESIS OF METAL CARBONYL CHALCOGENIDE CLUSTERS OF GROUP 8 ELEMENTS 179

I. Introduction 179

II. Experimental Section 180

1. Reagents 180

2. Physical Measurements 181

3. Syntheses 181

Preparation of $(Ph_4P)_2[Ru_6(Te_2)_7(CO)_{12}]$ (5·1) 181

Preparation of $(Ph_4P)_2[\{Fe_4Te_4(CO)_{10}\}_2(Te_2)]$ (5·2) 182

Preparation of $(Ph_4P)_2[\{Fe_2Se(CO)_6\}_2(Se_2)]$ (5·3) 182

4. X-ray Diffraction and Crystallographic Studies 183

III. Results 198

1. Description of Crystal and Molecular Structures of the Compounds 198

Structure of $(Ph_4P)_2[Ru_6(Te_2)_7(CO)_{12}]$ (5·1) 198

Structure of $(Ph_4P)_2[\{Fe_4Te_4(CO)_{10}\}_2(Te_2)]$ (5·2) 205

Structure of $(Ph_4P)_2[\{Fe_2Se(CO)_6\}_2(Se_2)]$ (5·3) 211

2. Spectroscopic Studies 217

3. Thermal Decompositions 217

IV. Discussion 224

REFERENCES 229

CHAPTER 6 MENTHANOTHERMAL SYNTHESIS OF CHALCOGENIDE-CONTAINING METAL CARBONYL CLUSTERS OF GROUP 7 ELEMENTS 235

I. Introduction 235

II. Experimental Section 238

1. Reagents 238

2. Physical Measurements 338

3. Syntheses 238

Preparation of $(Ph_4P)_2[Mn_3(S_2)_2(SH)(CO)_9]$ (**6·1**) 239

Preparation of $(Ph_4P)_2[Mn_3(S_2)_2(SCH_3)(CO)_9]$ (**6·2**) 239

Preparation of $(Ph_4P)_2[Mn_3(Se_2)_2(SeCH_3)(CO)_9]$ (**6·3**) 240

Preparation of α-$(Ph_4P)_2[Mn_3(Te_2)_2(TeCH_3)(CO)_9]$ (**6·4**) 240

Preparation of β-$(Ph_4P)_2[Mn_3(Te_2)_2(TeCH_3)(CO)_9]$ (**6·5**) 241

Preparation of $(Ph_4P)_3[Re_4(Te_2)_3(TeCH_3)(CO)_{12}].CH_3OH$ (**6·6**) 241

Preparation of $(Ph_4P)[Mn_2(SCH_3)_3(CO)_6]$ (**6·7**) 242

Preparation of $(Ph_4P)[Mn_2(SeCH_3)_3(CO)_6]$ (**6·8**) 242

Preparation of $(Ph_4P)[Mn_2(TeCH_3)_3(CO)_6]$ (**6·9**) 243

4. X-ray Diffraction and Crystallographic Studies 243

III. Results 286

1. Description of Crystal and Molecular Structures of the Compounds 286

Structures of $(Ph_4P)_2[Mn_3(S_2)_2(SH)(CO)_9]$ (**6·1**) and $(Ph_4P)_2[Mn_3(S_2)_2(SCH_3)(CO)_9]$ (**6·2**) 286

Structure of $(Ph_4P)_2[Mn_3(Se_2)_2(SeCH_3)(CO)_9]$ (**6·3**) 296

Structures of α-$(Ph_4P)_2[Mn_3(Te_2)_2(TeCH_3)(CO)_9]$ (**6·4**) and β-$(Ph_4P)_2[Mn_3(Te_2)_2(TeCH_3)(CO)_9]$ (**6·5**) 302

Structure of $(Ph_4P)_3[Re_4(Te_2)_3(TeCH_3)(CO)_{12}].CH_3OH$ (**6·6**) 313

Structures of $(Ph_4P)[Mn_2(SCH_3)_3(CO)_6]$ (**6·7**), $(Ph_4P)[Mn_2(SeCH_3)_3(CO)_6]$ (**6·8**) and $(Ph_4P)[Mn_2(TeCH_3)_3(CO)_6]$ (**6·9**) 319

2. Spectroscopic Studies 326

3. Thermal Decomposition 344

IV. Discussion 348

REFERENCES 355

CHAPTER 7 MENTHANOTHERMAL SYNTHESIS OF METAL CARBONYL SULFIDO CLUSTERS OF GROUP 6 ELEMENTS 358

I. Introduction 358

II. Experimental Section 359

1. Reagents 359

2. Physical Measurements 359

3. Syntheses 359

Preparation of $(Ph_4P)_2[(CO)_4Mo(MoS_4)]$ (**7·1**) 359

Preparation of $(Ph_4P)_2[(CO)_4W(WS_4)]$ (**7·2**) 360

Preparation of $(Ph_4P)_2[(CO)_4Mo(MoS_4)Mo(CO)_4]$ (**7·3**) 360

Preparation of $(Ph_4P)_2[(CO)_4W(WS_4)W(CO)_4]$ (**7·4**) 361

4. X-ray Diffraction and Crystallographic Studies 361

III. Results 379

1. Description of Crystal and Molecular Structures of the Compounds 379

Structure of $(Ph_4P)_2[(CO)_4W(WS_4)]$ (7·2) 379

Structure of $(Ph_4P)_2[(CO)_4Mo(MoS_4)Mo(CO)_4]$ (7·3) and $(Ph_4P)_2[(CO)_4W(WS_4)W(CO)_4]$ (7·4) 384

2. Spectroscopic Studies 389

3. Thermal Decomposition 395

IV. Discussion 398

REFERENCES 401

CHAPTER 8 CONCLUSIONS 405

REFERENCES 408

LISTING OF TABLES

Table 1·1. Typical Coordination Modes of Polysulfide Ligands 3

Table 1·2. ^{77}Se and ^{125}Te NMR data for the $[MX(Q_4)_2]^{2-}$ (M=Mo, W..... 18

Table 2·1. Data for Crystal Structure Analysis of $(PPN)_2[Au_2Se_2(Se_4)_2]$ (**2·1**), $(Ph_4P)_2[Au_2(Se_2)(Se_3)]$ (**2·2**) and $(PPN)_2[Au_2(Se_2)(Se_3)]$ (**2·3**) 44

Table 2·2. Data for Crystal Structure Analysis of $(Ph_4P)_2[Au_2(Se_2)(Se_4)]$ (**2·4**), $(Et_4N)_3[NaAu_{12}Se_8]$ (**2·5**) and $(Ph_4P)_2[Au_2(Te_2)_2]$ (**2·6**)..... 45

Table 2·3. Positional Parameters and B_{eq} Values for $(PPN)_2[Au_2Se_2(Se_4)_2]$ (**2·1**) 46

Table 2·4. Positional Parameters and B_{eq} Values for $(Ph_4P)_2[Au_2(Se_2)(Se_3)]$ (**2·2**) 48

Table 2·5. Positional Parameters and B_{eq} Values for $(PPN)_2[Au_2(Se_2)(Se_3)]$ (**2·3**) 50

Table 2·6. Positional Parameters and B_{eq} Values for $(Ph_4P)_2[Au_2(Se_2)(Se_4)]$ (**2·4**) 52

Table 2·7. Positional Parameters and B_{eq} Values for $(Et_4N)_3[NaAu_{12}Se_8]$ (**2·5**) 53

Table 2·8. Positional Parameters and B_{eq} Values for $(Ph_4P)_2[Au_2(Te_2)_2]$ (**2·6**) 54

Table 2·9. Calculated and Observed X-ray Powder Diffraction Patterns for $(PPN)_2[Au_2Se_2(Se_4)_2]$ (**2·1**)..... 55

Table 2·10. Calculated and Observed X-ray Powder Diffraction Patterns for $(Ph_4P)_2[Au_2(Se_2)(Se_3)]$ (**2·2**)..... 57

Table 2·11. Calculated and Observed X-ray Powder Diffraction Patterns for $(PPN)_2[Au_2(Se_2)(Se_3)]$ (**2·3**)..... 58

Table 2·12. Calculated and Observed X-ray Powder Diffraction Patterns for $(Ph_4P)_2[Au_2(Se_2)(Se_4)]$ (2·4) 59

Table 2·13. Calculated and Observed X-ray Powder Diffraction Patterns for $(Et_4N)_3[NaAu_{12}Se_8]$ (2·5) 61

Table 2·14. Calculated and Observed X-ray Powder Diffraction Patterns for $(Ph_4P)_2[Au_2(Te_2)_2]$ (2·6) 63

Table 2·15. Selected Geometric Data for $(PPN)_2[Au_2Se_2(Se_4)_2]$ (2·1) 65

Table 2·16. Selected Geometric Data for $(Ph_4P)_2[Au_2(Se_2)(Se_3)]$ (2·2) 65

Table 2·17. Selected Geometric Data for $(Ph_4P)_2[Au_2(Se_2)(Se_4)]$ (2·4) 74

Table 2·18. Selected Geometric Data for $(Et_4N)_3[NaAu_{12}Se_8]$ (2·5) 76

Table 2·19. Selected Geometric Data for $(Ph_4P)_2[Au_2(Te_2)_2]$ (2·6) and Comparison with $(PPN)_2[Au_2(Te_2)_2]$ 77

Table 2·20 Electronic Spectral Data for $(PPN)_2[Au_2Se_2(Se_4)_2]$ (2·1), $(Ph_4P)_2[Au_2(Se_2)(Se_3)]$ (2·2), $(PPN)_2[Au_2(Se_2)(Se_3)]$ (2·3), $(Ph_4P)_2[Au_2(Se_2)(Se_4)]$ (2·4), $(Et_4N)_3[NaAu_{12}Se_8]$ (2·5) and $(Ph_4P)_2[Au_2(Te_2)_2]$ (2·6) in DMF 83

Table 2·21. Thermal Gravimetric Analysis Data for $(PPN)_2[Au_2Se_2(Se_4)_2]$ (2·1), $(Ph_4P)_2[Au_2(Se_2)(Se_3)]$ (2·2), $(PPN)_2[Au_2(Se_2)(Se_3)]$ (2·3), $(Ph_4P)_2[Au_2(Se_2)(Se_4)]$ (2·4), $(Et_4N)_3[NaAu_{12}Se_8]$ (2·5) and $(Ph_4P)_2[Au_2(Te_2)_2]$ (2·6) 93

Table 3·1. Data for Crystal Structure Analysis of α-$(Ph_4P)_2[Se(Se_5)_2]$ (3·1) and β-$(Ph_4P)_2[Se(Se_5)_2]$ (3·2) 111

Table 3·2. Positional Parameters and B_{eq} Values for α-$(Ph_4P)_2[Se(Se_5)_2]$ (3·1) 112

Table 3·3. Positional Parameters and B_{eq} Values for β-$(Ph_4P)_2[Se(Se_5)_2]$ (3·2) 114

Table 3·4. Calculated and Observed X-ray Powder Diffraction Patterns for α-$(Ph_4P)_2[Se(Se_5)_2]$ (3·1) 116

Table 3·5. Calculated and Observed X-ray Powder Diffraction Patterns for β-$(Ph_4P)_2[Se(Se_5)_2]$ (**3·2**) and $(Ph_4P)_2[Te(Se_5)_2]$ (**3·3**) 117

Table 3·6. Selected Bond Distances (Å) and Bond Angles (deg) of α-$(Ph_4P)_2[Se(Se_5)_2]$ (**3·1**) and β-$(Ph_4P)_2[Se(Se_5)_2]$ (**3·2**)..... 124

Table 4·1. Data for Crystal Structure Analysis of $(Et_4N)_{1.5}Na_{0.5}[Ru(CO)_2(Se_4)_2]$ (**4·1**), $(Ph_4P)_2[Ru(CO)_2(Se_4)_2]$ (**4·2**) and $(Ph_4P)_2[Fe(CO)_2(Se_4)_2]$ (**4·3**) 146

Table 4·2. Positional Parameters and B_{eq} Values for $(Et_4N)_{1.5}Na_{0.5}[Ru(CO)_2(Se_4)_2]$ (**4·1**) 147

Table 4·3. Positional Parameters and B_{eq} Values for $(Ph_4P)_2[Fe(CO)_2(Se_4)_2]$ (**4·3**) 149

Table 4·4. Calculated and Observed X-ray Powder Diffraction Patterns for $(Et_4N)_{1.5}Na_{0.5}[Ru(CO)_2(Se_4)_2]$ (**4·1**) 152

Table 4·5. Calculated and Observed X-ray Powder Diffraction Patterns for $(Ph_4P)_2[Fe(CO)_2(Se_4)_2]$ (**4·3**) 153

Table 4·6. Selected Geometric Data for $(Et_4N)_{1.5}Na_{0.5}[Ru(CO)_2(Se_4)_2]$ (**4·1**)..... 155

Table 4·7. Selected Geometric Data for $(Ph_4P)_2[Fe(CO)_2(Se_4)_2]$ (**4·3**)..... 159

Table 4·8. Thermal Gravimetric Analysis Data for $(Et_4N)_{1.5}Na_{0.5}[Ru(CO)_2(Se_4)_2]$ (**4·1**), $(Ph_4P)_2[Ru(CO)_2(Se_4)_2]$ (**4·2**) and $(Ph_4P)_2[Fe(CO)_2(Se_4)_2]$ (**4·3**) 168

Table 5·1. Data for Crystal Structure Analysis of $(Ph_4P)_2[Ru_6(Te_2)_7(CO)_{12}]$ (**5·1**), $(Ph_4P)_2[\{Fe_4Te_4(CO)_{10}\}_2(Te_2)]$ (**5·2**) and $(Ph_4P)_2[\{Fe_2Se(CO)_6\}_2(Se_2)]$ (**5·3**)..... 184

Table 5·2. Positional Parameters and B_{eq} Values for $(Ph_4P)_2[Ru_6(Te_2)_7(CO)_{12}]$ (**5·1**) 185

Table 5·3. Positional Parameters and B_{eq} Values for $(Ph_4P)_2[\{Fe_4Te_4(CO)_{10}\}_2(Te_2)]$ (**5·2**) 187

Table 5·4. Positional Parameters and B_{eq} Values for $(Ph_4P)_2[\{Fe_2Se(CO)_6\}_2(Se_2)]$ (**5·3**) 191

Table 5·5. Calculated and Observed X-ray Powder Diffraction Patterns for $(Ph_4P)_2[Ru_6(Te_2)_7(CO)_{12}]$ (**5·1**) 194

Table 5·6. Calculated and Observed X-ray Powder Diffraction Patterns for $(Ph_4P)_2[\{Fe_4Te_4(CO)_{10}\}_2(Te_2)]$ (**5·2**) 195

Table 5·7. Calculated and Observed X-ray Powder Diffraction Patterns for $(Ph_4P)_2[\{Fe_2Se(CO)_6\}_2(Se_2)]$ (**5·3**) 196

Table 5·8. Selected Geometric Data for $(Ph_4P)_2[Ru_6(Te_2)_7(CO)_{12}]$ (**5·1**) 199

Table 5·9. Selected Geometric Data for $(Ph_4P)_2[\{Fe_4Te_4(CO)_{10}\}_2(Te_2)]$ (**5·2**) 206

Table 5·10. Selected Geometric Data for $(Ph_4P)_2[\{Fe_2Se(CO)_6\}_2(Se_2)]$ (**5·3**) 212

Table 6·1. Data for Crystal Structure Analysis of $(Ph_4P)_2[Mn_3(S_2)_2(SH)(CO)_9]$ (**6·1**), $(Ph_4P)_2[Mn_3(S_2)_2(SCH_3)(CO)_9]$ (**6·2**), $(Ph_4P)_2[Mn_3(Se_2)_2(SeCH_3)(CO)_9]$ (**6·3**) 245

Table 6·2. Data for Crystal Structure Analysis of α-$(Ph_4P)_2[Mn_3(Te_2)_2(TeCH_3)(CO)_9]$ (**6·4**), β-$(Ph_4P)_2[Mn_3(Te_2)_2(TeCH_3)(CO)_9]$ (**6·5**), $(Ph_4P)_3[Re_4(Te_2)_3(TeCH_3)(CO)_{12}].CH_3OH$ (**6·6**) 246

Table 6·3. Data for Crystal Structure Analysis of $(Ph_4P)[Mn_2(SCH_3)_3(CO)_6]$ (**6·7**), $(Ph_4P)[Mn_2(SeCH_3)_3(CO)_6]$ (**6·8**) and $(Ph_4P)[Mn_2(TeCH_3)_3(CO)_6]$ (**6·9**) 247

Table 6·4. Positional Parameters and B_{eq} Values for $(Ph_4P)_2[Mn_3(S_2)_2(SH)(CO)_9]$ (**6·1**) 248

Table 6·5. Positional Parameters and B_{eq} Values for $(Ph_4P)_2[Mn_3(S_2)_2(SCH_3)(CO)_9]$ (**6·2**) 251

Table 6·6. Positional Parameters and B_{eq} Values for $(Ph_4P)_2[Mn_3(Se_2)_2(SeCH_3)(CO)_9]$ (**6·3**) 256

Table 6·7. Positional Parameters and B_{eq} Values for α-$(Ph_4P)_2[Mn_3(Te_2)_2(TeCH_3)(CO)_9]$ (**6·4**) 259

Table 6·8. Positional Parameters and B_{eq} Values for β-$(Ph_4P)_2[Mn_3(Te_2)_2(TeCH_3)(CO)_9]$ (**6·5**) 262

Table 6·9. Positional Parameters and B_{eq} Values for $(Ph_4P)_3[Re_4(Te_2)_3(TeCH_3)(CO)_{12}].CH_3OH$ (**6·6**) 265

Table 6·10. Positional Parameters and B_{eq} Values for $(Ph_4P)[Mn_2(SCH_3)_3(CO)_6]$ (**6·7**) 269

Table 6·11. Positional Parameters and B_{eq} Values for $(Ph_4P)[Mn_2(SeCH_3)_3(CO)_6]$ (**6·8**) 271

Table 6·12. Positional Parameters and B_{eq} Values for $(Ph_4P)[Mn_2(TeCH_3)_3(CO)_6]$ (**6·9**) 273

Table 6·13. Calculated and Observed X-ray Powder Diffraction Patterns for $(Ph_4P)_2[Mn_3(S_2)_2(SH)(CO)_9]$ (**6·1**) 275

Table 6·14. Calculated and Observed X-ray Powder Diffraction Patterns for $(Ph_4P)_2[Mn_3(S_2)_2(SCH_3)(CO)_9]$ (**6·2**) 276

Table 6·15. Calculated and Observed X-ray Powder Diffraction Patterns for $(Ph_4P)_2[Mn_3(Se_2)_2(SeCH_3)(CO)_9]$ (**6·3**) 277

Table 6·16. Calculated and Observed X-ray Powder Diffraction Patterns for α-$(Ph_4P)_2[Mn_3(Te_2)_2(TeCH_3)(CO)_9]$ (**6·4**) 278

Table 6·17. Calculated and Observed X-ray Powder Diffraction Patterns for β-$(Ph_4P)_2[Mn_3(Te_2)_2(TeCH_3)(CO)_9]$ (**6·5**) 280

Table 6·18. Calculated and Observed X-ray Powder Diffraction Patterns for $(Ph_4P)_3[Re_4(Te_2)_3(TeCH_3)(CO)_{12}].CH_3OH$ (**6·6**) 281

Table 6·19. Calculated and Observed X-ray Powder Diffraction Patterns for $(Ph_4P)[Mn_2(SCH_3)_3(CO)_6]$ (**6·7**) and $(Ph_4P)[Mn_2(SeCH_3)_3(CO)_6]$ (**6·8**) 283

Table 6·20. Calculated and Observed X-ray Powder Diffraction Patterns for $(Ph_4P)[Mn_2(TeCH_3)_3(CO)_6]$ (**6·9**) 284

Table 6-21. Selected Bond Distances (Å) and Bond Angles (deg) of $(Ph_4P)_2[Mn_3(S_2)_2(SH)(CO)_9]$ (**6-1**) and $(Ph_4P)_2[Mn_3(S_2)_2(SCH_3)(CO)_9]$ (**6-2**)..... 288

Table 6-22. Selected Bond Distances (Å) and Bond Angles (deg) of $(Ph_4P)_2[Mn_3(Se_2)_2(SeCH_3)(CO)_9]$ (**6-3**) 297

Table 6-23. Selected Bond Distances (Å) and Bond Angles (deg) of α-$(Ph_4P)_2[Mn_3(Te_2)_2(TeCH_3)(CO)_9]$ (**6-4**) and β-$(Ph_4P)_2[Mn_3(Te_2)_2(TeCH_3)(CO)_9]$ (**6-5**) 303

Table 6-24. Selected Bond Distances (Å) and Bond Angles (deg) of $(Ph_4P)_3[Re_4(Te_2)_3(TeCH_3)(CO)_{12}].CH_3OH$ (**6-6**) 314

Table 6-25. Selected Bond Distances (Å) and Bond Angles (deg) of $(Ph_4P)[Mn_2(SCH_3)_3(CO)_6]$ (**6-7**), $(Ph_4P)[Mn_2(SeCH_3)_3(CO)_6]$ (**6-8**) and $(Ph_4P)[Mn_2(TeCH_3)_3(CO)_6]$ (**6-9**)..... 319

Table 6-26. IR Spectral Data for $(Ph_4P)_2[Mn_3(S_2)_2(SH)(CO)_9]$ (**6-1**), $(Ph_4P)_2[Mn_3(S_2)_2(SCH_3)(CO)_9]$ (**6-2**), $(Ph_4P)_2[Mn_3(Se_2)_2(SeCH_3)(CO)_9]$ (**6-3**), α-$(Ph_4P)_2[Mn_3(Te_2)_2(TeCH_3)(CO)_9]$ (**6-4**), β-$(Ph_4P)_2[Mn_3(Te_2)_2(TeCH_3)(CO)_9]$ (**6-5**), $(Ph_4P)_3[Re_4(Te_2)_3(TeCH_3)(CO)_{12}].CH_3OH$ (**6-6**), $(Ph_4P)[Mn_2(SCH_3)_3(CO)_6]$ (**6-7**), $(Ph_4P)[Mn_2(SeCH_3)_3(CO)_6]$ (**6-8**) and $(Ph_4P)[Mn_2(TeCH_3)_3(CO)_6]$ (**6-9**)..... 327

Table 6-27. Thermal Gravimetric Analysis Data for $(Ph_4P)_2[Mn_3(S_2)_2(SH)(CO)_9]$ (**6-1**), $(Ph_4P)_2[Mn_3(S_2)_2(SCH_3)(CO)_9]$ (**6-2**), $(Ph_4P)_2[Mn_3(Se_2)_2(SeCH_3)(CO)_9]$ (**6-3**), α-$(Ph_4P)_2[Mn_3(Te_2)_2(TeCH_3)(CO)_9]$ (**6-4**), β-$(Ph_4P)_2[Mn_3(Te_2)_2(TeCH_3)(CO)_9]$ (**6-5**), $(Ph_4P)_3[Re_4(Te_2)_3(TeCH_3)(CO)_{12}].CH_3OH$ (**6-6**), $(Ph_4P)[Mn_2(SCH_3)_3(CO)_6]$ (**6-7**), $(Ph_4P)[Mn_2(SeCH_3)_3(CO)_6]$ (**6-8**) and $(Ph_4P)[Mn_2(TeCH_3)_3(CO)_6]$ (**6-9**)..... 344

Table 7-1. Data for Crystal Structure Analysis of $(Ph_4P)_2[(CO)_4Mo(MoS_4)]$ (**7-1**), $(Ph_4P)_2[(CO)_4W(WS_4)]$ (**7-2**), $(Ph_4P)_2[(CO)_4Mo(MoS_4)Mo(CO)_4]$ (**7-3**) and $(Ph_4P)_2[(CO)_4W(WS_4)W(CO)_4]$ (**7-4**) 364

Table 7-2. Positional Parameters and B_{eq} Values for $(Ph_4P)_2[(CO)_4W(WS_4)]$ (**7-2**) 366

Table 7·3. Positional Parameters and B_{eq} Values for
$(Ph_4P)_2[(CO)_4Mo(MoS_4)Mo(CO)_4]$ (7·3) 369

Table 7·4. Positional Parameters and B_{eq} Values for
$(Ph_4P)_2[(CO)_4W(WS_4)W(CO)_4]$ (7·4) 372

Table 7·5. Calculated and Observed X-ray Powder Diffraction Patterns for
$(Ph_4P)_2[(CO)_4Mo(MoS_4)]$ (7·1) and $(Ph_4P)_2[(CO)_4W(WS_4)]$ (7·2) 376

Table 7·6. Calculated and Observed X-ray Powder Diffraction Patterns for
$(Ph_4P)_2[(CO)_4Mo(MoS_4)Mo(CO)_4]$ (7·3) and $(Ph_4P)_2[(CO)_4W(WS_4)W(CO)_4]$
(7·4) 378

Table 7·7. Comparison of Geometric Data Between $(Ph_4P)_2[(CO)_4W(WS_4)]$ (7·2)
and $(Et_4N)_2[(CO)_4W(WS_4)]$ 380

Table 7·8. Geometric Data of $(Ph_4P)_2[(CO)_4Mo(MoS_4)Mo(CO)_4]$ (7·3) and
$(Ph_4P)_2[(CO)_4W(WS_4)W(CO)_4]$ (7·4) 384

Table 7·9 Electronic Spectral Data for $[\{M(CO)_4\}_n(MS_4)]^{2-}$ (M=Mo, W) 395

LISTING OF FIGURES

Figure 2·1. Two Views of the $[Au_2Se_2(Se_4)_2]^{2-}$ Anion 66

Figure 2·2. The Packing Diagram in the Unit Cell of $(PPN)_2[Au_2Se_2(Se_4)_2]$ (Stereoview) 67

Figure 2·3. Two Views of the $[Au_2(Se_2)(Se_3)]^{2-}$ Anion 68

Figure 2·4. The Packing Diagram in the Unit Cell of $(Ph4P)_2[Au_2(Se_2)(Se_3)]$ (Stereoview) 69

Figure 2·5. The ORTEP Representation of the $[Au_2(Se_2)(Se_3)]^{2-}$ Anion in $(PPN)_2[Au_2(Se_2)(Se_3)]$, Showing Structural Disorder Caused By the Inversion Center 71

Figure 2·6. Two Views of the $[Au_2(Se_2)(Se_4)]^{2-}$ Anion 72

Figure 2·7. The Packing Diagram in the Unit Cell of $(Ph_4P)_2[Au_2(Se_2)(Se_4)]$ (Stereoview) 73

Figure 2·8. The Packing Diagram in the Unit Cell of $(Et_4N)_3[NaAu_{12}Se_8]$ (Stereoview). 78

Figure 2·9. The Structure of the $[NaAu_{12}Se_8]^{3-}$ Anion 79

Figure 2·10. Two Views of the $[Au_2(Te_2)_2]^{2-}$ Anion 80

Figure 2·11. The Packing Diagram in the Unit Cell of $(Ph_4P)_2[Au_2(Te_2)_2]$ (Stereoview) 81

Figure 2·12. The solid-state far IR spectra of (A) $(PPN)_2[Au_2Se_2(Se_4)_2]$, (B) $(Ph4P)_2[Au_2(Se_2)(Se_3)]$, (C) $(PPN)_2[Au_2(Se_2)(Se_3)]$, (D) $(Ph_4P)_2[Au_2(Se_2)(Se_4)]$, (E) $(Et_4N)_3[NaAu_{12}Se_8]$ and (F) $(Ph_4P)_2[Au_2(Te_2)_2]$ 86

Figure 2·13. The UV/vis Spectra of (A) $(PPN)_2[Au_2Se_2(Se_4)_2]$ and (B) $(Ph4P)_2[Au_2(Se_2)(Se_4)]$ in DMF 87

Figure 2·14. The UV/vis Spectra of (A) $(Ph_4P)_2[Au_2(Se_2)(Se_3)]$ and (B) $(PPN)_2[Au_2(Se_2)(Se_3)]$ in DMF 87

Figure 2·15. The UV/vis Spectrum of $(Ph_4P)_2[Au_2(Te_2)_2]$ in DMF 88

Figure 2·16. The ^{77}Se NMR Spectra of (A) $(Ph_4P)_2[Au_2(Se_2)(Se_3)]$, (B) $(PPN)_2[Au_2(Se_2)(Se_3)]$ and (C) $(Ph_4P)_2[Au_2(Se_2)(Se_4)]$ in DMF 89

Figure 2·17. The ^{77}Se NMR Spectrum (A) and ^{23}Na NMR Spectrum (B) of $(Et_4N)_3[NaAu_{12}Se_8]$ in DMF 90

Figure 2·18. The TGA Diagrams of (A) $(PPN)_2[Au_2Se_2(Se_4)_2]$, (B) $(Ph4P)_2[Au_2(Se_2)(Se_3)]$, (C) $(PPN)_2[Au_2(Se_2)(Se_3)]$ and (D) $(Ph_4P)_2[Au_2(Se_2)(Se_4)]$ 91

Figures 2·19. The TGA Diagrams of (A) $(Et_4N)_3[NaAu_{12}Se_8]$ and (B) $(Ph_4P)_2[Au_2(Te_2)_2]$ 92

Figure 3·1. The Packing Diagram in the Unit Cell of α-$(Ph_4P)_2[Se(Se_5)_2]$ (Stereoview) 120

Figure 3·2. The Packing Diagram in the Unit Cell of β-$(Ph_4P)_2[Se(Se_5)_2]$ (Stereoview) 121

Figure 3·3. The Structure of the $[Se(Se_5)_2]^{2-}$ Anion 122

Figure 3·4. Comparison of Selected Bond Distances (Å) and Bond Angles (deg) in (A) α- And (B) β-$(Ph_4P)_2[Se(Se_5)_2]$ 123

Figure 3·5. The Solid-State Far IR Spectra of (A) $(Ph_4P)_2[Se(Se_5)_2]$ and (B) $(Ph_4P)_2[Te(Se_5)_2]$ 126

Figure 3·6. The UV/vis Spectrum of $(Ph_4P)_2[Se(Se_5)_2]$ in DMF 127

Figure 3·7. The TGA diagrams of (A) $(Ph_4P)_2[Se(Se_5)_2]$ And (B) $(Ph_4P)_2[Te(Se_5)_2]$ 128

Figure 4·1. The Packing Diagram in the Unit Cell of $(Et_4N)_{1.5}Na_{0.5}[Ru(CO)_2(Se_4)_2]$ (Stereoview) 156

Figure 4·2. The Structure of the $[Ru(CO)_2(Se_4)_2]^{2-}$ Anion 157

Figure 4·3. ORTEP Representation of the $\{Na[Ru(CO)_2(Se_4)_2]_2\}^{3+}$ Structure, Showing the Coordination of a Na^+ by Two $[Ru(CO)_2(Se_4)_2]^{2-}$ Anions 158

Figure 4·4. The Packing Diagram in the Unit Cell of $(Ph_4P)_2[Fe(CO)_2(Se_4)_2]$ (Stereoview) 161

Figure 4·5. The Structure of the $[Fe(CO)_2(Se_4)_2]^{2-}$ Anion 162

Figure 4·6 The Solid-State IR Spectra in the CO Region for (—) $(Et_4N)_{1.5}Na_{0.5}[Ru(CO)_2(Se_4)_2]$, (-x-x-x-) $(Ph_4P)_2[Ru(CO)_2(Se_4)_2]$ and (----) $(Ph_4P)_2[Fe(CO)_2(Se_4)_2]$ 165

Figure 4·7 The Solid-State Far IR Spectra of (—) $(Et_4N)_{1.5}Na_{0.5}[Ru(CO)_2(Se_4)_2]$, (-x-x-x-) $(Ph_4P)_2[Ru(CO)_2(Se_4)_2]$ and (----)) $(Ph_4P)_2[Fe(CO)_2(Se_4)_2]$ 166

Figure 4·8. The ^{77}Se NMR Spectra of (A) $(Et_4N)_{1.5}Na_{0.5}[Ru(CO)_2(Se_4)_2]$ and (B) $(Ph_4P)_2[Ru(CO)_2(Se_4)_2]$, (C) $(Ph_4P)_2[Fe(CO)_2(Se_4)_2]$ and ^{23}Na NMR Spectrum of (D) $(Et_4N)_{1.5}Na_{0.5}[Ru(CO)_2(Se_4)_2]$ 167

Figure 4·9. The TGA diagrams of (A) $(Et_4N)_{1.5}Na_{0.5}[Ru(CO)_2(Se_4)_2]$, (B) $(Ph_4P)_2[Ru(CO)_2(Se_4)_2]$ and (C) $(Ph_4P)_2[Fe(CO)_2(Se_4)_2]$ 170

Figure 5·1. The Packing Diagram in the Unit Cell of $(Ph_4P)_2[Ru_6(Te_2)_7(CO)_{12}]$ (Stereoview) 201

Figure 5·2. The Structure of the $[Ru_6(Te_2)_7(CO)_{12}]^{2-}$ Anion 202

Figure 5·3. The Structure of the $[Ru_6(Te_2)_7(CO)_{12}]^{2-}$ Anion with CO Groups Omitted, Showing the Staggering Conformation of the Ru_3Te-$TeRu_3$ Fragment 203

Figure 5·4. Comparison Between the $[Ru_6(Te_2)_7]^{2-}$ Core and a Small-Core Fragment of $RuTe_2$ 204

Figure 5·5. The Packing Diagram in the Unit Cell of $(Ph_4P)_2[\{Fe_4Te_4(CO)_{10}\}_2(Te_2)]$ (Stereoview) 208

Figure 5·6. The Structure of the $[\{Fe_4Te_4(CO)_{10}\}_2(Te_2)]^{2-}$ Anion 209

Figure 5·7. The Structure of the $[\{Fe_4Te_4(CO)_{10}\}_2(Te_2)]^{2-}$ Anion with CO Groups Omitted, Emphasizing the Two Fe_4Te_4 Cores and Their Coupling via the Te_2^{2-} Ligand 210

Figure 5·8. The Packing Diagram in the Unit Cell of $(Ph_4P)_2[\{Fe_2Se(CO)_6\}_2(Se_2)]$ (Stereoview) 214

Figure 5·9. The Structure of the $[\{Fe_2Se(CO)_6\}_2(Se_2)]^{2-}$ Anion 215

Figure 5·10. A Different View of the $[\{Fe_2Se(CO)_6\}_2(Se_2)]^{2-}$ Anion, Showing the Double "Butterfly" Conformation of the Molecule 216

Figure 5·11. The Solid-State IR Spectra in the CO Region for (A) $(Ph_4P)_2[Ru_6(Te_2)_7(CO)_{12}]$, (B) $(Ph_4P)_2[\{Fe_4Te_4(CO)_{10}\}_2(Te_2)]$ and (C) $(Ph_4P)_2[\{Fe_2Se(CO)_6\}_2(Se_2)]$ 219

Figure 5·12. The Solid-State Far IR Spectrum of $(Ph_4P)_2[Ru_6(Te_2)_7(CO)_{12}]$ 220

Figure 5·13. The Solid-State Far IR Spectra for (—) $(Ph_4P)_2[\{Fe_4Te_4(CO)_{10}\}_2(Te_2)]$ and (---) $(Ph_4P)_2[\{Fe_2Se(CO)_6\}_2(Se_2)]$ 220

Figure 5·14. The UV/vis Spectrum of $(Ph_4P)_2[\{Fe_2Se(CO)_6\}_2(Se_2)]$ in DMF 221

Figure 5·15. The ^{77}Se NMR Spectrum of $(Ph_4P)_2[\{Fe_2Se(CO)_6\}_2(Se_2)]$ in DMF 222

Figure 5·16. The TGA diagrams of (A) $(Ph_4P)_2[Ru_6(Te_2)_7(CO)_{12}]$, (B) $(Ph_4P)_2[\{Fe_4Te_4(CO)_{10}\}_2(Te_2)]$ and (C) $(Ph_4P)_2[\{Fe_2Se(CO)_6\}_2(Se_2)]$ 223

Figure 6·1. The Packing Diagram in the Unit Cell of $(Ph_4P)_2[Mn_3(S_2)_2(SH)(CO)_9]$ (Stereoview) 292

Figure 6·2. The Packing Diagram in the Unit Cell of $(Ph_4P)_2[Mn_3(S_2)_2(SCH_3)(CO)_9]$ (Stereoview) 293

Figure 6·3. The Structure of the $[Mn_3(S_2)_2(SH)(CO)_9]^{2-}$ Anion 294

Figure 6-4. Structures of the Two Crystallographically Independent $[Mn_3(S_2)_2(SH)(CO)_9]^{2-}$ Anions Found in the $(Ph_4P)_2[Mn_3(S_2)_2(SH)(CO)_9]$ Unit Cell 295

Figure 6-5. The Packing Diagram in the Unit Cell of $(Ph_4P)_2[Mn_3(Se_2)_2(SeCH_3)(CO)_9]$ (Stereoview) 299

Figure 6-6. The Structure of the $[Mn_3(Se_2)_2(SeCH_3)(CO)_9]^{2-}$ Anion 300

Figure 6-7. Two Optical Isomers of the $[Mn_3(Se_2)_2(SeCH_3)(CO)_9]^{2-}$ Anion Found in the $(Ph_4P)_2[Mn_3(Se_2)_2(SeCH_3)(CO)_9]$ Unit Cell 301

Figure 6-8. The Packing Diagram in the Unit Cell of α-$(Ph_4P)_2[Mn_3(Te_2)_2(TeCH_3)(CO)_9]$ (Stereoview) 307

Figure 6-9. The Packing Diagram in the Unit Cell of β-$(Ph_4P)_2[Mn_3(Te_2)_2(TeCH_3)(CO)_9]$ (Stereoview) 308

Figure 6-10. Structure of the $(Ph_4P)_2[Mn_3(Te_2)_2(TeCH_3)(CO)_9]^{2-}$ Anion Found in α-$(Ph_4P)_2[Mn_3(Te_2)_2(TeCH_3)(CO)_9]$ 309

Figure 6-11. Structure of the $[Mn_3(Te_2)_2(TeCH_3)(CO)_9]^{2-}$ Anion Found in β-$(Ph_4P)_2[Mn_3(Te_2)_2(TeCH_3)(CO)_9]$ 310

Figure 6-12. Two Optical Isomers of the $[Mn_3(Te_2)_2(TeCH_3)(CO)_9]^{2-}$ Anion Found in the α-$(Ph_4P)_2[Mn_3(Te_2)_2(TeCH_3)(CO)_9]$ Unit Cell 311

Figure 6-13. Two Optical Isomers of the $[Mn_3(Te_2)_2(TeCH_3)(CO)_9]^{2-}$ Anion Found in the β-$(Ph_4P)_2[Mn_3(Te_2)_2(TeCH_3)(CO)_9]$ Unit Cell 312

Figure 6-14. The Packing Diagram in the Unit Cell of $(Ph_4P)_3[Re_4(Te_2)_3(TeCH_3)(CO)_{12}].CH_3OH$ (Stereoview) 316

Figure 6-15. The Structure of the $[Re_4(Te_2)_3(TeCH_3)(CO)_{12}]^{3-}$ Anion 317

Figure 6-16. The $[Re_4(Te_2)_3(Te)]^{4-}$ Cluster Core, Showing a Pseudo-C3 Axis 318

Figure 6-17. The Packing Diagram in the Unit Cell of $(Ph_4P)[Mn_2(QCH_3)_3(CO)_6]$ (Q=S and Se) (Stereoview) 322

Figure 6-18. The Packing Diagram in the Unit Cell of $(Ph_4P)[Mn_2(TeCH_3)_3(CO)_6]$ (Stereoview) 323

Figure 6-19. The Structure of the $[Mn_2(QCH_3)_3(CO)_6]^{2-}$ (Q=S and Se) Anions 324

Figure 6-20. The Structure of the $[Mn_2(TeCH_3)_3(CO)_6]^{2-}$ Anion 325

Figure 6-21. The Solid-State IR Spectra in the CO Region for (A) $(Ph_4P)_2[Mn_3(S_2)_2(SH)(CO)_9]$ and (B) $(Ph_4P)_2[Mn_3(S_2)_2(SCH_3)(CO)_9]$ 329

Figure 6-22. The Solid-State IR Spectra in the CO Region for (A) $(Ph_4P)_2[Mn_3(Se_2)_2(SeCH_3)(CO)_9]$ and (B) $(Ph_4P)_3[Re_4(Te_2)_3(TeCH_3)(CO)_{12}]\cdot CH_3OH$ 330

Figure 6-23. The Solid-State IR Spectra in the CO Region for (A) α-$(Ph_4P)_2[Mn_3(Te_2)_2(TeCH_3)(CO)_9]$ and (B) β-$(Ph_4P)_2[Mn_3(Te_2)_2(TeCH_3)(CO)_9]$ 331

Figure 6-24. The Solid-State IR Spectra in the CO Region for (A) $(Ph_4P)[Mn_2(SCH_3)_3(CO)_6]$, (B) $(Ph_4P)[Mn_2(SeCH_3)_3(CO)_6]$ and (C) $(Ph_4P)[Mn_2(TeCH_3)_3(CO)_6]$ 332

Figure 6-25. The Solid-State Far IR Spectra of (A) $(Ph_4P)_2[Mn_3(S_2)_2(SH)(CO)_9]$ and (B) $(Ph_4P)_2[Mn_3(S_2)_2(SCH_3)(CO)_9]$ 333

Figure 6-26. The Solid-State Far IR Spectrum of $(Ph_4P)_2[Mn_3(Se_2)_2(SeCH_3)(CO)_9]$ 334

Figure 6-27. The Solid-State Far IR Spectra of (A) α-$(Ph_4P)_2[Mn_3(Te_2)_2(TeCH_3)(CO)_9]$ and (B) β-$(Ph_4P)_2[Mn_3(Te_2)_2(TeCH_3)(CO)_9]$ 335

Figure 6-28. The Solid-State Far IR Spectrum of $(Ph_4P)_3[Re_4(Te_2)_3(TeCH_3)(CO)_{12}]\cdot CH_3OH$ 336

Figure 6-29. The Solid-State Far IR Spectrum of $(Ph_4P)[Mn_2(SCH_3)_3(CO)_6]$ 337

Figure 6-30. The Solid-State Far IR Spectrum of $(Ph_4P)[Mn_2(SeCH_3)_3(CO)_6]$ 338

Figure 6-31. The Solid-State Far IR Spectrum of $(Ph_4P)[Mn_2(TeCH_3)_3(CO)_6]$ 339

Figure 6·32. The UV/vis Spectra of (—) $(Ph_4P)[Mn_2(SCH_3)_3(CO)_6]$, (---) $(Ph_4P)[Mn_2(SeCH_3)_3(CO)_6]$ and (···) $(Ph_4P)[Mn_2(TeCH_3)_3(CO)_6]$ in CH_3CN 341

Figure 6·33. The UV/vis Spectrum of $(Ph_4P)_3[Re_4(Te_2)_3(TeCH_3)(CO)_{12}]\cdot CH_3OH$ in CH_3CN 341

Figure 6·34. The ^1H NMR Spectra of (A) $(Ph_4P)_2[Mn_3(S_2)_2(SCH_3)(CO)_9]$, (B) $(Ph_4P)_2[Mn_3(Se_2)_2(SeCH_3)(CO)_9]$, (C) $(Ph_4P)_2[Mn_3(Te_2)_2(TeCH_3)(CO)_9]$ and (D) $(Ph_4P)_3[Re_4(Te_2)_3(TeCH_3)(CO)_{12}]\cdot CH_3OH$ in $(CD_3)_2CO$ 342

Figure 6·35. The ^1H NMR Spectra of (A) $(Ph_4P)[Mn_2(SCH_3)_3(CO)_6]$, (B) $(Ph_4P)[Mn_2(SeCH_3)_3(CO)_6]$ and (C) $(Ph_4P)[Mn_2(TeCH_3)_3(CO)_6]$ in CDCl3 342

Figure 6·36. The TGA diagrams of (A) $(Ph_4P)_2[Mn_3(S_2)_2(SH)(CO)_9]$, (B) $(Ph_4P)_2[Mn_3(S_2)_2(SCH_3)(CO)_9]$, (C) $(Ph_4P)_2[Mn_3(Se_2)_2(SeCH_3)(CO)_9]$ and (D) $(Ph_4P)_2[Mn_3(Te_2)_2(TeCH_3)(CO)_9]$ 346

Figure 6·37. The TGA diagrams of (A) $(Ph_4P)_3[Re_4(Te_2)_3(TeCH_3)(CO)_{12}]\cdot CH_3OH$, (B) $(Ph_4P)[Mn_2(SCH_3)_3(CO)_6]$, (C) $(Ph_4P)[Mn_2(SeCH_3)_3(CO)_6]$ and (D) $(Ph_4P)[Mn_2(TeCH_3)_3(CO)_6]$ 347

Figure 7·1. The Packing Diagram in the Unit Cell of $(Ph_4P)_2[(CO)_4W(WS_4)]$ (Stereoview) 382

Figure 7·2. The Structure of the $[(CO)_4W(WS_4)]^{2-}$ Anion 383

Figure 7·3. The Packing Diagram in the Unit Cell of $(Ph_4P)_2[(CO)_4M(MS_4)M(CO)_4]$ (M=Mo and W) (Stereoview) 387

Figure 7·4. The Structure of the $[(CO)_4M(MS_4)M(CO)_4]^{2-}$ (M=Mo and W) Anions 388

Figure 7·5. The Solid-State IR Spectra in the CO Region for (A) $(Ph_4P)_2[(CO)_4Mo(MoS_4)]$ and (B) $(Ph_4P)_2[(CO)_4W(WS_4)]$ 390

Figure 7·6. The Solid-StateIR Spectra in the CO Region for (A) $(Ph_4P)_2[(CO)_4Mo(MoS_4)Mo(CO)_4]$ and (B) $(Ph_4P)_2[(CO)_4W(WS_4)W(CO)_4]$ 391

Figure 7·7. The Solid-State Far IR Spectra of (A) $(Ph_4P)_2[(CO)_4Mo(MoS_4)]$ and (B) $(Ph_4P)_2[(CO)_4W(WS_4)]$ 392

Figure 7·8. The Solid-State Far IR Spectra of (A) $(Ph_4P)_2[(CO)_4Mo(MoS_4)Mo(CO)_4]$ and (B) $(Ph_4P)_2[(CO)_4W(WS_4)W(CO)_4]$..... 393

Figure 7·9. The UV/vis Spectra of (—) $(Ph_4P)_2[(CO)_4Mo(MoS_4)]$ and (---) $(Ph_4P)_2[(CO)W(WS_4)]$..... 394

Figure 7·10. The UV/vis Spectra of (---) $(Ph_4P)_2[(CO)_4Mo(MoS_4)Mo(CO)_4]$ and (—) $(Ph_4P)_2[(CO)_4W(WS_4)W(CO)_4]$..... 394

Figure 7·11. The TGA diagrams of (A) $(Ph_4P)_2[(CO)_4Mo(MoS_4)]$, (B) $(Ph_4P)_2[(CO)_4W(WS_4)]$, (C) $(Ph_4P)_2[(CO)_4Mo(MoS_4)Mo(CO)_4]$ and (D) $(Ph_4P)_2[(CO)_4W(WS_4)W(CO)_4]$ 397

ABBREVIATION

Bu_4N^+=tetrabutylammonium cation

Bu_3P=tributylphosphine

Cp=cyclopentadienyl, C_5H_5

crypt =4,7,13,16,21,24-hexaoxa-1,10-diazabicyclo[8,8,8]hexacosane, $N(CH_2CH_2OCH_2CH_2OCH_2CH_2)_3N$

DMF=N,N'-dimethylformamide, $HC(O)N(CH_3)_2$

dmos=dimethyloctylsilyl, $(C_7H_{15}CH_2)Si(CH_3)_2$

dmpe=1,2-bis(dimethylphosphino)ethane, $(CH_3)_2PCH_2CH_2P(CH_3)_2$

DMSO=dimethyl sulfoxide, $(CH_3)_2SO$

dppe=1,2-bis(diphenylphosphino)ethane, $Ph_2PCH_2CH_2PPh_2$

en=ehylenediamine, $H_2NCH_2CH_2NH_2$

Et_4N^+=tetraethylammonium cation

Me_4N^+=tetramethylammonium cation

N-MeIm=N-methylimidazole,

Ph_3P=triphenylphosphine

Ph_4P^+=tetraphenylphosphonium cation

PPN^+=bis(triphenylphosphino)imidium cation, $[(Ph_3P)_2N]^+$

THF=tetrahydrofuran, C_4H_8O

tmeda=N,N,N',N'-tetramethylehylenediamine, $(CH_3)_2NCH_2CH_2N(CH_3)_2$

CHAPTER 1

INTRODUCTION

I. General Background

All three elements of group 16, S, Se and Te, have a tendency to catenate. This results not only in the rings or chains of their several elemental forms[1], but also in the polychalcogenide Q_n^{2-} (Q=S, Se, Te; n=2-6) ions that can exist in solutions[2-3] or in the solid-state[4-21] in various sizes. Among the earliest systematic investigators to study the solution chemistry of the electropositive metals and many post transition non-metals, including chalcogens, were Zintl and co-workers[2e]. So compounds like A_2Q_n (A=alkali metal) or BQ_n (B=alkaline-earth metal) are often called as Zintl phases. Many such polyhomoatomic anions have been isolated and structurally characterized as the alkali/alkaline-earth salts, alkali-cryptates, or as molecules with organic cations. These include S_n^{2-} (n=2-7)[4-9], Se_n^{2-} (n=2-9)[10-17], and Te_n^{2-} (n=2-5)[18-21]. All these anions are found to be unbranched helical chains in the solid-state. The homoatomic bonding in the polychalcogenide anions represents a retention, to a certain degree, of the characteristics of the element. In addition to the normal σ bonds that connect chalcogen atoms in the chain, the negative charges are expected to fill in a π molecular orbital and delocalize over the whole chain. However, with the increased chain length, the negative charge will primarily reside on the terminal atoms[22]. Nevertheless, the terminal atoms in the polychalcogenide chains are often simply considered to have the formal oxidation state -1, and the internal atoms 0. This formal description is especially effective in dealing with

the coordinating properties of these ligands, and accounts for their observed behavior towards metal ions.

The polychalcogenide Q_n^{2-} ligands are fascinating in view of their versatile chelating abilities towards virtually all metal ions. This has and continues to breed a new branch of coordination chemistry which is largely characterized by structural diversity and wealthiness. In the past two decades, the chemistry of metal polysulfides has been extensively studied because evidence has been accumulated that this system is relevant to many processes of biological, geological and catalytic importance, such as biosynthesis of metalloproteins[23], hydrothermal conversion of metals to their binary chalcogenide minerals in nature[24], hydrodesulfurization (HDS) of crude oil[25], and hydrogenations of unsaturated and aromatic hydrocarbons[26]. The chemistry of metal polysulfides is rich and diverse. Several comprehensive review articles have appeared in the literature[27-28]. In contrast, until *c.a.* 1987, the chemistry of metal heavy polychalcogenides (i. e. polyselenides and polytellurides) failed to keep abreast with that of metal polysulfides, as witnessed by the very few sporadic reports of metal compounds containing polyselenide or polytelluride ligands, namely $Me\text{-}C(CH_2PPh_2)_3Co(Se_4)$[29], $[(dmpe)_2Ir(Se_4)]Cl$ ($dmpe=Me_2PCH_2CH_2PMe_2$)[30], $(\eta^5\text{-}Cp)_2Ti(Se_5)$[31], $(\eta^5\text{-}Cp)_2V(Se_5)$[32], $(\eta^5\text{-}Cp)_2M(Se_4)$ (M=Mo, W)[33], $(Ph_4P)_2[Fe_2Se_2(Se_5)_2]$[34], $(Bu_4N)_4[Hg_4(Te)_2(Te_2)_2(Te_3)_2]$[35] and $(Ph_4P)_2[Hg_2(Te)(Te_2)_2]$[35]. Two reasons seem to be primarily responsible for this delayed development. First, there was a considerable synthetic difficulty in introducing heavy polychalcogenide ligands into the metal centers because the most convenient method for synthesizing metal polysulfide complexes involved the use of H_2S, and this was found to be unattractive for the polyselenide or polytelluride system (H_2Se is extremely poisonous, and H_2Te highly unstable). Second, initial perception that the chemistry of metal heavy polychalcogenides would more or less parallel that of metal polysulfides had greatly hindered research enthusiasm in this area. As a

result, much of our understanding of metal polychalcogenide chemistry up to the mid 80's had been derived from the metal polysulfide system. Table 1·1 summarizes the most commonly observed coordination modes for polysulfide ligands.

Table 1·1. Typical Coordination Modes of Polysulfide Ligands

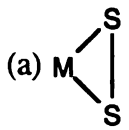
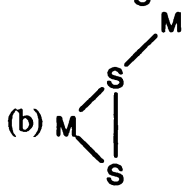
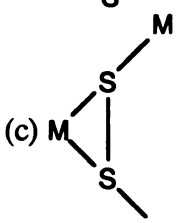
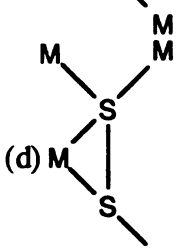
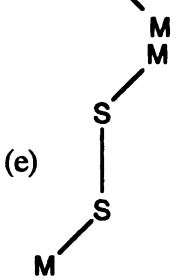
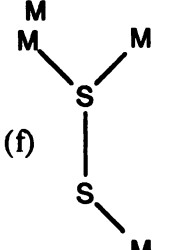
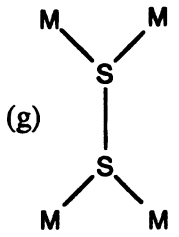
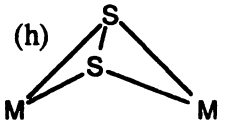
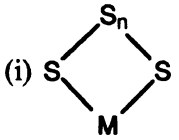
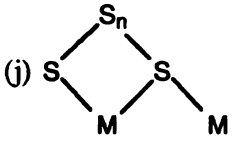
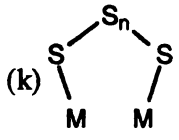
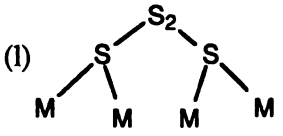
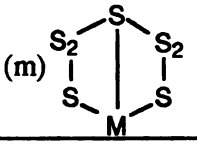
Type	Example	Reference
(a) 	$[(dppe)_2Ir(S_2)]^+$, $Cp_2Mo(S_2)$	[36a-b], [36c]
(b) 	$[Mo_4(NO)_4(S_2)_5S_3]^{4-}$, $Cp_2Fe_2(S_2)_2CO$	[37a], [37b]
(c) 	$Mn_4(S_2)_2(CO)_{15}$	[38]
(d) 	$Mn_4(S_2)_2(CO)_{15}$	[38]
(e) 	$[(NH_3)_5Ru(S_2)Ru(NH_3)_5]^{4+}$, $Cp(CO)_2Mn(S_2)Mn(CO)_2Cp$	[39a-b], [39c]
(f) 	$Cp_4Fe_4S_2(S_2)_2$, $Cp_4Co_4S_2(S_2)_2$	[40a-b], [40c]

Table 1·1. (cont'd)

Type	Example	Reference
 (g)	$[\{SMo_3(CO)_7\}_2S_2]$, $[CpMn(NO)(S_2)]_n$	[41a], [41b]
 (h)	$[Mo_2(S_2)]^{2-}$, $Fe_2(S_2)(CO)_6$	[42a-b], [42c]
 (i) n=1-4,7	$(Cp^*)_2Ti(S_3)$, $[Ni(S_4)_2]^{2-}$, $[Pt(S_5)_3]^{2-}$, $[Hg(S_6)_2]^{2-}$, $[AgS_9]^-$	[43a], [43b], [43c-d], [43e], [43f]
 (j) n=2 or 4	$[Cu_3(S_4)_3]^{3-}$, $[Ag_2(S_6)_2]^{2-}$	[44a], [44b]
 (k) n=1-6	$(MeCp)_4Ti_2(S_3)_2$, $[Au_2(S_4)_2]^{2-}$, $[Mo_2(OH)(NO)_2(S_2)_3(S_5)]^{3-}$, $[Bi_2(S_7)_4(S_6)]^{4-}$, $[Pd_2(S_7)_4]^{2-}$, $[Cu_2(S_6)_2(S_8)]^{4-}$	[45a], [45b], [45c], [45d], [45e], [45a]
 (l)	$[Cu_6(S_4)_3(S_5)]^{2-}$	[46]
 (m)	$(Me_3P)_3Os(S_7)$	[47]

The impetus to scrutinize the metal heavy polychalcogenide chemistry in the late 1980s came from the realization that this chemistry would be quite different from that of metal polysulfides. For most metal polyselenide (polytelluride) complexes synthesized by that time, few had sulfur analogues. In some cases, the structures of metal polyselenides or polytellurides turned out to be more novel. So compounds such as $(Et_4N)_2[V_2Se_{13}]$[48], $(Ph_4P)_3[NbTe_{10}]\cdot DMF$[49], $(Ph_4P)_3[Cr_3(Q_4)_6]$[Q=Se or Te][50], $(Bu_4N)_4[Hg_4(Te)_2(Te_2)_2(Te_3)_2]$[35] and $(Ph_4P)_2[Hg_2(Te)(Te_2)_2]$[35], to just name a few, had never been seen in the metal polysulfide chemistry. Plausible reasons for this different coordination chemistry of the heavy polychalcogenide ligands are:

(a) the propensity for catenation of chalcogen atoms decreases from S to Te, which greatly affects Q_x^{2-} ligand sizes. Thus far, the longest polysulfide chain observed in a metal complex is S_9^{2-}[43f]. Similar sized ligands have not yet been known for the metal polyselenide or polytelluride compounds;

(b) the reduction potentials required to split the Q-Q bonds vary with the nature of the element and the ligand size. This results in different internal redox chemistry in various metal/Q_x^{2-} systems;

(c) the increase in the Q-Q bond lengths from S to Te affects the chemical nature and dimensions of the Q_x^{2-} ligands.

The initial efforts needed in this field were the synthetic explorations in establishing viable routes to new compounds. We[51], and others[52-53], were among the first to devote attention to the development of synthetic methodology in this chemistry. Our broad interest in metal chalcogenide chemistry has prompted us to adopt multiple approaches to the novel metal polychalcogenide compounds. For instance, by using the molten salt technique, meta-stable solid-state compounds of metal polychalcogenides were sought by

several researchers in this group[54]. While the hydro(solvo)thermal method was employed to make metal polychalcogenide clusters[55-56], homoleptic complexes were prepared from the conventional solution synthesis[57]. As a reflection of the above diverse endeavor, the results presented in this dissertation can be essentially divided into two different types: (i) the conventional solution synthesis for making homoleptic species, and (ii) the hydro(solvo)thermal synthesis for making chalcogen-containing metal carbonyl clusters. To put the above two types of synthetic work into perspective, a brief evolution of various synthetic methods for making metal heavy polychalcogenide compounds is given below.

II. Summary of Synthetic Methods

1. Use of polychalcogenide anions generated *in situ* as reagents

The simplest method of producing polysulfide ligands is to pass a stream of H_2S through an aqueous NH_3 solution in the presence of elemental sulfur:

$$H_2S + (x\text{-}1)S + 2NH_3 \xrightarrow[x=2\text{-}6]{\text{aqueous}} (NH_4)_2S_x \quad \text{eq.}(1\cdot1)$$

The polysulfide anions generated from such a procedure can then react with appropriate metal salts. This has been very successful in preparing metal polysulfides. Thus, the most rational synthetic approach for metal heavy polychalcogenides would be to duplicate this reaction. However, H_2Se gas is expensive and poisonous, and H_2Te highly unstable. Such a preparative route is actually impractical, and potentially irreproducible.

In non-protic solvents, reactions of alkali metals with elemental chalcogens can also generate the polychalcogenide anions *in-situ*. Another advantage of using nonaqueous solvents is to allow the use of various organic counterions. When appropriate metal salts

are added to these solutions, metal complexes will form. The first compound prepared by this method was the $(Ph_4P)_2[Fe_2Se_2(Se_5)_2]$[34]:

$$6Na + 12Se + 2FeCl_2 \xrightarrow{DMF,\ 70\ ^\circ C} Na_2[Fe_2Se_2(Se_5)_2] + 4NaCl \quad \text{eq.(1·2)}$$

Many other metal complexes have now been prepared in a similar manner, they include $(Ph_4P)_2[Sn(Se_4)_3]$[58], $(Ph_4P)[(\eta^5\text{-Cp})Mo(Se_4)_2]$[58], $(Ph_4P)_2[M(Se_4)_2]$ (M=Ni, Zn, Cd, Hg and Pb)[59], $(Ph_2P)_2[Cu_4(Se_4)_{2.4}(Se_5)_{0.6}]$[60] and $(Ph_2P)_2[Ag_4(Se_4)_{2.1}(Se_5)_{0.9}]$[60]. Although the current preparative examples all involve polyselenide compounds, the method itself is extendable to the polytelluride system. The only drawback seems to be the use of reactive alkali metals, which makes the reaction heterogeneous and control of stoichiometry difficult. A synthetic modification of using A_2Se_x (A=alkali metal, x=1, 2) and elemental selenium is often adopted:

$$2Na_2Se + 6Se + M(Ac)_2 \xrightarrow[15\text{-crown-5}]{DMF} [Na(15\text{-crown-5})_2][M(Se_4)_2] + 2NaAc \quad \text{eq.(1·3)[61]}$$

M=Zn, Cd and Hg

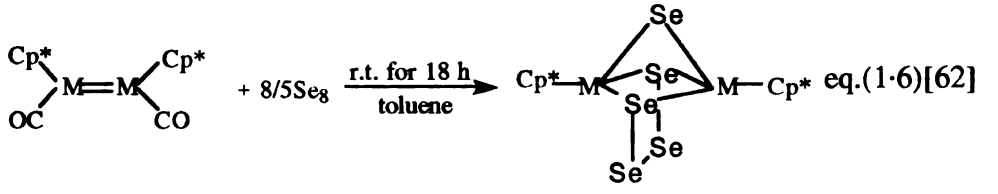
$$2Na_2Se_2 + 4Se + PdCl_2 \xrightarrow[2Ph_4PCl]{DMF} (Ph_4P)_2[Pd(Se_4)_2] + 4NaCl \quad \text{eq.(1·4)[13d]}$$

2. Use of elemental chalcogens as reagents

In order to achieve a successful addition of elemental chalcogen to a metal ion, the reaction requires that a coordinatively unsaturated electron-rich metal complex, or a compound containing metal-metal bonds be used as the starting material. Such a process often results in change of the oxidation state of the metal, and is bound to produce compounds with partial chalcogenide-coordination environment because no metathesis can take place between the all ancillary groups and the elemental chalcogen atoms. Thus, this

method is responsible for the syntheses of most organometallic compounds. Examples are given in eq. 1·5 and eq. 1·6:

$$[(dmpe)_2Ir]Cl + 1/2Se_8 \xrightarrow[THF/C_6H_6(1:1)]{\text{r.t. for 8 days}} [(dmpe)Ir(Se_4)]Cl \quad \text{eq.(1·5)[30]}$$



eq.(1·6)[62]

M=Co, Rh

Due to the lack of suitable starting metal complexes which possess enough reactivity towards elemental chalcogen, this method is far less than universal. No organometallic compounds of polytellurides have been reported to be prepared from this route, either because the reactivity of elemental tellurium is lower than that of selenium or, perhaps, because no such reactions have been extensively pursued.

Elemental selenium is readily incorporated into some metal monoselenide compounds, forming metal polyselenide rings via a redox process:

$$2[WSe_4]^{2-} + 1/4Se_8 \xrightarrow{CH_3CN,\ 85\ ^\circ C} [W_2Se_{10}]^{2-} \text{ (two isomers)} \quad \text{eq.(1·7)[63]}$$

$$[MoSe_4]^{2-} + 5Se \xrightarrow[2\ h]{\text{DMF, at r.t.}} [MoSe(Se_4)_2]^{2-} \quad \text{eq.(1·8)[64]}$$

The above results are analogous to those known for sulfur[65]. Similar reactions between complexes containing Se-Se bonds and elemental selenium can also take place, resulting in MSe_x ring augmentation:

$$[Mn(Se_2)_2(CO)_6]^{2-} + 4Se \xrightarrow{DMF} [Mn(Se_4)_2(CO)_6]^{2-} \quad \text{eq.(1·9)[66]}$$

Recently, Rauchfuss and co-workers have discovered that N-alkylimidazoles can greatly promote the reactivity of elemental chalcogens (i.e. S and Se) towards low valent metal species, particularly metal powders and metal carbonyls. Thus, the N-alkylimidazole suspension of elemental selenium is found to react with $Fe(CO)_5$ or even zinc dust to produce polyselenide complexes:

$$2Fe(CO)_5 + Se_8 \xrightarrow{\text{N-MeIm, 25 °C}} [Fe(\text{N-MeIm})_6][Fe(Se_4)_2(CO)_2] + 8CO \quad \text{eq.(1·10)[67]}$$

$$Zn + 1/2Se_8 \xrightarrow{\text{N-MeIm, 100 °C}} [Zn(Se_4)(\text{N-MeIm})_2] \quad \text{eq.(1·11)[68]}$$

The partial coordination of selenium ligand in $[Zn(Se_4)(\text{N-MeIm})_2]$ is the result of competition of the solvent N-methylimidazole which is a strong σ-donor ligand.

3. Extraction of transition metal/chalcogen-containing alloys

Some ternary or quaternary alkali metal alloys can be "solubilized" in polar organic solvents (e.g. en). Such a process often involves the disruption of solid-state bonding with the assistance of a strong coordination solvent. As a result, metal polychalcogenide clusters can be isolated by addition of organic counterions:

$$K_2Hg_2Te_3 \xrightarrow{en} \begin{cases} \xrightarrow{Bu_4NBr(MeOH)} (Bu_4N)_4[Hg_4(Te)_2(Te_2)_2(Te_3)_2] \\ \xrightarrow{Ph_4PBr(MeOH)} (Ph_4P)_2[Hg_2(Te)(Te_2)_2] \end{cases} \quad \text{eq.(1·12)[35]}$$

$$KAuTe_2(K_2AuAsTe_3 \text{ or } K_3AuGeTe_3) \xrightarrow{\text{en, PPNCl}} (PPN)_2[Au_2(Te_2)_2] \quad \text{eq.(1·13)[69]}$$

4. Use of other reagents

(i). Bis(trialkylsilyl)selenides

It is known that bis(trimethylsilyl)sulfide $(Me_3Si)_2S$ can be used in place of H_2S to synthesize sulfido complexes[70]. Ibers and co-workers explored the use of several bis(trialkylsilyl)selenides as possible "selenization" agents, and found that $[(CH_3)_2C_8H_{17}Si)]_2Se$ provides the best compromise[48, 71]. Use of this reagent as well as the other bis(trialkylsilyl)selenides (mainly $[Me_3Si]_2Se$) was found in the synthesis of $(Et_4N)_2[V_2(Se_2)_4(Se_5)]$[48], $[MSe_4]^{2-}$ (M=Mo, W)[71], $[(\eta^5\text{-}Cp)_4Ti_4(\mu_4\text{-}O)(\mu_2\text{-}Se)(\mu_3\text{-}Se)_2(\mu_3\text{-}Se_2)_2]$[72], $[\eta^5\text{-}MeCp_2V_2(\mu_2\text{-}Se)(\mu_2\text{-}Se_2)(\mu_2\text{-}\eta^2\text{-}Se_2)]$[73]. It should be pointed out that bis(trialkylsilyl)selenides are monoselenide-transfer agents, as can be seen in the synthesis of a large number of metal monoselenide clusters by Fenske[73].

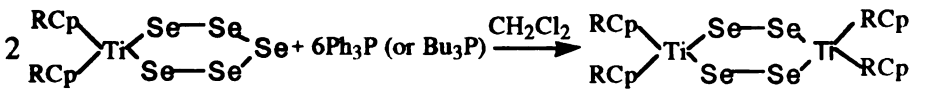
(ii). Hydrogen chalcogenides

H_2Se was employed to synthesize $[(\eta^5\text{-}MeCp)_2V_2(\mu_2\text{-}Se)(\mu_2\text{-}Se_2)(\mu_2\text{-}\eta^2\text{-}Se_2)]$[74]. Because of its poor stability, H_2Te is generated from reaction of Al_2Te_3 with HCl and used *in-situ* to prepare $[(\eta^5\text{-}Cp^*)_2Re_2(Te_2)(CO)_4]$[75]. Again, hydrogen chalcogenides are conceivably monoselenide-transfer agents. Generation of Q-Q bonds in the products must rely on a redox process during the reaction.

(iii). Reactivity of Q_x^{2-} ligands towards organic phosphines

With abstraction of internal selenium atoms from MSe_x rings, this reaction can lead to compounds with shorter Se_x^{2-} ligands. Sometimes these reactive intermediate species generated *in-situ* will condense to a larger cluster. For instance:

$$[(dmpe)_2Ir(Se_4)]Cl+2Ph_3P \xrightarrow{CH_3CN} [(dmpe)_2Ir(Se_2)]Cl+2Ph_3PSe \quad \text{eq.(1·14)[30]}$$



+ $6Ph_3PSe$ (or Bu_3PSe)

R=H, Me, *i*-Pr

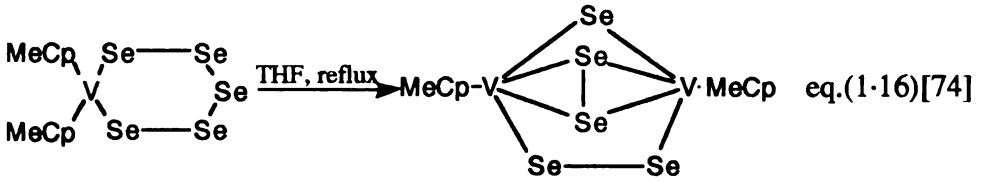
eq.(1·15)[76]

(iv). Other chalcogen-containing agents

Many other chalcogen-containing reagents, such as SeO_3^{2-}, TeO_3^{2-}, COSe and CSe_2, have all been occasionally used to synthesize metal chalcogenide complexes. Reactions involving these reagents lack rationale, so their synthetic value is limited[77].

5. Thermolysis

The thermal rearrangement reactions have been used to prepare new compounds. For example, $(\eta^5\text{-MeCp})_2V(Se_5)$ is transformed to $[(\eta^5\text{-MeCp})_2V_2(\mu_2\text{-Se})(\mu_2\text{-Se}_2)(\mu_2\text{-}\eta^2\text{-Se}_2)]$ upon refluxing in THF:



eq.(1·16)[74]

Heating a DMF solution of $[Mn_2(Se_4)_2(CO)_6]^{2-}$ at 90 °C leads to the homoleptic complex $[Mn(Se_4)_2]^{2-}$. IR spectroscopic studies suggest that the process is a thermally induced disproportionation reaction:

$$[Mn_2(Se_4)_2(CO)_6]^{2-} \xrightarrow{DMF,\ 90\ ^\circ C} [Mn(Se_4)_2]^{2-} + 1/2Mn_2CO_{10} + CO$$ eq.(1·17)[66]

6. The molten salt technique

The use of molten alkali metal polychalcogenides for making solid-state compounds is a very active area of research [54]. As far as the synthesis of molecular compounds is concerned, the molten salt method differs from conventional, non-aqueous, reactions in many respects. For example, reaction temperatures attainable by molten salts are often higher than those using organic solvents. This tends to increase the chemical reaction rates and even change the reaction pathways. The highly ionic nature of the melts provides enhanced solubility for many compounds and thus, high concentrations of reactants can be obtained. The main advantage is the elimination of any "wet" solvent, which makes the system oxygen-free. This may prove to be important in the synthesis of early transition metal, or lanthanide and actinide compounds. Thus far, there have seen several such examples:

$$U + 2K_2Se + 8Se \xrightarrow[10\ days]{300\ ^\circ C} K_4[U(Se_2)_4] \quad \text{eq.(1·18)[78]}$$

$$Nb + 3K_2Se + 10Se \xrightarrow[100\ h]{375\ ^\circ C} K_6[Nb_4Se_4(Se_2)_9] \quad \text{eq.(1·19)[79]}$$

The recent application of polychalcogenide salts of large organic cations (e.g. Ph_4P^+) as reactive fluxes opened up a new synthetic dimension in this research area. The use of organic counterions in place of alkali metal ions not only lowers the melting point, but also results in new and often open structure types (i.e. size or template effect). For example, three isotypical compounds with a layered structure have been prepared as follows:

$$2M + (Ph_4P)_2Se_5 + 8Se \xrightarrow[2\ days]{200\ ^\circ C} (Ph_4P)[M(Se_6)_2] \quad \text{eq.(1·20)[80]}$$

M=Ga, In and Tl

Large channels caused by the presence of Ph_4P^+ cations are found in the compounds. However, it should be noted that these compounds have an extended polymeric structure. In general, the molten salt technique favors formation of solid-state compounds. The synthesis of molecular compounds by the molten salt method has been purely serendipitous, and little is known about how to control the reactions from which new small molecular anions can be made reproducibly.

7. Use of Zintl phases of alkali metal polychalcogenides

By far, this is the most successful synthetic method for making metal heavy polychalcogenide compounds. It is generally applicable to sulfide, selenide and telluride systems. Most of these Zintl phases can be obtained from either high-temperature or liquid ammonia reactions of alkali metals and chalcogens. Our early method of preparing the starting materials of A_2Q_x was to react stoichiometric amounts of elemental chalcogens with alkali metals in sealed Pyrex tubes at elevated temperatures (i.e. 450 °C for polyselenide and 490 °C for polytelluride). However, the exothermic reactions at such high temperatures often caused cracks in the tubes and the alloy products usually left some insoluble residue, which made stoichiometric control difficult. Subsequently, we used a liquid-ammonia method:

$$xQ + 2A \xrightarrow[\text{-78 °C (dry-ice/acetone)}]{\text{Liq.NH}_3} A_2Q_x \qquad \text{eq(1·21)}$$

A=Li, Na, K, Rb, Cs; Q=S, Se, Te

In our hands this method provided excellent polychalcogenide anions for synthetic reactions. When simple metal salts such as halides or oxides are used as starting materials, the reactions leading to metal complexes are mostly metathetical. Occasionally, redox precesses can also occur:

$$SnCl_4 + 3Na_2Se_4 + 2Ph_4PCl \xrightarrow{DMF/Et_2O} (Ph_4P)_2[Sn(Se_4)_3] + 6NaCl \quad \text{eq.(1·22)[57e]}$$

$$K_2Te_4 + (Ph_3P)_3CuCl \xrightarrow[Me_4NCl]{DMF} (Me_4N)[Cu(Te_4)] + 2KCl + 3Ph_3P \quad \text{eq.(1·23)[81]}$$

$$2AuCN + 2Na_2Se_5 + 2PPNCl \xrightarrow{DMF/Et_2O} (PPN)_2[Au_2Se_2(Se_4)_2] + 2NaCl + 2NaCN \quad \text{eq.(1·24)[57c]}$$

Oxidative decarbonylation of metal carbonyls by polychalcogenide ligands Q_n^{2-} (Q=S, Se and Te; n=2-6) provides another convenient route for introducing chalcogen-atoms into metal centers[53]. Depending on the reactivity of the metal carbonyl and the polychalcogenide ligand, the product isolated can be either homoleptic or CO-containing complexes:

$$M(CO)_6 + nK_2Se_3 \xrightarrow{DMF} [MSe_4]^{2-} \text{ or } [MSe(Se_4)_2]^{2-} + 6CO \quad \text{eq.(1·25)[64]}$$

M=Mo, W

$$M(CO)_6 + K_2Te_4 + 2Ph_4PBr \xrightarrow{DMF/THF} (Ph_4P)_2[M(Te_4)(CO)_4] + 2CO + 2KBr \quad \text{eq.(1·26)[82]}$$

M=Cr, Mo, W

This shows that the reactions are often controlled by redox interplay between the metal center and the polychalcogenide ligand. Since most of the transition metal carbonyls are readily available, this synthetic method has been successfully applied to the preparations of many transition metal polychalcogenide compounds.

8. Hydro(solvo)thermal reactions

Despite the successful application of hydrothermal techniques to the preparation of many technologically important materials, such as α-quartz and zeolites, the hydrothermal synthesis of chalcogenides is little studied[56]. Several examples of preparing monochalcogenids under hydro(methano)thermal conditions are known[56]. These reactions often employ alkali carbonates as "mineralizers" (complexing agents) to increase dissolution of reactants as well as to facilitate crystal growth[56]. Researchers in our group have found that under hydro(solvo)thermal conditions, alkali metal polychalcogenides can act as reagents as well as "mineralizers". The latter help with or promote crystal growth. These reactions provide a unique route to novel metal polyselenide clusters, most of which have, thus far, proven to be inaccessible by other synthetic methods:

$$Mo + 2K_2Se_4 \xrightarrow[\text{sealed tube}]{H_2O,\ 140\ ^\circ C \text{ for } 60\ h} K_{12}[Mo_{12}Se_8(Se_2)_{18}(Se_3)_4] \quad \text{eq.(1·27)[55]}$$

This method was applied to transition metal carbonyl/polychalcogenide systems in attempt to synthesize chalcogen-containing metal carbonyl clusters. It turned out that the application of the hydro(solvo)thermal technique to the synthesis of metal carbonyl clusters is feasible. Many novel clusters have been synthesized by such technique. This chemistry will be discussed in detail in later chapters[83].

Research in polychalcogenide chemistry has been mostly driven by the need to expand our knowledge of structural principles and bonding in these ligands. Therefore, the emphasis is primarily placed on fundamental chemistry rather than on practical applications. For this reason, the full characterization of the newly synthesized compounds is prerequisite for the study of their chemistry. The use of different spectroscopic techniques for characterizing metal polychalcogenides is given in the following section.

III. Spectroscopic Studies of Metal Heavy Polychalcogenides

1. The IR and UV/vis Spectroscopy

Both IR and UV/vis spectroscopic studies are little informative in the characterization of metal heavy polychalcogenides. Unless CO groups are present in the molecules, the mid-IR region is invariably dominated by the hydrocarbon skeletons of ancillary ligands or the organic counterions. In the far IR region, M-Se and Se-Se often show absorptions in the 200-400 cm^{-1} with the corresponding M-Te and Te-Te bands shifted to even lower energies. IR spectroscopy could be used to confirm the presence of Q-Q bonds in the compound. However, one should be cautious in assigning these bands in view of the absence of any systematic studies using isotope labeling.

The problem associated with the UV/vis spectroscopy is two-fold. First, some metal complexes do not retain their identity in a polar solvent such as DMF or CH_3CN. If M^+ ions are involved, such a dissociation is likely. In this case, the UV/vis spectrum of the metal complex is similar to that of the free polychalcogenide ligand. Second, most compounds that remain intact in polar solvents show featureless UV/vis spectra yielding no information about the coordination environment of the metal ions. The following example is one of the very few occasions when the UV/vis spectra are useful in identifying the different species present in solutions. DMF solutions of the $[Fe_2Se_2(Se_5)_2]^{2-}$ give five absorption maxima at 312(sh), 386(sh), 415(sh), 498 and 670(sh) nm, which are characteristic of this Fe(III) species[34], while the UV/vis spectrum of the $[Fe(Se_4)_2]^{2-}$ in the same solvent is featureless [84].

2. NMR Spectroscopy

Both selenium and tellurium have spin-half nuclei with moderate NMR receptivity. ^{77}Se (I=1/2, natural abundance=7.58%, receptivity relative to ^{13}C=2.98), ^{125}Te (I=1/2, natural abundance=6.99%, receptivity relative to ^{13}C=12.5) and ^{123}Te (I=1/2, natural

abundance=0.87%, receptivity relative to ^{13}C=0.89) are all NMR active, but ^{123}Te is seldom used because of its lower natural abundance[85]. In ^{77}Se and ^{125}Te NMR studies, the convention is that their chemical shifts are referenced respectively to $(CH_3)_2Se$ and $(CH_3)_2Te$ at δ=0 ppm with the downfield shift associated with positive ppm values. ^{77}Se NMR spectroscopy has been applied to a larger extent than ^{125}Te, although both equally have the potential for characterizing metal complexes in solution. The chemical shifts of both ^{77}Se and ^{125}Te are found to be extremely sensitive to their chemical environments. Due to low natural abundance of these two nuclei, the Se-Se, or Te-Te couplings are often unobservable. Occasionally, M-Q bond coupling to an NMR active metal can be observed. In a typical metal polychalcogenide complex, the ligand atoms are often in very different chemical environments (metal-bound, internal or bridging, etc.), thus the resonance pattern in its NMR spectrum can be very complex. In the absence of any homo-nuclear coupling information, the assignment of the different NMR resonances is not easy but several assignments have been made. For example, in the series of $[MX(Q_4)_2]^{2-}$ (M=Mo, W; X=O, Se; Q=Se, Te) and $[M(Se_4)_2]^{2-}$ (M=Ni, Pd, Pt, Zn, Cd, Hg) complexes the NMR spectra have completely characterized.

Within the $[WQ(Se_4)_2]^{2-}$ (Q=O, S, Se) series, the resonances corresponding to the metal-bound seleniums all exhibit couplings to W (^{183}W, I=1/2, natural abundance=14.3%)[64a-b]. This observation helps in assigning the resonances of both the terminal and the internal selenium atoms in the compounds. By analogy, similar assignments are then extended to the Mo (two quadropolar nuclei: ^{95}Mo, I=5/2, natural abundance=15.7%; ^{97}Mo, I=5/2, natural abundance=9.5%) analogues of the above compounds[71], as well as to the $[MO(Te_4)_2]^{2-}$ (M=Mo, W) system, where the Mo-Se, Mo-Te or W-Te couplings are not observed[86]. Table 1·2. gives the NMR data of these compounds.

Within the $[M(Se_4)_2]^{2-}$ (M=Ni, Pd, Pt) series, Pt has a spin-half nucleus (^{195}Pt, I=1/2, natural abundance=33.8%). In solution the $[Pt(Se_4)_2]^{2-}$ species generated *in-situ* gives a two-line ^{77}Se NMR spectrum with δ=727 and 642 ppm. The resonance at 727 ppm shows coupling to ^{195}Pt, thus is assigned to metal-bound selenium and the remaining to the inner two selenium atoms of the Se_4^{2-} ligand. By analogy, similar assignments are made for the Ni and Pd analogues[87]. The detailed data are also given in Table 1·2.

Within the $[M(Se_4)_2]^{2-}$ (M=Zn, Cd, Hg) series, both Cd and Hg have spin-half nuclei (^{111}Cd, I=1/2, natural abundance=12.3%; ^{113}Cd, I=1/2, natural abundance=12.8% and^{119}Hg, I=1/2, natural abundance=16.8%). The observed couplings in these two complexes allow unequivocal assignments for their ^{77}Se NMR spectra. The ^{77}Se NMR spectrum of the $[Zn(Se_4)_2]^{2-}$ is then assigned by analogy as shown in Table 1·2[87].

Table 1·2. ^{77}Se and ^{125}Te NMR data for the $[MX(Q_4)_2]^{2-}$ (M=Mo, W; X=O, S, Se; Q=Se, Te) and $[M(Se_4)_2]^{2-}$ (M=Ni, Pd, Pt, Zn, Cd, Hg) series

Compound	Metal d electron configuration	δ($^1J_{Q-M}$, Hz), ppm			Reference
		Metal-bound	Ring	Apical	
$[WO(Se_4)_2]^{2-}$	d^2	828(98)	280	/	[71]
$[WS(Se_4)_2]^{2-}$	d^2	993(106)	313	/	[71]
$[WSe(Se_4)_2]^{2-}$	d^2	1034(108)	324	1787	[71]
$[MoO(Se_4)_2]^{2-}$	d^2	946	380	/	[71]
$[MoS(Se_4)_2]^{2-}$	d^2	1122	396	/	[71]
$[MoSe(Se_4)_2]^{2-}$	d^2	1163	403	2357	[71]
$[WO(Te_4)_2]^{2-}$	d^2	903	120	/	[86]

Table 1·2. (cont'd)

Compound	Metal d electron configuration		$\delta(^1J_{Q\text{-}M}$, Hz), ppm		Reference
$[MoO(Te_4)_2]^{2-}$	d^2	717(98)	89	/	[86]
$[Ni(Se_4)_2]^{2-}$	d^8	820	748	/	[87]
$[Pd(Se_4)_2]^{2-}$	d^8	893	758	/	[87]
$[Pt(Se_4)_2]^{2-}$	d^8	727(384)	642	/	[87]
$[Zn(Se_4)_2]^{2-}$	d^{10}	127	598	/	[87]
$[Cd(Se_4)_2]^{2-}$	d^{10}	62(255)	608	/	[87]
$[Hg(Se_4)_2]^{2-}$	d^{10}	76(1265)	594	/	[87]

By comparing the above assignments, a general shielding argument based on the metal d electron configuration has been advanced[87]. In the free Q_4^{2-} ligands, the shielding arguments would predict that the terminal atoms resonate upfield of the internal atoms in accordance with the formal charge assignments on these atoms. Upon chelating to a metal ion with partially filled d orbitals, the electron density of these terminal (now metal-bound) atoms will decrease because of electron donation from the Q_4^{2-} ligand to the d orbitals of the metal. This will lead to NMR signals downfield of the resonances due to non-metal bound selenium atoms (Table 1·2). However, if the metal ion has filled d orbitals (i.e. Zn, Cd or Hg), the electron donation from the ligand to the metal is claimed to be negligible leading to resonances upfield of the non-metal bound selenium atoms (Table 1·2). Though this argument is empirical, it appears to be consistent thus far.

It should be noted that the ^{77}Se NMR spectrum of $[Pt(Se_4)_3]^{2-}$ gives two signals at 680 and 790 ppm. The resonance at 680 ppm is assigned to the metal-bound Se atoms because of the observed Se-Pt coupling[88]. This is opposite to the above identified trend.

Apparently, other factors must also be operative in affecting the resonance positions of Se atoms in polyselenides.

^{77}Se NMR spectroscopy was also used to characterize the solution behavior of the In/Se_x^{2-} family of compounds[89-90]. The ^{77}Se NMR spectra of $[In_2(Se_4)_4(Se_5)]^{4-}$, $[In_3Se_3(Se_4)_3]^{3-}$ and $[In_2Se_2(Se_4)_2]^{2-}$ in DMF solutions are all identical and show three peaks in 2:2:1 ratio at 643 ppm, 197 ppm and -244 ppm respectively. Therefore, it has been proposed that the most stable complex in solution is $[In_3Se_3(Se_4)_3]^{3-}$. The peak at 643 ppm can be assigned to resonance from the terminal Se atoms of the chelating Se_4^{2-} ligands and 197 ppm from the inner atoms of the Se_4^{2-} ligands while the -244 ppm is more reasonably assigned to the bridging Se^{2-} ligand. This assignment is consistent with the ^{77}Se NMR results reported for other metal polyselenide complexes discussed above.

IV. Concluding Remarks

Thus far, research in metal heavy-polychalcogenides has covered almost every group of p-block and d-block elements with a fair degree of success at least for the polyselenide system. Yet, the field is still expanding, as evidenced by many new research papers constantly appearing in the literature[77]. Different synthetic methods, such as conventional solution reactions, hydro(solvo)thermal techniques and molten salt syntheses (i.e. by using the organic cations), are enjoying continued application in this research area. Exploration of these different methods has broadened the horizon of coordination chemistry of polychalcogenide ligands.

Since a large number of metal polychalcogenide compounds have been synthesized, many aspects of their reaction chemistry[30,76,86,91-92] as well as the potential of using some of these compounds as soluble low temperature precursors to solid-state materials[93-95] are being explored. For example, by using suitable metal polyselenide complexes, solid-state thin films or nanocluters of technologically relevant binary and

ternary metal chalcogenides[96-100] have been fabricated in this laboratory[93-95]. However, mechanistic issues in metal polychalcogenide chemistry have seldom been addressed thus far. Interest in this area, along with the synthesis of yet new metal heavy polychalcogenide compounds, is expected to grow[77].

In the following chapters, I will first discuss the synthesis, X-ray structures and spectroscopic characterization of metal heavy polychalcogenide complexes made by solution method, followed by those of transition metal carbonyl chalcogenide clusters prepared by hydro(solvo)thermal technique. For clarity, compounds are arranged in different chapters according to periodic groups.

REFERENCES

1. (a) N. N. Greenwood and A. Earnshaw, *Chemistry of the Elements,* Pergamon Press, Oxford UK, 1989, p757-917. (b) F. A. Cotton and G. Wilkinson, *Advanced Inorganic Chemistry,* 5th Ed.; John Wiley & Sons, New York, 1988, p491-543.

2. Early investigations on the existence of the homopolychalcogenide anions in liquid ammonia solution can be found in (a) C. C. Hugot *R, Hebd. Seances Acad. Sci,* (1899), 219, 299, 388. (b) C. C. Hugot, *Ann. Chim. Phys.*, 21(1900), 72. (c) C. A. Kraus and C. Y. Chiu, *J. Am. Chem. Soc,* 14(1922), 1999-2009. (d) F. W. Bergstrom, *J. Am. Chem. Soc.*, 48(1926), 146-151. (e) E. Zintl, J. Goubeau and W. Dullenkopf, *Z. Phys. Chem., Abt. A,* 154(1931), 1. (f) W. Klemm, H. Sodomann and P. Langmesser, *Z. Anorg. Allg. Chem.*, 241(1939), 281-304.

3. For recent spectroscopic studies of these species in polar solvents (i. e. en, NH_3 and MDF, etc.), see (a) F. Seel, H. J. Guttler, G. Simon and A. Wieckowski, *Pure Appl. Chem.*, 49(1977), 45-54. (b) K. W. Sharp and W. H. Koehler, *Inorg. Chem.*, 16(1977), 2528-2565. (c) L. D. Schultz and W. H. Koehler, *Inorg. Chem.*, 26(1987), 1989-1993. (d) P. Dubois, J. P. Lelieur and G. Lepoutre, *Inorg. Chem.*, 26(1987), 1897-1902. (e) P. Dubois, J. P. Lelieur and G. Lepoutre, *Inorg. Chem.*, 27(1987), 73-80. (f) P. Dubois, J. P. Lelieur and G. Lepoutre, *Inorg. Chem.*, 27(1988), 1883-1890. (g) V. Pinon and J. P. Lelieur, *Inorg. Chem.*, 30(1991), 2260-2264. (h) M. Bjorgvinsson and G. J. Schrobilgen, *Inorg. Chem.*, 30(1991), 2540-2547.

4. For S_2^{2-}, see (a) H. Föppl, *Angew. Chem.*, 70(1958), 401-401. (b) H. Föppl, E. Busmann and F.-K. Frorath, *Z. Anorg. Allg. Chem.*, 314(1962), 12-20.

5. For S_3^{2-}, see W. S. Miller and A. J. King, *Z. Kristallogr., Kristallgeom., Kristallphys., Kristallchem.*, 94(1936), 439.

6. For S_4^{2-}, see (a) S. C. Abrahams, *Acta Crystallogr.*, 7(1954), 423-429. (b) S. C. Abrahams and J. L. Bernstein, *Acta Crystallogr.*, 25B(1969), 2365-2370. (c) R. Tegman, *Acta Crystallogr.*, 29B(1973), 1463-1469.

7. For S_5^{2-}, see (a) B. Leclerc and T. S. Kabre, *Acta Crystallogr.*, 31B(1975), 1675-1677. (b) B. Kelly and P. Woodward, *J. Chem. Soc. Dalton Trans.*, (1976), 1314-1316. (c) P. Böttcher, *Kristallogr.*, 150(1974), 65-73. (d) P. Böttcher and K. Kruse, *J. Less-common Met.*, 83(1982), 115-125.

8. For S_6^{2-}, see (a) S. C. Abrahams and E. Grison, *Acta Crystallogr.*, 6(1953), 206-213. (b) A. Hordvik and E. Stetten, *Acta Chem. Scand.*, 22(1968), 3029-3052. (c) R. G. Teller, L. J. Krause and R. C. Haushalter, *Inorg. Chem.*, 22(1983), 1809-1812.

9. For S_7^{2-}, see (a) H. Krebs and K. H. Müller, *Z. Anorg. Allg. Chem.*, 275(1954), 147-151. (b) M. G. Kanatzidis, N. C. Baenziger and D. Coucouvanis, *Inorg. Chem.*, 22(1983), 290-292.

10. For Se_2^{2-}, see (a) G. Cordier, R. Cook and H. Schäfer, *Angew. Chem. Int. Ed. Engl.*, 19(1980), 324-325. (b) ref.[5b].

11. For Se_3^{2-}, see (a) H. G. Von Schnering and N. K. Goh, *Naturwissenshaften* , 61(1974), 272. (b) P. Böttcher, *Z. Anorg. Allg. Chem.*, 461(1980), 13-21.

12. For Se_4^{2-}, see (a) O. Foss and V. Janickis, *J. Chem. Soc. Dalton Trans.*, (1980), 620-623. (b) T. König, B. Eisenmann and H. Schäfer, *Z. Naturforsch.*, 37B(1982), 1245-1249. (c) T. König, B. Eisenmann and H. Schäfer, *Z. Anorg.*

Allg. Chem., 498(1983), 99-104. (d) N. E. Brese, C. R. Randall and J. A. Ibers, *Inorg. Chem.*, 27(1988), 940-943.

13. For Se_5^{2-}, see (a) U. Kretschmann and P. Böttcher, *Z. Naturforsch.*, 40B(1985), 895-899. (b) C.-N. Chau, R. W. M. Wardle and J. A. Ibers, *Acta Crystallogr.*, 44C(1988), 883-885. (c) W. S. Sheldrick and H. G. Braunback, *Z. Naturforsch.*, 44B(1989), 1397-1401. (d) G. Kräuter, K. Dehnicke and D. Fenske, *Chem.-Ztg.*, 114(1990), 7-9. (e) J. Dietz, U. Müller, V. Müller and K. Dehnicke, *Z. Naturforsch.*, 46B(1991), 1293-1299. (f) V. Müller, G. Frenzen, K. Dehnicke and D. Fenske, *Z. Naturforsch.*, 47B(1992), 205-210. (g) ref.[8c]. (h) ref.[13d].

14. For Se_6^{2-}, see (a) F. Weller, J. Adel and K. Dehnicke, *Z. Anorg. Allg. Chem.*, 548(1987), 125-132. (b) D. Fenske, C. Kraus and K. Dehnicke, *Z. Anorg. Allg. Chem.*, 607(1992), 109-112. (c) ref.[9c].

15. For Se_7^{2-}, see V. Müller, K. Dehnicke, D. Fenske and G. Baum, *Z. Naturforsch.*, 46B(1991), 63-67.

16. For Se_8^{2-}, see R. Staffel, U. Müller, A. Ahle and K. Dehnicke, *Z. Naturforsch.*, 46B(1991), 1287-1292.

17. For Se_9^{2-}, see V. Müller, C. Grebe, U. Müller and K. Dehnicke, *Z. Anorg. Allg. Chem.*, 619(1993), 416-420.

18. For Te_2^{2-}, see R. C. Burns and J. D. Corbett, *J. Am. Chem. Soc.*, 103(1981), 2627-2632.

19. For Te_3^{2-}, see (a) A. Cisar and J. D. Corbett, *Inorg. Chem.*, 16(1977), 632-635. (b) Eisenmann and H. Schäfer, *Angew. Chem. Int. Ed. Engl.*, 17(1978), 684-686. (c) P. Böttcher, *J. Less-common Met.*, 70(1980), 263-271.

20. For Te_4^{2-}, see (a) J. C. Huffman and R. C. Haushalter, *Z. Anorg. Allg. Chem.*, 518(1984), 203-209. (b) L. A. Devereux, G. J. Schrobilgen ans J. F. Sawyer, *Acta Crystallogr.*, 41C(1985), 1730-1733. (c) K. W. Klinkmammer and P. Böttcher, *Z. Naturforsch.*, 45B(1990), 141-147. (d) H. Wolker, B. Schreiner, R. Staffel, U. Müller and K. Dehnicke, *Z. Naturforsch.*, 46B(1991), 1015-1019. (e) B. Schreiner and K. Dehnicke, *Chem.-Ztg.*, 115(1991), 326. (f) D. Fenske, G. Baum, H. Wolkers, B. Schreiner, F. Weller and K. Dehnicke, *Z. Anorg. Allg. Chem.*, (1992), in press.

21. For Te_5^{2-}, see (a) P. Böttcher and U. Kretschmann, *J. Less-common Met.*, 95(1983), 81-91. (b) P. Böttcher and U. Kretschmann, *Z. Anorg. Allg. Chem.*, 491(1982), 39-46. (c) ref.[9c]. (d) ref.[21f].

22. A. Hordvik, *Acta Chem. Scand.*, 20(1966), 1885. (b) M. G. Kanatzidis, N. C. Baenziger and D. Coucouvanis *Inorg. Chem.*, 22(1983), 290-292.

23. D. Coucouvanis, D. Swenson, P. Stremple and C. N. Baenziger, *J. Am. Chem. Soc.*, 101(1979), 3392-3394.

24. K. B. Krauskopf, *Introduction to Geochemistry*, McGraw Hill, New York, 1979.

25. (a) R. R. Chianelli, *Catal. Rev-Sci. Eng.*, 26(1984), 361-393. (b) F. E. Massoth and G. Muralidhar, in *Proceedings of the Climax Fourth International Conference on the Chemistry and Uses of Molybdenum* , H. P. Barry and P. C. Mitchell, Eds.; p343, Climax Molybdenum Company, Ann Arbor, Michigan, 1982.

26. M. R. Dubois, *Chem. Rev.*, 89(1989), 1-8.

27. M. Draganjac and T. B. Rauchfuss, *Angew. Chem. Int. Ed. Engl* , 24(1985), 742-757.

28. (a) A. Müller, *Polyhedron* , 5(1986), 323-340. (b) A. Müller and E. Diemann, *Adv. Inorg. Chem.*, 31(1987), 89-122.

29. M. Schmidt and R. Höller, *Rev. Chim. Miner.*, 20(1983), 763-768.

30. A. P. Ginsberg, W. E. Lindsell, C. R. Sprinrle, K. W. West and R. L. Cohen, *Inorg. Chem.*, 22(1983), 1781-1790.

31. H. Köpf, B. Block and M. Schmidt, *Chem. Ber.*, 101(1968), 272-276.

32. H. Köpf, A. Wirl and W. Kahl, *Angew. Chem. Int. Ed. Engl.*, 10(1971), 137-138.

33. H. Köpf, W. Kahl and A. Wirl, *Angew. Chem. Int. Ed. Engl.*, 9(1970), 801-802.

34. H. Strasdeit, B. Krebs and G. Henkel, *Inorg. Chim. Acta* , 89(1984), L11-L13.

35. R. C. Haushalter, *Angew. Chem. Int. Ed. Engl.*, 24(1985), 433-435.

36. (a) A. P. Ginsberg and W. E. Lindsell, *J. Chem. Soc., Chem. Commun.*, 1971, 232-233. (b) W. D. Bonds, Jr. and J. A. Ibers, *J. Am. Chem. Soc.*, 94(1972), 3413-3419. (c) H. Köpf, S. K. S. Hazari and M. Leitner, *Z. Naturforsch.*, 33B(1978), 1398-1404.

37. (a) A. Müller, W. Eltzner and N. Mohan, *Angew. Chem. Int. Ed. Engl.*, 18(1979), 168-169. (b) C. Giannotti, A. M. Ducourant, H. Chanaud, A. Chiaroni and C. Riche, *J. Organomet. Chem.*, 140(1977), 289-295.

38. (a) V. Küllmer, E. Röttinger and H. Vahrenkamp, *J. Chem. Soc., Chem. Commun.*, 1977, 782-783. (b) V. Küllmer, E. Röttinger and H. Vahrenkamp *Z. Naturforsch* , 34B(1979), 224-229.

39. (a) C. R. Brulet, S. S. Isied and H. Taube, *J. Am. Chem. Soc.*, 95(1973), 4758-4759. (b) R. C. Elder and M. Trkula, *Inorg. Chem.*, 16(1977), 1048-1051. (c) M. Herberhold, D. Reiner, B. Zimmer-Gasser and U. Schubert *Z. Naturforsch.*, 35B(1980), 1281-1285.

40. (a) P. J. Vergamini and G. J. Kubas *Prog. Inorg. Chem.*, 21(1976), 261-282. (b) G. J. Kubas and P. J. Vergamini *Inorg. Chem.*, 20(1981), 2667-2676. (c) V. A. Uchtman and L. F. Dahl *J. Am. Chem. Soc.*, 91(1969), 3756-3763.

41. (a) D. L. Stevenson, V. R. Magnuson and L. F. Dahl, *J. Am. Chem. Soc.*, 89(1967), 3727-3732. (b) T. S. Piper and G. Wilkinson, *J. Am. Chem. Soc.*, 78(1956), 900-900.

42. (a) A. Müller, W.-O. Nolte and B. Krebs, *Angew. Chem. Int. Ed. Engl.*, 17(1978), 279-279. (b) A. Müller, W.-O. Nolte and B. Krebs, *Inorg. Chem.*, 19(1980), 2835-2836. (c) C. H. Wei and L. F. Dahl *Inorg. Chem.*, 4(1965), 1-11.

43. (a) P. H. Bird, J. M. McCall, A. Shaver and U. Siriwardane, *Angew. Chem. Int. Ed. Engl.*, 21(1982), 384-385. (b) D. Coucouvanis, P. R. Patil, M. G. Kanatzidis, B. Detering and N. C. Baenziger, *Inorg. Chem.*, 24(1985), 24-31. (c) P. E. Jones and L. Katz, *J. Chem. Soc. Chem. Commun.*, 1967, 842-843. (d) P. E. Jones and L. Katz, *Acta Crystallogr.*, 25B(1969), 745-753. (e) A. Müller, J. Schimanski, U. Schimanski, *Angew. Chem. Int. Ed. Engl.*, 23(1984), 159-160. (f) A. Müller, M. Römer, H. Bögge, E. Krickemeyer and M. Zimmermann, *Z. Anorg. Allg. Chem.*, 534(1986), 69-76.

44. (a) A. Müller, F.-W. Baumann, H. Bögge, M. Römer, E. Krickemeyer and K. Schmitz, *Angew. Chem. Int. Ed. Engl.*, 23(1984), 632-633. (b) A. Müller, E.

Krickemeyer, M. Zimmermann, M. Römer, H. Bögge, M. Penk and K. Schmitz, *Inorg. Chim. Acta* , 90(1984), L69-L71.

45. (a) C. M. Bolinger, T. B. Rauchfuss and S. R. Wilson, *J. Am. Chem. Soc.*, 103(1981), 5620-5621. (b) A. Müller, M. Römer, H. Bögge, E. Krickemeyer and K. Schmitz, *Inorg. Chim. Acta* , 85(1984), L39-L41. (c) A. Müller, W. Eltzner, H. Bögge and E. Krickemeyer, *Angew. Chem. Int. Ed. Engl.*, 22(1983), 884-885. (d) A. Müller, M. Zimmermann and H. Bögge, *Angew. Chem. Int. Ed. Engl.*, 25(1986), 273-273. (e) A. Müller, K. Schmitz, E. Krickemeyer, M. Penk and H. Bögge, *Angew. Chem. Int. Ed. Engl.*, 25(1986), 453-454.

46. A. Müller, M. Römer, H. Bögge, E. Krickemeyer and D. Bergmann, *J. Chem. Soc. Chem. Commun.*, 1984, 348-349.

47. J. Gotzig, A. L. Rheingold and H. Werner, *Angew. Chem. Int. Ed. Engl.*, 23(1984), 814-815.

48. C.-N. Chau, R. W. M. Wardle and J. A. Ibers, *Inorg. Chem.*, 26(1987), 2740-2741.

49. W. A. Flomer and J. W. Kolis, *J. Am. Chem. Soc.*, 110(1988), 3682-3683.

50. W. A. Flomer, S. C. O'Neal, W. T. Pennington, D. Jeter, A. W. Cordes and J. W. Kolis *Angew Chem. Int. Ed. Engl.*, 27(1988), 1702-1703.

51. M. G. Kanatzidis *Comments Inorg. Chem.*, 10(1990), 161-195.

52. M. A. Ansari and J. A. Ibers *Coord. Chem. Rev.*, 100(1990), 223-266.

53. J. W. Kolis *Coord. Chem. Rev.*, 105(1990), 195-219.

54. Synthesis of solid-state compounds by using molten alkali metal polychaocogenides as fluxes at mild temperatures (i.e. below 500 °C) is currently a very active area of research. For recent results from this research group see, M. G. Kanatzidis, *Chem. Mater.*, 2(1990), 353-363.

55. (a) J.-H. Liao and M. G. Kanatzidis, *J. Am. Chem. Soc.*, 112(1990), 7400-7402. (b) J.-H. Liao and M. G. Kanatzidis, *Inorg. Chem.*, 31(1992), 431-439.

56. Hydrothermal conditions have also been used to prepared metal monochalcogenides, see (a) W. S. Sheldrick, *Z. Anorg. Allg. Chem.*, 562(1988), 23-30. (b) W. S. Sheldrick and H.-J. Häuser, *Z. Anorg. Allg. Chem.*, 557(1988), 98-104. (c) W. S. Sheldrick and H.-J. Häuser, *Z. Anorg. Allg. Chem.*, 557(1988), 105-111. (d) W. S. Sheldrick and J. Kaub, *Z. Anorg. Allg. Chem.*, 535(1986), 179-185. (e) J. B. Parise, *Science*, 251(1991), 293-294. (f) J. B. Parise, *J. Chem. Soc., Chem. Commun.*, (1990), 1553-1554.

57. For early examples of the compounds made in solutions, see (a) M. G. Kanatzidis and S.-P. Huang, *J. Am. Chem. Soc.*, 111(1989), 760-761. (b) M. G. Kanatzidis and S.-P. Huang, *Angew. Chem. Int. Ed. Engl.*, 28(1989), 1513-1514. (c) M. G. Kanatzidis and S.-P. Huang, *Inorg. Chem.*, 28(1989), 4667-4669. (d) M. G. Kanatzidis and S. Dhingra, *Inorg. Chem.*, 28(1989), 2024-2026. (e) S.-P. Huang, S. Dhingra and M. G. Kanatzidis, *Polyhedron* , 9(1990), 1389-1395. (f) M. Draganjac, S. Dhingra, S.-P. Huang and M. G. Kanatzidis, *Inorg. Chem.*, 29(1990), 590-591.

58. R. M. H. Banda, J. Cusick, M. L. Scudder, D. C. Craig and I. G. Dance, *Polyhedron*, 8(1989), 1999-2001.

59. R. M. H. Banda, J. Cusick, M. L. Scudder, D. C. Craig and I. G. Dance, *Polyhedron,* 8(1989), 1995-1998.

60. J. Cusick, M. L. Scudder, D. C. Craig and I. G. Dance, *Polyhedron* , 8(1989), 1139-1141.

61. J. Adel, F. Weller and K. Dehnicke, *Z. Naturforsch.*, 43B(1988), 1094-1100.

62. W. A. Herrmann and J. Rohrmann, *Chem. Ber.*, 119(1986), 1437-1440.

63. (a) R. W. M. Wardle, C.-N. Chau and J. A. Ibers, *J. Am. Chem. Soc.*, 109(1987), 1859-1860. (b) R. W. M. Wardle, S. Bhaduri, C.-N. Chau and J. A. Ibers, *Inorg. Chem.*, 27(1988), 1747-1755.

64. S. C. O'Neal and J. W. Kolis, *J. Am. Chem. Soc.*, 110(1988), 1971-1973.

65. (a) W. Clegg, G. Christou, C. D. Garner and G. M. Sheldrick *Inorg. Chem.*, 20(1981), 1562-1566. (b) M. Draganjac, E. Simhon, L. T. Chan, M. G. Kanatzidis, N. C. Baenziger and D. Coucouvanis, *Inorg. Chem.*, 21(1982), 3321-3332. (c) W.-H. Pan, M. A. Harmer, T. R. Halbert and E. I. Stiefel ,*J. Am. Chem. Soc.*, 106(1984), 459-460.

66. S. C. O'Neal, W. T. Pennington and J. W. Kolis, *Inorg. Chem.*, 29(1990), 3134-3138.

67. T. A. Rauchfuss, S. Dev and S. R. Wilson, *Inorg. Chem.*, 31(1992), 153-154.

68. S. Dev, E. Ramli, T. B. Rauchfuss and C. L. Stern, *J. Am. Chem. Soc.*, 112(1990), 6385-6386.

69. R. C. Haushalter, *Inorg. Chim. Acta*, 102(1985), L37-L38.

70. J. Sola, Y. Do, J. M. Berg and R. H. Holm, *Inorg. Chem.*, 24(1985), 1706-1713.

71. R. W. M. Wardle, C. H. Mahler C.-N. Chau and J. A. Ibers, *Inorg. Chem.*, 27(1988), 2790-2795.

72. P. G. Maué and D. Fenske, *Z. Naturforsch.*, 43B(1988), 1213-1218.

73. D. Fenske, J. Ohmer, J. Hachgenei and K. Merzweiler, *Angew. Chem. Int. Ed. Engl.*, 27(1988), 1277-1296.

74. (a) C. M. Bolinger, T. B. Rauchfuss and A. L. Rheingold, *Organometallics*, 1(1982), 1551-1553. (b) A. L. Rheingold, C. M. Bolinger and T. B. Rauchfuss, *Acta Crystallogr.*, 42C(1986), 1878-1880.

75. W. A. Herrmann, C. Hecht, E. Herdtweck and H.-J. Kneuper, *Angew. Chem. Int. Ed. Engl.*, 26(1987), 132-134.

76. D. M. Giolando, M. Papavassiliou, J. Pickardt T. B. Rauchfuss and R. Steudel, *Inorg. Chem.*, 27(1988), 2596-2600.

77. M. G. Kanatzidis and S.-P. Huang, submitted to *Coord. Chem. Rev.*

78. A. C. Sutorik and M. G. Kanatzidis, *J. Am. Chem. Soc.*, 113(1991), 7754-7755.

79. S. Schreiner, L. E. Aleandri, D. Kang and J. A. Ibers, *Inorg. Chem.*, 28(1989), 392-393.

80. S. Dhingra and M. G. Kanatzidis, *Science*, 258(1992), 1769-1772.

81. K.-W. Kim and M. G. Kanatzidis, submitted to *J. Am. Chem. Soc.*

82. W. A. Flomer, S. C. O'Neal, J. W. Kolis, D. Jeter and A. W. Cordes, *Inorg. Chem.*, 27(1988), 971-973.

83. See chapters 5, 6 and 7.

84. K.-W. Kim and M. G. Kanatzidis, manuscript in preparation.

85. H. C. E. McFarlane and W. McFarlane, *NMR and the periodic table*, R. K. Harris and B. E. Mann, Eds.; Academic Press, New York, 1978, p402-419.

86. W. A. Flomer and J. W. Kolis, *Inorg. Chem.*, 28(1989), 2513-2517.

87. M. A. Ansari, C. H. Mahler, G. S. Chorghade, Y.-J. Lu and J. A. Ibers, *Inorg. Chem.*, 29(1990), 3832-3839.

88. M. A. Ansari and J. A. Ibers, *Inorg. Chem.*, 28(1989), 4068-4069.

89. S. Dhingra and M. G. Kanatzidis, *Inorg. Chem,* in press.

90. S. Dhingra, Ph.D. Thesis, Michigan State University, 1992.

91. M. A. Ansari, C. H. Mahler and J. A. Ibers, *Inorg. Chem.*, 28(1989), 2669-2674.

92. C. M. Bolinger and T. A. Rauchfuss, *Inorg. Chem.*, 21(1982), 3947-3954.

93. S. Dhingra and M. G. Kanatzidis in *Better Ceramics Through Chemistry IV, Mat. Res. Soc. Symp. Proc.*, 180(1990), 825-830.

94. S. Dhingra, K.-W. Kim and M. G. Kanatzidis in *Chemical Perspectives in Microelectronic Materials , Mat. Res. Soc. Symp. Proc.*, 204(1991), 163-168.

95. K.-W. Kim, J. A. Cowen, S. Dhingra and M. G. Kanatzidis in *Chemical Processes in Inorganic Materials: Metal and Semiconductor Clusters and Colloids*, *Mat. Res. Soc. Symp. Proc.*, 1992, in press.

96. (a) R. A. Smith in *Semiconductors*, Cambridge University Press, Cambridge UK, 1978, p438. (b) B. E. Bartlett, et al, *Infrared Phys.*, 9(1969), 35.

97. Z. K. Kun, *Solid State Technology*, 31(1988), L77-79.

98. A. A. Ballman, R. L. Byer, D. Eimerl, R. S. Feigelson, B. J. Feldman, L. S. Goldberg, N. Menyuk and C. L. Tang, *Applied Optics*, 26(1987), 224-227.

99. (a) J. R. Tuttle, D. S. Albin and R. Noufi, *Solar Cells*, 27(1989), 231-236. (b) K. Zeibel in *The Potential of $CuInSe_2$ and CdTe for Space Applications. 23rd Intersociety Energy Conversion Engineering Conference*, Vol. 3, p97-102. D. Y. Goswami Ed.: ASME, 1988.

100. (a) M. S. Whittingham, *Science*, 192(1976), 1126-1127. (b) M. S. Whittingham, *J. Solid State Chem.*, 29(1979), 303-310.

CHAPTER 2

POLYSELENIDE AND POLYTELLURIDE CHEMISTRY OF GOLD

I. Introduction

We chose coinage metals as our starting point for synthesizing new soluble homoleptic metal polyselenide and polytelluride compounds because prior to our work, there had been no reported polyselenide or polytelluride complexes of copper or silver[1-2]. As a matter of fact, $[Au_2(Te_2)_2]^{2-}$ was the only known heavy polychalcogenide compound from this group at that time[3], whereas the polysulfide complexes of this group represented one of the most fruitful triads in the periodic table[4].

In the gold polyselenide system, we encountered a vacillating redox chemistry between Au^{n+} (n=1, 3) and Se_x^{2-}. In DMF solution the reaction of $AuCl_3$ with Na_2Se_5 resulted in the isolation of α-$(Ph_4P)_2[Se(Se_5)_2]$, an oxidation product of the Se_5^{2-} by Au^{3+}. The structure of this compound will be discussed in a later chapter along with those in the $[A(Q_5)_2]^{2-}$ (A=Te, Q=S, Se or A=Se, Q=Se) family[5]. To avoid the above redox process and so as to isolate the gold-containing polyselenide complex, we used AuCN as the starting material. Surprisingly, a reverse redox reaction occurred in the second synthesis, that is, Au^+ is oxidized by the Se_5^{2-} to Au^{3+}, yielding the dimeric complex $(PPN)_2[Au_2Se_2(Se_4)_2]$ (**2·1**). In a further attempt at stabilizing a Au^+ polyselenide compound, shorter polyselenide Se_x^{2-} (x=2-4) ligands were used. Three new compounds containing Au^+ were then obtained. $(Ph_4P)_2[Au_2(Se_2)(Se_3)]$ (**2·2**) and $(PPN)_2[Au_2(Se_2)(Se_3)]$ (**2·3**) were synthesized by using Na_2Se_2 or Na_2Se_3, while $(Ph_4P)_2[Au_2(Se_2)(Se_4)]$ (**2·4**) was obtained by using Na_2Se_4. When the shortest possible

ligand Se^{2-} is used, both redox chemistry and ligand size effect cease to operate while surprisingly, a new factor, the interaction of Au^+ with an alkali ion (i.e. Na^+), emerges as a structure directing force. Consequently, a cryptand-like novel cluster $(Et_4N)_3[NaAu_{12}Se_8]$ (**2·5**) was isolated.

In the corresponding Au^+/Te_x^{2-} system, a very stable symmetric dimer seems to dominate the chemistry. Thus far, we have only been able to isolate and structurally characterize one compound, $(Ph_4P)_2[Au_2(Te_2)_2]$ (**2·6**). The anion in (**2·6**) was crystallized earlier as the PPN^+ salt through a different synthetic method[3].

In this chapter, we wish to describe the synthesis, X-ray structures and spectroscopic studies of the newly prepared homoleptic compounds, $(PPN)_2[Au_2Se_2(Se_4)_2]$ (**2·1**), $(Ph_4P)_2[Au_2(Se_2)(Se_3)]$ (**2·2**), $(PPN)_2[Au_2(Se_2)(Se_3)]$ (**2·3**), $(Ph_4P)_2[Au_2(Se_2)(Se_4)]$ (**2·4**), $(Et_4N)_3[NaAu_{12}Se_8]$ (**2·5**) and $(Ph_4P)_2[Au_2(Te_2)_2]$ (**2·6**).

II. Experimental Section

1. Reagents

Chemicals in this work other than solvents were used as obtained: (i) selenium powder, ~100 mesh, 99.5% purity, Aldrich Chemical Company, Inc., Milwaukee, WI; (ii) tellurium powder, ~200 mesh, 99.8% purity, Aldrich Chemical Company, Inc., Milwaukee, WI; (iii) sodium sticks in kerosene, 99% purity, Mallinckrodt Inc., Paris, Ky.; (iv) potassium sticks in mineral oil, 99% Mallinckrodt Inc., Paris, Ky.; (v) gold(III) chloride, Strem Chemicals, Inc., Newburyport, MA; (vi) gold(I) cyanide, Strem Chemicals, Inc., Newburyport, MA; (vii) tetraphenylphosphonium chloride (Ph_4PCl), 98% purity, Aldrich Chemical Company, Inc., Milwaukee, WI; (viii) bis(triphenylphosphoranylidene)ammonium chloride (PPNCl), 98% purity, Aldrich

Chemical Company, Inc., Milwaukee, WI; (ix) tetraethylammonium chloride hydrate ($Et_4NCl \cdot xH_2O$), 97% purity, Aldrich Chemical Company, Inc., Milwaukee, WI.

Dimethylformamide (DMF, analytical reagent, Mallinckrodt Inc., Paris, Ky) was stored over 4A Linde molecular sieves for several days and then distilled under reduced pressure at ~30 °C[6].

Diethyl ether (A.C.S. anhydrous, Columbus Chemical Industries Inc., Columbus, WI) was distilled under a dry N_2 blanket after being refluxed with potassium metal, benzophenone and triethylene glycol dimethyl ether for 12 hours[6].

Methanol (GR anhydrous, EM Science Inc., Gibbstown, NY) was refluxed for 4-5 h with magnesium methoxide (prepared from dry magnesium turnings and absolute methanol), and distilled under a nitrogen atmosphere[6].

2. Physical Measurements

Semi-quantitative elemental analyses for the elements having an atomic number≥11 were routinely performed on a JEOL JSM-35C scanning electron microscope (SEM) equipped with an X-ray microanalysis attachment. Samples were mounted on an aluminum stub with conductive carbon paint to avoid the charge buildup on samples under the electron beam. After obtaining the energy dispersive spectrum (EDS) for the sample, a program called "standardless quantitation" was used to analyze the energy and intensity of the characteristic X-rays in the spectrum, thus identifying the elements present and the atom percentage for each element. Such a method is often referred to as EDAX (Energy Dispersive Microanalysis of X-rays) in the literature. The typical working conditions for carrying out the elemental analysis on this type of SEM are as follows[7]:

X-ray detector position: 55 mm; Working distance: 39 mm; Accelerating voltage: 20 kV; Take-off angle: 27°; Beam current: 200 picoamps; Accumulation time: 60 sec.

Because the X-ray detector in the scanning electron microscope is protected with a beryllium window, the X-rays emitted by the element with an atomic number lower than 11 will be absorbed by the window. Therefore, the elemental analyses for such elements can not be performed.

FT-IR spectra of the compounds were determined as solids in the CsI matrix. Each sample was ground with dry alkali metal halide into a fine powder, and a pressure of about 6 tons was applied to the mixture to make a translucent pellet. The spectra were recorded in the region of 500 to 100 cm^{-1} with the use of a Nicolet 740 FT-IR spectrometer[8].

UV/vis spectra of the compounds were measured on a Hitachi U-2000 spectrophotometer[9]. The solutions to be measured had accurately known concentrations obtained by weighing the samples with a micro balance and dissolving them in volumetric flasks. These solutions were then measured in a cell whose pathlength is known to be 1.000±0.002 mm along with a second cell containing the pure solvent in the reference beam. The positions of the absorption peaks were plotted as absorbance (A, $\log I_O/I_t$) *vs.* wavelength (λ in nm). The molar extinction coefficients at maximum absorption were calculated according to the Beer-Lambert law:

$$A=\log I_O/I_t=\varepsilon cl$$

Where c is the concentration in moles per liter and l is the sample pathlength in cm.

^{77}Se (I=1/2, nat. abund. 7.58%) NMR spectra were obtained on a Varian VXR-500 pulse spectrometer equipped with Sun/360 workstation[10]. The spectra were

recorded at room temperature (25 °C). The observing frequency for ^{77}Se was 95.358 MHz. The acquisition time was 0.322 sec with spectral width of 38.35 KHz for ^{77}Se which gave data point resolution of 1.14 Hz. The pulse width used in these experiments was 6 msec and no relaxation delay was applied. The number of free induction decays accumulated were >70,000. The spectra were referenced relative to Me_2Se at δ=0 ppm in DMF. Solutions of Ph_2Se_2 (δ=460 ppm) in DMF were used as external reference. The convention used for the chemical shifts is that a positive sign signifies a shift to high frequency compared to the reference compound.

Thermal gravimetric analyses (TGA) of the compounds were performed on a Shimadzu TGA-50 system[11]. The solid samples were heated up to 800 °C from room temperature at a rate of 5 °C/min under a steady flow of dry nitrogen.

3. Syntheses

All syntheses were carried out under a dry nitrogen atmosphere in a Vacuum Atmospheres Dri-Lab glovebox.

(i). Preparation of alkali metal polychalcogenides in liquid ammonia

In a typical preparation of Na_2Se_5, 18.8 g (~0.239 mol) of elemental selenium was combined with 2.2 g (~0.0956 mol) of sliced sodium metal under nitrogen in a round-bottom flask equipped with a teflon valve and a stirbar. 80 ml liquid ammonia was then condensed to the flask at -78 °C (dry ice/acetone bath) through a specially designed condenser. The mixture was stirred for three to four hours until a dark green solution formed. Care was taken to ensure that all sodium metal had dissolved. The NH_3 was removed from the solution by evaporation at room temperature (by allowing the cold bath to warm up slowly) under a flow of nitrogen. The resulting solid was then flame-dried

under vacuum. The product was ground to a fine powder in the glovebox. The black microcrystalline powder dissolves in DMF and CH_3CN.

The other alkali metal polychalcogenides were prepared in a similar manner. These include Na_2Se, Na_2Se_2, Na_2Se_3, Na_2Se_4, K_2Te and K_2Te_2.

(ii). Preparation of $(PPN)_2[Au_2Se_2(Se_4)_2]$ (2·1)

A 67 mg (0.3 mmol) sample of solid AuCN was added to a 50 ml DMF solution of 270 mg (0.61 mmol) Na_2Se_5 in the presence of 345 mg (0.61 mmol) of PPNCl. After stirred for 2 h, the solution was filtered to remove NaCl and NaCN, and then diluted with 30 ml ether. When the mixture was allowed to stand for 3 days, analytically pure orange-brown needles of $(PPN)_2[Au_2Se_2(Se_4)_2]$ were isolated in 69% yield. Far IR spectrum (of solid-state): 276(w), 256(m, b) and 236(s) cm^{-1}; Semi-quantitative elemental analyses by EDAX (atom%): Au:Se:P=13:60:27; UV/vis spectrum (in DMF): 314 nm (ε=28600 M^{-1} cm^{-1}), 398 nm (ε=9690 M^{-1} cm^{-1}).

(iii). Preparation of $(Ph_4P)_2[Au_2(Se_2)(Se_3)]$ (2·2)

Method (A): A 45 mg (0.2 mmol) sample of solid AuCN was added to a 30 ml DMF suspension of 120 mg (0.6 mmol) Na_2Se_2 in the presence of 75 mg (0.2 mmol) of Ph_4PCl. Upon stirring, a red solution was gradually formed in about 1 h. Following filtration of any formed precipitates, 30 ml ether was added to the filtrate. Red, needle-shaped X-ray quality single crystals of $(Ph_4P)_2[Au_2(Se_2)(Se_3)]$ were obtained in 56% yield within two days.

Method (B): The reaction of AuCN with Na_2Se_3 in the same molar ratio and under the same conditions also gave (2·2) in 58% yield. Far IR spectrum (of solid-state): 264(m, b) and 236 (s) cm^{-1}; ^{77}Se NMR: 366 and 504 ppm. Semi-quantitative elemental

analyses by EDAX (atom%): Au:Se:P=25:47:28. UV/vis spectrum (in DMF): 497 nm (b, ε=3160 M^{-1} cm^{-1}).

(iv). Preparation of $(PPN)_2[Au_2(Se_2)(Se_3)]$ (2·3)

The reaction of 45 mg (0.2 mmol) of solid AuCN with 113 mg (0.4 mmol) Na_2Se_3 and 230 mg (0.4 mmol) PPNCl in 30 ml DMF gave a red solution within 1 h. Filtration of the reaction solution, followed by slow diffusion of 15 ml ether into the filtrate, resulted in red crystals of $(PPN)_2[Au_2(Se_2)(Se_3)]$ in 52% yield within 6 days. Far IR spectrum (of solid-state): 277(w), 264(m, sh) and 236 (s) cm^{-1}; ^{77}Se NMR: 366 and 504 ppm. Semi-quantitative elemental analyses by EDAX (atom%): Au:Se:P=18:45:37. UV/vis spectrum (in DMF): 501 nm (b, ε=2940 M^{-1} cm^{-1}).

(v). Preparation of $(Ph_4P)_2[Au_2(Se_2)(Se_4)]$ (2·4)

The procedure was identical with the one described above in method (A) except 140 mg (0.4 mmol) of K_2Se_4 was used. Analytically pure red needles of $(Ph_4P)_2[Au_2(Se_2)(Se_3)]$ were isolated in 76% yield within 4 days. Far IR spectrum (of solid-state): 278(w), 266(m), 257(m, b) and 236 (m) cm^{-1}; ^{77}Se NMR: -3, 146, 157, 365, 408, 421, 503, 635 and 702 ppm. Semi-quantitative elemental analyses by EDAX (atom%): Au:Se:P=20:54:26. UV/vis spectrum (in DMF): 292 nm (sh, ε=11500 M^{-1} cm^{-1}), 387 nm (b, ε=3930 M^{-1} cm^{-1}).

(vi). Preparation of $(Et_4N)_3[NaAu_{12}Se_8]$ (2·5)

A 45 mg (0.2 mmol) sample of solid AuCN was added to to a 20 ml methanol solution of 25 mg Na_2Se (0.2 mmol) and 33 mg Et_4NCl (0.2 mmol). A slow color change from red to light yellow was observed. Addition of 25 ml ether to this reaction mixture afforded a pale yellow powder in *ca* a day. Collection and recrystallization of the product with a slow diffusion technique in ~1:1 DMF/ether solution of a total 20 ml volume over a

(Et

on t

ppm

quar

DMI

(vii)

20 ml

A brow

addition

isolate

preser

reactio

spectru

(atom

4. X-ray

period of two weeks gave amber-colored, cube-like single crystals of $(Et_4N)_3[NaAu_{12}Se_8]$. The overall yield of the synthesis was estimated as *ca* 33% based on the AuCN. Far IR spectrum (of solid-state): 239 (m) cm^{-1}; ^{23}Na NMR: -12.0 (singlet) ppm (relative to $NaBPh_4$ in DMF at δ=0 ppm); ^{77}Se NMR: 758 (singlet) ppm; Semi-quantitative elemental analyses by EDAX (atom%): Au:Se=63:37; UV/vis spectrum (in DMF): featureless.

(vii). Preparation of $(Ph_4P)_2[Au_2(Te_2)_2]$ (2·6)

Method (A): A 10 ml DMF solution of 30 mg (0.1 mmol) $AuCl_3$ was added to a 20 ml DMF solution of 41 mg K_2Te (0.2 mmol) and 75 mg (0.2 mmol) Ph_4PCl dropwise. A brown solution was formed under vigorous stirring. The filtration was followed by addition of 10 ml ether to the filtrate. Dark brown platelets of $(Ph_4P)_2[Au_2(Te_2)_2]$ were isolated in ~40% yield from the solution after 4 days standing at room temperature.

Method (B): The reaction of AuCN with K_2Te_2 in a 1:2 molar ratio in the presence of Ph_4PCl in DMF gave (2·6) in 63% yield. The product isolated from such a reaction is often contaminated with tetraphenylphosphonium polytellurides. Far IR spectrum (of solid-state): 188 (w) cm^{-1}; Semi-quantitative elemental analyses by EDAX (atom%): Au:Te:P=28:44:28. UV/vis spectrum (in DMF): 530 nm (decomposing).

4. X-ray Diffraction and Crystallographic Studies

The single crystal X-ray diffraction studies were performed by using either a Nicolet P3 four-circle difractometer[12] or a Rigaku automated AFC6S four-circle single crystal diffractometer[13].

The crystallographic data sets of (2·1) and (2·2) were collected on the Nicolet P3 diffractometer using a θ-2θ scan mode and Mo Kα radiation, while those of (2·3), (2·4), (2·5) and (2·6) were collected on the Rigaku AFC6S diffractometer using ω–2θ scan

int

ref

dec

on

squa

atom

perio

Corpo

prograr

compo

refine

coord

Table

membe

molec

orienta

techniques and Mo Kα radiation. The stability of the experimental setup and crystal integrity for each data collection was monitored by measuring three representative reflections periodically (every 100 for Nicolet P3 and 150 for Rigaku AFC6S). No crystal decay was detected. Empirical absorption corrections were applied to all the data sets based on ψ scans of several strong reflections with $\chi \sim 90^{o}$.

The structures were solved with direct methods and refined with full-matrix least squares techniques. DIFABS corrections were applied to the structure-factors after all the atoms in the structures were located and refined isotropically[14]. The calculations were performed using the TEXSAN crystallographic software package of Molecular Structure Corporation[15] or the SHELXS-86 and SDP combined package of crystallographic programs[16]. Tables 2·1and 2·2 give crystal data and details for structure analysis of all compounds.

Atoms in the anions were refined anisotropically, and atoms in the cations were refined isotropically. The hydrogen positions were calculated but not refined. The final coordinates and average temperature factors of the atoms in each compound are given in Tables 2·3–2·8, respectively.

The structure of (2·3) was found to be disordered at the anion site. The seven membered ring of $[Au_2(Se_2)(Se_3)]^{2-}$ is positioned on an inversion center, causing the molecule to stack in two opposite directions in the crystal lattice. The two molecular orientations share a common Au–Au axis. The inversion center is situated in the middle of the Au–Au vector. The structure refinement for this compound was carried out on a disordered model with five Se atoms having half occupancy. No accurate structural parameters were obtained due to the close proximity of the disordered Se atoms.

(2·5) crystallizes in the space group P-1(#2) having an asymmetric unit of $(Et_4N)_{1.5}[Na_{0.5}Au_6Se_4]$. In addition to Na^+, one of the tetrahedral Et_4N^+ cations was

found to sit on a crystallographic inversion center, causing a positional disorder of the ethyl groups on this cation site. The refinement of the atoms in this cation was carried out with a disordered model where all the C atoms except for a terminal one (i.e. C16) possess half-occupancy. C16 could not be found, but its position was calculated and included in the structure factor calculation.

Finally, each compound was examined by X-ray powder diffraction for the purpose of phase characterization and identification. A Debye-Scherrer camera was employed to record the X-ray powder diffraction patterns. Ni-filtered Cu radiation was used. The crystals were ground to fine powder and packed into 0.5 mm glass capillaries which were sealed and mounted to the standard Debye-Scherrer powder camera which has a diameter of 114.6 mm (1 mm corresponds to 1 degree for 2θ). X-rays were generated by a Phillips Norelco XRG-5000 X-ray generator operating at 40 kV and 20 mA. Approximately, a six hour exposure time was used. Accurate d-spacings (Å) of each compound were calculated from the powder patterns recorded on a Phillips XRG-3000 computer controlled powder diffractometer[17]. To verify the homogeneities of the products, the d-spacings observed for the bulk materials were compared with the calculated d-spacings from the X-ray single-crystal structure analysis data[18]. Listings of calculated and observed d-spacings (Å) along with the observed relative diffraction intensities of these compounds are given in Tables 2·9–2·14.

Table 2·1. Data for Crystal Structure Analysis of $(PPN)_2[Au_2Se_2(Se_4)_2]$ (2·1), $(Ph_4P)_2[Au_2(Se_2)(Se_3)]$ (2·2) and $(PPN)_2[Au_2(Se_2)(Se_3)]$ (2·3)

compound	2·1	2·2	2·3
formula	$C_{72}H_{60}P_4N_2Au_2Se_{10}$	$C_{48}H_{40}P_2Au_2Se_5$	$C_{72}H_{60}P_4N_2Au_2Se_5$
a, Å	11.872(4)	10.381(4)	12.166(3)
b, Å	11.419(4)	11.002(5)	12.960(5)
c, Å	26.910(12)	21.181(9)	21.673(6)
α, deg	90.00	75.50(4)	90.00
β, deg	94.02(6)	74.74(3)	105.15(3)
γ, deg	90.00	81.40(4)	90.00
Z; V, $Å^3$	2; 3639(2)	2; 2250(2)	2; 3299(2)
space group	$P2_1/n$	P-1	$P2_1/n$
D_{calc}, g/cm^3	1.71	2.17	1.88
μ(Mo Kα), cm^{-1}	90	106	73
cryst size, mm	0.04, 0.75, 0.58	0.05, 0.08, 0.21	0.07, 0.10, 0.31
$2\theta_{max}$, deg	44	45	40
Temperature (°C)	25	-93	23
no. of data collcd	5187	5927	3473
no. of data used($F_o^2>3\sigma(F_o^2)$)	3276	3230	1351
min, max abs cor	0.78 , 0.99	0.78 , 0.98	0.73, 1.46
no. of variables	406	274	211
no. of atoms per asym uint (including H)	75	97	75
final R/R_w, %	4.6/5.7	5.5/6.8	6.2/6.5

Table 2·2. Data for Crystal Structure Analysis of $(Ph_4P)_2[Au_2(Se_2)(Se_4)]$ (2·4), $(Et_4N)_3[NaAu_{12}Se_8]$ (2·5) and $(Ph_4P)_2[Au_2(Te_2)_2]$ (2·6)

compound	2·4	2·5	2·6
formula	$C_{48}H_{40}P_2Au_2Se_6$	$C_{24}H_{60}N_3NaAu_{12}Se_8$	$C_{48}H_{40}P_2Au_2Te_2$
a, Å	28.409(7)	11.956(4)	10.526(3)
b, Å	10.97(1)	12.733(4)	11.237(2)
c, Å	19.762(5)	10.784(3)	10.453(4)
α, deg	90.00	103.94(3)	103.03(2)
β, deg	130.49(1)	108.96(3)	106.95(3)
γ, deg	90.00	113.63(2)	81.66(2)
Z; V, Å^3	4; 4680(5)	2; 1285(2)	2; 1148(1)
space group	C2/c	P-1	P-1
D_{calc}, g/cm^3	2.19	4.40	2.29
μ(Mo Kα), cm^{-1}	110	396	90
cryst size, mm	0.10, 0.13, 0.31	0.14, 0.14, 0.16	0.03, 0.09, 0.24
$2\theta_{max}$, deg	45	45	50
Temperature (°C)	23	23	-95
no. of data collcd	3358	3557	4303
no. of data used($F_o^2>3\sigma(F_o^2)$)	1475	1872	2609
min, max abs cor	0.67, 1.17	0.75, 1.39	0.75, 1.38
no. of variables	142	167	133
no. of atoms per asym uint (including H)	49	55	48
final R/R_w, %	7.6/7.9	7.2/8.4	5.2/5.9

Table 2·3. Positional Parameters and B_{eq} Values[a] for $(PPN)_2[Au_2Se_2(Se_4)_2]$ (2·1)
(Standard Deviations in Parentheses)

atom	x	y	z	B_{eq}, Å^2
Au	0.99332(5)	0.06784(6)	0.43833(3)	2.94(1)
Se1	0.8324(1)	0.0888(2)	0.37617(7)	3.60(4)
Se2	0.8958(2)	0.2231(2)	0.31779(8)	4.23(4)
Se3	1.0754(2)	0.1501(2)	0.31220(8)	5.05(5)
Se4	1.1408(2)	0.1688(2)	0.39560(8)	4.66(5)
Se5	0.8639(2)	-0.0182(2)	0.49493(8)	4.77(5)
P1	0.7376(3)	0.0866(4)	0.1125(2)	2.20(8)
P2	0.4506(3)	0.2844(4)	0.6014(2)	2.42(9)
N	0.3187(9)	0.308(1)	0.6025(5)	2.9(3)
C1	1.111(1)	0.354(1)	0.6361(5)	1.8(3)
C2	1.084(1)	0.237(1)	0.6304(6)	2.8(4)
C3	1.022(1)	-0.195(2)	0.3562(7)	4.2(4)
C4	0.903(1)	0.275(2)	0.6626(7)	3.5(4)
C5	0.930(1)	0.392(2)	0.6682(6)	3.5(4)
C6	1.033(1)	0.433(2)	0.6549(6)	3.0(3)
C7	1.294(1)	0.519(1)	0.6587(6)	2.4(3)
C8	1.338(1)	0.624(1)	0.6416(6)	2.8(4)
C9	1.385(1)	0.700(2)	0.6793(7)	3.4(4)
C10	1.389(1)	0.672(2)	0.7292(7)	3.6(4)
C11	1.346(1)	0.564(2)	0.7440(6)	3.2(4)
C12	1.299(1)	0.487(1)	0.7086(7)	3.1(4)
C13	1.194(1)	0.490(1)	0.5546(6)	2.2(3)
C14	1.211(1)	0.436(2)	0.5112(7)	3.7(4)
C15	1.170(1)	0.490(2)	0.4665(6)	3.6(4)
C16	0.888(1)	0.403(2)	0.5325(7)	3.7(4)
C17	0.907(1)	0.353(2)	0.4876(6)	3.5(4)
C18	0.866(1)	0.405(2)	0.4435(6)	3.0(4)
C19	-0.008(1)	0.336(1)	0.1418(6)	2.9(4)
C20	0.581(1)	-0.129(2)	0.3218(7)	4.0(4)
C21	0.549(2)	-0.031(2)	0.2934(8)	5.6(5)
C22	0.442(2)	0.020(2)	0.2959(8)	4.8(5)

Table 2-3. (cont'd)

atom	x	y	z	B_{eq}, Å^2
C23	1.373(2)	-0.019(2)	0.3304(7)	4.7(5)
C24	0.402(1)	-0.112(2)	0.3620(7)	3.9(4)
C25	0.462(1)	0.591(1)	0.3787(6)	2.5(3)
C26	1.583(1)	0.416(2)	0.6695(7)	3.4(4)
C27	1.638(1)	0.517(2)	0.6847(8)	4.6(5)
C28	1.656(1)	0.607(2)	0.6525(8)	5.2(5)
C29	1.386(1)	0.401(2)	0.3964(7)	3.7(4)
C30	1.553(2)	0.500(2)	0.5870(8)	4.5(4)
C31	1.487(1)	0.238(2)	0.5415(6)	3.2(4)
C32	1.406(1)	0.174(1)	0.5107(6)	3.0(4)
C33	0.566(2)	-0.123(2)	0.5319(7)	3.9(4)
C34	0.543(2)	0.138(2)	0.4510(7)	3.7(4)
C35	0.623(1)	0.199(2)	0.4802(7)	3.9(4)
C36	0.596(1)	0.257(2)	0.5232(7)	3.6(4)

a. B_{eq} is defined as $4/3[a^2\beta_{11}+b^2\beta_{22}+c^2\beta_{33}+ab(\cos\gamma)\beta_{12}+ac(\cos\beta)\beta_{13}+bc(\cos\alpha)\beta_{23}]$.

Table 2·4. Positional Parameters and B_{eq} Values[a] for $(Ph_4P)_2[Au_2(Se_2)(Se_3)]$ (2·2)
(Standard Deviations in Parentheses)

atom	x	y	z	B_{eq}, Å^2
Au1	0.0120(1)	0.1525(1)	0.24575(5)	2.30(2)
Au2	-0.0779(1)	-0.1051(1)	0.26774(6)	3.12(3)
Se1	0.0152(3)	0.0836(3)	0.3616(1)	3.42(7)
Se2	-0.0650(3)	-0.1194(3)	0.3808(2)	3.66(8)
Se3	-0.1041(3)	-0.0872(3)	0.1564(2)	4.52(7)
Se4	0.0583(4)	0.0419(4)	0.0940(2)	5.9(1)
Se5	0.0003(3)	0.2251(3)	0.1304(1)	3.51(7)
P1	0.4337(6)	0.6619(6)	0.3680(3)	1.6(1)
P2	0.5231(6)	0.3555(6)	0.1436(3)	1.6(1)
C1	0.405(2)	0.750(2)	0.434(1)	1.9(5)
C2	0.496(2)	0.742(2)	0.471(1)	1.6(4)
C3	0.472(3)	0.821(3)	0.514(1)	3.5(6)
C4	0.357(2)	0.899(2)	0.523(1)	1.9(5)
C5	0.258(2)	0.903(2)	0.487(1)	1.9(5)
C6	0.288(2)	0.826(2)	0.441(1)	2.2(5)
C7	0.406(2)	0.422(2)	0.642(1)	1.2(4)
C8	0.284(3)	0.367(3)	0.651(1)	3.1(6)
C9	0.165(3)	0.430(3)	0.661(2)	3.9(7)
C10	0.154(2)	0.559(2)	0.660(1)	1.7(5)
C11	0.265(3)	0.620(2)	0.647(1)	2.5(5)
C12	0.388(2)	0.552(2)	0.638(1)	2.1(5)
C13	0.422(2)	0.765(2)	0.292(1)	1.4(4)
C14	0.303(3)	0.817(2)	0.279(1)	2.5(5)
C15	0.291(2)	0.913(2)	0.222(1)	2.3(5)
C16	0.403(2)	0.955(2)	0.174(1)	2.2(5)
C17	0.525(3)	0.902(3)	0.187(1)	3.4(6)
C18	0.538(2)	0.810(2)	0.242(1)	2.3(5)
C19	0.308(2)	0.553(2)	0.392(1)	2.0(5)
C20	0.252(2)	0.509(2)	0.458(1)	1.7(5)
C21	0.168(3)	0.414(3)	0.476(2)	3.9(7)
C22	0.137(3)	0.362(2)	0.432(1)	2.9(6)

Table 2-4. (cont'd)

atom	x	y	z	B_{eq}, Å^2
C23	0.195(3)	0.410(3)	0.361(2)	3.9(7)
C24	0.276(3)	0.507(2)	0.342(1)	2.9(6)
C25	0.519(2)	0.243(2)	0.224(1)	1.5(4)
C26	0.403(3)	0.196(2)	0.263(1)	2.7(5)
C27	0.403(2)	0.101(2)	0.321(1)	3.1(6)
C28	0.518(3)	0.063(2)	0.340(1)	2.7(5)
C29	0.637(3)	0.110(3)	0.302(1)	3.1(6)
C30	0.639(2)	0.205(2)	0.243(1)	1.5(4)
C31	0.345(2)	0.547(2)	0.880(1)	1.8(5)
C32	0.316(3)	0.489(3)	0.832(1)	3.4(6)
C33	0.221(3)	0.406(3)	0.849(1)	3.6(6)
C34	0.150(3)	0.378(3)	0.917(1)	3.2(6)
C35	0.174(3)	0.430(3)	0.966(2)	3.7(6)
C36	0.268(2)	0.518(2)	0.944(1)	1.8(5)
C37	0.450(2)	0.739(2)	0.917(1)	1.1(4)
C38	0.333(3)	0.820(2)	0.924(1)	2.4(5)
C39	0.306(2)	0.892(2)	0.973(1)	2.1(5)
C40	0.394(3)	0.882(2)	1.012(1)	2.9(6)
C41	0.509(3)	0.803(2)	1.005(1)	2.5(5)
C42	0.539(2)	0.726(2)	0.959(1)	2.3(5)
C43	0.370(2)	0.454(2)	0.147(1)	2.1(5)
C44	0.365(2)	0.581(2)	0.146(1)	1.6(4)
C45	0.249(3)	0.660(2)	0.152(1)	2.7(5)
C46	0.132(3)	0.603(3)	0.165(1)	3.6(6)
C47	0.129(3)	0.484(2)	0.165(1)	2.8(6)
C48	0.244(2)	0.405(2)	0.157(1)	2.2(5)

a. B_{eq} is defined as $4/3[a^2\beta_{11}+b^2\beta_{22}+c^2\beta_{33}+ab(\cos\gamma)\beta_{12}+ac(\cos\beta)\beta_{13}+bc(\cos\alpha)\beta_{23}]$.

Table 2·5. Positional Parameters and B_{eq} Values[a] for $(PPN)_2[Au_2(Se_2)(Se_3)]$ (2·3) (Standard Deviations in Parentheses)

atom	x	y	z	B_{eq}, Å^2
Au	0.0773(1)	0.4106(1)	0.48505(7)	7.34(9)
Se1	0.143(3)	0.387(2)	0.609(1)	10(1)
Se2	-0.031(1)	0.464(1)	0.3697(8)	10(1)
Se3	0.139(2)	0.353(2)	0.5827(9)	7.6(8)
Se4	0.1470(7)	0.5094(7)	0.6352(4)	6.0(4)
Se5	0.045(1)	0.441(2)	0.3806(8)	6.2(6)
P1	-0.0755(6)	0.0893(6)	0.7224(3)	3.6(4)
P2	-0.2964(6)	0.1001(6)	0.6285(3)	3.2(4)
N	-0.199(2)	0.132(1)	0.690(1)	4(1)
C1	-0.011(2)	0.012(2)	0.671(1)	3.7(6)
C2	0.033(2)	0.065(2)	0.628(1)	4.2(6)
C3	0.067(2)	0.008(2)	0.582(1)	5.7(7)
C4	0.059(2)	-0.099(2)	0.580(1)	5.3(7)
C5	0.014(3)	-0.148(2)	0.624(1)	6.2(8)
C6	-0.024(2)	-0.094(2)	0.670(1)	4.1(6)
C7	0.018(2)	0.199(2)	0.746(1)	3.1(6)
C8	-0.023(2)	0.296(2)	0.744(1)	3.4(6)
C9	0.048(2)	0.378(2)	0.762(1)	4.5(7)
C10	0.168(2)	0.362(2)	0.787(1)	4.4(6)
C11	0.210(2)	0.262(2)	0.789(1)	4.4(6)
C12	0.135(2)	0.179(2)	0.769(1)	4.3(7)
C13	-0.077(2)	0.019(2)	0.796(1)	3.6(6)
C14	-0.174(2)	0.013(2)	0.816(1)	4.3(6)
C15	-0.171(3)	-0.034(2)	0.874(1)	5.5(7)
C16	-0.069(3)	-0.071(2)	0.911(2)	7.6(9)
C17	0.020(3)	-0.073(3)	0.890(2)	9(1)
C18	0.025(3)	-0.026(2)	0.831(2)	6.0(8)
C19	-0.290(2)	0.180(2)	0.563(1)	3.0(6)
C20	-0.205(2)	0.246(2)	0.562(1)	3.7(6)
C21	-0.198(2)	0.310(2)	0.515(1)	3.6(6)
C22	-0.286(3)	0.300(2)	0.459(1)	5.7(7)

Table 2·5. (cont'd)

atom	x	y	z	B_{eq}, Å^2
C23	-0.377(2)	0.234(2)	0.453(1)	4.8(7)
C24	-0.379(2)	0.175(2)	0.504(1)	4.5(7)
C25	-0.300(2)	-0.035(2)	0.604(1)	3.8(6)
C26	-0.318(2)	-0.107(2)	0.647(1)	3.5(6)
C27	-0.313(2)	-0.212(2)	0.632(1)	4.4(7)
C28	-0.286(2)	-0.242(2)	0.580(1)	4.9(7)
C29	-0.261(3)	-0.170(2)	0.536(1)	3.9(6)
C30	-0.266(2)	-0.065(2)	0.552(1)	4.4(7)
C31	-0.443(2)	0.120(2)	0.646(1)	2.7(5)
C32	-0.444(3)	0.183(2)	0.693(1)	5.4(7)
C33	-0.549(3)	0.198(2)	0.705(2)	7.2(9)
C34	-0.642(3)	0.153(2)	0.669(2)	6.5(8)
C35	-0.633(2)	0.086(2)	0.624(1)	5.4(7)
C36	-0.528(3)	0.066(2)	0.611(1)	4.6(6)

a. B_{eq} is defined as $4/3[a^2\beta_{11}+b^2\beta_{22}+c^2\beta_{33}+ab(\cos\gamma)\beta_{12}+ac(\cos\beta)\beta_{13}+bc(\cos\alpha)\beta_{23}]$.

Table 2·6. Positional Parameters and B_{eq} Values[a] for $(Ph_4P)_2[Au_2(Se_2)(Se_4)]$ (2·4)
(Standard Deviations in Parentheses)

atom	x	y	z	B_{eq}, Å^2
Au	0.93180(6)	0.1557(2)	0.6595(1)	5.23(7)
Se1	0.9571(2)	0.3702(4)	0.6689(3)	8.5(3)
Se2	0.8893(2)	-0.0390(4)	0.6387(2)	5.4(2)
Se3	0.9635(2)	-0.1731(4)	0.6735(2)	5.3(2)
P1	0.1748(3)	0.1276(7)	0.2022(5)	2.4(3)
C1	0.223(1)	0.137(3)	0.173(2)	2.2(5)
C2	0.197(1)	0.134(3)	0.086(2)	3.5(7)
C3	0.235(1)	0.141(3)	0.061(2)	3.7(7)
C4	0.299(1)	0.162(3)	0.132(2)	4.5(7)
C5	0.324(1)	0.169(3)	0.217(2)	3.9(7)
C6	0.286(1)	0.155(3)	0.239(2)	3.0(6)
C7	0.131(1)	0.266(3)	0.173(2)	3.0(6)
C8	0.122(1)	0.341(3)	0.110(2)	3.9(7)
C9	0.086(1)	0.451(3)	0.087(2)	4.4(8)
C10	0.061(1)	0.471(3)	0.125(2)	4.4(8)
C11	0.069(1)	0.393(4)	0.184(2)	5.6(9)
C12	0.104(1)	0.288(3)	0.212(2)	4.1(7)
C13	0.122(1)	-0.002(3)	0.143(2)	2.9(6)
C14	0.131(1)	-0.092(3)	0.099(2)	2.9(6)
C15	0.090(1)	-0.180(3)	0.057(2)	4.4(7)
C16	0.041(1)	-0.189(3)	0.055(2)	4.4(8)
C17	0.034(1)	-0.110(3)	0.096(2)	5.0(8)
C18	0.075(1)	-0.012(3)	0.146(2)	4.1(7)
C19	0.222(1)	0.112(3)	0.320(2)	1.9(5)
C20	0.248(1)	0.211(3)	0.374(2)	2.7(6)
C21	0.289(1)	0.201(3)	0.463(2)	3.9(7)
C22	0.313(1)	0.098(3)	0.502(2)	4.7(8)
C23	0.289(1)	-0.010(3)	0.450(2)	4.0(7)
C24	0.245(1)	0.002(3)	0.358(2)	3.3(7)

a. B_{eq} is defined as $4/3[a^2\beta_{11}+b^2\beta_{22}+c^2\beta_{33}+ab(\cos\gamma)\beta_{12}+ac(\cos\beta)\beta_{13}+bc(\cos\alpha)\beta_{23}]$.

Table 2·7. Positional Parameters and B_{eq} Values[a] for $(Et_4N)_3[NaAu_{12}Se_8]$ (2·5) (Standard Deviations in Parentheses)

atom	x	y	z	B_{eq}, Å^2
Au1	0.8339(2)	0.1495(2)	0.8752(2)	3.98(8)
Au2	0.6494(2)	-0.1651(2)	0.8038(2)	4.46(8)
Au3	0.8407(2)	-0.2231(2)	0.6710(2)	3.47(7)
Au4	0.9767(2)	-0.0934(2)	1.2622(2)	3.43(7)
Au5	0.8134(2)	-0.3164(2)	0.9303(2)	3.85(8)
Au6	0.8090(2)	0.0581(2)	1.1363(2)	3.50(7)
Se1	0.9788(7)	-0.2835(6)	1.1567(7)	5.2(2)
Se2	0.6425(7)	0.0203(7)	0.9072(8)	6.1(3)
Se3	0.6478(7)	-0.3552(5)	0.6995(7)	5.7(2)
Se4	0.9728(6)	0.0936(6)	1.3660(6)	4.5(2)
Na	1.0000	0	1.0000	2.789(9)
N1	0.468(3)	0.249(3)	0.738(3)	1.380(7)
N2	1.0000	1/2	1/2	2.867(4)
C1	0.596(6)	0.260(6)	0.748(6)	5.019(3)
C2	0.620(5)	0.279(5)	0.617(6)	3.716(4)
C3	0.453(5)	0.354(5)	0.729(6)	3.544(4)
C4	0.331(7)	0.361(7)	0.735(7)	6.715(3)
C5	0.444(5)	0.217(5)	0.847(6)	3.960(4)
C6	0.537(7)	0.329(6)	1.003(7)	6.207(3)
C7	0.353(6)	0.125(6)	0.599(7)	5.242(3)
C8	0.361(7)	0.006(7)	0.565(8)	6.415(3)
C9	1.052(7)	0.434(6)	0.408(7)	0.295(3)
C10	0.977(8)	0.431(8)	0.249(9)	2.129(3)
C11	0.844(8)	0.448(7)	0.429(8)	1.539(2)
C12	0.753(7)	0.302(7)	0.368(8)	0.878(3)
C13	1.042(6)	0.475(1)	0.619(9)	8.819(1)
C14	0.993(4)	0.543(3)	0.715(5)	6.704(5)
C15	1.10(2)	0.62(1)	0.57(2)	7.573(1)
C16	1.0574	0.7014	0.6649	9.6

a. B_{eq} is defined as $4/3[a^2\beta_{11}+b^2\beta_{22}+c^2\beta_{33}+ab(\cos\gamma)\beta_{12}+ac(\cos\beta)\beta_{13}+bc(\cos\alpha)\beta_{23}]$.

Table 2·8. Positional Parameters and B_{eq} Values[a] for $(Ph_4P)_2[Au_2(Te_2)_2]$ (2·6) (Standard Deviations in Parentheses)

atom	x	y	z	B_{eq}, Å^2
Au	0.54453(8)	0.62201(7)	0.0280(1)	2.17(3)
Te1	0.4641(1)	0.4080(1)	0.2257(1)	2.82(6)
Te2	0.5549(1)	0.6428(1)	0.2809(1)	3.01(6)
P	0.9608(4)	0.1588(4)	0.7727(4)	1.2(1)
C1	0.927(2)	0.250(1)	0.644(2)	1.6(3)
C2	0.812(2)	0.328(2)	0.629(2)	2.0(3)
C3	0.783(2)	0.400(2)	0.531(2)	2.3(3)
C4	0.867(2)	0.397(2)	0.453(2)	2.9(4)
C5	0.981(2)	0.321(2)	0.466(2)	2.7(3)
C6	1.014(2)	0.244(2)	0.563(2)	2.1(3)
C7	0.833(1)	0.056(1)	0.724(2)	1.4(3)
C8	0.763(2)	0.023(1)	0.591(2)	1.8(3)
C9	0.670(2)	-0.064(2)	0.552(2)	2.6(3)
C10	0.645(2)	-0.117(2)	0.651(1)	2.6(3)
C11	0.714(2)	-0.081(2)	0.790(2)	2.8(4)
C12	0.807(2)	0.006(2)	0.827(2)	2.2(3)
C13	0.957(1)	0.261(1)	0.930(2)	1.2(3)
C14	1.074(2)	0.309(1)	1.019(2)	2.0(3)
C15	1.068(2)	0.401(2)	1.132(2)	2.2(3)
C16	0.948(2)	0.443(1)	1.161(2)	1.9(3)
C17	0.833(2)	0.394(2)	1.074(2)	2.2(3)
C18	0.835(2)	0.302(1)	0.961(2)	1.6(3)
C19	1.118(2)	0.071(1)	0.788(2)	1.4(3)
C20	1.235(2)	0.128(1)	0.807(2)	1.7(3)
C21	1.358(2)	0.059(2)	0.828(2)	2.0(3)
C22	1.362(2)	-0.067(2)	0.826(2)	2.3(3)
C23	1.251(2)	-0.125(2)	0.806(2)	2.4(3)
C24	1.127(2)	-0.056(1)	0.785(2)	1.9(3)

a. B_{eq} is defined as $4/3[a^2\beta_{11}+b^2\beta_{22}+c^2\beta_{33}+ab(\cos\gamma)\beta_{12}+ac(\cos\beta)\beta_{13}+bc(\cos\alpha)\beta_{23}]$.

Table 2·9. Calculated and Observed X-ray Powder Diffraction Patterns for $(PPN)_2[Au_2Se_2(Se_4)_2]$ (2·1)

h k l	$d_{calc.}$ (Å)	$d_{obs.}$ (Å)	$I/I_{max.}$ (obs.)
0 0 2	13.42	13.59	31
-1 0 1	11.13	11.24	100
1 0 1	10.57	10.63	90
0 1 1	10.51	/	/
0 1 2	8.70	8.74	37
1 1 0	8.22	8.27	100
-1 1 1	7.97	8.03	50
1 1 1	7.76	7.81	21
1 0 3	6.910	6.915	26
0 0 4	6.711	6.743	24
-1 1 3	6.206	6.262	18
2 0 0	5.921	5.989	43
0 2 1	5.584	5.645	55
0 2 2	5.254	5.296	47
2 1 1	5.099	5.131	50
-1 2 1	5.079	/	/
1 2 1	5.022	5.065	27
-1 2 2	4.852	4.905	61
0 2 3	4.813	/	/
1 2 2	4.754	4.794	53
-1 2 3	4.519	4.561	53
1 2 3	4.401	4.442	39
0 1 6	4.166	4.193	18
-2 2 2	3.984	4.028	15
0 3 2	3.662	3.689	19
-1 3 2	3.517	3.545	23
0 3 4	3.311	3.328	26
-2 1 7	3.194	3.218	21
-2 3 4	2.933	2.983	11
2 3 4	2.848	2.853	31

Table 2·9. (cont'd)

h k l	$d_{calc.}$ (Å)	$d_{obs.}$ (Å)	$I/I_{max.}$ (obs.)
2 0 8	2.835	/	/
1 1 9	2.761	2.771	16
2 2 7	2.738	/	/
-3 2 6	2.703	2.720	19
-3 1 8	2.581	2.595	31
-3 3 5	2.490	2.499	16
3 1 8	2.417	2.424	13
-2 4 5	2.347	2.352	10
3 2 10	2.013	2.018	12
-2 6 2	1.801	1.813	12

Table 2·10. Calculated and Observed X-ray Powder Diffraction Patterns for $(Ph_4P)_2[Au_2(Se_2)(Se_3)]$ (2·2)

h k l	$d_{calc.}$ (Å)	$d_{obs.}$ (Å)	$I/I_{max.}$ (obs.)
0 1 0	10.6	10.7	48
1 0 0	9.9	10.1	100
0 0 2	9.9	/	/
0 1 2	8.23	8.35	45
1 1 0	7.62	7.67	23
-1 1 0	6.96	7.03	27
-1 0 2	6.34	6.40	18
1-1 2	5.76	5.87	12
2 0 0	4.99	5.05	35
2 0 2	4.95	/	/
2 1 2	4.87	4.86	12
-2 1 0	4.37	4.43	39
-2 1 1	4.17	4.21	27
0 2 4	4.11	4.10	12
-2 1 2	3.843	3.847	13
2 2 0	3.814	/	/
0 3 2	3.592	3.641	12
1 3 0	3.437	3.450	13
-3 1 0	3.091	3.116	11
2 3 0	3.010	3.013	10
1 4 2	2.728	2.732	11
1 1 8	2.646	2.618	10
3 3 0	2.536	2.529	10

Table 2·11. Calculated and Observed X-ray Powder Diffraction Patterns for $(PPN)_2[Au_2(Se_2)(Se_3)]$ (2·3)

h k l	$d_{calc.}$ (Å)	dobs. (Å)	$I/I_{max.}$ (obs.)
-1 0 1	11.6	11.8	57
0 1 1	11.0	11.2	73
0 0 2	10.5	10.6	24
1 0 1	9.26	9.36	66
1 1 0	8.70	8.77	74
-1 1 2	7.44	7.49	100
0 2 0	6.48	6.52	22
2 0 0	5.87	5.92	24
-2 1 1	5.51	5.57	52
2 1 0	5.35	5.36	43
1 2 1	5.31	/	/
2 2 0	4.35	4.39	21
0 2 4	4.07	4.11	33
-3 1 1	3.86	3.88	15
-1 3 3	3.65	3.69	28
2 3 0	3.48	3.50	16
-3 2 2	3.42	3.44	18
3 2 0	3.35	3.37	16
-3 3 1	2.95	2.96	22
-4 2 3	2.72	2.74	17

Table 2·12. Calculated and Observed X-ray Powder Diffraction Patterns for $(Ph_4P)_2[Au_2(Se_2)(Se_4)]$ (2·4)

h k l	$d_{calc.}$ (Å)	$d_{obs.}$ (Å)	$I/I_{max.}$ (obs.)
1 1 0	10.2	10.8	39
0 0 2	9.6	9.8	91
-1 1 1	9.3	/	/
-2 0 2	9.0	/	/
-1 1 2	7.31	7.49	30
-3 1 1	7.04	7.04	100
-4 0 2	6.35	/	/
-1 1 3	5.65	5.66	18
4 0 2	5.07	5.14	14
5 1 0	4.93	4.95	50
2 2 1	4.83	4.92	40
6 0 0	4.60	4.64	10
-4 0 4	4.46	/	/
3 1 3	4.37	4.40	90
2 0 4	4.24	4.23	21
1 1 4	4.21	/	/
-5 1 4	3.872	3.878	28
6 0 2	3.820	3.804	30
-6 0 4	3.786	3.764	30
1 3 0	3.627	3.620	25
-6 2 2	3.528	3.530	13
8 0 0	3.452	3.454	25
6 2 1	3.364	3.368	19
-2 0 6	3.286	3.277	11
-1 1 6	3.127	3.121	39
-9 1 1	3.031	3.036	34
4 2 4	2.989	2.974	20
-8 2 1	2.961	2.972	28
0 4 0	2.744	2.742	16
-8 0 6	2.682	2.690	25

Table 2·12. (cont'd)

h k l	$d_{calc.}$ (Å)	$d_{obs.}$ (Å)	$I/I_{max.}$ (obs.)
3 3 4	2.667	2.658	20
-4 4 2	2.523	2.537	18
4 4 1	2.503	2.510	24
-4 0 8	2.451	2.446	20
6 2 5	2.390	2.392	16
9 3 0	2.355	2.363	15
4 4 3	2.303	2.291	17
-1 5 1	2.180	2.175	27
-6 0 10	1.944	1.941	17
-14 2 1	1.891	1.890	14

Table 2·13. Calculated and Observed X-ray Powder Diffraction Patterns for $(Et_4N)_3[NaAu_{12}Se_8]$ (2·5)

h k l	$d_{calc.}$ (Å)	$d_{obs.}$ (Å)	$I/I_{max.}$ (obs.)
0 1 0	10.54	10.73	100
-1 1 0	10.27	10.45	67
1 0 0	9.64	9.82	53
0 0 1	9.21	9.32	83
-1 0 1	9.18	/	/
0-1 1	9.15	/	/
1 0 1	5.49	5.50	49
-2 0 1	5.47	/	/
-1-1 2	5.120	5.157	46
0-1 2	5.099	/	/
-1 2 1	4.716	4.758	56
-2 2 1	4.662	4.697	59
0 0 2	4.608	/	/
-1-2 1	4.439	4.478	32
2-2 1	4.327	4.326	63
-2-1 1	4.297	/	/
-2-1 2	4.105	4.134	76
1-2 2	4.104	4.101	81
1-1 2	4.073	4.036	45
-3 2 0	3.749	3.776	31
0-3 2	3.647	3.679	34
-2 0 3	3.423	3.485	42
-2 1 3	3.164	3.185	21
-3-1 2	3.131	3.147	19
1 2 1	3.052	3.071	41
0-3 3	3.048	3.015	47
1-4 2	2.994	2.996	40
-4 2 1	2.980	/	/
2 2 0	2.880	2.899	41
0-4 2	2.880	/	/

Table 2·13. (cont'd)

h k l	$d_{calc.}$ (Å)	$d_{obs.}$ (Å)	$I/I_{max.}$ (obs.)
-4 2 0	2.819	2.823	37
-4 3 0	2.776	2.785	54
-2 4 1	2.767	/	/
-3 4 1	2.746	2.760	42
-3-2 2	2.652	2.667	46
0-4 3	2.634	/	/
-2 0 4	2.617	2.626	53
-3-2 3	2.570	2.579	56
2-2 3	2.540	2.552	70
-2 1 4	2.427	2.428	67
-3 1 4	2.421	/	/
-4-1 3	2.400	2.404	57
-1 5 0	2.329	2.321	50
-3 5 1	2.285	2.296	46
-2-4 2	2.219	2.223	21
-4-2 3	2.156	2.162	30
2-2 4	2.037	2.040	30
-6 3 4	1.764	1.763	19
5 0 1	1.731	1.738	23

Table 2·14. Calculated and Observed X-ray Powder Diffraction Patterns for $(Ph_4P)[Au_2Te_4]$ (2·6)

h k l	$d_{calc.}$ (Å)	$d_{obs.}$ (Å)	$I/I_{max.}$ (obs.)
0 1 0	10.9	11.4	88
1 0 0	10.0	10.1	100
0 0 1	9.8	/	/
1 0-1	8.21	8.27	31
0 1-1	8.12	8.27	31
1 1 0	7.723	7.770	45
1-1 0	7.094	7.099	71
1 0 1	6.235	6.237	16
1-1-1	5.939	5.941	11
2 0-1	5.051	5.050	23
2 0 0	5.017	5.014	28
2-1 0	4.418	4.420	77
2 2 0	3.862	3.867	19
0 3 0	3.640	3.644	17
1 3 0	3.519	3.526	13
3-1 0	3.125	3.117	26
2 3 0	3.073	3.071	8
3-2 0	2.750	2.749	16
0 4 0	2.730	2.735	11
1 1-4	2.615	2.618	16
3 3 0	2.575	2.577	12
2 0-4	2.486	2.483	12
4-1 0	2.401	2.406	8
4 2 0	2.357	2.347	10
1-1 4	2.277	2.269	9
4 0-4	2.052	2.050	14
2-2 4	1.961	1.963	7
4-1-4	1.938	1.930	8
5-2 0	1.833	1.830	7

III. Results

1. Description of Crystal and Molecular Structures of the Compounds

(i). Structure of $(PPN)_2[Au_2Se_2(Se_4)_2]$ (2·1)

The crystal lattice of this compound is made up of well separated PPN^+ cations and $[Au_2Se_2(Se_4)_2]^{2-}$ anions. The PPN^+ cations have the normal structure, and warrant no further comments. The $[Au_2Se_2(Se_4)_2]^{2-}$ anion is situated on a crystallographically imposed inversion center. In the structure, two square-planar (d^8 configuration) Au^{3+} ions are bonded by two μ_2-Se^{2-} and two bidentate chelating Se_4^{2-} ligands. The molecule possesses idealized C_{2h} symmetry. Figure 2·1 shows two different views of this molecule, while a packing diagram of this compound is given in Figure 2·2. The four-membered $[Au_2Se_2]^{2+}$ core is perfectly planar because of the inversion center (at the midpoint of the Au···Au vector). The distance of 3.660(1) Å for the Au···Au separation in this structure represents a non-interacting situation of two gold atoms in the same molecule. The five-membered $AuSe_4$ ring has a twist-boat conformation. Selected bond distances and bond angles as given in Table 2·15.

(ii). Structure of $(Ph_4P)_2[Au_2(Se_2)(Se_3)]$ (2·2)

The structure of (2·2) is composed of well separated Ph_4P^+ cations and $[Au_2(Se_2)(Se_3)]^{2-}$ anions in the crystal lattice. The Ph_4P^+ cations have the normal tetrahedral structure, and will not be discussed further. The $[Au_2(Se_2)(Se_3)]^{2-}$ anion forms an envelope-shaped seven-membered ring which contains two gold and five selenium atoms. Two different views of this molecule are shown in Figure 2·3. Figure 2·4 is the packing diagram of this compound. Such a ring molecule features two linearly-coordinated Au^+ centers bridged by a Se_2^{2-} and a Se_3^{2-} ligand. Two Au^+ ions and their adjacent Se atoms (e.g. Au(1)/Se(1)/Se(2)/Au(2)/Se(3)/Se(5)) form almost a perfect plane with the

Se(4) atom lying 1.172 Å above it. The Au···Au distance of 3.004(2) Å indicates d^{10}–d^{10} interactions between the two atoms. The Se(1)-Se(2) distance in the diselenide unit is rather long at 2.402(5) Å. Other selected metric parameters are given in Table 2·16.

Table 2·15. Selected Geometric Data for $(PPN)_2[Au_2Se_2(Se_4)_2]$ (2·1)[b]

		Bond Distances (Å)	
Au-Se(1)	2.461(2)	Au-Se(4)	2.450(2)
Au-Se(5)	2.444(2)	Au-Se(5)'	2.449(2)
Au-Se(mean)	2.451(4)	Se(1)-Se(2)	2.357(3)
Se(2)-Se(3)	2.304(3)	Se(3)-Se(4)	2.332(3)
Se-Se(mean)	2.331(15)		
		Bond Angles (deg)	
Se(1)-Au-Se(4)	100.43(7)	Se(1)-Au-Se(5)	88.31(6)
Se(5)-Au-Se(5)'	82.95(6)		

Table 2·16. Selected Geometric Data for $(Ph_4P)_2[Au_2(Se_2)(Se_3)]$ (2·2)[b]

		Bond Distances (Å)	
Au(1)-Se(1)	2.388(3)	Au(1)-Se(5)	2.401(3)
Au(2)-Se(2)	2.399(4)	Au(2)-Se(3)	2.401(4)
Au-Se(mean)	2.397(3)	Se(1)-Se(2)	Se(1)-Se(2)
Se(3)-Se(4)	2.283(5)	Se(4)-Se(5)	2.279(6)
Se-Se(mean)	2.321(40)	Au(1)···Au(2)	3.004(2)
		Bond Angles (deg)	
Se(1)-Au(1)-Se(5)	177.9(1)	Se(2)-Au(2)-Se(3)	176.8(1)
Au(1)-Se(1)-Se(2)	97.7(2)	Au(2)-Se(2)-Se(1)	96.8(1)
Au(1)-Se(5)-Se(4)	100.8(1)	Au(2)-Se(3)-Se(4)	101.3(2)
Se(3)-Se(4)-Se(5)	105.2(2)		

b. The estimated standard deviations in the mean bond lengths and the mean bond angles are calculated by the equation $\sigma_l=\{\Sigma_n(l_n-l)^2/n(n-1)\}^{1/2}$, where l_n is the length (angle) of the *n*th bond, l the mean length (angle), and n the number of bonds.

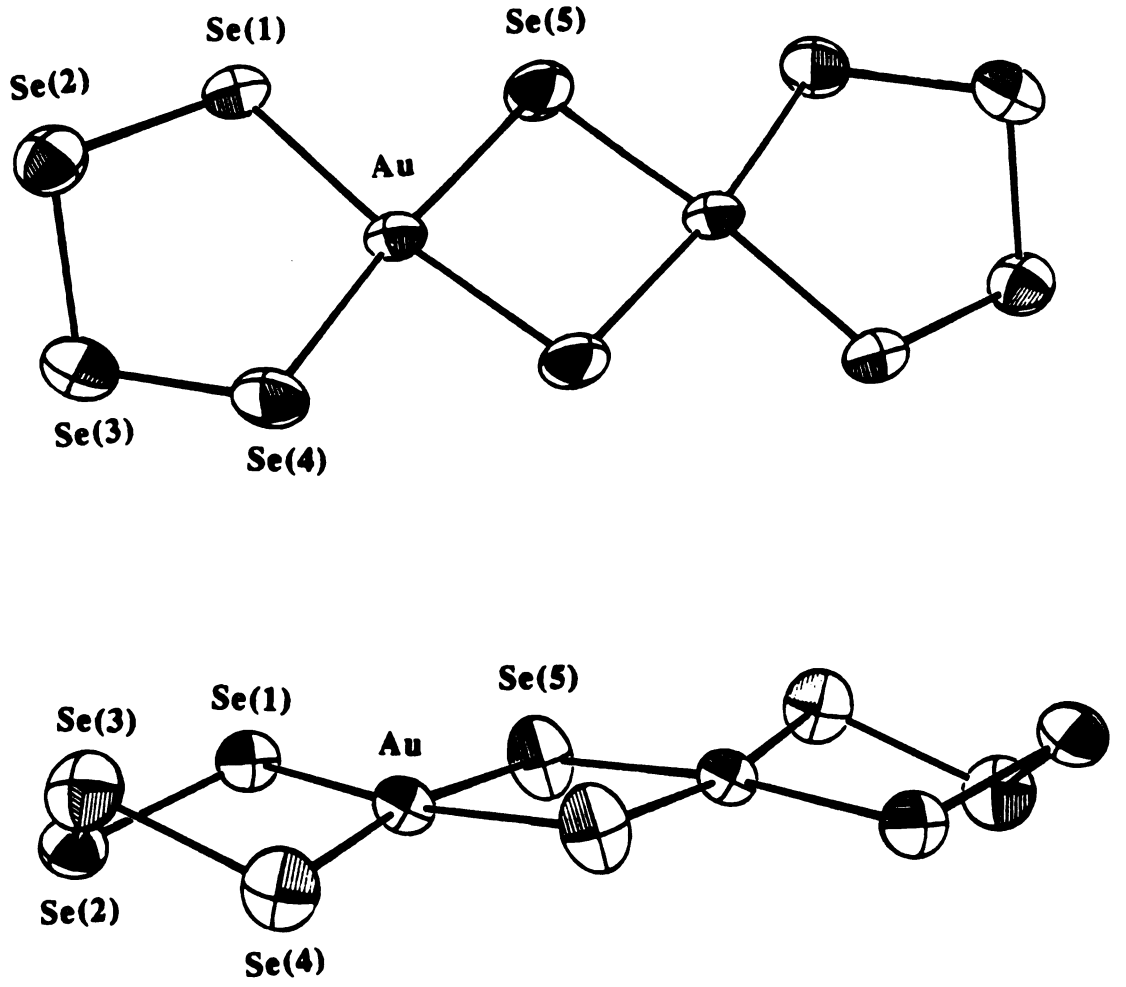


Figure 2·1. Two Views of the $[Au_2Se_2(Se_4)_2]^{2-}$ Anion

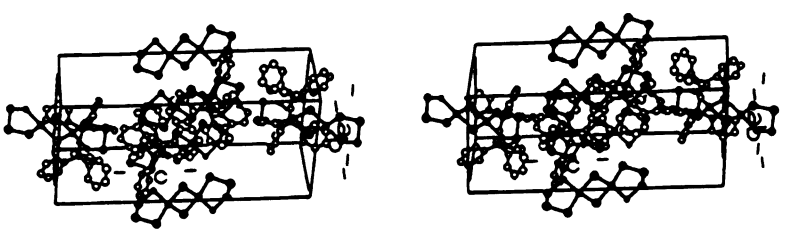


Figure 2·2. The Packing Diagram in the Unit Cell of $(PPN)_2[Au_2Se_2(Se_4)_2]$ (Stereoview)

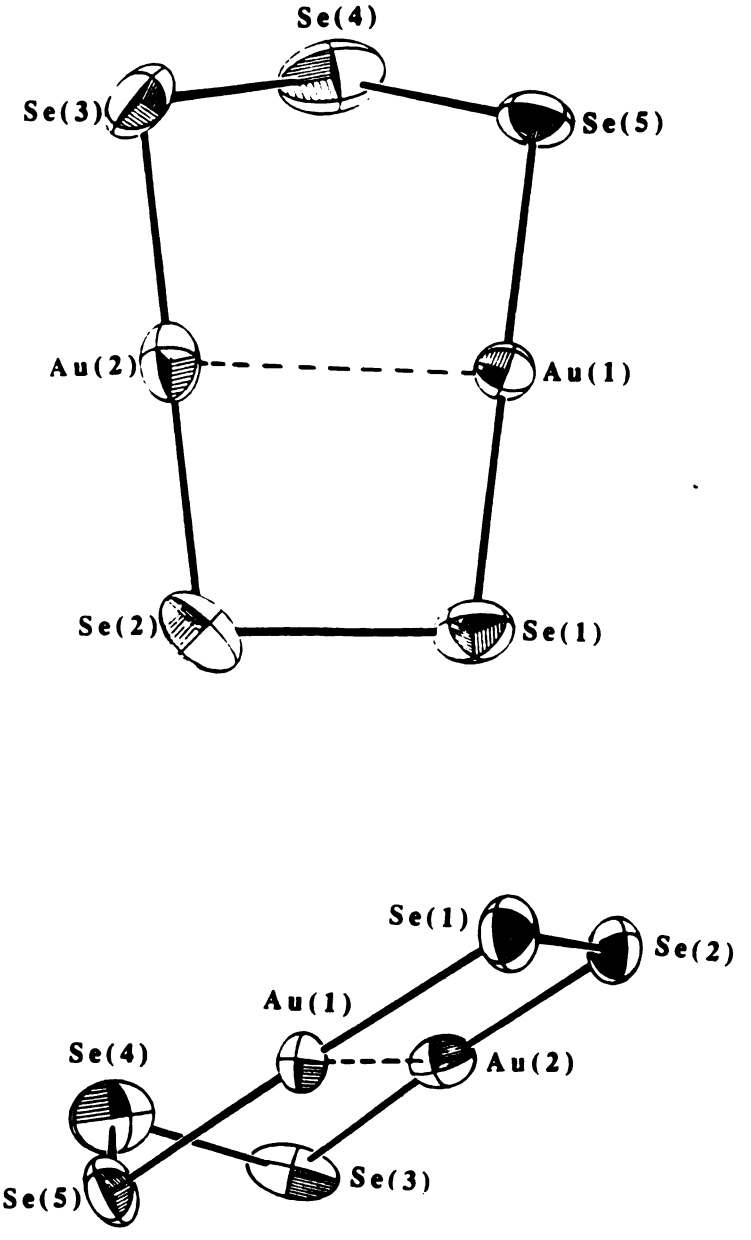


Figure 2-3. Two Views of the $[Au_2(Se_2)(Se_3)]^{2-}$ Anion

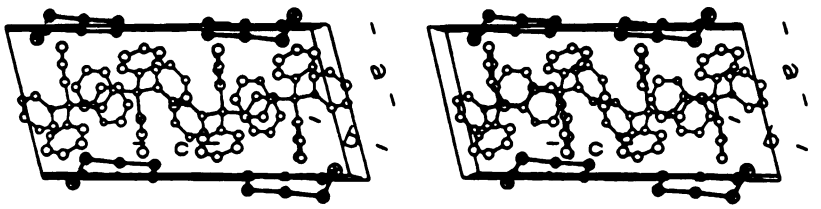


Figure 2-4. The Packing Diagram in the Unit Cell of $(Ph_4P)_2[Au_2(Se_2)(Se_3)]$ (Stereoview)

(iii). Structure of $(PPN)_2[Au_2(Se_2)(Se_3)]$ (2·3)

This compound is also consisted of PPN^+ cations and $[Au_2(Se_2)(Se_3)]^{2-}$ anions in the crystal lattice, and crystallizes in the centrosymmetic space group $P2_1/n$ (#14). Despite lacking of centrosymmetry, the $[Au_2(Se_2)(Se_3)]^{2-}$ anion is situated on the inversion center. This causes an orientation disorder on this molecule. Figure 2·5 is the ORTEP representation of the disordered anion. Two opposite molecular orientations share a common Au–Au axis. The inversion center is located at the middle of the Au–Au vector. No meaningful structural parameters can be obtained from the refinement. Nevertheless, this anion has essentially the same structure as that found in $(Ph_4P)_2[Au_2(Se_2)(Se_3)]$ (2·2).

(iv). Structure of $(Ph_4P)_2[Au_2(Se_2)(Se_4)]$ (2·4)

The $[Au_2(Se_2)(Se_4)]^{2-}$ anion in this compound is structurally similar to $[Au_2(Se_2)(Se_3)]^{2-}$ as shown in Figure 2·6. Figure 2·7 shows a packing diagram of the compound. The $[Au_2(Se_2)(Se_4)]^{2-}$ anion has a C_2 symmetry with the two-fold axis running across the centers of the Au···Au and Se(1)-Se(1) axes. The Au–Au separation between the two linearly-coordinated Au^+ ions at 3.132(3) Å (*vs.* 3.004 Å in (2·2)) is perhaps due to the longer Se_4^{2-} ligand present in the structure. Interestingly, the Au-Se bond lengths separate into two sets. The Au-Se bonds to Se_2^{2-} are long at 2.433(5) Å, while the Au-Se bonds to Se_4^{2-} are short at 2.355(5) Å. Although the Se-Se bond distances in Se_4^{2-} are all normal, the Se-Se distance of 2.46(1) Å in Se_2^{2-} is even longer than that in (2·2). The eight-membered ring is puckered. Other selected metric parameters are given in Figure 2·17.

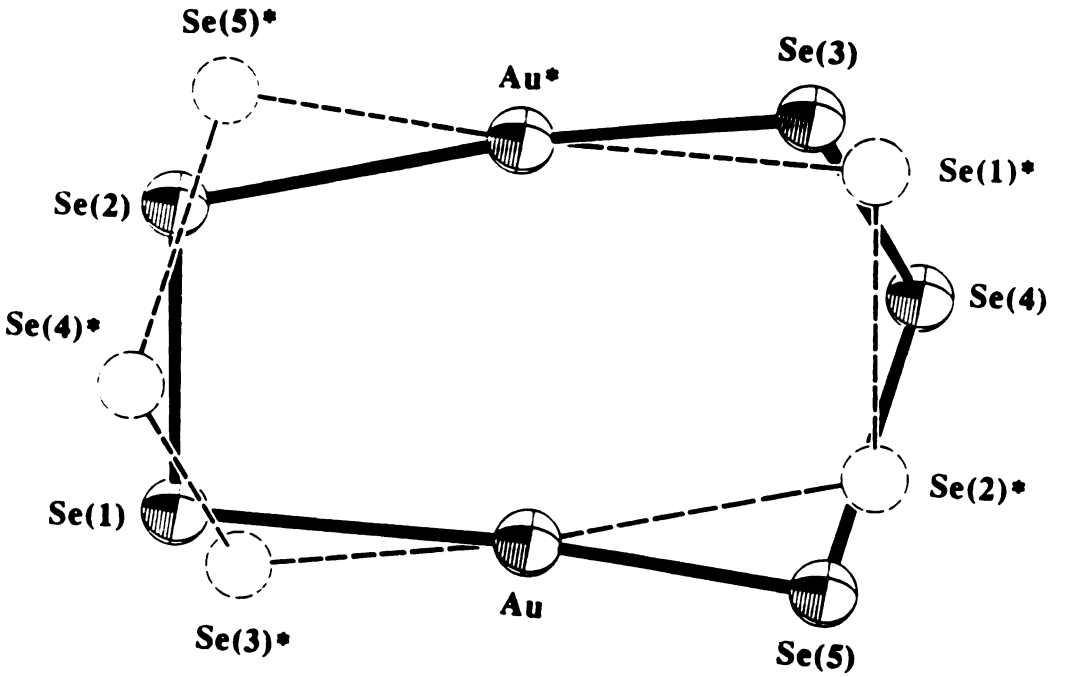


Figure 2-5. The ORTEP Representation of the $[Au_2(Se_2)(Se_3)]^{2-}$ Anion in $(PPN)_2[Au_2(Se_2)(Se_3)]$, Showing Structural Disorder Caused By the Inversion Center

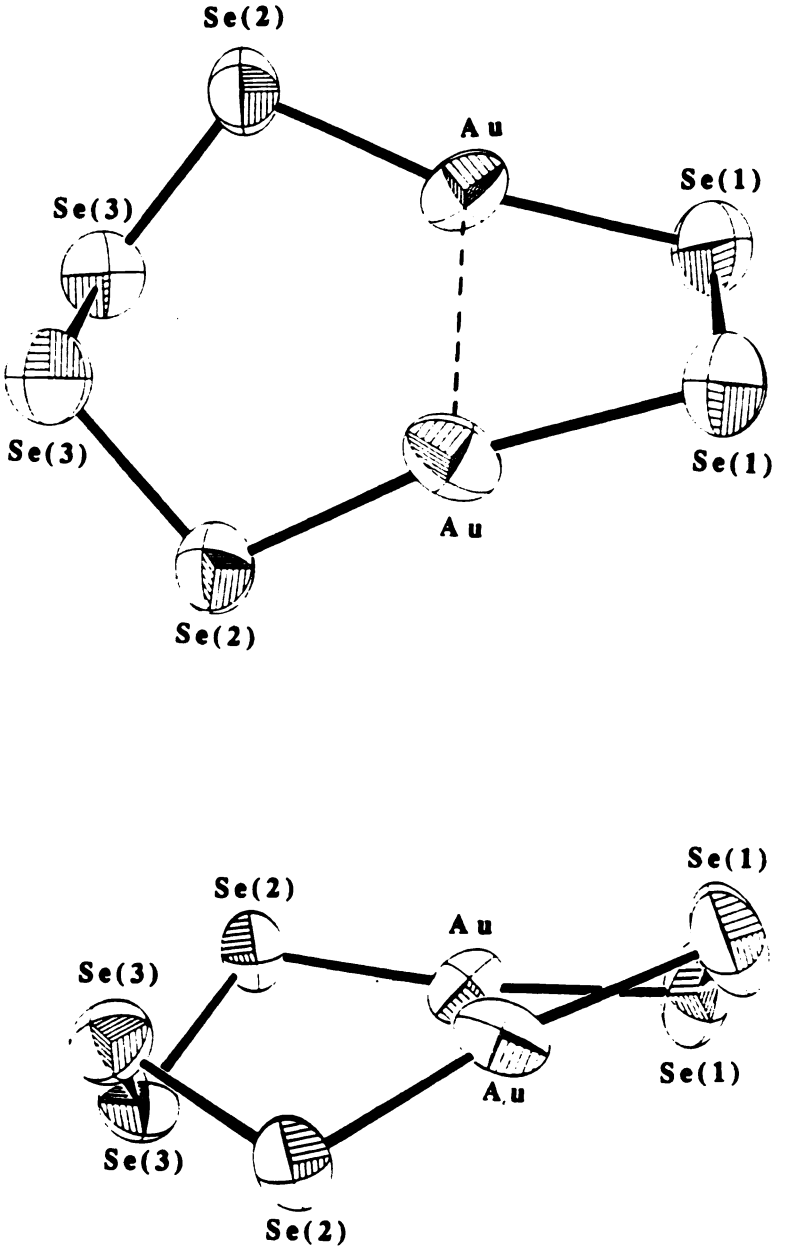


Figure 2·6. Two Views of the $[Au_2(Se_2)(Se_4)]^{2-}$ Anion

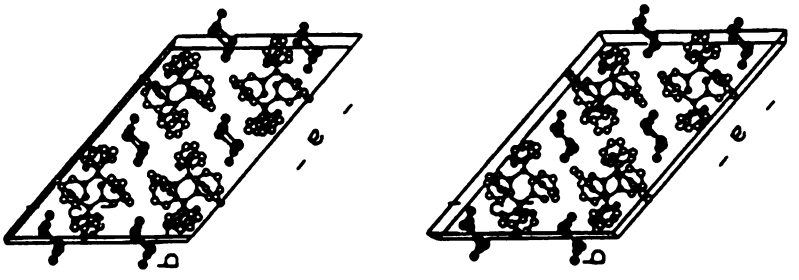


Figure 2·7. The Packing Diagram in the Unit Cell of $(Ph_4P)_2[Au_2(Se_2)(Se_4)]$ (Stereoview)

Table 2·17. Selected Geometric Data for $(Ph_4P)_2[Au_2(Se_2)(Se_4)]$ (2·4)[b]

		Bond Distances (Å)	
Au-Se(1)	2.433(5)	Au-Se(2)	2.355(5)
Au-Se(mean)	2.394(39)	Se(1)-Se(1)	2.46(1)
Se(2)-Se(2)	2.280(6)	Se(3)-Se(3)	2.301(7)
Se-Se(mean)	2.347(50)	Au···Au	3.132(3)
		Bond Angles (deg)	
Se(1)-Au-Se(2)	169.6(1)	Au-Se(1)-Se(1)	95.4(1)
Au-Se(2)-Se(3)	105.3(2)	Se(2)-Se(3)-Se(3)	105.3(2)

b. The estimated standard deviations in the mean bond lengths and the mean bond angles are calculated by the equation $\sigma_l=\{\Sigma_n(l_n-l)^2/n(n-1)\}^{1/2}$, where l_n is the length (angle) of the *n*th bond, l the mean length (angle), and n the number of bonds.

(v). Structure of $(Et_4N)_3[NaAu_{12}Se_8]$ (2·5)

The crystal lattice of (2·5) comprises of Et_4N^+ cations and $[NaAu_{12}Se_8]^{3-}$ anions. The compound crystallizes in the space group P-1 (#2). The Na^+ ion and one of the N atoms from the Et_4N cations are located, respectively, on the inversion centers 1, 0, 1 and 1, 1/2, 1/2. This imposes a structural disorder on the tetrahedral molecule Et_4N^+. Another Et_4N^+ cation is situated in a general position, and has the normal tetrahedral structure. Thus, the compound possesses an asymmetric unit of $(Et_4N)_{1.5}[Na_{0.5}Au_6Se_4]$. With the disordered model on this Et_4N^+ cation the structural refinement yielded satisfactory results, and the anion site was well resolved. A packing diagram of the compound is shown in Figure 2·8. Figure 2·9 is the ORTEP representation of the $[NaAu_{12}Se_8]^{3-}$ anion. The structure features an almost perfect cube with twelve linearly-coordinated Au^+ ions positioned at the mid-points of the edges and eight trigonal Se atoms occupying the corners of the cube. The molecule possesses an idealized O_h symmetry. The captured Na^+ ion is situated at the center of the cube, and interacts with the Au^+ at 3.327 (3) Å to 3.467 (3) Å.

The affinity of the $[Au_{12}Se_8]^{4-}$ cage for Na^+ is reminiscent of the behavior of organic-based cryptand molecules. Selected bond distances and bond angles as given in Table 2·18.

(vi). Structure of $(Ph_4P)_2[Au_2(Te_2)_2]$ (2·6)

The crystal lattice of (2·6) is made up of non-interacting Ph_4P^+ cations and $[Au_2(Te_2)_2]^{2-}$ anions. The Ph_4P^+ cations have the normal tetrahedral structure, and will not be discussed further. The structure of the $[Au_2(Te_2)_2]^{2-}$ anion is shown in Figure 2·10, while the packing diagram of the compound is shown in Figure 2·11. The $[Au_2(Te_2)_2]^{2-}$ anion is a perfectly planar molecule with D_{2h} symmetry because it is situated on an crystallographically imposed inversion center. The structural motif is analogous to the $[Au_2(Se_2)(Se_x)]^{2-}$ (x=3, 4) anions described above. The similar lengths of the Au-Au and Te-Te vectors in this structure are probably responsible for the stability of such a symmetric entity. The same molecule has been isolated as the PPN^+ salt, and structurally characterized before[3]. The metric parameters in the current anion are similar to those found in $(PPN)_2[Au_2(Te_2)_2]$, and are compared in Table 2·19.

Table 2·18. Selected Geometric Data for $(Et_4N)_3[NaAu_{12}Se_8]$ (2·5)[b]

		Bond Distances (Å)	
Au(1)-Se(1)	2.400(7)	Au(1)-Se(2)	2.414(8)
Au(2)-Se(2)	2.402(8)	Au(2)-Se(3)	2.400(8)
Au(3)-Se(3)	2.417(7)	Au(3)-Se(4)	2.408(6)
Au(4)-Se(1)	2.428(7)	Au(4)-Se(4)	2.401(6)
Au(5)-Se(1)	2.399(7)	Au(5)-Se(3)	2.404(7)
Au(6)-Se(2)	2.401(7)	Au(6)-Se(4)	2.402(6)
Au-Se(mean)	2.406(5)	Na···Au(1)	3.451(2)
Na···Au(2)	3.391(3)	Na···Au(3)	3.272(3)
Na··Au(4)	3.369(3)	Na···Au(5)	3.467(3)
Na···Au(6)	3.306(2)		
		Bond Angles (deg)	
Se(1)-Au(1)-Se(2)	177.8(2)	Se(2)-Au(2)-Se(3)	177.8(2)
Se(3)-Au(3)-Se(4)	178.0(2)	Se(1)-Au(4)-Se(4)	179.6(2)
Se(1)-Au(5)-Se(3)	178.2(3)	Se(2)-Au(6)-Se(4)	179.1(2)
Au(1)-Se(1)-Au(4)	85.8(2)	Au(1)-Se(1)-Au(5)	90.5(2)
Au(4)-Se(1)-Au(5)	85.9(2)	Au(1)-Se(2)-Au(2)	91.1(3)
Au(1)-Se(2)-Au(6)	88.2(2)	Au(2)-Se(2)-Au(6)	86.7(2)
Au(2)-Se(3)-Au(3)	86.0(2)	Au(2)-Se(3)-Au(5)	92.1(2)
Au(3)-Se(3)-Au(5)	88.0(2)	Au(3)-Se(4)-Au(4)	92.4(2)
Au(3)-Se(4)-Au(6)	89.5(2)	Au(4)-Se(4)-Au(6)	93.2(2)

b. The estimated standard deviations in the mean bond lengths and the mean bond angles are calculated by the equation $\sigma_l=\{\Sigma_n(l_n-l)^2/n(n-1)\}^{1/2}$, where l_n is the length (angle) of the *n*th bond, l the mean length (angle), and n the number of bonds.

Table 2·19. Selected Geometric Data for $(Ph_4P)_2[Au_2(Te_2)_2]$ (2·6) and Comparison with $(PPN)_2[Au_2(Te_2)_2]$[3]

	Ph_4P^+ salt	PPN^+ salt
Au···Au	2.905(2)	2.908
Au-Te(1)	2.573(2)	2.543
Au-Te(2)	2.572(2)	2.552
Te(1)-Te(1)	2.816(2)	2.781
Te(1)-Au-Te(2)	177.72(6)	176.64
Au-Te(1)-Te(2)	91.69(6)	88.79
Au-Te(2)-Te(1)	90.30(6)	94.05

b. The estimated standard deviations in the mean bond lengths and the mean bond angles are calculated by the equation $\sigma_l=\{\Sigma_n(l_n-l)^2/n(n-1)\}^{1/2}$, where l_n is the length (angle) of the *n*th bond, l the mean length (angle), and n the number of bonds.

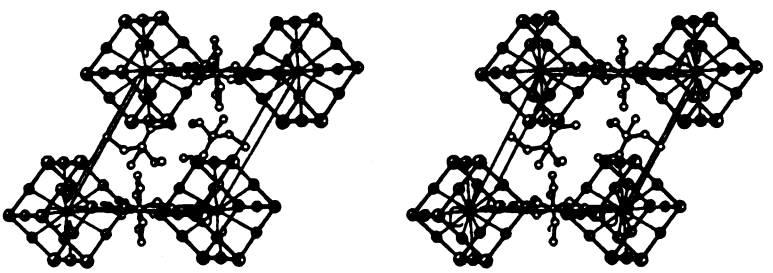


Figure 2·8. The Packing Diagram in the Unit Cell of $(Et_4N)_3[NaAu_{12}Se_8]$ (Stereoview). One Et_4N^+ Is Located on an Inversion Center (1, 1/2, 1/2), Showing Disorder

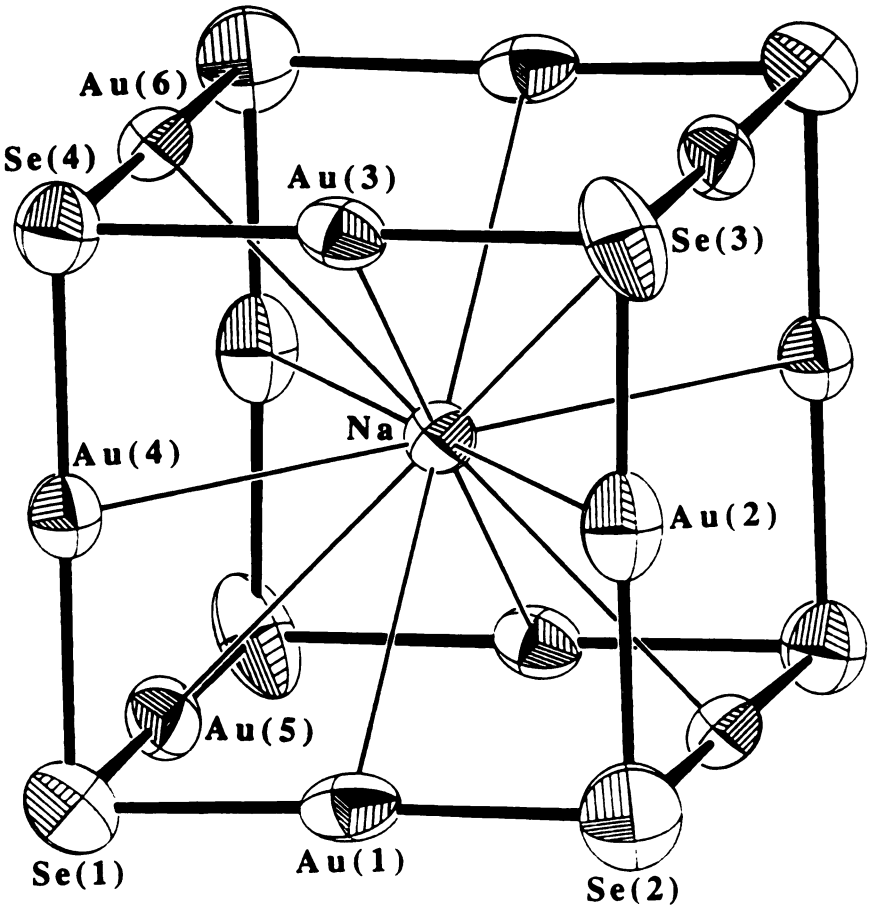


Figure 2-9. The Structure of the $[NaAu_{12}Se_8]^{3-}$ Anion

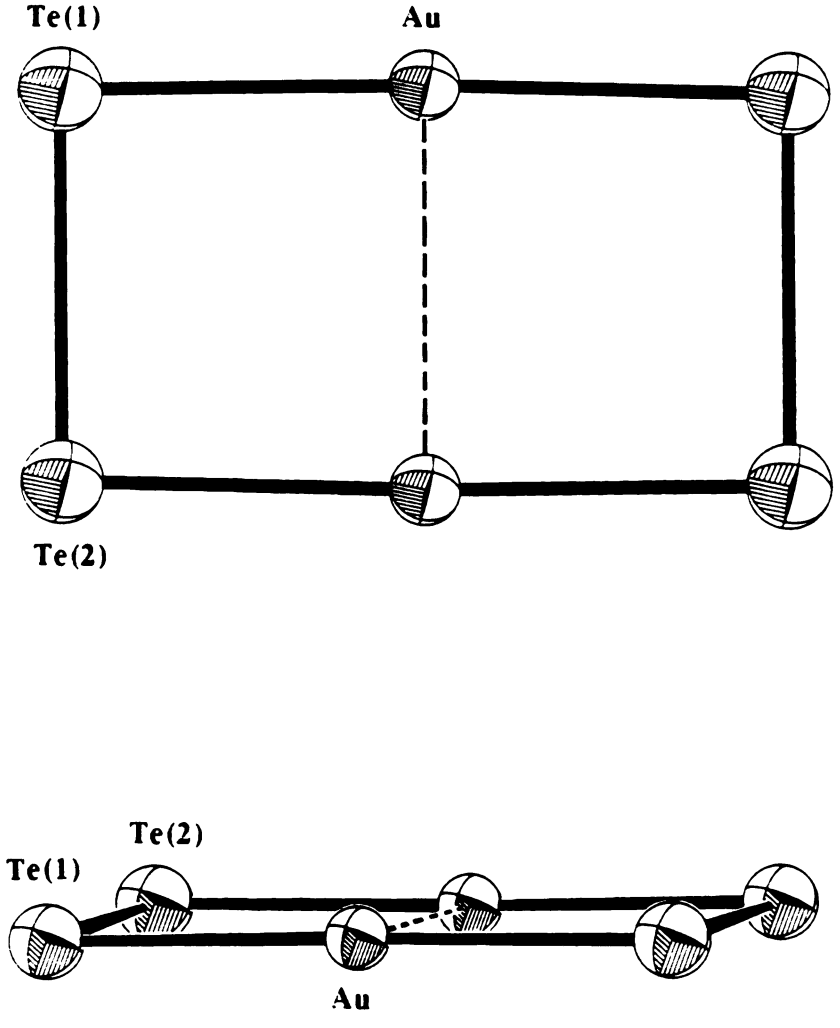


Figure 2·10. Two Views of the $[Au_2(Te_2)_2]^{2-}$ Anion

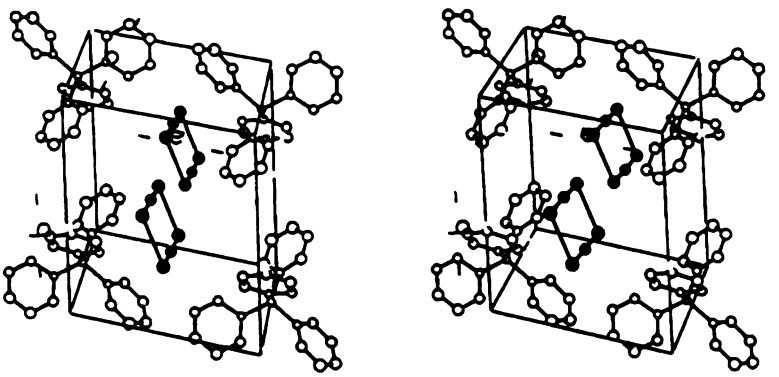


Figure 2·11. The Packing Diagram in the Unit Cell of $(Ph_4P)_2[Au_2(Te_2)_2]$ (Stereoview)

2. Spectroscopic Studies

The solid-state far IR spectra of all selenide compounds show a strong absorption at ~236 cm^{-1} as shown in Figure 2·12. This band is the only far IR absorption for $(Et_4N)_3[NaAu_{12}Se_8]$ (i.e. at 239 cm^{-1}). Based on this observation, the peak is assigned to the Au-Se stretching vibration. In addition, a broad peak centered around 202 cm^{-1} appears in all these spectra. Although this might be a good candidate for another Au-Se stretching vibration, the peak is not assigned at this stage due to lacking of any confirmatory evidence from other known gold selenide compounds. Compounds (2·1)–(2·4) also show absorptions in the region of 276 or/and 250 cm^{-1}, i.e. $(PPN)_2[Au_2Se_2(Se_4)_2]$ has two peaks at 276(w) and 256(m, broad). $(Ph_4P)_2[Au_2(Se_2)(Se_3)]$ and $(PPN)_2[Au_2(Se_2)(Se_3)]$ have a similar IR pattern in this region, being characterized by a peak at 265 cm^{-1} although this peak has two shoulders for $(PPN)_2[Au_2(Se_2)(Se_3)]$. The spectrum of $(Ph_4P)_2[Au_2(Se_2)(Se_4)]$ in the same region shows three peaks at 278(w), 266(m) and 257(m, broad) cm^{-1}. All these absorptions can be attributed to Se-Se stretching vibrations. The similar assignment has also been made in the far IR spectra of other metal polyselenide compounds or unbound ligands, $[Fe_2Se_{12}]^{2-}$ ($\nu_{se\text{-}se}$=258 cm^{-1})[19], $[SnSe_{12}]^{2-}$ ($\nu_{se\text{-}se}$=273 and 256 cm^{-1})[20], $[Ag_xSe_y]^{n-}$ ($\nu_{se\text{-}se}$=265 cm^{-1})[21], $[Se_x]^{2-}$ (x=2-6, $\nu_{se\text{-}se}$=285 cm^{-1})[22] and *cyclo*-Se_6 ($\nu_{se\text{-}se}$=253 cm^{-1})[23]. $(Ph_4P)_2[Au_2(Te_2)_2]$ shows a weak absorption at 188 cm^{-1}. This peak is tentatively assigned to the Te-Te stretching vibration. The similar assignment has been known in the literature, i.e. $\nu_{Te\text{-}Te}$=200 cm^{-1} for $(Ph_4P)_2[Pd(Te_4)_2]\cdot DMF$[24] and $\nu_{Te\text{-}Te}$=188 cm^{-1} for $(Ph_4P)_2[Te_4]$[25].

All polyselenide compounds in DMF give UV/vis absorptions in the 200–800 nm region as shown in Figures 2·13–2·14. The DMF solution of $(Et_4N)_3[NaAu_{12}Se_8]$ shows a featureless UV/vis spectrum. $(Ph_4P)_2[Au_2(Te_2)_2]$ is insoluble in common organic solvents, but decomposes in DMF, giving a UV/vis spectrum similar to that of polytelluride

as shown in Figure 2·15. Table 2·20 summarizes the solution UV/vis data for these compounds.

Table 2·20 Electronic Spectral Data for $(PPN)_2[Au_2Se_2(Se_4)_2]$ (2·1), $(Ph_4P)_2[Au_2(Se_2)(Se_3)]$ (2·2), $(PPN)_2[Au_2(Se_2)(Se_3)]$ (2·3), $(Ph_4P)_2[Au_2(Se_2)(Se_4)]$ (2·4), $(Et_4N)_3[NaAu_{12}Se_8]$ (2·5) and $(Ph_4P)_2[Au_2(Te_2)_2]$ (2·6) in DMF

compound	λ_{max}, nm (ε, $M^{-1}\cdot cm^{-1}$)
$(PPN)_2[Au_2Se_2(Se_4)_2]$	314(28600), 398(9690)
$(Ph_4P)_2[Au_2(Se_2)(Se_3)]$	497(broad, 3160)
$(PPN)_2[Au_2(Se_2)(Se_3)]$	501(broad, 2940)
$(Ph_4P)_2[Au_2(Se_2)(Se_4)]$	292(sh, 11500), 387(broad, 3930)
$(Et_4N)_3[NaAu_{12}Se_8]$	featureless
$(Ph_4P)_2[Au_2(Te_2)_2]$	530 (decomposing)

In DMF both $(Ph_4P)_2[Au_2(Se_2)(Se_3)]$ and $(PPN)_2[Au_2(Se_2)(Se_3)]$ give two ^{77}Se NMR resonances at 366 and 504 ppm as shown in Figure 2·16. In addition, a very weak peak at 410 ppm is observed for $(PPN)_2[Au_2(Se_2)(Se_3)]$, but not for $(Ph_4P)_2[Au_2(Se_2)(Se_3)]$. The peaks at 366 and 504 ppm also appear in the ^{77}Se NMR spectrum of $(Ph_4P)_2[Au_2(Se_2)(Se_4)]$ in DMF at 365 and 503 ppm, along with several other peaks, i.e. -3, 146, 157, 408, 421, 635 and 702 ppm. Due to the lack of coupling information and chemical shift parameters for other known Au/Se complexes, the spectra can not be easily interpreted. Three possible scenarios are (a) $(Ph_4P)_2[Au_2(Se_2)(Se_3)]$/$(PPN)_2[Au_2(Se_2)(Se_3)]$ remain intact in solution, but $(Ph_4P)_2[Au_2(Se_2)(Se_4)]$ dissociates to give $(Ph_4P)_2[Au_2(Se_2)(Se_3)]$ and other unknown species. Based on the ratio of peak intensities, a reasonable spectral assignment from this scenario would be that the peak at 504 ppm comes from four gold-bound Se atoms and the peak at 366 ppm from the internal Se atom; (b) All compounds dissociate in solution, giving at least one common species, which is responsible for the peaks at 504 and 366

ppm; (c) $[Au_2(Se_2)(Se_3)]^{2-}$ and $[Au_2(Se_2)(Se_4)]^{2-}$ dissociate via different pathways, but the chemical shifts of some species involved in both equilibria happen to coincide with one another. On any account, it is fair to conjecture that species generated in DMF solution of these compounds may not be necessarily the same as those in the solid-state. Finally, the weak resonance at 400 ppm for $(PPN)_2[Au_2(Se_2)(Se_3)]$, which happens to be the strongest resonance in the ^{77}Se NMR spectrum of $(Ph_4P)_2[Au_2(Se_2)(Se_4)]$, may be an indication that the sample contains a tiny amount of $(Ph_4P)_2[Au_2(Se_2)(Se_4)]$ which is not detected by XRD studies (i.e. < 5%).

$(PPN)_2[Au_2Se_2(Se_4)_2]$ is sparingly soluble in DMF. Addition of Bu_4NBr to the solution increases the solubility of this compound, but even the saturated solution is not concentrated enough to allow for ^{77}Se NMR study. The ^{77}Se NMR spectrum of $(Et_4N)_3[NaAu_{12}Se_8]$ in DMF shows a single resonance at 758 ppm (relative to Ph_2Se_2 in DMF at δ=460 ppm) as shown in Figure 2·17. The same solution gives a single ^{23}Na NMR signal at -12.0 ppm (relative to $NaBPh_4$ in DMF at δ=0 ppm) (see Figure 2·17). The upfield shift of the resonance indicates that the Na^+ ion is somewhat "naked" compared to the "free" sodium ion of the $NaBPh_4$ solution. The latter is actually highly shielded by solvent molecules. The NMR data suggest that in solution, $(Et_4N)_3[NaAu_{12}Se_8]$ retains its structural integrity and are consistent with a molecule possessing O_h symmetry.

3. Thermal Decomposition Properties

Figures 2·18 and 2·19 show the TGA diagrams of the six compounds in the temperature range of 25 to 800 °C. $(PPN)_2[Au_2Se_2(Se_4)_2]$, $(Ph_4P)_2[Au_2(Se_2)(Se_3)]$, $(PPN)_2[Au_2(Se_2)(Se_3)]$, and $(Ph_4P)_2[Au_2(Se_2)(Se_4)]$ undergo clean thermal decompositions below 530 °C, giving various intermediates as listed in Table 2·21. However, at temperatures higher than 720 °C, all intermediates start losing weight again– presumably giving up selenium. The final product in all the compounds at 830 °C was

any well-defined intermediates according to their TGA diagrams. In both cases, the weight loss continues after 800 °C.

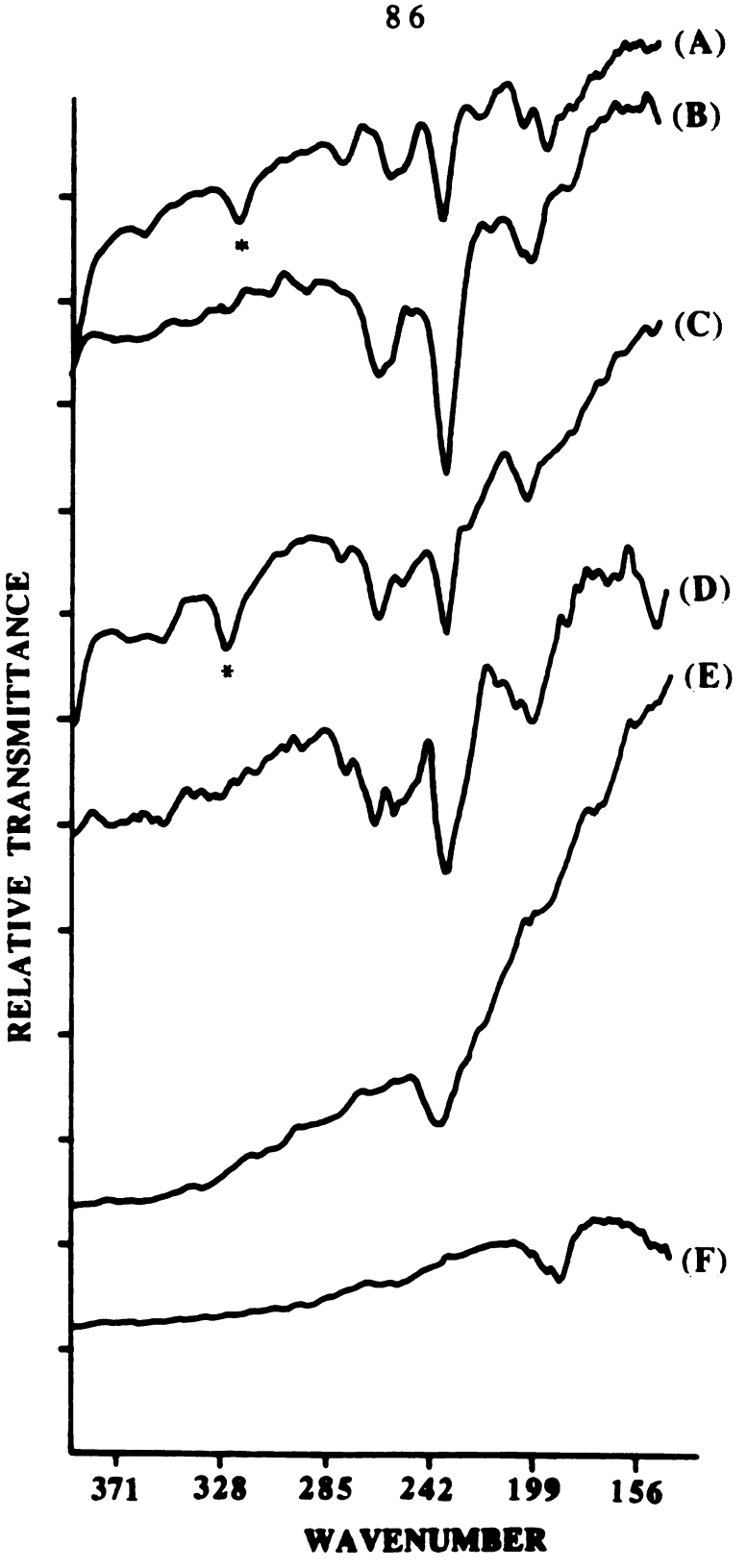


Figure 2·12. The solid-state far IR spectra of (A) $(PPN)_2[Au_2Se_2(Se_4)_2]$, (B) $(Ph_4P)_2[Au_2(Se_2)(Se_3)]$, (C) $(PPN)_2[Au_2(Se_2)(Se_3)]$, (D) $(Ph_4P)_2[Au_2(Se_2)(Se_4)]$, (E) $(Et_4N)_3[NaAu_{12}Se_8]$ and (F) $(Ph_4P)_2[Au_2(Te_2)_2]$. * absorption from the PPN^+ cation

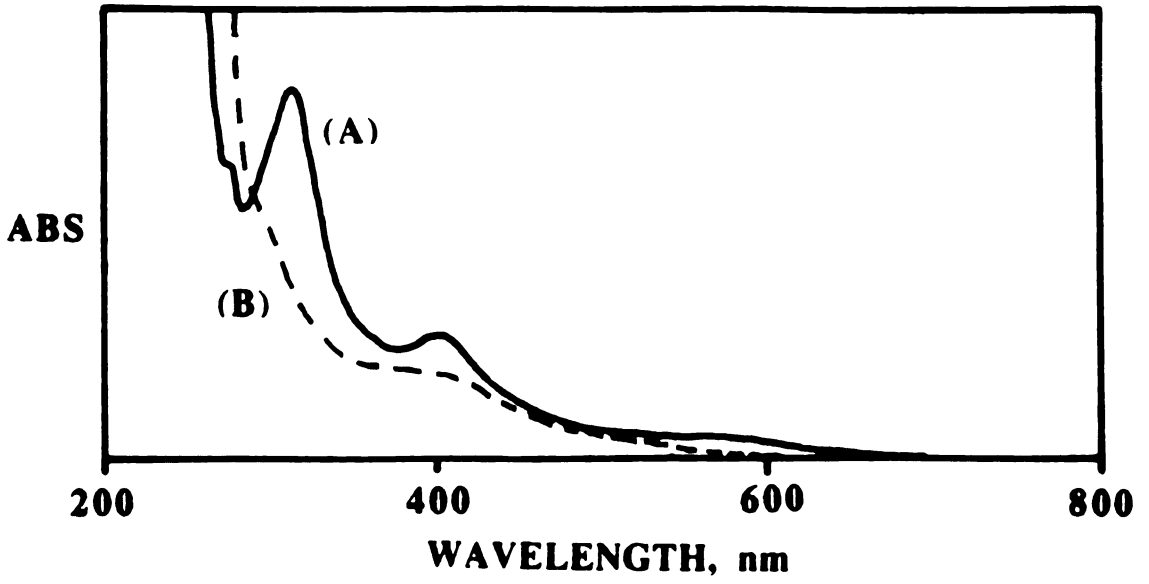


Figure 2·13. The UV/vis Spectra of (A) $(PPN)_2[Au_2Se_2(Se_4)_2]$ and (B) $(Ph_4P)_2[Au_2(Se_2)(Se_4)]$ in DMF

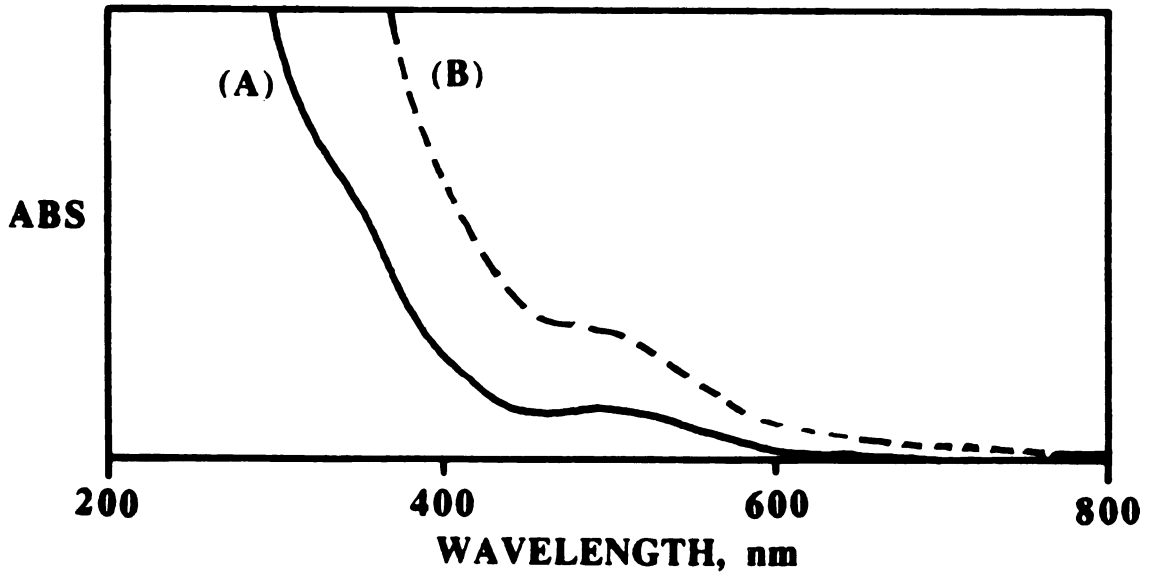


Figure 2·14. The UV/vis Spectra of (A) $(Ph_4P)_2[Au_2(Se_2)(Se_3)]$ and (B) $(PPN)_2[Au_2(Se_2)(Se_3)]$ in DMF

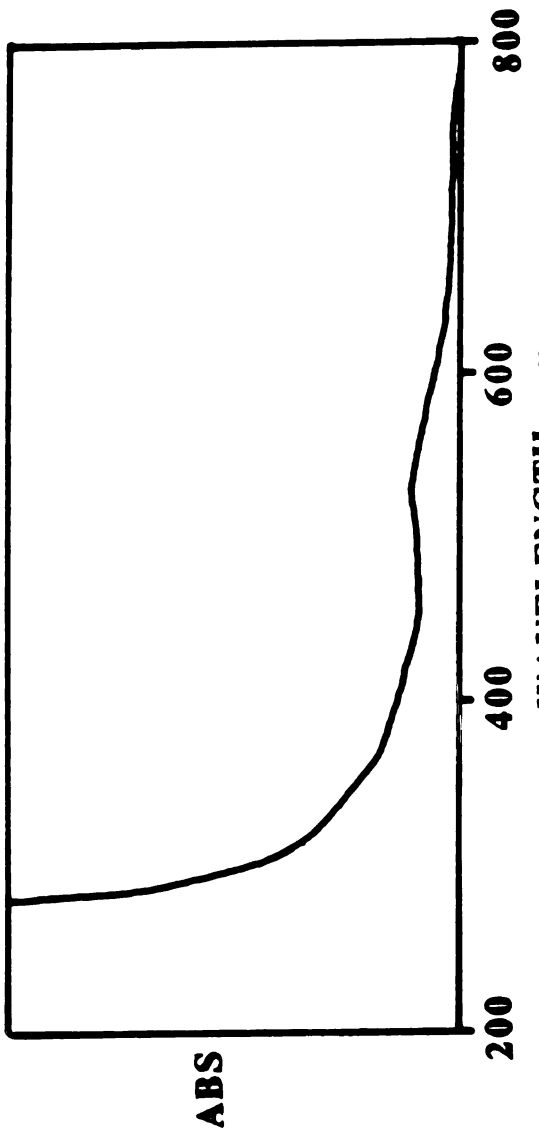


Figure 2·15. The UV/vis Spectrum of $(Ph_4P)_2[Au_2(Te_2)_2]$ in DMF

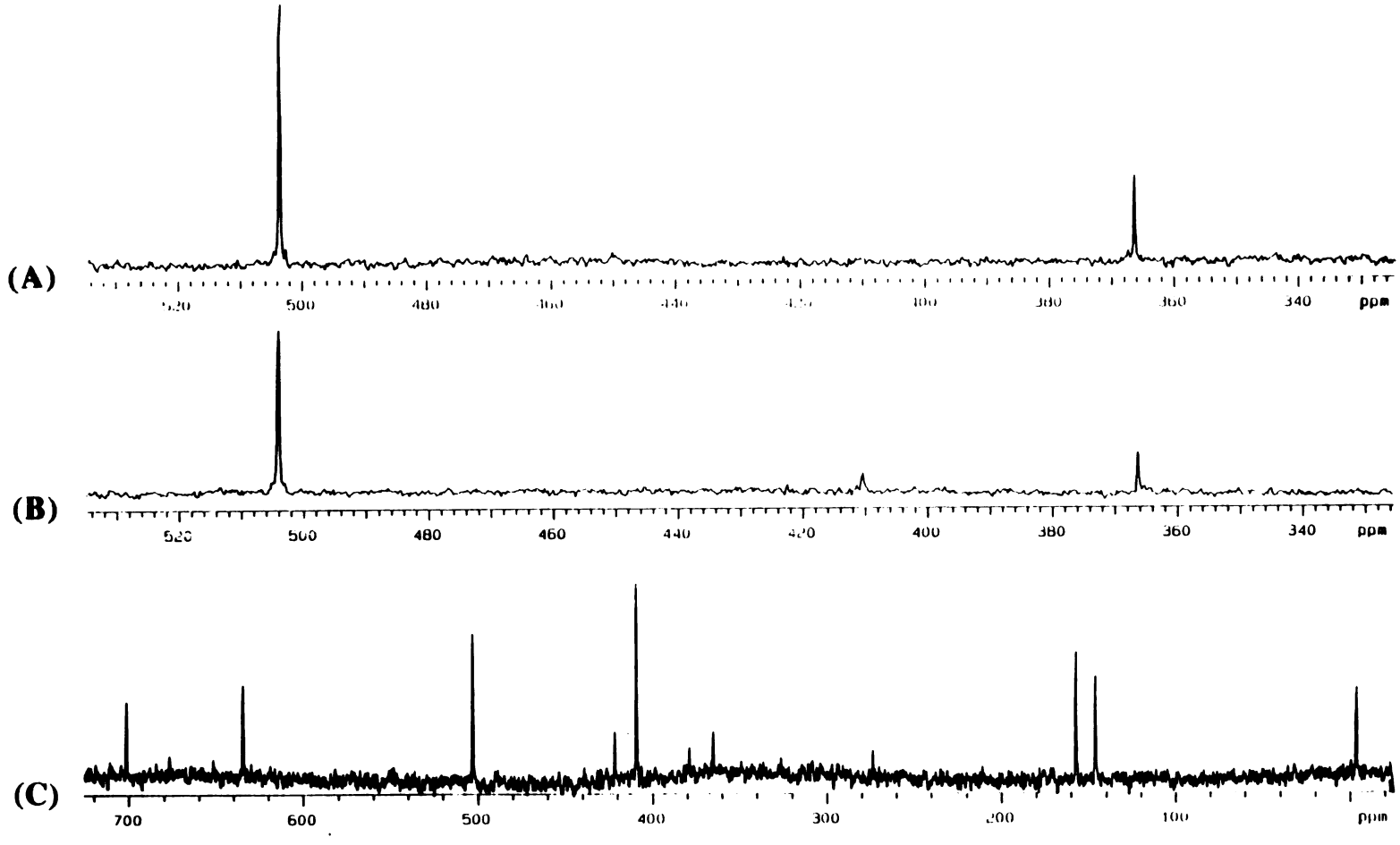


Figure 2·16. The ^{77}Se NMR Spectra of (A) $(Ph_4P)_2[Au_2(Se_2)(Se_3)]$, (B) $(PPN)_2[Au_2(Se_2)(Se_3)]$ and (C) $(Ph_4P)_2[Au_2(Se_2)(Se_4)]$ in DMF. Note That the ppm Scale Are the Same in (A) and (B), But different in (C).

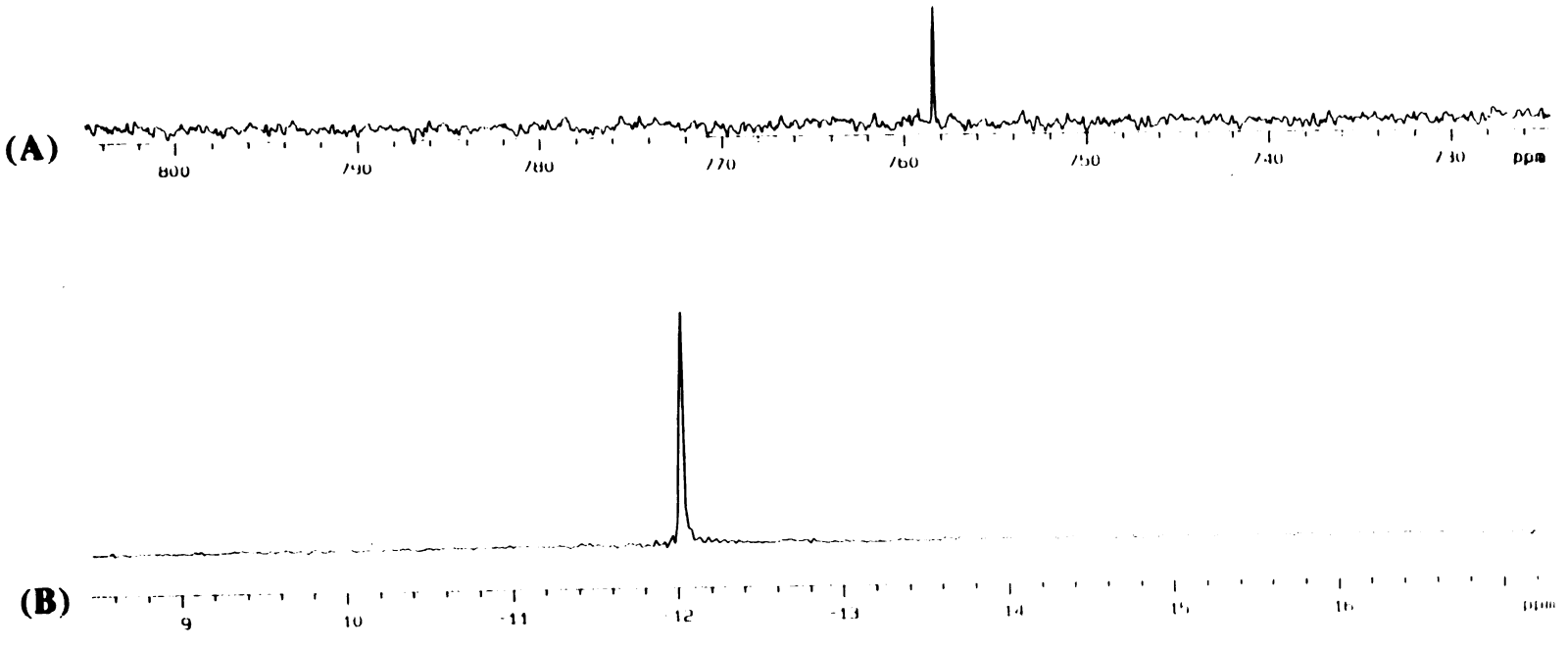


Figure 2-17. The ^{77}Se NMR Spectrum (A) and ^{23}Na NMR Spectrum (B) of $(Et_4N)_3[NaAu_{12}Se_8]$ in DMF

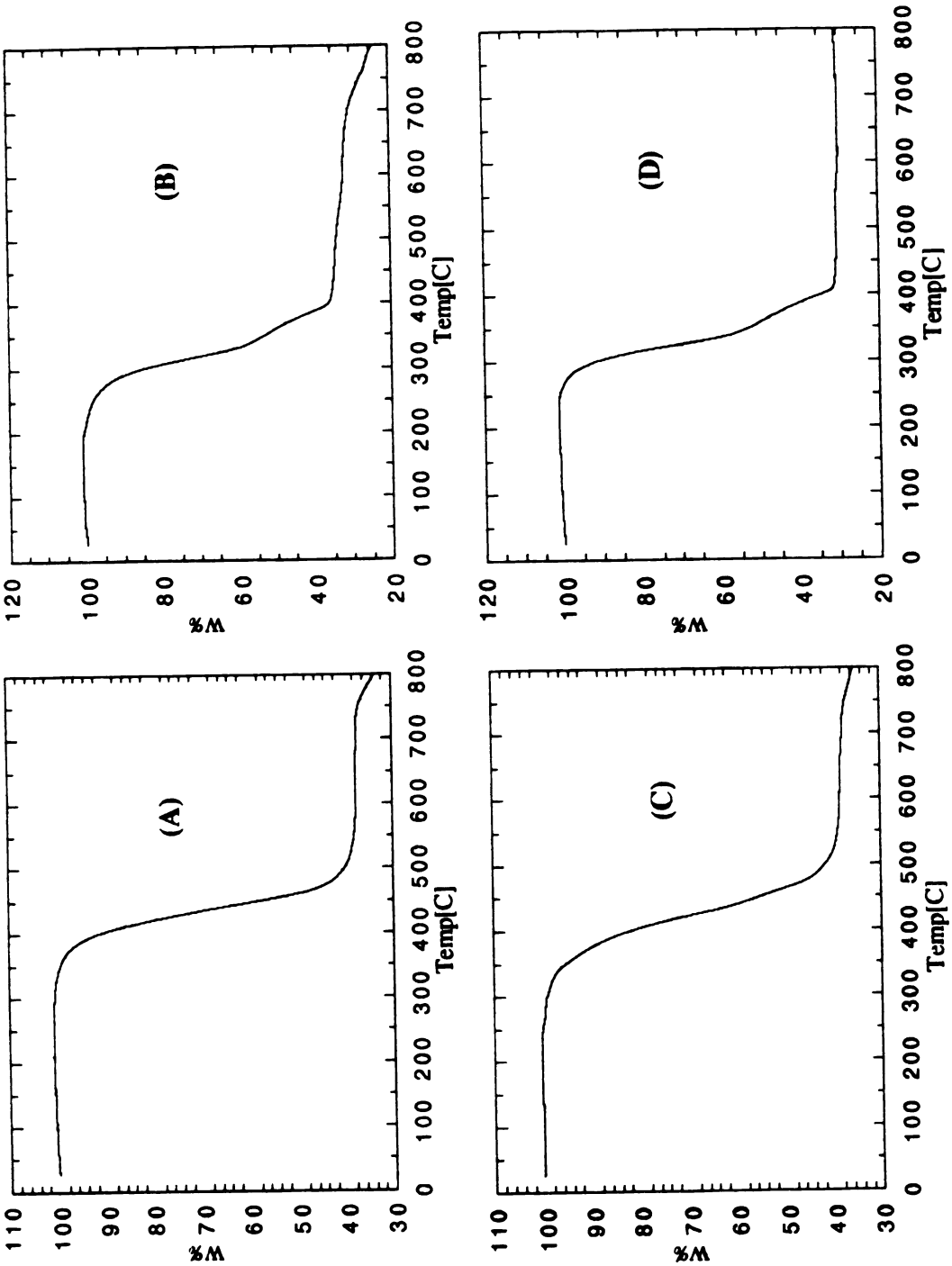
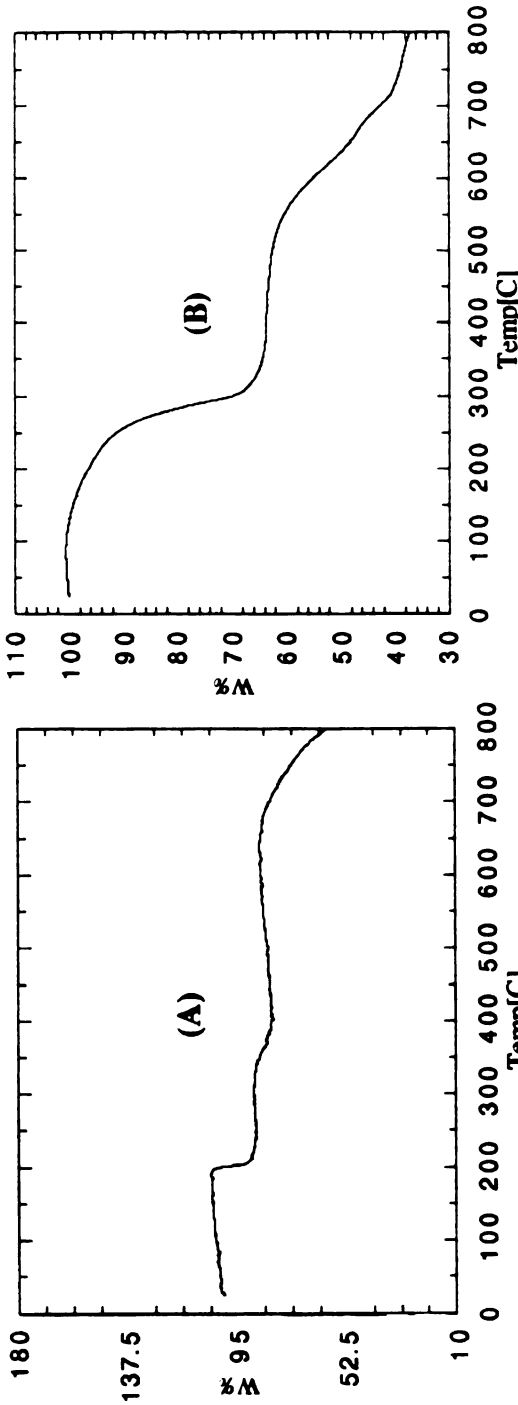


Figure 2·18. The TGA Diagrams of (A) $(PPN)_2[Au_2Se_2(Se_4)_2]$, (B) $(Ph_4P)_2[Au_2(Se_2)(Se_3)]$, (C) $(PPN)_2[Au_2(Se_2)(Se_3)]$ and (D) $(Ph_4P)_2[Au_2(Se_2)(Se_4)]$



Figures 2·19. The TGA Diagrams of (A) $(Et_4N)_3[NaAu_{12}Se_8]$ and (B) $(Ph_4P)_2[Au_2(Te_2)_2]$

Table 2·21. Thermal Gravimetric Analysis Data for $(PPN)_2[Au_2Se_2(Se_4)_2]$ (2·1), $(Ph_4P)_2[Au_2(Se_2)(Se_3)]$ (2·2) $(PPN)_2[Au_2(Se_2)(Se_3)]$ (2·3), $(Ph_4P)_2[Au_2(Se_2)(Se_4)]$ (2·4), $(Et_4N)_3[NaAu_{12}Se_8]$ (2·5) and $(Ph_4P)_2[Au_2(Te_2)_2]$ (2·6)

compd	onset temp °C	final temp °C	obsd % wt loss	calcd % wt loss	proposed residue formula
(2·1)	367	525	62.65	61.59	Au_2Se_6
(2·2)	235	408	66.15	67.78	Au_2Se_2
(2·3)	329	529	61.55	61.94	Au_2Se_4
(2·4)	260	417	69.69	69.41	Au_2Se
(2·5)	193	210	15.83	/	/
	341	379	5.64	/	/
	662	800	/		$AuTe_2$
(2·6)	159	362	36.62	/	/
	533	?			

IV. Discussion

The synthesis of four gold polyselenide complexes and a gold monoselenide cluster was readily accomplished through reactions between AuCN and suitable sodium polyselenides Na_2Se_x (x=2-5), or sodium monoselenide Na_2Se in the presence of the organic counterion such as Ph_4P^+, PPN^+ or Et_4N^+. Similar reactions of $AuCN/AuCl_3$ with K_2Te_2/K_2Te gave the Au^+ polytelluride $[Au_2(Te_2)_2]^{2-}$ complex:

$$Au^+ + 3Se_2^{2-}(\text{or } Se_3^{2-}) \xrightarrow[Ph_4P^+]{DMF} (Ph_4P)_2[Au_2(Se_2)(Se_3)] \quad \text{eq.(2·1)}$$

$$Au^+ + 2Se_4^{2-} \xrightarrow[Ph_4P^+]{DMF} (Ph_4P)_2[Au_2(Se_2)(Se_4)] \quad \text{eq.(2·2)}$$

$$Au^{+} + 2Se_5^{2-} \xrightarrow[PPN^{+}]{DMF} 1/2(PPN)_2[Au_2(Se)_2(Se_4)_2] \quad \text{eq.(2·3)}$$

$$Au^{+} + Na_2Se \xrightarrow[Et_4N^{+}]{MeOH/DMF} (Et_4N)_3[NaAu_{12}Se_8] \quad \text{eq.(2·4)}$$

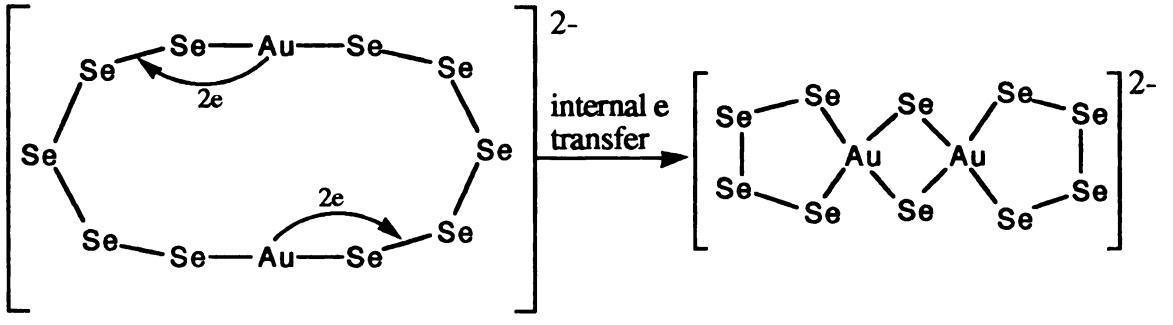
$$Au^{3+} + 2Te^{2-} \xrightarrow[Ph_4P^{+}]{DMF} 1/2(Ph_4P)_2[Au_2(Te_2)_2] \quad \text{eq.(2·5)}$$

$$Au^{+} + 2Te_2^{2-} \xrightarrow[Ph_4P^{+}]{DMF} 1/2(Ph_4P)_2[Au_2(Te_2)_2] \quad \text{eq.(2·6)}$$

Often the reactions between metal ions and polychalcogenide ligands cannot be balanced. This is the case for the majority of the equations presented here. Inability to do so reflects the complexity of the reactions. It is found that in polar solvents, such as NH_3 or DMF, the polyatomic anions of chalcogens (S, Se and Te) exist as various species involved in complex equilibria[26-29]. Many metal ions can take advantage of such equilibria, and "choose" the preferable ligand size from the equilibrium mixture of various Se_x^{2-} species to form a stable complex[30-31]. In other words, the type of Se_x^{2-} ligand present in the metal complex need not necessarily be the same as that used as the starting material. However, the isolation of several different gold complexes in this work, by just using different polyselenide ligands, seems to be an exception to the above widely accepted view. This is because, (a) there exists a vacillating redox reaction between Au^{n+} (n=1 or 3) and the Se_x^{2-} ligands, which influences the reaction outcome by changing the oxidation state of the metal ion. The longer the Se_x^{2-} chain is , the easier it is for the ligand to be reduced through the cleavage of Se-Se bonds. The redox chemistry slows down or shuts off in going from Se_5^{2-} to Se_4^{2-}. While use of Se_5^{2-} results in a Au^{3+} compound, the use of Se_4^{2-} affords a Au^{+} compound ,$[Au_2(Se_2)(Se_4)]^{2-}$, in the presence of Ph_4P^{+} cation, but a Au^{3+} compound, $[Au_2Se_2(Se_4)_2]^{2-}$, in the presence of PPN^{+} cation. Interestingly, the above redox reaction between Au^{n+} and Se_5^{2-} can be reversed, i.e. Se_5^{2-} can be oxidized by Au^{3+}, resulting in the isolation of an oxidation product of Se_5^{2-}[5] with the fate of Au^{+}

unknown; (b) given their structural similarity, $[Au_2(Se_2)(Se_3)]^{2-}$ and $[Au_2(Se_2)(Se_4)]^{2}$ should have comparable formation constants in solution. In this case, the equilibrium concentration of certain polyselenide ligand present in solution might have overridden the gold ion's ability of choosing suitable ligands. Therefore, the ultimate compositions of two Au^+ compounds $[Au_2(Se_2)(Se_3)]^{2-}$ and $[Au_2(Se_2)(Se_4)]^{2}$ can be determined by the polyselenide ligands used in the synthesis.

Assuming that the initial step in the reaction of AuCN with Se_5^{2-} is a simple coordination to form Au^+, the formation of $[Au_2Se_2(Se_4)_2]^{2-}$ can be speculated through an internal two-electron transfer from the Au^+ to the terminal Se-Se bond of the Se_5^{2-} ligand. This will result in the splitting of the Se-Se bond, creating Se^{2-} and Se_4^{2-} ligands as shown in the following scheme:



Scheme 2·1. Transformation From $[Au_2(Se_5)_2]^{2-}$ to $[Au_2Se_2(Se_4)_2]^{2-}$ via an Internal Electron Transfer Process

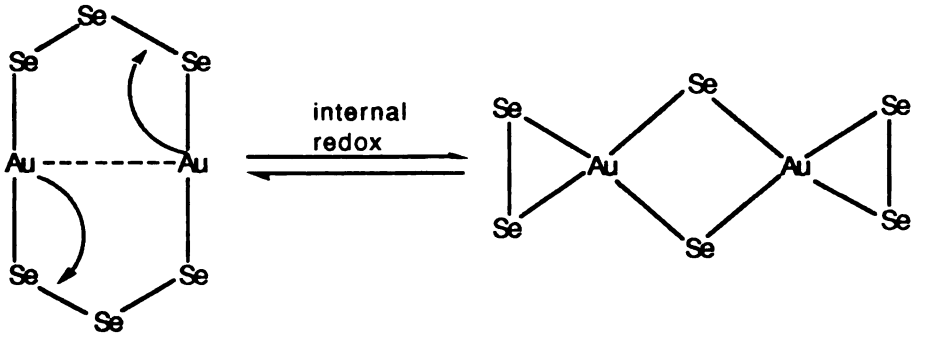
A similar process is also believed to be responsible for the generation of Tl^{3+} from Tl^+ with the concomitant formation of a trimeric complex $[Tl_3Se_3(Se_4)_3]^{3-}$ in the reaction of TlCl with Na_2Se_5[33-34]

Although the Au^+ intermediate $[Au_2(Se_5)_2]^{2-}$ has not been isolated or detected, the envisioning of such a complex, with same Se_x^{2-} ligand on either side of the Au–Au unit, is justified by the existence of $[Au_2(S_4)_2]^{2-}$ a close structural sulfur analogue, [32].

Other systems in which the metal ions undergo redox reactions with the polyselenide ligands include Fe^{n+}/Se_x^{2-} (n=2, or 3)[35], and Ni^{n+}/Se_x^{2-} (n=2 or 4)[36]. In both Fe^{n+}/Se_x^{2-} and Ni^{n+}/Se_x^{2-} systems, compounds containing Fe^{2+} or Fe^{3+}, and Ni^{2+} or Ni^{4+} are known, i.e. $[Fe(Se_4)_2]^{2-}$ *vs.* $[Fe_2Se_2(Se_5)]^{2-}$, and $[Ni(Se_4)_2]^{2-}$ *vs.* $[Ni_4Se_4(Se_3)_5(Se_4)]^{4-}$. Generally speaking, polyselenide ligands are more tolerant than their sulfur counterparts towards stabilizing metal centers in different oxidation states [30b].

When shorter polyselenide Se_x^{2-} (x=2-4) ligands are used, in order to avoid the above redox reaction, three compounds containing Au^+ can be obtained. Interestingly, these compounds are all unsymmetric dimers. Instead of forming a molecule with Se_2^{2-} ligands on both sides, (2·2) and (2·3) adopt a Se_3^{2-} ligand on one side and a Se_2^{2-} on the other. The Se-Se bond in Se_2^{2-} cannot be stretched to such a distance as to accommodate two Au atoms 2.9-3.0 Å apart, to form a planar molecule of $[Au_2(Se_2)_2]^{2-}$. This would cause severe deviations in the linear coordination of Au^+ ion. Such a structure is found possible in the Au^+/Te_2^{2-} system, i.e. $[Au_2(Te_2)_2]^{2-}$, where the Te-Te distance is 2.781 Å, closer to the Au-Au distance of 2.908 Å. In anticipation that a symmetric molecule such as $[Au_2(Se_3)_2]^{2-}$ or $[Au_2(Se_4)_2]^{2-}$ might form with higher concentration of longer polyselenides in solution, we used Se_4^{2-} instead of the original Se_2^{2-} and Se_3^{2-}. Unexpectedly, the isolated molecule, (2·4) contains a Se_2^{2-} unit bridging the two gold atoms while a Se_4^{2-} ligand is adopted on the other side. The fact that the more symmetric compound $(Ph_4P)_2[Au_2(Se_x)_2]$ (x=3 or 4) does not form in this reaction when Se_3^{2-} or even Se_4^{2-} are used is intriguing, in view of the apparent stability of the sulfur analogue, $[Au_2(S_4)_2]^{2-}$[32]. The reason of the preferential formation of (2·2)–(2·4) might rest on the stability of the $Au_2(Se_2)$ unit. It might be reasonably speculated that if indeed $[Au_2(Se_x)_2]^{2-}$ (x=3 or 4) formed in solution, it could be susceptible to internal redox electron transfer between Au^+ and Se-Se bonds according to Scheme 2·3. This is similar to

the above two-electron-transfer process which might be responsible for the formation of $(PPN)_2[Au_2Se_2(Se_4)_2]$:



Scheme 2·3 Hypothetical Internal Electron Transfer Process in $[Au_2(Se_x)_2]^{2-}$ (x=3 or 4)

It should be noted that it is more difficult to reduce the Se-Se bonds in Se_2^{2-} than those in Se_3^{2-} or Se_4^{2-}. The species of $[Au_2Se_2(Se_x)_2]^{2-}$ (x=2 or 3) formed by the internal electron transfer may not be favored under such conditions due to the small size of the Se_x^{2-} ligand which cannot span the square-planar gold coordination site.

At this point it is relevant to discuss the chemistry of Au^{n+} (n=1, 3) and A_2Se_x (A=alkali metal, x=1-5) in the solid-state[38]. It is found that similar Au^+/Au^{3+} redox reactions can also take place in A_2Se_x fluxes in the temperature range of 250 to 350 °C. Through proper control of the reaction temperature, the composition of polyselenide fluxes, and the nature of the alkali cation, both Au^+ and Au^{3+} compounds, having polymeric structures, can be synthesized. For example, $KAuSe_5$ and $CsAuSe_3$ are made up of dimeric one-dimensional $[AuSe_5]_n^{n-}$ or $[AuSe_3]_n^{n-}$ anionic chains with linearly-coordinated Au^+ atoms bridged by helical open chains of Se_5^{2-} or Se_3^{2-} ligands, while two selenium-rich phases K_3AuSe_{13} and Na_3AuSe_8 contain square-planar Au^{3+} centers bridged by a Se_3^{2-} (in K_3AuSe_{13}) or Se_2^{2-} (in Na_3AuSe_8), and coordinated by two Se_5^{2-} (in K_3AuSe_{13}) or Se_3^{2-} (in Na_3AuSe_8) ligands in a trans fashion via one of their terminal Se atoms. Although these compounds were prepared from molten Se_x^{2-} in which different equilibria

might be involved, the underlying redox chemistry between Au^{n+} and Se_x^{2-} seems to be of the same origin.

The $[NaAu_{12}Se_8]^{3-}$ is a rare example of an inorganic cryptand. Although one might be amazed by the structural simplicity of $[NaAu_{12}Se_8]^{3-}$, the assembly and stabilization of this unique complex reveal a chemical logic. First of all, the strong preference of Au^+ to linear coordination and the trigonal pyramidal geometry of Se^{2-} account for the buildup of a cube with edges and corners occupied by atoms. In addition, the cavity size of the cube, which is pre-determined by both the Au^+ and the Se^{2-} radii, happens to be a perfect fit for an alkali metal ion, a Na^+ in this case. A common feature worthy of note in a cube is that the distances from the center to its corners are longer than the distances from the center to the mid-points of its edges. Consequently, the Na^+ ion must interact with the twelve Au atoms rather than the eight Se atoms. It has been found that Au^+ has a remarked affinity to positively charged alkali metal ions. Such interactions have been observed in other Au^+ chalcogenide complexes, i.e. $[KAu_9Te_7]^{4-}$[40] $[K_2Au_4Te_4(en)_4]^{2-}$[39] and $[K_2Au_4Te_4(DMF)_2]^{2-}$[40]. Thus, the formation of $[NaAu_{12}Se_8]^{3-}$ may not be coincidental, but results instead from the combination of cube-cavity size and the tendency of Au^+ to interact with alkali-metal ions. It should be noted that the S^{2-} ligand can also form cube-like molecules with either Au^+ or Cu^+[41-42]. The $[Cu_{12}S_8]^{4-}$ cube is highly distorted on the edges because the Cu^+ atoms deviate from the ideal linear coordination geometry because of attractive Cu···Cu d^{10}-d^{10} interactions[43]. However, no alkali-metal ion is encapsulated in either of the compounds.

A comparison of the volume of the $[Au_{12}S_8]^{4-}$ and $[Au_{12}Se_8]^{4-}$ clusters shows that the sulfide cluster is 12% smaller than its selenide analogue (i.e. 98 $Å^3$ vs.111 $Å^3$). This explains why the corresponding $[NaAu_{12}S_8]^{3-}$ cannot be made. It suggests, however, that $[LiAu_{12}S_8]^{3-}$ may be accessible. On the other hand, the volume of the $[Au_{12}Te_8]^{4-}$ (i.e.

136 Å) is 23% larger than that of the $[Au_{12}Se_8]^{4-}$, which suggests that K^+, Rb^+, or even Cs^+ might be good candidates for inclusion.

The encapsulation of Na^+ ion in the $[Au_{12}Se_8]^{4-}$ may not be due only to the right cavity size but also to a tendency of the cube to reduce its high negative charge. When the synthesis was carried out with K_2Se, no corresponding $[KAu_{12}Se_8]^{3-}$ species was found, presumably because of the inability of K^+ to fit in the $[Au_{12}Se_8]^{4-}$ cage. The empty $[Au_{12}Se_8]^{4-}$ cage could not be isolated thus far. It should be mentioned that complete encapsulation of sodium ions by metal chalcogenide complexes was also found in $[Na_2(Fe_6S_9(SMe)_2)_2]^{6-}$[44] where the Na^+ ions cause the aggregation of two Fe_6S_9 clusters, and in the recently reported $[Na_2Fe_{18}S_{30}]^{8-}$[45], where two Na^+ ions are entirely complexed by the toroidal $Fe_{18}S_{30}$ cluster.

Through the synthesis of six gold polychalcogenide complexes we have shown that the reaction of Q_x^{2-} (Q=Se, x=1-5; Q=Te, x=1-2) solutions extracted from the Zintl phases A_2Q_x (A=Na or K) with metal salts is not only a rational but a far more convenient route to metal polychalcogenide complexes than any previous methods. In addition, we have noted that the variation of the nominal compositions of the starting materials can profoundly affect the reaction outcomes because of the intriguing redox interplay between $Au^{+/3+}$ and Q_x^{2-}. Analogous redox chemistry with corresponding S_x^{2-} ligands remains to be seen[46].

REFERENCES

1. M. Draganjac and T. B. Rauchfuss, *Angew. Chem. Int. Ed. Engl* , 24(1985), 742-757.

2. (a) A. Müller, *Polyhedron* , 5(1986), 323-340. (b) A. Müller and E. Diemann, *Adv. Inorg. Chem.*, 31(1987), 89-122.

3. R. C. Haushalter, *Inorg. Chim. Acta,* 102(1985), L37-L38.

4. (a) C. Burschka, *Z. Naturforsch*, B35(1980), 1511-1513. (b) A. Müller and U. Schimanski, *Inorg. Chim. Acta* , 77(1983), L187-L188. (c) A. Müller, F.-W. Baumann, H. Bögge, M. Römer, E. Krickemeyer and K. Schmitz, *Angew. Chem. Int. Ed. Engl.*, 23(1984), 632-633. (d) A. Müller, N. H. Schlanderbeck, E. Krickemeyer, H. Bögge K. Schmitz, E. Bill and A. X. Trautwein, *Z. Anorg. Allg. Chem.*, 570(1989), 7-36. (e) G. Kiel, G. Gattow and T. Dingeldein, *Z. Anorg. Allg. Chem.*, 596(1991), 111-119.

5. See chapter 3.

6. D. D. Perrin, W. L. F. Armarego and D. R. Perrin, *Purification of Laboratory Chemicals,* 2nd Ed., Pergamon Press, Oxford UK, 1980.

7. S. Flegler, *Instructions for Energy Dispersive X-ray Microanalysis,* Michigan State University, 1991.

8. *Introduction to the 740 Fourier Transform Infrared Spectrometer,* Nicolet Analytical Instruments, 1988, Madison, Wisconsin.

9. *Instruction Manual for Model U-2000 Double-Beam Spectrophotometer,* Hitachi, Ltd., Tokyo, Japan.

10. *VXR-Series S NMR Spectrometer Systems,* Varian NMR Instrument Division, 1987.

11. *TGA-50 Thermogravimetric Analyzer Instruction Manual,* Shimadzu Corporation, Kyoto, Japan.

12. *P3/V Data Collection Manual,* Siemens Analytical X-ray Instruments, Inc., 1989.

13. *MSC/AFC Diffractometer Control Software,* Molecular Structure Corporation, The Woodlands, Texas.

14. N. Walker and D. Stuart, *Acta Crystallogr.*, 39A(1983), 158-166.

15. *TEXSAN: Single Crystal Structure Analysis Software*, Version 5.0, Molecular Structure Corporation, The Woodlands, Texas.

16. (a) G. M. Sheldrick in *Crystallographic Computing,* G. M. Sheldrick, C. Kruger, and R. Doddard, Oxford University Press, 1985, p.175-189. (b) B. A. Frenz, The Enraf-Nonius CAD4 SDP System. in *Computing in Crystallography*; Delft University Press, Delft Holland, 1978; p.64-71.

17. H. P. Klug and L. E. Alexander, *X-ray Diffraction Procedures for Polycrystalline and Amorphous Materials,* John Wiley and Sons, New York, 1974.

18. D. K. Smith, M. C. Nichols and M. E. Zolensky, *POWD10: A Fortran IV Program for Calculating X-ray Powder Diffration Patterns,* Version 10, Pennsylvania State University, 1983.

19. H. Strasdeit, B. Krebs and G. Henkel, *Inorg. Chim. Acta* , 89(1984), L11-L13.

20. S.-P. Huang, S. Dhingra and M. G. Kanatzidis, *Polyhedron* , 9(1990), 1389-1395.

21. S.-P. Huang and M. G. Kanatzidis, *Inorg. Chem.*, 30(1991), 1455-1466.

22. F. Weller, J. Adel and K. Dehnicke, *Z. Anorg. Allg. Chem.*, 548(1987), 125-132.

23. K. Nagata, K. Tshibashi and Y. Miyamoto, *Jpn. J. Appl. Phys.*, 19(1980), 1569-1573.

24. H. Wolkers, K. Dehnicke, D. Fenske, A. Khassanov and S. S. Hafner, *Acta Crystallogr.*, 47C(1991), 1627-1632.

25. J. Dietz, U. Müller, V. Müller and K. Dehnicke, *Z. Naturforsch.*, 46B(1991), 1293-1299.

26. (a) F. Seel, H. J. Guttler, G. Simon and A. Wieckowski, *Pure Appl. Chem.*, 49(1977), 45-54. (b) K. W. Sharp and W. H. Koehler, *Inorg. Chem.*, 16(1977), 2528-2565.

27. L. D. Schultz and W. H. Koehler, *Inorg. Chem.*, 26(1987), 1989-1993.

28. (a) P. Dubois, J. P. Lelieur and G. Lepoutre, *Inorg. Chem.*, 26(1987), 1897-1902. (b) P. Dubois, J. P. Lelieur and G. Lepoutre, *Inorg. Chem.*, 27(1987), 73-80. (c) P. Dubois, J. P. Lelieur and G. Lepoutre, *Inorg. Chem.*, 27(1988), 1883-1890. (d) V. Pinon and J. P. Lelieur, *Inorg. Chem.*, 30(1991), 2260-2264.

29. M. Bjorgvinsson and G. J. Schrobilgen, *Inorg. Chem.*, 30(1991), 2540-2547.

30. (a) M. G. Kanatzidis, *Comments Inorg. Chem.*, 10(1990), 161-195. (b) M. G. Kanatzidis and S.-P. Huang, *Coord. Chem. Rev.*, in press.

31. M. A. Ansari and J. A. Ibers, *Coord. Chem. Rev.*, 100(1990), 223-266.

32. A. Müller, M. Römer, H. Bögge, E. Krickemeyer and K. Schmitz, *Inorg. Chim. Acta,* 85(1984), L39-L41.

33. S. Dhingra and M. G. Kanatzidis, *Inorg. Chem.,* in press.

34. S. Dhingra, Ph.D. Thesis, Michigan State University, 1992.

35. K.-W. Kim and M. G. Kanatzidis, manuscript in preparation.

36. (a) J. M. McConnachie, M. A. Ansari and J. A. Ibers, *J. Am. Chem. Soc.*, 113(1991), 7078-7079. (b) J. M. McConnachie, M. A. Ansari and J. A. Ibers, *Inorg. Chim. Acta*, 198-200(1992), 85-93.

37. G. Marbach, J. Strähler, *Angew. Chem. Int. Ed. Engl.,* 23(1984), 246-247.

38. Y. Park, Ph.D. Thesis, Michigan State University, 1992.

39. R. C. Haushalter, *Angew. Chem. Int. Ed. Engl.,* 24(1985), 432-433.

40. M. G. Kanatzidis, S.-P. Huang, *Phosphorous and Sulfur* , 64(1992), 153-160.

41. G. Marbach, J. Strahle, *Angew. Chem. Int. Ed. Engl.,* 23(1984), 715-716.

42. P. Betz, B. Krebs, G. Henkel, *Angew. Chem. Int. Ed. Engl.,* 23(1984), 311-312.

43. (a) P. K. Mehrotra and R. Hoffmann, *Inorg. Chem.*, 17(1978), 2187-2189. (b) K. M. Merz and R. Hoffmann, *Inorg. Chem.*, 27(1988), 2120-2127.

44. J.-F. You, B. S. Snyder, G. C. Papaefthymiou and R. H. Holm, *J. Am. Chem. Soc,* 112(1990), 6589-6591.

45. J. F. You, B. S. Snyder and R. H. Holm, *J. Am. Chem. Soc.*, 110(1988), 6589-6591.

46. S.-P. Huang and M. G. Kanatzidis, work continues.

CHAPTER 3

CHEMISTRY OF HOMO- AND HETEROPOLYCHALCOGENIDE COMPOUNDS

I. Introduction

It is generally recognized that in solutions of polar solvents such as NH_3 or DMF polychalcogenides exist as various species involved in complex equilibria[1-2]. By using different solvents, temperatures and counterions, a variety of polychalcogenides, S_n^{2-} (n=2-7)[3-8], Se_n^{2-} (n=2-9)[9-16], and Te_n^{2-} (n=2-5)[17-20], have been isolated and structurally characterized. With the exception of the bicyclic decaselenide $[Se_{10}]^{2-}$[21] all the anions are found to be unbranched helical chains in the solid state. However, under certain conditions, an oxidized chalcogen atom (in the +2 or +4 oxidation state) itself can be chelated by polychalcogenide ligands to form a closed cyclic structure—analogous to certain metal polychalcogenide complexes. For instance, in DMF solution the reaction of $AuCl_3$ with Na_2Se_5 resulted in the isolation of α-$(Ph_4P)_2[Se(Se_5)_2]$, an oxidation product of the Se_5^{2-} by Au^{3+}[22]. The existence of this peculiar molecule had been mentioned before in a review article[23]. However, its accurate parameters as well as the synthetic method were not revealed until our serendipitous discovery of this molecule during our investigation of the Au^{3+}/Na_2Se_5 chemistry[24]. To rationalize the synthesis of $(Ph_4P)_2[Se(Se_5)_2]$, I_2 was used as an oxidant to react with Na_2Se_5. Interestingly, a different crystal modification of undecaselenide, β-$(Ph_4P)_2[Se(Se_5)_2]$, was afforded using this procedure. To further investigate whether selenium and tellurium would form a similar heteropolychalcogenide to the above, we reacted polyselenide ligands with different tellurium sources. As a result of this effort, the tellurodecaselenide $(Ph_4P)_2[Te(Se_5)_2]$ was

obtained from the reaction between pentaselenide and elemental tellurium. This compound is isostructural to β-$(Ph_4P)_2[Se(Se_5)_2]$. In this chapter we describe the synthesis, spectroscopic studies of three mixed valence polychalcogenides, α-$(Ph_4P)_2[Se(Se_5)_2]$ (**3·1**), β-$(Ph_4P)_2[Se(Se_5)_2]$ (**3·2**) and $(Ph_4P)_2[Te(S_5)_2]$ (**3·3**), and the X-ray structures of α- and β-$(Ph_4P)_2[Se(Se_5)_2]$.

II. Experimental Section

1. Reagents

Chemicals in this work other than solvents were used as obtained: (i) selenium powder, ~100 mesh, 99.5% purity, Aldrich Chemical Company, Inc., Milwaukee, WI; (ii) tellurium powder, ~200 mesh, 99.8% purity, Aldrich Chemical Company, Inc., Milwaukee, WI; (iii) sodium sticks in kerosene, 99% purity, Mallinckrodt Inc., Paris, Ky.; (iv) iodine, 99.8% purity, Aldrich Chemical Company, Inc., Milwaukee, WI; (v) gold(III) chloride, Strem Chemicals, Inc., Newburyport, MA; (vi) tetraphenylphosphonium chloride (Ph_4PCl), 98% purity, Aldrich Chemical Company, Inc., Milwaukee, WI.

Dimethylformamide (DMF, analytical reagent, Mallinckrodt Inc., Paris, Ky) was stored over 4A Linde molecular sieves for several days and then distilled under reduced pressure at ~30 °C[25].

Diethyl ether (A.C.S. anhydrous, Columbus Chemical Industries Inc., Columbus, WI) was distilled under a dry N_2 blanket after being refluxed with potassium metal, benzophenone and triethylene glycol dimethyl ether for 12 hours[25].

2. Physical Measurements

Semi-quantitative elemental analyses, FT-IR and UV/vis spectroscopic studies, and thermal gravimetric analyses (TGA) of the compounds were carried out as described previously[24].

3. Syntheses

All syntheses were carried out under a dry nitrogen atmosphere in a Vacuum Atmospheres Dri-Lab glovebox.

(i). Preparation of sodium pentaselenide in liquid ammonia

This material was prepared by reacting stoichiometric amount of selenium and sodium metal in a routine procedure used in this laboratory[24].

(ii). Preparation of α-$(Ph_4P)_2[Se(Se_5)_2]$ (3·1)

The dropwise addition of a 20 ml DMF solution of 0.091 g (0.30 mmol) of $AuCl_3$ to a stirred 30 cml DMF solution of 0.270 g (0.60 mmol) Na_2Se_5 and 0.220 g (0.60 mmol) Ph_4PCl resulted in an immediate color change from dark green to brown. The stirring continued for 1 h, after which the solution was filtered to remove NaCl and then diluted with ether. When the mixture was allowed to stand for 3 days, red-brown needles of α-$(Ph_4P)_2[Se(Se_5)_2]$ were isolated in 50% yield. Far IR spectrum (of solid-state): 265 (s) and 216 (s) cm^{-1}; Semi-quantitative elemental analyses by EDAX (atom%): Se:P=81:19; UV/vis spectrum (in DMF): 653 nm (ε=2841 $M^{-1}cm^{-1}$), 457 nm (ε=9432 $M^{-1}cm^{-1}$) and 400 nm (sh, ε=9154 $M^{-1}cm^{-1}$).

(iii). Preparation of β-$(Ph_4P)_2[Se(Se_5)_2]$ (3·2)

A ~10 ml DMF solution of 0.076 g (0.30 mmol) I_2 was added dropwise to a ~50 ml deep green DMF solution of 0.270 g (0.60 mmol) Na_2Se_5 and 0.220 g (0.60 mmol)

Ph_4PCl. The resulting brown solution was filtered, and the filtrate was diluted with ~40 ml diethyl ether. The reaction mixture gave red-brown crystals within 2 days in 72% yield (based on Se content). Crystals suitable for X-ray single crystal structure analysis were grown from diethyl ether/DMF solution (1:1) at room temperature. Far IR spectrum (of solid-state): 265 (s) and 216 (s) cm^{-1}; Semi-quantitative elemental analyses by EDAX (atom%): Se:P=76:24; UV/vis spectrum (in DMF): 653 nm (ε=2841 $M^{-1}\cdot cm^{-1}$), 457 nm (ε=9432 $M^{-1}\cdot cm^{-1}$) and 400 nm (sh, ε=9154 $M^{-1}cm^{-1}$).

(iii). Preparation of $(Ph_4P)_2[Te(Se_5)_2]$ (3·3)

0.025 g (0.20 mmol) of elemental Te was added directly into a ~40 ml deep green DMF solution of 0.180 g (0.40 mmol) Na_2Se_5 and 0.146 g (0.40 mmol) Ph_4PCl. After 30 min. stirring, the solution turned slightly brown and was filtered. The filtrate was diluted with ~40 ml diethyl ether. Large dark brown single crystals were afforded within 2 days (60 % yield based on Te). Far IR spectrum (of solid-state): 277 cm^{-1} (s) and 258 (w, b) cm^{-1}; Semi-quantitative elemental analyses by EDAX (atom%): Te:Se:P=78:73:19; UV/vis spectrum (in DMF): featureless. X-ray powder diffraction (XRD) pattern: same as that of β-$(Ph_4P)_2[Se(Se_5)_2]$.

4. X-ray Diffraction and Crystallographic Studies

The single crystal X-ray diffraction studies were performed by using a Nicolet P3 four-circle diffractometer[26].

The crystallographic data sets of (3·1) and (3·2) were collected using a θ-2θ scan mode and Mo Kα radiation. The stability of the experimental setup and crystal integrity for each data collection was monitored by measuring three representative reflections periodically (every 100). No crystal decay was detected. Empirical absorption corrections were applied to all the data sets based on ψ scans of several strong reflections with χ~90°.

The structures were solved with direct methods and refined with full-matrix least squares techniques. DIFABS corrections were applied to the structure-factors after all the atoms in the structures were located and refined isotropically[27]. The calculations were performed using the SHELXS-86 and SDP combined package of crystallographic programs[28]. Table 3·1 gives crystal data and details for structure analysis of the two compounds.

All non-hydrogen atoms in these structures were refined either isotropically or anisotropically. The hydrogen positions were calculated but not refined. The final coordinates and average temperature factors of the atoms in each compound are given in Tables 3·2 and 3·3, respectively.

Compound (**3·3**) was found to be isostructural to β-$(Ph_4P)_2[Se(Se_5)_2]$ by X-ray powder diffraction (XRD) studies (vide infra). The single crystal structure analysis was not carried out for this compound because the same anion had been reported as its [K-222-crypt]$^+$ and [Ba-222-crypt]$^{2+}$ salts[29].

Finally, each compound was examined by X-ray powder diffraction for the purpose of phase characterization and identification. A Debye-Scherrer camera was employed to record the X-ray powder diffraction patterns. Ni-filtered Cu radiation was used. The crystals were ground to fine powder and packed into 0.5 mm glass capillaries which were sealed and mounted to the standard Debye-Scherrer powder camera which has a diameter of 114.6 mm (1 mm corresponds to 1 degree for 2θ). X-rays were generated by a Phillips Norelco XRG-5000 X-ray generator operating at 40 kV and 20 mA. Approximately, a six hour exposure time was used. Accurate d-spacings (Å) of each compound were calculated from the powder patterns recorded on a Phillips XRG-3000 computer controlled powder diffractometer[30]. To verify the homogeneities of the products, the d-spacings observed for the bulk materials were compared with the calculated d-spacings from the X-ray single-

crystal structure analysis data[31]. Listings of calculated and observed d-spacings (Å) along with the observed relative diffraction intensities of these compounds are given in Tables 3·4 and 3·5.

Table 3·1. Data for Crystal Structure Analysis of α-$(Ph_4P)_2[Se(Se_5)_2]$ (**3·1**) and β-$(Ph_4P)_2[Se(Se_5)_2]$ (**3·2**)

compound	**3·1**	**3·2**
formula	$C_{48}H_{40}P_2Se_{11}$	$C_{48}H_{40}P_2Se_{11}$
a, Å	12.871(3)	9.967(4)
b, Å	14.822(3)	13.889(4)
c, Å	14.144(3)	18.668(4)
α, deg	90.0	90.0
β, deg	108.67(2)	102.60(3)
γ, deg	90.0	90.0
Z; V, $Å^3$	2, 2556(2)	2, 2522(2)
space group	P 2_1/n(#14)	P 2_1/n(#14)
D_{calc}, g/cm^3	2.01	2.04
μ, cm^{-1} (Mo Kα)	114.6	80.0
cryst size, mm	0.04x0.06x0.38	0.12, 0.22, 0.45
$2\theta_{max}$, deg	48	45
temperature (°C)	25	23
no. of data collcd	3728	3717
no. of data used ($F_o^2>3\sigma(F_o^2)$)	1882	1538
min, max abs cor	0.49, 0.99	0.80, 1.12
no. of variables	277	204
no. of atoms per asym unit (including H)	51	51
final R/R_w, %	6.1/6.5	5.2/5.8

Table 3·2. Positional Parameters and B_{eq} Values[a] for α-$(Ph_4P)_2[Se(Se_5)_2]$ (3·1) (Standard Deviations in Parentheses)

atom	x	y	z	B_{eq}, Å^2
Se	0.000	0.000	0.500(1)	4.67(7)
Se(1)	0.0900(2)	-0.0578(2)	0.6863(2)	6.23(6)
Se(2)	-0.0435(2)	-0.1277(2)	0.7348(2)	6.28(6)
Se(3)	-0.1589(2)	-0.0128(3)	0.7510(2)	9.03(8)
Se(4)	-0.2709(2)	0.0069(2)	0.5868(2)	7.60(7)
Se(5)	-0.1763(2)	0.0942(2)	0.5040(2)	6.78(7)
P	0.6761(3)	0.1219(3)	-0.0512(3)	2.58(9)
C1	0.771(1)	0.192(1)	-0.080(1)	3.7(4)
C2	0.772(2)	0.217(1)	-0.172(1)	4.8(5)
C3	0.854(2)	0.271(2)	-0.190(1)	6.7(5)
C4	0.935(1)	0.304(1)	-0.108(2)	5.5(5)
C5	0.936(1)	0.285(1)	-0.015(1)	5.1(5)
C6	0.858(1)	0.232(1)	-0.001(1)	3.6(4)
C7	0.732(1)	0.009(1)	-0.025(1)	3.0(4)
C8	0.660(1)	-0.064(1)	-0.046(1)	3.2(4)
C9	0.701(2)	-0.153(1)	-0.029(1)	4.5(5)
C10	0.809(2)	-0.166(1)	0.016(1)	4.1(5)
C11	0.881(1)	-0.088(1)	0.039(1)	4.9(5)
C12	0.841(1)	-0.005(1)	0.019(1)	4.1(4)
C13	0.645(1)	0.165(1)	0.052(1)	2.5(4)
C14	0.616(1)	0.255(1)	0.056(1)	2.9(4)
C15	0.586(1)	0.290(1)	0.134(1)	3.6(4)
C16	0.595(1)	0.233(1)	0.215(1)	3.3(4)
C17	0.627(1)	0.147(1)	0.215(1)	4.1(5)
C18	0.651(1)	0.109(1)	0.133(1)	3.5(4)
C19	0.554(1)	0.116(1)	-0.155(1)	3.3(4)

Table 3·2. (cont'd)

atom	x	y	z	B_{eq}, Å^2
C20	0.456(1)	0.156(1)	-0.152(2)	3.4(4)
C21	0.362(1)	0.151(1)	-0.232(1)	4.8(5)
C22	0.360(1)	0.098(1)	-0.316(1)	5.1(5)
C23	0.454(1)	0.059(1)	-0.319(1)	4.4(5)
C24	0.551(1)	0.065(1)	-0.241(1)	3.5(4)

a. B_{eq} is defined as $4/3[a^2\beta_{11}+b^2\beta_{22}+c^2\beta_{33}+ab(\cos\gamma)\beta_{12}+ac(\cos\beta)\beta_{13}+bc(\cos\alpha)\beta_{23}]$.

Table 3·3. Positional Parameters and B_{eq} Values[a] for β-$(Ph_4P)_2[Se(Se_5)_2]$ (3·2) (Standard Deviations in Parentheses)

atom	x	y	z	B_{eq}, Å^2
Se	0.000	0.500	0.500	4.09(7)
Se(1)	0.1092(2)	0.3631(2)	0.5939(1)	3.69(5)
Se(2)	0.0350(2)	0.4037(2)	0.6986(1)	4.43(5)
Se(3)	-0.1897(2)	0.3439(2)	0.6789(1)	4.25(5)
Se(4)	-0.3177(2)	0.4606(2)	0.6042(1)	5.30(6)
Se(5)	-0.2645(2)	0.4513(2)	0.4917(1)	5.25(6)
P	0.2696(5)	0.4653(4)	0.1083(3)	2.8(1)
C1	0.573(2)	0.543(1)	0.8232(8)	2.4(3)
C2	0.542(2)	0.473(1)	0.7696(9)	3.2(4)
C3	0.427(2)	0.486(1)	0.712(1)	3.6(4)
C4	0.343(2)	0.565(1)	0.710(1)	3.9(4)
C5	0.376(2)	0.635(2)	0.763(1)	4.7(5)
C6	0.493(2)	0.623(1)	0.821(1)	3.5(4)
C7	0.789(2)	0.075(1)	0.5188(9)	2.5(4)
C8	0.765(2)	0.013(2)	0.460(1)	4.6(5)
C9	0.778(2)	0.046(2)	0.392(1)	5.2(5)
C10	0.816(2)	0.138(2)	0.383(1)	4.1(4)
C11	0.838(2)	0.203(2)	0.441(1)	4.4(5)
C12	0.820(2)	0.169(1)	0.5105(9)	3.1(4)
C13	0.643(2)	0.107(1)	0.638(1)	3.5(4)
C14	0.641(2)	0.107(1)	0.712(1)	4.1(5)
C15	0.541(2)	0.159(2)	0.737(1)	5.2(5)
C16	0.453(2)	0.216(2)	0.688(1)	4.6(5)
C17	0.458(2)	0.221(2)	0.616(1)	4.6(5)
C18	0.550(2)	0.164(1)	0.5893(9)	3.4(4)
C19	0.283(2)	0.089(1)	0.3988(9)	3.1(4)

Table 3·3. (cont'd)

atom	x	y	z	B_{eq}, Å^2
C20	0.411(2)	0.116(1)	0.382(1)	3.4(4)
C21	0.456(2)	0.209(2)	0.388(1)	5.5(5)
C22	0.372(3)	0.280(2)	0.409(1)	6.6(6)
C23	0.247(2)	0.255(2)	0.421(1)	5.4(5)
C24	0.197(2)	0.160(2)	0.415(1)	4.5(5)

a. B_{eq} is defined as $4/3[a^2\beta_{11}+b^2\beta_{22}+c^2\beta_{33}+ab(\cos\gamma)\beta_{12}+ac(\cos\beta)\beta_{13}+bc(\cos\alpha)\beta_{23}]$.

Table 3-4. Calculated and Observed X-ray Powder Diffraction Patterns for α-$(Ph_4P)_2[Se(Se_5)_2]$ (3-1)

h k l	$d_{calc.}$ (Å)	$d_{obs.}$ (Å)	$I/I_{max.}$ (obs.)
0 1 1	9.94	9.87	52
1 1 0	9.41	9.38	71
-1 1 1	8.79	8.74	21
1 0 1	7.85	7.76	70
0 2 0	7.41	7.39	57
1 2 0	6.33	6.24	24
1 2 1	5.39	5.42	51
1 3 0	4.58	4.51	32
-2 2 2	4.397	4.301	23
1 3 1	4.182	4.212	100
2 2 1	4.134	3.996	41
0 0 4	3.350	3.360	21
-3 3 2	3.158	3.160	45
2 0 2	2.927	3.008	32
1 1 4	2.935	2.945	25
-3 4 1	2.804	2.807	15
-4 3 1	2.687	2.691	12
-3 4 3	2.597	2.560	15
1 0 5	2.457	2.458	19
1 2 5	2.333	2.330	519
-3 3 6	2.079	2.077	30
-2 4 6	1.987	1.999	16

Table 3·5. Calculated and Observed X-ray Powder Diffraction Patterns for β-$(Ph_4P)_2[Se(Se_5)_2]$ (3·2) and $(Ph_4P)_2[Te(Se_5)_2]$ (3·3)

h k l	$d_{calc.}$ (Å)	$d_{obs.}$ (Å), I/I_{max} for (3·2)	$d_{obs.}$ (Å), I/I_{max} for (3·3)
0 1 1	11.05	11.18, 90	11.20, 52
0 0 2	9.11	9.15, 13	9.09, 20
1 1 0	7.97	7.98, 100	7.85, 100
1 0 1	7.90	/	/
-1 1 1	7.83	/	/
0 1 2	7.62	7.69, 60	7.64, 42
0 2 0	6.95	7.02, 44	7.02, 33
0 2 1	6.49	6.55, 60	6.54, 44
0 2 2	5.523	5.570, 26	5.517, 21
-1 2 2	5.100	5.131, 31	5.114, 27
2 0 0	4.863	4.893, 24	4.873, 19
0 2 3	4.571	4.591, 56	4.591, 29
0 1 4	4.330	4.353, 35	4.351, 20
1 3 0	4.181	/	4.220, 45
-1 3 1	4.163	4.191, 80	/
0 3 2	4.134	/	/
-2 1 3	4.091	/	/
-2 2 1	4.052	3.979, 71	3.964, 44
-2 0 4	3.765	3.773, 31	3.718, 49
-1 0 5	3.690	3.700, 54	/
0 1 5	3.522	3.541, 22	/
2 3 0	3.353	3.375, 42	3.313, 59
-1 2 5	3.268	3.266, 27	/
-3 1 2	3.204	3.210, 36	/
3 1 0	3.164	3.174, 29	/
1 4 2	3.003	3.021, 52	/
1 3 4	2.951	2.953, 34	2.980, 20
-1 2 6	2.833	2.833, 22	2.826, 29

III. Results

1. Description of Crystal and Molecular Structures of α- and β-$(Ph_4P)_2[Se(Se_5)_2]$

The crystal lattice of these two compounds is made up of well separated Ph_4P^+ cations and $[Se(Se_5)_2]^{2-}$ anions. Although two compounds crystallize as different unit cells, the structures of the anions in two crystal modifications are essentially the same. Figures 3·1 and 3·2 are the packing diagrams of the two compounds, while Figure 3·3 depicts the structure of the anion in both compounds. A comparison of selected bond distances and bond angles in two anions found in two crystal forms is given in Figure 3·4. The Ph_4P^+ cations have the normal tetrahedral structure and warrant no further comments. The $[Se(Se_5)_2]^{2-}$ anion can be thought of as a Se^{2+} ion, which is situated on a crystallographic inversion center, chelated by two Se_5^{2-} chains, forming a spirocyclic ring with C_{2h} symmetry. This assignment of oxidation state might be formal, but the argument here is well supported by the observed square-planar coordination geometry around the central Se atom. This geometry is predicted by valence-shell electron-pair repulsion theory (VSEPR) for Se^{2+}. The bonds of the central Se atom to the four ligands of the square-plane are very long. The two sets of Se-Se bond distances are, Se-Se(1)=2.659(2) Å and Se-Se(5)=2.680(3) Å in (**3·1**), and Se-Se(1)=2.653(2) Å and Se-Se(5)=2.693(3) Å in (**3·2**). These distances are considerably longer than their sum of the covalent radii of the atoms involved, suggesting a strong ionic character in the bonds. It is obvious that the Se-Se distances around Se central atoms are not equal. The difference, 0.021 Å in (**3·1**) and 0.040 Å in (**3·2**), is statistically significant. In contrast, no significant difference was found in the two $[Te(Se_5)_2]^{2-}$ anions that were crystallized with different counterions and in a different space group[29]. Therefore, it is tempting to attribute this effect to distortions effected by lattice packing. It is also noteworthy that the Se-Se distances of the Se_5^{2-} chelate in α-$(Ph_4P)_2[Se(Se_5)_2]$ show two short terminal bonds and two slightly longer

internal Se-Se bonds in contrast with the structure of α-$(Ph_4P)_2[Se(Se_5)_2]$ which shows no such differentiation. The conformation of the six-membered ring of Se/Se(1)/Se(2)/Se(3)/Se(4)/Se(5) can be best described as "chair" in both structures. In (**3·1**) the four Se atoms, Se(1), Se(2), Se(4) and Se(5) are lying almost on a plane, with the mean deviation of 0.034 Å from the least square plane. The remaining two atoms of the six-membered ring, Se(3) and Se are positioned 1.750 Å and 1.820 Å above and below the plane, respectively, while in (**3·2**) Se(1), Se(2), Se(4), and Se(5), form a plane with the mean deviation of 0.090 Å from the least square plane, the fifth and sixth atoms, Se(3) and Se, positioned 1.517 Å and 1.349 Å above and below the plane, respectively. The corresponding bond distances and bond angles in the two crystal modifications are similar but not identical. For comparison, selected bond distances and bond angles for the $[Se(Se_5)_2]^{2-}$ anion in the two compounds are given in Table 3·6.

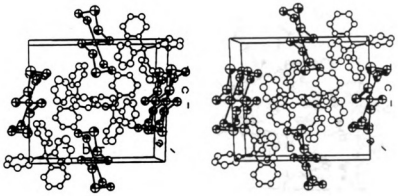


Figure 3·1. The Packing Diagram in the Unit Cell of α-$(Ph_4P)_2[Se(Se_5)_2]$ (Stereoview)

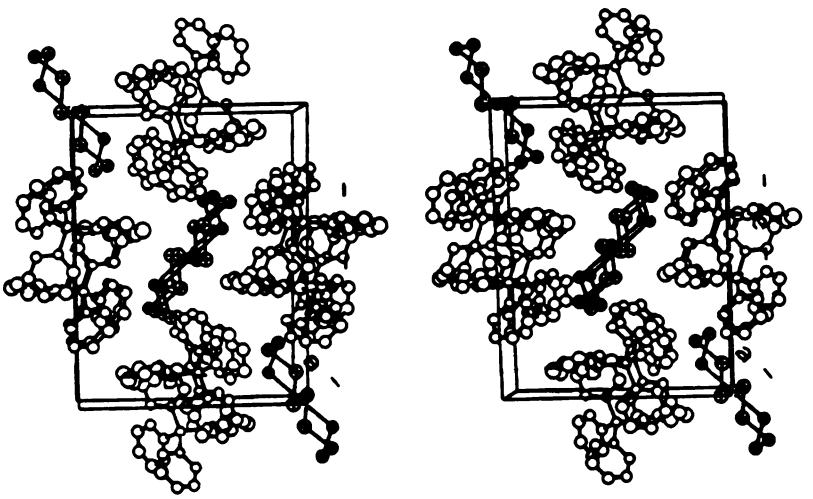


Figure 3·2. The Packing Diagram in the Unit Cell of β-$(Ph_4P)_2[Se(Se_5)_2]$ (Stereoview)

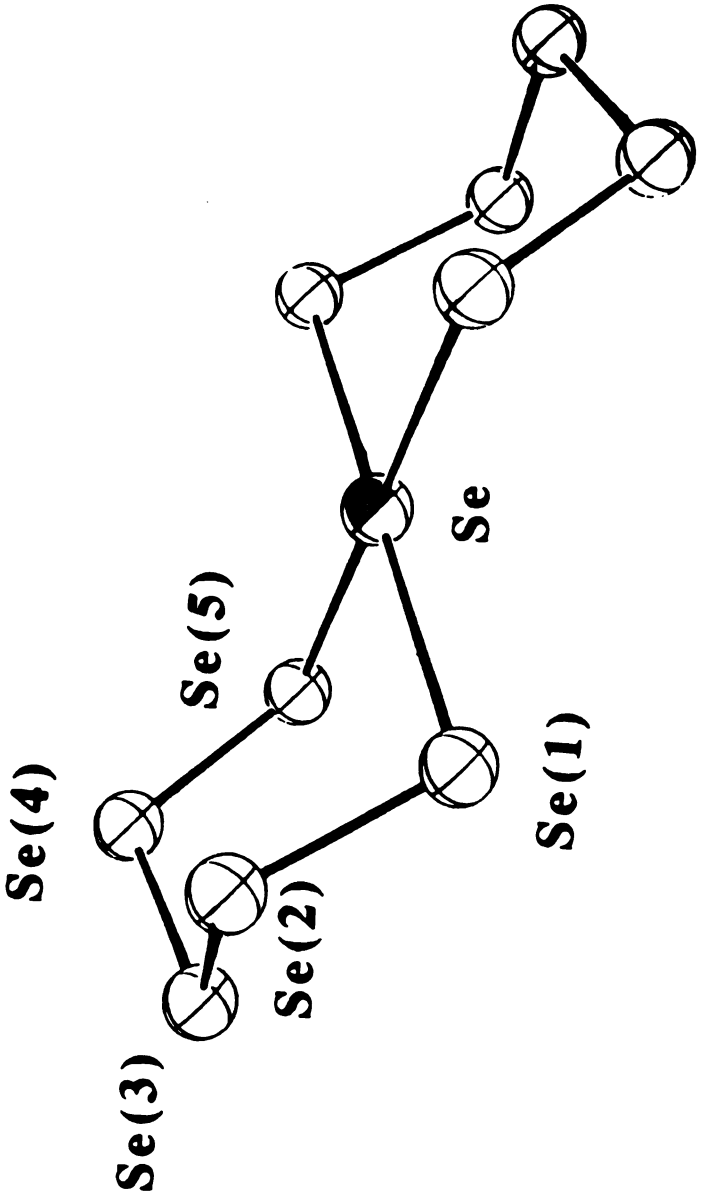


Figure 3:3. The Structure of the $[Se(Se_5)_2]^{2-}$ Anion

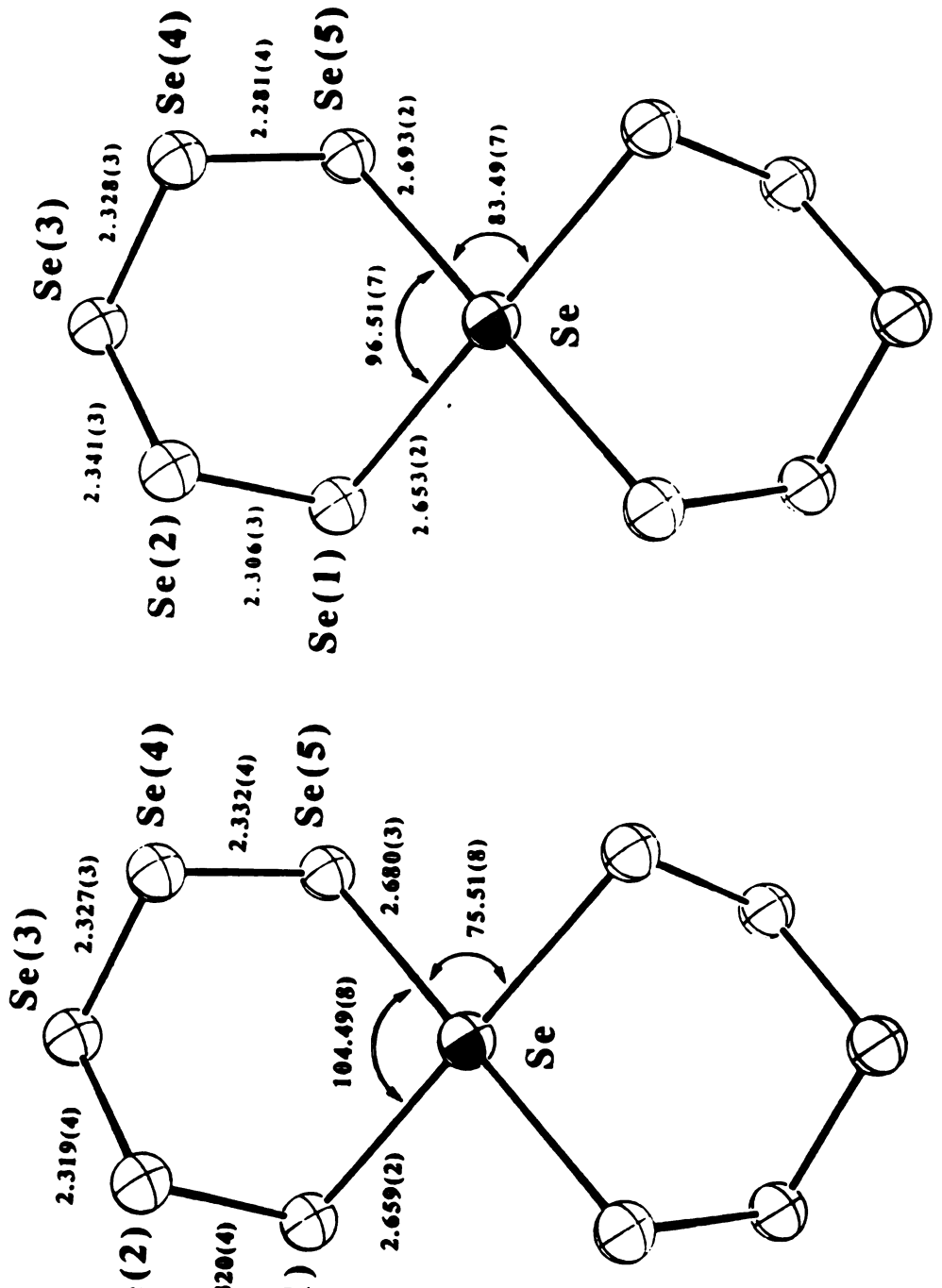
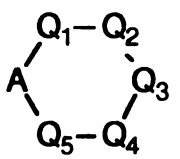


Figure 3-4. Comparison of Selected Bond Distances (Å) and Bond Angles (deg) in (A) α- And (B) β-$(Ph_4P)_2[Se(Se_5)_2]$

Table 3-6. Selected Bond Distances (Å) and Bond Angles (deg) of α-$(Ph_4P)_2[Se(Se_5)_2]$ and β-$(Ph_4P)_2[Se(Se_5)_2]$[a,b]

Compound	α-$(Ph_4P)[Se(Se_5)_2]$	β-$(Ph_4P)[Se(Se_5)_2]$
A-Q1	2.659(2)	2.653(2)
A-Q5	2.680(3)	2.693(2)
A-Q_{mean}	2.670(11)	2.673(20)
Q1-Q2	2.320(4)	2.306(3)
Q2-Q3	2.319(4)	2.341(3)
Q3-Q4	2.327(3)	2.328(3)
Q4-Q5	2.332(4)	2.281(4)
Q-Q_{mean}	2.325(4)	2.314(13)
Q1-A-Q5	104.49(8)	96.51(7)
A-Q1-Q2	108.19(9)	102.91(10)
Q1-Q2-Q3	105.24(15)	104.67(11)
Q2-Q3-Q4	101.86(14)	103.15(12)
Q3-Q4-Q5	108.33(13)	107.80(14)
Q4-Q5-A	107.66(12)	110.75(10)



Labeling Scheme: a. b. The estimated standard deviations in the mean bond lengths and the mean bond angles are calculated by the equation $\sigma_l=\{\Sigma_n(l_n-l)^2/n(n-1)\}^{1/2}$, where l_n is the length (angle) of the *n*th bond, l the mean length (angle), and n the number of bonds.

2. Spectroscopic Studies

The solid-state far IR spectra of α-and β-$(Ph_4P)_2[Se(Se_5)_2]$ are identical. Figure 3·5 shows the far IR spectra of $(Ph_4P)_2[Se(Se_5)_2]$ and $(Ph_4P)_2[Te(Se_5)_2]$. Two strong peaks at 265 and 216 cm^{-1} are observed for $(Ph_4P)_2[Se(Se_5)_2]$, while $(Ph_4P)_2[Te(Se_5)_2]$ gives two peaks at 277 cm^{-1} (strong) and 258 cm^{-1} (weak, broad). They are all assigned to the Se-Se stretching vibrations (vide infra).

The solution of $(Ph_4P)_2[Se(Se_5)_2]$ in DMF has a dense green tint, and shows a broad UV/vis absorption at 653 nm (ε=2841 $M^{-1}\cdot cm^{-1}$), and an extremely broad shoulder from ~380–480 nm with two identifiable absorption maxima at 457 nm (ε=9432 $M^{-1}\cdot cm^{-1}$) and 400 nm (sh, ε=9154 $M^{-1}cm^{-1}$) as shown in Figure 3·6, while the solution of $(Ph_4P)_2[Se(Se_5)_2]$ is reddish, and shows a featureless UV/vis spectrum with a rising absorbance.

3. Thermal Decomposition

Figure 3·7 shows thermal decomposition diagrams of $(Ph_4P)_2[Se(Se_5)_2]$ and $(Ph_4P)_2[Te(Se_5)_2]$ under nitrogen. Both compounds begin to lose weight at ~265 °C. The observed weight loss for $(Ph_4P)_2[Se(Se_5)_2]$ at 442 °C is 93.10%, which corresponds to *ca.* one equivalent elemental selenium (i.e. the calculated weight loss is 94.89%). At 557 °C, the weight loss for this compound starts again, presumably that the elemental selenium is evaporating. Up to ~800 °C, the observed weight loss approaches 100%, indicating that all selenium has been evaporated. The observed weight loss at 427°C for $(Ph_4P)_2[Te(Se_5)_2]$ is 91.64%, which corresponds to one equivalent elemental tellurium (i.e. the calculated weight loss is 92.00%). Further weight loss for this compound goes beyond 800 °C.

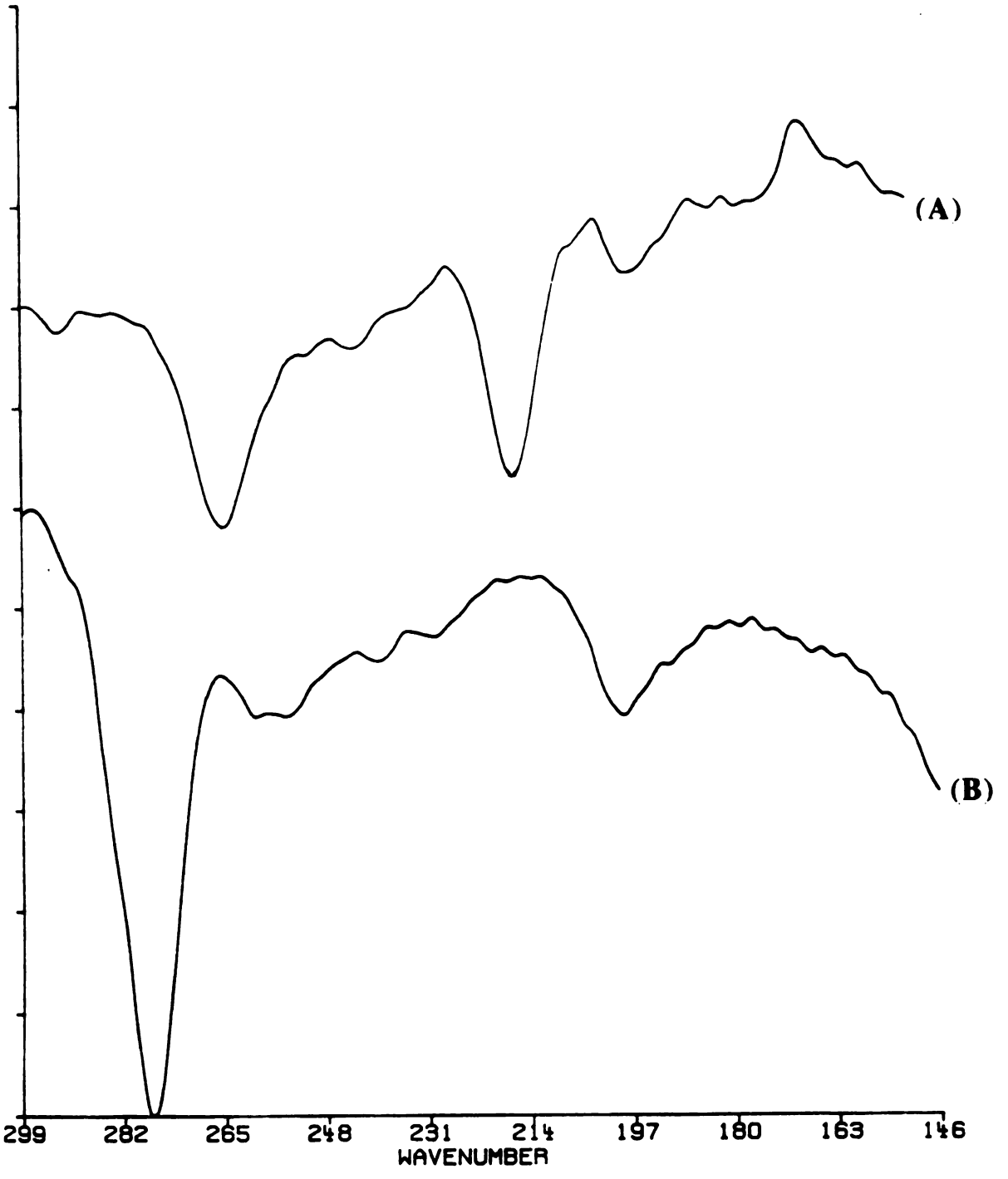


Figure 3-5. The Solid-State Far IR Spectra of (A) $(Ph_4P)_2[Se(Se_5)_2]$ and (B) $(Ph_4P)_2[Te(Se_5)_2]$

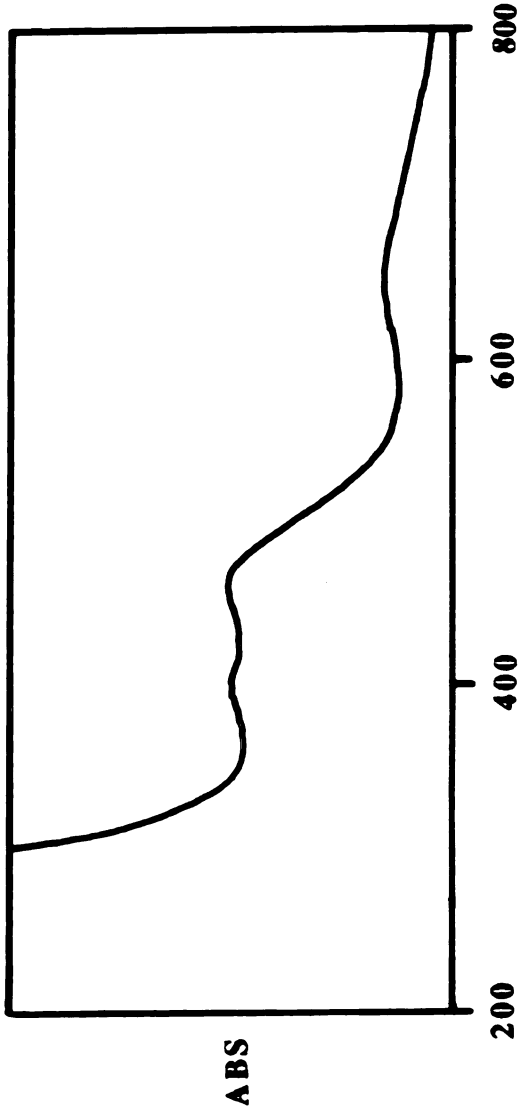


Figure 3-6. The UV/vis Spectrum of $(Ph_4P)_2[Se(Se_5)_2]$ in DMF

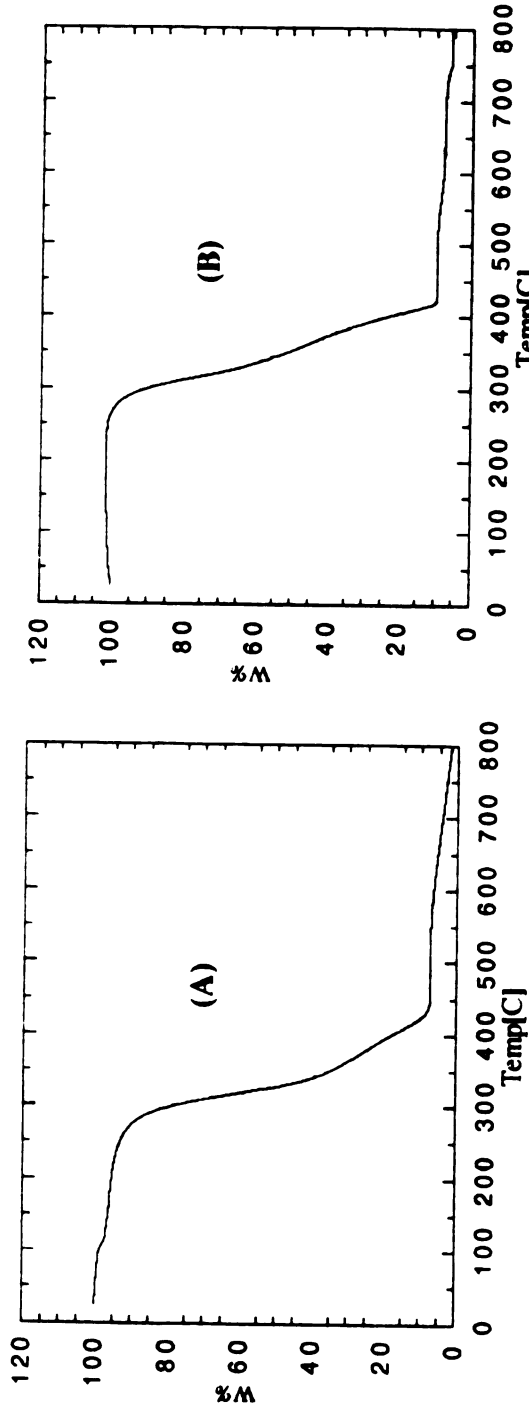


Figure 3·7. The TGA diagrams of (A) $(Ph_4P)_2[Se(Se_5)_2]$ And (B) $(Ph_4P)_2[Te(Se_5)_2]$

IV. Discussion

Three homo- or heteropolychalcogenide compounds in the $[A(Se_5)_2]^{2-}$ family (A=Se and Te) have been made by redox reactions in DMF solution. Either the external reagent $AuCl_3$, I_2 or the polychalcogenide ligand Se_5^{2-} were used as oxidant:

$$2Na_2Se_5+AuCl_3+2Ph_4PCl \xrightarrow{DMF} \alpha\text{-}(Ph_4P)_2[Se(Se_5)_2]+AuCl+NaCl \quad \text{eq.(3·1)}$$

$$2Na_2Se_5+I_2+2Ph_4PCl \xrightarrow{DMF} \beta\text{-}(Ph_4P)_2[Se(Se_5)_2]+NaI+NaCl \quad \text{eq.(3·2)}$$

$$Te+2Na_2Se_5+2Ph_4PCl \xrightarrow{DMF} (Ph_4P)_2[Te(Se_5)_2]+NaCl \quad \text{eq.(3·3)}$$

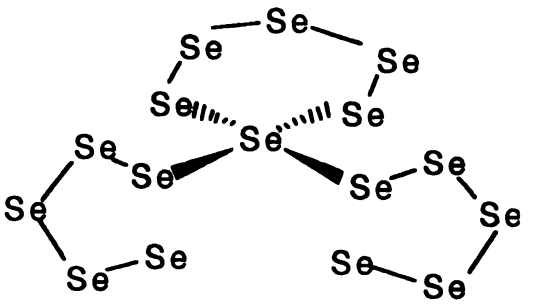
None of the above reactions is balanced. Inability to do so reflects the complexity of the reactions which polychalcogenide ligands undergo in solutions as frequently observed in metal/polychalcogenide systems[32-34].

The solid-state far IR spectra of α-$(Ph_4P)_2[Se(Se_5)_2]$ and β-$(Ph_4P)_2[Se(Se_5)_2]$ are identical to each other, showing two strong absorptions at 265 and 216 cm^{-1}, while $(Ph_4P)_2[Te(Se_5)_2]$ shows a strong band at 277 cm^{-1} and a weak broad absorption centered around 258 cm^{-1}. All these absorptions are assigned to the Se-Se stretching vibrations. This is based on the previously reported far IR assignment made for the other unliganded polyselenide compounds. For example, $[Se_x]^{2-}$ (x=2-6) shows a $\nu_{se\text{-}se}$ at 285 cm^{-1}[35], *cyclo*-Se_6 shows a $\nu_{se\text{-}se}$ at 253 cm^{-1}[36], and $(Ph_4P)_2[Se_5]$ shows a $\nu_{se\text{-}se}$ at 267 cm^{-1}[37].

The solution UV/vis absorptions of $(Ph_4P)_2[Se(Se_5)_2]$ at 653, 457 and 400 nm are associated with free Se_x^{2-} species in solution which are thought to be dissociated into radical anion chains. The presence of these absorption bands indicates that the compounds do not maintain their integrity in this solvent, but rather they dissociate to various Se_x^{2-}

species[37]. Interestingly, the red solution of $(Ph_4P)_2[Te(Se_5)_2]$ in DMF shows a a featureless UV/vis spectrum with a rising absorbance. This suggests that $(Ph_4P)_2[Te(Se_5)_2]$ does not undergo the same dissociation as α-$(Ph_4P)_2[Se(Se_5)_2]$ and β-$(Ph_4P)_2[Se(Se_5)_2]$, or at least not to the same extent.

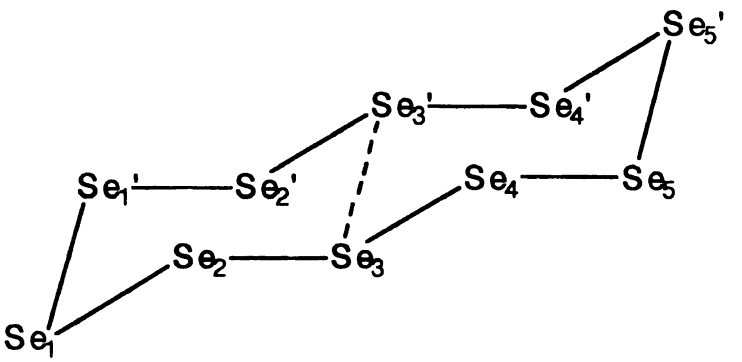
Four coordinated square-planar Se^{2+} with chalcogen ligands is scarce. To our knowledge the only example of mixed valence polyselenide containing a formal Se^{2+} unit is $Cs_4[Se_{16}]$ in which a square-planar Se^{2+} is chelated by three Se_5^{2-} chains, of which one acts as bidentate while the other two act as monodetate ligands, resulting in a structure of a six-membered ring on one side with two Se_5^{2-} "tails" dangling on other, as shown in Scheme 3·1[38]. As in $[Se(Se_5)_2]^{2-}$, $[Se_{16}]^{4-}$ shows four long Se-Se bond distances around the Se^{2+} atom.



Scheme 3·1. The Structure of $[Se_{16}]^{2-}$

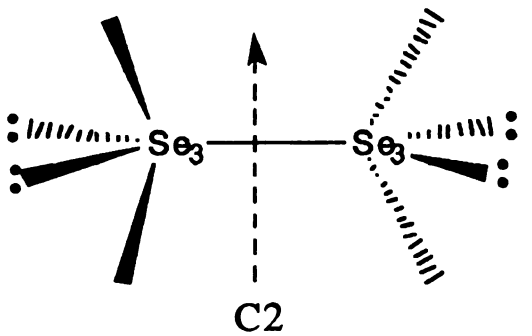
In order to put the above description of mixed-valence polychalcogenides in perspective, two more related free polyselenides must be discussed. The $(PPN)_2[Se_{10}]$·DMF[21] and $[Sr(15\text{-crown-}5)_2][Se_9]$[16], crystallized from a DMF solution of polyselenides with respectively PPN^+ or Sr^{2+} in the presence of the crown ether, represent two incredible examples of how large polyselenide ligands stabilize themselves in the absence of metal ions. The $[Se_{10}]^{2-}$ anion forms a decalin-like molecule, i.e. it consists of two fused six-membered Se_6 rings as shown in Scheme 3·2. The

molecule is situated on a crystallographic C_2 axis, and both individual rings have the chair conformation.



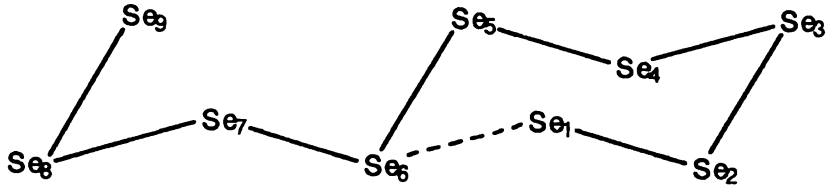
Scheme 3·2. The Structure of $[Se_{10}]^{2-}$

The reason for this is electronic. First, two selenium atoms in the central Se-Se unit have a distorted trigonal-bipyramidal geometry, and are linked together through one of the equatorial positions of each atom. The Se-Se bond distance of 2.4602(2) Å in the central Se_2 unit is slightly longer than typical Se-Se distances in most unbranched Se_x^{2-} chains (e.g.Se-Se=2.38(5) Å in Na_2Se_2). Secondly, Se(3) forms two long bonds with Se(2) and Se(4) at 2.759(3) and 2.572(3) Å. Therefore, the molecule might be conveniently described as a $\{Se_2\}^{2+}$ unit chelated by two Se_4^{2-} ligands with chemical bonds having certain ionic character. This also accounts for the coordination geometry observed for the central $\{Se_2\}^{+}$ unit as shown below, as well as the bond distance lengthening in this central unit.



Scheme 3·3. Geometry of the Ten Valence Electron Species $\{Se_2\}^{2+}$

In a large polyselenide system such as $[Se_{10}]^{2-}$, the catenation ability of selenium may not allow the anion to maintain an unbranched helical chain structure in the solid state. Stability is thus gained through internal electron transfer. This is also found to be operative in the $[Se_9]^{2-}$ system. Scheme 3·4 shows the structure of the $[Se_9]^{2-}$ anion[16]. Instead of being a zig-zag chain, this molecule has an astonishing resemblance to $[Se_{10}]^{2-}$. Topologically, $[Se_9]^{2-}$ can be viewed as formed through the $[Se_{10}]^{2-}$ by removing a terminal selenium atom from one of the Se_4^{2-} ligands. The remaining Se_6 ring still has the chair conformation. Although the distance of the "central" Se_2 unit, i.e. Se(5)-Se(6) at 2.473 Å, is comparable to that found in $[Se_{10}]^{2-}$, the normal bond distance of Se4-Se5 at 2.341(4) Å, as well as the weak interaction between Se(1) and Se(6) (i.e. 2.953(4) Å) renders the molecule certain characteristics of the open chain structure. This clearly indicates a transition state of the molecule from abandoning the unbranched helical chain structure by seeking a similar electronic configuration to that in $[Se_{10}]^{2-}$ or in $[Se_{11}]^{2-}$.



Scheme 3·4. The Structure of $[Se_9]^{2-}$

The isolation of two crystal modifications of the $[Se(Se_5)_2]^{2-}$ from polyselenide solutions in DMF with different oxidants suggests that this compound is the stable end-product of such solvent-extracted polyselenide solutions. Event in the presence of other organic counterion (i.e. Pr_4N^+), the same molecule can be isolated from the reaction of Na_2Se_2 with I_2[39]. Unlike the ordinary polyselenide solutions, this closed-ring molecule is much less reactive with metal ions to form complexes, which accounts for the failure to isolate any Au/Se_x^{2-} compounds from the $AuCl_3/Na_2Se_5$ system[24]. Furthermore, an analogous chemistry has been seen in the Te/Se_5^{2-} system. The formation of $[Te(Se_5)_2]^{2-}$

is also the result of a redox reaction between Se_5^{2-} and Te, a reasonable (but not necessarily expected) outcome determined by their electronegativities. The results presented here suggest that the stabilization of mixed $[Se_xTe_y]^{2-}$ ($x \geq y > 1$) anions with chain structures is probably unlikely because of the ensuing internal electron transfer to yield species with oxidized Te.

REFERENCES

1. Early investigations on the existence of the homopolychalcogenide anions in liquid ammonia solution can be found in (a) C. C. Hugot *R, Hebd. Seances Acad. Sci,* (1899), 219, 299, 388. (b) C. C. Hugot, *Ann. Chim. Phys.*, 21(1900), 72. (c) C. A. Kraus and C. Y. Chiu, *J. Am. Chem. Soc,* 14(1922), 1999-2009. (d) F. W. Bergstrom, *J. Am. Chem. Soc.,* 48(1926), 146-151. (e) E. Zintl, J. Goubeau and W. Dullenkopf, *Z. Phys. Chem., Abt. A,* 154(1931), 1. (f) W. Klemm, H. Sodomann and P. Langmesser, *Z. Anorg. Allg. Chem.*, 241(1939), 281-304.

2. For recent spectroscopic studies of these species in polar solvents (i. e. en, NH_3 and MDF, etc.), see (a) F. Seel, H. J. Guttler, G. Simon and A. Wieckowski, *Pure Appl. Chem.*, 49(1977), 45-54. (b) K. W. Sharp and W. H. Koehler, *Inorg. Chem.*, 16(1977), 2528-2565. (c) L. D. Schultz and W. H. Koehler, *Inorg. Chem.*, 26(1987), 1989-1993. (d) P. Dubois, J. P. Lelieur and G. Lepoutre, *Inorg. Chem.*, 26(1987), 1897-1902. (e) P. Dubois, J. P. Lelieur and G. Lepoutre, *Inorg. Chem.*, 27(1987), 73-80. (f) P. Dubois, J. P. Lelieur and G. Lepoutre, *Inorg. Chem.*, 27(1988), 1883-1890. (g) V. Pinon and J. P. Lelieur, *Inorg. Chem.*, 30(1991), 2260-2264. (h) M. Bjorgvinsson and G. J. Schrobilgen, *Inorg. Chem.*, 30(1991), 2540-2547.

3. For S_2^{2-}, see (a) H. Föppl, *Angew. Chem.*, 70(1958), 401-401. (b) H. Föppl, E. Busmann and F.-K. Frorath, *Z. Anorg. Allg. Chem.*, 314(1962), 12-20.

4. For S_3^{2-}, see W. S. Miller and A. J. King, *Z. Kristallogr., Kristallgeom., Kristallphys., Kristallchem.*, 94(1936), 439.

5. For S_4^{2-}, see (a) S. C. Abrahams, *Acta Crystallogr.*, 7(1954), 423-429. (b) S. C. Abrahams and J. L. Bernstein, *Acta Crystallogr.*, 25B(1969), 2365-2370. (c) R. Tegman, *Acta Crystallogr.*, 29B(1973), 1463-1469.

6. For S_5^{2-}, see (a) B. Leclerc and T. S. Kabre, *Acta Crystallogr.*, 31B(1975), 1675-1677. (b) B. Kelly and P. Woodward, *J. Chem. Soc. Dalton Trans.*, (1976), 1314-1316. (c) P. Böttcher, *Kristallogr.*, 150(1974), 65-73. (d) P. Böttcher and K. Kruse, *J. Less-common Met.*, 83(1982), 115-125.

7. For S_6^{2-}, see (a) S. C. Abrahams and E. Grison, *Acta Crystallogr.*, 6(1953), 206-213. (b) A. Hordvik and E. Stetten, *Acta Chem. Scand.*, 22(1968), 3029-3052. (c) R. G. Teller, L. J. Krause and R. C. Haushalter, *Inorg. Chem.*, 22(1983), 1809-1812.

8. For S_7^{2-}, see (a) H. Krebs and K. H. Müller, *Z. Anorg. Allg. Chem.*, 275(1954), 147-151. (b) M. G. Kanatzidis, N. C. Baenziger and D. Coucouvanis, *Inorg. Chem.*, 22(1983), 290-292.

9. For Se_2^{2-}, see (a) G. Cordier, R. Cook and H. Schäfer, *Angew. Chem. Int. Ed. Engl.*, 19(1980), 324-325. (b) ref.[3b].

10. For Se_3^{2-}, see (a) H. G. Von Schnering and N. K. Goh, *Naturwissenshaften* , 61(1974), 272. (b) P. Böttcher, *Z. Anorg. Allg. Chem.*, 461(1980), 13-21.

11. For Se_4^{2-}, see (a) O. Foss and V. Janickis, *J. Chem. Soc. Dalton Trans.*, (1980), 620-623. (b) T. König, B. Eisenmann and H. Schäfer, *Z. Naturforsch.*, 37B(1982), 1245-1249. (c) T. König, B. Eisenmann and H. Schäfer, *Z. Anorg. Allg. Chem.*, 498(1983), 99-104. (d) N. E. Brese, C. R. Randall and J. A. Ibers, *Inorg. Chem.*, 27(1988), 940-943.

12. For Se_5^{2-}, see (a) U. Kretschmann and P. Böttcher, *Z. Naturforsch.*, 40B(1985), 895-899. (b) C.-N. Chau, R. W. M. Wardle and J. A. Ibers, *Acta Crystallogr.*, 44C(1988), 883-885. (c) W. S. Sheldrick and H. G. Braunback, *Z. Naturforsch.*, 44B(1989), 1397-1401. (d) G. Kräuter, K. Dehnicke and D. Fenske, *Chem.-Ztg.*, 114(1990), 7-9. (e) J. Dietz, U. Müller, V. Müller and K. Dehnicke, *Z. Naturforsch.*, 46B(1991), 1293-1299. (f) V. Müller, G. Frenzen, K. Dehnicke and D. Fenske, *Z. Naturforsch.*, 47B(1992), 205-210. (g) ref.[6c]. (h) ref.[11d].

13. For Se_6^{2-}, see (a) F. Weller, J. Adel and K. Dehnicke, *Z. Anorg. Allg. Chem.*, 548(1987), 125-132. (b) D. Fenske, C. Kraus and K. Dehnicke, *Z. Anorg. Allg. Chem.*, 607(1992), 109-112. (c) ref.[7c].

14. For Se_7^{2-}, see V. Müller, K. Dehnicke, D. Fenske and G. Baum, *Z. Naturforsch.*, 46B(1991), 63-67.

15. For Se_8^{2-}, see R. Staffel, U. Müller, A. Ahle and K. Dehnicke, *Z. Naturforsch.*, 46B(1991), 1287-1292.

16. For Se_9^{2-}, see V. Müller, C. Grebe, U. Müller and K. Dehnicke, *Z. Anorg. Allg. Chem.*, 619(1993), 416-420.

17. For Te_2^{2-}, see R. C. Burns and J. D. Corbett, *J. Am. Chem. Soc.*, 103(1981), 2627-2632.

18. For Te_3^{2-}, see (a) A. Cisar and J. D. Corbett, *Inorg. Chem.*, 16(1977), 632-635. (b) Eisenmann and H. Schäfer, *Angew. Chem. Int. Ed. Engl.*, 17(1978), 684-686. (c) P. Böttcher, *J. Less-Common Met.*, 70(1980), 263-271.

19. For Te_4^{2-}, see (a) J. C. Huffman and R. C. Haushalter, *Z. Anorg. Allg. Chem.*, 518(1984), 203-209. (b) L. A. Devereux, G. J. Schrobilgen ans J. F. Sawyer,

Acta Crystallogr., 41C(1985), 1730-1733. (c) K. W. Klinkmammer and P. Böttcher, *Z. Naturforsch.*, 45B(1990), 141-147. (d) H. Wolker, B. Schreiner, R. Staffel, U. Müller and K. Dehnicke, *Z. Naturforsch.*, 46B(1991), 1015-1019. (e) B. Schreiner and K. Dehnicke, *Chem.-Ztg.*, 115(1991), 326. (f) D. Fenske, G. Baum, H. Wolkers, B. Schreiner, F. Weller and K. Dehnicke, *Z. Anorg. Allg. Chem.*, (1992), in press.

20. For Te_5^{2-}, see (a) P. Böttcher and U. Kretschmann, *J. Less-common Met.*, 95(1983), 81-91. (b) P. Böttcher and U. Kretschmann, *Z. Anorg. Allg. Chem.*, 491(1982), 39-46. (c) ref.[7c]. (d) ref.[19f].

21. D. Fenske, G. Kräuter and K. Dehnicke, *Angew. Chem. Int. Ed. Engl.*, 29(1990), 390-301.

22. M. G. Kanatzidis and S.-P. Huang, *Inorg. Chem.*, 28(1989), 4667-4669.

23. P. Böttcher, *Angew. Chem. Int. Ed. Engl.*, 27(1988), 759-864.

24. See chapter 2.

25. D. D. Perrin, W. L. F. Armarego and D. R. Perrin, *Purification of Laboratory Chemicals,* 2nd Ed., Pergamon Press, Oxford UK, 1980.

26. *P3/V Data Collection Manual,* Siemens Analytical X-ray Instruments, Inc., 1989.

27. N. Walker and D. Stuart, *Acta Crystallogr.*, 39A(1983), 158-166.

28. (a) G. M. Sheldrick in *Crystallographic Computing,* G. M. Sheldrick, C. Kruger, and R. Doddard, Oxford University Press, 1985, p.175-189. (b) B. A. Frenz, The Enraf-Nonius CAD4 SDP System. in *Computing in Crystallography*; Delft University Press, Delft Holland, 1978; p.64-71.

29. R. Zagler and B. Eisenmann, *Z. Naturforsch.*, 46B(1991), 593-601.

30. H. P. Klug and L. E. Alexander, *X-ray Diffraction Procedures for Polycrystalline and Amorphous Materials,* John Wiley and Sons, New York, 1974.

31. D. K. Smith, M. C. Nichols and M. E. Zolensky, *POWD10: A Fortran IV Program for Calculating X-ray Powder Diffration Patterns,* Version 10, Pennsylvania State University, 1983.

32. (a) M. G. Kanatzidis, *Comments Inorg. Chem.*, 10(1990), 161-195. (b) M. G. Kanatzidis and S.-P. Huang, *Coord. Chem. Rev.*, in press.

33. M. A. Ansari and J. A. Ibers, *Coord. Chem. Rev.*, 100(1990), 223-266.

34. J. W. Kolis, *Coord. Chem. Rev.*, 105(1990), 195-219.

35. F. Weller, J. Adel and K. Dehnicke, *Z. Anorg. Allg. Chem.*, 548(1987), 125-132.

36. K. Nagata, K. Tshibashi and Y. Miyamoto, *Jpn. J. Appl. Phys.*, 19(1980), 1569-1573.

37. S.-P. Huang and M. G. Kanatzidis, *Inorg. Chem.*, 30(1991), 1455-1466.

38. W. S. Sheldrick and H. G. Braunbeck, *Z. Naturforsch.*, 44B(1989), 1397-1401.

39. J. Dietz, U. Müller, V. Müller and K.Dehnicke *Z. Naturforsch.*, 46B(1991), 1293-1299.

CHAPTER 4

CHEMISTRY OF POLYSELENIDE LIGANDS WITH IRON AND RUTHENIUM CARBONYLS IN SOLUTION

I. Introduction

In parallel to our systematic investigations on the heavy polychalcogenide chemistry of coinage metals[1], we also explored the corresponding transition metal carbonyls in order to prepare CO-containing compounds in which the metal centers have a *partial* polychalcogenide environment. Syntheses of such compounds represent the interface between organometallic chemistry of the transition metals and the chemistry of main group elements. Research in this particular field of organometallic chemistry has been active[2-5].

The simplest method for synthesizing metal chalcogenide compounds with organometallic ligands in general, and carbonyl groups in particular, has been to react elemental chalcogen with coordinatively unsaturated electron-rich metal complexes, or with compounds containing metal-metal bonds[3, 5, 6-12]. Such a process often results in a change in the oxidation state of the metal, and usually produces compounds with partial chalcogenide-coordination environment because no metathesis can take place between the all ancillary groups and the elemental chalcogen atoms. Due to the lack of suitable starting metal complexes which possess enough reactivity towards the elemental chalcogens, this method is less than universal[13]. On the other hand, oxidative decarbonylation of metal carbonyls by polychalcogenide ligands Q_n^{2-} (Q=S, Se and Te; n=2-6) provides a convenient route for introducing chalcogen-atoms into metal centers[14]. This approach

was first initiated by Kolis and co-workers in the synthesis of group 6 metal carbonyl polychalcogenide complexes[15-18]. Since most of the transition metal carbonyls are readily available, this synthetic method is potentially extendable to the preparation of other transition metal carbonyl polychalcogenide compounds.

Our interest in synthesizing soluble ruthenium polychalcogenide, especially polysulfide, complexes stems from the hydrodesulfurization (HDS) problem[19]. RuS_2 is one of the most active catalysts known for the hydrodesulfurization of crude oil[20]. As with the other HDS catalysts (i.e. MoS_2, WS_2 and "CoMoS"), the mechanism of its action is currently unkown[21]. We were interested in probing the RuS_2/HDS problem from the standpoint of mimicking the active sites present in RuS_2 by using soluble homoleptic ruthenium polysulfides as model compounds[22]. However, Ru/S chemistry has proven to be somewhat recalcitrant to study in the sense that, to date, no homoleptic Ru/S complexes have been isolated in pure form and/or structurally characterized. Numerous attempts made in our group to prepare homoleptic polysulfido(selenido) complexes of ruthenium by reacting polysulfido(selenido) ligands with various ruthenium salts such as $RuCl_3$, $Ru(DMSO)_2Cl_2$ or $Ru(acac)_3$, etc. were also unsuccessful[23]. Due to complex electron transfer processes between Ru^{n+} and Q_x^{2-}(Q=S or Se, x=2-4), these reactions often yielded very ill-defined mixtures possibly containing ruthenium in different oxidation states. No pure species could be extracted from such mixtures by fractional crystallization. By exploring the fundamentals of Ru^{2+}/polychalcogenide chemistry, we aimed to establish the current unknown coordination preferences of this metal with chalcogenide ligands. To minimize the above electron transfer between Ru^{n+} ions and polychalcogenide ligands, one of the strategies we adopted was to introduce CO groups into the target molecule by using oxidative decarbonylation reaction in the hope that such a strong π-acid could eliminate the multiple electron transfer, thus stabilizing a ruthenium complex that contains polychalcogenide ligands. This resulted in isolation of the first stable anionic

Ru^{2+}/polyselenide complex, $[Ru(CO)_2(Se_4)_2]^{2-}$. Later, similar chemistry was successfully extended to the Fe^{2+}/polyselenide system. In this chapter, we describe the synthesis, X-ray diffraction studies and spectroscopic characterization of $(Et_4N)_{1.5}Na_{0.5}[Ru(CO)_2(Se_4)_2]$ (**4·1**), $(Ph_4P)_2[Ru(CO)_2(Se_4)_2]$ (**4·2**) and $(Ph_4P)_2[Fe(CO)_2(Se_4)_2]$ (**4·3**). Although CO and Se ligands are not HDS-relevant, structures stabilized only by these ligands may represent difficulty in isolating reactive intermediates in sulfur chemistry, and thus provide useful insight into that chemistry.

II. Experimental Section

1. Reagents

Chemicals in this work other than solvents were used as obtained: (i) selenium powder, ~100 mesh, 99.5% purity, Aldrich Chemical Company, Inc., Milwaukee, WI; (ii) sodium sticks in kerosene, 99% purity, Mallinckrodt Inc., Paris, Ky.; (iii) iron pentacarbonyl, $Fe(CO)_5$, Strem Chemicals, Inc., Newburyport, MA; (iv) ruthenium carbonyl, $Ru_3(CO)_{12}$, Strem Chemicals, Inc., Newburyport, MA; (v) tetraphenylphosphonium chloride (Ph_4PCl), 98% purity, Aldrich Chemical Company, Inc., Milwaukee, WI; (vi) tetraethylammonium chloride hydrate ($Et_4NCl{\cdot}xH_2O$), 97% purity, Aldrich Chemical Company, Inc., Milwaukee, WI.

Acetone (analytical reagent, Mallinckrodt Inc., Paris, Ky) was degassed, and used without further purification.

Diethyl ether (A.C.S. anhydrous, Columbus Chemical Industries Inc., Columbus, WI) was distilled under a dry N_2 blanket after being refluxed with potassium metal, benzophenone and triethylene glycol dimethyl ether for 12 hours[24].

2. Physical Measurements

Semi-quantitative elemental analyses, FT-IR, UV/vis, Se ^{77}NMR spectroscopic studies, and thermal gravimetric analyses (TGA) of the compounds were carried out as described previously[25].

3. Syntheses

All syntheses were carried out under a dry nitrogen atmosphere in a Vacuum Atmospheres Dri-Lab glovebox.

(i). Preparation of sodium pentaselenide in liquid ammonia

This material was prepared by reacting stoichiometric amount of selenium and sodium metal in a routine procedure used in this laboratory[25].

(ii). Preparation of $(Et_4N)_{1.5}Na_{0.5}[Ru(CO)_2(Se_4)_2]$ (4·1)

A 15 ml acetone suspension of 64 mg (0.10 mmol) $Ru_3(CO)_{12}$ was added dropwise to a 50 ml acetone solution of 270 mg (0.60 mmol) Na_2Se_5 in the presence of 100 mg (0.60 mmol) of Et_4NCl. After stirred for 10 h, the resulting brown solution was filtered to remove NaCl, and then diluted with 30 ml ether. When the mixture was allowed to stand for 3 days, analytically pure red-orange crystals of $(Et_4N)_{1.5}Na_{0.5}[Ru(CO)_2(Se_4)_2]$ were isolated in 70% yield. Mid-IR spectrum (KBr pellet): 1999(s,b) and 1939(m,b) cm^{-1}; Far IR spectrum (CsI pellet): 268(s) and 249(m) cm^{-1}; Semi-quantitative elemental analyses by EDAX (atom%): Ru:Se=14:86; ^{77}Se NMR (in DMF): 717, 650, 630 and 395 ppm; ^{13}C NMR (in DMF): 199 ppm; ^{23}Na NMR (in DMF): 0.7 (singlet) ppm.

(iii). Preparation of $(Ph_4P)_2[Ru(CO)_2(Se_4)_2]$ (4·2)

This compound is prepared in a similar manner as above, except that 220 (0.6 mmol) Ph_4PCl was used in place of Et_4NCl. Analytically pure red-orange crystals of $(Ph_4P)_2[Ru(CO)_2(Se_4)_2]$ were obtained in 83% yield. Mid-IR spectrum (KBr pellet): 1981(s) and 1915(m) cm^{-1}; Semi-quantitative elemental analyses by EDAX (atom%): Ru:Se:P=14:64:22; Far IR spectrum (CsI pellet): 269(m), 250 (s) and 199(m) cm^{-1}; ^{77}Se NMR (in DMF): 717, 650, 630 and 395 ppm.

(iv). Preparation of $(Ph_4P)_2[Fe(CO)_2(Se_4)_2]$ (4·3)

To a 50 ml acetone solution of 270 mg (0.60 mmol) Na_2Se_5 and 220 mg (0.60 mmol) Ph_4PCl at the boiling point, 0.1 ml (0.76 mmol) neat $Fe(CO)_5$ was added. The solution was kept stirring below the boiling point until a brown solution was gradually formed in about 1 hour. Following filtration of any formed precipitates, 30 ml ether was added to the filtrate. Dark brown, needle-shaped X-ray quality single crystals of $(Ph_4P)_2[Fe(CO)_2(Se_4)_2]$ were obtained in 43% yield within two days. Mid-IR spectrum (KBr pellet): 1958(s) and 1905(m) cm^{-1}; Far IR spectrum (CsI pellet): 268(s), 250(m) and 207(m) cm^{-1}; Semi-quantitative elemental analyses by EDAX (atom%): P:Fe:Se=26:17:57; ^{77}Se NMR (in DMF): 720, 706, 679 and 445 ppm ; ^{13}C NMR (in DMF): 209 ppm.

4. X-ray Diffraction and Crystallographic Studies

The single crystal X-ray diffraction studies were performed by using a Nicolet P3 four-circle difractometer.

The crystallographic data sets of (4·1), (4·2) and (4·3) were collected using a θ-2θ scan mode. The stability of the experimental setup and crystal integrity for each data collection was monitored by measuring three representative reflections periodically (every 100). The intensities of the three standard reflections in (4·1) and (4·2) showed no statistically significant change. A ~ 33% decay in the intensities of three standard

reflections in (4·3) was observed. Linear decay correction was applied to the data set. Empirical absorption corrections were applied to both data sets based on ψ scans of several strong reflections with χ~90°.

The structures were solved with direct methods and refined with full-matrix least squares techniques. DIFABS corrections were applied to the structure-factors after all the atoms in the structures were located and refined isotropically[26]. The calculations were performed using the SHELXS-86 and SDP combined package of crystallographic programs[27]. Table 4·1 gives crystal data and details for structure analysis of the two compounds.

All non-hydrogen atoms in these structures were refined either isotropically or anisotropically. The hydrogen positions were calculated but not refined. The final coordinates and average temperature factors of the atoms in each compound are given in Tables 4·2 and 4·3, respectively.

(4·1) crystallizes in the space group P-1(#2) having an asymmetric unit of $(Et_4N)_{1.5}Na_{0.5}[Ru(CO)_2(Se_4)_2]$. In addition to the Na^+ (0, 1/2, 0), one of the tetrahedral Et_4N^+ cations was found to sit on a crystallographic inversion center (0, 0, 1/2), causing a positional disorder of the ethyl groups on this cation site. The refinement of the atoms in this cation was carried out with a disorder model.

Thus far, we have been unsuccessful in solving the structure of (4·2). Structural solutions obtained from direct methods often revealed two crystallographically independent octahedral fragments of $[Ru(CO)_2(Se_4)_2]^{2-}$ which are situated in general positions, but no Ph_4P^+ cations could be found. Although the initial Fourier difference map showed a fragment resembling the Ph_4P^+ cation. The structural refinement including such a group would become divergent. The possible reason for this might be that the P atom is situated to close to a crystallographic inversion center. Based on ^{77}Se NMR, Mid- and far-IR,

elemental analysis by EDAX and TGA, this compound is formulated as $(Ph_4P)_2[Ru(CO)_2(Se_4)_2]$ (vide infra).

Finally, each compound was examined by X-ray powder diffraction for the purpose of phase characterization and identification. A Debye-Scherrer camera was employed to record the X-ray powder diffraction patterns. Ni-filtered Cu radiation was used. The crystals were ground to fine powder and packed into 0.5 mm glass capillaries which were sealed and mounted to the standard Debye-Scherrer powder camera which has a diameter of 114.6 mm (1 mm corresponds to 1 degree for 2θ). X-rays were generated by a Phillips Norelco XRG-5000 X-ray generator operating at 40 kV and 20 mA. Approximately, a six hour exposure time was used. Accurate d-spacings (Å) of each compound were calculated from the powder patterns recorded on a Phillips XRG-3000 computer controlled powder diffractometer[28]. To verify the homogeneities of the products, the d-spacings observed for the bulk materials were compared with the calculated d-spacings from the X-ray single-crystal structure analysis data[29]. Listings of calculated and observed d-spacings (Å) along with the observed relative diffraction intensities of these compounds are given in Tables 4·4 and 4·5.

Table 4·1. Data for Crystal Structure Analysis of $(Et_4N)_{1.5}Na_{0.5}[Ru(CO)_2(Se_4)_2]$ (**4·1**), $(Ph_4P)_2[Ru(CO)_2(Se_4)_2]$ (**4·2**) and $(Ph_4P)_2[Fe(CO)_2(Se_4)_2]$ (**4·3**)

compound	**4·1**	**4·2**	**4·3**
formula	$C_{14}H_{30}N_{1.5}Na_{0.5}O_2RuSe_8$	$C_{50}H_{40}P_2O_2RuSe_8$	$C_{50}H_{40}P_2O_2FeSe_8$
a, Å	10.986(3)	15.752(4)	11.525(2)
b, Å	10.979(2)	18.211(4)	14.951(3)
c, Å	13.876(4)	31.172(5)	16.553(5)
α, deg	102.12(2)	90.00	93.87(2)
β, deg	104.09(1)	99.98(2)	103.89(2)
γ, deg	113.33(1)	90.00	111.56(2)
Z; V, Å^3	2, 1399.61	4; 8806(3)	2, 2537(1)
space group	P-1(#2)	C2/c(#15)	P-1(#2)
D_{calc}, g/cm^3	2.43	2.22(D_{obs})	1.86
μ(Mo Kα), cm^{-1}	110.3 (Mo Kα)	/	100.9 (Cu Kα)
cryst size, mm	0.05x0.09x0.11	0.02x0.37x1.17	0.05x0.48x0.62
$2\theta_{max}$, deg	48.3	45	105.1
Temperature (°C)	25	-95	20
no. of data collcd	4472	8231	5812
no. of data used($F_o^2>3\sigma(F_o^2)$)	2821	5310	2502
min, max abs cor	0.40, 0.99	0.78 , 0.98	0.41, 1.49
no. of variables	240	/	308
no. of atoms per asym unit (including H)	72	/	103
final R/R_w, %	5.4/6.1	/	10.5/11.9

Table 4·2. Positional Parameters and B_{eq} Values[a] for $(Et_4N)_{1.5}Na_{0.5}[Ru(CO)_2(Se_4)_2]$ (4·1) (Standard Deviations in Parentheses)

atom	x	y	z	B_{eq}, Å^2
Ru	0.7135(1)	0.3174(1)	0.7074(1)	3.40(3)
Se1	0.5844(2)	0.1714(2)	0.8027(2)	4.71(5)
Se2	0.7662(2)	0.1871(2)	0.9432(1)	4.75(5)
Se3	0.8997(2)	0.1358(2)	0.8504(2)	4.96(5)
Se4	0.9553(2)	0.3278(2)	0.7888(1)	3.76(4)
Se5	0.8557(2)	0.4802(2)	0.6279(1)	4.92(5)
Se6	0.1855(2)	0.3273(2)	0.3198(2)	6.08(5)
Se7	0.0926(2)	0.2671(2)	0.1380(2)	5.25(5)
Se8	0.7558(2)	0.5146(2)	0.8714(1)	3.74(4)
Na	0.000	0.500	0.000	4.2(2)
O1	0.654(1)	0.063(1)	0.535(1)	7.7(5)
O2	0.449(1)	0.328(1)	0.598(1)	6.4(4)
N1	0.000	0.000	0.500	3.3(4)
N2	0.569(1)	0.297(1)	0.187(1)	3.6(3)
C1	0.676(2)	0.159(2)	0.599(1)	5.1(5)
C2	0.550(1)	0.325(2)	0.641(1)	5.2(5)
C3	0.097(4)	0.145(4)	0.506(3)	5.3(8)
C4	0.071(3)	0.264(3)	0.542(2)	3.9(6)
C5'	0.152(3)	0.055(3)	0.582(2)	4.0(7)
C5	0.971(3)	0.002(3)	0.606(3)	5.1(8)
C6	0.131(3)	0.061(2)	0.697(2)	8.4(8)

Table 4·2. (cont'd)

atom	x	y	z	B_{eq}, Å^2
C7	0.941(3)	0.103(3)	0.525(3)	5.1(8)
C8	1.008(3)	0.240(3)	0.519(3)	4.3(7)
C9	0.721(3)	0.336(3)	0.241(3)	4.8(8)
C9'	0.597(4)	0.169(4)	0.155(3)	6.0(9)
C10	0.744(2)	0.201(2)	0.230(2)	7.0(6)
C11	0.561(3)	0.438(3)	0.209(3)	4.5(7)
C11'	0.660(4)	0.407(4)	0.141(3)	5.7(9)
C12	0.632(2)	0.532(2)	0.151(2)	7.8(7)
C13	0.471(3)	0.207(3)	0.239(3)	4.4(7)
C13'	0.599(4)	0.363(4)	0.297(3)	7(1)
C14	0.517(2)	0.259(2)	0.353(2)	7.7(7)
C15'	0.410(3)	0.238(3)	0.120(3)	4.8(8)
C15	0.509(3)	0.218(3)	0.072(3)	4.7(8)
C16	0.363(2)	0.188(2)	0.004(2)	6.1(6)

a. B_{eq} is defined as $4/3[a^2\beta_{11}+b^2\beta_{22}+c^2\beta_{33}+ab(\cos\gamma)\beta_{12}+ac(\cos\beta)\beta_{13}+bc(\cos\alpha)\beta_{23}]$.

Table 4·3. Positional Parameters and B_{eq} Values[a] for $(Ph_4P)_2[Fe(CO)_2(Se_4)_2]$ (**4·3**)
(Standard Deviations in Parentheses)

atom	x	y	z	B_{eq}, Å^2
Se1	0.3693(4)	0.8887(3)	0.2959(3)	5.6(1)
Se2	0.5510(5)	1.0116(3)	0.3942(3)	6.4(1)
Se3	0.6873(5)	1.0485(4)	0.3078(4)	6.7(2)
Se4	0.6846(4)	0.8913(4)	0.2775(3)	5.7(1)
Se5	0.5463(5)	0.6783(4)	0.1771(3)	7.1(2)
Se6	0.4861(6)	0.5432(4)	0.2437(4)	9.1(2)
Se7	0.5706(5)	0.6294(4)	0.3812(4)	8.0(2)
Se8	0.4517(4)	0.7265(3)	0.3669(3)	5.6(1)
Fe	0.4535(6)	0.7828(5)	0.2335(4)	5.2(2)
P1	0.0940(9)	0.0367(7)	0.1865(7)	4.3(3)
P2	0.096(1)	0.5128(7)	0.6887(7)	4.9(3)
O1	0.435(3)	0.876(2)	0.087(2)	9(1)
O2	0.200(3)	0.627(2)	0.171(2)	8.6(9)
C1	0.551(4)	0.169(3)	0.859(3)	7(1)
C2	0.712(5)	0.323(4)	0.806(3)	9(2)
C3	0.961(3)	0.095(2)	0.855(2)	4.3(9)
C4	1.062(4)	0.156(3)	0.828(3)	6(1)
C5	1.111(4)	0.255(3)	0.862(3)	8(1)
C6	1.055(4)	0.288(3)	0.913(3)	6(1)
C7	0.955(4)	0.227(3)	0.941(3)	8(1)
C8	0.911(4)	0.126(3)	0.914(3)	7(1)
C9	0.140(3)	0.062(2)	0.298(2)	4.3(9)

Table 4·3. (cont'd)

atom	x	y	z	B_{eq}, Å^2
C10	0.259(3)	0.084(3)	0.347(2)	4.7(9)
C11	0.287(3)	0.103(2)	0.435(2)	4.7(9)
C12	0.196(3)	0.092(3)	0.474(2)	4.9(9)
C13	0.068(4)	0.069(3)	0.420(3)	6(1)
C14	0.039(3)	0.045(3)	0.334(2)	4.8(9)
C15	0.041(3)	0.930(3)	0.856(2)	5.0(9)
C16	0.020(4)	0.834(3)	0.816(3)	6(1)
C17	0.115(4)	0.798(3)	0.841(3)	6(1)
C18	0.234(4)	0.859(3)	0.901(3)	6(1)
C19	0.252(3)	0.952(3)	0.930(3)	5(1)
C20	0.155(3)	0.988(2)	0.902(2)	4.7(9)
C21	0.235(3)	0.102(2)	0.150(2)	4.3(9)
C22	0.336(3)	0.080(3)	0.162(3)	5(1)
C23	0.444(4)	0.131(3)	0.135(3)	5(1)
C24	0.441(4)	0.202(3)	0.089(3)	6(1)
C25	0.336(4)	0.221(3)	0.072(3)	6(1)
C26	0.225(3)	0.176(3)	0.102(3)	5(1)
C27	0.016(3)	0.431(3)	0.346(2)	4.7(9)
C28	0.138(4)	0.464(3)	0.329(3)	6(1)
C29	0.218(3)	0.412(3)	0.354(3)	5(1)
C30	0.175(4)	0.332(3)	0.391(3)	6(1)
C31	0.062(3)	0.304(3)	0.410(3)	5(1)

Table 4-3. (cont'd)

atom	x	y	z	B_{eq}, Å^2
C32	-0.015(4)	0.351(3)	0.387(3)	6(1)
C33	0.237(3)	0.569(2)	0.653(2)	4.4(9)
C34	0.248(3)	0.530(3)	0.578(2)	4.8(9)
C35	0.346(4)	0.575(3)	0.545(3)	7(1)
C36	0.440(4)	0.668(3)	0.591(3)	8(1)
C37	0.429(4)	0.708(3)	0.664(3)	8(1)
C38	0.326(4)	0.662(3)	0.697(3)	7(1)
C39	-0.016(4)	0.615(3)	0.356(3)	6(1)
C40	0.113(3)	0.659(3)	0.410(3)	5(1)
C41	0.159(4)	0.766(3)	0.443(3)	6(1)
C42	0.092(3)	0.814(3)	0.424(3)	6(1)
C43	-0.035(4)	0.773(2)	0.378(3)	7(1)
C44	-0.096(4)	0.671(3)	0.343(3)	6(1)
C45	0.155(3)	0.534(3)	0.804(3)	6(1)
C46	0.086(3)	0.551(3)	0.853(3)	5(1)
C47	0.135(4)	0.567(3)	0.941(3)	6(1)
C48	0.247(4)	0.566(3)	0.976(3)	7(1)
C49	0.317(3)	0.540(3)	0.926(3)	5(1)
C50	0.263(4)	0.524(3)	0.836(3)	7(1)

a. B_{eq} is defined as $4/3[a^2\beta_{11}+b^2\beta_{22}+c^2\beta_{33}+ab(\cos\gamma)\beta_{12}+ac(\cos\beta)\beta_{13}+bc(\cos\alpha)\beta_{23}]$.

Table 4-4. Calculated and Observed X-ray Powder Diffraction Patterns for $(Et_4N)_{1.5}Na_{0.5}[Ru(CO)_2(Se_4)_2]$ (4-1)

h k l	$d_{calc.}$ (Å)	$d_{obs.}$ (Å)	$I/I_{max.}$ (obs.)
0 0 1	12.6	12.9	17
0 1 0	9.5	/	41
1 0-1	9.34	9.47	100
1-1 0	9.17	/	/
1-1-1	7.35	7.39	30
1 0 1	6.49	6.54	69
0 0 2	6.319	6.327	17
2-1 0	5.326	5.332	32
1-1-2	5.257	5.271	14
0 2-1	5.038	5.038	8
0 2 0	4.733	4.740	13
1-2-1	4.643	4.646	7
2-1 2	3.693	3.691	11
3-1 1	3.159	3.157	18
1-2-3	3.054	3.055	21
3-2 2	2.865	2.868	9
1 3-3	2.776	2.788	18
2 0 3	2.689	2.692	10
1-4 3	2.556	2.557	7
4-2 1	2.498	2.493	9
2 3-3	2.375	2.377	13
2 3-4	2.285	2.286	11
1 2-6	2.254	2.253	9

Table 4·5. Calculated and Observed X-ray Powder Diffraction Patterns for $(Ph_4P)_2[Fe(CO)_2(Se_4)_2]$ (4·3)

h k l	$d_{calc.}$ (Å)	$d_{obs.}$ (Å)	$I/I_{max.}$ (obs.)
0 1 0	13.7	13.9	22
0 1-1	11.4	11.6	54
1 0 0	10.27	10.47	100
0 1 1	9.57	9.59	77
1-1-1	9.43	/	/
1-1 1	8.14	8.22	49
0 0 2	7.914	7.926	81
1 0 1	7.675	7.663	31
1 1 1	5.819	/	/
2-1-1	5.722	5.741	20
2 0 0	5.136	5.137	24
2 0-2	5.011	4.980	27
2-1 1	4.915	/	/
0 2-3	4.578	4.581	9
1-1 3	4.434	4.437	26
0 3 1	4.198	4.197	11
2-3 1	4.140	4.159	13
0 0 4	3.957	3.962	10
2 1-3	3.935	/	/
2 0-4	3.684	3.693	9
2-4 0	3.577	3.587	13
1-3 4	3.172	3.181	7

III. Results

1. Description of Crystal and Molecular Structures of the Compounds

(i). Structure of $(Et_4N)_{1.5}Na_{0.5}[Ru(CO)_2(Se_4)_2]$ (4·1)

The crystal lattice of this compound is made up of non-interacting Et_4N^+ cations, interacting Na^+ ions and $[Ru(CO)_2(Se_4)_2]^{2-}$ anions as shown in Figure 4·1. There are two crystallographically independent Et_4N^+ ions. One is situated in a general position, and has the normal tetrahdedral structure. Another Et_4N^+ cation is located on an inversion center 0, 0, 1/2. This causes a structural disorder on the tetrahedral molecule Et_4N^+. The Na^+ ion is found in the second inversion center 0, 1/2, 0, closely associated with two $[Ru(CO)_2(Se_4)_2]^{2-}$ anions. $[Ru(CO)_2(Se_4)_2]^{2-}$ adopts an octahedral geometry with two cis CO groups and two chelating Se_4^{2-} ligands as shown Figure 4·2. The molecule possesses a noncrystallographic 2-fold axis that bisects the C(1)-Ru-C(2) and Se(4)-Ru-Se(8) angles. The Ru-C(1) and Ru-C(2) distances are 1.858(7) and 1.846(7) Å, respectively, with a C(1)-Ru-C(2) angle of 95.0(2)°. The Ru-Se bonds are divided into two sets of short and long distances. The Ru-Se(1) and Ru-Se(5) bonds are trans to each other at 2.517(1) and 2.513(1) Å, and are shorter than the corresponding cis Ru-Se(4) and Ru-Se(8) at 2.566(1) and 2.588(1) Å, respectively. The lengthening of the Ru-Se bonds that are disposed trans to the CO groups reflects the effective competition between the latter and the Se_4^{2-} ligands for both σ (xy orbital) and to a lesser extent π (xz and yz orbitals) bonding to the metal center. The Se_4^{2-} ligands adopt both half-boat (Se(1)/Se(2)/Se(3)/Se(4)) and envelope (Se(5)/Se(6)/Se(7)/Se(8)) conformations. In both Se_4^{2-} ligands there is an alternation of a long Se(external)-Se(internal) average 2.352 (11) Å and a short Se(internal)-Se(internal) average of 2.319(4) Å. The Na^+ is coordinated by two centrosymmetrically disposed $[Ru(CO)_2(Se_4)_2]^{2-}$ anions through the Se(2), Se(4) and Se(8) atoms as shown in Figure 4·3. The six Se atoms create an excellent octahedral pocket for Na^+. The Se···Na distances

range from 2.921(1) to 3.148(1) Å. Selected bond distances and bond angles are given in Table 4·6.

Table 4·6. Selected Geometric Data for $(Et_4N)_{1.5}Na_{0.5}[Ru(CO)_2(Se_4)_2]$ (**4·1**)[b]

		Bond Distances (Å)	
Ru-Se(1)	2.517(1)	Ru-Se(4)	2.566(1)
Ru-Se(5)	2.513(1)	Ru-Se(8)	2.588(1)
Ru-Se(mean)	2.546(18)	Se(1)-Se(2)	2.346(2)
Se(2)-Se(3)	2.323(1)	Se(3)-Se(4)	2.353(1)
Se(5)-Se(6)	2.339(2)	Se(6)-Se(7)	2.315(2)
Se(7)-Se(8)	2.369(1)	Se-Se(mean)	2.341(8)
Se(2)-Na	3.148(1)	Se(4)-Na	2.9395(9)
Se(8)-Na	2.9215(9)	Ru-C(1)	1.858(7)
Ru-C(2)	1.846(7)		
		Bond Angles (deg)	
Se(1)-Ru-Se(4)	97.32(4)	Se(1)-Ru-Se(5)	174.95(5)
Se(1)-Ru-Se(8)	79.45(4)	Se(4)-Ru-Se(5)	80.72(4)
Se(4)-Ru-Se(8)	93.58(3)	Se(5)-Ru-Se(8)	95.99(4)
Se(1)-Se(2)-Se(3)	99.25(5)	Se(2)-Se(3)-Se(4)	97.19(5)
Se(5)-Se(6)-Se(7)	99.64(5)	Se(6)-Se(7)-Se(8)	97.28(5)
C(1)-Ru-Se(1)	93.4(2)	C(1)-Ru-Se(4)	85.4(2)
C(1)-Ru-Se(5)	91.1(2)	C(1)-Ru-Se(8)	172.6(2)
C(2)-Ru-Se(1)	89.4(2)	C(2)-Ru-Se(4)	173.2(2)
C(2)-Ru-Se(5)	92.5(2)	C(2)-Ru-Se(8)	86.9(2)
C(1)-Ru-C(2)	95.0(2)		

b. The estimated standard deviations in the mean bond lengths and the mean bond angles are calculated by the equation $\sigma_l=\{\Sigma_n(l_n-l)^2/n(n-1)\}^{1/2}$, where l_n is the length (angle) of the *n*th bond, l the mean length (angle), and n the number of bonds.

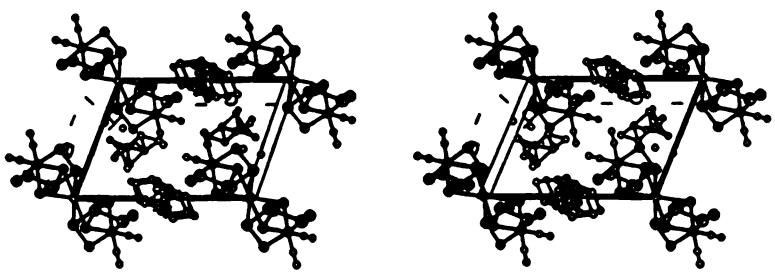


Figure 4·1. The Packing Diagram in the Unit Cell of $(Et_4N)_{1.5}Na_{0.5}[Ru(CO)_2(Se_4)_2]$ (Stereoview). One Et_4N^+ Is Located on an Inversion Center ((0, 0, 1/2)), Showing Disorder

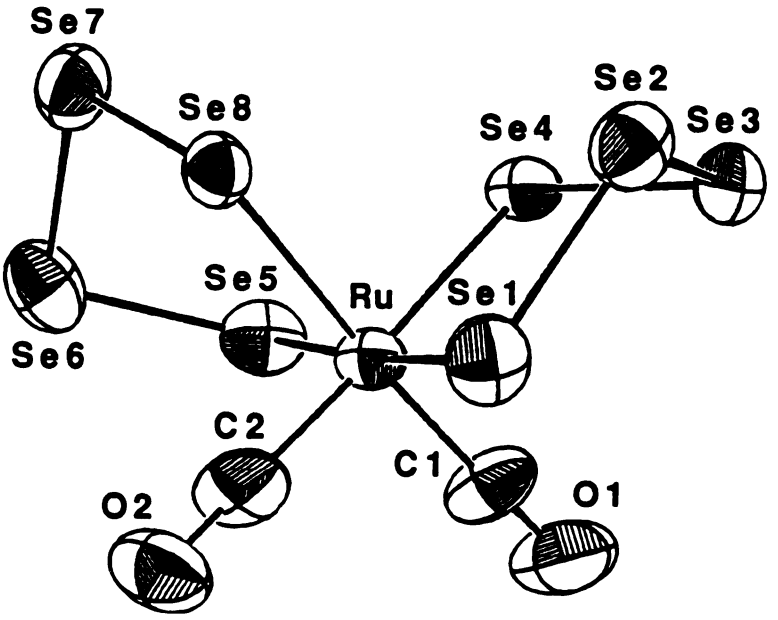


Figure 4·2. The Structure of the $[Ru(CO)_2(Se_4)_2]^{2-}$ Anion

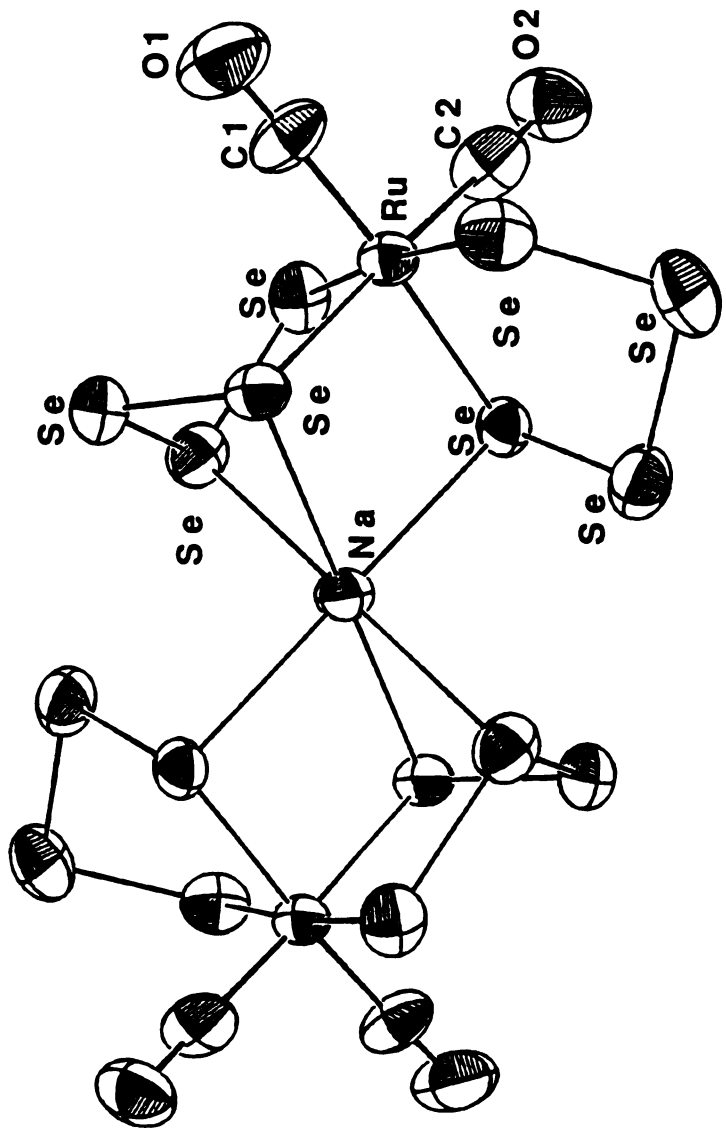


Figure 4-3. ORTEP Representation of the $\{Na[Ru(CO)_2(Se_4)_2]_2\}^{3+}$ Structure, Showing the Coordination of a Na^+ by Two $[Ru(CO)_2(Se_4)_2]^{2-}$ Anions

(ii). Structure of $(Ph_4P)_2[Fe(CO)_2(Se_4)_2]$ (4·3)

The structure of (4·3) is composed of well separated Ph_4P^+ cations and $[Fe(CO)_2(Se_4)_2]^{2-}$ anions in the crystal lattice as shown in Figure 4·4. The Ph_4P^+ cations have the normal tetrahedral structure, and will not be discussed further. The $[Fe(CO)_2(Se_4)_2]^{2-}$ is analogous to its ruthenium counterpart. Figure 4·5 shows the structure of the $[Fe(CO)_2(Se_4)_2]^{2-}$ anion. Due to the large standard deviations in the metric parameters resulted from the crystal decay, a meaningful discussion on the bond distances and bond angles for the structure cannot be made. However, the similar structural features observed in the ruthenium analogue seem to appear in the current structure also. Selected metric parameters for this anion are given in Table 4·7.

Table 4·7. Selected Geometric Data for $(Ph_4P)_2[Fe(CO)_2(Se_4)_2]$ (4·3)[b]

		Bond Distances (Å)	
Fe-Se(1)	2.44(1)	Fe-Se(4)	2.448(7)
Fe-Se(5)	2.44(1)	Fe-Se(8)	2.417(9)
Se(1)-Se(2)	2.354(5)	Se(2)-Se(3)	2.316(9)
Se(3)-Se(4)	2.357(8)	Se(5)-Se(6)	2.327(9)
Se(6)-Se(7)	2.325(9)	Se(7)-Se(8)	2.323(9)
Se-Se(mean)	2.334(7)	Fe-C(1)	1.73(5)
Fe-C(2)	1.90(4)		
		Bond Angles (deg)	
Se(1)-Fe-Se(4)	98.9(3)	Se(1)-Fe-Se(5)	177.3(3)
Se(1)-Fe-Se(8)	80.0(3)	Se(4)-Fe-Se(5)	79.2(3)
Se(4)-Fe-Se(8)	95.7(3)	Se(5)-Fe-Se(8)	98.3(3)

Table 4·7. (con't)

Bond Angles (deg)			
Se(1)-Se(2)-Se(3)	97.5(3)	Se(2)-Se(3)-Se(4)	97.4(3)
Se(5)-Se(6)-Se(7)	96.6(3)	Se(6)-Se(7)-Se(8)	97.8(3)
C(1)-Fe-Se(1)	95(2)	C(1)-Fe-Se(4)	85(1)
C(1)-Fe-Se(5)	87(2)	C(1)-Fe-Se(8)	175(2)
C(2)-Fe-Se(1)	94(2)	C(2)-Fe-Se(4)	167(2)
C(2)-Fe-Se(5)	88(2)	C(2)-Fe-Se(8)	84(2)
C(1)-Fe-C(2)	97(2)		

b. The estimated standard deviations in the mean bond lengths and the mean bond angles are calculated by the equation $\sigma_l=\{\Sigma_n(l_n-l)^2/n(n-1)\}^{1/2}$, where l_n is the length (angle) of the *n*th bond, l the mean length (angle), and n the number of bonds.

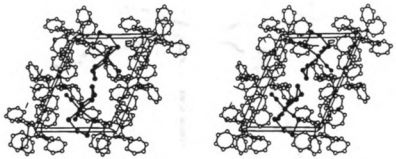


Figure 4-4. The Packing Diagram in the Unit Cell of $(Ph_4P)_2[Fe(CO)_2(Se_4)_2]$ (Stereoview)

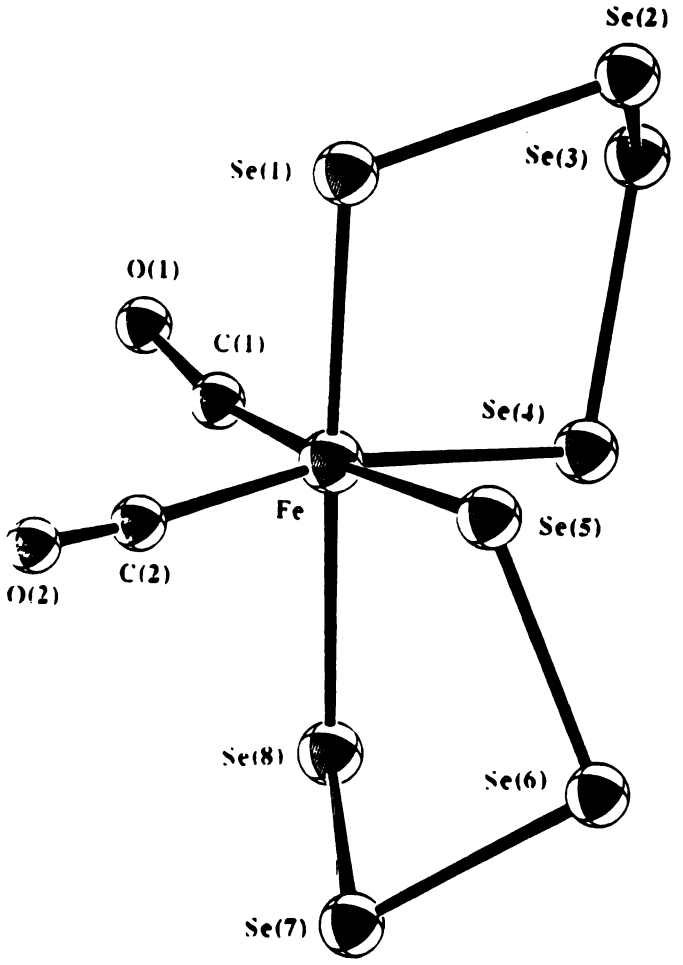


Figure 4·5. The Structure of the $[Fe(CO)_2(Se_4)_2]^{2-}$ Anion

2. Spectroscopic Studies

Three compounds each give two well-resolved peaks for the CO groups as expected for the *cis*-$ML_4(CO)_2$ type molecule. Figure 4·6 show the solid-state IR spectra of $(Et_4N)_{1.5}Na_{0.5}[Ru(CO)_2(Se_4)_2]$ (**4·1**), $(Ph_4P)_2[Ru(CO)_2(Se_4)_2]$ (**4·2**) and $(Ph_4P)_2[Fe(CO)_2(Se_4)_2]$ (**4·3**), respectively, in the CO region. The two peaks at 1999 and 1939 cm^{-1} for (**4·1**), 1981 and 1915 for (**4·2**), and 1958 and 1905 cm^{-1} for (**4·3**) are assigned to the symmetric and anti-symmetric CO stretching vibrations, respectively. The blue shift of two CO vibrations in $(Et_4N)_{1.5}Na_{0.5}[Ru(CO)_2(Se_4)_2]$ with respect to those in $(Ph_4P)_2[Ru(CO)_2(Se_4)_2]$ is consistent with the reduced electron-withdrawing ability of the Se_4^{2-} ligands in this compound because they are corrdinated to a Na^+ ion. In the far IR spectrum of $(Et_4N)_{1.5}Na_{0.5}[Ru(CO)_2(Se_4)_2]$ two strong absorptions are observed at 268 and 248 cm^{-1}, while the far IR spectra of $(Ph_4P)_2[Ru(CO)_2(Se_4)_2]$ and $(Ph_4P)_2[Fe(CO)_2(Se_4)_2]$ are almost superimposable, each showing three absorptions at 269(m), 250 (s) and 199(m) for Ru compound, and 268(s), 255(m) and 207(m) cm^{-1} for Fe compound, respectively (Figure 4·7). The two peaks between 270-250 in each compound are assigned to Se-Se stretching vibrations . The similar assignment has also been made in the far IR spectra of other metal polyselenide compounds or unbound ligands, $[Fe_2Se_{12}]^{2-}$ (ν_{se-se}=258 cm^{-1})[30], $[SnSe_{12}]^{2-}$ (ν_{se-se}=273 and 256 cm^{-1})[31], $[Ag_xSe_y]^{n-}$ (ν_{se-se}=265 cm^{-1})[32], $[Se_x]^{2-}$ (x=2-6, ν_{se-se}=258 cm^{-1})[33] and *cyclo*-Se_6 (ν_{se-se}=258 cm^{-1})[34]. However, the medium peak at 199 cm^{-1} for $(Ph_4P)_2[Ru(CO)_2(Se_4)_2]$ and 207 cm^{-1} for $(Ph_4P)_2[Fe(CO)_2(Se_4)_2]$ cannot be assigned at this time.

All three compounds are soluble in CH_3CN and DMF, giving featureless UV/vis spectra. The absence of any absorptions due to Se_x^{2-} species suggests that the compounds maintain their integrity in these solvents. The DMF solution of each compound gives a single ^{13}C resonance, attributable to two CO groups, at 199 for Ru, and 209 for the Fe, as

expected for a species with C_2 symmetry. Consistent with the C_2 group symmetry, four peaks are observed at 717, 650, 630 and 395 ppm for Ru, and 720, 706, 679 and 445 ppm for the Fe in the ^{77}Se NMR spectra of DMF solutions as shown in Figure 4·8. The DMF solution of $(Et_4N)_{1.5}Na_{0.5}[Ru(CO)_2(Se_4)_2]$ shows a single ^{23}Na resonance at 0.7 ppm (see Figure 4·8), indicating that in solution the Na^+ ion is no longer associated with the the anions.

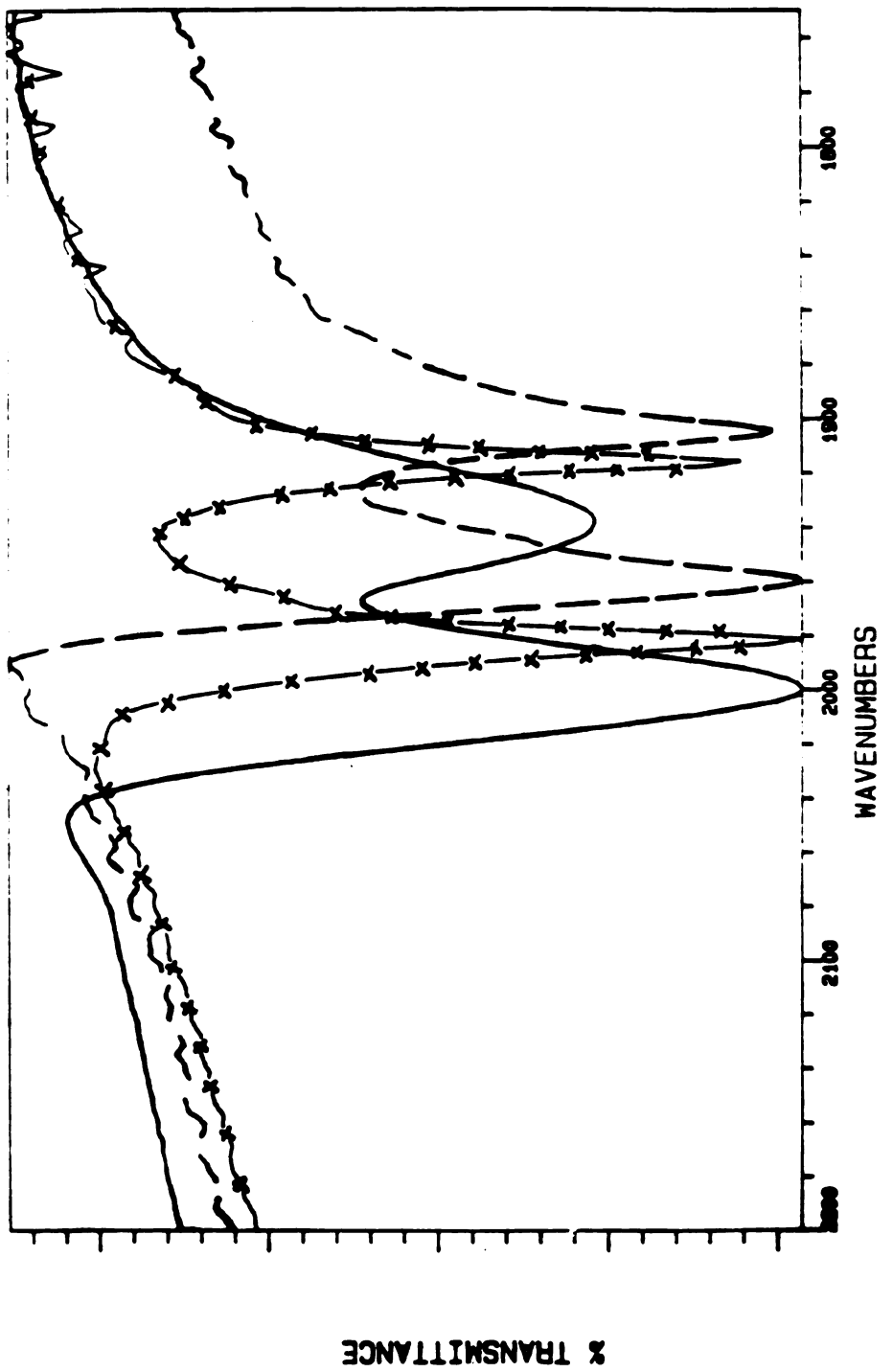


Figure 4-6 The Solid-State IR Spectra in the CO Region for (—) $(Et_4N)_{1.5}Na_{0.5}[Ru(CO)_2(Se_4)_2]$, (-x-x-x-) $(Ph_4P)_2[Ru(CO)_2(Se_4)_2]$ and (----)) $(Ph_4P)_2[Fe(CO)_2(Se_4)_2]$

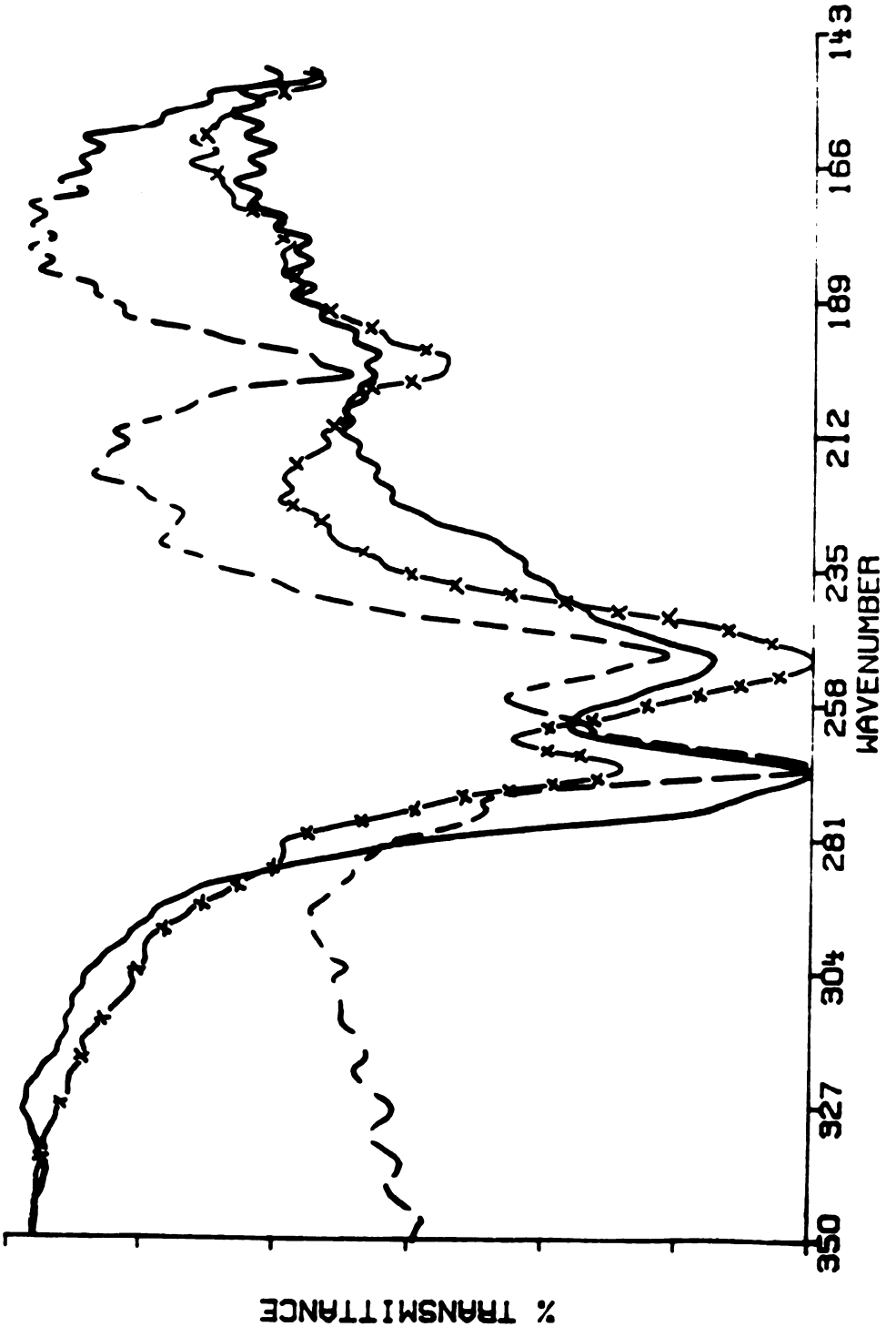


Figure 4·7 The Solid-State Far IR Spectra of (—) $(Et_4N)_{1.5}Na_{0.5}[Ru(CO)_2(Se_4)_2]$, (-x-x-x-) $(Ph_4P)_2[Ru(CO)_2(Se_4)_2]$ and (----)) $(Ph_4P)_2[Fe(CO)_2(Se_4)_2]$

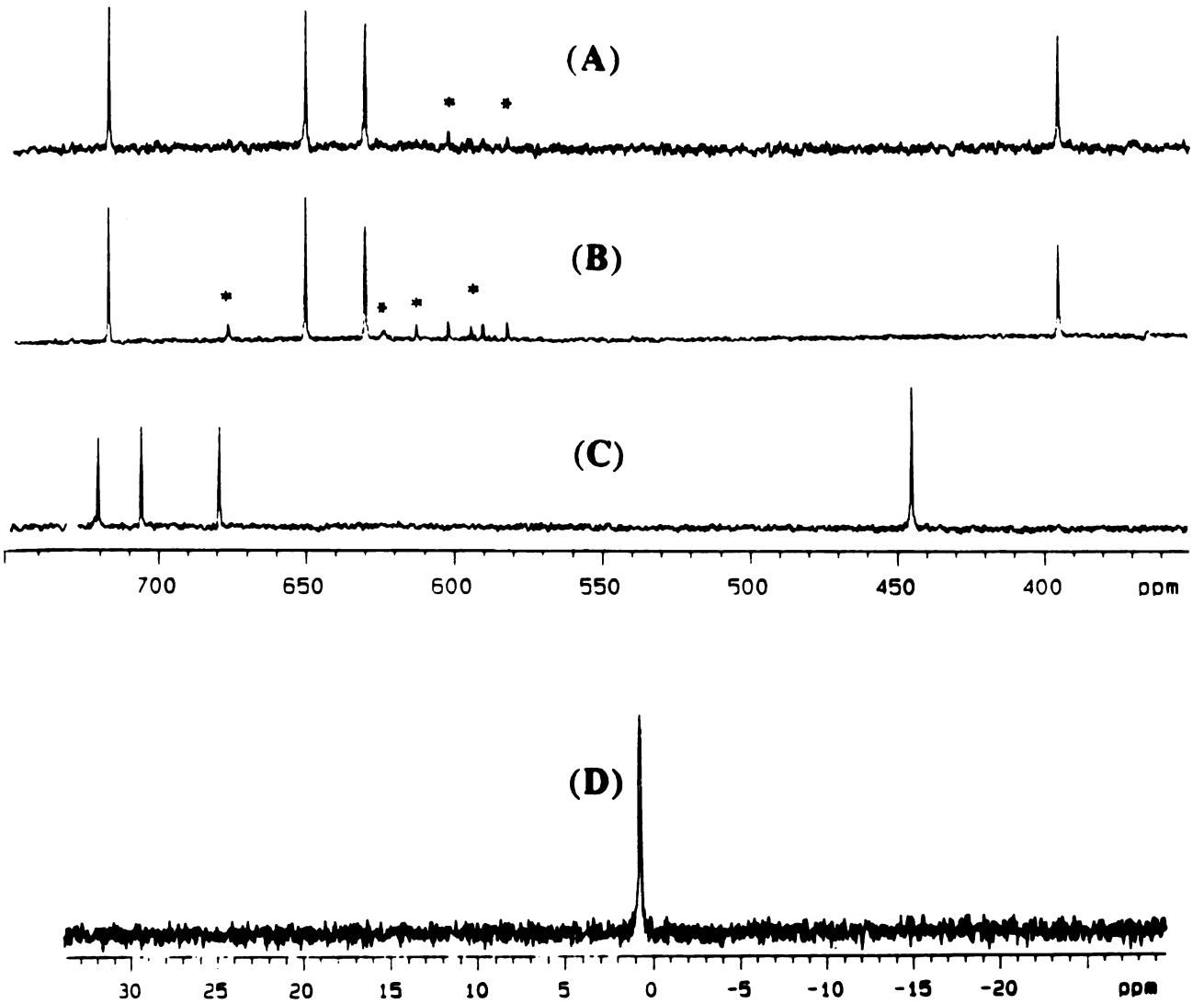


Figure 4-8. The ^{77}Se NMR Spectra of (A) $(Et_4N)_{1.5}Na_{0.5}[Ru(CO)_2(Se_4)_2]$ and (B) $(Ph_4P)_2[Ru(CO)_2(Se_4)_2]$, (C) $(Ph_4P)_2[Fe(CO)_2(Se_4)_2]$ and ^{23}Na NMR Spectrum of (D) $(Et_4N)_{1.5}Na_{0.5}[Ru(CO)_2(Se_4)_2]$. * Peak From Impurities.

3. Thermal Decomposition

Under N_2 flow, all three compounds undergo multiple-step thermal decompositions as shown in Figure 4·9. The observed and calculated values of weight loss for each step of thermolysis are compared in Table 4·8 along with the proposed residue formula.

The final product from the thermolysis of $(Et_4N)_{1.5}Na_{0.5}[Ru(CO)_2(Se_4)_2]$ corresponds to a composition $Na_{0.5}RuSe$. The XRD studies showed the product does not contain $RuSe_2$–the only known Ru/Se binary phase[35a]. Since there is no known ternary Na/Ru/Se phase the XRD pattern can not be indexed at this moment. Both $(Ph_4P)_2[Ru(CO)_2(Se_4)_2]$ and $(Ph_4P)_2[Fe(CO)_2(Se_4)_2]$ follow a similar thermal decomposition pathway. The final products deduced from the weight loss have the formulas $RuSe_2$ and $FeSe_2$, respectively. The XRD patterns confirmed that they are ruthenium selenide $RuSe_2$[35b] and ferroselite $FeSe_2$[35c].

Table 4·8. Thermal Gravimetric Analysis Data for $(Et_4N)_{1.5}Na_{0.5}[Ru(CO)_2(Se_4)_2]$ (4·1), $(Ph_4P)_2[Fe(CO)_2(Se_4)_2]$ (4·2) and $(Ph_4P)_2[Fe(CO)_2(Se_4)_2]$ (4·3)

Step	onset temp °C	final temp °C	obsd % wt loss*	calcd % wt loss*	proposed residue formula
			(4·1)		
1	135	275	44.26	43.87	$1/4Na_2Se+RuSe_{5.4}$
2	350	484	71.60	70.84	$1/4Na_2Se+RuSe_2$
3	484	772	81.67	80.75	$Na_{0.5}RuSe$
			(4·2)		
1	193	224	4.02	3.82	$(Ph_4P)_2[RuSe_8]$
2	224	423	61.52	60.84	$FeSe_6$
3	423	698	84.96	82.35	$RuSe_2$

Table 4·8. (cont'd)

Step	onset temp °C	final temp °C	obsd % wt loss*	calcd % wt loss*	proposed residue formula
			(4·3)		
1	148	175	4.01	3.94	$(Ph_4P)_2[FeSe_8]$
2	265	329	58.38	57.20	$FeSe_7$
3	329	402	76.65	76.63	$FeSe_{3.5}$
4	525	745	86.47	84.96	$FeSe_2$

* initial sample weight=100%

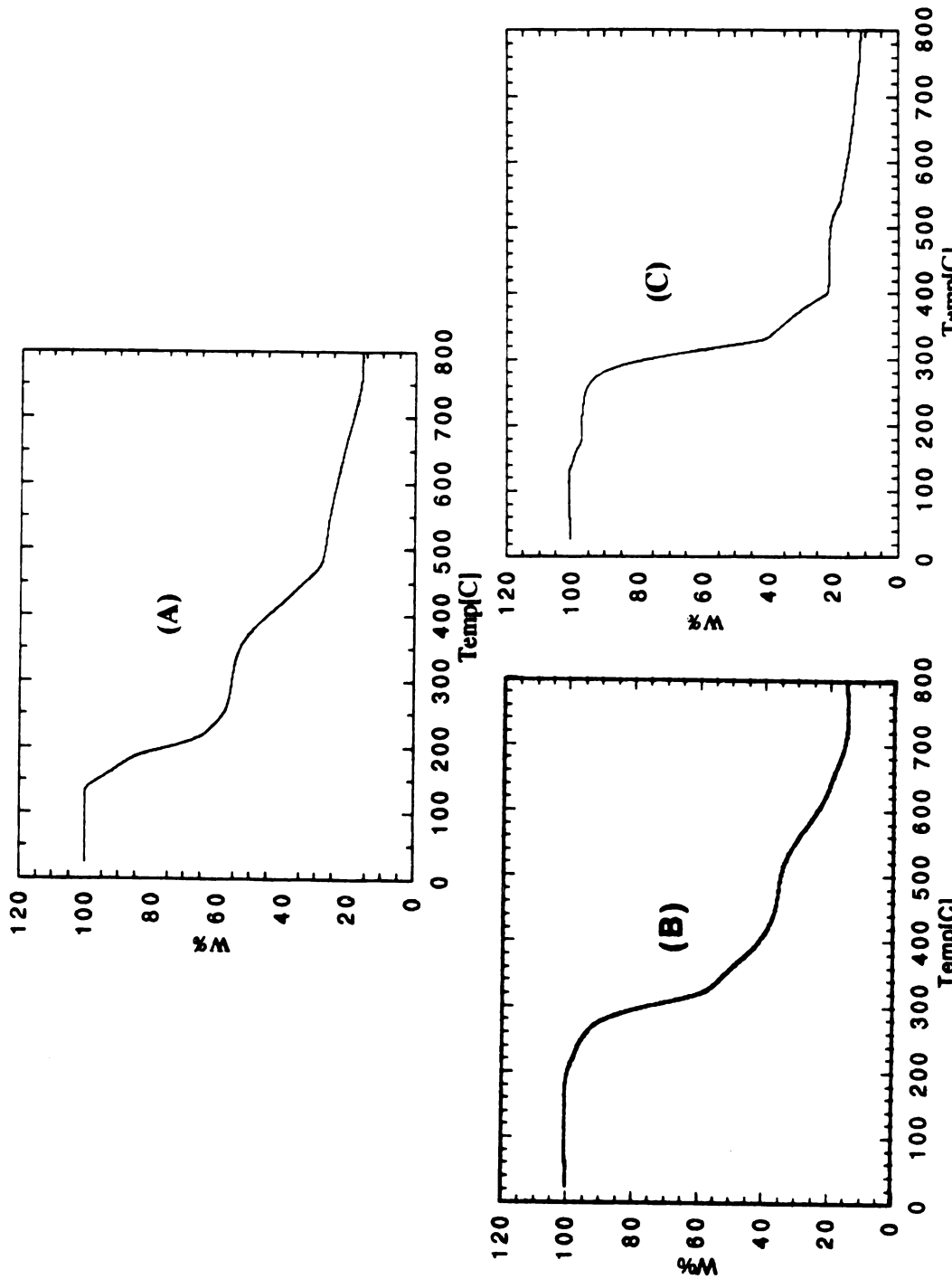


Figure 4-9. The TGA diagrams of (A) $(Et_4N)_{1.5}Na_{0.5}[Ru(CO)_2(Se_4)_2]$, (B) $(Ph_4P)_2[Ru(CO)_2(Se_4)_2]$ and (C) $(Ph_4P)_2[Fe(CO)_2(Se_4)_2]$

IV. Discussion

$Ru_3(CO)_{12}$ and $Fe(CO)_5$ react readily with sodium pentaselenide in acetone to form the anionic complexes $[M(CO)_2(Se_4)_2]$ (M=Ru and Fe). Such oxidative decarbonylation reactions result in a change in the oxidation state of the metal center with concomitant partial loss of its CO groups:

$$Ru_3(CO)_{12}+Na_2Se_5 \xrightarrow[Et_4NCl]{\text{acetone, r.t.}} (Et_4N)_{1.5}Na_{0.5}[Ru(CO)_2(Se_4)_2]+NaCl+CO \qquad \text{eq.(4·1)}$$

$$Ru_3(CO)_{12}+Na_2Se_5 \xrightarrow[Ph_4PCl]{\text{acetone, r.t.}} (Ph_4P)_2[Ru(CO)_2(Se_4)_2]+NaCl+CO \qquad \text{eq.(4·2)}$$

$$Fe(CO)_5+Na_2Se_5 \xrightarrow[Ph_4PCl]{\text{acetone, b.p.}} (Ph_4P)_2[Fe(CO)_2(Se_4)_2]+NaCl+CO \qquad \text{eq.(4·3)}$$

The structures of both $(Et_4N)_{1.5}Na_{0.5}[Ru(CO)_2(Se_4)_2]$ and $(Ph_4P)_2[Fe(CO)_2(Se_4)_2]$ are established by X-ray single crystal analysis. Although we have not been able to solve the X-ray structure of $(Ph_4P)_2[Ru(CO)_2(Se_4)_2]$, there is little doubt from the spectroscopic data that this compound is analogous to $(Ph_4P)_2[Fe(CO)_2(Se_4)_2]$. In the preparation of all these compounds, the Se_5^{2-} ligand is believed to act as oxidant by splitting its Se-Se bonds[14]. Similar reactions have been observed to occur between $Ru_3(CO)_{12}$/$Fe(CO)_5$ and K_2Te_4. In each case, the IR spectrum in the CO region suggests that the $[M(CO)_2(Te_n)_2]^{2-}$-type molecule also forms. Thus far we have not been successful in isolating any of these products in pure form. Although semi-quantitative elemental analyses by EDAX on the freshly formed products indicate that they contain the metal and tellurium in the 1:8–1:10 ratios, upon standing during crystallization/recrystallization, the products often decompose to give elemental tellurium.

Recently, Rauchfuss and co-workers have discovered that N-alkylimidazoles can greatly promote the reactivity of elemental chalcogens (i.e. S and Se) towards low valent metal species, particularly metal powders and metal carbonyls[36]. The N-alkylimidazole suspension of elemental selenium is found to react with $Fe(CO)_5$ to produce a polyselenide compound[36b]:

$$2Fe(CO)_5 + Se_8 \xrightarrow{\text{N-MeIm, 25 °C}} [Fe(\text{N-MeIm})_6][Fe(Se_4)_2(CO)_2] + 8CO \quad \text{eq.(4·4)}$$

The identity of this compound has been established by X-ray single crystal analysis. The anion of this compound has essentially the same structure as that in (**4·3**). The above reaction constitutes another useful synthetic route to the octahedral complex of the iron polyselenide.

It is interesting to note that compounds (**4·1**)–(**4·3**) contain Se_4^{2-} ligands while the nominal composition of the ligand used was Na_2Se_5. This is because a complex equilibrium of different Se_n^{2-} species is established in solution[37-40], which allows for the metal to choose a preferable chain length. Such a phenomenon has been observed for many other metal polysulfide, polyselenide and polytelluride systems[13-14, 32, 37-38, 41-42].

The $[Ru(Se_4)_2(CO)_2]^{2-}$ is the first structurally characterized ruthenium polyselenide complex. Two cationic species containing the diselenide, $[\{CpRu(Ph_3P)_2\}_2Se_2](OTf)_2$ and $[\{(MeCp)Ru(Ph_3P)\}_2(Se_2)_2](OTf)_2$, have been recently reported[12], whereas iron polyselenide complexes are relatively common. Structurally characterized compounds include $[Fe_2(Se_2)(CO)_6]$[43], $(Ph_4P)_2[Fe_4Se_2(Se_2)(CO)_{12}]$[44], $(Ph_4P)_2[Fe_2Se_2(Se_5)_2]$[30] and $(Ph_4P)_2[Fe(Se_4)_2]$[45]. It should be noted that the latter two homoleptic compounds contain Se_5^{2-} and Se_4^{2-}, respectively, with the metal center having a formal oxidation state 3+ and 2+. It appears that in the $Fe^{n+}(n=2, 3)/Se_x^{2-}$

system, the high oxidation state of the metal center favors the six-membered $FeSe_5$ ring, while the five-membered $FeSe_4$ ring is formed if the metal center is in the low oxidation state. The ring size of the current iron carbonyl polyselenide compound seems to be consistent with this notion.

Coordination of a Na^+ ion by two $[Ru(CO)_2(Se_4)_2]^{2-}$ molecules in the crystal lattice is, in a sense, reminiscent of organic crown ethers. The similar interactions between the Na^+ and the Se^{2-} ligands have also been observed in an indium polyselenide cluster $[NaIn_6Se_{30}]^{5-}$[38c], where a Na^+ ion is encapsulated in an octahedral pocket created by six Se^{2-} ligands from the twelve-membered $[In_6Se_6]^{6+}$ ring. Other known inorganic crown ether-like metal chalcogenide complexes that act as chelates to encapsulate alkali-metal ions are $[Na_2(Fe_6S_9(SMe)_2)_2]^{6-}$[46] and $[Na_2Fe_{18}S_{30}]^{8-}$[47].

In summary, both $Ru_3(CO)_{12}$ and $Fe(CO)_5$ exhibit well behaved reactivity towards polyselenide ligands in solution at ambient temperatures. The partial oxidative decarbonylation of the metal center by polyselenide ligands in such reactions retains two strong π ligands, i.e. CO, in the isolated complex. This has so far proven to be necessary in preventing the complex electron transfer between Ru^{n+} (n=2, 3 and 4) ions and polychalcogenide ligands, thus allowing for the isolation of the first ruthenium complex containing Se_4^{2-} ligands. This finding also defines new opportunities in Ru^+/S_x^{2-} chemistry.

REFERENCES

1. See chapter 2.

2. H. Vahrenkamp, *Adv. Organomet. Chem.*, 22(1983), 169-208.

3. W. A. Herrmann, *Angew. Chem. Int. Ed. Engl.*, 25(1986), 56-76.

4. K. H. Whitmire, *J. Coord. Chem.*, 17(1988), 95-203.

5. J. Wachter, *Angew. Chem. Int. Ed. Engl.*, 28(1989), 1613-1626.

6. D. H. Farrar, K. R. Grundy, N. C. Payne, W. R. Roper and A. Walker, *J. Am. Chem. Soc.*, 101(1979), 6577-6582.

7. (a) A. P. Ginsberg, W. E. Lindsell, C. R. Sprinrle, K. W. West and R. L. Cohen,.*Inorg. Chem.*, 21(1982), 3666-3681. (b) A. P. Ginsberg, W. E. Lindsell, C. R. Sprinrle, K. W. West and R. L. Cohen, *Inorg. Chem.*, 22(1983), 1781-1790.

8. M. Herberhold, D. Reiner and U. Thewalt, *Angew. Chem. Int. Ed. Engl.*, 22(1983), 1000-1001.

9. L. Y. Goh, C. Wei and E. Sinn, *J. Chem. Soc., Chem. Commun.*, (1985), 462-464.

10. W. A. Herrmann and J. Rohrmann, *Chem. Ber.*, 119(1986), 1437-1440.

11. (a) H. Brunner, W. Meier, B. Nuber, J. Wachter and M. L. Ziegler, *Angew. Chem. Int. Ed. Engl.*, 25(1986), 907-908. (b) H. Brunner, N. Janietz, W. Meier, J. Wachter, E. Herdtweck, W. A. Herrmann, O. Serhadli and M. L. Ziegler, *J. Organomet. Chem.*, 347(1988), 237-252.

12. J. Amarasekera, E. J. Houser, T. A. Rauchfuss and C. L. Stern, *Inorg. Chem.*, 31(1992), 1614-1620.

13. M. G. Kanatzidis and S.-P. Huang, submitted to *Coord. Chem. Rev.*

14. J. W. Kolis, *Coord. Chem. Rev.*, 105(1990), 195-219.

15. S. C. O'Neal and J. W. Kolis, *J. Am. Chem. Soc.*, 110(1988), 1971-1973.

16. W. A. Flomer, S. C. O'Neal, J. W. Kolis, D. Jeter, and A. W. Cordes, *Inorg. Chem.*, 27(1988) , 969-971.

17. S. C. O'Neal and J. W. Kolis, *Inorg. Chem.*, 28(1989), 2780-2783.

18. L. C. Roof, W. T. Pennington and J. W. Kolis, *J. Am. Chem. Soc.*, 112(1990), 8172-8174.

19. (a) B. C. Gates, J. R. Katzer and G. C. A. Schuit, *Chemistry of Catalytic Processes*, McGraw-Hill, New York, 1979. (b) O. Weisser and S. Landa,*Sulfide Catalytsis : Their Properties and Applications*, Pergamon, Oxford, 1973.

20. (a) R. R. Chianelli, *Catal. Rev-Sci. Eng.*, 26(1984), 361-393. (b) R. R. Chianelli, T. A. Pecoraro, T. R. Halbert, W.-H. Pan and E. I. Stieflel, *J. Catal.*, 86(1984), 226-230. (c) S. Harris and R. R. Chianelli, *J. Catal.*, 86(1984), 400-412. (d) T. A. Pecoraro and R. R. Chianelli, *J. Catal.*, 67(1981), 430-445.

21. (a) E. G. Derouane, E. Pedersen, B. S. Clausen, Z. Gabelica, R. Candia and H. Topsoe, *J. Catal.*, 99(1986), 253-261. (b) J. T. Roberts and C. M. Frien, *J. Am. Chem. Soc.*, 108(1986), 7204-7210.

22. R. J. Angelici, *Acc. Chem. Res.*, 21(1988), 387-394.

23. S.-P. Huang and M. G. Kanatzidis, unpublished results.

24. D. D. Perrin, W. L. F. Armarego and D. R. Perrin, *Purification of Laboratory Chemicals,* 2nd Ed., Pergamon Press, Oxford UK, 1980.

25. See chapter 2.

26. N. Walker and D. Stuart, *Acta Crystallogr.,* 39A(1983), 158-166.

27. (a) G. M. Sheldrick in *Crystallographic Computing,* G. M. Sheldrick, C. Kruger, and R. Doddard, Oxford University Press, 1985, p.175-189. (b) B. A. Frenz, The Enraf-Nonius CAD4 SDP System. in *Computing in Crystallography*; Delft University Press, Delft Holland, 1978; p.64-71.

28. H. P. Klug and L. E. Alexander, *X-ray Diffraction Procedures for Polycrystalline and Amorphous Materials,* John Wiley and Sons, New York, 1974.

29. D. K. Smith, M. C. Nichols and M. E. Zolensky, *POWD10: A Fortran IV Program for Calculating X-ray Powder Diffration Patterns,* Version 10, Pennsylvania State University, 1983.

30. H. Strasdeit, B. Krebs and G. Henkel, *Inorg. Chim. Acta* , 89(1984), L11-L13.

31. S.-P. Huang, S. Dhingra and M. G. Kanatzidis, *Polyhedron* , 9(1990), 1389-1395.

32. S.-P. Huang and M. G. Kanatzidis, *Inorg. Chem.*, 30(1991), 1455-1466.

33. F. Weller, J. Adel and K. Dehnicke, *Z. Anorg. Allg. Chem.*, 548(1987), 125-132.

34. K. Nagata, K. Tshibashi and Y. Miyamoto, *Jpn. J. Appl. Phys.*, 19(1980), 1569-1573.

35. JCPDS International Center for Diffration Data, (a) Powder Diffration File 3-1198 (b) Powder Diffration File 3-1198. (c) Powder Diffration File 21-432.

36. (a) S. Dev, E. Ramli, T. B. Rauchfuss and C. L. Stern, *J. Am. Chem. Soc.*, 112(1990), 6385-6386. (b) T. A. Rauchfuss, S. Dev and S. R. Wilson, *Inorg. Chem.*, 31(1992), 153-154.

37. M. G. Kanatzidis, *Comments Inorg. Chem.*, 10(1990), 161-195.

38. (a) M. G. Kanatzidis and S. Dhingra, *Inorg. Chem.*, 28(1989), 2024-2026. (b) S. Dhingra and M. G. Kanatzidis, submitted to *Inorg. Chem.* (c) S. Dhingra, Ph.D. Thesis, Michigan State University, 1992.

39. L. D. Schultz and W. H. Koehler, *Inorg. Chem.*, 26(1987), 1989-1993.

40. M. Bjorgvinsson and G. J. Schrobilgen, *Inorg. Chem.*, 30(1991), 2540-2547.

41. M. Draganjac and T. B. Rauchfuss, *Angew. Chem. Int. Ed. Engl* , 24(1985), 742-757.

42. (a) A. Müller, *Polyhedron* , 5(1986), 323-340. (b) A. Müller and E. Diemann, *Adv. Inorg. Chem.*, 31(1987), 89-122.

43. (a) W. Hieber and J. Gruber, *Z. Anorg. Allg. Chem.*, 296(1958), 91-103. (b) C. F. Campana, F. Y.-K Lo and L. F. Dahl, *Inorg. Chem.*, 18(1979), 3060-3064.

44. See Chapter 5.

45. K.-W. Kim and M. G. Kanatzidis, manuscript in preparation.

46. J.-F. You, B. S. Snyder, G. C. Papaefthymiou and R. H. Holm, *J. Am. Chem. Soc,* 112(1990), 6589-6591.

47. J. F. You, B. S. Snyder and R. H. Holm, *J. Am. Chem. Soc.*, 110(1988), 6589-6591.

CHAPTER 5

HYDRO(METHANO)THERMAL SYNTHESIS OF METAL CARBONYL CHALCOGENIDE CLUSTERS OF GROUP 8 ELEMENTS

I. Introduction

Recently, research carried out in this group has demonstrated that the application of hydrothermal technique to the synthesis of transition metal polychalcogenide compounds can afford novel metal polychalcogenide clusters inaccessible by solution method[1-2]. This was first shown by the preparation of a large cluster $K_{12}[Mo_{12}Se_8(Se_2)_{18}(Se_3)_4]$ as the prelude[2], followed by the syntheses of several other transition metal polyselenide clusters[3]. Such a discovery has opened up a new avenue to the cluster chemistry of transition metal polychalcogenides.

Encouraged by the above results, we set out to explore the possibility of applying hydro(solvo)thermal technique to the synthesis of chalcogen-containing transition metal carbonyl clusters. The incorporation of main group elements into transition metal clusters often introduces unique structural features and unusual reactivities, thus providing many new opportunities for studies of structural principles and new chemical reactions[4-6]. One particular area of current interest is the preparation of chalcogen-containing metal carbonyl clusters[7-10]. Syntheses designed to produce novel metal carbonyl clusters containing chalcogens have imposed a great challenge to the cluster chemist and still occupy a prominent position in this research area[6-10]. A common approach to obtaining large clusters is to react a chalcogen-containing cluster either with a complex having labile groups or with a coordinatively unsaturated species generated *in-situ* by UV irradiation[11]. This

has been particularly successful in the synthesis of many sulfur-containing metal clusters[6, 7b, 11b-c]. However, such reactions often suffer low yields and require lengthy separation procedures. We demonstrated for the first time that under the hydro(solvo)thermal conditions direct reactions between metal carbonyls and polychalcogenide ligands can lead to the formation of novel metal carbonyl chalcogenide clusters. In this chapter we wish to describe three novel metal carbonyl/heavy polychalcogenide clusters of group 8 elements, $(Ph_4P)_2[Ru_6(Te_2)_7(CO)_{12}]$ (**5·1**), $(Ph_4P)_2[\{Fe_4Te_4(CO)_{10}\}_2(Te_2)]$ (**5·2**) and $(Ph_4P)_2[\{Fe_2Se(CO)_6\}_2(Se_2)]$ (**5·3**), obtained from hydro(methano)thermal reactions.

II. Experimental Section

1. Reagents

Chemicals in this work other than solvents were used as obtained: (i) selenium powder, ~100 mesh, 99.5% purity, Aldrich Chemical Company, Inc., Milwaukee, WI; (ii) tellurium powder, ~200 mesh, 99.8% purity, Aldrich Chemical Company, Inc., Milwaukee, WI; (iii) sodium sticks in kerosene, 99% purity, Mallinckrodt Inc., Paris, Ky.; (iv) iron pentacarbonyl, $Fe(CO)_5$, Strem Chemicals, Inc., Newburyport, MA; (v) ruthenium carbonyl, $Ru_3(CO)_{12}$, Strem Chemicals, Inc., Newburyport, MA; (vi) tetraphenylphosphonium chloride, Ph_4PCl, 98% purity, Aldrich Chemical Company, Inc., Milwaukee, WI.

Diethyl ether (A.C.S. anhydrous, Columbus Chemical Industries Inc., Columbus, WI) was distilled under a dry N_2 blanket after being refluxed with potassium metal, benzophenone and triethylene glycol dimethyl ether for 12 hours[12].

Methanol (GR anhydrous, EM Science Inc., Gibbstown, NY) was refluxed for 4-5 h with magnesium methoxide (prepared from dry magnesium turnings and absolute methanol), and distilled under a nitrogen atmosphere[12].

2. Physical Measurements

Semi-quantitative elemental analyses, FT-IR, UV/vis and ^{77}Se NMR spectroscopic studies, and thermal gravimetric analyses (TGA) of the compounds were carried out as described previously[13].

3. Syntheses

All syntheses were carried out under a dry nitrogen atmosphere in a Vacuum Atmospheres Dri-Lab glovebox.

(i). Preparation of Na_2Se_2 and Na_2Te_2

These materials were prepared by reacting stoichiometric amount of chalcogen and sodium metal in a routine procedure used in this laboratory[13].

(ii). Preparation of $(Ph_4P)_2[Ru_6(Te_2)_7(CO)_{12}]$ (5·1)

64 mg (0.1 mmol) $Ru_3(CO)_{12}$ was mixed with 150 mg (0.5 mmol) Na_2Te_2 and 220 mg (0.6 mmol) Ph_4PCl. The reactants were sealed with 0.5 ml H_2O in a 25 cm long thick-walled Pyrex tube (~4 ml volume) by freezing with liquid N_2, and evacuated. The tube was heated at 110 °C for 65 hours. Washing of the reaction mixture with methanol and diethyl-ether afforded black needle-like single crystals of $(Ph_4P)_2[Ru_6(Te_2)_7(CO)_{12}]$ (~70 mg) and some dark brown crystalline powder (~60 mg). Crystals suitable for X-ray single-crystal analysis were harvested by mechanical separation. Later, the X-ray powder diffraction (XRD) and IR spectroscopic studies showed that the dark brown powder is

identical to the black crystals (total yield of 71 % based on Ru). Mid-IR spectrum (of solid-state):1997(s), 1966(w), 1957(sh) and 1948(m) cm^{-1}; Far IR spectrum (of solid-state): 228(m, b), 188(s), 175(s) and 164(w) cm^{-1}; Semi-quantitative elemental analyses by EDAX (atom%): Te:Ru:P=59:29:12.

(iii). Preparation of $(Ph_4P)_2[\{Fe_4Te_4(CO)_{10}\}_2(Te_2)]$ (5·2)

120 mg (0.4 mmol) Na_2Te_2 and 220 mg (0.6 mmol) Ph_4PCl were thoroughly mixed and loaded into a 25 cm long thick-walled Pyrex tube (9 mm in diameter) in which 0.15 ml (1.14 mmol) $Fe(CO)_5$ had already been added. After 0.5 ml H_2O was syringed in, the tube was frozen with liquid N_2, then evacuated and sealed (the total volume is ~ 4 ml after sealing). Continuous heating of the tube at 110 °C for 60 h resulted in large plate-like black crystals. Successive washing of the product with MeOH and ether afforded 100 mg analytically pure single crystals (67% yield based on Na_2Te_2). Mid-IR spectrum (of solid-state): 2013(s, multiple), 1968(s), 1951(sh), 1940(sh), 1912(m) and 1900(m) cm^{-1}; Far IR spectrum (of solid-state): 209(w, b and triplet), 151(m) and 140(m) cm^{-1}; Semi-quantitative elemental analyses by EDAX (atom%): Te:Fe:P=14:36:50.

(iv). Preparation of $(Ph_4P)_2[\{Fe_2Se(CO)_6\}_2(Se_2)]$ (5·3)

This compound is prepared in a similar manner as above, except that the sealed tube contained 0.15 ml (1.14 mmol) $Fe(CO)_5$, 82mg (0.4 mmol) Na_2Se_2, 220 (0.6 mmol) Ph_4PCl and 0.8 ml MeOH. The reaction was carried out at 80 °C for 96 h. During this time, the tube had been taken out and shaken three times in a ~24 h interval to homogenize the tube content. 117 mg needle-like black crystals were obtained (75% yield based on Na_2Se_2). Mid-IR spectrum (of solid-state): 2020(m), 1984(s) and1939(s) and 1917(sh) cm^{-1}; Far IR spectrum (of solid-state): 243(m), 224(w) 206(w) and 198(w, doublet) cm^{-1}; Semi-quantitative elemental analyses by EDAX (atom%): Se:Fe:P=31:44:25; ^{77}Se NMR (in DMF): 450 and -32 ppm.

4. X-ray Diffraction and Crystallographic Studies

The single crystal X-ray diffraction studies were performed by using either a Nicolet P3 four-circle difractometer or a Rigaku automated AFC6S single crystal diffractometer.

The crystallographic data set of (5·1) was collected on the Nicolet P3 diffractometer using a θ-2θ scan mode and Mo Kα radiation. The crystallographic data sets of (5·2) and (5·3) were collected on a Rigaku AFC6S four-circle diffractometer using $\omega-2\theta$ scan techniques and Mo Kα radiation. A crystal of (5·2) was mounted in a glass capillary and sealed. Crystals of (5·1) and (5·3) were each affixed to the tip of a glass fiber, and the intensity data were measured at low temperatures. The stability of the experimental setup and crystal integrity for each data collection was monitored by measuring three representative reflections periodically (every 150). No statistically significant change of intensities was detected for the standards. Empirical absorption corrections based on ψ scans of three strong reflections with χ~90° were applied to each data set.

The structures were solved with direct methods and refined with full-matrix least squares techniques. DIFABS corrections, after isotropic refinement of all atoms, were then applied[14]. The calculations were performed on a VAXstation 3100 computer using the TEXSAN crystallographic software package of Molecular Structure Corporation[15]. Table 5·1 gives crystal data and details for structure analysis of the three compounds. All non-hydrogen atoms were refined either isotropically or anisotropically. The hydrogen positions were calculated but not refined. The final coordinates and average temperature factors (B_{iso}) of the atoms in (5·1), (5·2) and (5·3) are given in Tables 5·2-5·4, respectively.

Table 5·1. Data for Crystal Structure Analysis of $(Ph_4P)_2[Ru_6(Te_2)_7(CO)_{12}]$ (**5·1**), $(Ph_4P)_2[\{Fe_4Te_4(CO)_{10}\}_2(Te_2)]$ (**5·2**) and $(Ph_4P)_2[\{Fe_2Se(CO)_6\}_2(Se_2)]$ (**5·3**)

compound	**5·1**	**5·2**	**5·3**
formula	$C_{60}H_{40}O_{12}P_2Ru_6Te_{14}$	$C_{68}H_{40}O_{20}P_2Fe_8Te_{10}$	$C_{60}H_{40}P_2O_{12}Fe_4Se_4$
a, Å	13.492(3)	14.930(4)	10.561(6)
b, Å	13.474(4)	24.070(3)	14.021(5)
c, Å	14.438(3)	13.045(2)	20.46(1)
α, deg	114.77(2)	93.19(1)	90.00
β, deg	116.50(2)	113.36(1)	91.89(4)
γ, deg	90.74(2)	76.61(2)	90.00
Z; V, Å^3	2, 2067(3)	2, 4183(3)	4, 3028(2)
space group	P-1(#2)	P-1(#2)	$P2_1/n$(#14)
D_{calc}, g/cm^3	2.74	2.35	1.71
μ(Mo Kα), cm^{-1}	59.9	48.8	34.3
cryst size, mm	0.07x0.10x0.21	0.13x0.19x0.37	0.09x0.11x0.20
$2\theta_{max}$, deg	45.0	50.0	45.0
Temperature (°C)	-94	23	-100
no. of data collcd	5743	15332	4422
no. of data used($F_o^2>3\sigma(F_o^2)$)	4368	8757	1273
min, max abs cor	0.78, 1.27	0.76, 1.11	0.79, 1.17
no. of variables	424	973	220
no. of atoms per asym unit (including H)	67	148	61
final R/R_w, %	5.2/5.8	4.3/5.7	6.0/7.0

Table 5·2. Positional Parameters and B_{eq} Values[a] for $(Ph_4P)_2[Ru_6(Te_2)_7(CO)_{12}]$ (5·1) (Standard Deviations in Parentheses)

atom	x	y	z	B_{eq}, Å^2
Te1	1.1565(1)	0.79106(9)	1.2321(1)	1.66(3)
Te2	1.3418(1)	0.7438(1)	1.2018(1)	1.98(4)
Te3	1.2676(1)	0.53625(9)	1.25672(9)	1.73(3)
Te4	0.8109(1)	0.6829(1)	0.8023(1)	2.21(4)
Te5	0.8282(1)	0.70274(9)	1.0595(1)	1.78(3)
Te6	0.9397(1)	0.7410(1)	1.2892(1)	2.00(4)
Te7	0.9588(1)	0.46380(9)	1.0537(1)	1.51(3)
Ru1	1.1001(1)	0.6283(1)	1.2795(1)	1.60(4)
Ru2	1.2600(1)	0.5203(1)	1.0584(1)	1.66(4)
Ru3	0.9960(1)	0.7444(1)	1.0141(1)	1.68(4)
P	0.2463(4)	0.2253(4)	0.5016(4)	1.8(1)
O1	1.019(1)	0.483(1)	1.355(1)	3.5(5)
O2	1.268(1)	0.796(1)	1.534(1)	3.2(4)
O3	1.290(1)	0.551(1)	0.875(1)	4.0(5)
O4	1.485(1)	0.467(1)	1.151(1)	3.2(5)
O5	0.956(1)	0.980(1)	1.084(1)	3.3(5)
O6	1.160(1)	0.799(1)	0.944(1)	3.8(5)
C1	0.095(2)	0.181(1)	0.422(1)	2.3(6)
C2	0.039(1)	0.088(1)	0.417(2)	2.2(6)
C3	-0.078(2)	0.055(2)	0.355(2)	3.1(7)
C4	-0.140(1)	0.107(2)	0.298(2)	2.7(6)
C5	-0.088(2)	0.201(2)	0.301(2)	3.5(7)
C6	0.031(2)	0.235(2)	0.364(2)	2.7(6)
C7	0.307(1)	0.199(1)	0.626(1)	1.8(5)
C8	0.349(1)	0.289(1)	0.738(1)	2.2(6)
C9	0.396(2)	0.269(2)	0.833(2)	2.6(6)
C10	0.394(2)	0.159(2)	0.816(2)	2.7(7)
C11	0.350(2)	0.070(1)	0.701(2)	2.6(6)
C12	0.310(1)	0.090(1)	0.612(1)	2.2(6)
C13	0.288(1)	0.372(1)	0.551(1)	2.2(6)

Table 5·2. (cont'd)

atom	x	y	z	B_{eq}, Å^2
C14	0.231(2)	0.446(2)	0.599(2)	2.8(6)
C15	0.264(2)	0.556(2)	0.632(2)	4.2(8)
C16	0.355(2)	0.601(2)	0.628(2)	4.2(8)
C17	0.409(2)	0.529(2)	0.583(2)	4.2(8)
C18	0.376(2)	0.417(2)	0.544(2)	3.1(7)
C19	0.302(1)	0.148(1)	0.407(1)	2.0(5)
C20	0.412(2)	0.136(2)	0.455(2)	3.5(7)
C21	0.455(2)	0.080(2)	0.385(2)	3.1(7)
C22	0.388(2)	0.037(2)	0.262(2)	3.5(8)
C23	0.277(2)	0.047(2)	0.213(2)	2.9(6)
C24	0.234(2)	0.104(1)	0.287(2)	2.2(6)
C25	1.054(2)	0.532(1)	1.328(1)	2.3(6)
C26	1.204(2)	0.734(2)	1.436(2)	2.6(6)
C27	1.275(2)	0.536(1)	0.939(2)	2.6(6)
C28	1.405(2)	0.490(1)	1.123(2)	2.4(6)
C29	0.971(1)	0.894(2)	1.062(1)	2.6(7)
C30	1.099(2)	0.776(1)	0.970(2)	2.5(6)

a. B_{eq} is defined as $4/3[a^2\beta_{11}+b^2\beta_{22}+c^2\beta_{33}+ab(\cos\gamma)\beta_{12}+ac(\cos\beta)\beta_{13}+bc(\cos\alpha)\beta_{23}]$.

Table 5·3. Positional Parameters and B_{eq} Values[a] for $(Ph_4P)_2[\{Fe_4Te_4(CO)_{10}\}_2(Te_2)]$ (5·2) (Standard Deviations in Parentheses)

atom	x	y	z	B_{eq}, Å^2
Te1	0.83882(7)	0.14515(5)	0.69324(8)	3.41(5)
Te2	1.08027(7)	0.12777(5)	0.88306(8)	3.74(5)
Te3	0.98921(8)	0.22016(5)	0.64491(8)	4.04(6)
Te4	0.92219(7)	0.26139(5)	0.86222(8)	3.45(5)
Te5	0.50657(7)	0.29658(4)	0.85363(8)	3.08(5)
Te6	0.59419(7)	0.31444(5)	1.13779(8)	3.36(5)
Te7	0.55071(7)	0.42676(4)	0.95403(7)	2.94(4)
Te8	0.75459(7)	0.31640(4)	1.00937(7)	2.90(4)
Te9	0.65687(7)	0.27354(4)	0.70376(7)	3.01(5)
Te10	0.72188(7)	0.18640(4)	0.87126(8)	3.03(5)
Fe1	0.8143(2)	0.2551(1)	0.6523(2)	3.5(1)
Fe2	0.9130(2)	0.1594(1)	0.9093(2)	3.2(1)
Fe3	1.0092(2)	0.1099(1)	0.6668(2)	4.1(1)
Fe4	1.1027(2)	0.2300(1)	0.8561(2)	4.2(1)
Fe5	0.6126(1)	0.36068(9)	0.8199(2)	2.8(1)
Fe6	0.6612(2)	0.2389(1)	1.0196(2)	3.2(1)
Fe7	0.4307(1)	0.3678(1)	0.9738(2)	3.3(1)
Fe8	0.6994(2)	0.3891(1)	1.1443(2)	3.4(1)
P1	0.8135(3)	0.5937(2)	0.6662(3)	3.6(2)
P2	0.4052(4)	0.0099(2)	0.2359(4)	4.6(2)
O1	0.800(1)	0.3739(6)	0.612(1)	8(1)
O2	0.705(1)	0.2389(7)	0.415(1)	9(1)
O3	0.912(1)	0.0426(5)	0.967(1)	7.4(8)
O4	1.000(1)	0.1915(6)	1.140(1)	8(1)
O5	1.029(1)	-0.0096(6)	0.727(1)	8(1)
O6	0.890(1)	0.1038(7)	0.426(1)	9(1)
O7	1.204(1)	0.0925(6)	0.648(1)	6.4(8)
O8	1.107(1)	0.3449(6)	0.798(1)	8(1)
O9	1.193(1)	0.2391(7)	1.101(1)	9(1)
O10	1.291(1)	0.1815(8)	0.831(1)	10(1)

Table 5·3. (cont'd)

atom	x	y	z	B_{eq}, Å^2
O11	0.743(1)	0.4300(5)	0.802(1)	6.2(8)
O12	0.4341(8)	0.4135(6)	0.6285(8)	6.6(7)
O13	0.535(1)	0.1626(6)	1.017(1)	6.9(9)
O14	0.832(1)	0.1793(6)	1.213(1)	8(1)
O15	0.340(1)	0.2805(6)	1.019(1)	8(1)
O16	0.2706(9)	0.4176(5)	0.762(1)	6.5(7)
O17	0.3743(8)	0.4532(5)	1.122(1)	5.3(7)
O18	0.8031(9)	0.4713(5)	1.113(1)	6.0(7)
O19	0.871(1)	0.3241(6)	1.333(1)	8.1(9)
O20	0.6067(9)	0.4656(5)	1.280(1)	6.0(8)
C1	0.867(1)	0.5313(6)	0.613(1)	3.7(8)
C1'	0.804(1)	0.3284(8)	0.629(2)	6(1)
C2	0.964(1)	0.4991(8)	0.669(1)	4.6(9)
C2'	0.749(1)	0.2467(9)	0.509(1)	6(1)
C3	1.007(1)	0.4548(6)	0.626(1)	4.4(8)
C3'	0.915(1)	0.0869(8)	0.944(1)	5(1)
C4	0.952(1)	0.4343(6)	0.523(1)	4.6(8)
C4'	0.966(1)	0.1767(7)	1.049(1)	3.9(8)
C5	0.852(1)	0.4644(8)	0.465(1)	5(1)
C5'	1.018(1)	0.035(1)	0.700(2)	5(1)
C6	0.814(1)	0.5110(7)	0.509(1)	4.5(9)
C6'	0.937(1)	0.1057(8)	0.520(2)	6(1)
C7	0.822(1)	0.6590(8)	0.605(1)	5(1)
C7'	1.130(1)	0.0996(8)	0.659(1)	5(1)
C8	0.839(2)	0.7030(7)	0.663(1)	7(1)
C8'	1.102(1)	0.2980(9)	0.818(2)	6(1)
C9	0.844(2)	0.754(1)	0.615(2)	9(2)
C9'	1.158(1)	0.2362(8)	1.006(2)	5(1)
C10	0.828(2)	0.751(1)	0.505(2)	9(2)
C10'	1.217(1)	0.1986(7)	0.839(1)	5(1)
C11	0.809(2)	0.7070(7)	0.443(2)	6(1)

Table 5·3. (cont'd)

atom	x	y	z	B_{eq}, Å^2
C11'	0.691(1)	0.4025(7)	0.808(1)	3.7(8)
C12	0.804(2)	0.657(1)	0.491(1)	7(1)
C12'	0.506(1)	0.3906(8)	0.704(1)	4.5(9)
C13	0.685(1)	0.5978(7)	0.635(1)	3.8(8)
C13'	0.585(1)	0.1931(7)	1.017(1)	5(1)
C14	0.651(1)	0.548(1)	0.631(1)	6(1)
C14'	0.765(1)	0.2039(7)	1.137(1)	4.2(8)
C15	0.550(1)	0.552(1)	0.611(1)	6(1)
C15'	0.371(1)	0.3164(8)	0.996(1)	5(1)
C16	0.487(1)	0.610(1)	0.597(2)	9(2)
C16'	0.334(1)	0.3982(7)	0.845(1)	4.0(8)
C17	0.522(2)	0.649(1)	0.597(2)	9(2)
C17'	0.400(1)	0.4170(8)	1.066(1)	4(1)
C18	0.620(1)	0.6500(8)	0.620(1)	6(1)
C18'	0.762(1)	0.4407(7)	1.124(1)	3.8(8)
C19	0.883(1)	0.5928(6)	0.816(1)	3.6(7)
C19'	0.802(1)	0.3476(8)	1.258(1)	5(1)
C20	0.974(1)	0.6050(7)	0.861(1)	4.4(9)
C20'	0.640(1)	0.4383(7)	1.225(1)	4.2(9)
C21	1.026(1)	0.5995(7)	0.978(1)	5(1)
C22	0.989(1)	0.5821(8)	1.046(1)	5(1)
C23	0.900(1)	0.5669(8)	0.999(1)	5(1)
C24	0.844(1)	0.5733(7)	0.886(1)	4.1(9)
C25	0.304(1)	0.0453(6)	0.273(1)	3.7(7)
C26	0.327(1)	0.0708(8)	0.377(1)	5(1)
C27	0.248(2)	0.0928(8)	0.411(2)	6(1)
C28	0.152(2)	0.0894(9)	0.344(2)	6(1)
C29	0.131(1)	0.0667(8)	0.239(2)	6(1)
C30	0.207(1)	0.0435(9)	0.204(1)	6(1)
C31	0.456(1)	-0.0612(7)	0.301(1)	4.0(8)
C32	0.425(1)	-0.0773(8)	0.379(1)	5(1)

Table 5·3. (cont'd)

atom	x	y	z	B_{eq}, Å^2
C33	0.463(1)	-0.1359(9)	0.424(1)	6(1)
C34	0.532(1)	-0.1709(8)	0.391(1)	5(1)
C35	0.563(1)	-0.154(1)	0.316(2)	6(1)
C36	0.526(1)	-0.0973(9)	0.270(2)	6(1)
C37	0.364(1)	0.0013(9)	0.088(1)	5(1)
C38	0.308(2)	-0.0388(8)	0.042(2)	6(1)
C39	0.272(1)	-0.0441(8)	-0.071(1)	6(1)
C40	0.289(2)	-0.0134(9)	-0.141(1)	6(1)
C41	0.343(1)	0.029(1)	-0.095(2)	7(1)
C42	0.381(1)	0.0361(9)	0.020(2)	6(1)
C43	0.500(2)	0.0522(8)	0.281(1)	5(1)
C44	0.468(2)	0.1082(8)	0.250(2)	6(1)
C45	0.539(2)	0.143(1)	0.279(2)	9(2)
C46	0.637(2)	0.115(1)	0.349(2)	8(2)
C47	0.670(2)	0.057(1)	0.385(2)	7(1)
C48	0.598(2)	0.032(1)	0.352(2)	6(1)

a. B_{eq} is defined as $4/3[a^2\beta_{11}+b^2\beta_{22}+c^2\beta_{33}+ab(\cos\gamma)\beta_{12}+ac(\cos\beta)\beta_{13}+bc(\cos\alpha)\beta_{23}]$.

Table 5-4. Positional Parameters and B_{eq} Values[a] for $(Ph_4P)_2[\{Fe_2Se(CO)_6\}_2(Se_2)]$ (5-3) (Standard Deviations in Parentheses)

atom	x	y	z	B_{eq}, Å^2
Se1	0.0374(3)	0.4205(2)	0.4834(1)	2.8(2)
Se2	0.1013(3)	0.2696(2)	0.3975(1)	3.0(2)
Fe1	-0.0719(4)	0.3812(3)	0.3850(2)	2.8(2)
Fe2	0.1590(4)	0.4359(3)	0.3894(2)	2.6(2)
P	0.7181(7)	-0.0144(6)	0.3962(4)	2.5(4)
O1	-0.301(2)	0.316(2)	0.449(1)	6(1)
O2	-0.100(2)	0.297(2)	0.254(1)	6(1)
O3	-0.166(2)	0.574(2)	0.347(1)	5(1)
O4	0.422(2)	0.432(1)	0.440(1)	5(1)
O5	0.197(2)	0.401(1)	0.251(1)	4(1)
O6	0.148(2)	0.646(2)	0.3784(9)	4(1)
C1	0.647(3)	-0.129(2)	0.406(1)	3.0(7)
C1'	-0.215(3)	0.340(2)	0.426(2)	4.0(9)
C2	0.714(2)	-0.206(2)	0.426(1)	2.9(6)
C2'	-0.091(3)	0.329(2)	0.307(2)	4.3(8)
C3	0.653(3)	-0.292(2)	0.433(1)	3.2(7)
C3'	-0.132(3)	0.498(2)	0.364(1)	3.4(7)
C4	0.533(3)	-0.301(2)	0.422(2)	4.7(8)
C4'	0.318(3)	0.433(2)	0.420(1)	2.7(6)
C5	0.455(3)	-0.227(2)	0.401(1)	3.8(7)
C5'	0.184(3)	0.414(3)	0.305(2)	4.9(9)
C6	0.516(3)	-0.136(2)	0.393(1)	3.4(7)
C6'	0.147(3)	0.563(2)	0.384(1)	3.0(7)
C7	0.790(2)	0.021(2)	0.471(1)	2.8(6)
C8	0.857(2)	0.101(2)	0.477(1)	2.9(6)
C9	0.904(3)	0.142(2)	0.534(1)	3.3(7)

Table 5·4. (cont'd)

atom	x	y	z	B_{eq}, Å^2
C10	0.874(3)	0.097(2)	0.591(1)	3.8(7)
C11	0.805(3)	0.015(2)	0.590(2)	4.6(8)
C12	0.762(3)	-0.025(2)	0.530(1)	4.3(7)
C13	0.602(2)	0.073(2)	0.373(1)	2.3(6)
C14	0.559(3)	0.071(3)	0.309(1)	5.0(8)
C15	0.457(3)	0.133(2)	0.291(1)	4.4(8)
C16	0.404(2)	0.194(2)	0.339(1)	2.8(6)
C17	0.451(3)	0.191(2)	0.398(1)	2.7(6)
C18	0.545(2)	0.130(2)	0.417(1)	2.4(6)
C19	0.818(3)	-0.024(2)	0.331(1)	3.3(7)
C20	0.879(3)	0.059(2)	0.309(1)	4.6(8)
C21	0.963(3)	0.066(3)	0.257(2)	6.0(9)
C22	0.981(3)	-0.022(3)	0.226(2)	5.5(9)
C23	0.922(3)	-0.103(2)	0.245(2)	5.0(8)
C24	0.846(3)	-0.102(2)	0.299(1)	3.9(7)

a. B_{eq} is defined as $4/3[a^2\beta_{11}+b^2\beta_{22}+c^2\beta_{33}+ab(\cos\gamma)\beta_{12}+ac(\cos\beta)\beta_{13}+bc(\cos\alpha)\beta_{23}]$.

Finally, all compounds were examined by X-ray powder diffraction for the purpose of phase characterization and identification. A Debye-Scherrer camera was employed to record the X-ray powder diffraction patterns. Ni-filtered Cu radiation was used. The crystals were ground to fine powder and packed into 0.5 mm glass capillaries which were sealed and mounted to the standard Debye-Scherrer powder camera which has a diameter of 114.6 mm (1 mm corresponds to 1 degree for 2θ). X-rays were generated by a Phillips Norelco XRG-5000 X-ray generator operating at 40 kV and 20 mA. Approximately, a six hour exposure time was used. Accurate d-spacings (Å) of each compound were calculated from the powder patterns recorded on a Phillips XRG-3000 computer controlled powder diffractometer[16]. To verify the homogeneities of the products, the d-spacings observed for the bulk materials were compared with the calculated d-spacings from the X-ray single-crystal structure analysis data[17]. Listings of calculated and observed d-spacings (Å) along with the observed relative diffraction intensities of these compounds are given in Tables 5·5–5·7.

Table 5·5. Calculated and Observed X-ray Powder Diffraction Patterns for $(Ph_4P)_2[Ru_6(Te_2)_7(CO)_{12}]$ (5·1)

h k l	$d_{calc.}$ (Å)	$d_{obs.}$ (Å)	$I/I_{max.}$ (obs.)
0 1 0	11.85	/	/
1 0 0	11.70	11.69	100
-1 0 1	11.50	11.46	44
0 0 1	11.37	/	/
0-1 1	11.32	11.24	63
-1-1 1	9.46	9.34	34
-2-2 3	4.29	4.13	37
0-4 1	3.272	3.266	35
-4 1 1	3.250	/	/
1 0 3	3.173	3.190	36
-1 4 0	3.058	3.037	22
0 4 0	2.964	2.949	34
-1-4 4	2.930	2.931	19
-4 2 0	2.924	2.918	17
-2-4 1	2.711	2.707	23
0-5 1	2.579	2.551	13
-5 2 3	2.388	2.346	35
1-3 5	2.320	2.321	16
-2-5 1	2.235	2.224	18
5-2 1	2.200	2.203	10
-4 2 6	1.824	1.826	16

Table 5·6. Calculated and Observed X-ray Powder Diffraction Patterns for $(Ph_4P)_2[\{Fe_4Te_4(CO)_{10}\}_2(Te_2)]$ (5·2)

h k l	$d_{calc.}$ (Å)	$d_{obs.}$ (Å)	$I/I_{max.}$ (obs.)
1 1 0	12.93	13.07	70
0 0 1	11.96	12.05	47
0 2 0	11.70	11.91	57
0 1 1	10.83	10.85	41
0-1 1	10.48	10.50	80
-1-2 1	8.90	9.11	31
0-2 1	8.20	8.37	32
1 0 1	7.549	7.681	100
1 1 1	7.533	7.546	24
1 3 0	7.523	7.537	21
0-3 1	6.416	6.433	23
2-2 2	3.439	3.478	16
-2 5 3	2.993	3.002	27
-3 4 3	2.985	2.988	44
-5-1 2	2.962	2.973	25
-5 1 2	2.801	2.821	25
-5 0 3	2.783	2.796	21
2-3-3	2.646	2.648	24
-1-9 1	2.626	2.629	17
-2 5 4	2.589	2.583	12
2-5 3	2.359	2.370	15
0 3 5	2.314	2.311	13

Table 5·7. Calculated and Observed X-ray Powder Diffraction Patterns for $(Ph_4P)_2[\{Fe_2Se(CO)_6\}_2(Se_2)]$ (5·3)

h k l	$d_{calc.}$ (Å)	$d_{obs.}$ (Å)	$I/I_{max.}$ (obs.)
0 1 1	11.6	11.7	45
0 0 2	10.2	10.4	41
1 0-1	9.49	9.51	67
1 0 1	9.23	9.27	54
1 1 0	8.42	8.50	100
0 1 2	8.26	8.24	43
1 1-1	7.862	7.867	37
0 1 0	7.012	7.017	13
0 2 1	6.633	6.586	29
1 1 2	6.416	6.427	57
1 2-1	5.641	5.646	8
1 1-3	5.369	5.378	11
0 0 4	5.111	5.113	37
1 2-2	5.110	/	/
0 2 3	4.887	4.873	22
2 1 1	4.758	4.761	15
2 0 2	4.618	4.616	10
1 1-4	4.423	4.428	14
1 3 0	4.273	4.280	11
2 1-3	4.056	4.053	14
1 3 2	3.923	3.927	21
2 0 4	3.607	3.601	8
0 2 5	3.532	3.537	12
0 0 6	3.407	3.404	17
1 4 0	3.326	3.324	23
2 2-4	3.294	3.288	14
3 0 3	3.079	3.075	20
3 2-2	3.027	3.021	9
3 2 2	2.976	2.983	7
2 3-4	2.916	2.919	9

Table 5·7. (cont'd)

h k l	$d_{calc.}$ (Å)	$d_{obs.}$ (Å)	$I/I_{max.}$ (obs.)
3 2-3	2.885	2.886	11
1 0-7	2.839	2.837	15
2 4-2	2.820	/	/
3 1 4	2.792	2.788	11
1 5-1	2.690	2.669	7
3 3-3	2.620	2.617	10
2 5 0	2.476	2.477	12
2 5-3	2.339	2.337	9

III. Results

1. Description of Crystal and Molecular Structures of the Compounds

(i). Structure of $(Ph_4P)_2[Ru_6(Te_2)_7(CO)_{12}]$ (5·1)

The structure of (**5·1**) is composed of well separated Ph_4P^+ cations and $[Ru_6(Te_2)_7(CO)_{12}]^{2-}$ anions in the crystal lattice as shown in Figure 5·1. The Ph_4P^+ cations have the normal tetrahedral structure, and will not be discussed further. The centrosymmetric cluster $[Ru_6(Te_2)_7(CO)_{12}]^{2-}$, with an idealized S_6 molecular symmetry, contains an octahedral array of six ruthenium atoms upheld by a central ditelluride Te_2^{2-} as shown in Figure 5·2. The tellurium atoms in this unit each bind to three ruthenium atoms, forming a Ru_3Te-$TeRu_3$ ethane-like fragment with a staggered conformation. Furthermore, the ruthenium atoms are bridged by six Te_2^{2-} units in the periphery. In the bridging Te_2^{2-} ligands, one Te atom bonds to a ruthenium atom while the other Te atom bridges two ruthenium atoms, acting on the whole as μ_3-type chelating ligands. An ORTEP representation of the cluster core with all CO groups omitted is given in Figure 5·3. Finally, the octahedral coordination geometry of all the Ru atoms is each completed by two *cis* CO groups. The cluster core $\{Ru_6(Te_2)_7\}^{2-}$ has a striking resemblance to the $RuTe_2$ lattice. Figure 5·4 compares the $[Ru_6(Te_2)_7(CO)_{12}]^{2-}$ cluster core with a small fragment of $RuTe_2$. The Te-Te bond distances from 2.717Å to 2.763 Å are in the normal range of the Te-Te single bond[18-20], while the Ru-Te bond distances, ranging from 2.673(2) Å to 2.747(2) Å, can be compared with the Ru-Te distances of 2.755 Å (mean) in $Ru_4(CO)_{10}(Ph_3P)(Te)_2$[21], and 2.678 Å (mean) in $Ru_3(CO)_6(Ph_3P)_3(Te)_2$[21]. Other important bond distances and bond angles ae given in Table 5·8.

Table 5·8. Selected Geometric Data for $(Ph_4P)_2[Ru_6(Te_2)_7(CO)_{12}]$ (5·1)[b]

		Bond Distances (Å)	
Ru(1)-Te(1)	2.747(2)	Ru(1)-Te(3)	2.673(2)
Ru(1)-Te(6)	2.681(2)	Ru(1)-Te(7)	2.733(4)
Ru(2)-Te(2)	2.690(3)	Ru(2)-Te(3)	2.735(2)
Ru(2)-Te(5)	2.678(3)	Ru(2)-Te(7)	2.721(2)
Ru(3)-Te(1)	2.683(3)	Ru(3)-Te(4)	2.696(3)
Ru(3)-Te(5)	2.737(2)	Ru(3)-Te(7)	2.734(2)
Ru-Te(mean)	2.709(8)	Te(1)-Te(2)	2.763(2)
Te(3)-Te(4)	2.754(3)	Te(5)-Te(6)	2.758(3)
Te(7)-Te(7)	2.717(2)	Te-Te(mean)	2.748(10)
Ru(1)-C(25)	1.91(2)	Ru(1)-C(26)	1.87(2)
Ru(2)-C(27)	1.91(2)	Ru(2)-C(28)	1.89(2)
Ru(3)-C(29)	1.93(2)	Ru(3)-C(30)	1.87(2)
		Bond Angles (deg)	
Ru(1)-Te(7)-Ru(2)	117.74(7)	Ru(1)-Te(7)-Ru(3)	118.08(8)
Ru(2)-Te(7)-Ru(3)	118.75(9)	Te(7)-Te(7)-Ru(1)	97.84(9)
Te(1)-Ru(1)-Te(3)	90.55(6)	Te(1)-Ru(1)-Te(6)	80.40(6)
Te(1)-Ru(1)-Te(7)	98.65(8)	Te(1)-Ru(1)-C(26)	83.4(5)
Te(3)-Ru(1)-C(25)	97.0(5)	Te(2)-Ru(2)-Te(3)	79.21(8)
Te(2)-Ru(2)-Te(7)	93.72(9)	Te(3)-Ru(2)-Te(5)	92.17(8)
Te(5)-Ru(2)-C(27)	98.0(5)	Te(5)-Ru(2)-C(28)	87.3(5)
Te(4)-Ru(3)-Te(5)	80.45(8)	Te(4)-Ru(3)-Te(7)	93.7(1)
Te(4)-Ru(3)-C(29)	87.4(5)	Te(4)-Ru(3)-C(30)	93.7(5)

Table 5·8. (cont'd)

Bond Angles (deg)			
Ru(1)-Te(1)-Ru(3)	108.24(9)	Te(2)-Te(1)-Ru(1)	104.36(6)
Te(1)-Te(2)-Ru(2)	98.82(8)	Ru(1)-Te(3)-Ru(2)	108.73(7)
Te(4)-Te(3)-Ru(2)	104.10(8)	Te(3)-Te(4)-Ru(3)	98.7(1)
Ru(2)-Te(5)-Ru(3)	107.69(7)	Te(6)-Te(5)-Ru(3)	105.83(7)
Te(5)-Te(6)-Ru(1)	98.12(7)		

b. The estimated standard deviations in the mean bond lengths and the mean bond angles are calculated by the equation $\sigma_l=\{\Sigma_n(l_n-l)^2/n(n-1)\}^{1/2}$, where l_n is the length (angle) of the *n*th bond, l the mean length (angle), and n the number of bonds.

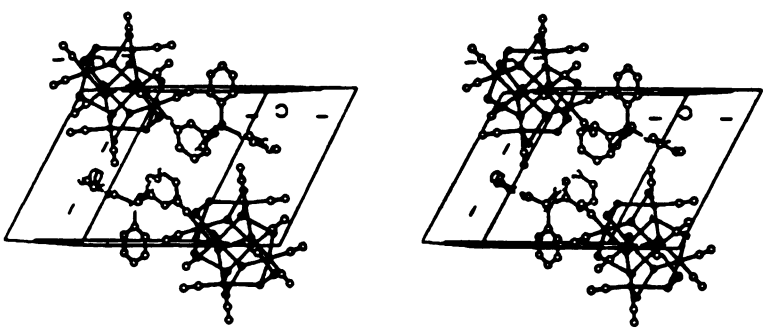


Figure 5·1. The Packing Diagram in the Unit Cell of $(Ph_4P)_2[Ru_6(Te_2)_7(CO)_{12}]$ (Stereoview)

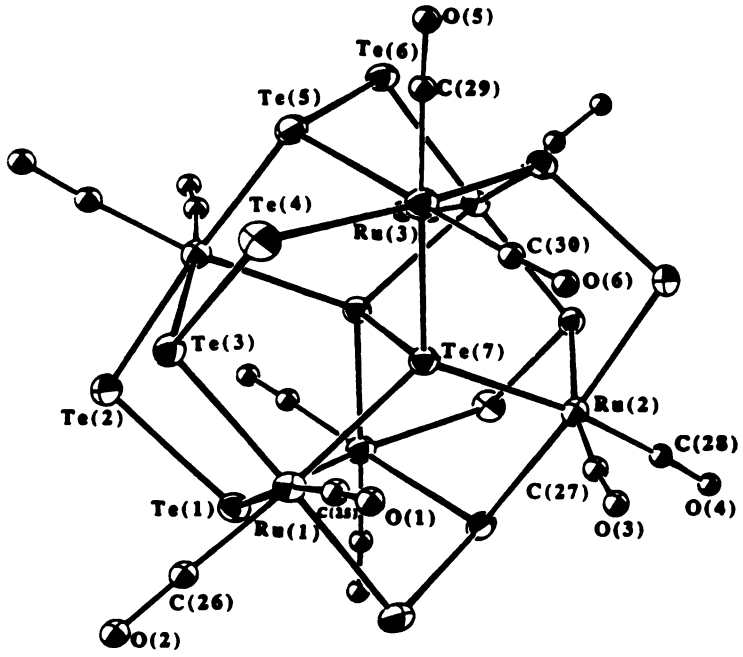


Figure 5-2. The Structure of the $[Ru_6(Te_2)_7(CO)_{12}]^{2-}$ Anion

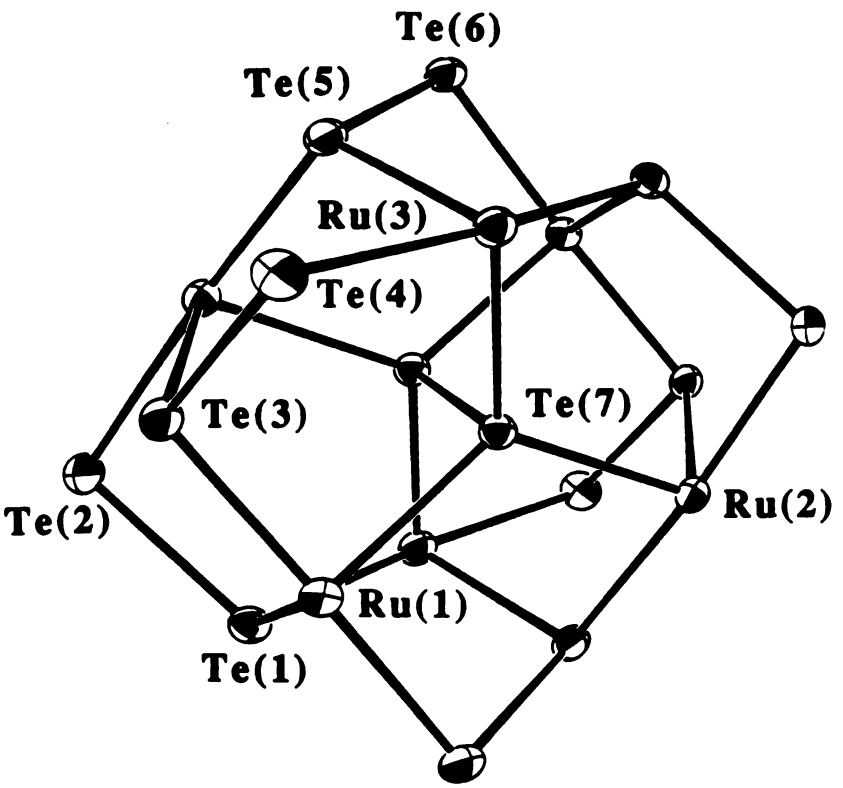


Figure 5-3. The Structure of the $[Ru_6(Te_2)_7(CO)_{12}]^{2-}$ Anion with CO Groups Omitted, Showing the Staggering Conformation of the Ru_3Te-$TeRu_3$ Fragment

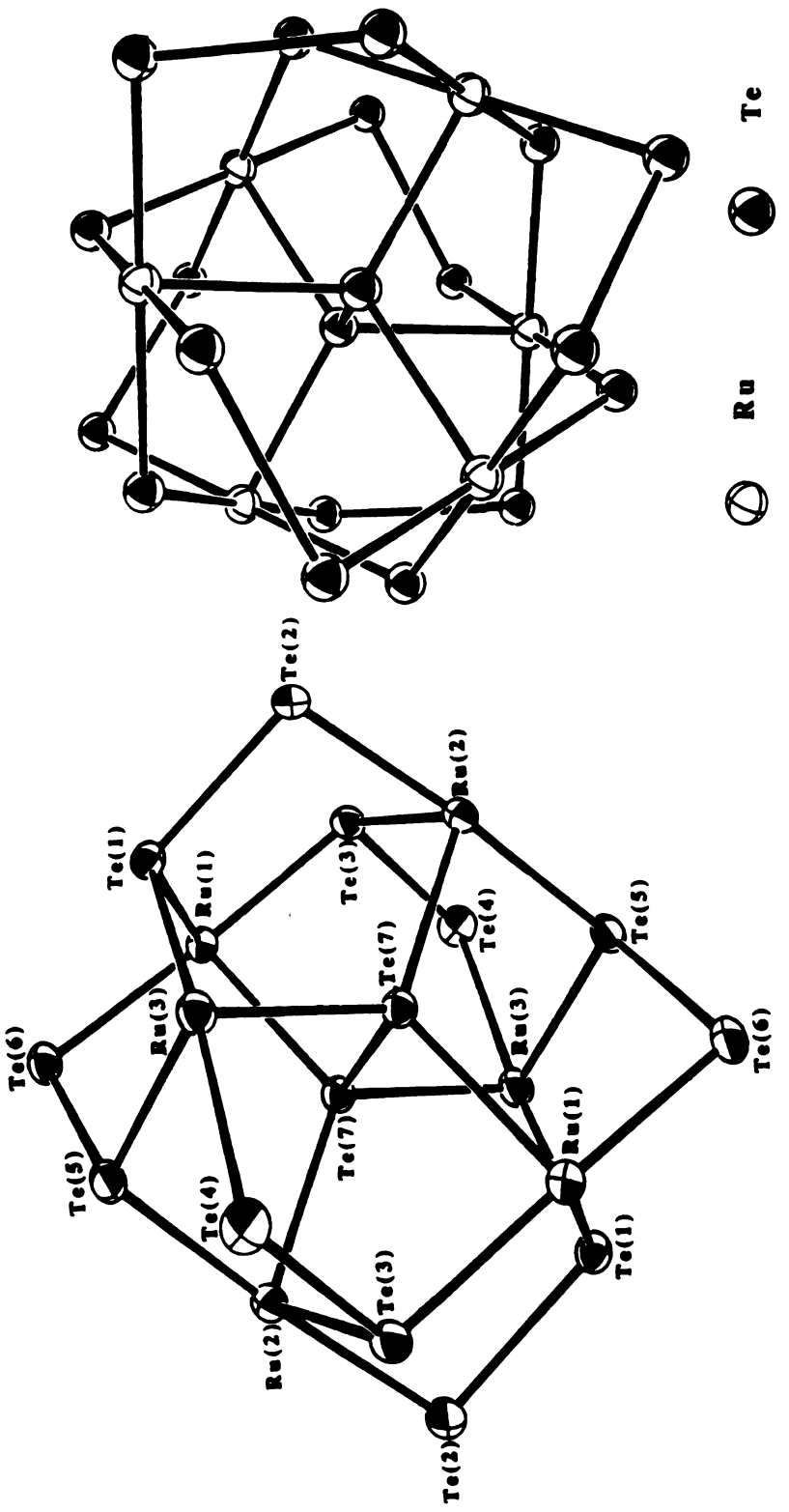


Figure 5-4. Comparison Between the $[Ru_6(Te_2)_7]^{2-}$ Core (Left) and a Small-Core Fragment of $RuTe_2$ (Right)

(ii). Structure of $(Ph_4P)_2[\{Fe_4Te_4(CO)_{10}\}_2(Te_2)]$ (5·2)

The structure of (5·2) comprises of Ph_4P^+ cations and $[\{Fe_4Te_4(CO)_{10}\}_2(Te_2)]^{2-}$ anions in the crystal lattice as shown in Figure 5·5. The $[\{Fe_4Te_4(CO)_{10}\}_2(Te_2)]^{2-}$ anion contains two Fe_4Te_4 cubane-like cages bridged by a Te_2^{2-} unit as shown in Figure 5·6. An ORTEP representation of the cluster core with all CO groups omitted is given in Figure 5·7. The Te_2^{2-} acts overall as a μ_4-type ligand. These cages can be each described as being formed by the interpenetrating tetrahedral arrays of four iron and tellurium atoms. Such a structure is an almost omnipresent theme in iron-sulfur chemistry[22]. However, the octahedral coordination geometry of all the iron atoms, being completed by terminal CO groups, differs from many iron-sulfur cubanes[22]. The Te-Te distance in the bridging unit is 2.829(2) Å, and can be considered a normal single bond[23]. Other compounds containing such a μ_4 type Te_2^{2-} ligand are $[K\text{-(crypt)}]_2Mo_4Te_{16}(en)_4$[27] and $(Bu_4N)_4[Hg_4Te_{12}]$[24]. The Fe-Te bond distances, ranging from 2.585(2) Å to 2.657(2) Å (average 2.619(4) Å), are rather uniform, and comparable with those found in $Cs_7[Fe_4Te_4(Te)_4]$[25a] and a number of iron-telluride-tellurolate complexes having cubane-like cores[25b-c]. Other selected bond distances and bond angles are given in Table 5·9. If the charge of both the ditelluride and the monotelluride ligands in this structure is taken as 2-, the eight iron atoms would have a formal oxidation state 2+. Consistent with this oxidation state, the observed long Fe-Fe distances in both cubanes (the shortest distance is 3.75 Å) exclude any possible M-M bonding in (5·2). As a result, the two Fe_4Te_4 cubes have approximate local T_d symmetry (see Figure 5·7).

Table 5-9. Selected Geometric Data for $(Ph_4P)_2[\{Fe_4Te_4(CO)_{10}\}_2(Te_2)]$ (5-2)[b]

		Bond Distances (Å)	
Fe(1)-Te(1)	2.642(3)	Fe(1)-Te(3)	2.590(2)
Fe(1)-Te(4)	2.585(2)	Fe(1)-Te(9))	2.628(2)
Fe(2)-Te(1)	2.623(2)	Fe(2)-Te(2)	2.589(2)
Fe(2)-Te(4)	2.612(3)	Fe(2)-Te(4)	2.620(2)
Fe(3)-Te(1)	2.641(2)	Fe(3)-Te(2)	2.640(2)
Fe(3)-Te(3)	2.620(3)	Fe(4)-Te(2)	2.620(3)
Fe(4)-Te(3)	2.632(3)	Fe(4)-Te(4)	2.657(2)
Fe(5)-Te(5)	2.615(2)	Fe(5)-Te(7)	2.595(2)
Fe(5)-Te(8)	2.613(2)	Fe(5)-Te(9)	2.633(2)
Fe(6)-Te(5)	2.614(2)	Fe(6)-Te(6)	2.598(2)
Fe(6)-Te(8)	2.612(2)	Fe(6)-Te(10)	2.599(2)
Fe(7)-Te(5)	2.625(2)	Fe(7)-Te(6)	2.627(2)
Fe(7)-Te(7)	2.622(2)	Fe(8)-Te(6)	2.625(3)
Fe(8)-Te(7)	2.619(2)	Fe(8)-Te(8)	2.641(2)
Fe-Te (mean)	2.619(4)	Te(9)-Te(10)	2.829(2)
Fe-C (mean)	1.78(7)		
		Bond Angles (deg)	
Fe(1)-Te(1)-Fe(2)	90.97(7)	Fe(1)-Te(1)-Fe(3)	96.98(8)
Fe(2)-Te(1)-Fe(3)	98.39(7)	Fe(2)-Te(2)-Fe(3)	99.29(7)
Fe(2)-Te(2)-Fe(4)	97.41(8)	Fe(3)-Te(2)-Fe(4)	93.78(8)
Fe(1)-Te(3)-Fe(3)	98.80(8)	Fe(1)-Te(3)-Fe(4)	99.40(8)
Fe(3)-Te(3)-Fe(4)	93.95(8)	Fe(1)-Te(4)-Fe(2)	92.52(8)
Fe(1)-Te(4)-Fe(4)	98.90(8)	Fe(2)-Te(4)-Fe(4)	95.94(8)

Table 5-9. (cont'd)

Bond Angles (deg)			
Fe(5)-Te(5)-Fe(6)	92.52(7)	Fe(5)-Te(5)-Fe(7)	97.42(7)
Fe(6)-Te(5)-Fe(7)	97.28(7)	Fe(6)-Te(6)-Fe(7)	97.61(7)
Fe(6)-Te(6)-Fe(8)	98.28(7)	Fe(7)-Te(6)-Fe(8)	95.26(7)
Fe(5)-Te(7)-Fe(7)	98.00(7)	Fe(5)-Te(7)-Fe(8)	99.29(7)
Fe(7)-Te(7)-Fe(8)	95.52(7)	Fe(5)-Te(8)-Fe(6)	92.60(7)
Fe(5)-Te(8)-Fe(8)	98.26(7)	Fe(6)-Te(8)-Fe(8)	97.51(7)
Fe-Te-Fe (mean)	96.5(5)	Fe(1)-Te(9)-Fe(5)	122.94(8)
Fe(2)-Te(10)-Fe(6)	120.47(7)	Te(1)-Fe(1)-Te(3)	82.17(7)
Te(1)-Fe(1)-Te(4)	87.15(7)	Te(1)-Fe(1)-Te(9)	87.60(8)
Te(1)-Fe(2)-Te(2)	81.77(7)	Te(1)-Fe(2)-Te(4)	87.01(7)
Te(1)-Fe(2)-Te(10)	80.94(7)	Te(1)-Fe(3)-Te(2)	80.49(7)
Te(1)-Fe(3)-Te(3)	81.64(8)	Te(2)-Fe(3)-Te(3)	84.32(8)
Te(2)-Fe(4)-Te(3)	84.48(8)	Te(2)-Fe(4)-Te(4)	82.31(7)
Te(3)-Fe(4)-Te(4)	79.74(7)	Te(5)-Fe(5)-Te(7)	82.41(6)
Te(5)-Fe(5)-Te(8)	86.40(7)	Te(5)-Fe(5)-Te(9)	82.39(7)
Te(5)-Fe(6)-Te(6)	82.79(7)	Te(5)-Fe(6)-Te(8)	86.47(7)
Te(5)-Fe(6)-Te(10)	87.34(7)	Te(5)-Fe(7)-Te(6)	82.01(7)
Te(5)-Fe(7)-Te(7)	81.72(7)	Te(6)-Fe(7)-Te(7)	83.23(7)
Te(6)-Fe(8)-Te(7)	83.34(7)	Te(6)-Fe(8)-Te(8)	81.37(7)
Te(7)-Fe(8)-Te(8)	80.57(6)	Te-Fe-Te (mean)	83.3(5)
C-Fe-C (mean)	97(6)		

b. The estimated standard deviations in the mean bond lengths and the mean bond angles are calculated by the equation $\sigma_l=\{\Sigma_n(l_n-l)^2/n(n-1)\}^{1/2}$, where l_n is the length (angle) of the *n*th bond, l the mean length (angle), and n the number of bonds.

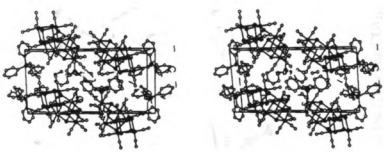


Figure 5·5. The Packing Diagram in the Unit Cell of $(Ph_4P)_2[\{Fe_4Te_4(CO)_{10}\}_2(Te_2)]$ (Stereoview)

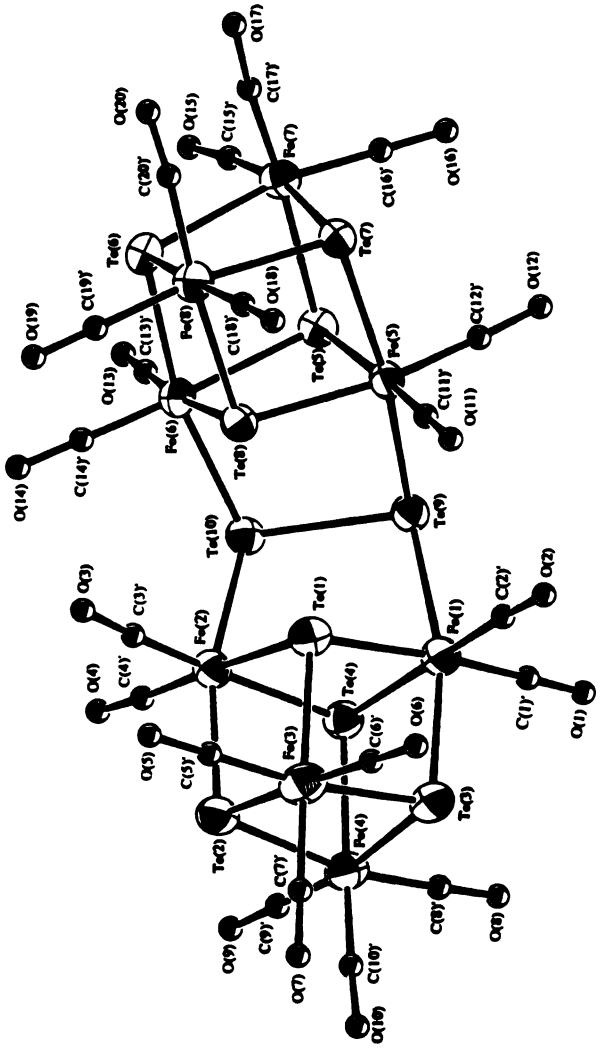


Figure 5-6. The Structure of the $[\{Fe_4Te_4(CO)_{10}\}_2(Te_2)]^{2-}$ Anion

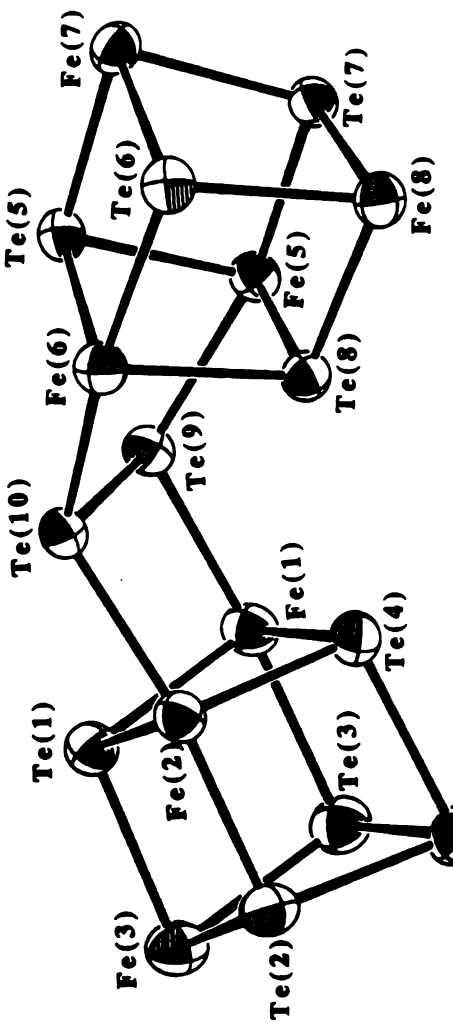


Figure 5·7. The Structure of the $[\{Fe_4Te_4(CO)_{10}\}_2(Te_2)]^{2-}$ Anion with CO Groups Omitted, Emphasizing the Two Fe_4Te_4 Cores and Their Coupling via the Te_2^{2-} Ligand

(iii). Structure of $(Ph_4P)_2[\{Fe_2Se(CO)_6\}_2(Se_2)]$ (5·3)

The lattice of (5·3) is made up of Ph_4P^+ cations and discrete $[\{Fe_2Se(CO)_6\}_2(Se_2)]^{2-}$ anions as shown in Figure 5·8. The latter has a known sulfur analog $[\{Fe_2S(CO)_6\}_2(S_2)]^{2-}$[26]. The $[\{Fe_2Se(CO)_6\}_2(Se_2)]^{2-}$, as depicted in Figure 5·9, possesses a Se-Se linkage (also a μ_4-type ligand) between two $Fe_2Se_2(CO)_6$ units which are crystallographically related to each other by an inversion center at the midpoint of the diselenide Se_2^{2-} ligand. The asymmetric unit $[Fe_2Se_2(CO)_6]^-$ can be viewed as being formed by two square pyramids of the $FeSe_2(CO)_3$ fragments through sharing one edge (i. e. Se(1)-Se(2)) of their basal planes. These basal planes of the pyramids are each defined by Se(1)/Se(2)/C(2)/C(3) or Se(1)/Se(2)/C(5)/C(6), and the apexes by C(1) or C(4), respectively. The planarity of two basal planes is as following: Se(1), Se(2), C(2) and C(3) deviate from the best least-squares plane by -0.003, 0.004, -0.301 and 0.249 Å respectively, and Fe(1) is displaced from the plane by -0.372 Å; Se(1), Se(2), C(5) and C(6) deviate from the best least-squares plane by -0.001, 0.001, -0.112 and 0.083 Å respectively with Fe(2) lying 0.343 Å above it. If the charge of the diselenide and the monoselenide ligands is each taken as 2-, the four iron atoms would have a formal oxidation state 1+. The coordination geometry around the iron atoms is best described as distorted octahedral because, in addition to the normal chemical bonds to the corners of the square pyramids, the iron atoms are very close at 2.555(6) Å to each other. This is consistent with an Fe-Fe single bond, and comparable with that found in $Fe_2(Se_2)(CO)_6$ (2.575(2) Å)[27] and in $(Ph_4As)_2[\{Fe_2S(CO)_6\}_2(S_2)]$ (2.516(1) Å)[26]. The short Fe-Fe bond gives rise to the non-planar conformation of two Fe_2Se_2 units, hence the whole molecule looks like two butterflies joining their wings in a side-by-side fashion as shown in Figure 5·10. The bond distance of the Se_2^{2-} unit (i. e. Se(1)-Se(1)=2.467(7) Å) approaches the upper limit of a single Se-Se bond [28-29] while the intra-molecular Se-Se distance (i. e. Se(1)-Se(2)) of 2.847(5) is significantly shorter than their van der Waals

contact (i.e. 4.00 Å)[30]. This indicates that the valence electrons in the Se atoms are more or less delocalized among these four Se atoms. The same structural feature has also been observed in the sulfur analog[26]. It appears that Se(1) and Se(2) form a partial bond by removal of electron density from these atoms and transfer to the Se(1)-Se(1) bond and to the CO ligands. Selected bond distances and bond angles are summarized in Table 5·10.

Table 5·10. Selected Geometric Data for $(Ph_4P)_2[\{Fe_2Se(CO)_6\}_2(Se_2)]$ (5·3)[b]

		Bond Distances (Å)	
Fe(1)-Fe(2)	2.555(6)	Se(1)-Se(1)	2.467(7)
Fe(1)-Se(2)	2.415(5)	Fe(2)-Se(1)	2.358(5)
Fe(1)-Se(1)	2.354(5)	Fe(2)-Se(2)	2.417(5)
Fe-Se (mean)	2.386(17)	Fe-C (mean)	1.80(1)
Se(1)···Se(2)	2.847(5)		
		Bond Angles (deg)	
Fe(1)-Se(1)-Fe(2)	65.7(2)	Fe(1)-Se(2)-Fe(2)	63.8(2)
Se(1)-Se(1)-Fe(1)	107.1(2)	Se(1)-Se(1)-Fe(2)	109.2(2)
Se(1)-Fe(1)-Se(2)	73.3(2)	Se(1)-Fe(2)-Se(2)	73.2(2)
Se(1)-Fe(1)-C(1)'	94(1)	Se(1)-Fe(1)-C(2)'	156(1)
Se(1)-Fe(1)-C(3)'	98.5(9)	Se(1)-Fe(2)-C(4)'	104.0(8)
Se(1)-Fe(2)-C(5)'	151(1)	Se(1)-Fe(2)-C(6)'	96.1(9)
Se(2)-Fe(1)-C(1)'	112(1)	Se(2)-Fe(1)-C(2)'	84(1)

Table 5·10. (cont'd)

Bond Angles (deg)			
Se(2)-Fe(1)-C(3)'	151(1)	Se(2)-Fe(2)-C(4)'	101(1)
Se(2)-Fe(2)-C(5)'	87(1)	Se(2)-Fe(2)-C(6)'	161(1)
Fe(2)-Fe(1)-C(1)'	112(1)	Fe(2)-Fe(1)-C(2)'	84(1)
Fe(2)-Fe(1)-C(3)'	151(1)	Fe(1)-Fe(2)-C(4)'	153.8(9)
Fe(1)-Fe(2)-C(5)'	95(1)	Fe(1)-Fe(2)-C(6)'	103.5(9)
C(1)'-Fe(1)-C(2)'	102(1)	C(1)'-Fe(1)-C(3)'	96(1)
C(2)'-Fe(1)-C(3)'	98(1)	C(4)'-Fe(2)-C(5)'	100(1)
C(4)'-Fe(2)-C(6)'	96(1)	C(5)'-Fe(2)-C(6)'	97(1)
C(4)'-Fe(2)-C(6)'	96(1)	C(5)'-Fe(2)-C(6)'	97(1)

b. The estimated standard deviations in the mean bond lengths and the mean bond angles are calculated by the equation $\sigma_l=\{\Sigma_n(l_n-l)^2/n(n-1)\}^{1/2}$, where l_n is the length (angle) of the *n*th bond, l the mean length (angle), and n the number of bonds.

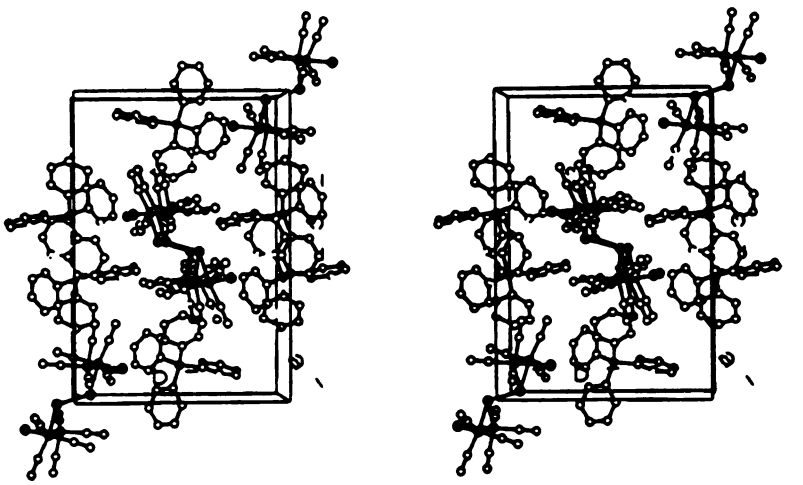


Figure 5·8. The Packing Diagram in the Unit Cell of $(Ph_4P)_2[\{Fe_2Se(CO)_6\}_2(Se_2)]$ (Stereoview)

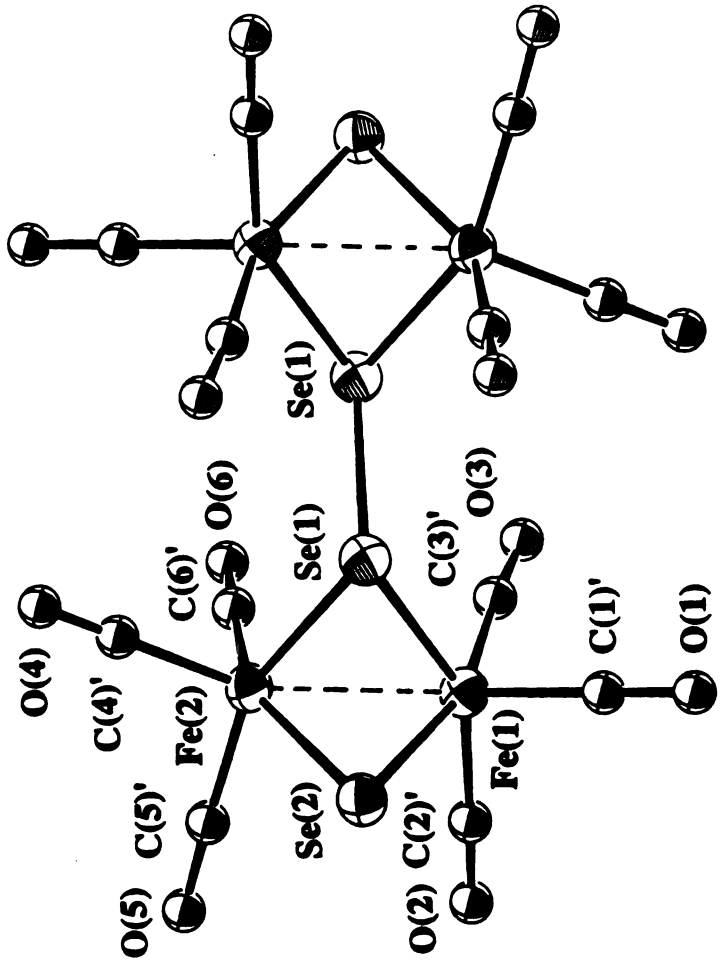


Figure 5-9. The Structure of the $[\{Fe_2Se(CO)_6\}_2(Se_2)]^{2-}$ Anion

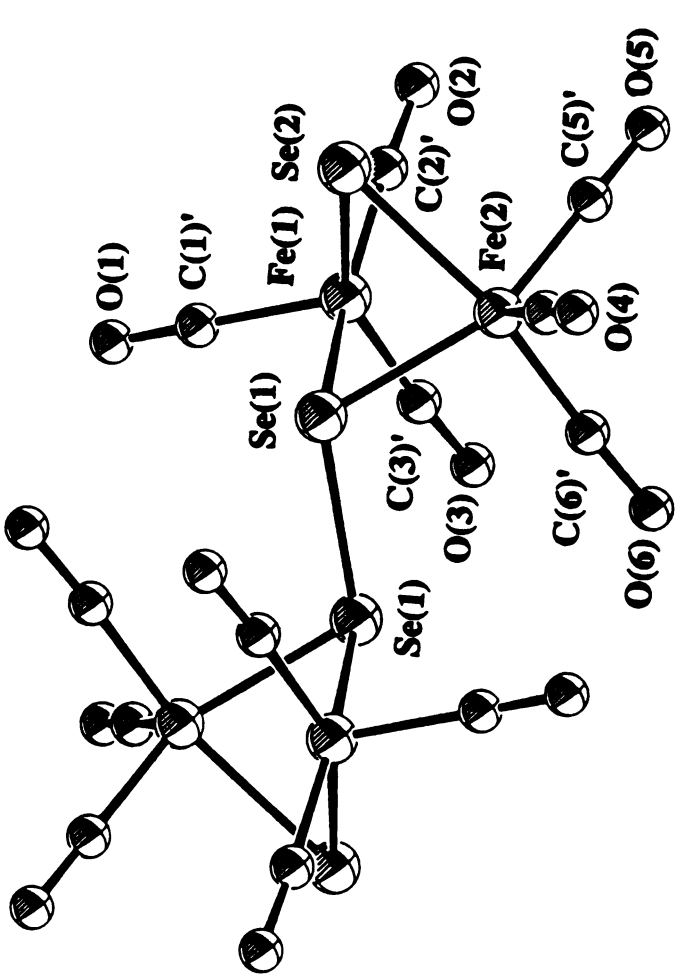


Figure 5-10. A Different View of the [{Fe2Se(CO)6}2(Se2)]$^{2-}$ Anion, Showing the Double "Butterfly" Conformation of the Molecule

2. Spectroscopic Studies

Figure 5·11 shows the solid-state IR spectra of the three compounds in the CO region. $(Ph_4P)_2[Ru_6(Te_2)_7(CO)_{12}]$ shows an overlapped absorption pattern in this region, a broad peak centered at 1997 cm^{-1} and three superimposed peaks at 1966, 1957 and 1948 cm^{-1}. Four broad bands are identifiable for $(Ph_4P)_2[\{Fe_4Te_4(CO)_{10}\}_2(Te_2)]$ at 2013, 1968, 1912 and 1900 cm^{-1}, while $(Ph_4P)_2[\{Fe_2Se(CO)_6\}_2(Se_2)]$ gives three absorptions at 2020, 1984 and 1939 cm^{-1}. Figure 5·12-5·13 show the far IR spectra of the three compounds. $(Ph_4P)_2[Ru_6(Te_2)_7(CO)_{12}]$ shows two strong absorptions at 188 and 175 cm^{-1}, a medium absorption at 228 cm^{-1}, and a weak absorption at 164 cm^{-1}. In the spectrum of $(Ph_4P)_2[\{Fe_4Te_4(CO)_{10}\}_2(Te_2)]$, three weak bands are observed at 209(w), 151(m) and 140(m) cm^{-1}, while $(Ph_4P)_2[\{Fe_2Se(CO)_6\}_2(Se_2)]$ gives four absorptions at 243(m), 224(w), 206(w) and 198(w) cm^{-1}. The assignment of these far-IR peaks is given in the next section.

The UV/vis spectra of $(Ph_4P)_2[Ru_6(Te_2)_7(CO)_{12}]$ and $(Ph_4P)_2[\{Fe_4Te_4(CO)_{10}\}_2(Te_2)]$ in DMF solution are both featureless, while $(Ph_4P)_2[\{Fe_2Se(CO)_6\}_2(Se_2)]$ in the same solution shows a plateau in the region 300 to 385 nm (Figures 5·14).

The ^{77}Se NMR spectrum of (5·3) in DMF gave two peaks at 450 and -32 ppm, as shown in Figure 5·15, and is consistent with two types of Se ligands present in this cluster. However, no unambiguous assignment of the peaks can be given based on the resonance frequencies.

3. Thermal Decomposition

Figure 5·16 shows the TGA diagrams of compounds (5·1)–(5·3) in the temperature range of 25 to 800 °C. For all compounds, the weight loss continues beyond

800 °C. Although a well-defined plateau can be found in each diagram, the residual weight does not suggest a simple binary metal chalcogenide. Instead, such an intermediate may contain carbon as well.

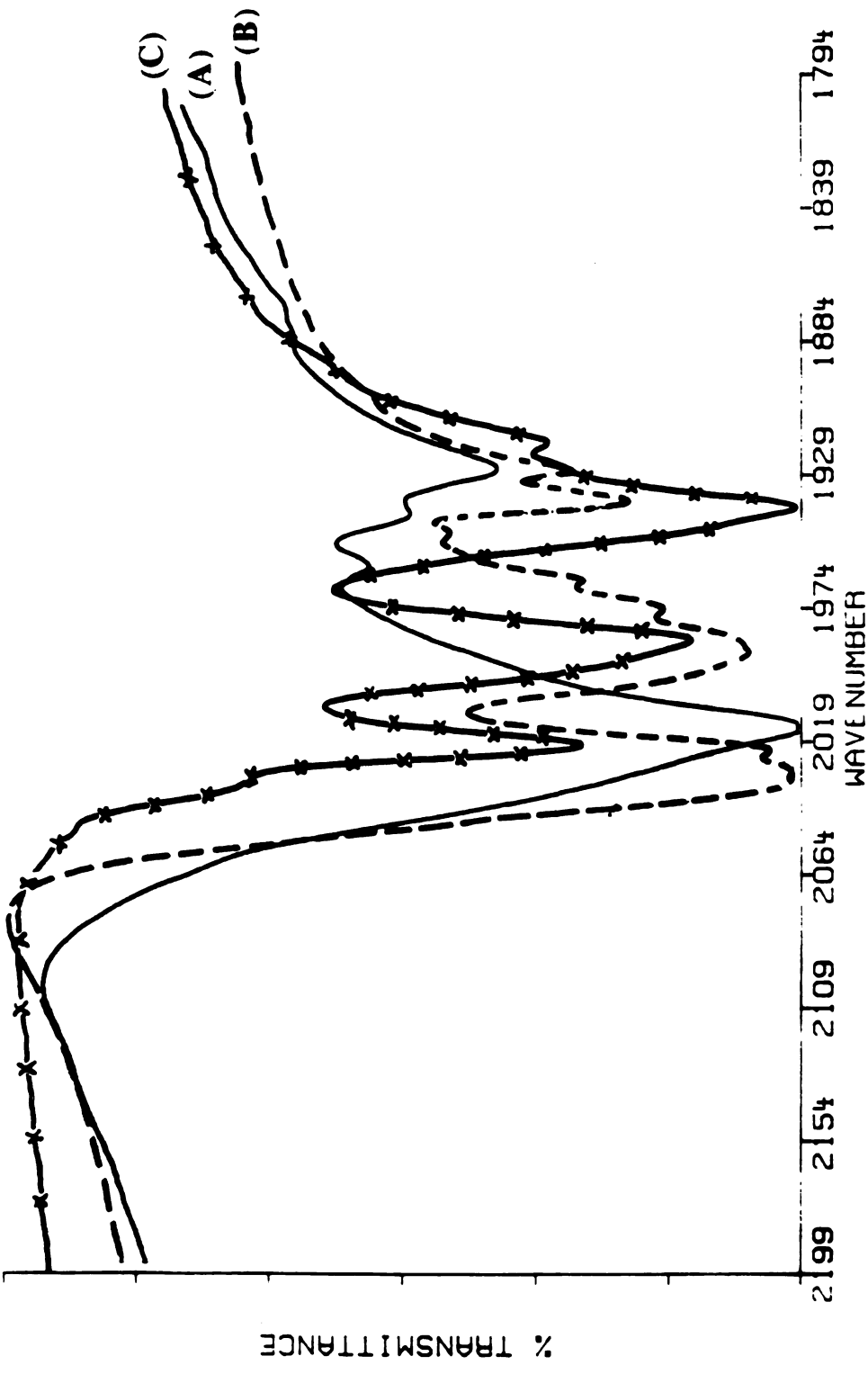


Figure 5·11. The Solid-State IR Spectra in the CO Region for (A) $(Ph_4P)_2[Ru_6(Te_2)_7(CO)_{12}]$, (B) $(Ph_4P)_2[\{Fe_4Te_4(CO)_{10}\}_2(Te_2)]$ and (C) $(Ph_4P)_2[\{Fe_2Se(CO)_6\}_2(Se_2)]$

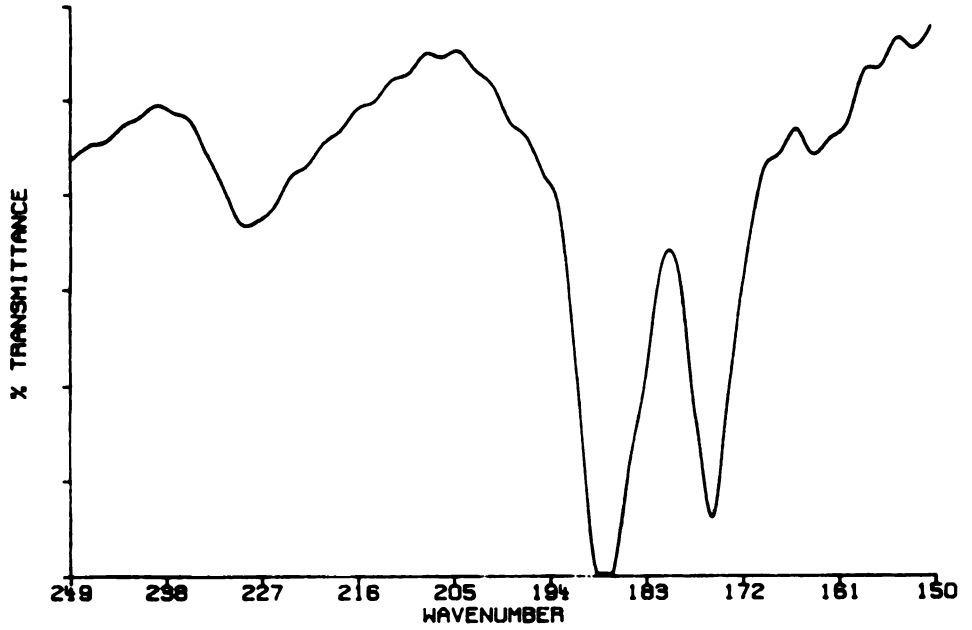


Figure 5·12. The Solid-State Far IR Spectrum of $(Ph_4P)_2[Ru_6(Te_2)_7(CO)_{12}]$

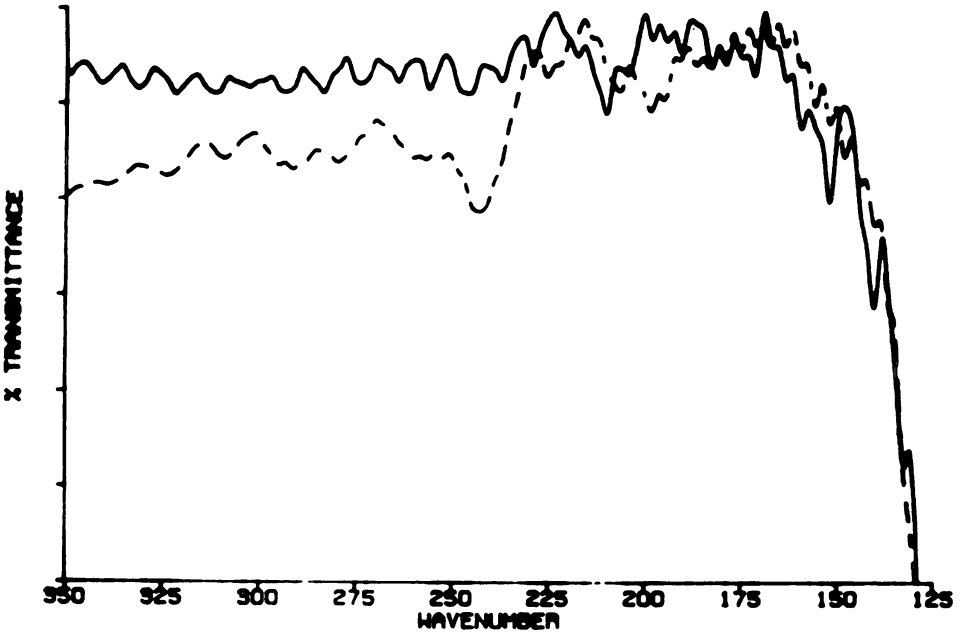


Figure 5·13. The Solid-State Far IR Spectrum for (—) $(Ph_4P)_2[\{Fe_4Te_4(CO)_{10}\}_2(Te_2)]$ and (---) $(Ph_4P)_2[\{Fe_2Se(CO)_6\}_2(Se_2)]$

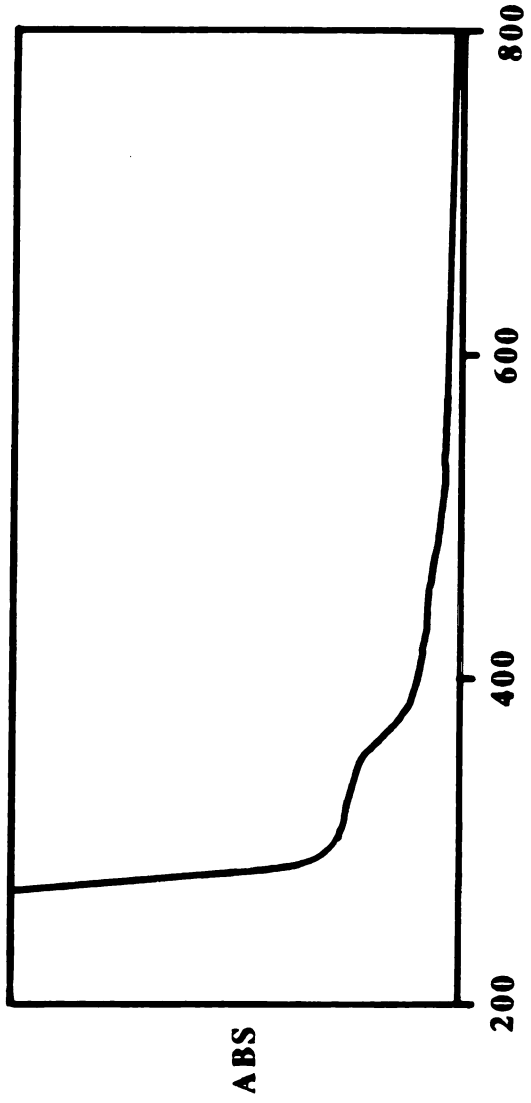


Figure 5·14. The UV/vis Spectrum of $(Ph_4P)_2[\{Fe_2Se(CO)_6\}_2(Se_2)]$ in DMF

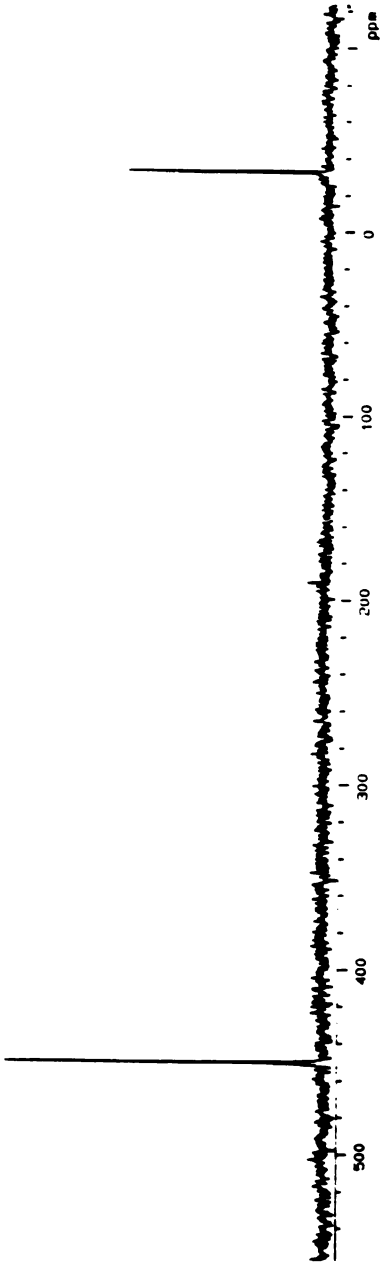


Figure 5-15. The ^{77}Se NMR Spectrum of $(Ph_4P)_2[\{Fe_2Se(CO)_6\}_2(Se_2)]$ in DMF

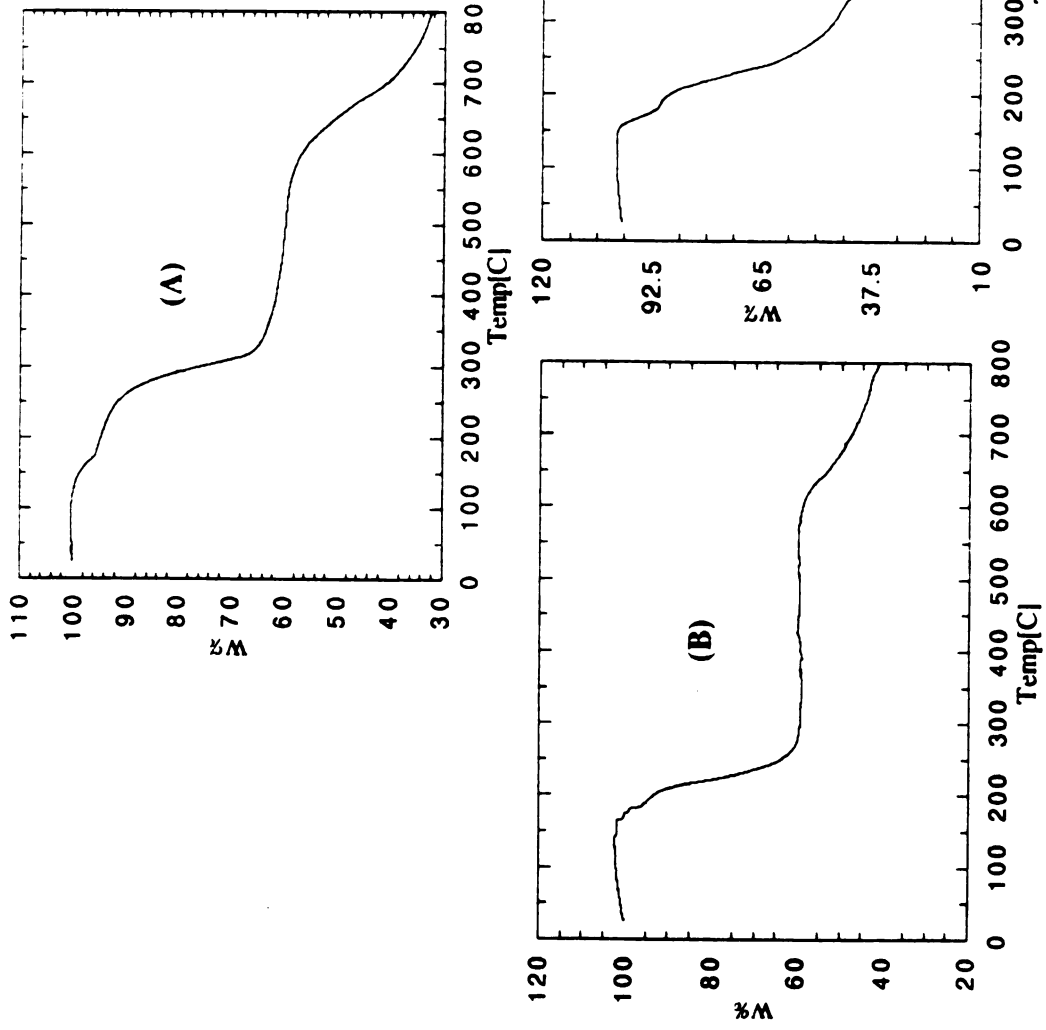


Figure 5.16. The TGA diagrams of (A) $(Ph_4P)_2[Ru_6(Te_2)_7(CO)_{12}]$, (B) $(Ph_4P)_2[\{Fe_4Te_4(CO)_{10}\}_2(Te_2)]$ and (C) $(Ph_4P)_2[\{Fe_2Se(CO)_6\}_2(Se_2)]$

IV. Discussion

The one-step assembly of three transition metal carbonyl polychalcogenide clusters is readily accomplished through oxidative decarbonylation of $Fe(CO)_5$ by Na_2Q_2 (Q=Te or Se) under hydro(methano)thermal conditions:

$$Ru_3(CO)_{12} + 5Na_2Te_2 \xrightarrow[6Ph_4PCl,\ \text{sealed tube}]{H_2O,\ 110\ ^\circ C\ \text{for}\ 65\ h} (Ph_4P)_2[Ru_6(Te_2)_7(CO)_{12}] \quad \text{eq.(5·1)}$$

$$Fe(CO)_5(\text{excess}) + Na_2Te_2 \xrightarrow[Ph_4PCl,\ \text{sealed tube}]{H_2O,\ 110\ ^\circ C\ \text{for}\ 60\ h} (Ph_4P)_2[\{Fe_4Te_4(CO)_{10}\}_2(Te_2)] \quad \text{eq.(5·2)}$$

$$Fe(CO)_5(\text{excess}) + Na_2Se_2 \xrightarrow[Ph_4PCl,\ \text{sealed tube}]{MeOH,\ 80\ ^\circ C\ \text{for}\ 96\ h} (Ph_4P)_2[\{Fe_2Se(CO)_6\}_2(Se_2)] \quad \text{eq.(5·3)}$$

The most intriguing feature of these reactions is the concomitant growth of single crystals of the products. Under hydro(solvo)thermal conditions the chemical reaction is combined with a transport process. The latter can facilitate crystallization of the reaction product. Generally, both solubility and crystallization process of a hydrothermal reaction are improved by the presence of a complexing agent–a "mineralizer" in geological terminology. In the the above reactions, dichalcogenide ligands act as reagents as well as mineralizers.

The ultimate molar ratio of the reactants in each synthesis was determined by optimizing the synthetic yield, and/or by avoiding the formation of polychalcogenide/elemental chalcogen crystals. In the synthetic reactions that involve Na_2Se_2, H_2O is found to cause decomposition of the ligand, affording single crystals of elemental selenium. The use of MeOH gave satisfactory result.

The $(Ph_4P)_2[Ru_6(Te_2)_7(CO)_{12}]$ has so far proven to be inaccessible by conventional solution reactions. Attempts to synthesize $[Ru_6(Te_2)_7(CO)_{12}]^{2-}$ by reacting $Ru_3(CO)_{12}$ or $(Ph_3P)_2Ru(CO)_2Cl_2$ with Na_2Te_x (X=2 or 4) in non-aqueous solutions (i.e. DMF or CH_3CN) at ambient temperatures yielded $[Ru(CO)_2(Te_4)_2]^{2-}$, isomorphous to $[Ru(CO)_2(Se_4)_2]^{2-}$[31]. Recently, Kolis and co-workers have successfully synthesized $(Ph_4P)_2[\{Fe_4Te_4(CO)_{10}\}_2(Te_2)]$ through a solution reaction[32]. The $(Ph_4P)_2[\{Fe_2Se(CO)_6\}_2(Se_2)]$ may also be accessible by conventional solution reactions in light that its sulfur analogue has been done so by Averill *et al*[26]. The significance of our synthetic discoveries lies in the methodology itself. In addition, it does provide an interesting alternative for making these two compounds. For a long time, the hydro(methano)thermal technique has been perceived to be unsuitable for the syntheses of compounds containing transition metal carbonyls, presumably, such a process will be hindered by either the poor thermal stability of metal carbonyls, or the low solubility of both reactants and products in H_2O or MeOH. Through the successful syntheses of these compounds, we have proven the applicability of the hydro(methano)thermal technique to the preparation of inorganic compounds involving organometallic molecules.

The structure of $[Ru_6(Te_2)_7(CO)_{12}]^{2-}$ is peculiar in that its central $\{Ru_6(Te_2)_7\}^{2-}$ core is reminiscent of an excised fragment of the $RuTe_2$ pyrite-type lattice. The mid-point of the central Te_2^{2-} unit in $[Ru_6(Te_2)_7(CO)_{12}]^{2-}$ is situated at the octahedral center with six Ru atoms being its neighbors. This is exactly the same environment for the Te_2^{2-} units found in pyrite[33]. It is tempting to conjecture that if further aggregation takes place to form the pyrite structure, this cluster core could be acting as the nucleus for crystallite growth. The close resemblance of this cluster core to the corresponding pyrite solid-state lattice imposes an unprecedented bonding feature on the central ditelluride Te_2^{2-} which has not been found in any molecular species containing either S_2^{2-} or Se_2^{2-} ligands[34-35]. The only example which can be cited for comparison is $[W_6(Te_2)_4(CO)_{18}]^{2-}$[36], where the

tellurium atoms in the center Te_2^{2-} each bind to three metal atoms. However, the six tungsten atoms are in trigonal prismatic arrangement due to the W-W metal bonds, which constrains the W_3Te-TeW_3 fragment to an eclipse conformation. The μ_3-type bridging mode of the six peripheral Te_2^{2-} units in $[Ru_6(Te_2)_7(CO)_{12}]^{2-}$ is not known for polytellurides[37].

Thus far, the majority of the $[Fe_4Q_4(X)_4]^{n-}$ (Q=S, Se and Te) cubanes found in the literature are mixed-valent with extensive M-M bonding in the Fe_4Q_4 cores[22, 25]. Therefore, the formal oxidation state of iron atoms is often a non-integral value between 2 and 3. Dahl and co-workers showed that when the nitrosyl clusters $[Fe_4Q_4(NO)_4]$ (Q=S, Se) were reacted with CO to form $[Fe_4Q_4(CO)_{12}]$ (Q=S, Se), the Fe-Fe distances expanded from 2.65 Å to 3.47 Å (for Q=S), or 2.71 Å to 3.62 Å (for Q=Se)[38]. This was in accordance with the analysis of the qualitative MO's of cubane-like Fe_4Q_4 clusters (Q=S, Se and Te), which had predicted that if the 60e nitrosyl cubane cluster was to expand to a 72e cluster, the additional 12 valence electrons would have to occupy the six empty tetra-iron antibonding MO's (i. e. t_1+t_2) of the cluster, resulting in complete breakage of the M-M bonding[39]. A similar argument applies in (**5·2**). Elimination of the metal-metal bonding in (**5·2**) liberates the two cubanes from severe distortion.

It has been shown that the Fe_2Q_2 (Q=S or Se) unit is a fundamental building block to a large family of iron-sulfur (-selenium) clusters[40], where the Fe_2Q_2 rhomb can be either planar or non-planar. However, when two iron atoms are each coordinated by three CO groups and two μ_2-type bridging ligands acting overall as 3-electron donors, the molecule will invariably adopt a "butterfly" conformation with an Fe-Fe single bond[41]. This salient feature has been manifested by a variety of structurally related compounds containing amido, phosphido and thiolato ligands[42]. In view of its electronic structure, the $\{Fe_2Se(CO)_6\}_2(Se_2)]^{2-}$ molecule apparently falls into this category. It is worthwhile to note that the iron-tellurium cluster $[Fe_2(Te)(Te_2)(CO)_6]^{2-}$ also belongs to this group[43].

The unusual Te_2^{2-} acts as a μ_2-η^1-ligand which bridges two iron centers using one tellurium atom while another tellurium atom assumes a terminal position. This molecule has a "butterfly" structure too.

The solid-state IR spectra of these compounds all showed overlapped absorption patterns in the CO region because they are complicated by the overlap of the CO absorptions from different metal centers in the crystal lattice. However, the overall pattern of each spectrum is very characteristic of the compound and the absorption energies are consistent with the terminal ligation for all CO groups. In the far IR region, three absorptions at 188, 175, 164 cm^{-1} for (**5·1**), and a weak absorption at 209 (w, b and triplet) cm^{-1} for (**5·2**), are tentatively assigned to the Te-Te stretching vibrations. The similar assignment has also been made before for other polytelluride compounds, i.e. ν_{Te-Te}=200 cm^{-1} for $(Ph_4P)_2[Pd(Te_4)_2]\cdot DMF$[44] and ν_{Te-Te}=188 cm^{-1} for $(Ph_4P)_2[Te_4]$[45]. The peak observed at higher energy, i.e. 228 cm^{-1} for (**5·1**) is a good candidate for the Ru-Te stretching vibration. However, two peaks observed at 151 and 140 cm^{-1} for (**5·2**) can not be interpreted. The weak absorption at 243 cm^{-1} for (**5·3**) can be assigned to the Se-Se stretching vibration, for example, $[Fe_2Se_{12}]^{2-}$ (ν_{se-se}=258 cm^{-1})[46], $[SnSe_{12}]^{2-}$ (ν_{se-se}=273 and 256 cm^{-1})[47], $[Ag_xSe_y]^{n-}$ (ν_{se-se}=265 cm^{-1})[48], $[Se_x]^{2-}$ (x=2-6, ν_{se-se}=285 cm^{-1})[49] and *cyclo*-Se_6 (ν_{se-se}=253 cm^{-1})[50]. Similarly, three weak absorptions for (**5·3**) at 224, 206 and 198 cm^{-1} cannot be assigned.

In conclusion, three metal carbonyl chalcogenide clusters have been made hydro(methano)thermally. The successful synthesis of these clusters illustrates the applicability of the hydrothermal technique to the preparation of inorganic compounds involving organometallic molecules. The reactions reported here are unexpected in two ways: (a) traditionally, water and methanol are believed to be poor solvents for metal carbonyls at ambient temperatures and thus undesirable for chemical reactions, (b) in general Ph_4P^+ salts of inorganic clusters are also insoluble in water or methanol. Thus, we

demonstrate for the first time, that with the altered solvent behavior of water or methanol at superheated conditions and in the presence of alkali polychalcogenides, the disadvantage of insufficient solubility of metal carbonyls and Ph_4P^+ salts can be overcome. This may prove to be significant as it opens up a new dimension in synthetic organometallic research. Such a method may create new exciting synthetic opportunities for organometallic-main group compounds. Applications of this technique to organometallic synthesis should by no means be limited to metal carbonyls[51].

REFERENCES

1. Hydrothermal conditions have also been used to prepared metal monochalcogenides, see (a) W. S. Sheldrick, *Z. Anorg. Allg. Chem.*, 562(1988), 23-30. (b) W. S. Sheldrick and H.-J. Häuser, *Z. Anorg. Allg. Chem.*, 557(1988), 98-104. (c) W. S. Sheldrick and H.-J. Häuser, *Z. Anorg. Allg. Chem.*, 557(1988), 105-111. (d) W. S. Sheldrick and J. Kaub, *Z. Anorg. Allg. Chem.*, 535(1986), 179-185. (e) J. B. Parise, *Science*, 251(1991), 293-294. (f) J. B. Parise, *J. Chem. Soc., Chem. Commun.*, (1990), 1553-1554.

2. J.-H. Liao and M. G. Kanatzidis, *J. Am. Chem. Soc.*, 112(1990), 7400-7402.

3. (a) J.-H. Liao and M. G. Kanatzidis, *Inorg. Chem.*, 31(1992), 431-439. (b) J.-H. Liao, L. Hill and M. G. Kanatzidis, submitted to *Inorg. Chem.* (c) J.-H. Liao and M. G. Kanatzidis, manuscript in preparation.

4. See, for example: (a) *Comprehensive Organometallic Chemistry,* Vol. 6, Chapter 41-43, p879-1043, G. Wilkinson, F. G. A. Stone, E. Abel, Eds., Pergamon, Oxford, England, 1982. (b) H. Vahrenkamp, *Adv. Organomet. Chem.*, 22(1983), 169-208.

5. W. A. Herrmann, *Angew. Chem. Int. Ed. Engl.*, 25(1986), 56-76.

6. K. H. Whitmire, *J. Coord. Chem.*, 17(1988), 95-203.

7. (a) H. Vahrenkamp, *Angew. Chem. Int. Ed. Engl.*, 14(1975), 322-329. (b) R. D. Adams, *Polyhedron,* 4(1985), 2003-2025. (c) J. Wachter, *J. Coord. Chem.*, 15(1987), 219-235. (d) A. Müller, *Polyhedron* , 5(1986), 323-340. (e) J. Wachter, *Angew. Chem. Int. Ed. Engl* ., 28(1989), 1613-1626.

8. D. Fenske, J. Ohmer, J. Hachgenei and K. Merzweiler, *Angew. Chem. Int. Ed. Engl.*, 27(1988), 1277-1296.

9. (a) V. W. Day, D. A. Lesch and T. B. Rauchfuss, *J. Am. Chem. Soc.*, 104(1982), 1290-1295. (b) D. A. Lesch and T. B. Rauchfuss, *Inorg. Chem.*, 22(1983), 1854-1857. (c) L. E. Bogan, Jr, T. B. Rauchfuss and A. L. Rheingold, *J. Am. Chem. Soc.*, 107(1985), 3843-3850.

10. (a) P. Mathur, I. J. Mavunkal and V. Rugmini, *Inorg. Chem.*, 28(1989), 3616-3618. (b) P. Mathur, I. J. Mavunkal and A. L. Rheingold, *J. Chem. Soc., Chem.Commun.*, 1989, 382-384. (c) P. Mathur, B. H. S. Thimmappa and A. L. Rheingold, *Inorg. Chem.*, 29(1990), 4658-4665. (d) P. Mathur, I. J. Mavunkal, V. Rugmini and M. F. Mahon, *Inorg. Chem.*, 29(1990), 4838-4840.

11. For recent examples, see (a) P. Mathur, D. Chakrabarty, Md. M. Hossain and R. S. Rashid, *J. Organomet. Chem.*, 420(1991), 79-86. (b) R. D. Adams, J. E. Babin, J.-G. Wang and W. Wu, *Inorg. Chem.*, 28(1989), 703-709. (c) R. D. Adams, J. E. Babin, J. Estrada, J.-G. Wang, M. B. Wang and A. A. Low, *Polyhedron*, 8(1989), 1885-1890.

12. D. D. Perrin, W. L. F. Armarego and D. R. Perrin, *Purification of Laboratory Chemicals*, 2nd Ed., Pergamon Press, Oxford UK, 1980.

13. See chapter 2.

14. N. Walker and D. Stuart, *Acta Crystallogr.*, 39A(1983), 158-166.

15. *TEXSAN: Single Crystal Structure Analysis Software*, Version 5.0, Molecular Structure Corporation, The Woodlands, Texas.

16. H. P. Klug and L. E. Alexander, *X-ray Diffraction Procedures for Polycrystalline and Amorphous Materials,* John Wiley and Sons, New York, 1974.

17. D. K. Smith, M. C. Nichols and M. E. Zolensky, *POWD10: A Fortran IV Program for Calculating X-ray Powder Diffration Patterns,* Version 10, Pennsylvania State University, 1983.

18. H. D. Lutz, M. Jung and G. Waschenbach, *Z. Anorg. Allg. Chem.,* 554(1987), 87-91.

19. M. Di Vaira, M. Peruzzini and P. Stoppioni, *Angew. Chem. Int. Ed. Engl.,* 26(1987), 916-917.

20. B. W. Eichhorn, R. C. Haushalter, F. A. Cotton and B. Wilson, *Inorg. Chem.,* 27(1988), 4084-4085.

21. P. Mathur, B. H. S. Thimmappa and A. L. Rheingold, *Inorg. Chem.,* 29(1990), 4658-4665.

22. (a) J. M. Berg and R. H. Holm in *Iron-Sulfur Proteins*, Chapter 1, T. G. Spiro, Ed., John Wiley and Sons, Inc., New York, 1982. (b) B. Krebs, G. Henkel, *Angew. Chem. Int. Ed. Engl.,* 30(1991), 769-788.

23. M. Di Vaira, M. Peruzzini and P. Stoppioni, *Angew. Chem. Int. Ed. Engl.,* 26(1987), 916-917.

24. R. C. Haushalter, *Angew. Chem. Int. Ed. Engl.,* 24(1985), 433-435.

25. (a) W. Bronger, M. Kimpel and D. Schmitz, *Angew. Chem. Int. Ed. Engl.,* 21(1982), 544-545. (b) W. Simon, A. Wilk, B Krebs and G. Henkel, *Angew.*

Chem. Int. Ed. Engl., 26(1987), 1009-1010. (c) G. Henkel, W. Simon and B. Krebs, *Z. Kristallogr.*, 186(1989), 125-127.

26. K. S. Rose, E. Sinn, B. A. Averill, *Organometallicss,* 3(1984), 1126-1128.

27. C. F. Campana, F. Y.-K. Lo and L. F. Dahl, *Inorg. Chem.*, 18(1979), 3060-3064.

28. S.-P. Huang and M. G. Kanatzidis, *Inorg. Chem.*, 30(1991), 3572-3575.

29. (a) M. G. Kanatzidis, *Comments Inorg. Chem.*, 10(1990), 161-195. (b) M. A. Ansari and J. A. Ibers, *Coord. Chem. Rev.*, 100(1990), 223-266.

30. L. Pauling, *The Nature of the Chemical Bond*, 2nd Ed., Cornell University Press, Ithaca, New York, 1960, p260.

31. See chapter 3.

32. L. A. Roof, W. T. Pennington and J. W. Kolis, *Angew. Chem. Int. Ed. Engl.*, 31(1992), 913-91915.

33. A. F. Wells, *Structural Inorganic Chemistry*, 5th Ed., Clarendon Press, Oxford UK, 1984, p758-759.

34. (a) M. Draganjac and T. B. Rauchfuss, *Angew. Chem. Int. Ed. Engl.*, 24(1985), 742-757. (b) A. Müller, *Polyhedron,* 5(1986), 323-340. (c) A. Müller and E. Diemann, *Adv. Inorg. Chem.*, 31(1987), 89-122.

35. (a) M. G. Kanatzidis, *Comments Inorg. Chem.*, 10(1990), 161-195. (b) M. A. Ansari and J. A. Ibers, *Coord. Chem. Rev.*, 100(1990), 223-266. (c) J. W. Kolis, *Coord. Chem. Rev.*, 105(1990), 195-219.

36. L. C. Roof, W. T. Pennington and J. W. Kolis, *J. Am. Chem. Soc.*, 112(1990), 8172-8174.

37. This bridging mode has been observed in sulfur and selenium chemistry, see (a) P. J. Vergamini and G. J. Kubas, *Prog. Inorg. Chem.*, 21(1976), 261-282. (b) V. A. Uchtman and L. F. Dahl, *J. Am. Chem. Soc.*, 91(1969), 3756-3763. (c) P. M. Fritz, W. Beck, U. Nagel, K. Polborn, W. A. Herrmann, C. Hecht and J. Rohrmann, *Z. Naturforsch*, 43B(1988), 665-670.

38. L. Nelson, F. Y.-K. Lo, A. D. Rae and L. F. Dahl, *J. Organomet. Chem.*, 225(1982), 309-329.

39. (a) Trinh-Toan, Ph.D. Thesis, University of Wisconsin-Madison, 1972. (b) B. K. Teo, Ph.D. Thesis, University of Wisconsin-Madison, 1973.

40. (a) J.-F. You, B. S. Snyder, G. C. Papaefthymiou and R. H. Holm, *J. Am. Chem. Soc.*, 112(1990), 1067-1076. (b) S.-B. Yu, G. C. Papaefthymiou and R. H. Holm, *Inorg. Chem.*, 30(1991), 3476-3485.

41. M. R. Adams, J. Gallucci and A. Wojcicki, *Inorg. Chem.*, 31(1992), 2-4.

42. D. F. Shriver and K. H. Whitmire in *Comprehensive Organometallic Chemistry*, Vol. 4, Chapter 31.1, p243-324., G. Wilkinson, F. G. A. Stone, E. Abel, Eds., Pergamon, Oxford, England, 1982.

43. B. W. Eichhorn, R. C. Haushalter and J. S. Merola, *Inorg. Chem.*, 29(1990), 728-731.

44. H. Wolkers, K. Dehnicke, D. Fenske, A. Khassanov and S. S. Hafner, *Acta Crystallogr.*, 47C(1991), 1627-1632.

45. J. Dietz, U. Müller, V. Müller and K. Dehnicke, *Z. Naturforsch.*, 46B(1991), 1293-1299.

46. H. Strasdeit, B. Krebs and G. Henkel, *Inorg. Chim. Acta* , 89(1984), L11-L13.

47. S.-P. Huang, S. Dhingra and M. G. Kanatzidis, *Polyhedron* , 9(1990), 1389-1395.

48. S.-P. Huang and M. G. Kanatzidis, *Inorg. Chem.*, 30(1991), 1455-1466.

49. F. Weller, J. Adel and K. Dehnicke, *Z. Anorg. Allg. Chem.*, 548(1987), 125-132.

50. K. Nagata, K. Tshibashi and Y. Miyamoto, *Jpn. J. Appl. Phys.*, 19(1980), 1569-1573.

51. See chapter 8.

MICHIGAN STATE UNIV. LIBR
3129300903215

THESIS
pt. 2



LIBRARY
Michigan State
University

PLACE IN RETURN BOX to remove this checkout from your record.
TO AVOID FINES return on or before date due.

DATE DUE	DATE DUE	DATE DUE

MSU Is An Affirmative Action/Equal Opportunity Institution
c:\circ\datedue.pm3-p.1

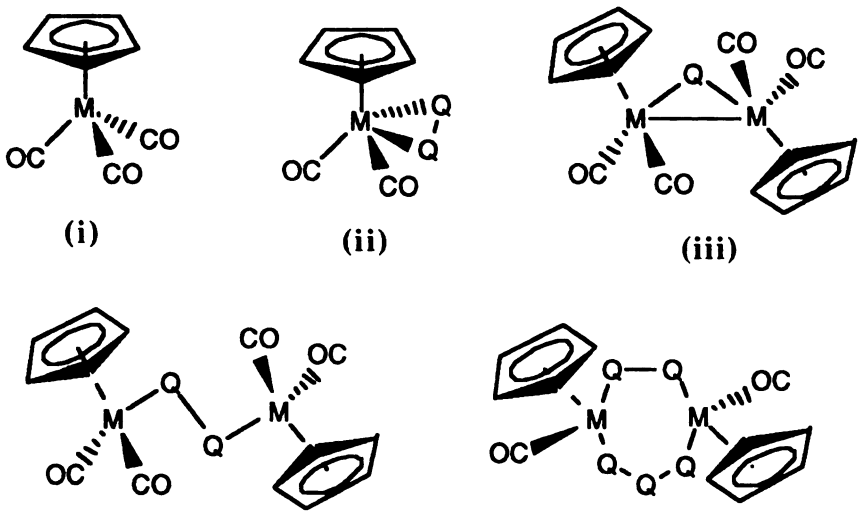
CHAPTER 6

MENTHANOTHERMAL SYNTHESIS OF CHALCOGENIDE-CONTAINING METAL CARBONYL CLUSTERS OF GROUP 7 ELEMENTS

I. Introduction

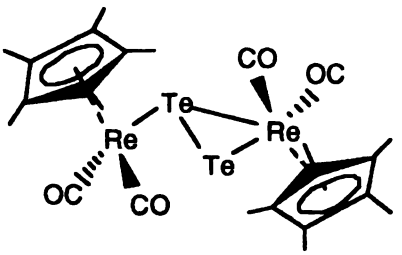
Through oxidative decarbonylation reactions of metal carbonyls by polychalcogenide ligands Q_n^{2-} (Q=S, Se and Te; n=2-6) *at hydro(solvo)thermal conditions,* we have opened up a new avenue for cluster chemistry of chalcogen-containing transition metal carbonyls[1]. With the technical expertise gained in the study of group 8 metal carbonyl/polychalcogenide chemistry, we moved on to explore similar synthetic opportunities in group 7.

Compared to elements in group 6 and 8, the organometallic chemistry of group 7 metals with polychalcogenides has not enjoyed extensive development[2-5]. Thus far, only a few CO/Cp-containing polychalcogenide complexes of Mn or Re have been described in the literature. For instance, Herberhold and co-workers once explored the reactivity of $CpM(CO)_2(L)$ (M=Mn or Re; L=CO or THF) with COQ (Q=S or Se) or elemental sulfur (selenium)[6-8]. Compounds isolated from these reactions are often monomers or dimers containing either monochalcogenide or dichalcogenide ligands, such as $CpM(CO)_2(Q_2)$ (when M=Mn, Q=S and Se; when M=Re, Q=S)[6-7], $Cp_2M_2(CO)_4(\mu\text{-}Q)$ (when M=Mn, Q=S and Se; when M=Re, Q=S)[6-7], $Cp_2Mn_2(CO)_4(\mu\text{-}Q_2)$ (Q=S and Se)[6-7] and $Cp_2Re_2(CO)_2(\mu\text{-}S_2)(\mu\text{-}S_3)$[8]. The structures of these compounds can be viewed as being formed by replacing CO groups in the $CpM(CO)_3$ molecule with chalcogenide ligands as shown in the following scheme:



Scheme 6·1. Structures of $CpM(CO)_3$ (i), and the Chalcogen-Containing Compounds Derived From This Molecule

A similar reaction between $CpRe(CO)_2(THF)$ and H_2Te (generated with Al_2Te_3/HCl) gave $Cp^*_2Re_2(CO)_4(Te_2)$[9]. The structure of this compound is slightly different from that of $Cp_2Mn_2(CO)_4(\mu\text{-}Q_2)$ (Q=S and Se) as shown below:



Scheme 6·2. The Structure of $Cp^*_2Re_2(CO)_4(Te_2)$

A large manganese carbonyl disulfide cluster $[Mn_4(S_2)_2(CO)_{15}]$ was prepared by the oxidative removal of $SnMe_3$ groups from the S-$SnMe_3$ ligands in $[(CO)_4Mn(\mu\text{-}SSnMe_3)_2Mn(CO)_4]$ by I_2[10]. It contains four $Mn(CO)_x$ (x=3, 4 or 5) fragments bridged by two disulfide ligands in different coordination modes (see section iv of this chapter). Recently, Kolis and co-workers have shown that group 7 metal carbonyl complexes

containing longer polysulfide or polyselenide chains (i.e. S_4^{2-} or Se_4^{2-}) can be obtained by oxidative decarbonylation of $M_2(CO)_{10}$ (M=Mn or Re) with polychalcogenides[4, 11-12]. The compounds $(Ph_4P)_2[M_2(Q_4)_2(CO)_6]$ (M=Mn or Re and Q=S or Se), prepared from the corresponding dimetal decacarbonyl and K_2Q_x (Q=s or Se; x=3 or 4) in DMF, are comprised of two $M(CO)_3$ fragments bridged by two Q_4^{2-} ligands (also see section iv of this chapter). Given these interesting results we set out to investigate similar reactivity patterns under superheated but subcritical hydro(methano)thermal conditions.

In the methanothermal synthesis of group 7 metal carbonyl polychalcogenide complexes, we encountered an unusual methylation reaction of coordinated chalcogenide ligands, the Me-group originating most probably from MeOH. Reactions of $Mn_2(CO)_{10}$ with Na_2Q_2 (Q=S, Se and Te) under super-heated methanol (i.e. at 80 °C in a sealed tube) gave a series of novel cluster compounds $(Ph_4P)_2[Mn_3(Q_2)_2(QR)(CO)_9]$ (R=H or CH_3 when Q=S; R=CH_3 when Q=Se and Te). These clusters can be further transformed, under the same conditions, into dinuclear methylchalcogenide complexes $(Ph_4P)[Mn_2(QCH_3)_3(CO)_6]$. The reaction of $CpRe(CO)_3$ with K_2Te_4 under the same conditions gave $(Ph_4P)_3[Re_4(Te_2)_3(TeCH_3)(CO)_{12}]\cdot CH_3OH$. This compound could not be transformed into the corresponding dimeric methyltelluride compound. In this chapter we describe the methanothermal synthesis, spectroscopic and thermal characterization and X-ray structures of nine clusters: $(Ph_4P)_2[Mn_3(S_2)_2(SH)(CO)_9]$ (**6-1**), $(Ph_4P)_2[Mn_3(S_2)_2(SCH_3)(CO)_9]$ (**6-2**), $(Ph_4P)_2[Mn_3(Se_2)_2(SeCH_3)(CO)_9]$ (**6-3**), α-$(Ph_4P)_2[Mn_3(Te_2)_2(TeCH_3)(CO)_9]$ (**6-4**), β-$(Ph_4P)_2[Mn_3(Te_2)_2(TeCH_3)(CO)_9]$ (**6-5**), $(Ph_4P)_3[Re_4(Te_2)_3(TeCH_3)(CO)_{12}]\cdot CH_3OH$ (**6-6**), $(Ph_4P)[Mn_2(SCH_3)_3(CO)_6]$ (**6-7**), $(Ph_4P)[Mn_2(SeCH_3)_3(CO)_6]$ (**6-8**) and $(Ph_4P)[Mn_2(TeCH_3)_3(CO)_6]$ (**6-9**). Among them, (**6-4**), (**6-5**) and (**6-9**) are the first structurally characterized manganese carbonyl telluride compounds, and (**6-6**) the first structurally characterized rhenium carbonyl polytelluride.

II. Experimental Section

1. Reagents

Chemicals in this work other than solvents were used as obtained: (i) sulfur powder, ~100 mesh, 99.9% purity, Aldrich Chemical Company, Inc., Milwaukee, WI; (ii) selenium powder, ~100 mesh, 99.5% purity, Aldrich Chemical Company, Inc., Milwaukee, WI; (iii) tellurium powder, ~200 mesh, 99.8% purity, Aldrich Chemical Company, Inc., Milwaukee, WI; (iv) sodium sticks in kerosene, 99% purity, Mallinckrodt Inc., Paris, Ky.; (v) dimanganese decacarbonyl, $Mn_2(CO)_{10}$, Strem Chemicals, Inc., Newburyport, MA; (vi) cyclopentadienyl rhenium tricarbonyl, $CpRe(CO)_3$, Strem Chemicals, Inc., Newburyport, MA; (vii) tetraphenylphosphonium chloride, Ph_4PCl, 98% purity, Aldrich Chemical Company, Inc., Milwaukee, WI.

Diethyl ether (A.C.S. anhydrous, Columbus Chemical Industries Inc., Columbus, WI) was distilled under a dry N_2 blanket after being refluxed with potassium metal, benzophenone and triethylene glycol dimethyl ether for 12 hours[12].

Methanol (A.C.S. anhydrous, Columbus Chemical Industries Inc., Columbus, WI) was refluxed for 4-5 h with magnesium methoxide (prepared from dry magnesium turnings and absolute methanol), and distilled under a nitrogen atmosphere[13].

2. Physical Measurements

Semi-quantitative elemental analyses, FT-IR, UV/vis and ^{77}Se NMR spectroscopic studies, and thermal gravimetric analyses (TGA) of the compounds were carried out as described previously[14].

3. Syntheses

All syntheses were carried out under a dry nitrogen atmosphere in a Vacuum Atmospheres Dri-Lab glovebox.

(i). Preparation of Na_2S_2, K_2Te_4, Na_2Se_2 and Na_2Te_2

These materials were prepared by reacting stoichiometric amount of chalcogen and alkali metal in a routine procedure used in this laboratory[14].

(ii). Preparation of $(Ph_4P)_2[Mn_3(S_2)_2(SH)(CO)_9]$ (6·1)

Method (A). 40 mg (0.1 mmol) $Mn_2(CO)_{10}$, 44 mg (0.4 mmol) Na_2S_2 and 220 mg (0.6 mmol) Ph_4PCl were mixed and sealed with 0.5 ml MeOH in a 25 cm long thick-walled Pyrex tube under vacuum, while the charge was kept frozen with liquid N_2. After the tube was heated at 80 °C for 8 hours, single crystals were found to deposit on the glass wall from a yellow solution. Washing of the reaction mixture with methanol and diethyl-ether afforded analytically pure orange single crystals of $(Ph_4P)_2[Mn_3(S_2)_2(SH)(CO)_9]$ **(6·1)** in 76% yield.

Method (B). If 0.5 ml EtOH is used in place of MeOH, this compound can also be prepared in the same manner as above in ~40% yield. Mid-IR spectrum in the CO region: 2002(w), 1974(s),1953(s), 1913(m), 1900(s), 1877(s), 1859(s) and 1853(s) cm^{-1}; UV/vis spectrum (in CH_3CN): featureless; Semi-quantitative elemental analyses by EDAX (atom%): Mn:S:P=27:56:17.

(iii). Preparation of $(Ph_4P)_2[Mn_3(S_2)_2(SCH_3)(CO)_9]$ (6·2)

40 mg (0.1 mmol) $Mn_2(CO)_{10}$, 99 mg (0.9 mmol) Na_2S_2 and 220 mg (0.6 mmol) Ph_4PCl were mixed and sealed with 0.5 ml MeOH in a 25 cm long thick-walled Pyrex tube under vacuum, while the charge was kept frozen with liquid N_2. After the reaction was carried out at 80 °C for 70 hours, orange red crystals were found to deposit on the glass wall. A small amount of yellow powder was also present. Analytically pure single crystals of $(Ph_4P)_2[Mn_3(S_2)_2(SCH_3)(CO)_9]$ **(6·2)** were obtained in 62% yield by washing the

reaction mixture with methanol and diethyl-ether, while the powder was readily removed by decanting the first two washings. Mid-IR spectrum in the CO region: 1998(w), 1969(s), 1956(s) and 1885(s), 1863(s) cm^{-1}; UV/vis spectrum (in CH_3CN): featureless; ^1H NMR (in acetone): 2.16 ppm (singlet, 3H); Semi-quantitative elemental analyses by EDAX (atom%): Mn:S:P=30:51:19.

(iv). Preparation of $(Ph_4P)_2[Mn_3(Se_2)_2(SeCH_3)(CO)_9]$ (6·3)

This compound was prepared in a similar manner, except that the sealed tube contained 40 mg (0.1 mmol) $Mn_2(CO)_{10}$, 82 mg (0.4 mmol) Na_2Se_2 and 220 mg (0.6 mmol) Ph_4PCl. The reaction was carried out at 80 °C for 46 hours. The tube contained dark brown single crystals, some brownish powder and a reddish solution. Pure single crystals of $(Ph_4P)_2[Mn_3(Se_2)_2(SeCH_3)(CO)_9]$ (**6·3**) were obtained in 38% yield by washing the reaction mixture with methanol and diethyl-ether. Mid-IR spectrum in the CO region: 1960(s), 1906(m), 1894(m), 1885(m) and 1864(s) cm^{-1}; UV/vis spectrum (in CH_3CN): featureless; ^1H NMR (in acetone): 2.00 ppm (singlet, 3H); Semi-quantitative elemental analyses by EDAX (atom%): Mn:Se:P=27:47:26.

(v). Preparation of α-$(Ph_4P)_2[Mn_3(Te_2)_2(TeCH_3)(CO)_9]$ (6·4)

This compound was prepared in a similar manner, except that the sealed tube contained 40 mg (0.1 mmol) $Mn_2(CO)_{10}$, 120 mg (0.4 mmol) Na_2Te_2 and 220 mg (0.6 mmol) Ph_4PCl. After the reaction was carried out at 80 °C for 14 days, black crystals separated from a purple-red solution in the tube. Analytically pure single crystals of α-$(Ph_4P)_2[Mn_3(Te_2)_2(TeCH_3)(CO)_9]$ (**6·4**) were obtained in 61% yield by washing the reaction mixture with methanol and diethyl-ether. Mid-IR spectrum in the CO region: 1979(sh), 1948(s), 1891(m), 1881(m), 1872(m) and 1857(m) cm^{-1}; UV/vis spectrum (in CH_3CN): featureless; ^1H NMR (in acetone): 1.96 ppm (singlet, 3H); Semi-quantitative elemental analyses by EDAX (atom%): Mn:Te:P=28:48:24.

(vi). Preparation of β-$(Ph_4P)_2[Mn_3(Te_2)_2(TeCH_3)(CO)_9]$ (6·5)

This compound was prepared in a similar manner, except that the sealed tube contained 80 mg (0.2 mmol) $Mn_2(CO)_{10}$, 120 mg (0.4 mmol) Na_2Te_2 and 220 mg (0.6 mmol) Ph_4PCl. The reaction was carried out at 80 °C for 10 days. Black single crystals of β-$(Ph_4P)_2[Mn_3(Te_2)_2(TeCH_3)(CO)_9]$ (**6·5**), along with red platelets of $(Ph_4P)[Mn_2(TeCH_3)_3(CO)_6]$ (**6·9**) (vide infra) in a weight percentage ratio of 60%:40% (total 192 mg), were found to be mixed together and separate from a purple-red solution. After washing the reaction mixture with methanol and diethyl-ether, crystals of (**6·5**) and (**6·9**) were separeted from each other by hand. The yield is estimated 49% for (**6·5**), and 37% for (**6·9**), respectively. The amount of $(Ph_4P)[Mn_2(TeCH_3)_3(CO)_6]$ can be reduced by using a shorter reaction time, e.g. heating between 6-8 days resulted in >90% β-$(Ph_4P)_2[Mn_3(Te_2)_2(TeCH_3)(CO)_9]$ in the reaction mixture. However, the compound thus obtained was microcrystalline. Mid-IR spectrum in the CO region: 1948(s), 1897(m), 1879(m), 1865(m) and 1843(m) cm^{-1}; UV/vis spectrum (in CH_3CN): featureless; ^1H NMR (in acetone): 1.96 ppm (singlet, 3H); Semi-quantitative elemental analyses by EDAX (atom%): Mn:Te:P=29:50:21.

(vii). Preparation of $(Ph_4P)_3[Re_4(Te_2)_3(TeCH_3)(CO)_{12}]\cdot CH_3OH$ (6·6)

This compound was prepared in a similar manner, except that the sealed tube contained 17 mg (0.05 mmol) $CpRe(CO)_3$,118 mg (0.2 mmol) K_2Te_4 and 146 mg (0.4 mmol) Ph_4PCl. The reaction was carried out at 80 °C for 9 days. Dark red needles of $(Ph_4P)_3[Re_4(Te_2)_3(TeCH_3)(CO)_{12}]\cdot CH_3OH$ (**6·6**) were found to be mixed with black crystals of $(Ph_4P)_2Te_4$, and separate from the mother liquor which remained dark red. After washing the reaction mixture with methanol and diethyl-ether, the two products were easily separated by hand. The estimated yield for $(Ph_4P)_3[Re_4(Te_2)_3(TeCH_3)(CO)_{12}]\cdot CH_3OH$ is 46%. Mid-IR spectrum in the CO region:

1996(w), 1969(s), 1883(sh) and 1864(m) cm^{-1}; UV/vis spectrum (in CH_3CN): 361(ε=1.27x10^3 M·cm^{-1}) nm; ^1H NMR (in acetone): 2.40 ppm (singlet, 3H); Semi-quantitative elemental analyses by EDAX (atom%): Re:Te:P=24:48:28.

(viii). Preparation of $(Ph_4P)[Mn_2(SCH_3)_3(CO)_6]$ (6·7)

See **Preparation of $(Ph_4P)_2[Mn_3(S_2)_2(SH)(CO)_9]$ (6·1).** When the reaction was carried out at 80 °C for 48 hours, pale yellow single crystals were separated from a greenish yellow solution. Analytically pure crystals of $(Ph_4P)[Mn_2(SCH_3)_3(CO)_6]$ (**6·7**) were obtained in 90% yield by washing the reaction mixture with methanol and diethyl-ether. Mid-IR spectrum in the CO region: 2001(w), 1977(m), 1903(m), 1882(s) and 1864(m) cm^{-1}; UV/vis spectrum (in CH_3CN): 379 nm (br, ε=2.29x10^3 M·cm^{-1}) and 288 nm (sh, ε=7.69x10^3 M·cm^{-1}); ^1H NMR (in $CDCl_3$): 1.99 ppm (singlet, 9H); Semi-quantitative elemental analyses by EDAX (atom%): Mn:S:P=31:55:14.

(ix). Preparation of $(Ph_4P)[Mn_2(SeCH_3)_3(CO)_6]$ (6·8)

See **Preparation of $(Ph_4P)_2[Mn_3(Se_2)_2(SeCH_3)(CO)_9]$ (6·3).** When the reaction was carried out at 80 °C for 21 days, orange-red single crystals were separated from a colorless solution which contained a considerable amount of grey and pink powder. By washing the reaction mixture and decanting the first few washings with methanol, analytically pure crystals of $(Ph_4P)[Mn_2(SeCH_3)_3(CO)_6]$ (**6·8**) were obtained in 43% yield . Mid-IR spectrum in the CO region: 1993(w), 1966(m), 1896(m), 1876(s) and 1859(m) cm^{-1}; UV/vis spectrum (in CH_3CN): 395 nm (br, ε=3.13x10^3 M·cm^{-1}) and 289 nm (sh, ε=1.22x10^4 M·cm^{-1}); ^1H NMR (in $CDCl_3$): 1.73 ppm (singlet, 9H); Semi-quantitative elemental analyses by EDAX (atom%): Mn:Se:P=41:46:13.

(xi). Preparation of $(Ph_4P)[Mn_2(TeCH_3)_3(CO)_6]$ (6·9)

See **Preparation of β-$(Ph_4P)_2[Mn_3(Te_2)_2(TeCH_3)(CO)_9]$ (6·5).** The yield of $(Ph_4P)[Mn_2(TeCH_3)_3(CO)_6]$ (**6·9**) increases with the reaction time. Up to 27 days the product isolated was mainly $(Ph_4P)_2[Mn_3(Te_2)_2(TeCH_3)(CO)_9]$ although a few single crystals of β-$(Ph_4P)_2[Mn_3(Te_2)_2(TeCH_3)(CO)_9]$ were still found. In this case, the product of $(Ph_4P)[Mn_2(TeCH_3)_3(CO)_6]$ was microcrystalline, and a large amount of elemental tellurium formed. This makes the separation of (**6·9**) from the elemental Te very difficult. Mid-IR spectrum in the CO region: 1951(s), 1875(m) and 1861(m) cm^{-1}; UV/vis spectrum (in CH_3CN): 404 nm (sh, $\varepsilon=2.74\times10^3$ $M\cdot cm^{-1}$) and 298 nm (br sh, $\varepsilon=1.13\times10^4$ $M\cdot cm^{-1}$); ^1H NMR (in $CDCl_3$): 1.38 ppm (singlet, 9H); Semi-quantitative elemental analyses by EDAX (atom%): Mn:S:P=32:51:17.

4. X-ray Diffraction and Crystallographic Studies

The single crystal X-ray diffraction studies were performed by using either a Nicolet P3 four-circle difractometer or a Rigaku automated AFC6S single crystal diffractometer[15-16].

The crystallographic data set of (**6·7**) was collected on the Nicolet P3 diffractometer using a θ-2θ scan mode. The crystallographic data sets of (**6·1**)–(**6·6**) and (**6·8**)–(**6·9**) were collected on a Rigaku AFC6S four-circle diffractometer using ω−2θ scan techniques. Mo Kα radiation was used in the data collection of (**6·1**)–(**6·7**) and (**6·9**), while Cu Kα radiation was used for (**6·8**). The stability of the experimental setup and crystal integrity for each data collection was monitored by measuring three representative reflections periodically. No statistically significant change of intensities was detected for the standards. An empirical absorption correction based on ψ scans of three strong reflections with $\chi\sim90^o$ was applied to all data sets.

The structures were solved with direct methods and refined with full-matrix least squares techniques. DIFABS correction after isotropic refinement of all atoms was then applied to all data[17]. The calculations were performed on a VAXstation 3100 computer using the TEXSAN crystallographic software package of Molecular Structure Corporation[18]. Tables 6·1–6·3 give crystal data and details for structure analysis of the compounds. All non-hydrogen atoms were refined either isotropically or anisotropically. The hydrogen positions were calculated but not refined. The final coordinates and average temperature factors (B_{eq}) of the atoms in compounds (**6·1**)–(**6·9**) are given in Tables 6·4-6·12, respectively.

Finally, all compounds were examined by X-ray powder diffraction for the purpose of phase characterization and identification. A Debye-Scherrer camera was employed to record the X-ray powder diffraction patterns. Ni-filtered Cu radiation was used. The crystals were ground to fine powder and packed into 0.5 mm glass capillaries which were sealed and mounted to the standard Debye-Scherrer powder camera which has a diameter of 114.6 mm (1 mm corresponds to 1 degree for 2θ). X-rays were generated by a Phillips Norelco XRG-5000 X-ray generator operating at 40 kV and 20 mA. Approximately, a six hour exposure time was used. Accurate d-spacings (Å) of each compound were calculated from the powder patterns recorded on a Phillips XRG-3000 computer controlled powder diffractometer. To verify the homogeneities of the products, the d-spacings observed for the bulk materials were compared with the calculated d-spacings from the X-ray single-crystal structure analysis data. Listings of calculated and observed d-spacings (Å) along with the observed relative diffraction intensities of these compounds are given in Tables 6·13–6·20.

Table 6·1. Data for Crystal Structure Analysis of $(Ph_4P)_2[Mn_3(S_2)_2(SH)(CO)_9]$ (**6·1**), $(Ph_4P)_2[Mn_3(S_2)_2(SCH_3)(CO)_9]$ (**6·2**), $(Ph_4P)_2[Mn_3(Se_2)_2(SeCH_3)(CO)_9]$ (**6·3**)

compound	**6·1**	**6·2**	**6·3**
formula	$C_{57}H_{41}O_9P_2S_5Mn_3$	$C_{58}H_{43}O_9P_2S_5Mn_3$	$C_{58}H_{43}O_9P_2Se_5Mn_3$
a, Å	26.741(8)	20.70(1)	11.089(6)
b, Å	16.055(6)	23.40(1)	29.844(8)
c, Å	12.985(4)	12.837(5)	18.123(5)
α, deg	90.00	91.86(4)	90.00
β, deg	97.01(2)	90.50(4)	95.80(3)
γ, deg	90.00	69.84(4)	90.00
Z; V, Å^3	4, 5533(6)	2, 5835(9)	4, 5966(2)
space group	$P2_1/a$(#14)	P-1(#2)	$P2_1/n$(#14)
D_{calc}, g/cm^3	1.51	1.45	1.68
μ(Mo Kα), cm^{-1}	9.4	8.9	37.3
cryst size, mm	0.07x0.08x0.11	0.09x0.20x0.28	0.06x0.06x0.12
$2\theta_{max}$, deg	45.1	45.1	45.0
Temperature (°C)	-96	23	23
no. of data collcd	7739	12309	7852
no. of data used($F_o^2>3\sigma(F_o^2)$)	3736	4398	2411
min, max abs cor	0.84, 1.11	0.81, 1.11	0.83, 0.98
no. of variables	305	807	349
no. of atoms per asym unit (including H)	117	240	120
final R/R_w, %	6.4/6.2	9.2/11.5	8.3/9.8

Table 6-2. Data for Crystal Structure Analysis of α-$(Ph_4P)_2[Mn_3(Te_2)_2(TeCH_3)(CO)_9]$ (**6-4**), β-$(Ph_4P)_2[Mn_3(Te_2)_2(TeCH_3)(CO)_9]$ (**6-5**), $(Ph_4P)_3[Re_4(Te_2)_3(TeCH_3)(CO)_{12}]\cdot CH_3OH$ (**6-6**)

compound	**6-4**	**6-5**	**6-6**
formula	$C_{58}H_{43}O_9P_2Te_5Mn_3$	$C_{58}H_{43}O_9P_2Te_5Mn_3$	$C_{86}H_{66}P_3O_{13}Te_7Re_4$
a, Å	11.437(1)	12.285(5)	15.454(4)
b, Å	12.007(2)	27.591(6)	22.401(4)
c, Å	24.300(3)	18.076(3)	14.810(5)
α, deg	103.72(1)	90.00	95.17(2)
β, deg	97.742(9)	100.86(3)	115.46(2)
γ, deg	103.66(1)	90.00	80.12(2)
Z; V, Å^3	2, 3085(3)	4, 6017(5)	2, 4560(2)
space group	P-1(#2)	$P2_1/n$(#14)	P-1(#2)
D_{calc}, g/cm^3	1.88	1.93	2.21
μ(Mo Kα), cm^{-1}	30.1	30.8	76.7
cryst size, mm	0.18x0.35x0.53	0.51x0.53x0.65	0.11x0.11x0.50
$2\theta_{max}$, deg	45.1	45.0	50.0
Temperature (°C)	23	-100	-90
no. of data collcd	8585	7479	16448
no. of data used($F_o^2>3\sigma(F_o^2)$)	5081	5660	11313
min, max abs cor	0.80, 1.18	0.80, 1.14	0.43, 1.18
no. of variables	454	454	523
no. of atoms per asym unit (including H)	120	120	179
final R/R_w, %	4.2/4.7	8.0/11.4	6.4/8.7

Table 6·3. Data for Crystal Structure Analysis of $(Ph_4P)[Mn_2(SCH_3)_3(CO)_6]$ (**6·7**), $(Ph_4P)[Mn_2(SeCH_3)_3(CO)_6]$ (**6·8**) and $(Ph_4P)[Mn_2(TeCH_3)_3(CO)_6]$ (**6·9**)

compound	**6·7**	**6·8**	**6·9**
formula	$C_{33}H_{29}O_6PS_3Mn_2$	$C_{33}H_{29}O_6PSe_3Mn_2$	$C_{33}H_{29}O_6PTe_3Mn_2$
a, Å	10.162(6)	10.192(4)	10.375(2)
b, Å	11.667(7)	11.937(5)	26.629(5)
c, Å	16.665(9)	16.822(4)	13.147(2)
α, deg	107.15(5)	107.24(2)	90.00
β, deg	92.75(5)	93.16(2)	97.90(1)
γ, deg	113.44(4)	112.92(2)	90.00
Z; V, Å^3	2, 1701(4)	2, 1766(3)	4, 3598(1)
space group	P-1(#2)	P-1(#2)	$P2_1/c$(#14)
D_{calc}, g/cm^3	1.18	1.69	1.93
μ, cm^{-1}	9.8 (Mo Kα)	102.9 (Cu Kα)	31.5 (Mo Kα)
cryst size, mm	0.09x0.11x0.30	0.06x0.07x0.11	0.05x0.23x0.26
$2\theta_{max}$, deg	45.0	110.1	45.0
Temperature (°C)	-94	23	-100
no. of data collcd	4800	4710	5139
no. of data used($F_o^2>3\sigma(F_o^2)$)	3664	3282	3892
min, max abs cor	0.91, 1.08	0.77, 1.34	0.75, 1.19
no. of variables	286	286	286
no. of atoms per asym unit (including H)	74	74	74
final R/R_w, %	4.6/5.7	5.8/6.8	3.5/5.5

Table 6·4. Positional Parameters and B_{eq} Values[a] for $(Ph_4P)_2[Mn_3(S_2)_2(SH)(CO)_9]$ (6·1)
(Standard Deviations in Parentheses)

atom	x	y	z	B_{eq}, Å^2
Mn1	0.11007(6)	0.6867(1)	0.2766(1)	2.38(4)
Mn2	0.08365(6)	0.8619(1)	0.0573(1)	2.40(4)
Mn3	0.03982(6)	0.9074(1)	0.2953(1)	2.53(4)
S1	0.0590(1)	0.7350(2)	0.1278(2)	2.59(6)
S2	0.0341(1)	0.7622(2)	0.2706(2)	2.40(6)
S3	0.1171(1)	0.9031(2)	0.2257(2)	2.62(6)
S4	0.1607(1)	0.8072(2)	0.2914(2)	2.76(6)
S5	0.0080(1)	0.9148(2)	0.1152(2)	2.80(6)
P1	0.2095(1)	0.2195(2)	0.2473(2)	2.26(6)
P2	-0.1209(1)	0.6122(2)	0.3327(2)	2.54(6)
O1	0.1428(3)	0.6665(5)	0.5011(6)	3.6(2)
O2	0.1939(3)	0.5990(5)	0.1989(6)	4.2(2)
O3	0.0565(3)	0.5263(6)	0.2694(6)	5.0(2)
O4	0.1170(3)	1.0225(5)	-0.0182(6)	4.7(2)
O5	0.0414(3)	0.8160(5)	-0.1541(7)	4.9(2)
O6	0.1791(3)	0.7892(5)	0.0107(6)	4.5(2)
O7	0.0470(3)	1.0885(6)	0.3116(6)	5.0(2)
O8	-0.0588(3)	0.9224(5)	0.3739(6)	5.0(2)
O9	0.0881(3)	0.8849(6)	0.5078(7)	6.0(2)
C1	0.2550(4)	0.3024(6)	0.2436(7)	1.8(2)
C2	0.2423(4)	0.3779(7)	0.2003(8)	2.6(2)
C3	0.2790(4)	0.4389(7)	0.1970(8)	3.4(3)
C4	0.3281(4)	0.4224(7)	0.2381(8)	3.3(3)
C5	0.3417(4)	0.3461(7)	0.2800(8)	3.1(2)
C6	0.3051(4)	0.2854(7)	0.2837(8)	3.0(2)
C7	0.2316(4)	0.1321(6)	0.1790(7)	1.8(2)
C8	0.2113(4)	0.0534(7)	0.1906(8)	3.2(3)
C9	0.2273(4)	-0.0147(7)	0.1343(9)	3.4(3)
C10	0.2624(4)	-0.0011(7)	0.0670(8)	2.5(2)
C11	0.2810(4)	0.0761(7)	0.0550(8)	2.5(2)

Table 6-4. (cont'd)

atom	x	y	z	B_{eq}, Å^2
C12	0.2655(4)	0.1432(7)	0.1083(8)	2.5(2)
C13	0.1489(4)	0.2525(6)	0.1877(7)	2.1(2)
C14	0.1201(5)	0.3076(8)	0.2384(9)	3.7(3)
C15	0.0734(5)	0.3329(8)	0.192(1)	4.7(3)
C16	0.0541(4)	0.3034(7)	0.097(1)	3.6(3)
C17	0.0803(5)	0.2471(9)	0.047(1)	5.0(3)
C18	0.1286(4)	0.2191(7)	0.0936(9)	3.6(3)
C19	0.2025(4)	0.1921(6)	0.3798(7)	2.0(2)
C20	0.1619(4)	0.1402(7)	0.3947(8)	2.5(2)
C21	0.1553(4)	0.1153(7)	0.4959(8)	2.8(2)
C22	0.1891(4)	0.1432(7)	0.5783(8)	2.9(2)
C23	0.2284(4)	0.1941(7)	0.5637(8)	3.1(2)
C24	0.2355(4)	0.2197(7)	0.4635(8)	2.8(2)
C25	-0.1069(4)	0.5310(7)	0.2466(8)	2.8(2)
C26	-0.1132(4)	0.4478(8)	0.2697(9)	3.6(3)
C27	-0.1002(5)	0.3862(8)	0.202(1)	4.5(3)
C28	-0.0809(5)	0.4076(8)	0.114(1)	4.6(3)
C29	-0.0758(5)	0.489(1)	0.086(1)	5.4(3)
C30	-0.0875(5)	0.5517(8)	0.156(1)	4.6(3)
C31	-0.1649(4)	0.5755(7)	0.4172(9)	3.1(3)
C32	-0.1478(4)	0.5578(7)	0.5179(9)	3.5(3)
C33	-0.1821(5)	0.5318(8)	0.5846(9)	4.1(3)
C34	-0.2304(5)	0.5244(8)	0.555(1)	4.2(3)
C35	-0.2487(6)	0.543(1)	0.456(1)	7.4(4)
C36	-0.2132(6)	0.567(1)	0.386(1)	7.2(4)
C37	-0.0652(4)	0.6420(7)	0.4138(7)	2.3(2)
C38	-0.0668(4)	0.7133(7)	0.4766(9)	3.8(3)
C39	-0.0249(5)	0.7359(8)	0.545(1)	4.3(3)
C40	0.0181(5)	0.6866(8)	0.5510(9)	3.7(3)
C41	0.0187(4)	0.6176(7)	0.4928(9)	3.3(3)
C42	-0.0216(4)	0.5948(7)	0.4223(8)	2.5(2)

Table 6-4. (cont'd)

atom	x	y	z	B_{eq}, Å^2
C43	-0.1437(4)	0.7002(6)	0.2564(7)	1.9(2)
C44	-0.1939(4)	0.7064(7)	0.2114(9)	3.3(3)
C45	-0.2088(4)	0.7766(7)	0.1507(8)	3.1(3)
C46	-0.1760(4)	0.8369(7)	0.1345(8)	2.5(2)
C47	-0.1265(4)	0.8306(7)	0.1787(8)	3.0(2)
C48	-0.1101(4)	0.7610(7)	0.2395(8)	2.7(2)
C49	0.1307(4)	0.6749(7)	0.4125(9)	3.1(2)
C50	0.1617(4)	0.6354(7)	0.2304(8)	3.1(3)
C51	0.0769(4)	0.5927(7)	0.2707(8)	3.1(2)
C52	0.1022(4)	0.9585(8)	0.0100(9)	3.6(3)
C53	0.0559(5)	0.8337(8)	-0.068(1)	4.1(3)
C54	0.1406(4)	0.8172(7)	0.0302(8)	3.2(3)
C55	0.0447(4)	1.0158(8)	0.3068(9)	3.6(3)
C56	-0.0196(5)	0.9124(8)	0.3408(9)	3.7(3)
C57	0.0684(5)	0.8939(8)	0.420(1)	4.0(3)

a. B_{eq} is defined as $4/3[a^2\beta_{11}+b^2\beta_{22}+c^2\beta_{33}+ab(\cos\gamma)\beta_{12}+ac(\cos\beta)\beta_{13}+bc(\cos\alpha)\beta_{23}]$.]

Table 6-5. Positional Parameters and B_{eq} Values[a] for $(Ph_4P)_2[Mn_3(S_2)_2(SCH_3)(CO)_9]$ (6-2) (Standard Deviations in Parentheses)

atom	x	y	z	B_{eq}, Å^2
Mn1A	0.1188(3)	0.6947(2)	0.6027(4)	4.8(4)
Mn1B	0.3261(3)	0.1820(2)	0.0029(4)	4.5(4)
Mn2A	0.1819(2)	0.8288(2)	0.5029(4)	4.0(4)
Mn2B	0.3901(3)	0.3249(2)	-0.0219(4)	4.1(4)
Mn3A	0.1275(3)	0.7453(2)	0.3101(4)	4.4(4)
Mn3B	0.3793(3)	0.2774(2)	0.2315(4)	4.2(4)
S1A	0.0939(4)	0.7993(4)	0.5758(6)	4.2(6)
S1B	0.4149(4)	0.2190(3)	-0.0323(6)	4.0(6)
S2A	0.0630(4)	0.7506(4)	0.4621(6)	4.7(7)
S2B	0.4124(4)	0.1906(4)	0.1178(6)	4.4(6)
S3A	0.2251(4)	0.7319(4)	0.4188(7)	5.1(7)
S3B	0.3050(4)	0.3321(3)	0.1014(6)	4.1(6)
S4A	0.2285(4)	0.6677(4)	0.5251(8)	5.9(7)
S4B	0.2485(4)	0.2784(4)	0.0487(7)	5.0(7)
S5A	0.1223(4)	0.8472(4)	0.3411(6)	4.3(6)
S5B	0.4530(4)	0.3166(4)	0.1375(6)	4.4(6)
P1	0.5468(4)	0.4413(4)	0.2905(6)	3.5(6)
P2	0.8325(5)	0.0515(4)	0.9439(7)	4.6(7)
P3	0.0528(5)	0.4331(4)	0.7865(7)	4.4(7)
P4	0.3354(5)	0.0742(4)	0.5179(7)	4.6(7)
O1A	0.120(1)	0.570(1)	0.547(2)	9(2)
O1B	0.245(1)	0.134(1)	0.137(2)	8(2)
O2A	0.191(1)	0.669(1)	0.803(2)	9(2)
O2B	0.245(1)	0.193(1)	-0.187(2)	11(3)
O3A	-0.008(1)	0.716(1)	0.719(2)	8(2)
O3B	0.412(1)	0.056(1)	-0.056(2)	9(2)
O4A	0.294(1)	0.864(1)	0.412(2)	7(2)
O4B	0.365(1)	0.454(1)	-0.008(2)	7(2)
O5A	0.116(1)	0.951(1)	0.595(2)	7(2)
O5B	0.502(1)	0.309(1)	-0.174(2)	8(2)

Table 6·5. (cont'd)

atom	x	y	z	B_{eq}, Å^2
O6A	0.261(1)	0.793(1)	0.696(2)	8(2)
O6B	0.289(1)	0.343(1)	-0.190(2)	7(2)
O7A	0.207(1)	0.738(1)	0.122(2)	9(2)
O7B	0.327(1)	0.385(1)	0.371(2)	8(2)
O8A	-0.001(1)	0.777(1)	0.198(2)	9(2)
O8B	0.483(1)	0.209(1)	0.381(2)	9(2)
O9A	0.150(1)	0.613(1)	0.290(2)	9(3)
O9B	0.275(1)	0.237(1)	0.328(2)	7(2)
C1	0.604(2)	0.475(1)	0.341(2)	4.0(7)
C2	0.624(2)	0.511(1)	0.272(3)	6(1)
C3	0.670(2)	0.541(2)	0.306(3)	7(1)
C4	0.697(2)	0.531(2)	0.404(3)	7(1)
C5	0.679(2)	0.495(1)	0.469(2)	4.7(8)
C6	0.635(1)	0.466(1)	0.435(2)	3.4(7)
C7	0.461(2)	0.498(1)	0.280(2)	4.4(7)
C8	0.451(2)	0.556(1)	0.311(2)	4.7(8)
C9	0.383(2)	0.601(1)	0.311(2)	5.6(8)
C10	0.333(2)	0.577(1)	0.274(2)	4.8(8)
C11	0.339(2)	0.524(2)	0.241(2)	5.4(8)
C12	0.407(1)	0.477(1)	0.244(2)	3.3(7)
C13	0.581(2)	0.411(1)	0.160(3)	5.5(8)
C14	0.649(2)	0.365(2)	0.155(3)	7(1)
C15	0.669(2)	0.344(2)	0.056(3)	8(1)
C16	0.633(2)	0.357(2)	-0.029(3)	7(1)
C17	0.571(2)	0.400(1)	-0.022(2)	5.4(8)
C18	0.540(2)	0.429(1)	0.074(3)	5.6(9)
C19	0.542(2)	0.384(1)	0.378(2)	4.5(8)
C20	0.605(2)	0.331(2)	0.393(3)	6.0(9)
C21	0.604(2)	0.289(2)	0.462(3)	7(1)
C22	0.542(2)	0.296(1)	0.518(2)	5.0(8)
C23	0.487(2)	0.346(1)	0.503(2)	4.3(7)
C24	0.489(2)	0.389(1)	0.433(2)	4.2(7)

Table 6·5. (cont'd)

atom	x	y	z	B_{eq}, Å^2
C25	0.870(2)	0.014(1)	0.825(2)	5.0(8)
C26	0.830(2)	0.027(1)	0.734(3)	6.0(9)
C27	0.866(2)	-0.010(2)	0.642(3)	7(1)
C28	0.931(2)	-0.046(1)	0.650(3)	7(1)
C29	0.972(2)	-0.055(2)	0.736(3)	7(1)
C30	0.940(2)	-0.027(2)	0.829(3)	7(1)
C31	0.844(1)	-0.006(1)	1.036(2)	4.2(7)
C32	0.867(2)	-0.002(1)	1.138(3)	5.4(8)
C33	0.870(2)	-0.049(2)	1.205(3)	7(1)
C34	0.862(2)	-0.101(1)	1.171(3)	5.6(9)
C35	0.843(2)	-0.104(1)	1.069(3)	5.7(9)
C36	0.832(2)	-0.058(2)	1.003(3)	6.1(9)
C37	0.741(2)	0.093(1)	0.927(2)	5.7(9)
C38	0.722(2)	0.149(2)	0.869(3)	8(1)
C39	0.652(2)	0.182(2)	0.859(3)	8(1)
C40	0.606(2)	0.164(2)	0.910(3)	7(1)
C41	0.618(2)	0.111(2)	0.959(3)	9(1)
C42	0.691(2)	0.077(1)	0.972(2)	5.4(8)
C43	0.873(2)	0.104(1)	0.991(2)	4.0(7)
C44	0.835(2)	0.143(1)	1.076(3)	6.1(9)
C45	0.874(2)	0.179(2)	1.124(3)	10(1)
C46	0.928(2)	0.182(2)	1.081(3)	7(1)
C47	0.960(2)	0.148(2)	0.998(3)	6(1)
C48	0.930(2)	0.109(2)	0.951(3)	7(1)
C49	0.084(2)	0.390(1)	0.673(2)	4.7(8)
C50	0.054(3)	0.356(3)	0.628(4)	14(2)
C51	0.080(3)	0.317(2)	0.534(4)	13(2)
C52	0.139(3)	0.317(2)	0.496(3)	10(1)
C53	0.174(2)	0.350(2)	0.539(4)	10(1)
C54	0.151(2)	0.384(2)	0.634(3)	9(1)
C55	0.036(2)	0.385(1)	0.875(2)	3.8(7)
C56	0.084(2)	0.332(2)	0.904(3)	5.9(9)

Table 6·5. (cont'd)

atom	x	y	z	B_{eq}, Å^2
C57	0.074(2)	0.291(2)	0.980(3)	7(1)
C58	0.014(2)	0.308(2)	1.024(3)	7(1)
C59	-0.041(2)	0.360(2)	0.999(3)	7(1)
C60	-0.031(2)	0.399(1)	0.922(2)	5.9(9)
C61	-0.027(1)	0.493(1)	0.761(2)	3.7(7)
C62	-0.044(2)	0.546(2)	0.817(3)	8(1)
C63	-0.101(2)	0.596(1)	0.799(3)	6.0(9)
C64	-0.149(2)	0.584(2)	0.738(3)	8(1)
C65	-0.138(2)	0.539(2)	0.677(3)	9(1)
C66	-0.070(2)	0.488(2)	0.685(3)	8(1)
C67	0.112(1)	0.464(1)	0.840(2)	3.5(7)
C68	0.142(2)	0.449(1)	0.936(2)	5.1(8)
C69	0.188(2)	0.487(1)	0.975(2)	5.2(8)
C70	0.206(2)	0.516(1)	0.917(3)	5.9(9)
C71	0.177(2)	0.533(2)	0.822(3)	7(1)
C72	0.124(2)	0.509(1)	0.784(3)	6.0(9)
C73	0.341(2)	0.013(2)	0.602(3)	7(1)
C74	0.345(3)	0.021(2)	0.703(5)	13(2)
C75	0.349(4)	-0.028(4)	0.775(6)	21(2)
C76	0.355(2)	-0.082(2)	0.730(4)	10(1)
C77	0.355(4)	-0.086(3)	0.645(7)	19(2)
C78	0.358(3)	-0.043(3)	0.565(5)	16(2)
C79	0.362(2)	0.130(2)	0.578(2)	5.2(8)
C80	0.426(3)	0.114(2)	0.631(4)	12(1)
C81	0.458(3)	0.149(3)	0.676(4)	15(2)
C82	0.421(3)	0.215(2)	0.667(4)	11(1)
C83	0.361(2)	0.232(2)	0.625(3)	8(1)
C84	0.337(2)	0.189(2)	0.576(3)	8(1)
C85	0.248(2)	0.109(1)	0.488(3)	4.6(8)
C86	0.197(3)	0.121(2)	0.567(3)	11(1)
C87	0.132(3)	0.150(2)	0.542(4)	11(1)
C88	0.110(2)	0.167(1)	0.441(3)	6.0(9)

Table 6-5. (cont'd)

atom	x	y	z	B_{eq}, Å^2
C89	0.157(2)	0.156(1)	0.366(2)	5.1(8)
C90	0.229(2)	0.125(1)	0.389(3)	6.0(9)
C91	0.381(2)	0.050(2)	0.393(3)	5.8(9)
C92	0.365(3)	-0.002(2)	0.342(4)	14(2)
C93	0.406(4)	-0.019(3)	0.238(5)	17(2)
C94	0.435(3)	0.011(2)	0.209(4)	10(1)
C95	0.455(2)	0.052(2)	0.252(4)	12(1)
C96	0.429(2)	0.073(2)	0.365(4)	11(1)
C97A	0.124(2)	0.616(1)	0.570(2)	4.3(8)
C97B	0.278(2)	0.151(1)	0.081(2)	4.0(8)
C98A	0.166(2)	0.678(2)	0.719(3)	7(1)
C98B	0.279(2)	0.188(2)	-0.113(3)	6(1)
C99A	0.038(2)	0.709(1)	0.673(2)	3.8(8)
C99B	0.376(2)	0.108(2)	-0.032(3)	5(1)
C100A	0.249(2)	0.851(1)	0.445(2)	3.6(7)
C100B	0.373(2)	0.401(2)	-0.010(3)	7(1)
C101A	0.145(2)	0.902(2)	0.559(3)	7(1)
C101B	0.457(2)	0.316(1)	-0.113(3)	5.0(9)
C102A	0.228(2)	0.809(1)	0.619(3)	4.3(8)
C102B	0.327(2)	0.333(1)	-0.122(3)	4.5(9)
C103A	0.178(2)	0.740(2)	0.195(3)	7(1)
C103B	0.352(2)	0.343(2)	0.314(3)	6(1)
C104A	0.052(3)	0.760(2)	0.236(4)	10(8)
C104B	0.450(2)	0.231(2)	0.316(3)	5(1)
C105A	0.141(2)	0.668(2)	0.297(2)	4.6(8)
C105B	0.315(2)	0.252(1)	0.289(3)	4.6(8)
C106A	0.031(2)	0.896(2)	0.362(3)	7(1)
C106B	0.540(2)	0.252(2)	0.131(3)	8(1)

a. B_{eq} is defined as $4/3[a^2\beta_{11}+b^2\beta_{22}+c^2\beta_{33}+ab(\cos\gamma)\beta_{12}+ac(\cos\beta)\beta_{13}+bc(\cos\alpha)\beta_{23}$

Table 6-6. Positional Parameters and B_{eq} Values[a] for $(Ph_4P)_2[Mn_3(Se_2)_2(SeCH_3)(CO)_9]$ (6-3) (Standard Deviations in Parentheses)

atom	x	y	z	B_{eq}, Å^2
Se1	0.8433(4)	0.0851(1)	0.8773(2)	3.7(2)
Se2	0.6664(4)	0.0595(1)	0.8060(2)	3.6(2)
Se3	0.8140(4)	0.1486(1)	0.7259(2)	3.5(2)
Se4	0.6063(4)	0.1530(1)	0.6844(2)	4.0(2)
Se5	0.6234(4)	0.1740(1)	0.8642(2)	3.5(2)
Mn1	0.8524(6)	0.0678(2)	0.7430(3)	3.8(4)
Mn2	0.8450(6)	0.1672(2)	0.8609(3)	3.7(3)
Mn3	0.5094(5)	0.1175(2)	0.7846(3)	3.5(3)
P1	1.043(1)	-0.1530(4)	0.5889(6)	3.3(2)
P2	0.474(1)	0.1043(4)	0.1824(6)	3.8(3)
O1	0.907(3)	-0.027(1)	0.759(2)	6.2(8)
O2	0.775(4)	0.054(1)	0.586(2)	11(1)
O3	1.102(3)	0.077(1)	0.722(2)	9(1)
O4	0.893(3)	0.181(1)	1.022(2)	6.5(8)
O5	0.845(2)	0.2639(8)	0.837(1)	4.7(7)
O6	1.104(3)	0.160(1)	0.845(2)	7.1(9)
O7	0.396(3)	0.078(1)	0.908(2)	6.4(8)
O8	0.322(3)	0.184(1)	0.765(2)	5.7(7)
O9	0.393(3)	0.057(1)	0.673(2)	9(1)
C1	1.086(3)	-0.097(1)	0.585(2)	2.0(8)
C2	1.004(4)	-0.062(1)	0.588(2)	5(1)
C3	1.042(5)	-0.018(2)	0.592(3)	8(1)
C4	1.159(4)	-0.005(1)	0.590(2)	5(1)
C5	1.244(4)	-0.040(1)	0.588(2)	5(1)
C6	1.209(4)	-0.086(1)	0.585(2)	5(1)
C7	1.164(3)	-0.189(1)	0.564(2)	3.2(9)
C8	1.177(4)	-0.194(1)	0.489(3)	6(1)
C9	1.273(5)	-0.219(2)	0.467(3)	8(1)
C10	1.361(5)	-0.236(2)	0.521(3)	9(2)
C11	1.344(4)	-0.229(1)	0.595(3)	5(1)

Table 6·6. (cont'd)

atom	x	y	z	B_{eq}, Å^2
C12	1.249(4)	-0.205(1)	0.617(2)	3.3(9)
C13	1.006(3)	-0.171(1)	0.683(2)	3.2(9)
C14	0.995(5)	-0.216(2)	0.700(3)	7(1)
C15	0.968(5)	-0.228(2)	0.767(3)	10(2)
C16	0.945(4)	-0.190(1)	0.816(2)	5(1)
C17	0.962(4)	-0.146(1)	0.802(2)	4(1)
C18	1.003(4)	-0.129(1)	0.731(2)	5(1)
C19	0.907(4)	-0.161(1)	0.526(2)	4(1)
C20	0.894(4)	-0.133(1)	0.462(2)	5(1)
C21	0.787(4)	-0.139(1)	0.414(2)	6(1)
C22	0.706(4)	-0.171(2)	0.427(2)	6(1)
C23	0.718(4)	-0.201(1)	0.485(3)	6(1)
C24	0.823(5)	-0.194(1)	0.536(3)	7(1)
C25	0.587(4)	0.067(1)	0.152(2)	4(1)
C26	0.586(4)	0.056(1)	0.080(3)	6(1)
C27	0.682(4)	0.028(1)	0.058(3)	6(1)
C28	0.767(4)	0.021(1)	0.114(3)	6(1)
C29	0.775(4)	0.026(1)	0.188(2)	4(1)
C30	0.675(4)	0.054(2)	0.208(3)	6(1)
C31	0.447(4)	0.095(2)	0.275(2)	5(1)
C32	0.429(4)	0.054(1)	0.293(2)	5(1)
C33	0.395(6)	0.035(2)	0.365(4)	12(2)
C34	0.409(5)	0.066(2)	0.415(3)	9(2)
C35	0.425(5)	0.111(2)	0.404(3)	9(1)
C36	0.447(4)	0.126(1)	0.333(3)	6(1)
C37	0.531(4)	0.159(1)	0.183(2)	5(1)
C38	0.451(4)	0.196(2)	0.191(2)	6(1)
C39	0.496(4)	0.236(2)	0.186(2)	6(1)
C40	0.607(4)	0.250(1)	0.177(2)	5(1)
C41	0.684(3)	0.215(1)	0.166(2)	4(1)
C42	0.653(4)	0.170(1)	0.166(2)	5(1)

Table 6·6. (cont'd)

atom	x	y	z	B_{eq}, Å^2
C43	0.337(4)	0.101(1)	0.119(2)	5(1)
C44	0.308(3)	0.133(1)	0.068(2)	2.5(8)
C45	0.205(4)	0.127(1)	0.018(2)	4(1)
C46	0.135(4)	0.088(2)	0.016(3)	7(1)
C47	0.171(4)	0.054(1)	0.068(2)	5(1)
C48	0.277(3)	0.060(1)	0.121(2)	3.3(9)
C49	0.887(4)	0.009(1)	0.756(2)	4(1)
C50	0.799(5)	0.058(2)	0.645(4)	10(2)
C51	1.004(6)	0.077(2)	0.727(3)	10(2)
C52	0.870(4)	0.177(1)	0.960(3)	5(1)
C53	0.838(4)	0.221(1)	0.845(2)	5(1)
C54	0.999(4)	0.163(1)	0.848(2)	5(1)
C55	0.445(4)	0.097(1)	0.862(3)	6(1)
C56	0.403(4)	0.159(2)	0.772(2)	6(1)
C57	0.435(3)	0.082(1)	0.716(2)	1.9(8)
C58	0.593(3)	0.162(1)	0.969(2)	3.2(9)

a. B_{eq} is defined as $4/3[a^2\beta_{11}+b^2\beta_{22}+c^2\beta_{33}+ab(\cos\gamma)\beta_{12}+ac(\cos\beta)\beta_{13}+bc(\cos\alpha)\beta_{23}$

Table 6·7. Positional Parameters and B_{eq} Values[a] for α-$(Ph_4P)_2[Mn_3(Te_2)_2(TeCH_3)(CO)_9]$ (6·4) (Standard Deviations in Parentheses)

atom	x	y	z	B_{eq}, Å^2
Te1	0.89243(8)	1.04569(7)	0.19382(3)	3.42(3)
Te2	0.64427(8)	1.01612(7)	0.17223(3)	3.49(3)
Te3	0.82487(8)	1.23631(7)	0.31693(3)	3.44(3)
Te4	0.59354(8)	1.12912(7)	0.32762(4)	4.17(3)
Te5	0.74933(7)	0.89821(7)	0.30116(3)	3.26(3)
Mn1	0.8011(2)	1.2344(2)	0.20647(8)	3.31(7)
Mn2	0.9471(2)	1.0723(2)	0.30676(8)	3.27(7)
Mn3	0.5416(2)	0.9220(2)	0.24821(8)	3.26(7)
P1	0.2867(3)	0.3476(3)	0.5628(1)	3.5(1)
P2	0.1552(3)	0.3468(3)	0.0589(1)	3.4(1)
O1	0.7549(9)	1.2472(9)	0.0865(4)	5.8(4)
O2	0.6747(9)	1.4209(9)	0.2287(4)	6.5(5)
O3	1.0406(9)	1.4094(8)	0.2367(4)	5.3(4)
O4	1.100(1)	0.9087(9)	0.2855(4)	5.7(4)
O5	0.990(1)	1.1105(9)	0.4326(4)	6.4(5)
O6	1.169(1)	1.267(1)	0.3227(5)	7.0(5)
O7	0.4868(8)	0.6833(8)	0.1657(4)	5.5(4)
O8	0.419(1)	0.8192(8)	0.3308(4)	6.0(4)
O9	0.308(1)	0.957(1)	0.2020(5)	6.7(5)
C1	0.152(1)	0.309(1)	0.5919(5)	2.8(2)
C2	0.076(1)	0.196(1)	0.5761(5)	4.1(3)
C3	-0.032(1)	0.173(1)	0.5986(6)	5.0(3)
C4	-0.061(1)	0.263(1)	0.6350(6)	5.2(3)
C5	0.017(1)	0.376(1)	0.6505(6)	4.8(3)
C6	0.120(1)	0.399(1)	0.6292(5)	4.3(3)
C7	0.423(1)	0.404(1)	0.6176(5)	3.5(2)
C8	0.420(1)	0.421(1)	0.6749(6)	4.4(3)
C9	0.531(1)	0.465(1)	0.7174(6)	4.9(3)
C10	0.640(1)	0.487(1)	0.6997(6)	5.7(3)
C11	0.642(1)	0.466(1)	0.6417(7)	5.7(3)

Table 6·7. (cont'd)

atom	x	y	z	B_{eq}, Å^2
C12	0.535(1)	0.423(1)	0.5998(6)	5.3(3)
C13	0.307(1)	0.221(1)	0.5131(5)	3.7(3)
C14	0.304(1)	0.217(1)	0.4540(6)	4.9(3)
C15	0.328(1)	0.115(1)	0.4199(7)	6.5(4)
C16	0.347(1)	0.030(1)	0.4391(7)	6.2(4)
C17	0.346(1)	0.030(1)	0.4959(7)	6.7(4)
C18	0.328(1)	0.128(1)	0.5340(6)	4.6(3)
C19	0.264(1)	0.460(1)	0.5281(5)	3.7(3)
C20	0.157(1)	0.430(1)	0.4864(6)	5.6(3)
C21	0.129(1)	0.519(1)	0.4624(7)	6.7(4)
C22	0.209(2)	0.632(2)	0.4815(8)	7.4(4)
C23	0.313(1)	0.659(1)	0.5209(7)	6.4(4)
C24	0.346(1)	0.573(1)	0.5457(6)	5.4(3)
C25	0.111(1)	0.465(1)	0.1054(5)	3.1(2)
C26	0.202(1)	0.549(1)	0.1496(5)	4.2(3)
C27	0.167(1)	0.639(1)	0.1833(6)	5.0(3)
C28	0.048(1)	0.646(1)	0.1752(6)	5.9(3)
C29	-0.037(1)	0.562(1)	0.1320(6)	4.7(3)
C30	-0.009(1)	0.471(1)	0.0980(5)	3.6(2)
C31	0.239(1)	0.402(1)	0.0101(5)	3.6(2)
C32	0.261(1)	0.319(1)	-0.0366(6)	4.7(3)
C33	0.332(1)	0.362(1)	-0.0739(7)	6.1(3)
C34	0.373(1)	0.476(1)	-0.0669(6)	5.7(3)
C35	0.351(1)	0.558(1)	-0.0239(7)	6.1(4)
C36	0.284(1)	0.521(1)	0.0157(6)	4.5(3)
C37	0.023(1)	0.232(1)	0.0186(5)	4.0(3)
C38	-0.029(2)	0.238(1)	-0.0348(7)	6.9(4)
C39	-0.140(2)	0.145(2)	-0.0677(8)	9.0(5)
C40	-0.185(2)	0.060(1)	-0.0447(8)	6.9(4)
C41	-0.136(1)	0.055(1)	0.0069(7)	6.7(4)
C42	-0.030(1)	0.140(1)	0.0405(6)	5.2(3)

Table 6-7. (cont'd)

atom	x	y	z	B_{eq}, Å^2
C43	0.252(1)	0.293(1)	0.1033(5)	3.2(2)
C44	0.358(1)	0.275(1)	0.0907(6)	4.5(3)
C45	0.433(1)	0.237(1)	0.1289(6)	5.4(3)
C46	0.399(1)	0.217(1)	0.1792(6)	5.1(3)
C47	0.290(1)	0.231(1)	0.1911(6)	5.0(3)
C48	0.218(1)	0.273(1)	0.1543(6)	4.5(3)
C49	0.777(1)	1.238(1)	0.1328(6)	4.0(5)
C50	0.720(1)	1.343(1)	0.2216(5)	4.0(5)
C51	0.946(1)	1.340(1)	0.2248(6)	3.9(5)
C52	1.034(1)	0.967(1)	0.2927(5)	4.0(5)
C53	0.972(1)	1.095(1)	0.3837(6)	4.1(5)
C54	1.081(1)	1.193(1)	0.3146(5)	4.0(5)
C55	0.509(1)	0.777(1)	0.1967(5)	3.6(5)
C56	0.472(1)	0.861(1)	0.2995(5)	4.0(5)
C57	0.402(1)	0.944(1)	0.2186(6)	4.4(6)
C58	0.783(1)	0.749(1)	0.2438(6)	4.6(5)

a. B_{eq} is defined as $4/3[a^2\beta_{11}+b^2\beta_{22}+c^2\beta_{33}+ab(\cos\gamma)\beta_{12}+ac(\cos\beta)\beta_{13}+bc(\cos\alpha)\beta_{23}]$.]

Table 6·8. Positional Parameters and B_{eq} Values[a] for β-$(Ph_4P)_2[Mn_3(Te_2)_2(TeCH_3)(CO)_9]$ (6·5) (Standard Deviations in Parentheses)

atom	x	y	z	B_{eq}, Å^2
Te1	0.5432(1)	0.17192(7)	0.2890(1)	2.49(7)
Te2	0.6828(1)	0.14483(7)	0.41799(9)	2.46(7)
Te3	0.7769(1)	0.11403(7)	0.23370(9)	2.54(7)
Te4	0.9601(2)	0.13080(7)	0.3433(1)	3.05(8)
Te5	0.8198(1)	0.24334(7)	0.3097(1)	2.59(8)
Mn1	0.6237(3)	0.0817(1)	0.3071(2)	2.6(2)
Mn2	0.6787(3)	0.1992(1)	0.1997(2)	2.3(2)
Mn3	0.8743(3)	0.1896(2)	0.4333(2)	2.5(2)
P1	0.5436(6)	0.1194(2)	0.6824(4)	2.4(3)
P2	0.9710(6)	0.1129(3)	0.9616(4)	3.2(3)
O1	0.460(2)	0.044(1)	0.389(1)	6(1)
O2	0.764(2)	-0.0039(8)	0.361(1)	6(1)
O3	0.505(2)	0.0425(7)	0.163(1)	4(1)
O4	0.560(2)	0.2912(6)	0.170(1)	4(1)
O5	0.836(2)	0.2183(8)	0.097(1)	5(1)
O6	0.522(2)	0.1542(7)	0.076(1)	3.6(9)
O7	0.789(2)	0.2672(7)	0.522(1)	5(1)
O8	1.087(2)	0.2433(8)	0.468(1)	5(1)
O9	0.944(2)	0.1232(8)	0.560(1)	4(1)
C1	0.504(2)	0.110(1)	0.771(1)	2.9(5)
C2	0.431(2)	0.076(1)	0.782(2)	3.5(6)
C3	0.399(2)	0.068(1)	0.851(2)	3.8(6)
C4	0.435(3)	0.100(1)	0.909(2)	4.1(6)
C5	0.505(2)	0.138(1)	0898(2)	3.5(6)
C6	0.537(2)	0.144(1)	0.829(1)	3.2(6)
C7	0.422(2)	0.119(1)	0.614(1)	2.1(5)
C8	0.407(2)	0.088(1)	0.550(2)	3.7(6)
C9	0.310(2)	0.088(1)	0.499(2)	3.5(6)
C10	0.221(3)	0.114(1)	0.512(2)	5.1(8)
C11	0.229(3)	0.145(1)	0.574(2)	5.8(8)

Table 6·8. (cont'd)

atom	x	y	z	B_{eq}, Å^2
C12	0.330(3)	0.145(1)	0.626(2)	4.6(7)
C13	0.638(2)	0.072(1)	0.669(1)	2.9(5)
C14	0.679(2)	0.043(1)	0.727(2)	3.5(6)
C15	0.762(3)	0.009(1)	0.719(2)	5.9(9)
C16	0.804(3)	0.007(1)	0.653(2)	5.0(8)
C17	0.764(3)	0.040(1)	0.596(2)	4.8(7)
C18	0.682(3)	0.071(1)	0.604(2)	4.0(6)
C19	0.615(2)	0.177(1)	0.683(2)	3.2(6)
C20	0.731(2)	0.174(1)	0.690(2)	3.8(6)
C21	0.787(2)	0.222(1)	0.697(2)	3.3(6)
C22	0.728(3)	0.264(1)	0.697(2)	4.9(7)
C23	0.613(3)	0.262(1)	0.688(2)	4.9(7)
C24	0.556(3)	0.218(1)	0.684(2)	4.6(7)
C25	0.851(2)	0.076(1)	0.970(1)	2.5(5)
C26	0.785(2)	0.091(1)	1.020(1)	2.2(5)
C27	0.695(2)	0.063(1)	1.029(2)	3.4(6)
C28	0.663(2)	0.024(1)	0.984(1)	3.0(5)
C29	0.732(3)	0.007(1)	0.933(2)	3.8(6)
C30	0.826(2)	0.035(1)	0.926(2)	3.4(6)
C31	1.079(2)	0.105(1)	1.043(1)	2.4(5)
C32	1.048(3)	0.099(1)	1.115(2)	4.0(6)
C33	1.132(3)	0.098(1)	1.179(2)	4.0(6)
C34	1.244(2)	0.110(1)	1.172(1)	2.9(5)
C35	1.268(3)	0.117(1)	1.103(2)	4.0(6)
C36	1.189(3)	0.116(1)	1.038(2)	4.1(6)
C37	0.933(2)	0.177(1)	0.951(1)	2.2(1)
C38	1.003(2)	0.214(1)	0.982(1)	2.7(5)
C39	0.972(3)	0.258(1)	0.972(2)	3.9(6)
C40	0.872(3)	0.270(1)	0.931(2)	5.6(8)
C41	0.799(3)	0.235(1)	0.899(2)	4.5(7)
C42	0.828(2)	0.186(1)	0.910(2)	3.7(6)

Table 6·8. (cont'd)

atom	x	y	z	B_{eq}, Å^2
C43	1.023(2)	0.092(1)	0.881(1)	2.6(5)
C44	0.996(2)	0.114(1)	0.813(2)	3.7(6)
C45	1.026(3)	0.098(1)	0.750(2)	4.7(7)
C46	1.079(3)	0.052(1)	0.753(2)	5.2(8)
C47	1.105(3)	0.025(1)	0.823(2)	5.0(7)
C48	1.078(3)	0.046(1)	0.886(2)	3.9(6)
C49	0.525(3)	0.0619(8)	0.356(2)	3(1)
C50	0.713(3)	0.0325(7)	0.342(2)	3(1)
C51	0.552(3)	0.059(1)	0.221(2)	4(2)
C52	0.607(3)	0.253(1)	0.182(2)	4(1)
C53	0.775(3)	0.2134(8)	0.142(2)	4(1)
C54	0.583(3)	0.169(1)	0.125(1)	4(2)
C55	0.819(3)	0.230(2)	0.489(2)	5(2)
C56	1.004(3)	0.221(2)	0.453(2)	4(2)
C57	0.916(3)	0.151(1)	0.510(1)	3(1)
C58	0.719(3)	0.151(1)	0.510(1)	3(1)

a. B_{eq} is defined as $4/3[a^2\beta_{11}+b^2\beta_{22}+c^2\beta_{33}+ab(\cos\gamma)\beta_{12}+ac(\cos\beta)\beta_{13}+bc(\cos\alpha)\beta_{23}]$.]

Table 6-9. Positional Parameters and B_{eq} Values[a] for $(Ph_4P)_3[Re_4(Te_2)_3(TeCH_3)(CO)_{12}]\cdot CH_3OH$ (6-6) (Standard Deviations in Parentheses)

atom	x	y	z	B_{eq}, Å^2
Re1	0.78161(6)	0.13423(4)	0.19807(7)	1.61(3)
Re2	1.08740(6)	0.17135(4)	0.24165(7)	1.59(3)
Re3	0.80536(7)	0.28725(5)	0.01163(7)	1.99(4)
Re4	0.89431(7)	0.31470(4)	0.36004(7)	1.73(4)
Te1	0.9222(1)	0.12532(7)	0.3937(1)	2.09(6)
Te2	1.0323(1)	0.20906(7)	0.39631(1)	1.74(6)
Te3	1.1008(1)	0.29234(7)	0.2335(1)	2.21(6)
Te4	0.9144(1)	0.34484(7)	0.1915(1)	2.02(6)
Te5	0.6541(1)	0.30973(8)	0.0690(1)	2.39(7)
Te6	0.7356(1)	0.25345(7)	0.2499(1)	1.65(6)
Te7	0.8899(1)	0.18074(7)	0.1183(1)	1.56(5)
P1	0.3912(4)	0.0888(3)	0.7370(5)	1.9(2)
P2	0.2362(4)	0.3409(3)	0.9628(5)	1.9(2)
P3	0.5287(4)	0.3545(3)	0.4799(4)	1.8(2)
O1	0.618(1)	0.1379(9)	-0.011(1)	3.5(4)
O2	0.863(2)	0.004(1)	0.172(2)	4.4(4)
O3	0.647(1)	0.0933(8)	0.276(1)	3.1(3)
O4	1.076(1)	0.0356(8)	0.245(1)	2.6(3)
O5	1.146(1)	0.148(1)	0.068(2)	3.9(4)
O6	1.300(2)	0.156(1)	0.396(2)	4.5(5)
O7	0.967(1)	0.2596(9)	-0.060(1)	3.4(4)
O8	0.679(2)	0.220(1)	-0.175(2)	4.9(5)
O9	0.722(2)	0.410(1)	-0.091(2)	4.8(5)
O10	0.748(1)	0.4304(9)	0.333(1)	3.5(4)
O11	0.864(2)	0.288(1)	0.543(2)	4.1(4)
O12	1.064(1)	0.383(1)	0.491(2)	3.9(4)
O13	0.018(2)	0.491(1)	0.289(2)	5.4(5)
C1	0.295(2)	0.057(1)	0.635(2)	2.2(4)
C2	0.215(2)	0.048(1)	0.651(2)	2.5(4)
C3	0.142(2)	0.023(2)	0.576(3)	4.3(7)

Table 6-9. (cont'd)

atom	x	y	z	B_{eq}, Å^2
C4	0.151(3)	0.002(2)	0.485(3)	5.0(7)
C5	0.233(2)	0.012(2)	0.472(3)	4.2(6)
C6	0.303(2)	0.038(1)	0.548(2)	3.7(6)
C7	0.380(2)	0.169(1)	0.717(2)	2.6(5)
C8	0.442(2)	0.203(1)	0.789(2)	2.2(4)
C9	0.438(2)	0.262(1)	0.770(2)	3.9(6)
C10	0.369(2)	0.290(1)	0.678(2)	3.3(5)
C11	0.308(2)	0.252(1)	0.604(2)	3.1(5)
C12	0.316(2)	0.190(1)	0.622(2)	2.0(4)
C13	0.375(2)	0.081(1)	0.847(2)	1.9(4)
C14	0.396(2)	0.026(1)	0.889(2)	2.8(5)
C15	0.372(2)	0.016(1)	0.966(2)	2.5(4)
C16	0.328(2)	0.063(1)	1.000(2)	3.1(5)
C17	0.309(2)	0.119(1)	0.962(2)	3.7(6)
C18	0.334(2)	0.130(1)	0.890(2)	3.2(5)
C19	0.505(2)	0.049(1)	0.743(2)	1.7(4)
C20	0.519(2)	-0.013(1)	0.732(2)	2.4(4)
C21	0.604(2)	-0.046(1)	0.731(2)	2.7(5)
C22	0.676(2)	-0.014(2)	0.756(2)	4.1(6)
C23	0.670(3)	0.048(2)	0.763(3)	5.0(7)
C24	0.582(2)	0.077(1)	0.756(2)	3.1(5)
C25	0.178(2)	0.296(1)	0.857(2)	1.8(4)
C26	0.138(2)	0.247(1)	0.867(2)	2.4(4)
C27	0.095(2)	0.209(1)	0.788(2)	2.9(5)
C28	0.085(2)	0.223(2)	0.691(2)	4.2(6)
C29	0.126(3)	0.268(2)	0.681(3)	4.8(7)
C30	0.172(2)	0.307(1)	0.762(2)	3.9(6)
C31	0.289(2)	0.398(1)	0.932(2)	2.1(4)
C32	0.237(3)	0.450(2)	0.898(3)	5.7(8)
C33	0.271(3)	0.501(2)	0.874(3)	5.9(9)
C34	0.362(2)	0.488(1)	0.882(2)	2.8(5)
C35	0.421(2)	0.433(1)	0.916(2)	3.2(5)

Table 6-9. (cont'd)

atom	x	y	z	B_{eq}, Å^2
C36	0.383(2)	0.386(1)	0.940(2)	3.3(5)
C37	0.147(2)	0.382(1)	1.002(2)	2.0(4)
C38	0.050(2)	0.379(1)	0.947(2)	1.9(4)
C39	-0.013(2)	0.409(1)	0.983(2)	2.5(4)
C40	0.017(2)	0.442(1)	1.072(2)	2.8(5)
C41	0.114(2)	0.446(1)	1.126(2)	3.9(6)
C42	0.184(2)	0.412(1)	1.097(2)	1.6(4)
C43	0.322(2)	0.290(1)	1.058(2)	1.6(4)
C44	0.301(2)	0.280(1)	1.138(2)	3.5(6)
C45	0.367(2)	0.237(1)	1.213(2)	3.5(6)
C46	0.449(2)	0.207(1)	1.205(2)	4.1(6)
C47	0.467(2)	0.218(1)	1.124(2)	2.9(5)
C48	0.406(2)	0.258(1)	1.053(2)	3.1(5)
C49	0.553(2)	0.275(1)	0.476(2)	2.0(4)
C50	0.498(2)	0.236(1)	0.490(2)	3.5(6)
C51	0.527(2)	0.173(2)	0.492(3)	4.3(6)
C52	0.607(2)	0.150(1)	0.482(2)	3.6(6)
C53	0.666(2)	0.188(1)	0.467(2)	2.8(5)
C54	0.639(2)	0.249(1)	0.463(2)	2.5(4)
C55	0.434(2)	0.379(1)	0.520(2)	1.5(4)
C56	0.339(2)	0.370(1)	0.459(2)	2.4(4)
C57	0.262(2)	0.395(1)	0.476(2)	3.5(5)
C58	0.280(2)	0.431(1)	0.559(2)	2.9(5)
C59	0.371(2)	0.444(1)	0.623(2)	2.6(5)
C60	0.450(2)	0.415(1)	0.604(2)	2.0(4)
C61	0.642(2)	0.379(1)	0.568(2)	2.1(4)
C62	0.679(2)	0.424(1)	0.542(2)	2.3(4)
C63	0.770(2)	0.436(1)	0.605(2)	3.1(5)
C64	0.820(2)	0.408(1)	0.696(2)	3.1(5)
C65	0.784(2)	0.366(1)	0.722(2)	3.7(6)
C66	0.694(2)	0.347(1)	0.654(2)	3.8(6)
C67	0.489(1)	0.392(1)	0.362(2)	1.4(3)

Table 6-9. (cont'd)

atom	x	y	z	B_{eq}, Å^2
C68	0.426(2)	0.446(1)	0.343(2)	2.0(4)
C69	0.401(2)	0.474(1)	0.256(2)	1.9(4)
C70	0.443(2)	0.449(1)	0.189(2)	2.7(5)
C71	0.502(2)	0.396(1)	0.204(2)	3.9(6)
C72	0.528(2)	0.366(1)	0.296(2)	2.9(5)
C73	0.681(2)	0.138(1)	0.067(2)	2.3(4)
C74	0.832(2)	0.054(1)	0.182(2)	2.6(5)
C75	0.702(2)	0.109(1)	0.249(2)	1.7(4)
C76	1.077(2)	0.085(1)	0.245(2)	1.8(4)
C77	1.123(2)	0.158(1)	0.134(2)	2.6(5)
C78	1.220(2)	0.162(1)	0.339(2)	3.0(1)
C79	0.909(2)	0.272(1)	-0.029(2)	2.6(5)
C80	0.725(2)	0.246(1)	-0.106(2)	3.0(5)
C81	0.754(2)	0.362(1)	-0.053(2)	3.0(5)
C82	0.807(2)	0.385(1)	0.344(2)	2.5(4)
C83	0.877(2)	0.298(1)	0.474(2)	2.1(4)
C84	1.000(2)	0.357(1)	0.441(2)	2.7(5)
C85	0.888(2)	0.112(1)	0.002(2)	3.2(5)
C86	-0.015(3)	0.527(2)	0.360(3)	6(1)

a. B_{eq} is defined as $4/3[a^2\beta_{11}+b^2\beta_{22}+c^2\beta_{33}+ab(\cos\gamma)\beta_{12}+ac(\cos\beta)\beta_{13}+bc(\cos\alpha)\beta_{23}$

Table 6·10. Positional Parameters and B_{eq} Values[a] for $(Ph_4P)[Mn_2(SCH_3)_3(CO)_6]$ (6·7)
(Standard Deviations in Parentheses)

atom	x	y	z	B_{eq}, Å^2
Mn1	0.4775(1)	0.8224(1)	0.13834(6)	1.74(3)
Mn2	0.2668(1)	0.9356(1)	0.23209(6)	1.69(3)
S1	0.2541(2)	0.7184(2)	0.1823(1)	1.79(5)
S2	0.3473(2)	0.9347(2)	0.1002(1)	2.02(6)
S3	0.5164(2)	0.9835(2)	0.2759(1)	1.90(6)
P	0.0947(2)	0.4055(2)	0.3144(1)	1.61(6)
O1	0.7514(5)	0.9836(5)	0.0938(3)	3.4(2)
O2	0.6202(6)	0.6879(5)	0.2071(4)	4.3(2)
O3	0.3832(6)	0.6158(5)	-0.0317(3)	4.1(2)
O4	0.3256(5)	1.2182(5)	0.2899(3)	3.4(2)
O5	0.1802(6)	0.9137(5)	0.3951(3)	3.8(2)
O6	-0.0401(6)	0.8489(6)	0.1570(3)	3.9(2)
C1	-0.0584(7)	0.4427(6)	0.3077(4)	1.9(1)
C2	-0.1835(7)	0.3800(6)	0.3381(4)	2.1(1)
C3	-0.3010(8)	0.4098(7)	0.3297(5)	3.2(2)
C4	-0.2940(8)	0.5046(7)	0.2935(5)	3.3(2)
C5	-0.1692(8)	0.5686(8)	0.2639(5)	3.4(2)
C6	-0.0532(8)	0.5387(7)	0.2714(5)	2.8(1)
C7	0.0456(7)	0.2696(6)	0.3543(4)	1.5(1)
C8	0.0737(7)	0.2993(7)	0.4429(4)	2.3(1)
C9	0.0224(8)	0.1954(7)	0.4752(4)	2.6(1)
C10	-0.0558(7)	0.0666(7)	0.4215(4)	2.5(1)
C11	-0.0822(7)	0.0379(7)	0.3349(4)	2.2(1)
C12	-0.0310(7)	0.1390(6)	0.3014(4)	2.2(1)
C13	0.2464(7)	0.5445(6)	0.3896(4)	1.8(1)
C14	0.2290(8)	0.6572(7)	0.4350(4)	2.7(1)
C15	0.3434(8)	0.7604(7)	0.4984(5)	3.0(1)
C16	0.4736(9)	0.7548(8)	0.5154(5)	3.5(2)
C17	0.4913(8)	0.6428(7)	0.4694(5)	3.0(1)
C18	0.3775(7)	0.5375(6)	0.4087(4)	2.1(1)

Table 6·10. (cont'd)

atom	x	y	z	B_{eq}, Å^2
C19	0.1380(7)	0.3646(6)	0.2095(4)	1.6(1)
C20	0.0225(7)	0.2743(7)	0.1411(4)	2.4(1)
C21	0.0550(8)	0.2369(7)	0.0615(5)	3.1(1)
C22	0.1948(8)	0.2907(7)	0.0466(5)	3.0(1)
C23	0.3070(8)	0.3849(7)	0.1138(4)	2.6(1)
C24	0.2769(7)	0.4221(6)	0.1947(4)	1.6(1)
C25	0.6440(8)	0.9216(7)	0.1112(4)	2.3(2)
C26	0.5612(7)	0.7401(7)	0.1788(4)	2.3(2)
C27	0.4210(8)	0.6975(7)	0.0356(5)	2.6(3)
C28	0.3024(7)	1.1067(7)	0.2664(4)	2.1(2)
C29	0.2166(7)	0.9211(6)	0.3307(4)	2.0(2)
C30	0.0825(8)	0.8823(7)	0.1851(4)	2.2(2)
C31	0.1110(8)	0.6159(7)	0.0876(5)	2.8(3)
C32	0.4765(8)	1.1031(7)	0.1124(5)	3.1(3)
C33	0.5180(8)	0.9011(7)	0.3526(5)	3.3(3)

a. B_{eq} is defined as $4/3[a^2\beta_{11}+b^2\beta_{22}+c^2\beta_{33}+ab(\cos\gamma)\beta_{12}+ac(\cos\beta)\beta_{13}+bc(\cos\alpha)\beta_{23}$

Table 6·11. Positional Parameters and B_{eq} Values[a] for $(Ph_4P)[Mn_2(SeCH_3)_3(CO)_6]$ (6·8)
(Standard Deviations in Parentheses)

atom	x	y	z	B_{eq}, Å^2
Se1	0.2622(1)	0.7177(1)	0.18958(7)	3.15(4)
Se2	0.3506(1)	0.9350(1)	0.09916(7)	3.34(4)
Se3	0.5352(1)	0.9932(1)	0.28292(7)	2.99(4)
Mn1	0.4899(2)	0.8236(2)	0.1417(1)	2.88(6)
Mn2	0.2737(2)	0.9399(2)	0.2379(1)	2.80(6)
P	0.0927(3)	0.3988(3)	0.3132(2)	2.74(9)
O1	0.754(1)	0.9794(9)	0.0960(5)	5.5(4)
O2	0.631(1)	0.693(1)	0.2114(7)	7.3(5)
O3	0.393(1)	0.616(1)	-0.0263(6)	7.2(4)
O4	0.329(1)	1.214(1)	0.2901(6)	5.7(4)
O5	0.193(1)	0.921(1)	0.4006(5)	6.1(4)
O6	-0.031(1)	0.848(1)	0.1597(6)	7.2(4)
C1	-0.060(1)	0.437(1)	0.3053(6)	2.8(2)
C2	-0.180(1)	0.378(1)	0.3375(7)	4.3(3)
C3	-0.299(1)	0.409(1)	0.3299(7)	4.8(3)
C4	-0.295(2)	0.496(1)	0.2915(8)	5.4(3)
C5	-0.173(2)	0.556(1)	0.2606(9)	6.5(3)
C6	-0.058(1)	0.521(1)	0.2670(8)	5.2(3)
C7	0.047(1)	0.270(1)	0.3549(6)	2.5(2)
C8	0.074(1)	0.300(1)	0.4421(7)	4.1(2)
C9	0.022(1)	0.198(1)	0.4743(7)	4.6(3)
C10	-0.047(1)	0.074(1)	0.4225(8)	4.7(3)
C11	-0.071(1)	0.043(1)	0.3370(7)	4.1(2)
C12	-0.023(1)	0.141(1)	0.3020(6)	3.5(2)
C13	0.242(1)	0.536(1)	0.3888(6)	3.1(2)
C14	0.225(1)	0.647(1)	0.4324(7)	3.8(2)
C15	0.339(1)	0.749(1)	0.4927(8)	5.2(3)
C16	0.465(1)	0.742(1)	0.5089(8)	5.2(3)
C17	0.486(1)	0.633(1)	0.4670(8)	4.9(3)
C18	0.372(1)	0.528(1)	0.4063(7)	3.9(2)

Table 6·11. (cont'd)

atom	x	y	z	B_{eq}, Å^2
C19	0.136(1)	0.359(1)	0.2097(6)	2.8(2)
C20	0.025(1)	0.269(1)	0.1413(7)	4.4(3)
C21	0.054(1)	0.232(1)	0.0608(8)	5.2(3)
C22	0.191(2)	0.288(1)	0.0479(8)	5.4(3)
C23	0.302(1)	0.380(1)	0.1147(8)	4.7(3)
C24	0.273(1)	0.415(1)	0.1955(6)	3.2(2)
C25	0.649(1)	0.918(1)	0.1147(7)	3.7(4)
C26	0.578(1)	0.745(1)	0.1836(8)	4.3(5)
C27	0.430(1)	0.700(1)	0.0406(8)	4.7(5)
C28	0.307(1)	1.106(1)	0.2687(7)	3.6(4)
C29	0.228(1)	0.928(1)	0.3363(7)	4.1(4)
C30	0.086(1)	0.884(1)	0.1895(7)	4.6(5)
C31	0.110(1)	0.610(1)	0.0870(7)	4.8(5)
C32	0.488(1)	1.111(1)	0.1140(7)	4.9(5)
C33	0.538(1)	0.905(1)	0.3662(7)	4.6(5)

a. B_{eq} is defined as $4/3[a^2\beta_{11}+b^2\beta_{22}+c^2\beta_{33}+ab(\cos\gamma)\beta_{12}+ac(\cos\beta)\beta_{13}+bc(\cos\alpha)\beta_{23}$

Table 6·12. Positional Parameters and B_{eq} Values[a] for $(Ph_4P)[Mn_2(TeCH_3)_3(CO)_6]$ (6·9)
(Standard Deviations in Parentheses)

atom	x	y	z	B_{eq}, Å^2
Te1	0.14023(5)	0.69412(2)	0.54200(4)	2.25(3)
Te2	0.01029(5)	0.57265(2)	0.55542(4)	2.23(3)
Te3	-0.06280(6)	0.66568(2)	0.72362(4)	2.76(3)
Mn1	-0.1042(1)	0.66199(5)	0.5201(1)	2.21(5)
Mn2	0.1640(1)	0.62678(5)	0.6939(1)	2.41(6)
P	0.4517(2)	0.61989(9)	0.1269(2)	2.1(1)
O1	-0.3688(7)	0.6261(3)	0.5318(7)	6.6(5)
O2	-0.1921(6)	0.7671(3)	0.4995(6)	4.2(3)
O3	-0.1204(7)	0.6433(3)	0.2971(5)	4.4(4)
O4	0.1498(6)	0.5465(3)	0.8469(5)	4.0(3)
O5	0.2990(7)	0.6954(3)	0.8488(6)	5.3(4)
O6	0.4044(6)	0.5914(3)	0.6210(5)	4.4(3)
C1	0.2786(8)	0.6083(3)	0.1069(6)	2.5(2)
C2	0.1925(9)	0.6472(4)	0.0852(7)	3.4(2)
C3	0.059(1)	0.6375(5)	0.0699(9)	4.8(2)
C4	0.016(1)	0.5890(5)	0.0767(8)	4.8(2)
C5	0.102(1)	0.5500(4)	0.0984(7)	3.8(2)
C6	0.2338(8)	0.5590(4)	0.1131(7)	2.9(2)
C7	0.4879(8)	0.6839(3)	0.1591(6)	2.1(1)
C8	0.5402(9)	0.6970(4)	0.2590(7)	3.3(2)
C9	0.571(1)	0.7467(4)	0.2814(8)	4.1(2)
C10	0.5510(9)	0.7832(4)	0.2068(7)	3.4(2)
C11	0.4984(9)	0.7696(4)	0.1097(7)	3.1(2)
C12	0.4675(8)	0.7209(3)	0.0850(6)	2.8(2)
C13	0.5271(8)	0.5800(3)	0.2272(6)	2.3(2)
C14	0.462(1)	0.5684(4)	0.3099(7)	3.4(2)
C15	0.523(1)	0.5416(4)	0.3915(8)	4.2(2)
C16	0.649(1)	0.5243(4)	0.3907(8)	4.7(2)
C17	0.712(1)	0.5356(4)	0.3084(7)	3.6(2)
C18	0.6525(8)	0.5629(3)	0.2262(7)	2.9(2)

Table 6-12. (cont'd)

atom	x	y	z	B_{eq}, Å^2
C19	0.5193(7)	0.6060(3)	0.0117(6)	2.1(1)
C20	0.6335(8)	0.6296(3)	-0.0055(7)	2.8(2)
C21	0.6908(9)	0.6182(4)	-0.0925(7)	3.6(2)
C22	0.633(1)	0.5830(4)	-0.1606(7)	3.6(2)
C23	0.5200(8)	0.5583(4)	-0.1435(7)	3.1(2)
C24	0.4638(8)	0.5705(3)	-0.0562(6)	2.6(2)
C25	-0.265(1)	0.6384(4)	0.5268(8)	3.6(5)
C26	-0.1569(8)	0.7266(4)	0.5077(6)	2.7(4)
C27	-0.1144(8)	0.6507(3)	0.3828(8)	2.7(4)
C28	0.1544(8)	0.5787(4)	0.7891(7)	2.9(4)
C29	0.248(1)	0.6691(4)	0.7872(7)	3.4(4)
C30	0.3108(9)	0.6048(3)	0.6508(7)	2.8(4)
C31	0.224(1)	0.6593(4)	0.4180(7)	3.7(5)
C32	-0.115(1)	0.5310(4)	0.6467(7)	3.4(4)
C33	-0.025(1)	0.7432(4)	0.7625(9)	4.7(5)

a. B_{eq} is defined as $4/3[a^2\beta_{11}+b^2\beta_{22}+c^2\beta_{33}+ab(\cos\gamma)\beta_{12}+ac(\cos\beta)\beta_{13}+bc(\cos\alpha)\beta_{23}$

Table 6·13. Calculated and Observed X-ray Powder Diffraction Patterns for $(Ph_4P)_2[Mn_3(S_2)_2(SH)(CO)_9]$ (6·1)

h k l	$d_{calc.}$ (Å)	$d_{obs.}$ (Å)	$I/I_{max.}$ (obs.)
2 1 0	10.2	10.7	88
0 1 1	10.0	10.3	70
1 1-1	9.69	9.66	31
2 0 1	8.72	8.86	19
2 1-1	8.40	8.47	38
0 2 0	8.03	8.06	100
4 0 0	6.64	6.72	60
0 0 2	6.43	6.39	68
4 1 0	6.13	6.18	81
3 2 0	5.95	6.01	72
4 1-1	5.80	5.82	60
3 2 1	5.23	5.20	98
1 2-2	5.019	5.017	96
4 1-2	4.711	4.713	90
5 2-1	4.324	4.312	80
0 1 3	4.142	4.143	67
3 1-3	3.934	3.933	74
6 0-2	3.872	3.869	66
1 4-1	3.811	3.802	49
4 1-3	3.716	3.713	50
4 3-2	3.625	3.626	30
5 3 1	3.535	3.529	28
6 0 2	3.453	3.454	33
8 0 0	3.317	3.320	30
2 0 4	3.043	3.040	24
3 5-1	2.966	2.967	20
4 3 3	2.879	2.877	11
8 3 0	2.820	2.822	18
5 5 0	2.747	2.744	10
4 5-2	2.690	2.702	22
1 4-4	2.501	2.501	24
9 4 1	2.297	2.296	41

Table 6·14. Calculated and Observed X-ray Powder Diffraction Patterns for $(Ph_4P)_2[Mn_3(S_2)_2(SCH_3)(CO)_9]$ (6·2)

h k l	$d_{calc.}$ (Å)	$d_{obs.}$ (Å)	$I/I_{max.}$ (obs.)
1 1-1	10.6	10.6	38
2 1 0	10.3	10.3	28
2 2 0	8.97	8.95	57
1 2 1	8.39	8.43	39
2-1 0	7.93	7.95	100
1-2-1	7.11	7.15	27
0 0 2	6.42	6.44	13
0 1 2	6.107	6.104	16
3 2 1	5.883	5.890	23
1-3 1	5.630	5.639	18
2 0-2	5.347	5.350	26
2-3 0	5.067	5.059	27
4 0 0	4.859	4.847	63
3 4 1	4.738	4.736	59
4 0-1	4.540	4.546	22
2 4-2	4.325	4.327	18
0 4-2	4.237	4.231	22
4-2 0	3.966	3.961	24
4 4-2	3.716	3.719	28
3 0 3	3.573	3.561	19
6 2 0	3.446	3.442	16
1 7 1	3.153	3.156	37
2-4 3	3.034	3.037	20
2-1 4	2.987	2.981	25
5 4-3	2.894	2.892	27
0 6 3	2.739	2.740	10
4 5-4	2.540	2.541	14
4 9 1	2.498	2.490	18
2 3-5	2.438	2.432	19
8 3 2	2.393	2.391	18

Table 6·15. Calculated and Observed X-ray Powder Diffraction Patterns for $(Ph_4P)_2[Mn_3(Se_2)_2(SeCH_3)(CO)_9]$ (6·3)

h k l	$d_{calc.}$ (Å)	$d_{obs.}$ (Å)	$I/I_{max.}$ (obs.)
0 2 1	11.5	11.6	100
1 0-1	9.87	9.90	21
0 0 2	9.02	9.02	68
1 0 1	9.01	/	/
1 2 0	8.87	8.91	57
0 1 2	8.63	8.70	31
0 4 0	7.46	7.47	21
1 1-2	7.15	7.15	13
1 2-2	6.603	6.601	19
1 3-2	5.918	5.914	23
1 4 1	5.745	5.748	20
0 2 3	5.579	5.577	18
1 5-1	5.105	5.109	27
2 2 1	4.851	4.849	21
0 4 3	4.682	4.680	14
2 0 2	4.506	4.511	25
1 5-3	4.053	4.055	16
1 7-1	3.912	3.921	11
0 8 0	3.728	3.723	20
2 2-4	3.575	3.574	17
2 7-3	3.023	3.031	15
0 10 1	2.942	2.944	22
4 2-1	2.723	2.722	13
4 3-1	2.668	2.664	18

Table 6-16. Calculated and Observed X-ray Powder Diffraction Patterns for α-$(Ph_4P)_2[Mn_3(Te_2)_2(TeCH_3)(CO)_9]$ (6-4)

h k l	$d_{calc.}$ (Å)	$d_{obs.}$ (Å)	$I/I_{max.}$ (obs.)
0 0 2	11.6	11.6	100
0 1-1	11.4	/	/
0 1 0	11.2	/	/
1 0-1	10.8	10.8	50
0 1-2	9.50	9.54	45
1 0 1	9.19	9.21	80
0 1 1	9.15	/	/
1-1 1	8.73	8.77	36
1-1-1	8.39	8.40	41
1-1 2	7.42	7.47	23
0 1 2	7.125	7.135	46
1 1-3	6.165	6.163	18
1-2 0	5.675	5.677	26
1-1 4	5.032	5.028	18
1-2-2	4.772	4.774	13
1 1-5	4.533	4.542	21
2-2 2	4.368	4.375	26
0 2 3	4.035	4.030	23
0 0 6	3.857	3.861	46
1-1 6	3.633	3.632	24
3-2 1	3.486	3.483	42
0 1 6	3.369	3.371	22
3 1-1	3.305	3.309	30
3-1 3	3.253	3.249	42
0 2 5	3.164	3.172	40
3 1 1	3.079	3.077	33
0 1-8	3.012	3.018	42
0 0 8	2.893	2.898	41
3 2-2	2.850	2.850	42
4-1 1	2.776	2.788	23

Table 6·16. (cont'd)

h k l	$d_{calc.}$ (Å)	$d_{obs.}$ (Å)	$I/I_{max.}$ (obs.)
4-2-3	2.674	2.671	16
4-2 3	2.558	2.558	21
3 3-2	2.412	2.409	27
3 2-8	2.354	2.356	25
4 2-3	2.319	2.320	27
4-4-2	2.234	2.234	31
1 5-2	2.174	2.175	22
5 1-2	2.101	2.100	19
3-4 8	2.053	2.054	17

Table 6-17. Calculated and Observed X-ray Powder Diffraction Patterns for β-$(Ph_4P)_2[Mn_3(Te_2)_2(TeCH_3)(CO)_9]$ (6-5)

h k l	$d_{calc.}$ (Å)	$d_{obs.}$ (Å)	$I/I_{max.}$ (obs.)
0 2 0	13.8	14.2	18
1 0-1	11.0	11.1	78
0 2 1	10.9	/	/
1 0 1	9.20	9.31	100
1 2 0	9.08	/	/
1 2-1	8.59	8.63	34
1 1-2	7.59	7.60	19
0 4 0	6.90	6.87	22
1 2-2	6.85	/	/
0 4 1	6.43	6.47	20
1 3-2	5.99	6.02	31
0 1 3	5.79	5.81	24
1 1-3	5.64	5.66	26
2 2-2	5.10	5.18	27
2 1-3	4.62	4.61	26
2 3-3	4.177	4.179	21
1 7-1	3.710	3.717	14
1 7 1	3.623	3.625	9
1 7 2	3.382	3.383	7
2 4-4	3.211	3.214	11
3 3-4	3.111	3.107	10

Table 6·18. Calculated and Observed X-ray Powder Diffraction Patterns for $(Ph_4P)_3[Re_4(Te_2)_3(TeCH_3)(CO)_{12}]\cdot CH_3OH$ (6·6)

h k l	$d_{calc.}$ (Å)	$d_{obs.}$ (Å)	$I/I_{max.}$ (obs.)
1 0 0	13.7	13.8	48
1 0-1	12.6	12.9	52
1 1 0	12.6	/	/
1 1-1	11.8	11.8	46
0 1-1	11.5	11.4	100
0 1 1	11.3	/	/
0 2 0	11.0	11.1	83
1-1 0	10.98	/	/
1-1-1	10.29	10.40	86
1 2 0	9.33	9.41	37
1 2-1	9.02	9.07	21
0 2 1	8.44	8.45	18
1 0 1	8.05	8.07	36
1-2 0	8.047	8.053	15
1 1 1	7.759	7.764	13
2 0-1	7.560	7.562	27
1-1 1	7.382	7.385	12
1 3 0	6.939	6.936	8
1 2 1	6.758	6.761	14
0 1 2	6.365	6.372	14
2 3-1	5.803	5.803	12
2 0 1	5.286	5.284	7
1 1 2	5.123	5.121	9
2 2 1	4.983	4.982	17
2 2-3	4.585	4.581	6
1 3 2	4.344	4.341	22
0 5-1	4.214	4.214	16
1-5-1	3.981	3.982	13
3 1-4	3.520	3.521	24
1-6 0	3.429	3.427	19

Table 6·18. (cont'd)

h k l	$d_{calc.}$ (Å)	$d_{obs.}$ (Å)	$I/I_{max.}$ (obs.)
3-4-2	3.373	3.375	8
1 4 3	3.168	3.170	13
3-1 2	3.132	3.131	8
2-6-1	3.102	3.104	13
5 3-2	2.999	3.002	8
3 2-5	2.888	2.890	13

Table 6·19. Calculated and Observed X-ray Powder Diffraction Patterns for $(Ph_4P)[Mn_2(SCH_3)_3(CO)_6]$ (**6·7**) and $(Ph_4P)[Mn_2(SeCH_3)_3(CO)_6]$ (**6·8**)

h k l	$d_{calc.}$ (Å)	$d_{obs.}$ (Å), I/I_{max} for (**6·7**)	$d_{obs.}$ (Å), I/I_{max} for (**6·8**)
0 1 0	10.3	10.5, 17	10.5, 11
1 0 0	9.20	9.34, 26	9.38, 32
1-1 0	9.04	9.12, 100	9.10, 100
0 0 2	7.88	7.94, 68	7.89, 49
0 1-2	7.67	7.70, 39	7.68, 44
1 0 1	7.354	7.367, 33	7.369, 12
1 0-2	6.659	6.662, 9	6.658, 5
1-1 2	6.302	6.307, 21	6.309, 12
1-2 0	5.638	5.644, 19	5.641, 20
0 2-1	5.496	5.499, 17	5.495, 21
0 2-2	5.222	5.219, 14	5.226, 18
1 1 1	4.933	4.937, 23	4.936, 20
0 2-3	4.550	4.554, 9	4.559, 11
0 1-4	4.196	4.201, 13	4.205, 7
1-3 2	3.909	3.903, 11	3.905, 9
2 1-2	3.742	3.740, 9	3.739, 11
1-3 3	3.640	3.646, 14	3.646, 10
2-3 3	3.297	3.293, 22	3.287, 20
0 2 3	3.173	3.177, 14	3.179, 16
3-2-2	3.057	3.058, 29	3.053, 25
3-1 2	2.984	2.991, 20	2.997, 16
2-4 1	2.909	2.909, 12	2.902, 13
2 2-4	2.777	2.771, 15	2.774, 17
3-4 2	2.607	2.609, 13	2.612, 13
3-4 3	2.514	2.510, 21	2.518, 19
1 1 5	2.459	2.461, 17	2.463, 14
0 2 5	2.352	2.362, 8	2.357, 13
1 2-7	2.317	2.316, 14	2.321, 11

Table 6·20. Calculated and Observed X-ray Powder Diffraction Patterns for $(Ph_4P)[Mn_2(TeCH_3)_3(CO)_6]$ (**6·9**)

h k l	$d_{calc.}$ (Å)	$d_{obs.}$ (Å)	$I/I_{max.}$ (obs.)
0 2 0	13.3	13.7	29
0 1 1	11.7	11.9	89
1 0 0	10.3	10.6	100
0 2 1	9.31	9.42	93
1 1-1	8.24	8.32	98
0 3 1	7.33	7.39	43
1 1 1	7.29	/	/
1 2-1	7.26	/	/
0 4 0	6.66	6.70	65
1 2 1	6.58	/	/
0 1 2	6.32	6.35	44
1 3-1	6.19	6.22	38
0 4 1	5.93	5.97	19
1 0-2	5.87	/	/
1 3 1	5.762	5.768	32
1 4 0	5.586	5.582	27
0 3 2	5.250	5.256	18
2 0 0	5.134	5.136	36
1 4 1	5.000	5.007	18
1 3-2	4.899	4.902	26
1 4 2	4.091	4.088	22
1 6 0	4.074	/	/
2 1 2	3.749	3.741	31
2 5 0	3.696	3.689	23
2 2 2	3.643	3.647	37
1 6-2	3.541	3.541	21
1 7-1	3.483	3.481	18
3 1 0	3.395	3.398	20
0 8 0	3.328	3.321	26
1 0-4	3.234	3.237	29

Table 6·20. (cont'd)

h k l	$d_{calc.}$ (Å)	$d_{obs.}$ (Å)	$I/I_{max.}$ (obs.)
3 3-1	3.198	3.198	36
3 1-2	3.193	3.191	26
1 8 0	3.166	3.167	39
0 2 4	3.163	/	/
1 8-1	3.107	3.105	28
1 7 2	3.067	3.069	32
2 3 3	2.936	2.935	25
1 6 3	2.893	2.891	36
3 5-1	2.882	/	/
1 7-3	2.823	2.830	28
3 4-3	2.649	2.641	26
1 9 2	2.570	2.567	21
4 3-1	2.483	2.486	26
1 8-4	2.319	2.313	19
1 1-6	2.178	2.177	16

III. Results

1. Description of Crystal and Molecular Structures of the Compounds

(i). Structures of $(Ph_4P)_2[Mn_3(S_2)_2(SH)(CO)_9]$ (6·1) and $(Ph_4P)_2[Mn_3(S_2)_2(SCH_3)(CO)_9]$ (6·2)

The crystal lattice of these two compounds is made up of non-interacting Ph_4P^+ cations and $[Mn_3(S_2)_2(SH)(CO)_9]^{2-}$ or $[Mn_3(S_2)_2(SCH_3)(CO)_9]^{2-}$ cluster anions. Figures 6·1 and 6·2 show the packing diagrams of the two compounds. (**6·1**) belongs to the space group $P2_1/a$ (#14), while (**6·2**) crystallizes in the space group P-1 (#2) with two crystallographically independent, but structurally similar $[Mn_3(S_2)_2(SCH_3)(CO)_9]^{2-}$ anions found in the unit cell. Nevertheless, these anions have essentially the same structure as shown in Figures 6·3 and 6·4. Each molecule contains a triangle of Mn atoms bridged by two disulfide S_2^{2-} ligands, and a methylsulfide CH_3S^- in (**6·2**) or a protonated sufide HS^- in (**6·1**). In the latter, the H atom could not be located from the X-ray structure. Its presence was revealed by other experimental evidence (vide infra). Two disulfide units in each cluster adapt different coordination modes, i.e. one is μ_3-η^1,η^1,η^2-type and another is overall μ_3-type. The hydrosulfide HS^- or methylsulfide CH_3S^- acts as a μ_2-type ligand. These clusters possess C_s molecular symmetry with the mirror running through O(3)/C(51)/Mn(1)/S(4)/S(3)/S(5) in (**6·1**), and O(3A)/C(99A)/Mn(1A)/S(4A)/S(3A)/S(5A)/C(106A)/H(83) or O(3B)/C(99B)/Mn(1B)/S(4B)/S(3B)/S(5B)/C(106B)/H(84) in (**6·2**), respectively. All Mn atoms, being bonded by three S ligands and three *cis* CO groups, are in an approximately octahedral environment. The observed M–M distances in the clusters range from 3.51 to 4.04 Å, which excludes any possible M–M bonding. All Mn atoms in these clusters have a +1 formal oxidation state. The Mn-S bond distances are split into two groups. The distances of Mn atoms to the hydrosulfide/methylsulfide ligands are longer, averaging

2.396(3) in (**6·1**), and 2.375(6) Å for molecule A and 2.392(2) Å for molecule B in (**6·2**), than the Mn-S bonds associated with the disulfide units, which average 2.356(9) in (**6·2**), and 2.356(7) Å for molecule A and 2.345(5) Å for molecule B in (**6·2**). Such Mn-S distances are comparable to those of 2.34–2.38 Å found in $[Mn_4(S_2)_2(CO)_{15}]$[10]. The S-S bond distances, averaging 2.073(20) Å in (**6·1**), 2.055(5) and 2.07(2) Å in (**6·2**), can be considered normal single bonds[19]. Selected bond distances and bond angles for the $[Mn_3(S_2)_2(SR)(CO)_9]^{2-}$ (R=H, CH_3) anions in the two compounds are comparatively shown in Table 6·21. Due to higher standard deviations of the bond distances in (**6·2**), comparison with those will not be meaningful. The bond angles of these anions are similar to each other, except for those angles that involve S(5) atom. The noticeable difference is that the S(1)-Mn(2)-S(5) and S(2)-Mn(3)-S(5) angles are larger in (**6·2**) than in (**6·1**), while S(3)-Mn(2)-S(5) and S(3)-Mn(3)-S(5) are smaller in (**6·2**) than in (**6·1**) (see Table 6·20). This may originate from the need of the methyl group to avoid the steric repulsion with the cluster. The methyl group can thus be viewed as an envelop flap in the motion of being opened up (see Figures 6·3 and 6·4).

Table 6-21. Selected Bond Distances (Å) and Bond Angles (deg) of $(Ph_4P)_2[Mn_3(S_2)_2(SH)(CO)_9]$ (**6-1**) and $(Ph_4P)_2[Mn_3(S_2)_2(SCH_3)(CO)_9]$ (**6-2**)[a,b]

compound	$[Mn_3(S_2)_2(SH)(CO)_9]^{2-}$ in (**6-1**)	molecule A of $[Mn_3(S_2)_2(SH)(CO)_9]^{2-}$ in (**6-2**)	molecule B of $[Mn_3(S_2)_2(SH)(CO)_9]^{2-}$ in (**6-2**)
Mn(1)-S(1)	2.357(3)	2.359(9)	2.338(9)
Mn(1)-S(2)	2.359(3)	2.320(9)	2.365(9)
Mn(1)-S(4)	2.355(3)	2.36(1)	2.33(1)
Mn(2)-S(1)	2.360(3)	2.367(9)	2.351(9)
Mn(2)-S(3)	2.354(3)	2.358(9)	2.337(9)
Mn(2)-S(5)	2.399(3)	2.38(1)	2.393(9)
Mn(3)-S(2)	2.355(4)	2.350(9)	2.363(9)
Mn(3)-S(3)	2.355(3)	2.38(1)	2.352(9)
Mn(3)-S(5)	2.393(3)	2.369(9)	2.39(1)
Mn-S(mean)(to S_2^{2-})	2.356(9)	2.356(7)	2.348(5)
Mn-S(mean).(to S^{2-})	2.396(3)	2.375(6)	2.392(2)
S(1)-S(2)	2.093(4)	2.05(1)	2.05(1)
S(3)-S(4)	2.053(4)	2.06(1)	2.09(1)
S-S(mean)	2.073(20)	2.055(5)	2.07(2)
S(5)-Cj	/	1.86(4)	1.92(4)
Mn(1)-Ca	1.79(1)	1.84(3)	1.76(3)
Mn(1)-Cb	1.77(1)	1.75(4)	1.76(4)
Mn(1)-Cc	1.75(1)	1.82(3)	1.74(4)
Mn(2)-Cd	1.76(1)	1.82(3)	1.70(4)

Table 6·21. (cont'd)

compound	$[Mn_3(S_2)_2(SH)(CO)_9]^{2-}$ in (6·1)	molecule A of $[Mn_3(S_2)_2(SH)(CO)_9]^{2-}$ in (6·2)	molecule B of $[Mn_3(S_2)_2(SH)(CO)_9]^{2-}$ in (6·2)
Mn(2)-Ce	1.76(1)	1.75(4)	1.77(4)
Mn(2)-Cf	1.76(1)	1.75(3)	1.78(3)
Mn(3)-Cg	1.75(1)	1.80(4)	1.76(4)
Mn(3)-Ch	1.76(1)	1.77(5)	1.85(4)
Mn(3)-Ci	1.71(1)	1.74(3)	1.80(4)
Mn-C(mean).	1.76(7)	1.78(10)	1.77(14)
S(1)-Mn(1)-S(2)	52.7(1)	52.1(3)	52.1(3)
S(1)-Mn(1)-S(4)	93.8(1)	92.8(3)	93.3(3)
S(2)-Mn(1)-S(4)	93.7(1)	93.6(4)	93.9(3)
S(1)-Mn(2)-S(3)	88.5(1)	88.4(3)	88.7(3)
S(1)-Mn(2)-S(5)	84.2(1)	90.5(3)	91.2(3)
S(3)-Mn(2)-S(5)	81.3(1)	78.4(3)	78.5(3)
S(2)-Mn(3)-S(3)	88.0(1)	87.9(3)	88.9(3)
S(2)-Mn(3)-S(5)	84.7(1)	90.3(3)	89.2(3)
S(3)-Mn(3)-S(5)	81.4(1)	78.2(3)	78.3(3)
S(1)-Mn(1)-Ca	156.8(4)	157(1)	155(1)
S(2)-Mn(1)-Cb	158.5(4)	159(1)	158(1)
S(4)-Mn(1)-Cc	175.2(4)	174(1)	173(1)
S(1)-Mn(2)-Cd	177.6(4)	179.1(9)	178(1)

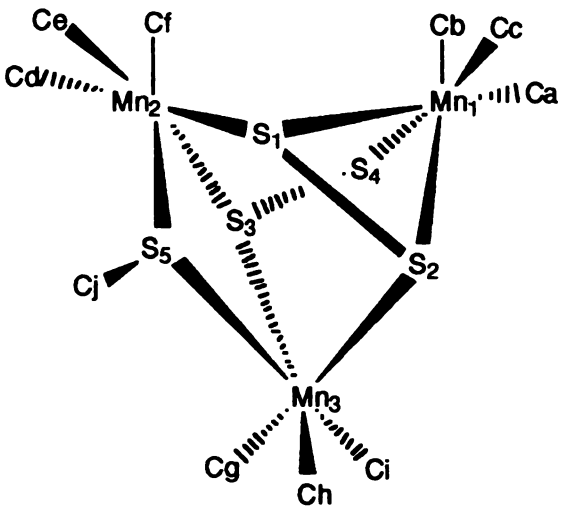
Table 6·21. (cont'd)

compound	$[Mn_3(S_2)_2(SH)(CO)_9]^{2-}$ in (**6·1**)	molecule A of $[Mn_3(S_2)_2(SH)(CO)_9]^{2-}$ in (**6·2**)	molecule B of $[Mn_3(S_2)_2(SH)(CO)_9]^{2-}$ in (**6·2**)
S(3)-Mn(2)-Ce	177.2(4)	176(1)	177(1)
S(5)-Mn(2)-Cf	172.8(4)	175(1)	167(1)
S(2)-Mn(3)-Cg	177.0(4)	179(1)	178(1)
S(3)-Mn(3)-Ch	176.9(4)	176(1)	170(1)
S(5)-Mn(3)-Ci	172.7(4)	173(1)	172(1)
Ca-Mn(1)-Cb	97.2(5)	96(1)	98(1)
Ca-Mn(1)-Cc	92.6(5)	91(1)	87(1)
Cb-Mn(1)-Cc	89.7(5)	91(1)	90(1)
Cd-Mn(2)-Ce	90.6(5)	91(1)	92(1)
Cd-Mn(2)-Cf	90.1(5)	92(1)	93(1)
Ce-Mn(2)-Cf	89.3(5)	87(1)	93(1)
Cg-Mn(3)-Ch	89.2(6)	91(2)	97(2)
Cg-Mn(3)-Ci	91.4(6)	90(2)	89(1)
Ch-Mn(3)-Ci	90.4(5)	89(2)	94(1)
Mn(1)-S(1)-Mn(2)	116.2(1)	117.4(4)	118.1(4)
Mn(1)-S(2)-Mn(3)	117.6(1)	117.8(4)	115.7(4)
Mn(2)-S(3)-Mn(3)	96.5(1)	95.8(3)	96.7(3)
Mn(2)-S(5)-Mn(3)	94.3(1)	95.5(3)	94.3(3)
Mn(1)-S(1)-S(2)	63.7(1)	63.0(3)	64.6(3)
Mn(2)-S(1)-S(2)	107.3(1)	107.2(4)	107.1(4)

Table 6·21. (cont'd)

compound	$[Mn_3(S_2)_2(SH)(CO)_9]^{2-}$ in (**6·1**)	molecule A of $[Mn_3(S_2)_2(SH)(CO)_9]^{2-}$ in (**6·2**)	molecule B of $[Mn_3(S_2)_2(SH)(CO)_9]^{2-}$ in (**6·2**)
Mn(1)-S(2)-S(1)	63.6(1)	64.9(3)	63.3(3)
Mn(3)-S(2)-S(1)	107.7(1)	108.9(4)	108.4(4)
Mn(2)-S(3)-S(4)	107.9(2)	108.3(5)	108.5(4)
Mn(3)-S(3)-S(4)	110.0(2)	108.1(5)	106.7(4)
Mn(1)-S(4)-S(3)	106.9(2)	108.0(4)	107.9(4)
Mn(2)-S(5)-Cj	/	110(1)	113(1)
Mn(3)-S(5)-Cj	/	109(1)	105(1)

a. Labeling scheme:



b. The estimated standard deviations in the mean bond lengths and the mean bond angles are calculated by the equation $\sigma_l=\{\Sigma_n(l_n-l)^2/n(n-1)\}^{1/2}$, where l_n is the length (angle) of the *n*th bond, l the mean length (angle), and n the number of bonds.

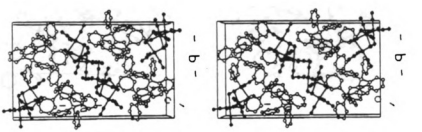


Figure 6-1. The Packing Diagram in the Unit Cell of $(Ph_4P)_2[Mn_3(S_2)_2(SH)(CO)_9]$ (Stereoview)

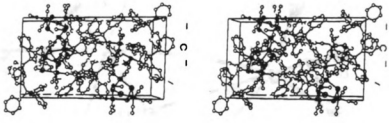


Figure 6-2. The Packing Diagram in the Unit Cell of $(Ph_4P)_2[Mn_3(S_2)_2(SCH_3)(CO)_9]$ (Stereoview)

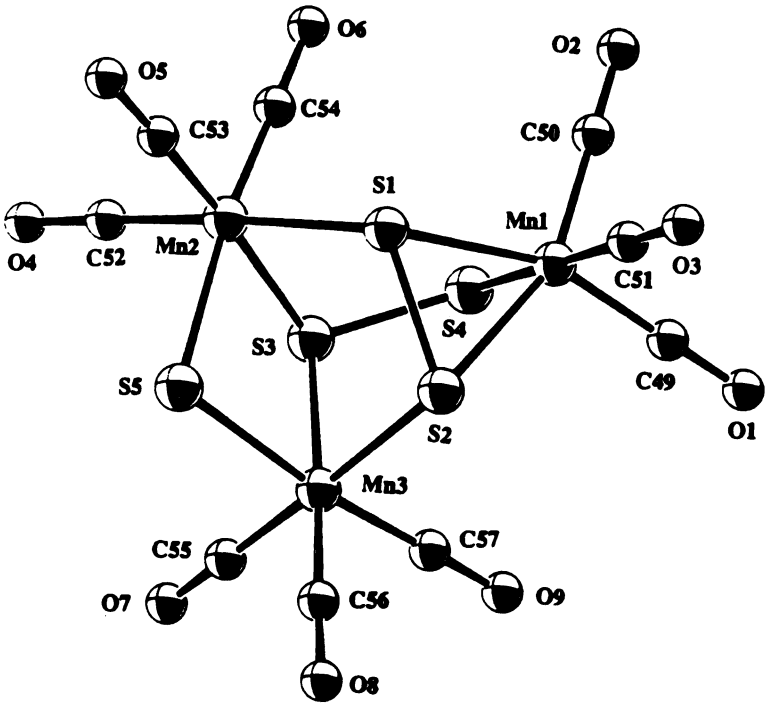


Figure 6-3. The Structure of the $[Mn_3(S_2)_2(SH)(CO)_9]^{2-}$ Anion

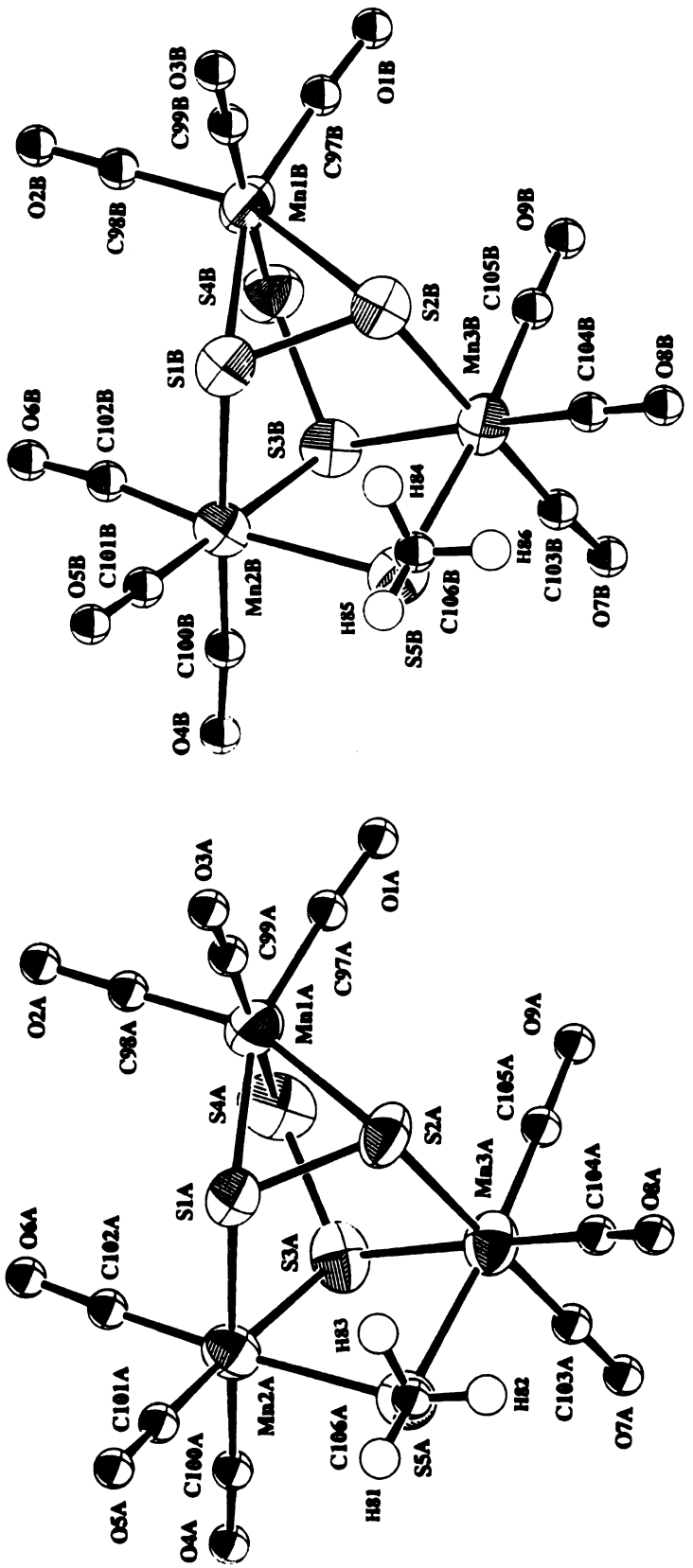
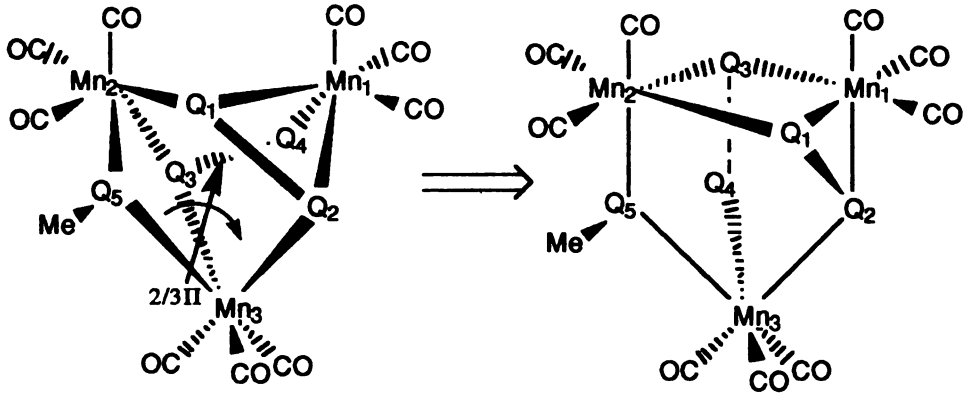


Figure 6-4. Structures of the Two Crystallographically Independent $[Mn_3(S_2)_2(SCH_3)(CO)_9]^{2-}$ Anions Found in the $(Ph_4P)_2[Mn_3(S_2)_2(SCH_3)(CO)_9]$ Unit Cell

(ii). Structure of $(Ph_4P)_2[Mn_3(Se_2)_2(SeCH_3)(CO)_9]$ (6·3)

The structure of (6·3) comprises of Ph_4P^+ cations and $[Mn_3(Se_2)_2(SeCH_3)(CO)_9]^{2-}$ anions in the crystal lattice as shown in Figure 6·5. The Ph_4P^+ cations have the normal tetrahedral structure, and will not be discussed further. The $[Mn_3(Se_2)_2(SeCH_3)(CO)_9]^{2-}$ cluster anion, although containing the same type of ligands as found in (6·2), is assembled differently. Figure 6·6 shows the structure of this anion. This cluster can be easily derived from its sulfide counterparts in (6·2) by rotating the μ_3-dichalcogenide ligand 120° clockwise as shown below:



S-Cluster Se-Cluster

Scheme 6·3. Structural Relationship Between $[Mn_3(S_2)_2(SCH_3)(CO)_9]^{2-}$ and $[Mn_3(Se_2)_2(SeCH_3)(CO)_9]^{2-}$

The Q(3) (Q=S, Se) atom is turned from bridging Mn(2) and Mn(3) to bridging Mn(1) and Mn(2), and Q(4) is moved from Mn(1) to Mn(3). Such an action removes the mirror plane from the structure. As a result, the current cluster is a chiral molecule. However, (6·3) crystallizes in the centrosymmetric space group $P2_1/n$ (#14) which necessitates a racemic mixture in the solid state. Figure 6·7 shows the two optical isomers of the cluster found in the unit cell. The average Mn-Se bond distance at 2.468(6) Å can be compared with 2.478(4) Å found in $(Ph_4P)_2[Mn_2(Se_2)_2(CO)_6]\cdot Et_2O$[11], while the Se-Se distances of 2.365(6) and 2.353(6) Å are in the range of normal single bond[5]. The Mn–

Mn distances of Mn(1)-Mn(2)=3.66 Å, Mn(2)-Mn(3)=4.11 Å and Mn(1)-Mn(3)=4.22 Å suggest no M–M bonding. Selected bond distances and bond angles are given in Table 6·22.

Table 6·22. Selected Bond Distances (Å) and Bond Angles (deg) of $(Ph_4P)_2[Mn_3(Se_2)_2(SeCH_3)(CO)_9]$ (**6·3**)[b]

		Bond Distances (Å)	
Mn(1)-Se(1)	2.500(8)	Mn(1)-Se(2)	2.468(8)
Mn(1)-Se(3)	2.463(8)	Mn(2)-Se(1)	2.467(7)
Mn(2)-Se(3)	2.463(8)	Mn(2)-Se(5)	2.472(8)
Mn(3)-Se(2)	2.458(7)	Mn(3)-Se(4)	2.442(7)
Mn(3)-Se(5)	2.480(8)	Mn-Se(mean)	2.468(6)
Se(1)-Se(2)	2.365(6)	Se(3)-Se(4)	2.353(6)
Se-Se(mean)	2.359(6)	Se(5)-C(58)	2.00(3)
Mn(1)-C(49)	1.80(4)	Mn(1)-C(50)	1.84(6)
Mn(1)-C(51)	1.75(6)	Mn(2)-C(52)	1.82(5)
Mn(2)-C(53)	1.63(4)	Mn(2)-C(54)	1.75(5)
Mn(3)-C(55)	1.74(5)	Mn(3)-C(56)	1.71(5)
Mn(3)-C(57)	1.78(3)	Mn-C(mean)	1.76(2)
		Bond Angles (deg)	
Se(1)-Mn(1)-Se(2)	56.8(2)	Se(1)-Mn(1)-Se(3)	84.0(2)
Se(2)-Mn(1)-Se(3)	90.8(2)	Se(1)-Mn(2)-Se(3)	84.0(2)
Se(1)-Mn(2)-Se(5)	93.4(2)	Se(3)-Mn(2)-Se(5)	90.2(2)
Se(2)-Mn(3)-Se(4)	93.7(3)	Se(2)-Mn(3)-Se(5)	94.3(2)
Se(4)-Mn(3)-Se(5)	84.3(2)	Se(1)-Mn(1)-C(50)	159(2)

Table 6·22. (cont'd)

Bond Angles (deg)

Se(2)-Mn(1)-C(51)	162(2)	Se(3)-Mn(1)-C(49)	178(1)
Se(1)-Mn(2)-C(53)	Se(3)-Mn(2)-C(52)	Se(3)-Mn(2)-C(52)	176(1)
Se(5)-Mn(2)-C(54)	174(1)	Se(2)-Mn(3)-C(56)	178(2)
Se(4)-Mn(3)-C(55)	174(1)	Se(5)-Mn(3)-C(57)	171(1)
C(49)-Mn(1)-C(50)	91(2)	C(49)-Mn(1)-C(51)	89(2)
C(50)-Mn(1)-C(51)	95(3)	C(52)-Mn(2)-C(53)	91(2)
C(52)-Mn(2)-C(54)	95(2)	C(53)-Mn(2)-C(54)	94(2)
C(55)-Mn(3)-C(56)	92(2)	C(55)-Mn(3)-C(57)	98(2)
C(56)-Mn(3)-C(57)	94(2)	Mn(1)-Se(1)-Mn(2)	95.0(3)
Mn(1)-Se(2)-Mn(3)	117.9(3)	Mn(1)-Se(3)-Mn(2)	95.1(3)
Mn(2)-Se(5)-Mn(3)	112.4(3)	Mn(1)-Se(1)-Se(2)	60.9(2)
Mn(1)-Se(2)-Se(1)	62.3(2)	Mn(2)-Se(1)-Se(2)	105.8(2)
Mn(1)-Se(3)-Se(4)	104.2(2)	Mn(2)-Se(3)-Se(4)	109.5(2)
Mn(3)-Se(4)-Se(3)	103.2(2)	Mn(2)-Se(5)-C(58)	106(1)
Mn(3)-Se(5)-C(58)	108(1)		

b. The estimated standard deviations in the mean bond lengths and the mean bond angles are calculated by the equation $\sigma_l=\{\Sigma_n(l_n-l)^2/n(n-1)\}^{1/2}$, where l_n is the length (angle) of the *n*th bond, l the mean length (angle), and n the number of bonds.

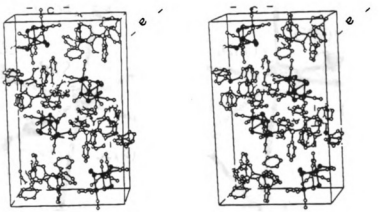


Figure 6-5. The Packing Diagram in the Unit Cell of $(Ph_4P)_2[Mn_3(Se_2)_2(SeCH_3)(CO)_9]$ (Stereoview)

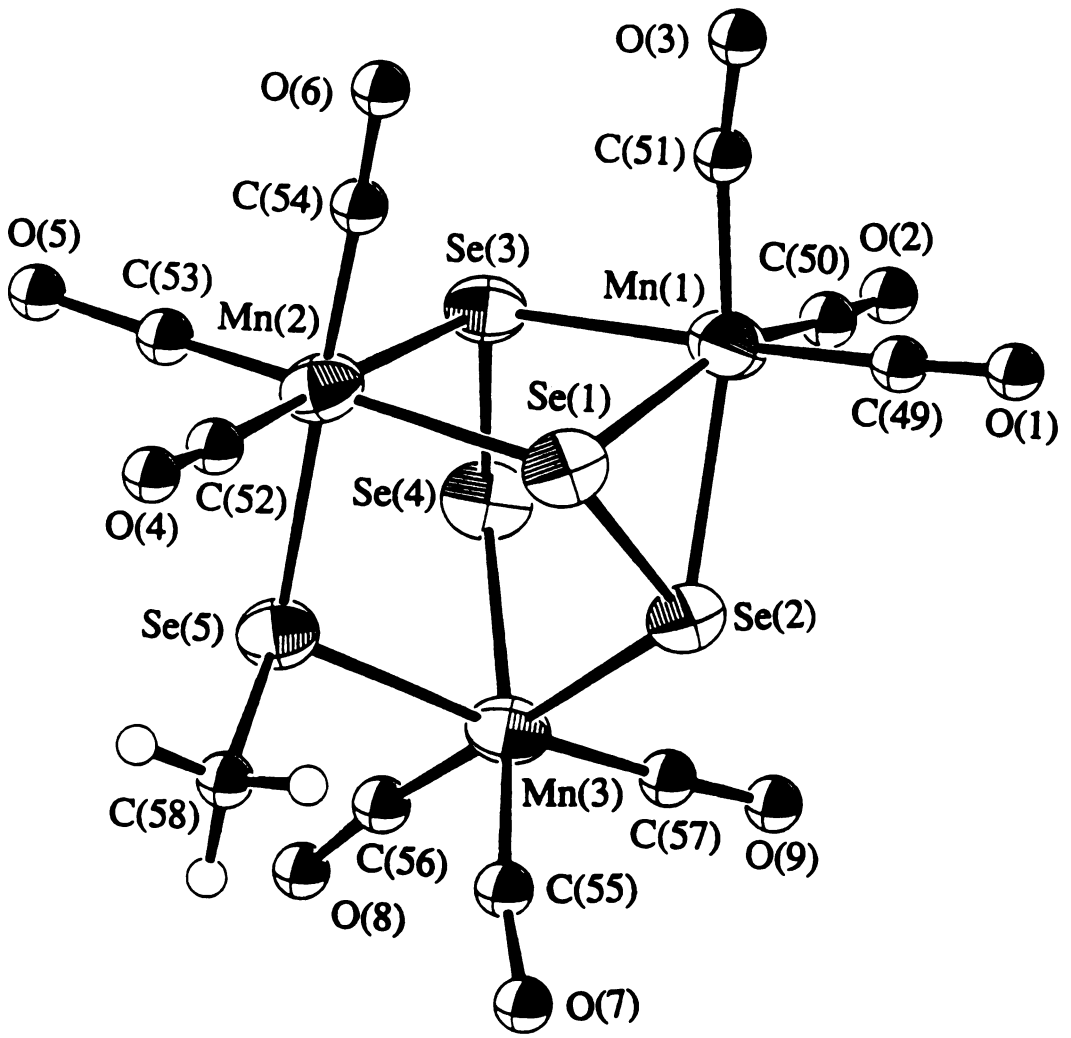


Figure 6-6. The Structure of the $[Mn_3(Se_2)_2(SeCH_3)(CO)_9]^{2-}$ Anion

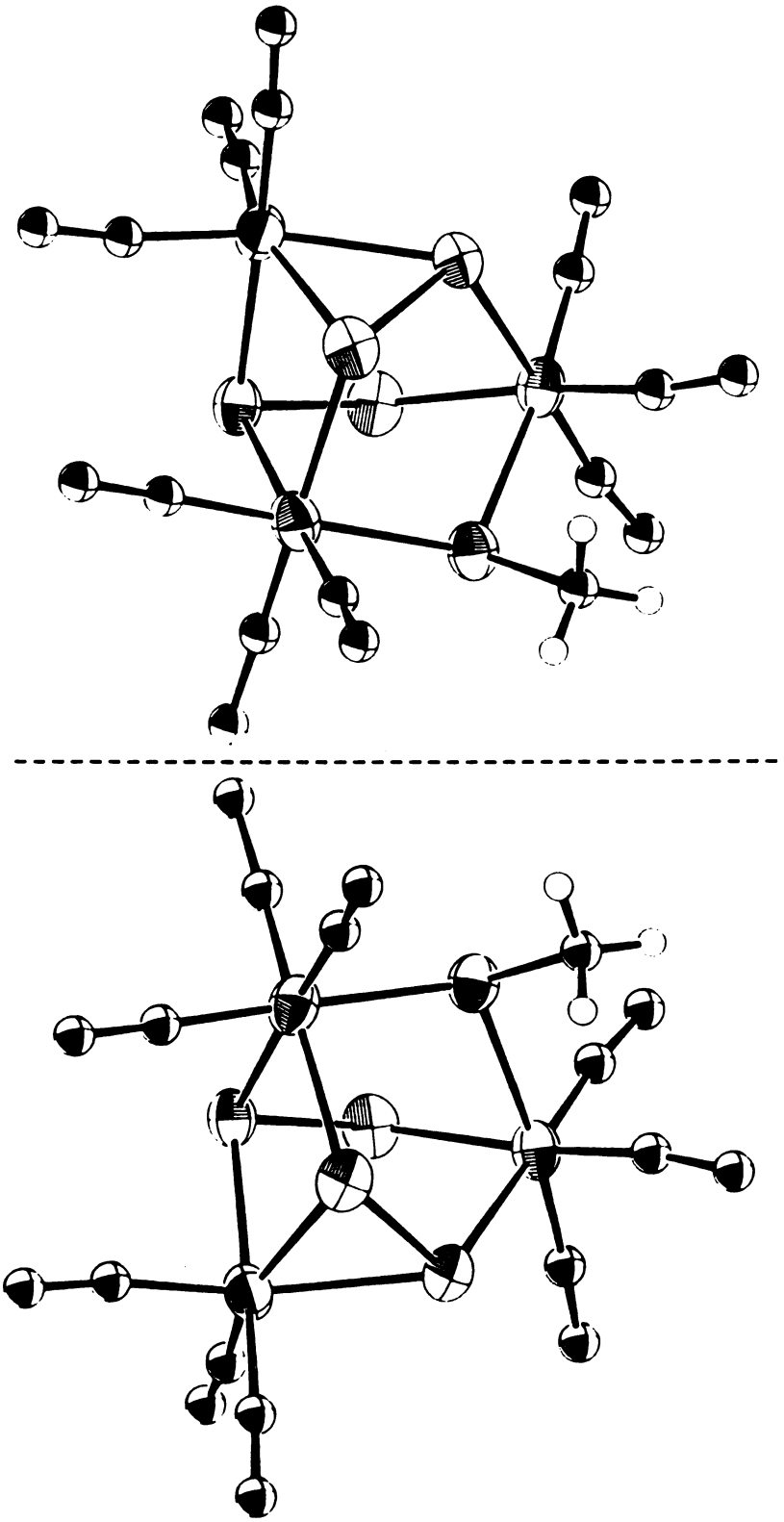


Figure 67. Two Optical Isomers of the $[Mn_3(Se_2)_2(SeCH_3)(CO)_9]^{2-}$ Anion Found in the $(Ph_4P)_2[Mn_3(Se_2)_2(SeCH_3)(CO)_9]$ Unit Cell

(iii). Structures of α-$(Ph_4P)_2[Mn_3(Te_2)_2(TeCH_3)(CO)_9]$ (6·4) and β-$(Ph_4P)_2[Mn_3(Te_2)_2(TeCH_3)(CO)_9]$ (6·5)

Compounds (6·4) and (6·5) are two crystal modifications of the same compound that crystallizes in different space groups, i.e. P-1 for (6·4) and $P2_1/n$ for (6·5). The crystal lattice of the two phases is made up of well separated Ph_4P^+ cations and $[Mn_3(Te_2)_2(TeCH_3)(CO)_9]^{2-}$ anions as shown in Figures 6·8 and 6·9. The Ph_4P^+ cations have the normal tetrahedral structure and warrant no further comments, while the $[Mn_3(Te_2)_2(TeCH_3)(CO)_9]^{2-}$ anions have exactly the same structure as their selenide analogue. Figures 6·10 and 6·11 are ORTEP representations of the anions found in each unit cell. It should be noted that each compound must be a racemic mixture in the crystal lattice because both crystal modifications belong to centrosymmetric space groups. Figures 6·12 and 6·13 show two optical isomers for the cluster anion found in each unit cell, respectively. The average Mn-Te bond distance are 2.655(2) Å in (6·4) and 2.660(4) Å in (6·5). No structural data for Mn-Te bond lengths from manganese polytellurride compounds are available for comparison because such molecules are hitherto unknown. As a matter of fact, the two compounds reported in this work are the first examples. A heteronuclear cluster $Cp^*Mn(CO)_2(Te)Fe_2(CO)_6$ featuring a μ_3-Te bonded to the three metal centers was found to have a Mn-Te distance at 2.518(1) Å and two Fe-Te distances at 2.472(1) and 2.476(1) Å[20], while the average Te-Te distances of 2.734(3) in (6·4) and 2.735(9) Å in (6·5) are in the range of normal single bond[5, 21]. The Mn–Mn distances, ranging from 3.90 to 4.61 Å, indicate that there are no M–M bonding interactions in the clusters. The corresponding bond distances and bond angles in the two crystal modifications are similar but not identical. For comparison, selected bond distances and bond angles for the $[Mn_3(Te_2)_2(TeCH_3)(CO)_9]$ anions in the two compounds are given in Table 6·23.

Table 6·23. Selected Bond Distances (Å) and Bond Angles (deg) of α-$(Ph_4P)_2[Mn_3(Te_2)_2(TeCH_3)(CO)_9]$ (**6·4**) and β-$(Ph_4P)_2[Mn_3(Te_2)_2(TeCH_3)(CO)_9]$ (**6·5**)[b]

compound	$[Mn_3(Te_2)_2(TeCH_3)(CO)_9]^{2-}$ in (**6·4**)	$[Mn_3(Te_2)_2(TeCH_3)(CO)_9]^{2-}$ in (**6·5**)
Mn(1)-Te(1)	2.682(2)	2.675(4)
Mn(1)-Te(2)	2.669(2)	2.651(4)
Mn(1)-Te(3)	2.655(2)	2.654(4)
Mn(2)-Te(1)	2.656(2)	2.638(4)
Mn(2)-Te(3)	2.656(2)	2.660(4)
Mn(2)-Te(5)	2.655(2)	2.673(4)
Mn(3)-Te(2)	2.648(2)	2.625(5)
Mn(3)-Te(4)	2.642(2)	2.653(4)
Mn(3)-Te(5)	2.655(2)	2.660(4)
Mn-Te(mean)	2.658(4)	2.654(5)
Te(1)-Te(2)	2.737(1)	2.726(3)
Te(3)-Te(4)	2.731(1)	2.743(3)
Te-Te(mean).	2.734(3)	2.735(9)
Te(5)-C(58)	2.14(1)	2.12(3)
Mn(1)-C(49)	1.79(1)	1.72(3)
Mn(1)-C(50)	1.77(1)	1.78(3)
Mn(1)-C(51)	1.76(1)	1.76(3)
Mn(2)-C(52)	1.78(1)	1.72(3)
Mn(2)-C(53)	1.80(1)	1.76(3)

Table 6·23. (cont'd)

compound	$[Mn_3(Te_2)_2(TeCH_3)(CO)_9]^{2-}$ in (**6·4**)	$[Mn_3(Te_2)_2(TeCH_3)(CO)_9]^{2-}$ in (**6·5**)
Mn(2)-C(54)	1.79(1)	1.81(3)
Mn(3)-C(55)	1.81(1)	1.72(4)
Mn(3)-C(56)	1.77(1)	1.79(4)
Mn(3)-C(57)	1.77(1)	1.75(3)
Mn-C(mean)	1.78(6)	1.76(1)
Te(1)-Mn(1)-Te(2)	61.53(5)	61.6(1)
Te(1)-Mn(1)-Te(3)	84.98(6)	84.7(1)
Te(2)-Mn(1)-Te(3)	92.03(6)	92.2(1)
Te(1)-Mn(2)-Te(3)	85.48(6)	85.3(1)
Te(1)-Mn(2)-Te(5)	91.97(6)	94.0(1)
Te(3)-Mn(2)-Te(5)	93.19(6)	91.6(1)
Te(2)-Mn(3)-Te(4)	93.99(6)	95.7(1)
Te(2)-Mn(3)-Te(5)	94.46(6)	95.5(1)
Te(4)-Mn(3)-Te(5)	86.09(6)	83.8(1)
Te(1)-Mn(1)-C(50)	168.6(4)	160.2(9)
Te(2)-Mn(1)-C(51)	156.0(4)	158(1)
Te(3)-Mn(1)-C(49)	176.2(4)	178.7(8)
Te(1)-Mn(2)-C(53)	174.9(4)	175.8(9)
Te(3)-Mn(2)-C(52)	173.2(4)	175(1)
Te(5)-Mn(2)-C(54)	176.9(4)	179.9(9)
Te(2)-Mn(3)-C(56)	179.0(4)	174.7(9)

Table 6·23. (cont'd)

compound	$[Mn_3(Te_2)_2(TeCH_3)(CO)_9]^{2-}$ in (**6·4**)	$[Mn_3(Te_2)_2(TeCH_3)(CO)_9]^{2-}$ in (**6·5**)
Te(4)-Mn(3)-C(55)	177.2(4)	177(1)
Te(5)-Mn(3)-C(57)	175.3(4)	175(1)
C(49)-Mn(1)-C(50)	88.5(6)	91(1)
C(49)-Mn(1)-C(51)	93.3(6)	93(1)
C(50)-Mn(1)-C(51)	94.1(6)	102(1)
C(52)-Mn(2)-C(53)	95.9(6)	94(1)
C(52)-Mn(2)-C(54)	90.5(6)	91(1)
C(53)-Mn(2)-C(54)	91.0(6)	94(1)
C(55)-Mn(3)-C(56)	92.9(5)	90(2)
C(55)-Mn(3)-C(57)	92.1(6)	91(1)
C(56)-Mn(3)-C(57)	90.9(6)	91(1)
Mn(1)-Te(1)-Mn(2)	93.86(6)	94.5(1)
Mn(1)-Te(2)-Mn(3)	120.31(6)	120.1(1)
Mn(1)-Te(3)-Mn(2)	94.46(6)	94.5(1)
Mn(2)-Te(5)-Mn(3)	114.00(6)	113.3(1)
Mn(1)-Te(1)-Te(2)	59.00(5)	58.8(1)
Mn(1)-Te(2)-Te(1)	59.47(5)	59.7(1)
Mn(2)-Te(1)-Te(2)	103.49(5)	103.5(1)
Mn(1)-Te(3)-Te(4)	104.46(5)	105.0(1)
Mn(2)-Te(3)-Te(4)	107.02(5)	107.0(1)
Mn(3)-Te(4)-Te(3)	101.46(5)	100.3(1)

Table 6·23. (cont'd)

compound	$[Mn_3(Te_2)_2(TeCH_3)(CO)_9]^{2-}$ in (**6·4**)	$[Mn_3(Te_2)_2(TeCH_3)(CO)_9]^{2-}$ in (**6·5**)
Mn(2)-Te(5)-C(58)	101.4(3)	101.8(9)
Mn(3)-Te(5)-C(58)	105.2(4)	103.5(9)

b. The estimated standard deviations in the mean bond lengths and the mean bond angles are calculated by the equation $\sigma_l=\{\Sigma_n(l_n-l)^2/n(n-1)\}^{1/2}$, where l_n is the length (angle) of the *n*th bond, l the mean length (angle), and n the number of bonds.

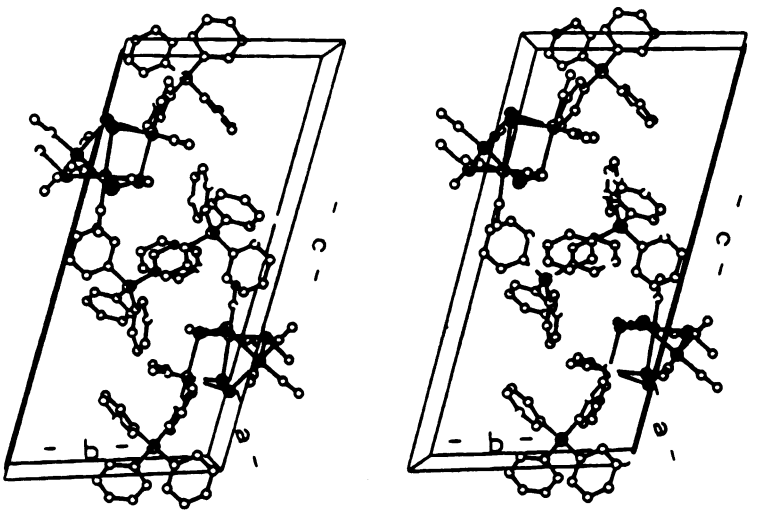


Figure 6-8. The Packing Diagram in the Unit Cell of α-$(Ph_4P)_2[Mn_3(Te_2)_2(TeCH_3)(CO)_9]$ (Stereoview)

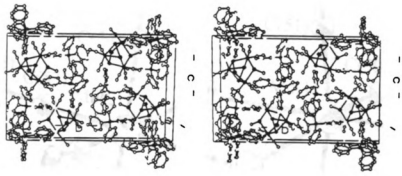


Figure 6-9. The Packing Diagram in the Unit Cell of β-$(Ph_4P)_2[Mn_3(Te_2)_2(TeCH_3)(CO)_9]$ (Stereoview)

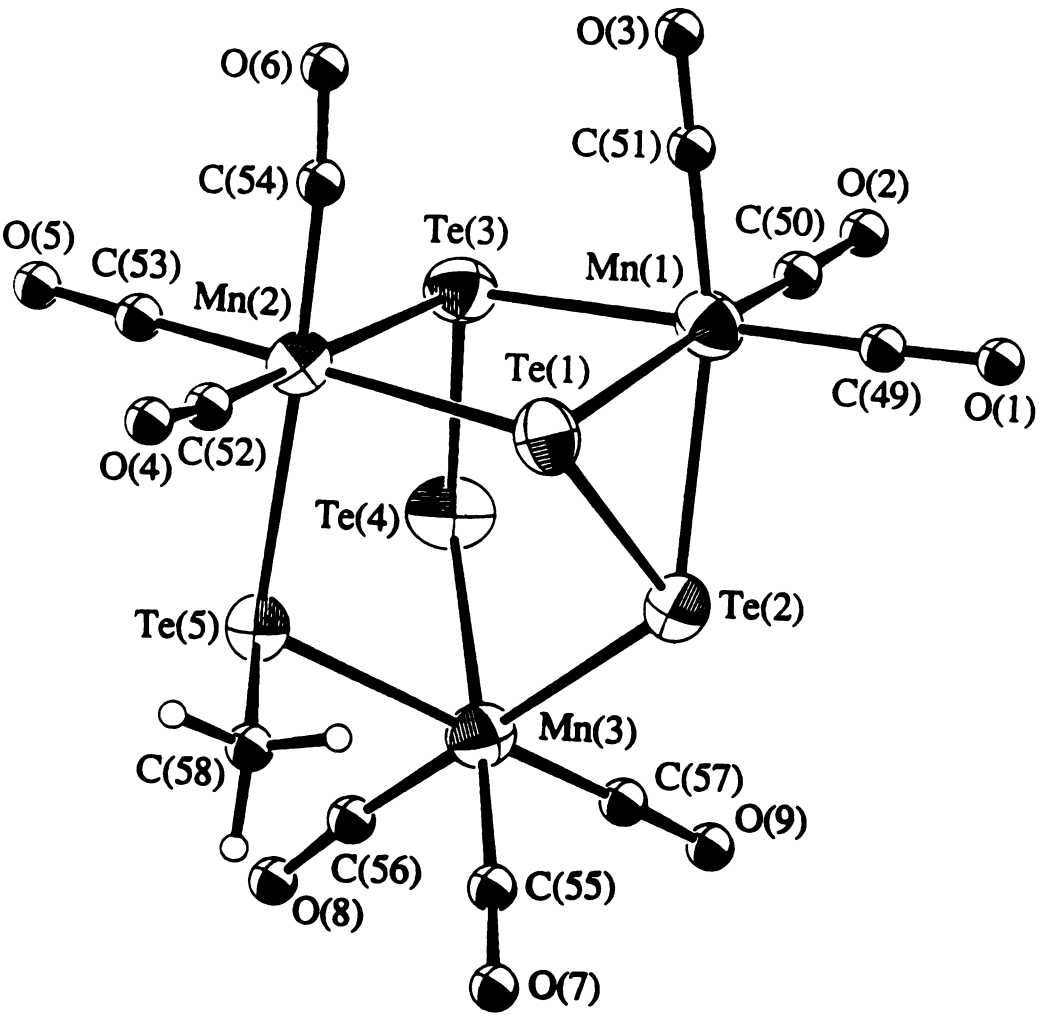


Figure 6-10. Structure of the $[Mn_3(Te_2)_2(TeCH_3)(CO)_9]^{2-}$ Anion Found in α-$(Ph_4P)_2[Mn_3(Te_2)_2(TeCH_3)(CO)_9]$

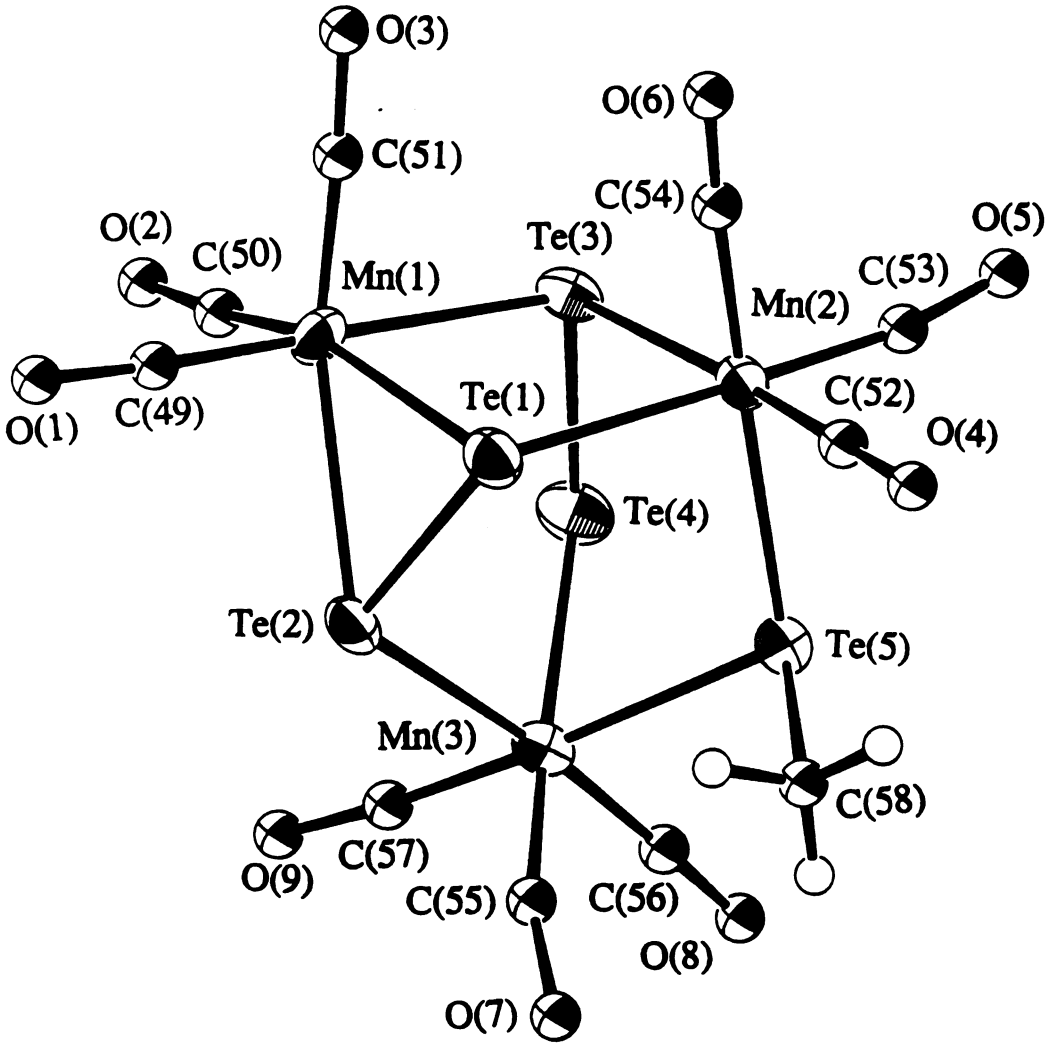


Figure 6-11. Structure of the $[Mn_3(Te_2)_2(TeCH_3)(CO)_9]^{2-}$ Anion Found in β-$(Ph_4P)_2[Mn_3(Te_2)_2(TeCH_3)(CO)_9]$

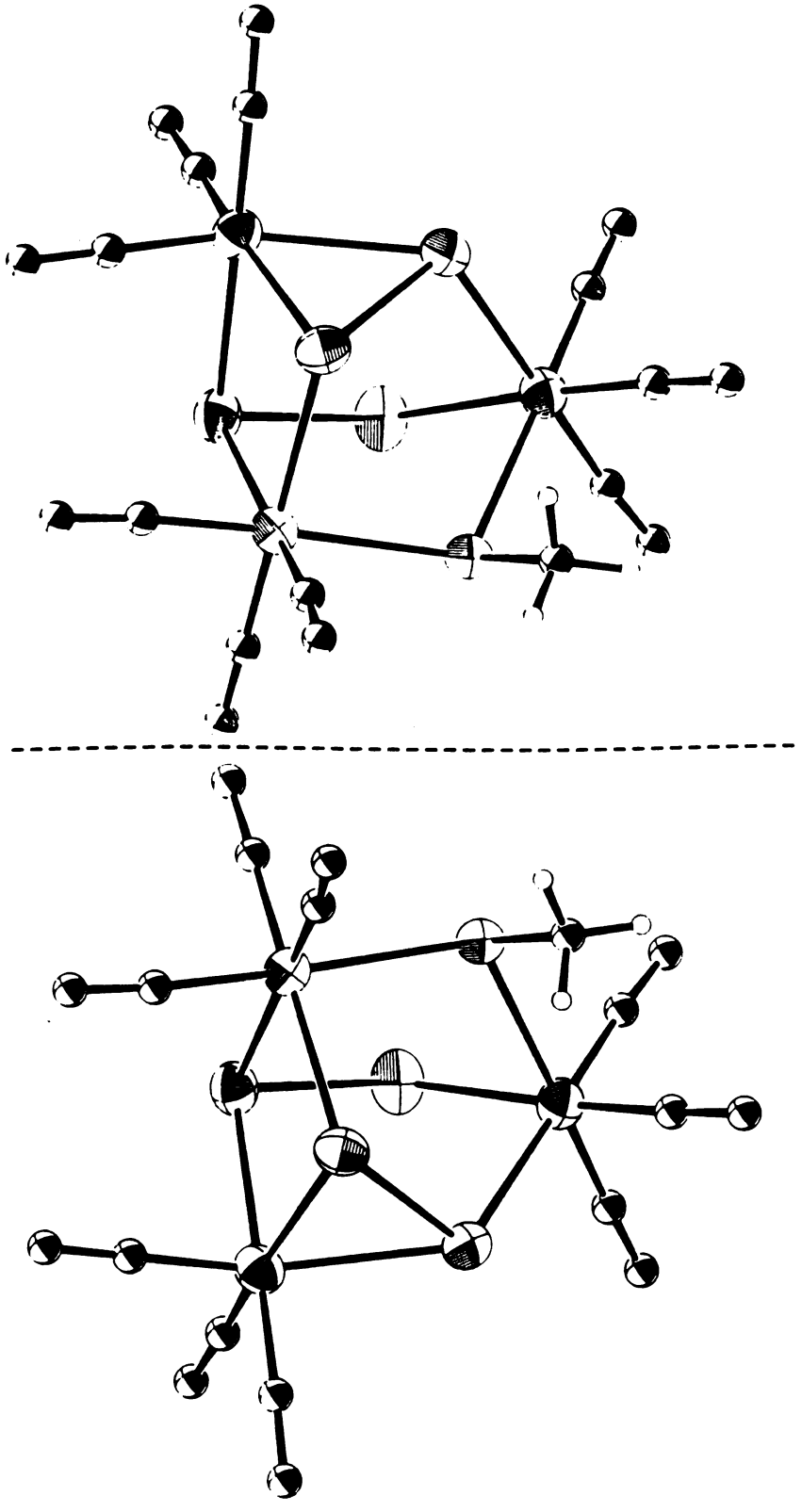


Figure 6-12. Two Optical Isomers of the $[Mn_3(Te_2)_2(TeCH_3)(CO)_9]^{2-}$ Anion Found in the α-$(Ph_4P)_2[Mn_3(Te_2)_2(TeCH_3)(CO)_9]$ Unit Cell

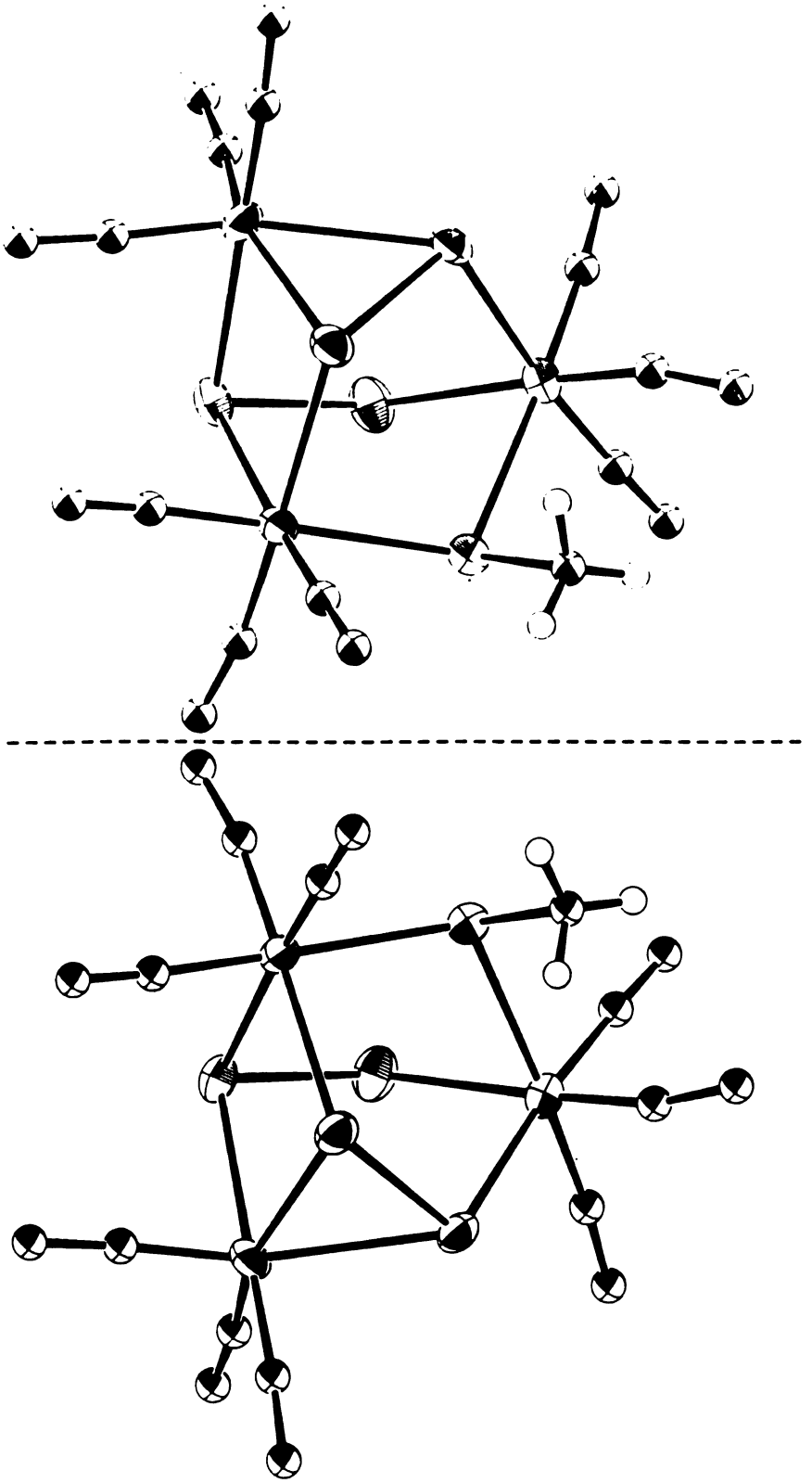


Figure 6-13. Two Optical Isomers of the $[Mn_3(Te_2)_2(TeCH_3)(CO)_9]^{2-}$ Anion Found in the β-$(Ph_4P)_2[Mn_3(Te_2)_2(TeCH_3)(CO)_9]$ Unit Cell

(iv). Structure of $(Ph_4P)_3[Re_4(Te_2)_3(TeCH_3)(CO)_{12}]\cdot CH_3OH$ (6·6)

This compound comprises of Ph_4P^+ cations, solvent CH_3OH molecules, and $[Re_4(Te_2)_3(TeCH_3)(CO)_{12}]^{3-}$ anions in the crystal lattice as shown in Figure 6·14. The $[Re_4(Te_2)_3(TeCH_3)(CO)_{12}]^{3-}$ anion consists of a tetrahedral array of Re atoms held by a μ_3-type methyltelluride CH_3Te^-, three μ_3-type ditelluride Te_2^{2-} ligands, and nine terminal CO groups as shown in Figure 6·15. The molecule possesses a pseudo-C_3 axis which passes through Te(7) and Re(4), thus dividing four Re atoms into two different types (see Figure 6·16). Three of them are in the triangular base of the tetrahedron bridged by the μ_3-CH_3Te^- ligand. Three μ_3-type Te_2^{2-} ligands each bridge two basal Re atoms and the fourth Re atom which occupies the top tetrahedral vertex. Alternatively, the cluster core $[Re_4(Te_2)_3(Te)]^{4-}$ can be described as being formed by capping each face of the Re tetrahedron with a μ_3-Te^{2-} and three μ_3-Te_2^{2-} ligands. The Re metal centers have the formal oxidation state +1, and are octahedrally surrounded by three Te atoms and three *cis* CO groups. The average bond distances of Re-Te at 2.788(10) Å may be considered normal single bond, although a more extensive comparison of this distance with other known Re-Te bonds can not be made at this stage. The only other structurally characterized rhenium polytelluride compound, $[(\eta^5\text{-}Cp^*)_2Re_2(Te_2)(CO)_4]$, contains three different Re-Te distances at 2.793(1), 2.806(1) Å and 2.632 Å[9]. The latter was interpreted as a Re-Te double bond[9]. The average Te-Te at 2.736(4) Å is in the normal range of the Te-Te single bond[5, 21]. Again, the Re atoms do not form M–M bonds to one another in this cluster because the shortest Re–Re distance is 4.70 Å. Selected bond distances and bond angles are given in Table 6·24.

Table 6-24. Selected Bond Distances (Å) and Bond Angles (deg) of $(Ph_4P)_3[Re_4(Te_2)_3(TeCH_3)(CO)_{12}]\cdot CH_3OH$ (**6-6**)[b]

		Bond Distances (Å)	
Re(1)-Te(1)	2.774(2)	Re(1)-Te(6)	2.771(2)
Re(1)-Te(7)	2.793(2)	Re(2)-Te(2)	2.787(2)
Re(2)-Te(3)	2.771(2)	Re(2)-Te(7)	2.784(2)
Re(3)-Te(4)	2.805(2)	Re(3)-Te(5)	2.769(2)
Re(3)-Te(7)	2.781(2)	Re(4)-Te(2)	2.820(2)
Re(4)-Te(4)	2.797(2)	Re(4)-Te(6)	2.805(2)
Re-Te(mean)	2.788(10)	Te(1)-Te(2)	2.727(2)
Te(3)-Te(4)	2.738(2)	Te(5)-Te(6)	2.742(2)
Te-Te(mean)	2.736(4)	Te(7)-C(85)	2.19(3)
Re(1)-C(73)	1.90(2)	Re(1)-C(74)	1.87(3)
Re(1)-C(75)	1.87(2)	Re(2)-C(76)	1.97(2)
Re(2)-C(77)	1.88(3)	Re(2)-C(78)	1.93(3)
Re(3)-C(79)	1.91(3)	Re(3)-C(80)	1.92(3)
Re(3)-C(81)	1.88(3)	Re(4)-C(82)	1.86(3)
Re(4)-C(83)	1.89(2)	Re(4)-C(84)	1.91(3)
Re-C(mean)	1.90(1)		
		Bond Angles (deg)	
Te(1)-Re(1)-Te(6)	85.14(6)	Te(1)-Re(1)-Te(7)	96.93(6)
Te(6)-Re(1)-Te(7)	85.38(5)	Te(2)-Re(2)-Te(3)	85.02(6)
Te(2)-Re(2)-Te(7)	85.91(5)	Te(3)-Re(2)-Te(7)	95.95(6)
Te(4)-Re(3)-Te(5)	86.73(6)	Te(4)-Re(3)-Te(7)	84.99(6)
Te(5)-Re(3)-Te(7)	94.64(6)	Te(2)-Re(4)-Te(4)	93.66(5)
Te(2)-Re(4)-Te(6)	94.25(5)	Te(4)-Re(4)-Te(6)	94.38(6)

Table 6·24. (cont'd)

Bond Angles (deg)

Te(1)-Re(1)-C(73)	176.6(7)	Te(6)-Re(1)-C(74)	170.5(8)
Te(7)-Re(1)-C(75)	175.0(7)	Te(2)-Re(2)-C(77)	171.7(8)
Te(3)-Re(2)-C(76)	179.0(7)	Te(7)-Re(2)-C(78)	173.1(8)
Te(4)-Re(3)-C(80)	175.3(8)	Te(5)-Re(3)-C(79)	179.4(8)
Te(7)-Re(3)-C(81)	176.4(9)	Te(2)-Re(4)-C(82)	176.7(8)
Te(4)-Re(4)-C(83)	177.1(7)	Te(6)-Re(4)-C(84)	176.6(8)
C(73)-Re(1)-C(74)	94(1)	C(73)-Re(1)-C(75)	91(1)
C(74)-Re(1)-C(75)	92(1)	C(76)-Re(2)-C(77)	92(1)
C(76)-Re(2)-C(78)	94(1)	C(77)-Re(2)-C(78)	93(1)
C(79)-Re(3)-C(80)	90(1)	C(79)-Re(3)-C(81)	94(1)
C(80)-Re(3)-C(81)	91(1)	C(82)-Re(4)-C(83)	88(1)
C(82)-Re(4)-C(84)	91(1)	C(83)-Re(4)-C(84)	91(1)
Re(1)-Te(6)-Re(4)	115.38(6)	Re(2)-Te(2)-Re(4)	115.53(6)
Re(3)-Te(4)-Re(4)	115.75(6)	Re(1)-Te(7)-Re(2)	114.77(6)
Re(1)-Te(7)-Re(3)	116.71(6)	Re(2)-Te(7)-Re(3)	116.09(6)
Re(1)-Te(1)-Te(2)	100.91(6)	Re(2)-Te(3)-Te(4)	100.92(6)
Re(3)-Te(5)-Te(6)	101.53(6)	Re(1)-Te(6)-Te(5)	102.38(7)
Re(2)-Te(2)-Te(1)	104.12(6)	Re(3)-Te(4)-Te(3)	103.19(7)
Re(4)-Te(2)-Te(1)	99.78(6)	Re(4)-Te(4)-Te(3)	101.50(7)
Re(4)-Te(6)-Te(5)	102.33(7)	Re(1)-Te(7)-C(85)	101.0(7)
Re(2)-Te(7)-C(85)	101.4(7)	Re(3)-Te(7)-C(85)	103.3(7)

b. The estimated standard deviations in the mean bond lengths and the mean bond angles are calculated by the equation $\sigma_l=\{\Sigma_n(l_n-l)^2/n(n-1)\}^{1/2}$, where l_n is the length (angle) of the *n*th bond, l the mean length (angle), and n the number of bonds.

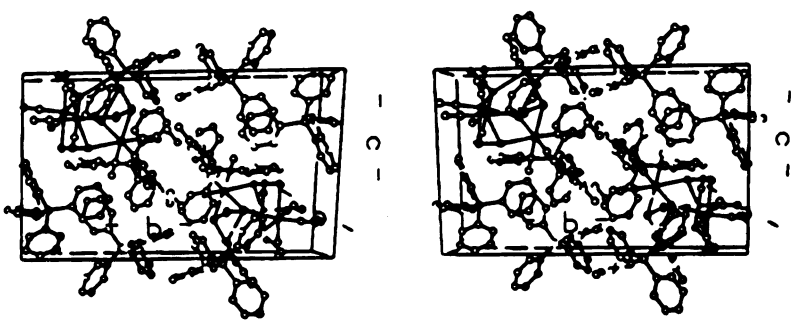


Figure 6-14. The Packing Diagram in the Unit Cell of $(Ph_4P)_3[Re_4(Te_2)_3(TeCH_3)(CO)_{12}]\cdot CH_3OH$ (Stereoview)

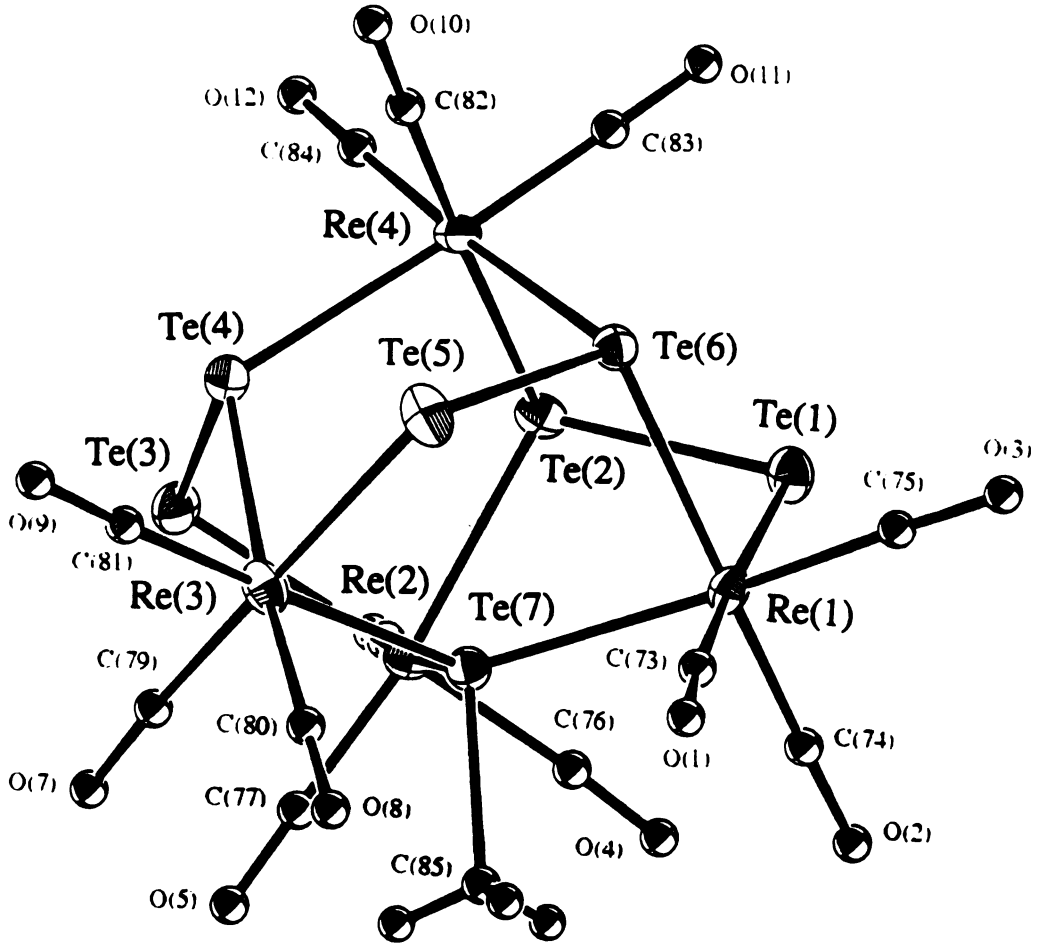


Figure 6-15. The Structure of the $[Re_4(Te_2)_3(TeCH_3)(CO)_{12}]^{3-}$ Anion

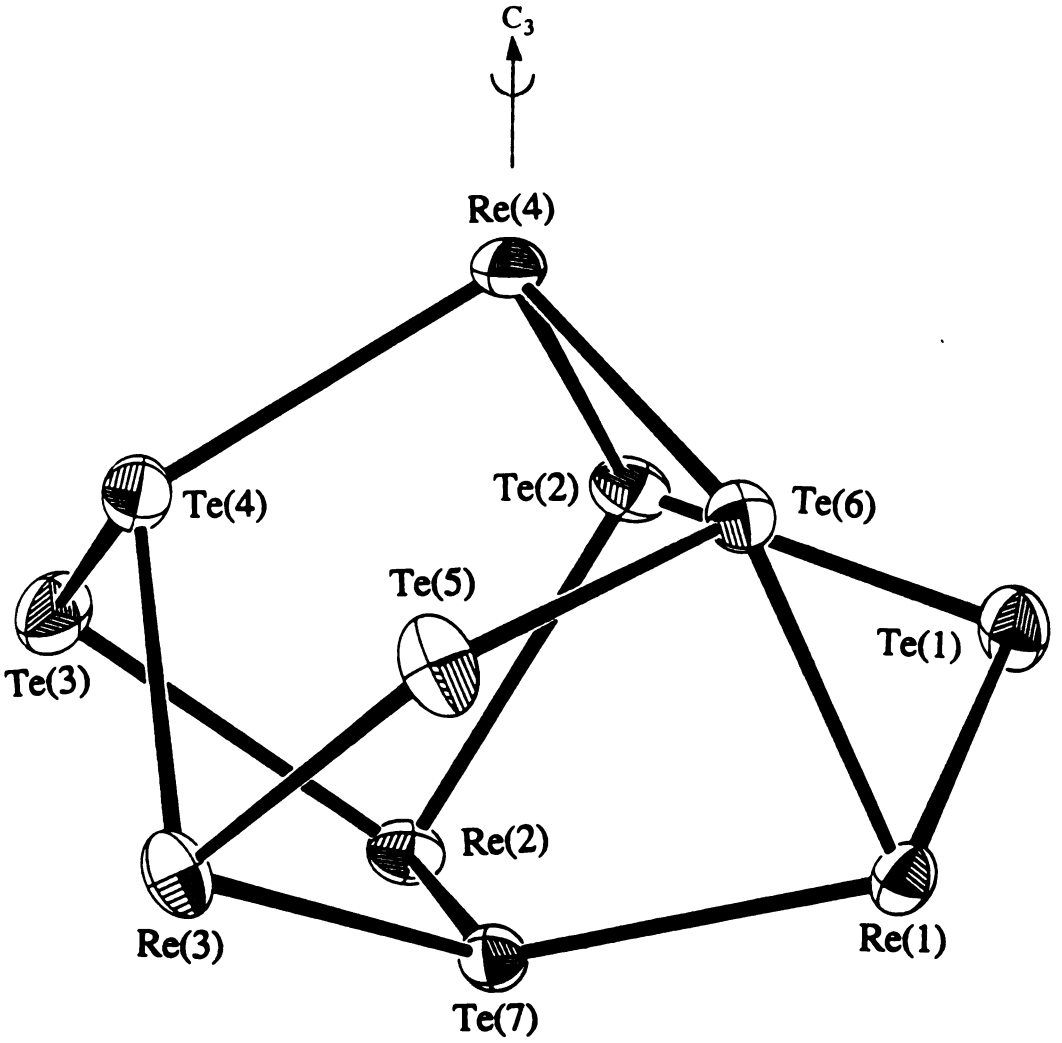


Figure 6-16. The $[Re_4(Te_2)_3(Te)]^{4-}$ Cluster Core, Showing a Pseudo-C_3 Axis

(v). Structures of $(Ph_4P)[Mn_2(SCH_3)_3(CO)_6]$ (6·7), $(Ph_4P)[Mn_2(SeCH_3)_3(CO)_6]$ (6·8) and $(Ph_4P)[Mn_2(TeCH_3)_3(CO)_6]$ (6·9)

(6·7) and (6·8) are isostructural to each other (space group P-1, #2), while (6·9) crystallizes in a different space group ($P2_1/c$, #14). Nevertheless, they are all made up of non-interacting Ph_4P^+ cations and $[Mn_2(QCH_3)_3(CO)_6]^{2-}$ (Q=S, Se or Te) anions. Figures 6·17 and 6·18 show the packing diagrams of the three compounds. The anions $[Mn_2(SCH_3)_3(CO)_6]^{2-}$, $[Mn_2(SeCH_3)_3(CO)_6]^{2-}$ and $[Mn_2(TeCH_3)_3(CO)_6]^{2-}$, shown in Figures 6·19 and 6·20, have essentially the same structure. Two Mn(I) centers are bridged by three μ_2-CH_3Q^- (Q=S, Se or Te) ligands. The octahedral coordination of the Mn atoms are then each completed by three *cis* CO groups. These molecules are analogous to the cationic species $[Fe_2(SCH_3)_3(CO)_6]^+$T[32]. If H atoms of the methyl groups were ignored, such a molecule would have C_{3h} symmetry. The Mn–Mn distances of 3.18 Å in (6·7), 3.29 Å in (6·8) and 3.48 Å in (6·9) suggest no M–M bonding interactions. Selected bond distances and bond angles are given in Table 6·25.

Table 6·25. Selected Bond Distances (Å) and Bond Angles (deg) of $(Ph_4P)[Mn_2(SCH_3)_3(CO)_6]$ (6·7), $(Ph_4P)[Mn_2(SeCH_3)_3(CO)_6]$ (6·8) and $(Ph_4P)[Mn_2(TeCH_3)_3(CO)_6]$ (6·9)[b]

compound	$[Mn_2(SCH_3)_3(CO)_6]^{2-}$ in (6·7)	$[Mn_2(SeCH_3)_3(CO)_6]^{2-}$ in (6·8)	$[Mn_2(TeCH_3)_3(CO)_6]^{2-}$ in (6·9)
Mn(1)-Q(1)	2.378(2)	2.482(2)	2.654(1)
Mn(1)-Q(2)	2.379(2)	2.494(2)	2.671(1)
Mn(1)-Q(3)	2.392(3)	2.502(2)	2.653(1)
Mn(2)-Q(1)	2.369(2)	2.486(2)	2.670(1)
Mn(2)-Q(2)	2.380(2)	2.494(2)	2.671(1)

Table 6·25. (cont'd)

compound	$[Mn_2(SCH_3)_3(CO)_6]^{2-}$ in (6·7)	$[Mn_2(SeCH_3)_3(CO)_6]^{2-}$ in (6·8)	$[Mn_2(TeCH_3)_3(CO)_6]^{2-}$ in (6·9)
Mn(2)-Q(3)	2.393(3)	2.500(2)	2.649(1)
Mn-Q(mean)	2.381(4)	2.493(3)	2.661(4)
Mn(1)-C(25)	1.755(7)	1.76(1)	1.79(1)
Mn(1)-C(26)	1.798(7)	1.78(1)	1.81(1)
Mn(1)-C(27)	1.776(7)	1.77(1)	1.82(1)
Mn(2)-C(28)	1.782(7)	1.78(1)	1.80(1)
Mn(2)-C(29)	1.780(7)	1.78(1)	1.80(1)
Mn(2)-C(30)	1.776(7)	1.81(1)	1.794(9)
Mn-C(mean)	1.778(6)	1.78(1)	1.80(1)
Q(1)-C(31)	1.823(7)	1.97(1)	2.161(9)
Q(2)-C(32)	1.820(7)	1.94(1)	2.185(8)
Q(3)-C(33)	1.814(7)	1.99(1)	2.15(1)
Q-C(mean)	1.819(3)	1.97(4)	2.165(10)
Q(1)-Mn(1)-Q(2)	80.25(8)	81.37(7)	82.71(4)
Q(1)-Mn(1)-Q(3)	79.46(9)	80.42(7)	81.90(4)
Q(2)-Mn(1)-Q(3)	81.01(8)	81.55(6)	81.44(4)
Q(1)-Mn(2)-Q(2)	80.40(8)	81.30(6)	82.40(4)
Q(1)-Mn(2)-Q(3)	79.61(9)	80.37(7)	81.67(4)
Q(2)-Mn(2)-Q(3)	80.95(8)	81.57(7)	81.51(4)
Mn(1)-Q(1)-Mn(2)	84.14(8)	83.08(7)	81.56(4)
Mn(1)-Q(2)-Mn(2)	83.89(7)	82.65(7)	81.21(4)

Table 6·25. (cont'd)

compound	$[Mn_2(SCH_3)_3(CO)_6]^{2-}$ in (**6·7**)	$[Mn_2(SeCH_3)_3(CO)_6]^{2-}$ in (**6·8**)	$[Mn_2(TeCH_3)_3(CO)_6]^{2-}$ in (**6·9**)
Mn(1)-Q(3)-Mn(2)	83.32(9)	82.37(7)	81.97(4)
Q(1)-Mn(1)-C(25)	172.3(2)	170.9(3)	170.9(3)
Q(2)-Mn(1)-C(26)	172.0(2)	170.5(3)	170.5(3)
Q(3)-Mn(1)-C(27)	171.6(2)	170.6(3)	170.6(3)
Q(1)-Mn(2)-C(28)	171.7(2)	171.7(4)	171.1(3)
Q(2)-Mn(2)-C(29)	172.4(2)	172.6(4)	171.8(3)
Q(2)-Mn(2)-C(30)	171.3(2)	170.7(4)	169.7(3)
C(25)-Mn(1)-C(26)	92.1(3)	92.5(6)	93.8(4)
C(25)-Mn(1)-C(27)	92.2(3)	93.4(5)	93.6(4)
C(26)-Mn(1)-C(27)	91.4(3)	92.2(6)	95.3(4)
C(28)-Mn(2)-C(29)	91.9(3)	93.0(5)	92.2(4)
C(28)-Mn(2)-C(30)	92.9(3)	93.3(6)	96.8(4)
C(29)-Mn(2)-C(30)	91.6(3)	92.5(5)	93.9(4)

b. The estimated standard deviations in the mean bond lengths and the mean bond angles are calculated by the equation $\sigma_l=\{\Sigma_n(l_n-l)^2/n(n-1)\}^{1/2}$, where l_n is the length (angle) of the *n*th bond, l the mean length (angle), and n the number of bonds.

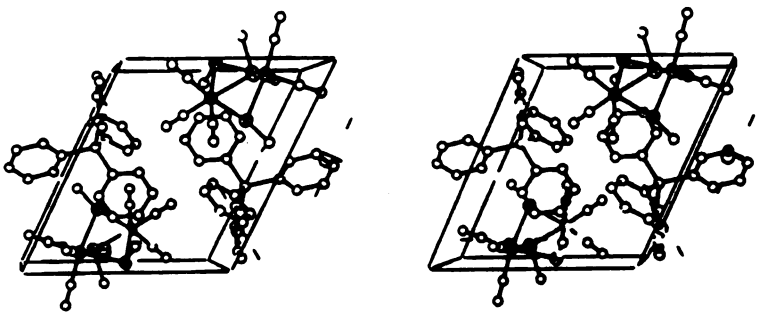


Figure 6-17. The Packing Diagram in the Unit Cell of $(Ph_4P)[Mn_2(QCH_3)_3(CO)_6]$ (Q=S and Se) (Stereoview)

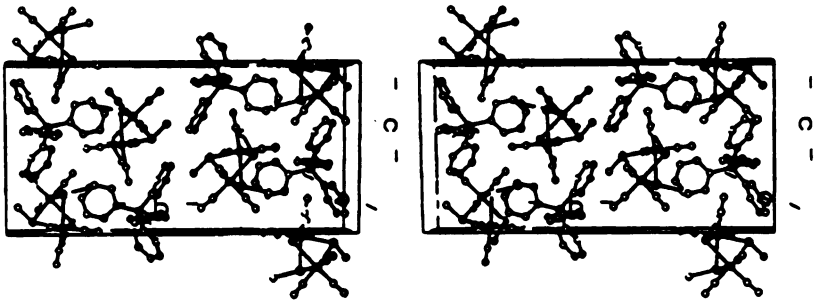


Figure 6-18. The Packing Diagram in the Unit Cell of $(Ph_4P)[Mn_2(TeCH_3)_3(CO)_6]$ (Stereoview)

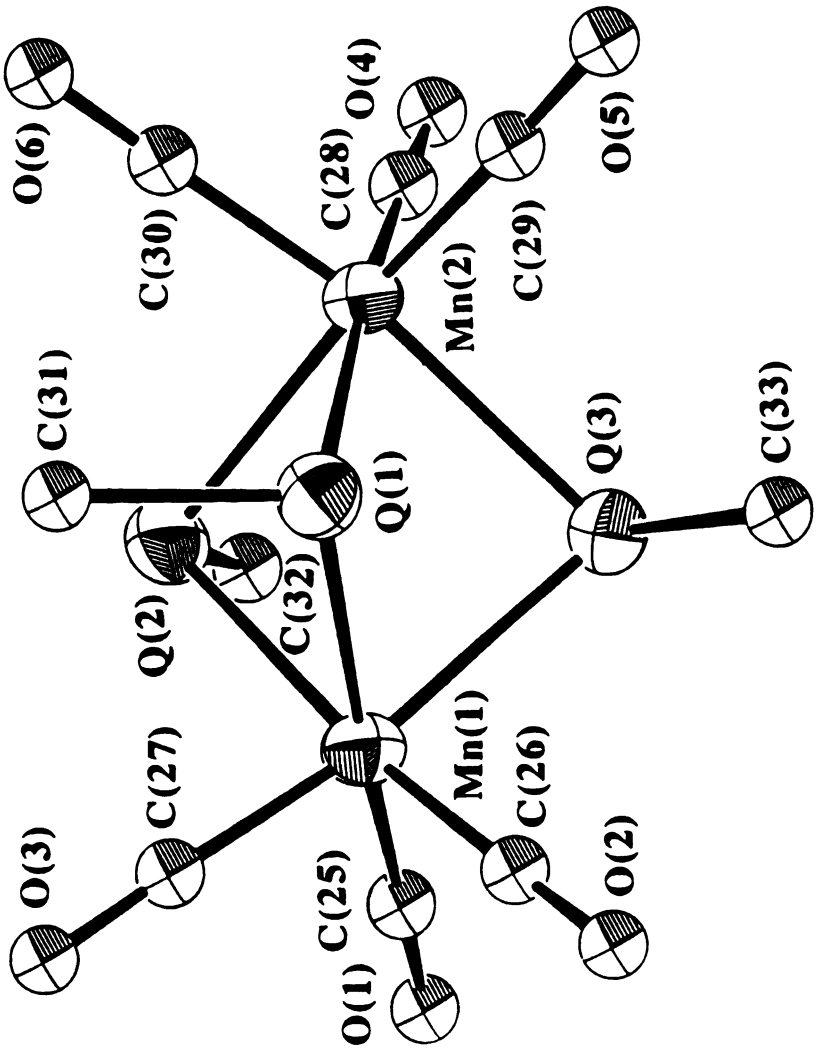


Figure 6-19. The Structure of the $[Mn_2(QCH_3)_3(CO)_6]^{2-}$ (Q=S and Se) Anions

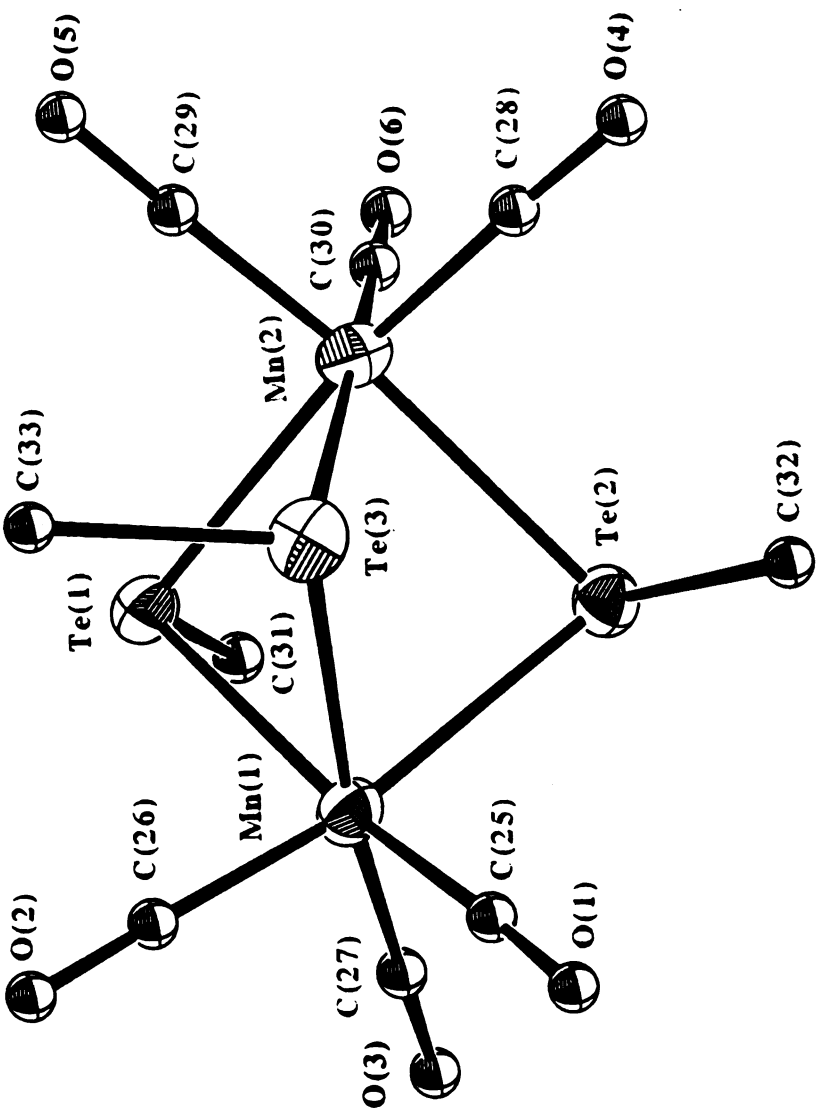


Figure 6-20. The Structure of the $[Mn_2(TeCH_3)_3(CO)_6]^{2-}$ Anion

2. Spectroscopic Studies

Figures 6·21–6·24 show the solid-state IR spectra of (**6·1**)–(**6·9**) in the CO region, while the far IR spectra of these compounds are shown in Figures 6·25-6·31. All these clusters contain metal centers with localized C_{3v} symmetry, which are expected to give two stretching vibrations for the CO groups. The assignment of the CO vibrations according to the symmetric and antisymmetric stretchings is given in Table 6·26, along with the far IR spectral data of the nine compounds. In general, the $Q_3M(CO)_3$ fragments are all crystallographically different in the lattice. Their CO absorptions often overlap each other, resulting in a certain pattern characteristic of the compound. Such a feature has been used, along with their XRD patterns, for the purpose of phase identification. On the other hand, interpretation of the far IR spectra of these compounds is much more difficult. The spectra are often complicated by the overlap of the Q-Q stretching modes with the other IR vibrations, e.g. ν_{M-Q}, etc. It is known that metal complexes containing disulfide units usually show the ν_{S-S} frequencies in 480 to 600 cm^{-1} region[19]. However, no identifiable IR peaks in this region, except a strong broad band from the Ph_4P^+ cation at 525 cm^{-1}, are present in the IR spectra of $(Ph_4P)_2[Mn_3(S_2)_2(SH)(CO)_9]$ and $(Ph_4P)_2[Mn_3(S_2)_2(SCH_3)(CO)_9]$. The IR peaks observed in the lower energy region in their IR spectra may be ν_{Mn-S} stretching modes. Similar vibrations in this region are also present in the spectrum of $(Ph_4P)[Mn_2(SCH_3)_3(CO)_6]$. When comparing the IR spectrum of $(Ph_4P)_2[Mn_3(Se_2)_2(SeCH_3)(CO)_9]$ with that of $(Ph_4P)[Mn_2(SeCH_3)_3(CO)_6]$, two peaks at 267 and 260 cm^{-1} present in the former, but absent in the latter, can be assigned to the ν_{Se-Se} vibrations. This assignment is consistent with other observations, e.g. ν_{se-se}=258 cm^{-1} for $[Fe_2Se_{12}]^{2-}$[22] and ν_{se-se}=265 cm^{-1} for $[Ag_xSe_y]^{n-}$[23]. Two other peaks in this area appear in both spectra at ~275 and 244 cm^{-1}, and might be candidates for the ν_{Mn-Se} vibrations. In the spectra of α-$(Ph_4P)_2[Mn_3(Te_2)_2(TeCH_3)(CO)_9]$ and β-$(Ph_4P)_2[Mn_3(Te_2)_2(TeCH_3)(CO)_9]$, a group of strong absorptions show in the 200-179

cm^{-1} region. These may contain the ν_{Te-Te} vibrations because the Te–Te stretching frequencies are known to be in the range of 200 to180 cm^{-1}[24]. However, a clear assignment of these peaks is hampered by the presence of two strong peaks in the same area in the IR spectrum of $(Ph_4P)[Mn_2(TeCH_3)_3(CO)_6]$ which does not contain Te-Te bonds. In the IR spectrum of $(Ph_4P)_3[Re_4(Te_2)_3(TeCH_3)(CO)_{12}]\cdot CH_3OH$, the strong peak centered at 180 cm^{-1} is tentatively assignment to the ν_{Te-Te} vibrations, while peaks at 170 and 148 cm^{-1} probably originate from Re–Te stretching. However, a medium peak at 260 cm^{-1} can not be interpreted.

Table 6·26. IR Spectral Data for $(Ph_4P)_2[Mn_3(S_2)_2(SH)(CO)_9]$ (**6·1**), $(Ph_4P)_2[Mn_3(S_2)_2(SCH_3)(CO)_9]$ (**6·2**), $(Ph_4P)_2[Mn_3(Se_2)_2(SeCH_3)(CO)_9]$ (**6·3**), α-$(Ph_4P)_2[Mn_3(Te_2)_2(TeCH_3)(CO)_9]$ (**6·4**), β-$(Ph_4P)_2[Mn_3(Te_2)_2(TeCH_3)(CO)_9]$ (**6·5**), $(Ph_4P)_3[Re_4(Te_2)_3(TeCH_3)(CO)_{12}]\cdot CH_3OH$ (**6·6**), $(Ph_4P)[Mn_2(SCH_3)_3(CO)_6]$ (**6·7**), $(Ph_4P)[Mn_2(SeCH_3)_3(CO)_6]$ (**6·8**) and $(Ph_4P)[Mn_2(TeCH_3)_3(CO)_6]$ (**6·9**)

compound	Mid-IR in the CO region, cm^{-1}		Far-IR, cm^{-1}
	Sym ν_{CO}	Antisym ν_{CO}	
(**6·1**)	2002(w), 1974(s), 1953(s)	1913(m), 1900(s), 1877(s),1859(s), 1853(s)	308(w), 299(w), 276(w), 261(s), 198(multiple, m),
(**6·2**)	1998(w), 1969(s), 1956(s)	1885(s), 1863(s)	344(m), 332(m), 306(m), 290(m), 277(m), 256(m), 244(sh), 229(w), 217(w), 214(w), 198(multiple, m), 178(w), 171(w), 167(w),
(**6·3**)	1960(s)	1906(m), 1885(m), 1864(s), 1894(m)	277(m), 267(m), 260(m), 244(w), 223(m), 198(multiple, s)

Table 6·26. (cont'd)

compound	Mid-IR in the CO region, cm^{-1}		Far-IR, cm^{-1}
	Sym ν_{CO}	Antisym ν_{CO}	
(6·4)	1979(sh), 1948(s)	1891(m),1881(m), 1872(m), 1857(m)	210(sh), 202(s), 198(s), 190(m), 179(s)
(6·5)	1948(s)	1897(m), 1879(m), 1865(m), 1843(m)	214(sh), 202(s), 198(s), 189(s), 179(s)
(6·6)	1996(w), 1969(s),	1883(sh),1864(m)	260(m), 187(sh), 180(s), 170(m), 148(multiple, m)
(6·7)	2001(w), 1977(m)	1903(m), 1882(s), 1864(m)	313(m), 298(w), 290(m), 279(s), 259(s), 245(w), 193(br, m)
(6·8)	1993(w), 1966(m)	1896(m), 1876(s), 1859(m)	290(w), 274(w), 257(w), 244(w), 225(w), 203(s), 194(m), 170(multiple, m)
(6·9)	1951(s)	1875(m), 1861(m)	281(w), 256(m), 249(sh),200(s), 195(sh), 187(m)

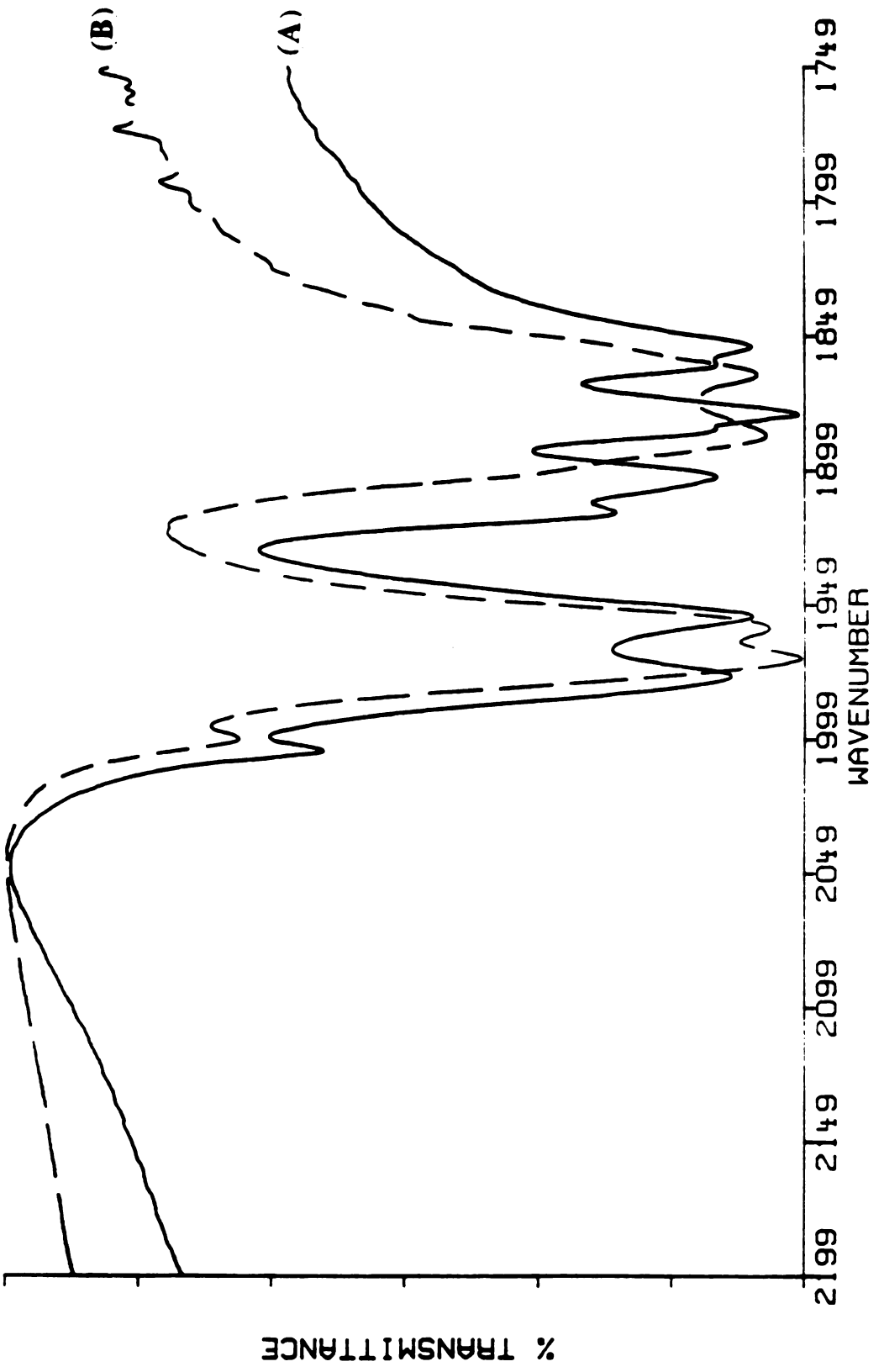


Figure 6-21. The Solid-State IR Spectra in the CO Region for (A) $(Ph_4P)_2[Mn_3(S_2)_2(SH)(CO)_9]$ and (B) $(Ph_4P)_2[Mn_3(S_2)_2(SCH_3)(CO)_9]$

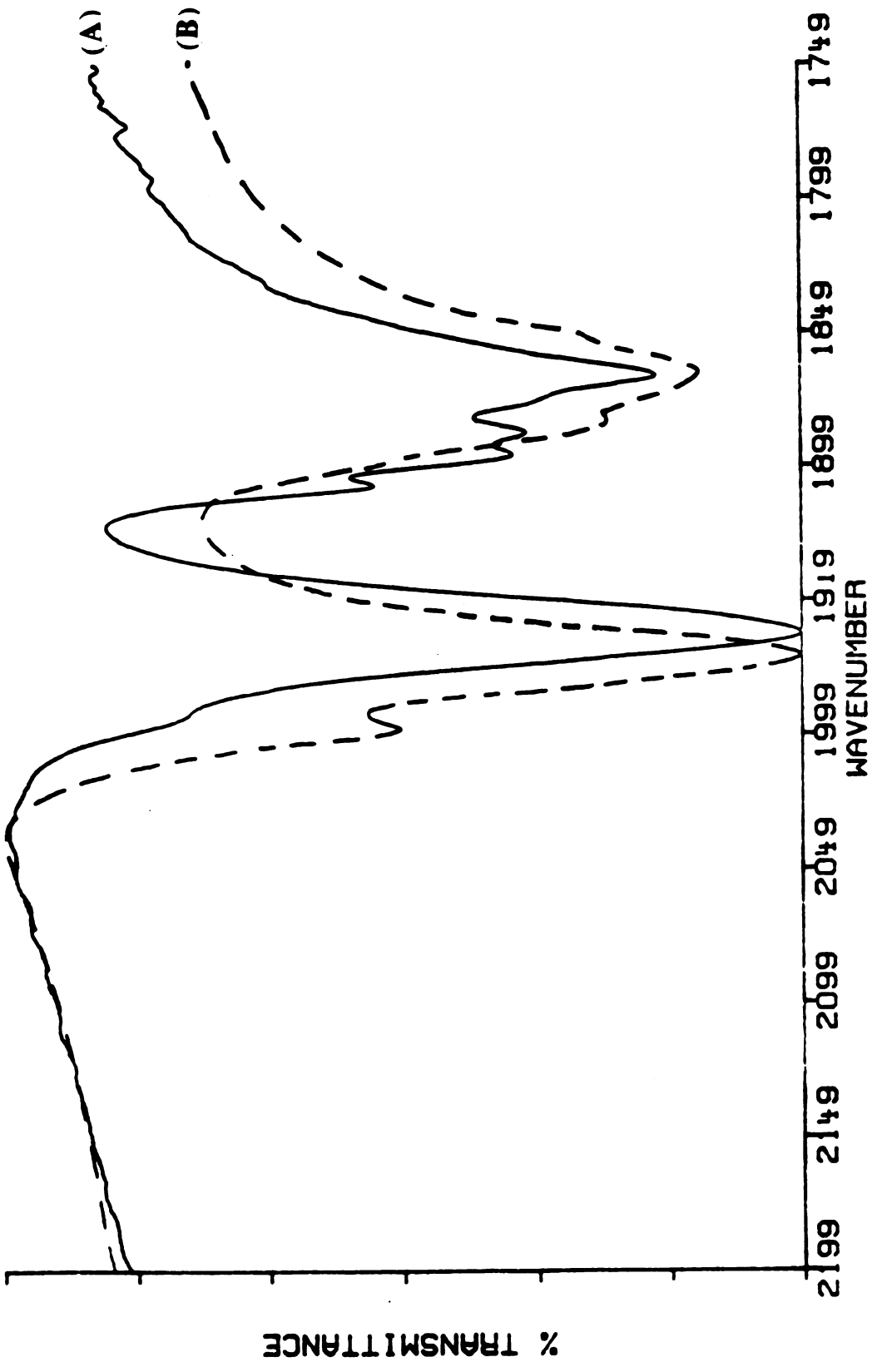


Figure 6-22. The Solid-State IR Spectra in the CO Region for (A) $(Ph_4P)_2[Mn_3(Se_2)_2(SeCH_3)(CO)_9]$ and (B) $(Ph_4P)_3[Re_4(Te_2)_3(TeCH_3)(CO)_{12}]\cdot CH_3OH$

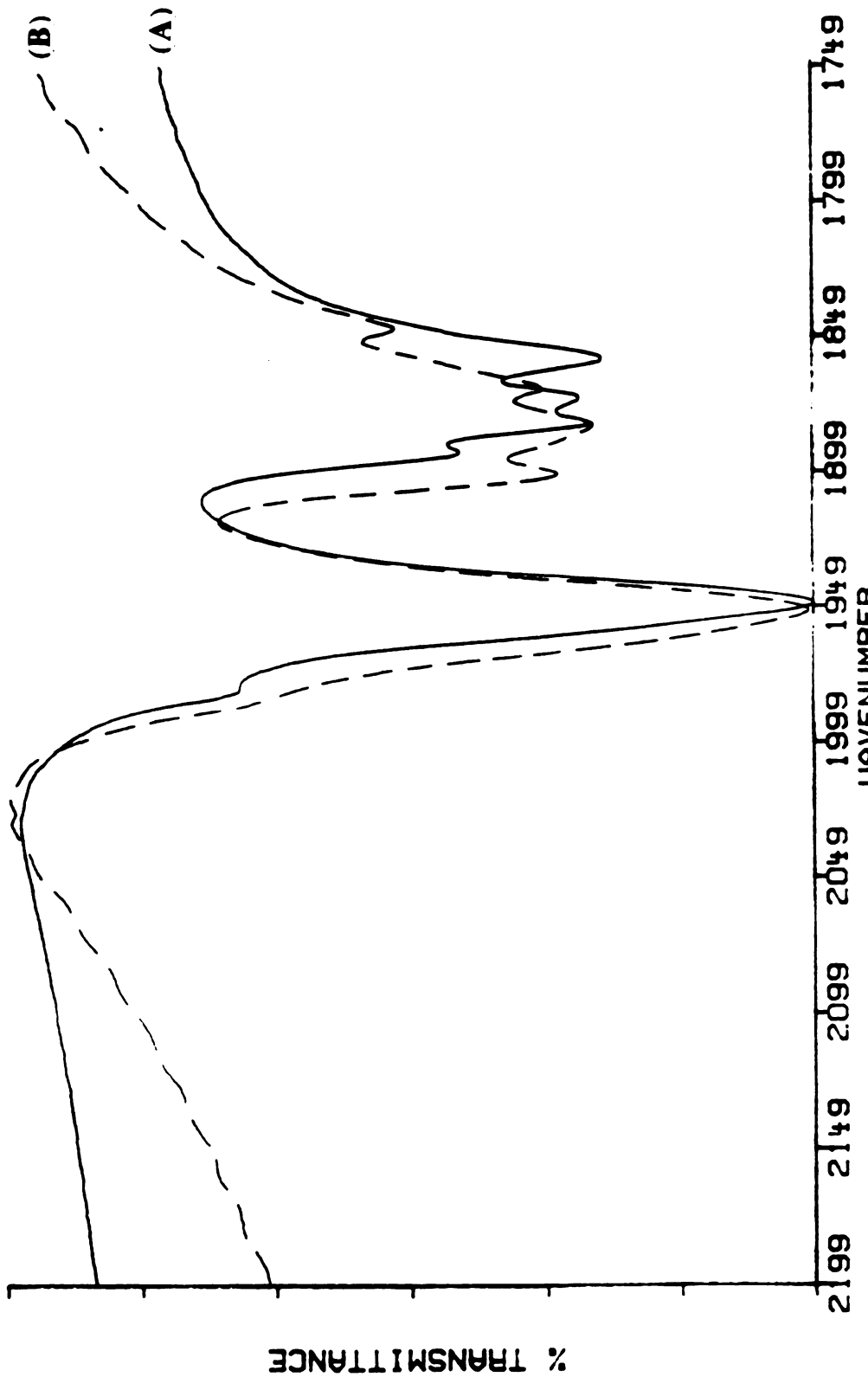


Figure 6-23. The Solid-State IR Spectra in the CO Region for (A) α-$(Ph_4P)_2[Mn_3(Te_2)_2(TeCH_3)(CO)_9]$ and (B) β-$(Ph_4P)_2[Mn_3(Te_2)_2(TeCH_3)(CO)_9]$

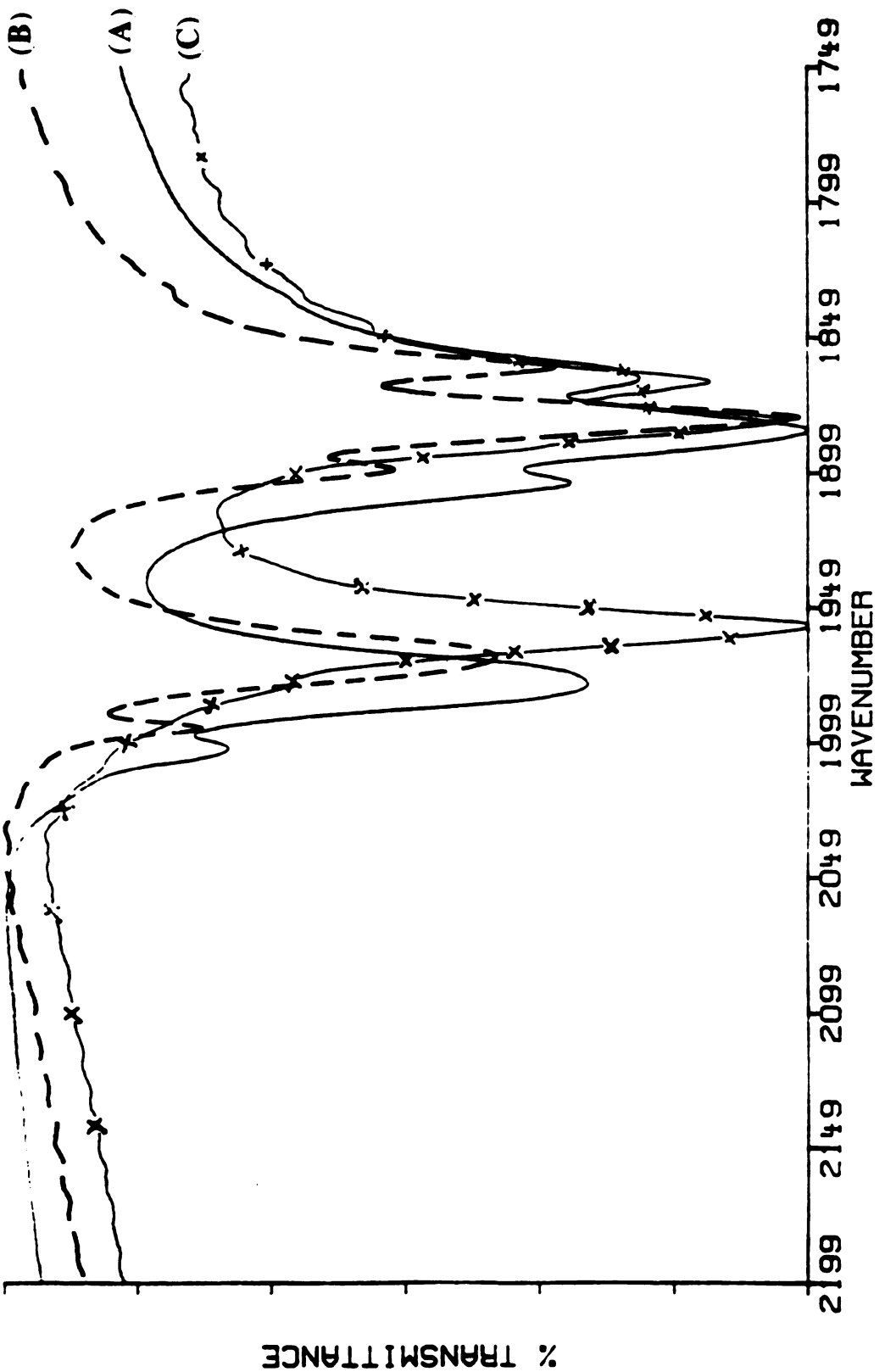


Figure 6·24. The Solid-State IR Spectra in the CO Region for (A) $(Ph_4P)[Mn_2(SCH_3)_3(CO)_6]$, (B) $(Ph_4P)[Mn_2(SeCH_3)_3(CO)_6]$ and (C) $(Ph_4P)[Mn_2(TeCH_3)_3(CO)_6]$

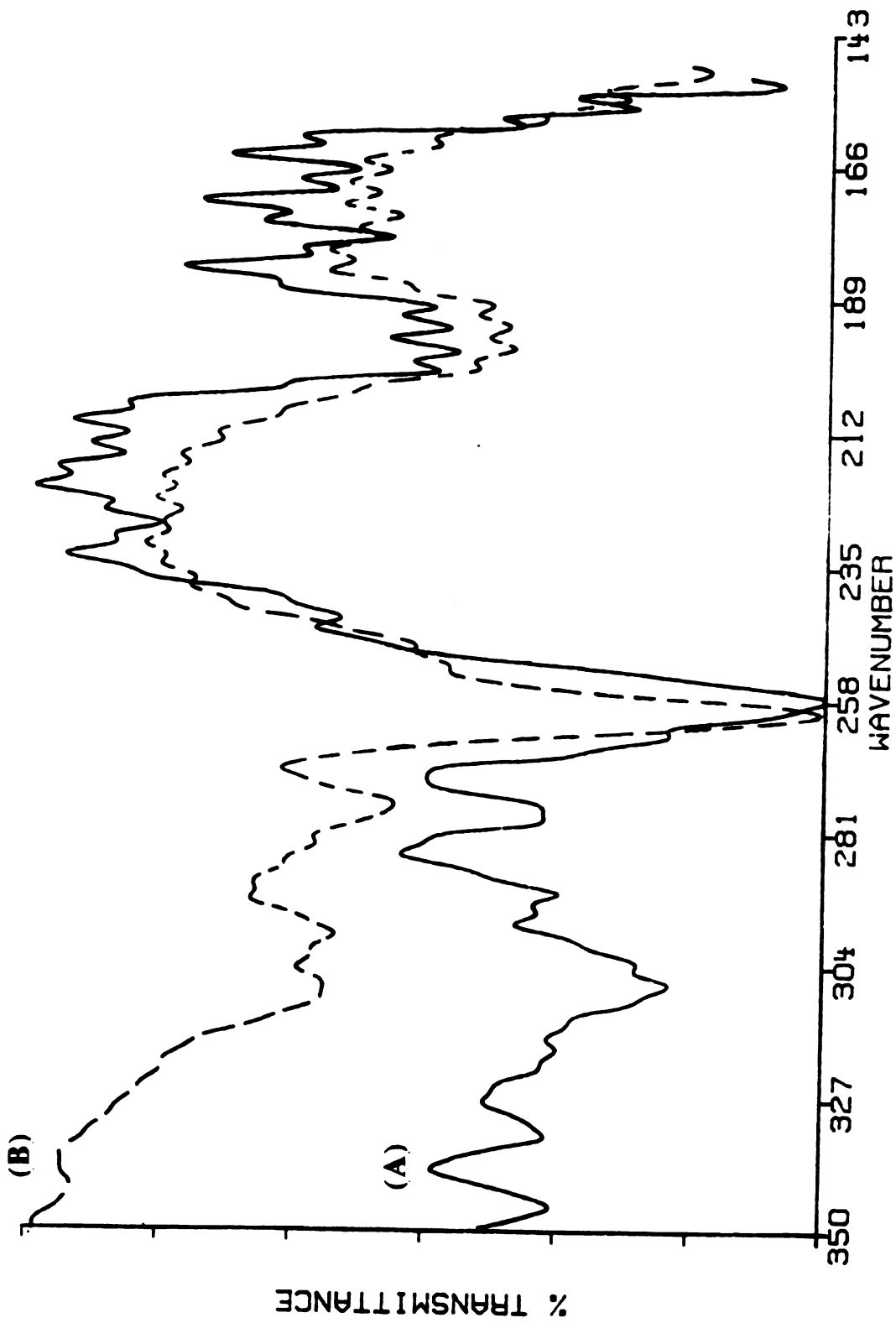


Figure 6-25. The Solid-State Far IR Spectra of (A) $(Ph_4P)_2[Mn_3(S_2)_2(SH)(CO)_9]$ and (B) $(Ph_4P)_2[Mn_3(S_2)_2(SCH_3)(CO)_9]$

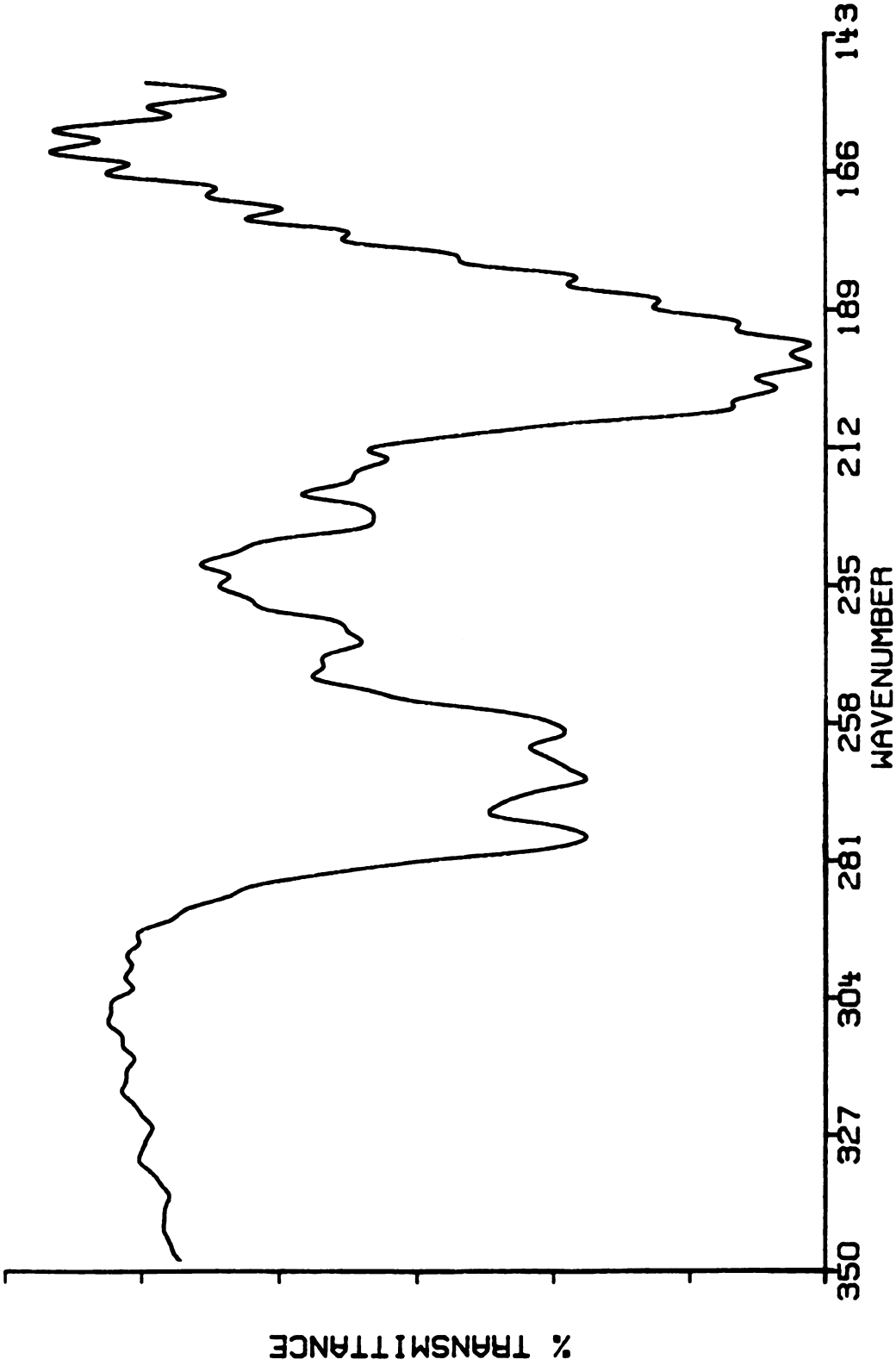


Figure 6·26. The Solid-State Far IR Spectrum of $(Ph_4P)_2[Mn_3(Se_2)_2(SeCH_3)(CO)_9]$

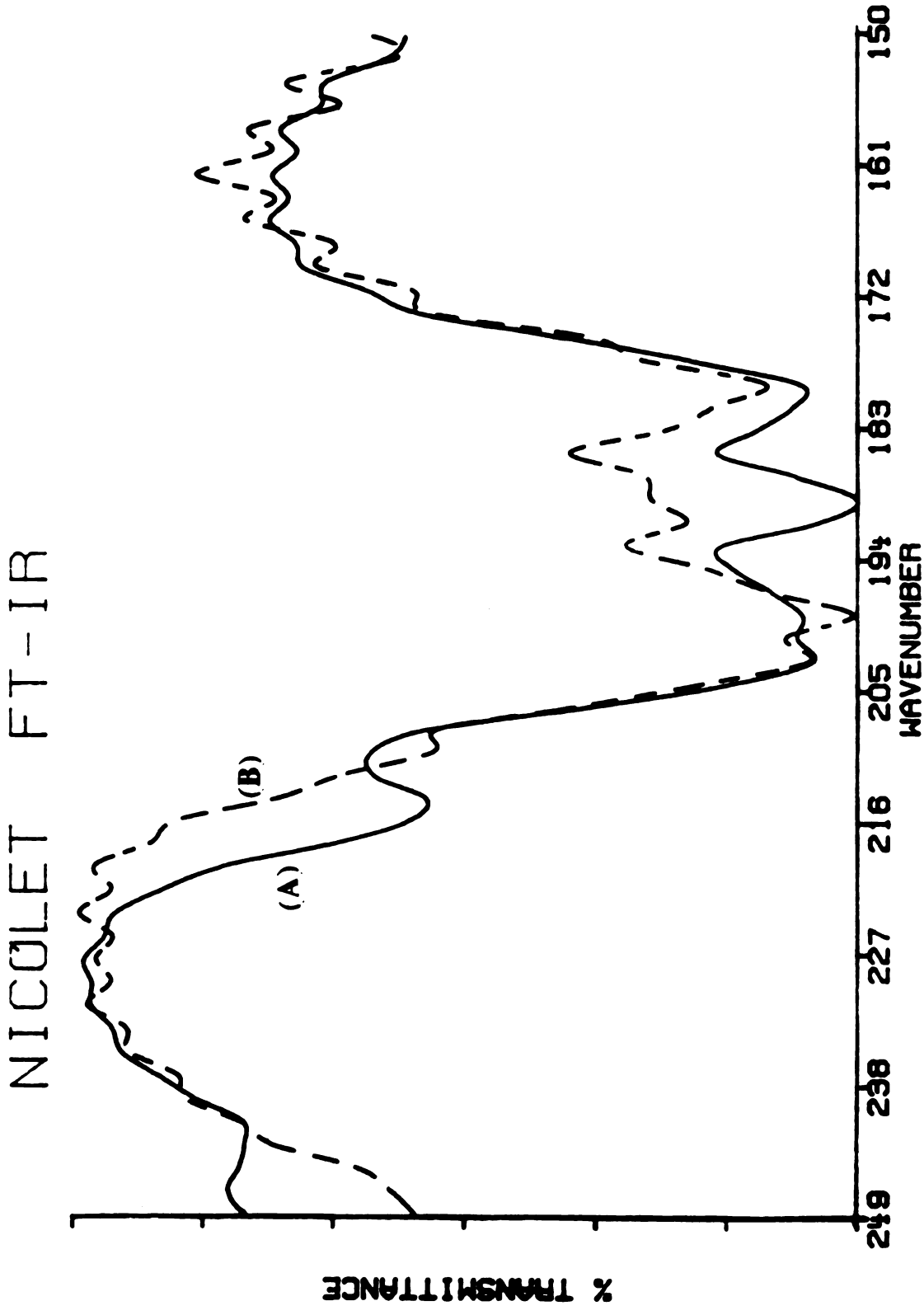


Figure 6-27. The Solid-State Far IR Spectra of (A) α-$(Ph_4P)_2[Mn_3(Te_2)_2(TeCH_3)(CO)_9]$ and (B) β-$(Ph_4P)_2[Mn_3(Te_2)_2(TeCH_3)(CO)_9]$

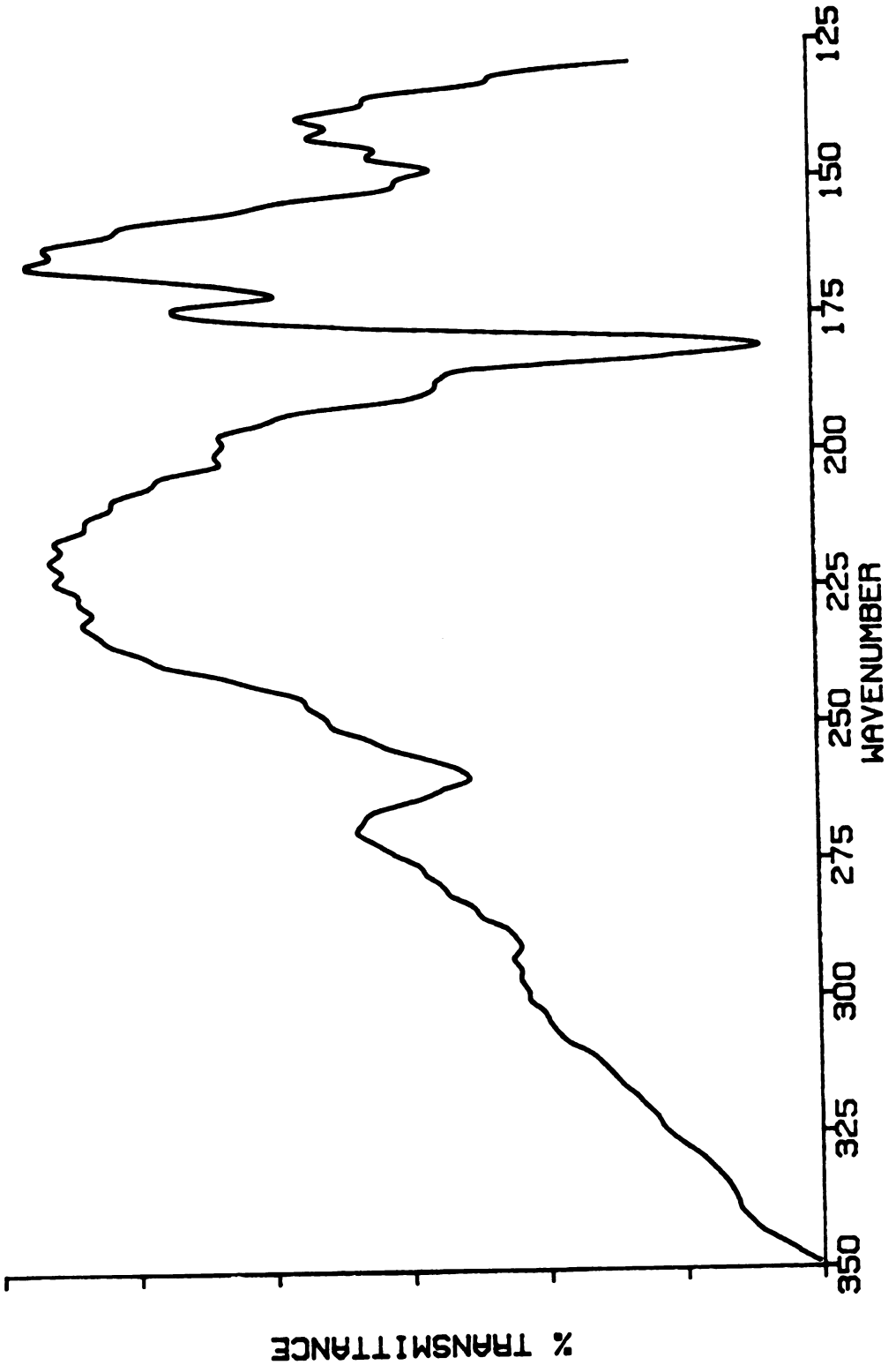


Figure 6-28. The Solid-State Far IR Spectrum of $(Ph_4P)_3[Re_4(Te_2)_3(TeCH_3)(CO)_{12}]\cdot CH_3OH$

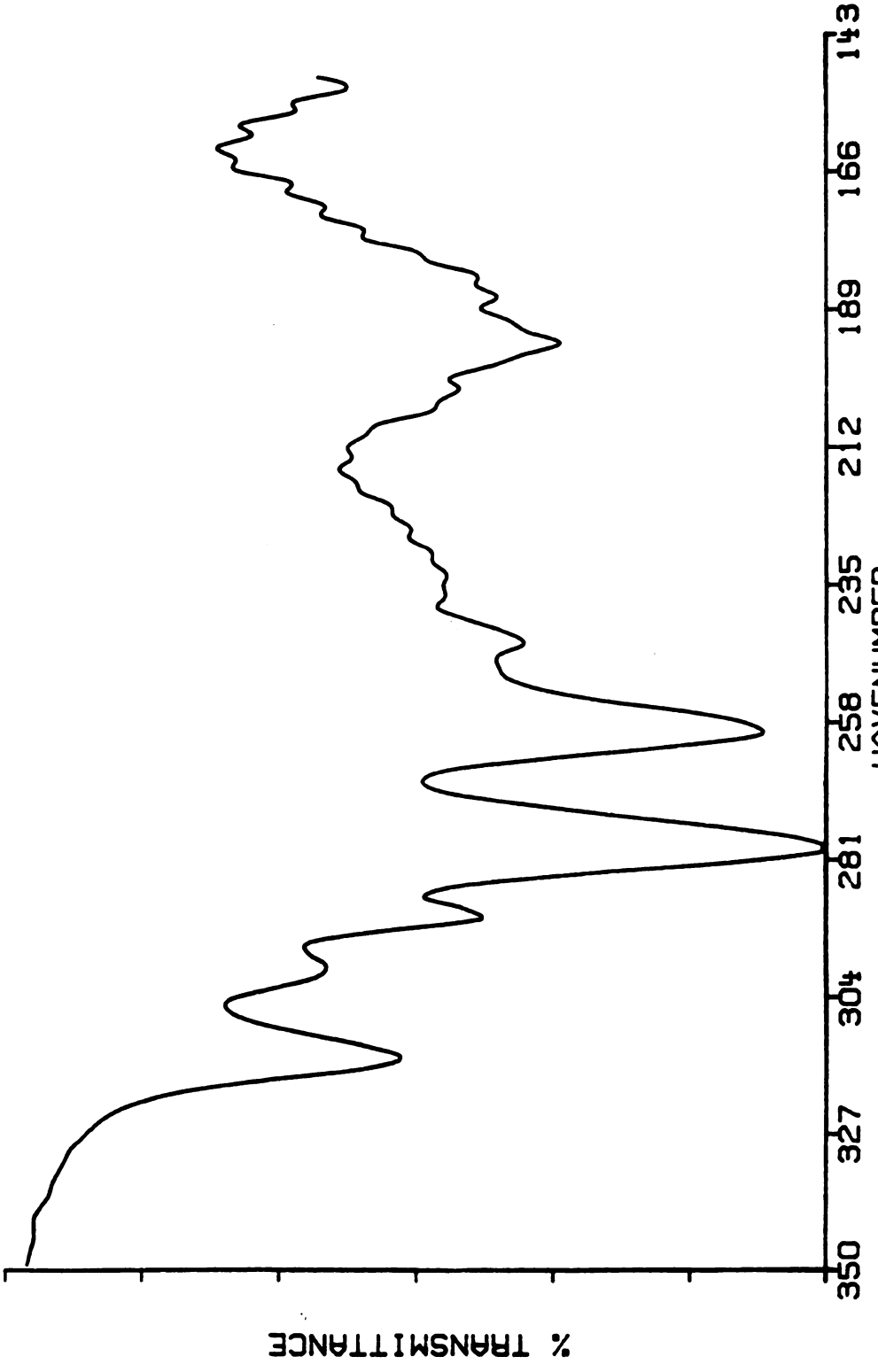


Figure 6.29. The Solid-State Far IR Spectrum of $(Ph_4P)[Mn_2(SCH_3)_3(CO)_6]$

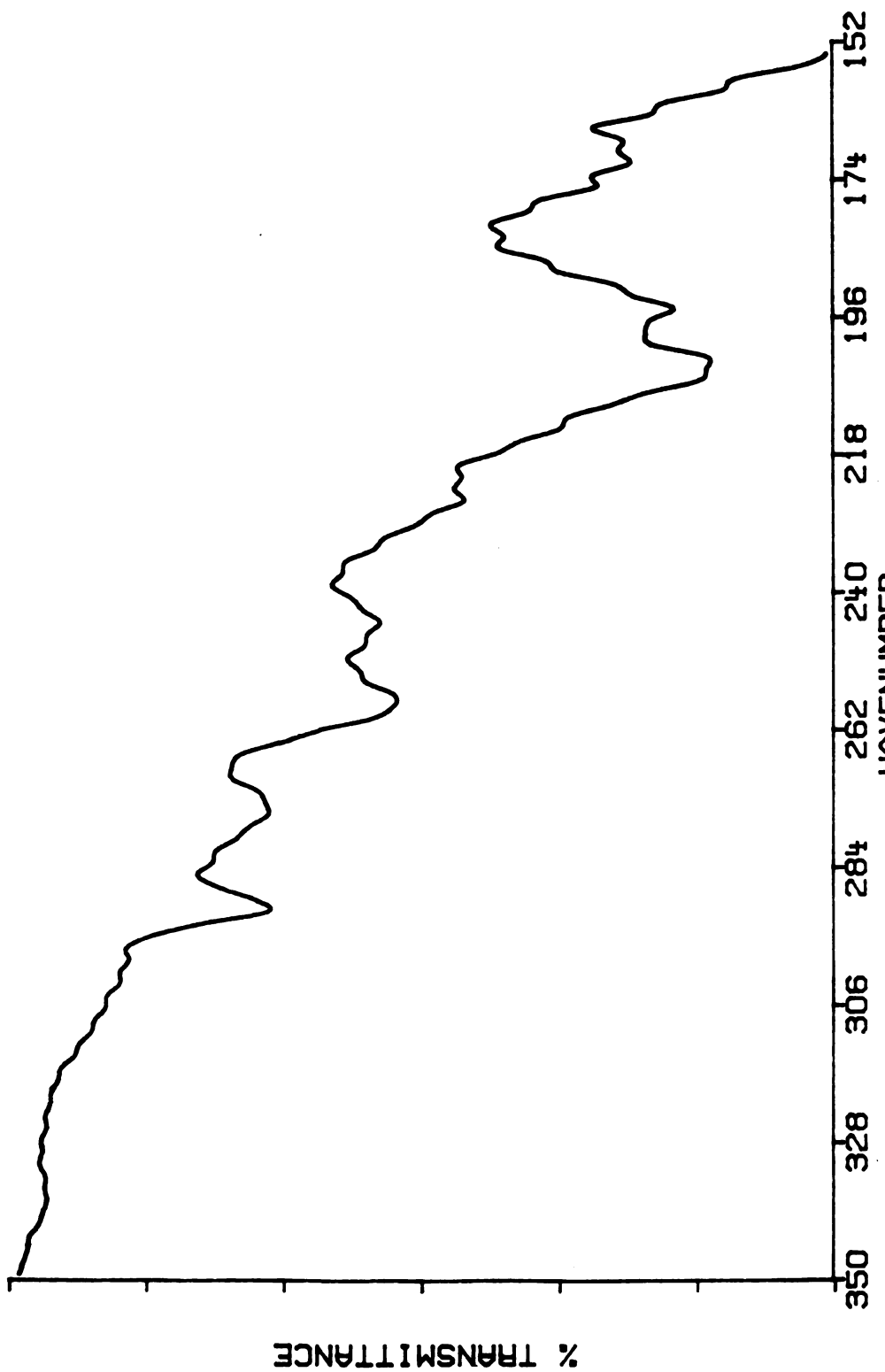


Figure 6-30. The Solid-State Far IR Spectrum of $(Ph_4P)[Mn_2(SeCH_3)_3(CO)_6]$

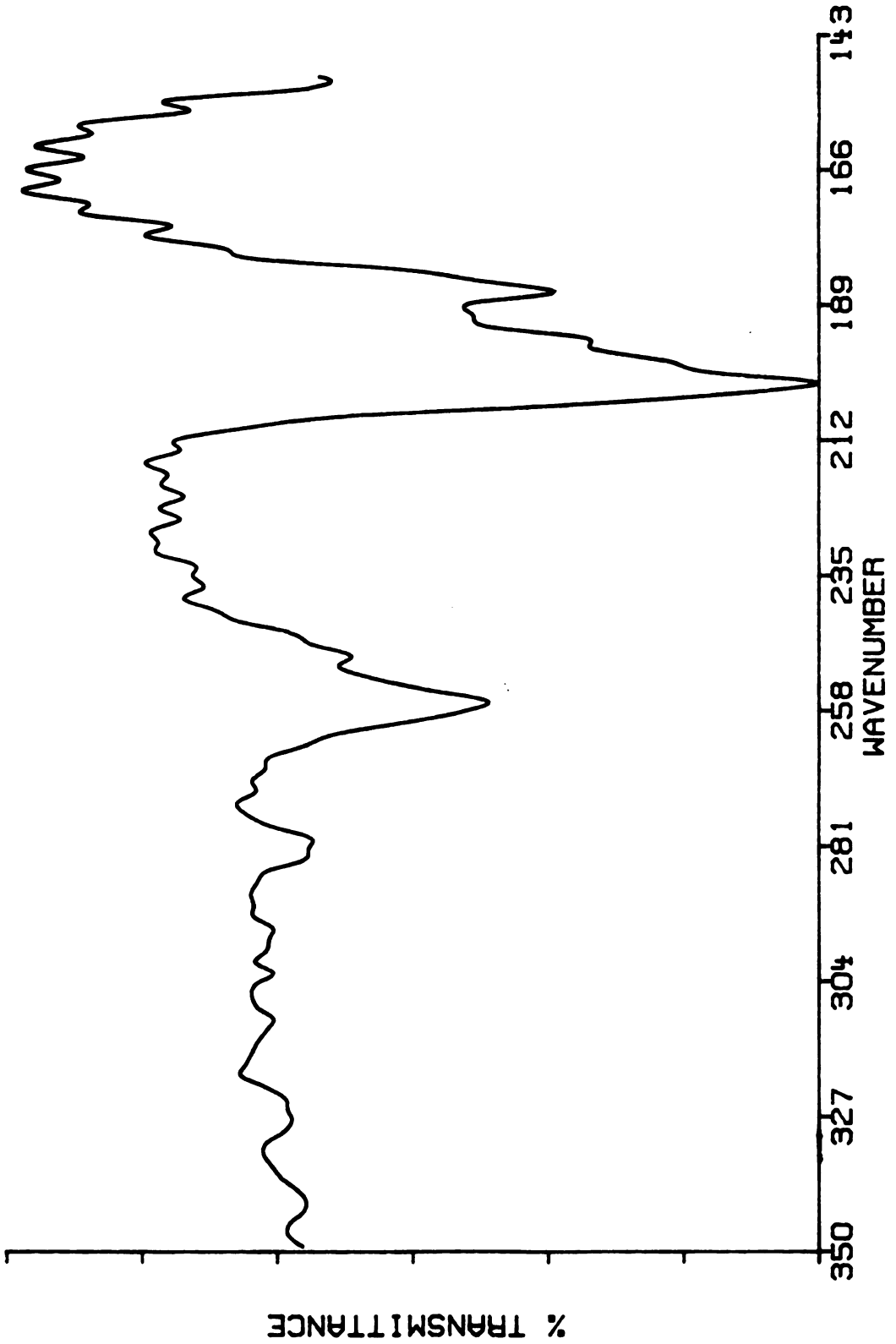


Figure 6:31. The Solid-State Far IR Spectrum of $(Ph_4P)[Mn_2(TeCH_3)_3(CO)_6]$

Compounds in the $(Ph_4P)_2[Mn_3(Q_2)_2(QR)(CO)_9]$ (Q=S, R=H or CH_3; Q=Se or Te, R=CH_3) family show featureless UV/vis spectra in CH_3CN, while compounds $(Ph_4P)[Mn_2(QCH_3)_3(CO)_6]$ (Q=S, Se or Te) each give a broad absorption at ~400 nm and a shoulder at ~290 nm in the same solvent (Figure 6·32). The absorption maxima for these two bands are 379 nm (br, $\varepsilon=2.29\times10^3$ M·cm^{-1}) and 288 nm (sh, $\varepsilon=7.69\times10^3$ M·cm^{-1}) for $(Ph_4P)[Mn_2(SCH_3)_3(CO)_6]$, 395 nm (br, $\varepsilon=3.13\times10^3$ M·cm^{-1}) and 289 nm (sh, $\varepsilon=1.22\times10^4$ M·cm^{-1}) for $(Ph_4P)[Mn_2(SeCH_3)_3(CO)_6]$ and 404 nm (sh, $\varepsilon=2.74\times10^3$ M·cm^{-1}) and 298 nm (broad sh, $\varepsilon=1.13\times10^4$ M·cm^{-1}) for $(Ph_4P)[Mn_2(TeCH_3)_3(CO)_6]$. The UV/vis spectrum of $(Ph_4P)_3[Re_4(Te_2)_3(TeCH_3)(CO)_{12}]\cdot CH_3OH$ shows a shoulder at 361nm (broad, $\varepsilon=1.27\times10^3$ M·cm^{-1}) as shown in Figure 6·33.

^{1}H NMR spectra of $(Ph_4P)_m[M_n(Q_2)_x(QR)(CO)_y]$ (when M=Mn and Q=S, R=H or CH_3, m=2, n=3, x=2, y=9; or 12) in d_6-acetone all show a singlet for the QCH_3^- at δ=2.16 ppm for $(Ph_4P)_2[Mn_3(S_2)_2(SCH_3)(CO)_9]$, δ=2.00 ppm for $(Ph_4P)_2[Mn_3(Se_2)_2(SeCH_3)(CO)_9]$, δ=1.96 ppm for $(Ph_4P)_2[Mn_3(Te_2)_2(TeCH_3)(CO)_9]$ and δ=2.40 ppm for $(Ph_4P)_3[Re_4(Te_2)_3(TeCH_3)(CO)_{12}]\cdot CH_3OH$ respectively, along with multiplets for the Ph_4P^+ cations in 7-8 ppm region (see Figure 6·34). The integration in $(Ph_4P)_2[Mn_3(Q_2)_2(QCH_3)(CO)_9]$ (Q=S, Se and Te) gives a ratio of methyl proton *vs.* phenyl proton ~3:40, while the ratio in $(Ph_4P)_3[Re_4(Te_2)_3(TeCH_3)(CO)_{12}]\cdot CH_3OH$ is ~3:60. In d_3-chloroform, the methyl groups in $(Ph_4P)[Mn_2(QCH_3)_3(CO)_6]$ (Q=S, Se and Te) also give a singlet ^{1}H NMR signal at δ=1.99 ppm for $(Ph_4P)[Mn_2(SCH_3)_3(CO)_6]$, δ=1.73 ppm for $(Ph_4P)[Mn_2(SeCH_3)_3(CO)_6]$ and δ=1.38 ppm $(Ph_4P)[Mn_2(TeCH_3)_3(CO)_6]$ respectively, as expected for a molecule with three-fold symmetry (see Figure 6·35). The change in the chemical shifts of the methyl groups in all manganese compounds can be explained by the decreased shielding effect of the different chalcogen atoms (i.e. from S to Te). The ^{1}H signal of the $TeCH_3^-$ group in $(Ph_4P)_3[Re_4(Te_2)_3(TeCH_3)(CO)_{12}]\cdot CH_3OH$ appears in the downfield. It should be noted that the $TeCH_3^-$ group in this compound is a μ_3-type ligand.

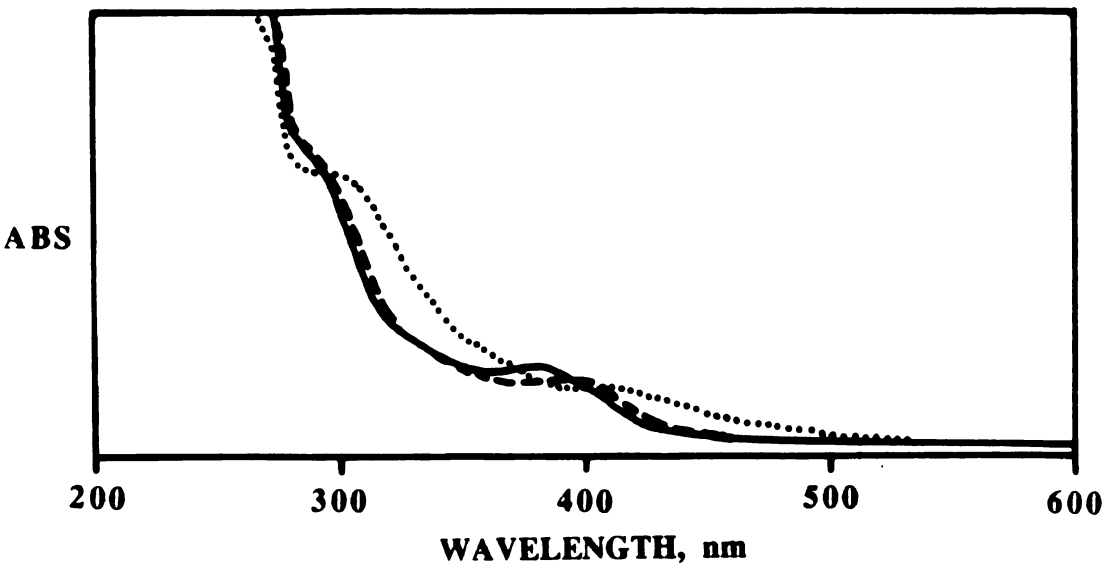


Figure 6-32. The UV/vis Spectra of (—) $(Ph_4P)[Mn_2(SCH_3)_3(CO)_6]$, (---) $(Ph_4P)[Mn_2(SeCH_3)_3(CO)_6]$ and (···) $(Ph_4P)[Mn_2(TeCH_3)_3(CO)_6]$ in CH_3CN

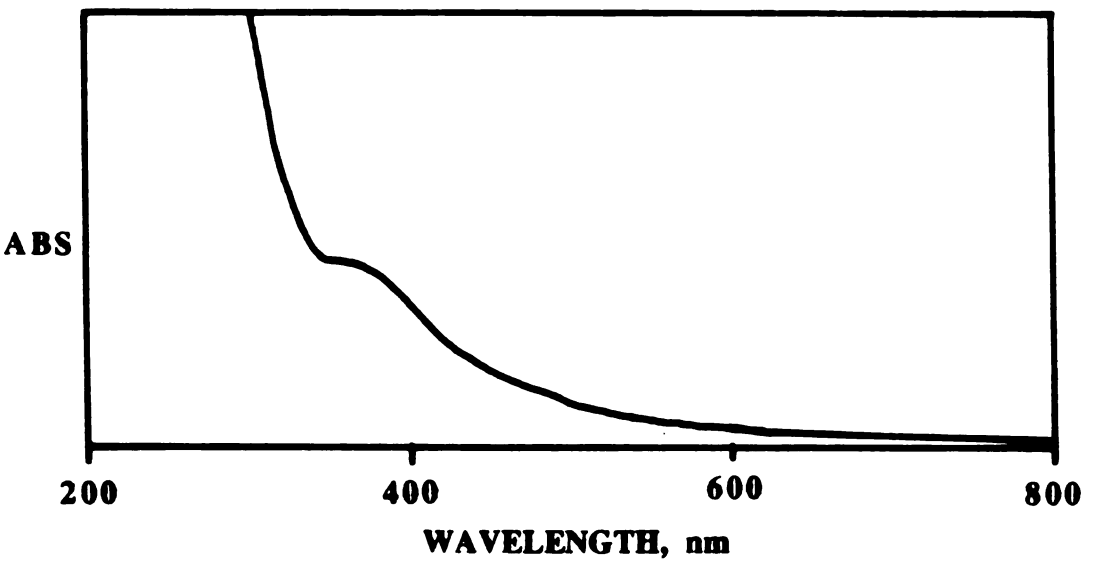


Figure 6-33. The UV/vis Spectrum of $(Ph_4P)_3[Re_4(Te_2)_3(TeCH_3)(CO)_{12}]\cdot CH_3OH$ in CH_3CN

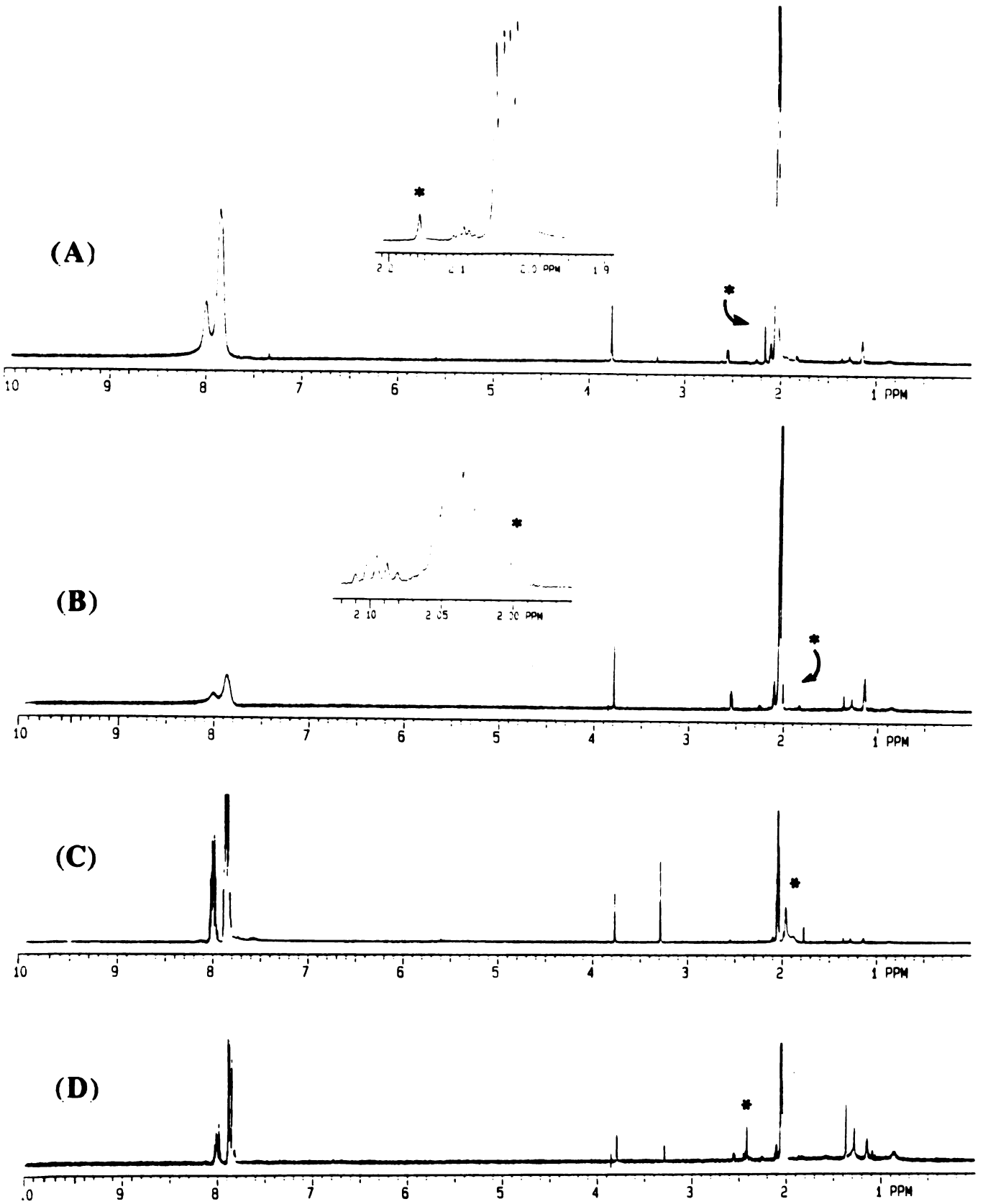


Figure 6-34. The ^1H NMR Spectra of (A) $(Ph_4P)_2[Mn_3(S_2)_2(SCH_3)(CO)_9]$, (B) $(Ph_4P)_2[Mn_3(Se_2)_2(SeCH_3)(CO)_9]$, (C) $(Ph_4P)_2[Mn_3(Te_2)_2(TeCH_3)(CO)_9]$ and (D) $(Ph_4P)_3[Re_4(Te_2)_3(TeCH_3)(CO)_{12}]\cdot CH_3OH$ in $(CD_3)_2CO$. * Signal of QCH_3^- (Q=S, Se and Te). The Insets Show the Expanded Areas Aroun the Methyl Groups

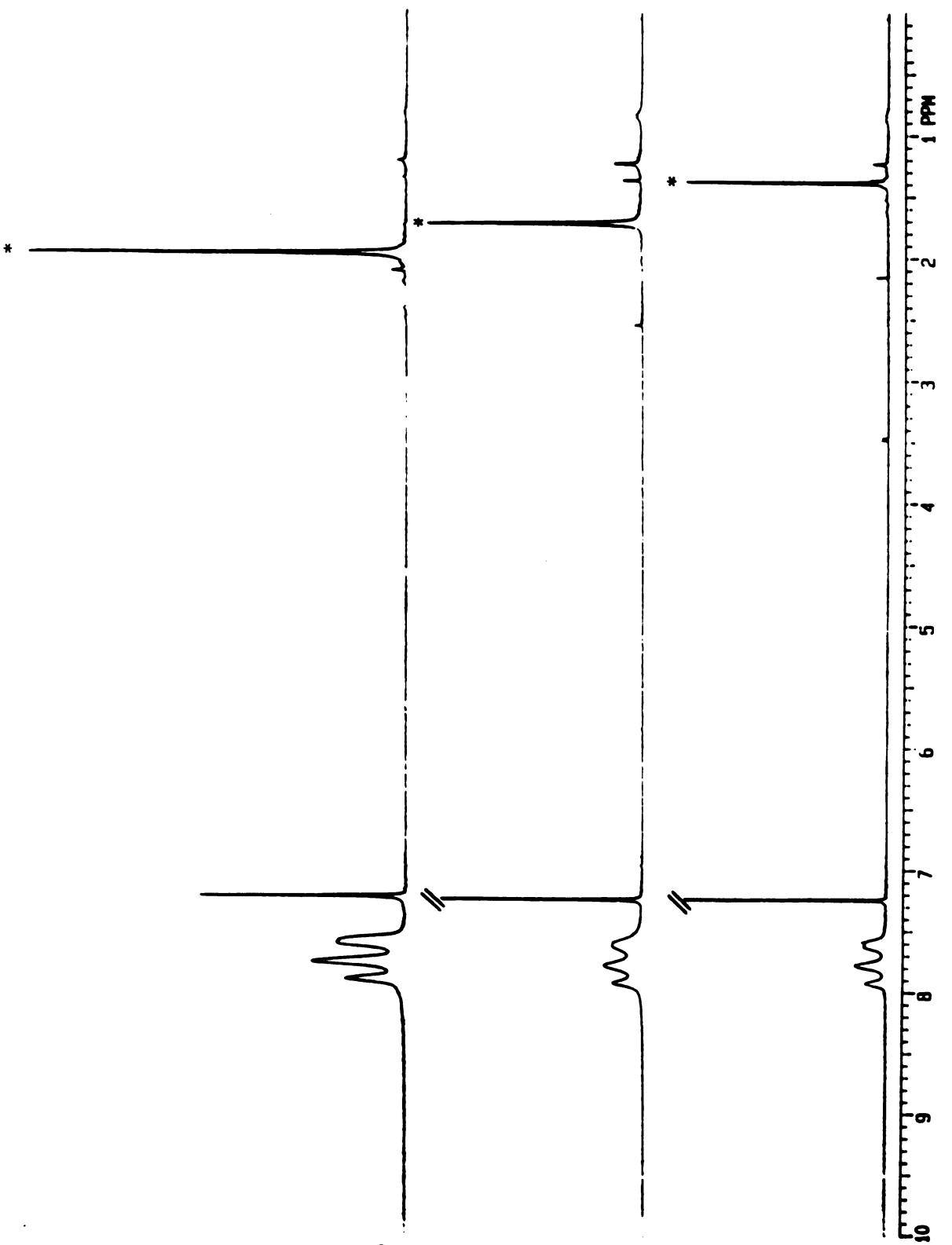


Figure 6·35. The ^1H NMR Spectra of (A) $(Ph_4P)[Mn_2(SCH_3)_3(CO)_6]$, (B) $(Ph_4P)[Mn_2(SeCH_3)_3(CO)_6]$ and (C) $(Ph_4P)[Mn_2(TeCH_3)_3(CO)_6]$ in $CDCl_3$. *Signal of QCH_3^- (Q=S, Se and Te)

3. Thermal Decomposition

Compounds (6·1) through (6·9) undergo stepwise or continuous thermal decompositions under N_2 flow in the temperature range of 25 to 800 °C as shown in Figures 6·36 and 6·37. For most of the compounds, the weight loss often continues beyond 800 °C. Table 6·27 summarizes the thermolysis data for these compounds. Although well-defined plateaus can be found in the TGA diagrams of the series $(Ph_4P)_m[M_n(Q_2)_x(QR)(CO)_y]$ (when M=Mn and Q=S, R=H or CH_3, m=2, n=3, x=2, y=9; or 12), their residual weights do not correspond to any simple binary metal chalcogenides, suggesting that carbon is still retained in the decomposition products. Similarly, residual products from thermal decompositions of $(Ph_4P)[Mn_2(QCH_3)_3(CO)_6]$ (Q=S, Se and Te) are not single phases or mixtures of binary manganese chalcogenides, as shown by their observed weight losses and the XRD studies. These products may also be Mn carbide phases.

Table 6·27. Thermal Gravimetric Analysis Data for $(Ph_4P)_2[Mn_3(S_2)_2(SH)(CO)_9]$ (6·1), $(Ph_4P)_2[Mn_3(S_2)_2(SCH_3)(CO)_9]$ (6·2), $(Ph_4P)_2[Mn_3(Se_2)_2(SeCH_3)(CO)_9]$ (6·3), α-$(Ph_4P)_2[Mn_3(Te_2)_2(TeCH_3)(CO)_9]$ (6·4), β-$(Ph_4P)_2[Mn_3(Te_2)_2(TeCH_3)(CO)_9]$ (6·5), $(Ph_4P)_3[Re_4(Te_2)_3(TeCH_3)(CO)_{12}]\cdot CH_3OH$ (6·6), $(Ph_4P)[Mn_2(SCH_3)_3(CO)_6]$ (6·7), $(Ph_4P)[Mn_2(SeCH_3)_3(CO)_6]$ (6·8) and $(Ph_4P)[Mn_2(TeCH_3)_3(CO)_6]$ (6·9)

compd	onset temp °C	final temp °C	obsd % wt loss
(6·1)	171	197	25.78
	197	333	69.81
	687	/	/
(6·2)	185	388	72.55
	650	/	/
(6·3)	170	352	73.71
	744	/	/

Table 6·27. (cont'd)

compd	onset temp °C	final temp °C	obsd % wt loss
(6·4)	193	286	54.06
	704	/	/
(6·5)	193	286	54.06
	704	/	/
(6·6)	246	299	16.37
	299	377	42.99
	377	526	46.90
	757	/	/
(6·7)	197	383	69.15
(6·8)	200	523	77.64
(6·9)	202	533	68.25

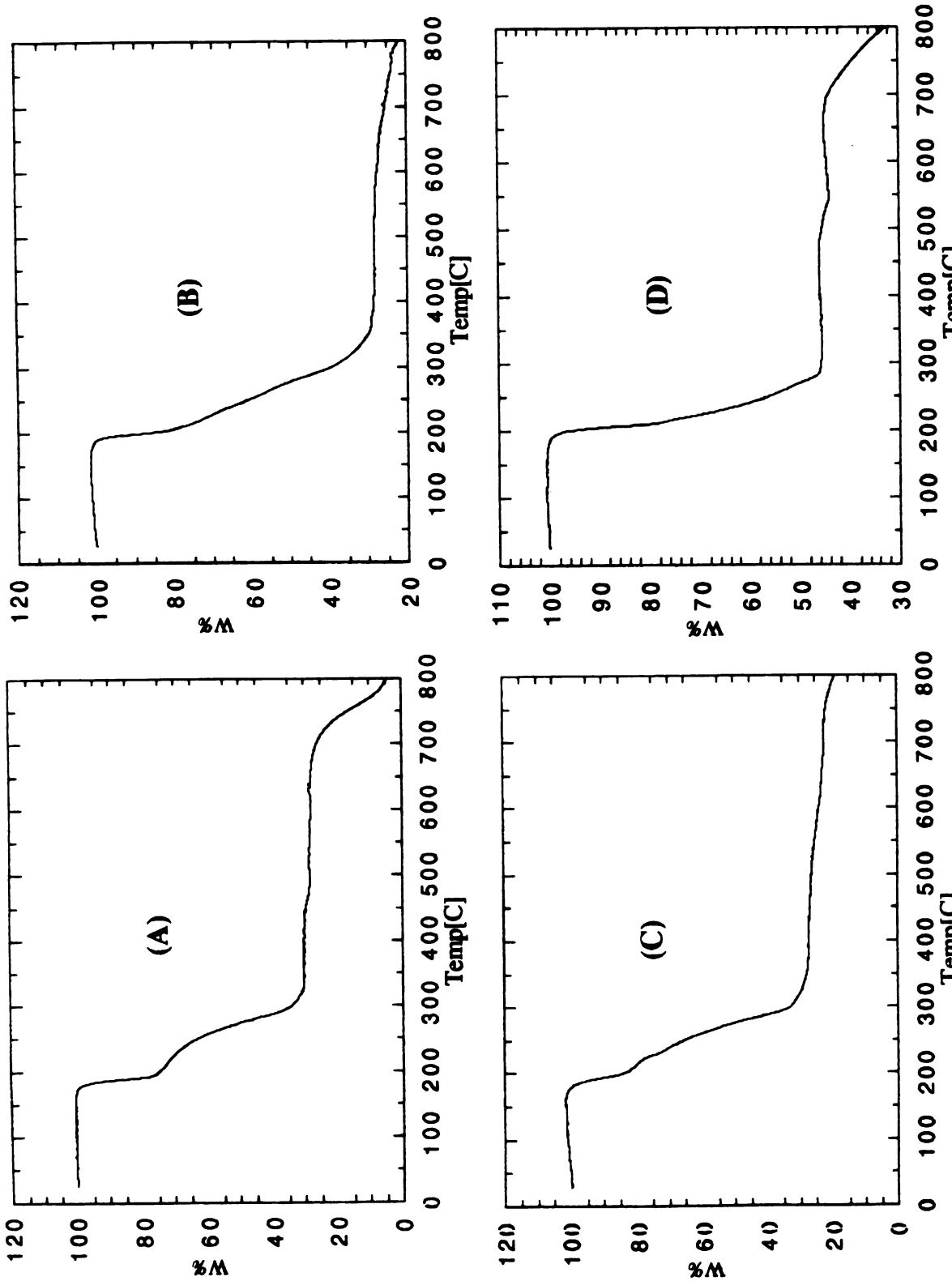


Figure 6·36. The TGA diagrams of (A) $(Ph_4P)_2[Mn_3(S_2)_2(SH)(CO)_9]$, (B) $(Ph_4P)_2[Mn_3(S_2)_2(SCH_3)(CO)_9]$, (C) $(Ph_4P)_2[Mn_3(Se_2)_2(SeCH_3)(CO)_9]$ and (D) $(Ph_4P)_2[Mn_3(Te_2)_2(TeCH_3)(CO)_9]$

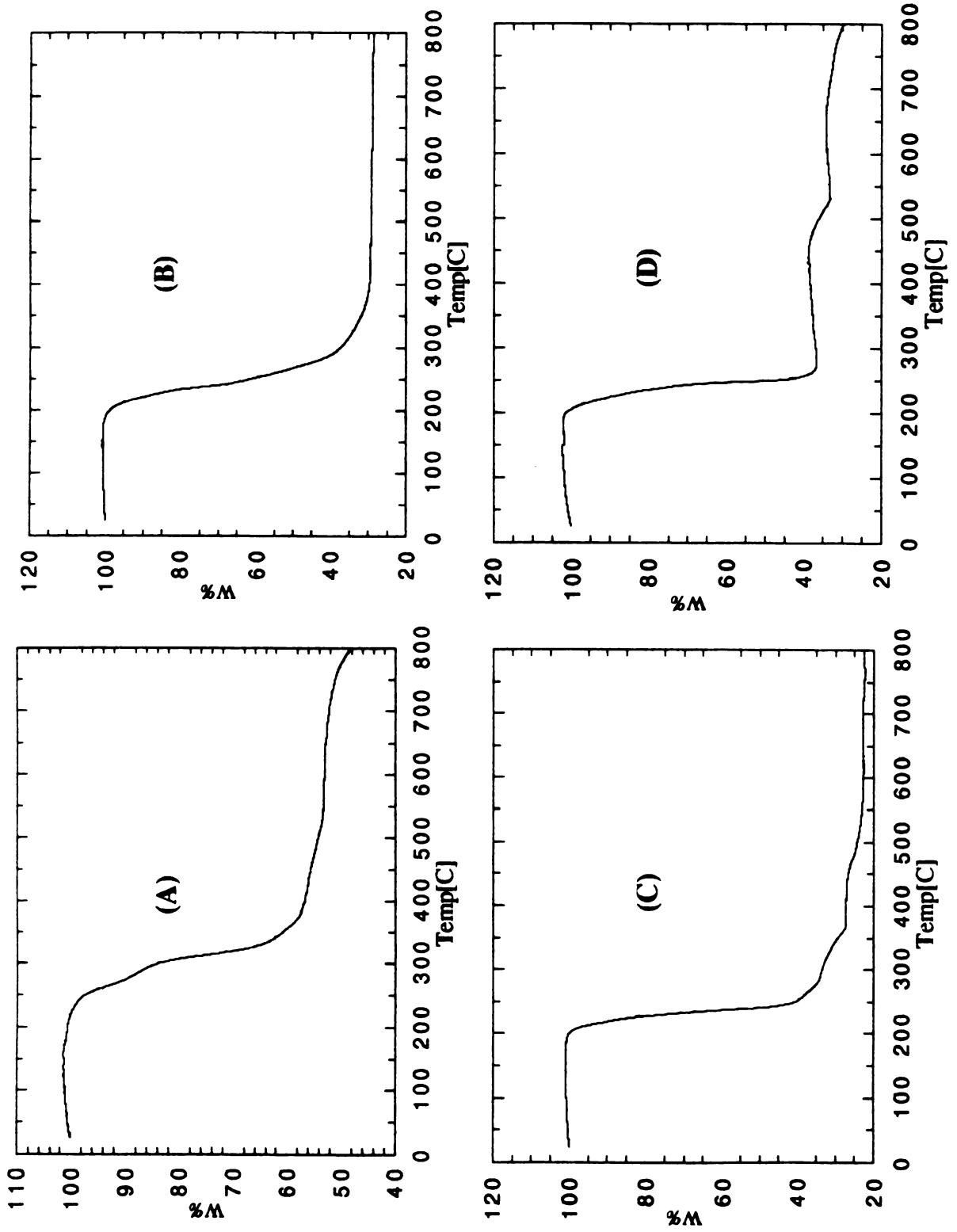
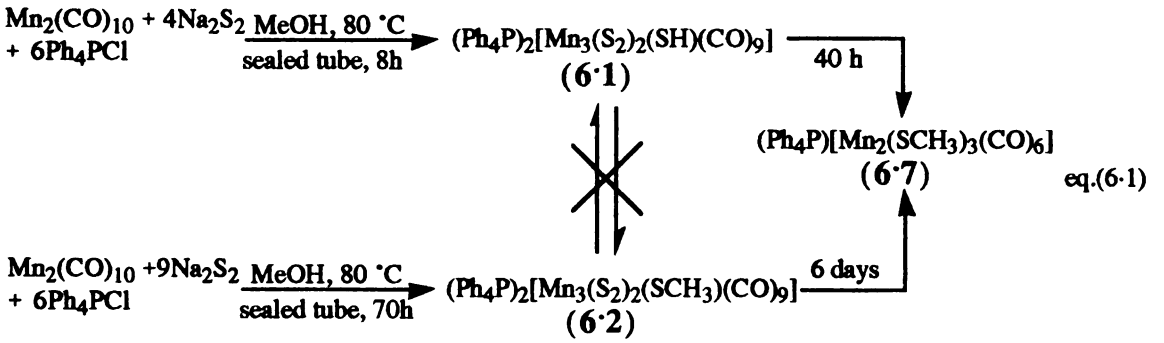


Figure 6-37. The TGA diagrams of (A) $(Ph_4P)_3[Re_4(Te_2)_3(TeCH_3)(CO)_{12}]\cdot CH_3OH$, (B) $(Ph_4P)[Mn_2(SCH_3)_3(CO)_6]$, (C) $(Ph_4P)[Mn_2(SeCH_3)_3(CO)_6]$ and (D) $(Ph_4P)[Mn_2(TeCH_3)_3(CO)_6]$

IV. Discussion

Nine group 7 metal carbonyl polychalcogenide/alkylchalcogenide compounds have been synthesized through methanothermal reactions. The most unexpected outcome of these reactions is that the compounds, except for $(Ph_4P)_2[Mn_3(S_2)_2(SH)(CO)_9]$, contain the methylated monochalcogenide ligands. The methylation probably originates from the electrophilic attack of CH_3OH on the chalcogenide ligand under the reaction conditions because if CH_3CH_2OH is used in place of CH_3OH the isolated compounds contain no alkylated chalcogenide ligands as confirmed by ^1H NMR studies. Alkylation of coordinated chalcogenide ligands can readily occur in some metal sulfide[25], selenide[26], and telluride[9] complexes. Among various alkylating agents such as CH_3SO_3F, $CH_3SO_3CF_3$, CH_3I, etc., however, CH_3OH is by no means a suitable choice. To the best of our knowledge, the current reactions are the first examples of coordinated chalcogenides being alkylated by CH_3OH. The results of this work underscore the intrinsic difference of the chemistry under hydro(solvo)thermal conditions and that at ambient temperatures and pressures. This also provides a convenient entry into the metal alkylchalcogenide complexes, especially those of metal alkyltellurides where the foul-smelling, air-sensitive liquids of free organotellurides with lower alkyl chains have long discouraged attempts at exploring its coordination chemistry[27].

In the $Mn_2(CO)_{10}/Na_2S_2$ system, the formation of either $(Ph_4P)_2[Mn_3(S_2)_2(SH)(CO)_9]$ (**6-1**) or $(Ph_4P)_2[Mn_3(S_2)_2(SCH_3)(CO)_9]$ (**6-2**) was found to be entirely dependent on the molar ratio of $Mn_2(CO)_{10}$ to Na_2S_2 in the reaction. For instance, the ratio 1:4 gave exclusively (**6-1**), while the ratio 1:9 yielded (**6-2**). Any ratios between these two would result in a mixture of the two compounds. Moreover, under the reaction conditions, the two compounds did not interchange to each other, instead they were both transformed to $(Ph_4P)[Mn_2(SCH_3)_3(CO)_6]$ (**6-7**), as shown in the following equation:

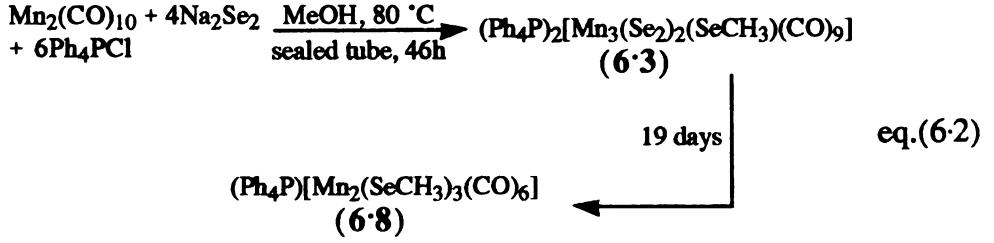


The transformation of (**6·1**) into (**6·7**) started after heating the reaction for ~12 hours, and were complete in ~ 40 hours. During this time, the product was a mixture with the ratio of (**6·7**) to (**6·1**) increasing with the heating time. A similar transformation also occurred in (**6·2**), but was relatively slow. Complete conversion of (**6·2**) to (**6·7**) often takes ~ 6 days. All these reactions must have involved, besides CH_3OH, some unidentified intermediate species generated in the reaction because under the same conditions, pure (**6·1**) or (**6·2**) failed to react with CH_3OH to give (**6·7**).

The protonated monosulfide ligand in (**6·1**) was formulated from the results of X-ray single crystal analysis, ^1H NMR and magnetic susceptibility measurements. Because a methyl group was found on the monochalcogenide ligand in all other anions of this series, a great deal of attention was paid to the difference Fourier maps of (**6·1**) at various stage of its refinement to discern possible methyl groups. However, the surrounding area of the monosulfide was quite clear of residual electron density, providing the first evidence of its absence. Of course, such evidence could be easily undermined by the disorder of this C atom, or inaccuracy of the difference Fourier maps resulting from the domination of the heavy atoms, i.e. Mn's and S's. However, the following observations should be more convincing: (i) our control reaction of preparing (**6·1**) by using EtOH as solvent gave the same product, albeit in a lower yield, as confirmed by X-ray powder diffraction (XRD), FT-IT and ^1H NMR studies; (ii) the ^1H NMR spectrum of this compound, unlike the other

compounds in this series, gave no CH_3 resonance in the expected region, while it is diamagnetic as measured by superconducting quantum interference device (SQUID) and EPR. These data strongly suggest that the monosulfide ligand is protonated. It should be noted that, like methylation of coordinated chalcogenide ligands, protonation of such ligands is also known to occur with the use of a strong acid[26c, 28]. However, attempts to use IR and ^1H NMR to confirm/locate this H atom have thus far been unsuccessful. The IR spectrum of the dimeric SH-bridged complex $[Mn_2(SH)_2(CO)_8]$ gave three weak ν_{SH} vibrations at 2571, 2531 and 2481 cm^{-1}[29]. However, (**6·1**) showed no identifiable IR bands in this region. It is generally accepted that ν_{SH} stretching modes are so weak that their absorptions in the IR spectrum are often obscured[30]. On the other hand, a trace amount of acids or bases in solution could cause exchange broadening and collapse of the SH proton NMR signal, as it has been proven to be the case in other metal hydrosulfido complexes[31]. This may account for the failure of observing the ^1H NMR peak of the SH group in (**6·1**).

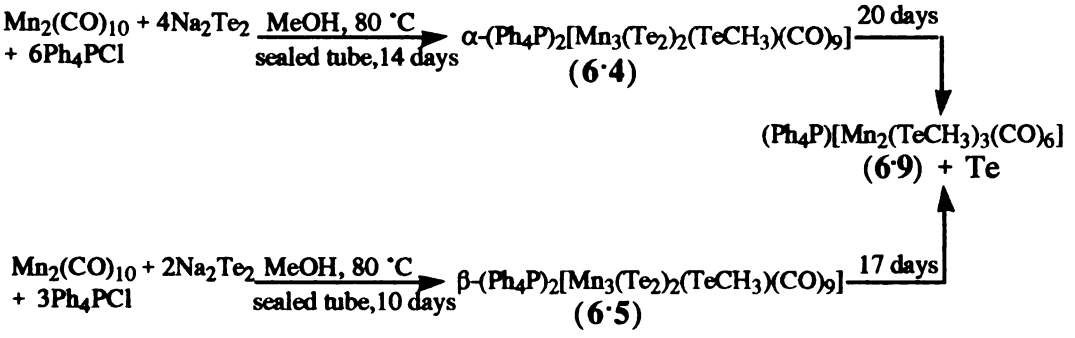
Reactions between $Mn_2(CO)_{10}$ and Na_2Se_2 proceed in a similar manner as the S-analogues above:



eq.(6·2)

Thus far we have not been able to isolated the protonated species analogous to (**6·1**), although various molar ratios of $Mn_2(CO)_{10}$ to Na_2Se_2 and different reaction times are examined. This is consistent with the higher nucleophilicity of the coordinated selenium ligands. Similarly, the search for such a protonated species in the $Mn_2(CO)_{10}/Na_2Te_2$ system resulted in isolation of two different crystal modifications of

the same compound, α- and β-$(Ph_4P)_2[Mn_3(Te_2)_2(TeCH_3)(CO)_9]$. They are both methylated products:



eq.(6·3)

Interestingly, the transformation of both (**6·4**) and (**6·5**) into (**6·9**) was found to be slow and often incomplete. Because the products formed in the first step of these reactions are much less soluble in MeOH than their sulfide or selenide counterparts, reaction of such compounds with the methylating agent should take longer time. In this case, the second-step reaction to (**6·9**) often competes with the thermal degradation of (**6·4**) and (**6·5**).

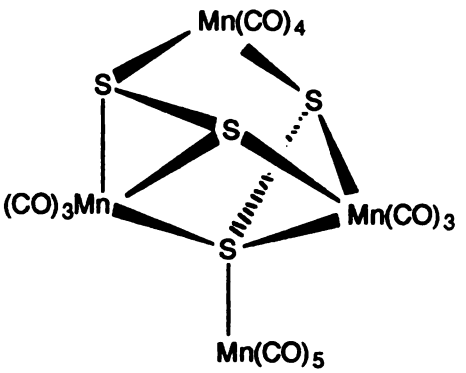
Unlike the reactions of $Mn_2(CO)_{10}$ with Na_2Q_2 (S, Se and Te) which are redox in nature, the reaction of $CpRe(CO)_3$ with K_2Te_4 is metathetical:

$$CpRe(CO)_3 + 8K_2Te_4 + 8Ph_4PCl \xrightarrow[\text{sealed tube}]{\text{MeOH, 80 °C}} (Ph_4P)_3[Re_4(Te_2)_3(TeCH_3)(CO)_{12}] + (Ph_4P)_2Te_4 \qquad \text{eq.(6·4)}$$

However, use of Na_2Te_2 as the starting material in the above reaction failed to give any rhenium telluride complex except $(Ph_4P)_2Te_4$, suggesting that the reaction mechanism may be more complicated than it appears. Furthermore, it was found that K_2Te_4 needs to be in excess. This means that the reaction would give $(Ph_4P)_2Te_4$ as a by-product. A ratio of $CpRe(CO)_3$ to K_2Te_4 lower than 1:8 would lead to a product containing $(Ph_4P)_2Te_4$ and Te powder only. (**6·6**) does not undergo similar transformation to the corresponding completely methylated monotelluride compound. Prolonged heating degrades the

compound slowly. After heated at 80 °C for 28 days, only $(Ph_4P)_2Te_4$ (crystal form) and elemental Te (microcrystalline) can be found in the solid phase of the product.

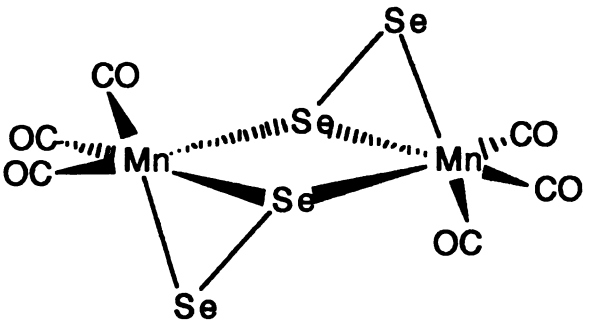
All structures in the homologous series of $(Ph_4P)_m[M_n(Q_2)_x(QR)(CO)_y]$ (when M=Mn and Q=S, R=H or CH_3, m=2, n=3, x=2, y=9; or 12) are hitherto unknown. Manganese or rhenium carbonyl clusters containing polychalcogenide ligands are relatively scarce. Among the structurally characterized compounds are $[Mn_4(S_2)_2(CO)_{15}]$[10] and $(Ph_4P)_2[M_2(Se_n)_2(CO)_6]$ (when M=Mn, n=2 or 4; when M=Re, n=4)[11-12]. The neutral cluster $[Mn_4(S_2)_2(CO)_{15}]$ contains a μ_4-$\eta^1,\eta^1,\eta^1,\eta^2$-type, and a μ_3-η^1,η^1,η^2-type S_2^{2-} ligands. The latter is the same as one of those found in either (**6·1**) or (**6·2**). Although $[Mn_4(S_2)_2(CO)_{15}]$ bears certain structural similarity to both (**6·1**) and (**6·2**), the most noticeable feature of this tetramer is the presence of a S-bound $Mn(CO)_5$ fragment in the structure as shown in the following scheme:



Scheme 6·3. The Structure of $[Mn_4(S_2)_2(CO)_{15}]$

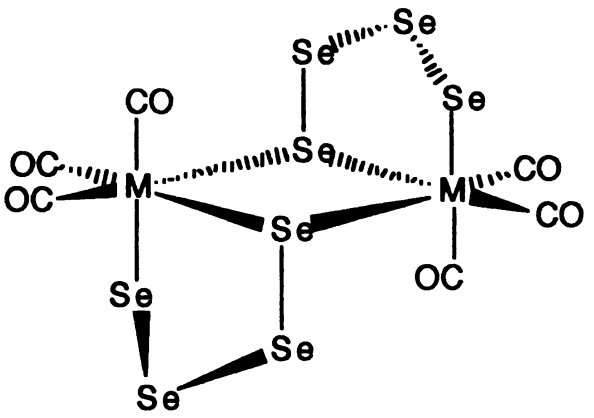
All Mn atoms in this cluster, having a +1 formal oxidation state, do not form M-M bonds. The octahedral coordination of the metal centers is completed by various S ligands and CO groups. The $(Ph_4P)_2[Mn_2(Se_2)_2(CO)_6]$ and $(Ph_4P)_2[M_2(Se_2)_2(CO)_6]$ (M=Mn or Re) are structurally related dimers. The centrosymmetric $[Mn_2(Se_2)_2(CO)_6]^{2-}$ anion is formed from two $Mn(CO)_3$ fragments bridged by two Se_2^{2-} ligands as shown in Scheme 6·3. The coordination mode of these two Se_2^{2-} ligands can be described as μ-η^1,η^2-type,

i.e. the Se_2^{2-} is bonded to a manganese center in the side-on fashion, while one selenium atom bridges another manganese center.



Scheme 6-4. The Structure of $[Mn_2(Se_2)_2(CO)_6]^{2-}$ Anion

The structure of $[M_2(Se_4)_2(CO)_6]^{2-}$ (M=Mn or Re), as shown in Scheme 6-4, is similar to that of $[Mn_2(Se_2)_2(CO)_6]^{2-}$. The molecule is also centrosymmetric, and the MSe_4 ring adopts a puckered conformation.



Scheme 6-5. The Structure of $[M_2(Se_4)_2(CO)_6]^{2-}$ (M=Mn or Re) Anion

We note that the two non-interacting Mn atoms in each of these compounds also have the +1 formal oxidation state with octahedral coordination. Interestingly, heating of $[Mn_2(Se_4)_2(CO)_6]^{2-}$ at 90 °C in DMF leads to complete decarbonylation of the metal centers via an internal redox process, producing the homoleptic complex $[Mn(Se_4)_2]^{2-}$.

The $[Mn_2(QCH_3)_3(CO)_6]^-$ (Q=S, Se or Te) anions are isoelectronic to the cationic species $[Fe_2(SCH_3)_3(CO)_6]^+$. The latter was prepared from reaction of $Fe_2(CO)_6(SCH_3)_2$

with dithietene $S_2C_2(CF_3)_2$, and its structure was shown to be essentially the same as the Mn analogues of the current series, i.e a C_{3h} molecule containing two non-interacting iron centers in the formal +2 oxidation state[32].

In closing, it is worthwhile once again pointing out the intrinsic difference of the organometallic-polychalcogenide chemistry under hydro(solvo)thermal conditions as opposed to ambient temperatures and pressures. On the other hand, this synthetic method has provided an easy access to some new metal complexes of alkylated chalcogenides which could serve as excellent starting materials for other chemistry. While the current results are very encouraging, further study is needed to extend this chemistry to other systems and to clarify the mechanism of the methylation reactions. The latter may prove to be of fundamental interest. All this promises many new opportunities for the exploratory synthetic chemistry.

REFERENCES

1. See chapters 5 & 7.

2. H. Vahrenkamp, *Angew. Chem. Int. Ed. Engl.*, 14(1975), 322-329.

3. J. Wachter, *Angew. Chem. Int. Ed. Engl.*, 28(1989), 1613-1626.

4. J. W. Kolis, *Coord. Chem. Rev.*, 105(1990), 195-219.

5. M. G. Kanatzidis and S.-P. Huang, submitted to *Coord. Chem. Rev.*

6. M. Herberhold, D. Reiner and U. Thewalt, *Z. Naturforsch.*, 35B(1980), 1281-1285.

7. M. Herberhold, D. Reiner and U. Thewalt, *Angew. Chem. Int. Ed. Engl.*, 22(1983), 1000-1001

8. M. Herberhold, D. Reiner, K. Ackermann, U. Thewalt and T.Debaerdemaeker, *Z. Naturforsch.*, 39B(1984), 1199-1205.

9. W. A. Herrmann, C. Hecht, E. Herdtweck and H.-J. Kneuper, *Angew. Chem. Int. Ed. Engl.*, 26(1987), 132-134.

10. V. Küllmer, E. Röttinger and H. Vahrenkamp, *J. Chem. Soc., Chem. Commun.*, (1977), 782-783.

11. S. C. O'Neal, W. T. Pennington and J. W. Kolis, *Inorg. Chem.*, 29(1990), 3134-3138.

12. S. C. O'Neal, W. T. Pennington and J. W. Kolis, *Can. J. Chem.*, 67(1989), 1980-1983.

13. D. D. Perrin, W. L. F. Armarego and D. R. Perrin, *Purification of Laboratory Chemicals,* 2nd Ed., Pergamon Press, Oxford UK, 1980.

14. See chapter 2.

15. *P3/V Data Collection Manual,* Siemens Analytical X-ray Instruments, Inc., 1989.

16. *MSC/AFC Diffractometer Control Software,* Molecular Structure Corporation, The Woodlands, Texas.

17. N. Walker and D. Stuart, *Acta Crystallogr.,* 39A(1983), 158-166.

18. *TEXSAN: Single Crystal Structure Analysis Software*, Version 5.0, Molecular Structure Corporation, The Woodlands, Texas.

19. A. Müller, W. Jaegermann and J. H. Enemark, *Coord. Chem. Rev.*, 46(1982), 245-280.

20. W. A. Herrmann and C. Hecht, *J. Organomet. Chem.*, 273(1984), 323-331.

21. (a) H. D. Lutz, M. Jung and G. Waschenbach, *Z. Anorg. Allg. Chem.,* 554(1987), 87-91. (b) M. Di Vaira, M. Peruzzini and P. Stoppioni, *Angew. Chem. Int. Ed. Engl.,* 26(1987), 916-917. (c) B. W. Eichhorn, R. C. Haushalter, F. A. Cotton and B. Wilson, *Inorg. Chem.*, 27(1988), 4084-4085.

22. H. Strasdeit, B. Krebs and G. Henkel, *Inorg. Chim. Acta* , 89(1984), L11-L13.

23. S.-P. Huang and M. G. Kanatzidis, *Inorg. Chem.*, 30(1991), 1455-1466.

24. (a) H. Wolkers, K. Dehnicke, D. Fenske, A. Khassanov and S. S. Hafner, *Acta Crystallogr.*, 47C(1991), 1627-1632. (b) J. Dietz, U. Müller, V. Müller and K. Dehnicke, *Z. Naturforsch.*, 46B(1991), 1293-1299.

25. (a) P. M. Treichel and G. P. Werber, *J. Am. Chem. Soc.*, 90(1968), 1753-1756. (b) G. R. Clark and D. R. Russell, *J. Organomet. Chem.*, 173(1979), 377-386. (c) K. L. K. Plute, R. C. Haltiwanger and M. Rakowski DuBois, *Inorg. Chem.*, 18(1979), 3246-3251.

26. (a) D. H. Farrar, K. R. Grundy, N. C. Payne, W. R. Roper and A. Walker, *J. Am. Chem. Soc.*, 101(1979), 6577-6579. (b) G. R. Clark and D. R. Russell, W. R. Roper and A. Walker, *J. Organomet. Chem.*, 136(1977), C1-C3. (c) J. E. Hoots and T. B. Rauchfuss, *Inorg. Chem.*, 22(1983), 2806-2812.

27. H. J. Gysling, *Coord. Chem. Rev.*, 42(1982), 133-244.

28. I. K. Adzamli, D. L. Nosco and E. Deutsch, *J. Inorg. Nucl. Chem.*, 42(1980), 1364-1366.

29. W. Beck, W. Danzer and R. Höfer, *Angew. Chem. Int. Ed. Engl.*, 12(1973), 77-78.

30. H.-J. Bach, H. Brunner, J. Wachter, M. M. Kubicki, J.-C. Leblanc, C. Moise and F. Volpato, *Organometallics*, 11(1992), 1403-1407.

31. D. Kwon, J. Real, D. Curtis, A. Rheingold and B. S. Haggerty, *Organometallics*, 10(1991), 143-148.

32. A. J. Schultz and R. Eisenberg, *Inorg. Chem.*, 12(1973), 518-525.

CHAPTER 7

MENTHANOTHERMAL SYNTHESIS OF METAL CARBONYL SULFIDO CLUSTERS OF GROUP 6 ELEMENTS

I. Introduction

Organometallic chemistry of group 6 metals with polychalcogenides has been recently developed to some extent by Kolis and co-workers[1]. Through oxidative decarbonylation of metal carbonyls by polychalcogenides Q_n^{2-} (Q=S, Se and Te; n=2-6) several new compounds of this group have been prepared and structurally characterized[2-5]. The products isolable from solution reactions often contain the metal center with its formal oxidation state tuned by redox chemistry. For instance, the reaction of tetratelluride Te_4^{2-} with group 6 metal carbonyls in DMF afforded carbonyl-containing metal polytellurides $[M(CO)_4Te_4]^{2-}$ (M=Cr, Mo or W)[2], whereby the metal centers are at their lowest oxidation state (0). However, when similar reactions were carried out with polysulfides or polyselenides in place of polytellurides, the products isolated were exclusively tetrathio(seleno)metalates $[MQ_4]^{2-}$ (M=Mo , W; Q=S, Se)[1, 4]. This requires an oxidation of the metal center from 0 to its maximum value of +6, along with the loss of all CO groups. Although the spectroscopic data pointed out that the formation of the $[MQ_4]^{2-}$ species involves some intermediates in which the metal centers have a lower oxidation state[6], none of these intermediates can be isolated from solution[4]. On the other hand, Rosenhein and McDonald have found that group 6 metals (Mo, W) form a series of polynuclear, sulfido-bridged carbonyl clusters where the metal centers have widely separated formal charges[7]. Based on the elemental analyses and spectroscopic

data, these clusters were formulated as $[\{Mo(CO)_4\}_n(MS_4)]^{2-}$ (M=Mo, W; n=1, 2)[7]. Later, the structures of two dimers, $[(CO)_4Mo(WS_4)]^{2-}$[8] and $[(CO)_4W(WS_4)]^{2-}$[9] from this homologous family, were confirmed by X-ray single crystal analysis. The rest of the clusters, especially the trimers, have not been structurally authenticated. We have discovered that under hydro(solvo)thermal conditions, the oxidative decarbonylation of metal carbonyls by polychalcogenides can often proceed via different pathways, presumably influenced by the altered solvent behavior under the super-heated conditions[10]. Furthermore, due to limited solubilities of both reactants and products under these conditions, such a process is often capable of intercepting insoluble intermediates in a multiple-step reaction. We have succeeded in synthesizing four clusters from the homonuclear family $[\{M(CO)_4\}_n(MS_4)]^{2-}$ (M=Mo, W; n=1, 2) in pure single crystal form using hydro(solvo)thermal conditions. In this chapter we describe the one-step methanothermal synthesis, spectroscopic characterization of the clusters $(Ph_4P)_2[(CO)_4Mo(MoS_4)]$ (7·1), $(Ph_4P)_2[(CO)_4W(WS_4)]$ (7·2), $(Ph_4P)_2[(CO)_4Mo(MoS_4)Mo(CO)_4]$ (7·3) and $(Ph_4P)_2[(CO)_4W(WS_4)W(CO)_4]$ (7·4). The X-ray structures of (7·2), (7·3) and (7·4) are reported. These multinuclear clusters are characterized by the presence of the well known tetrathiometalate $[MS_4]^{2-}$ (M=Mo, W) ligand whose chemistry has been extensively developed by Müller *et al* [11-12] and Coucouvanis *et al*[13-14].

II. Experimental Section

1. Reagents

Chemicals in this work other than solvents were used as obtained: (i) sulfur powder, ~100 mesh, 99.9% purity, Aldrich Chemical Company, Inc., Milwaukee, WI; (iii) sodium sticks in kerosene, 99% purity, Mallinckrodt Inc., Paris, Ky.; (iv) molybdenum hexacarbonyl, $Mo(CO)_6$, Strem Chemicals, Inc., Newburyport, MA; (v)

tungsten hexacarbonyl, $W(CO)_6$, Strem Chemicals, Inc., Newburyport, MA; (vi) tetraphenylphosphonium chloride, Ph_4PCl, 98% purity, Aldrich Chemical Company, Inc., Milwaukee, WI.

Diethyl ether (A.C.S. anhydrous, Columbus Chemical Industries Inc., Columbus, WI) was distilled under a dry N_2 blanket after being refluxed with potassium metal, benzophenone and triethylene glycol dimethyl ether for 12 hours[15].

Acetonitrile (GR anhydrous, EM Science Inc., Gibbstown, NY) was distilled under a dry N_2 atmosphere from CaH_2[15].

Methanol (GR anhydrous, EM Science Inc., Gibbstown, NY) was refluxed for 4-5 h with magnesium methoxide (prepared from dry magnesium turnings and absolute methanol), and distilled under a nitrogen atmosphere[15].

2. Physical Measurements

Semi-quantitative elemental analyses, FT-IR and UV/vis spectroscopic studies, and thermal gravimetric analyses (TGA) of the compounds were carried out as described previously[16].

3. Syntheses

All syntheses were carried out under a dry nitrogen atmosphere in a Vacuum Atmospheres Dri-Lab glovebox.

(i). Preparation of sodium disulfide Na_2S_2

This material was prepared by reacting stoichiometric amount of sulfur and sodium metal in a routine procedure used in this laboratory[16].

(ii). Preparation of $(Ph_4P)_2[(CO)_4Mo(MoS_4)]$ (7·1)

53 mg (0.2 mmol) $Mo(CO)_6$, 44 mg (0.4 mmol) Na_2S_2 and 145 mg (0.4 mmol) Ph_4PCl were thoroughly mixed and loaded into a 25 cm long thick-walled Pyrex tube (9 mm in diameter). After 0.3 ml MeOH was added, the tube was frozen with liquid N_2, then evacuated and sealed (the total volume is ~ 4 ml after sealed). Continuous heating of the tube at 80 °C for 3 h resulted in black thin needles. Successive washing of the product with MeOH and ether afforded 71 mg analytically pure single crystals of $(Ph_4P)_2[(CO)_4Mo(MoS_4)]$ (64% yield). IR spectrum (in KBr), ν_{co} : 2004(m), 1902(s), 1867(s) and 1837(s) cm^{-1}; ν_{m-s}: 477(s) and 431(m) cm^{-1}; Semi-quantitative elemental analyses by EDAX (atom%): Mo:S:P=36.5:35.8:27.7.

(iii). Preparation of $(Ph_4P)_2[(CO)_4W(WS_4)]$ (7·2)

As described above, the sealed Pyrex tube contained 70 mg (0.2 mmol) $W(CO)_6$, 44 mg (0.4 mmol) Na_2S_2, 147 mg (0.4 mmol) Ph_4PCl and 0.5 ml MeOH. The reaction was carried out at 80 °C for 8 h. 68 mg purple plate-like single crystals of $(Ph_4P)_2[(CO)_4W(WS_4)]$ were obtained by a similar isolation procedure (53% yield). IR spectrum (in KBr), ν_{co} : 1998(m), 1880(s), 1856(s) and 1826(s) cm^{-1}; ν_{m-s}: 481(sh), 474(s), 426(m) and 420(sh) cm^{-1}; Semi-quantitative elemental analyses by EDAX (atom%): W:S:P=24.8:48.8:26.4.

(iv). Preparation of $(Ph_4P)_2[Mo(CO)_4(MoS_4)Mo(CO)_4]$ (7·3)

Method (A). As described above, the sealed Pyrex tube contained 79 mg (0.3 mmol) $Mo(CO)_6$, 33 mg (0.3 mmol) Na_2S_2, 110 mg (0.3 mmol) Ph_4PCl and 0.5 ml MeOH. The reaction was carried out at 80 °C for 14 h. 79 mg large black crystals of $(Ph_4P)_2[Mo(CO)_4(MoS_4)Mo(CO)_4]$ were obtained by a similar isolation procedure (59% yield). IR spectrum (in KBr), ν_{co} : 2017(sh), 1998(m), 1903(s), 1875(sh) and 1859(s)

cm^{-1}; ν_{m-s}: 433(m) cm^{-1}; Semi-quantitative elemental analyses by EDAX (atom%): Mo:S:P=22.7:49.9:27.4.

Method (B). 30 mg (0.027 mmol) (**7·1**), 15 mg (0.054 mmol) $Mo(CO)_6$ and 0.5 ml MeOH were sealed in a Pyrex tube. After heated at 80 °C for 12 hours, pure single crystals of (**7·3**) were obtained in a quantitative yield.

(v). Preparation of $(Ph_4P)_2[W(CO)_4(WS_4)W(CO)_4]$ (7·4)

Method (A). As described above, the sealed Pyrex tube contained 106 mg (0.3 mmol) $W(CO)_6$, 33 mg (0.3 mmol) Na_2S_2, 110 mg (0.3 mmol) Ph_4PCl and 0.7 ml MeOH. The reaction was carried out at 80 °C for 24 h. 64 mg large dark red hexagonal prism-like single crystals of $(Ph_4P)_2[W(CO)_4(WS_4)W(CO)_4]$, along with 5 mg purple crystals of (**7·2**), were obtained by a similar isolation procedure (40% yield). Two compounds were easily separated mechanically. IR spectrum (in KBr), ν_{co} : 2017(sh), 1998(m), 1903(s), 1875(sh) and 1859(s) cm^{-1}; ν_{m-s}: 430(s) cm^{-1}; Semi-quantitative elemental analyses by EDAX (atom%): W:S:P=25.6:51.5:22.9.

Method (B). 20 mg (0.015 mmol) (**8·2**), 10 mg (0.03 mmol) $W(CO)_6$ and 0.3 ml MeOH were sealed in a Pyrex tube. After heated at 80 °C for 5 days, pure single crystals of (**7·4**) were obtained in a quantitative yield.

4. X-ray Diffraction and Crystallographic Studies

The single crystal X-ray diffraction studies were performed by using a Rigaku automated AFC6S single crystal diffractometer which was controlled by an integrated software package[17].

Crystal were either affixed to the tip of glass fibers (for low temperature data collection) or sealed in glass capillaries (for room temperature data collection).

Unit cell constants of all compounds were obtained from a least-squares refinement using the setting angles of 20-24 carefully centered reflections in the range $15.0^{\circ}<2\theta<39.9^{\circ}$. Intensity data of (7·2), (7·3) and (7·4) were collected with $\omega-2\theta$ scan techniques and Mo Kα radiation. The stability of the experimental setup and crystal integrity for each data collection was monitored by measuring three representative reflections periodically (every 150). No crystal decay was detected. Empirical absorption corrections were applied to all data based on ψ scans of several strong reflections with $\chi\sim90^{o}$. Crystals of (7·1) are sensitive to X-rays. They lose crystallinity within 4-5 hours under the X-ray beam, which does not allow for intensity data collection. Several attempts were made, only unit cell parameters obtained.

The structures were solved with direct methods and refined with full-matrix least squares techniques[18]. DIFABS corrections after isotropic refinement of all atoms were then applied[19]. The calculations were performed with the TEXSAN crystallographic software package of Molecular Structure Corporation[20]. Table 7·1 gives crystal data of all compounds, and information of structure analysis for (7·2), (7·3) and (7·4).

All non-hydrogen atoms were refined either isotropically or anisotropically. The hydrogen positions were calculated but not refined. The final coordinates and average temperature factors of the atoms in (7·2), (7·3) and (7·4) are given in Tables 7·2, & 7·3 and 7·4, respectively.

Table 7·1. Data for Crystal Structure Analysis of $(Ph_4P)_2[(CO)_4Mo(MoS_4)]$ (7·1), $(Ph_4P)_2[(CO)_4W(WS_4)]$ (7·2), $(Ph_4P)_2[(CO)_4Mo(MoS_4)Mo(CO)_4]$ (7·3) and $(Ph_4P)_2[(CO)_4W(WS_4)W(CO)_4]$ (7·4)

compound	7·1	7·2	7·3	7·4
formula	$C_{52}H_{40}O_4P_2S_4Mo_2$	$C_{52}H_{40}O_4P_2S_4W_2$	$C_{56}H_{40}O_8P_2S_4Mo_3$	$C_{56}H_{40}O_8P_2S_4W_3$
a, Å	12.393(8)	12.390(3)	11.416(3)	11.498(1)
b, Å	19.303(9)	19.314(4)	22.524(4)	22.600(4)
c, Å	11.909(6)	11.866(2)	10.815(4)	10.864(3)
α, deg	102.39(5)	102.66(2)	91.03(2)	90.92(2)
β, deg	111.54(5)	111.49(1)	100.57(3)	100.85(1)
γ, deg	73.61(5)	73.40(2)	88.96(2)	88.58(1)
Z; V, Å^3	2; 2522(3)	2; 2511(1)	2; 2733(1)	2; 2771(2)
space group	P-1(#2)	P-1(#2)	P-1(#2)	P-1(#2)
D_{calc}, g/cm^3	1.46	1.70	1.60	1.90
μ(Mo Kα), cm^{-1}	63.3	49.4	88.9	65.9
cryst size, mm	0.09, 0.14, 0.17	0.22, 0.23, 0.27	0.21, 0.26, 0.33	0.25, 0.25, 0.30

Table 7·1. (cont'd)

$2\theta_{max}$, deg	/	45.0	50,0	45.0
Temperature (°C)	23	23	-100	23
no. of data collcd				
no. of data used($F_o^2>3\sigma(F_o^2)$)	/	3291	6552	4703
min, max abs cor	/	0.78, 1.16	0.70, 1.28	0.61, 1.32
no. of variables	/	317	658	378
no. of atoms per asym uint (including H)	/	104	113	113
final R/R_w, %	/	4.6/5.5	5.4/8.0	6.9/9.2

Table 7·2. Positional Parameters and B_{eq} Values[a] for $(Ph_4P)_2[(CO)_4W(WS_4)]$ (7·2)
(Standard Deviations in Parentheses)

atom	x	y	z	B_{eq}, Å^2
W1	0.52284(7)	0.76078(4)	0.03379(7)	4.26(5)
W2	0.76034(7)	0.72709(4)	0.23397(7)	4.59(5)
S1	0.6993(4)	0.7154(2)	0.0029(4)	5.1(3)
S2	0.5464(5)	0.7781(3)	0.2319(5)	6.1(3)
S3	0.4073(5)	0.6864(3)	-0.0605(5)	5.7(3)
S4	0.4408(5)	0.8637(3)	-0.0371(6)	6.8(3)
P1	0.2645(4)	0.4495(3)	0.3320(4)	4.2(2)
P2	0.1676(4)	0.0169(3)	0.3124(5)	4.6(3)
O1	0.843(1)	0.7409(8)	0.518(1)	8(1)
O2	1.024(1)	0.6636(9)	0.239(2)	10(1)
O3	0.733(2)	0.5690(8)	0.225(2)	10(1)
O4	0.809(1)	0.8806(8)	0.255(1)	9(1)
C1	0.376(1)	0.3693(9)	0.379(1)	4.0(4)
C2	0.373(2)	0.338(1)	0.469(2)	5.7(5)
C3	0.450(2)	0.269(1)	0.496(2)	6.9(5)
C4	0.532(2)	0.237(1)	0.436(2)	7.1(5)
C5	0.535(2)	0.269(1)	0.348(2)	7.1(5)
C6	0.455(2)	0.336(1)	0.317(2)	5.7(4)
C7	0.314(2)	0.501(1)	0.260(2)	4.5(4)
C8	0.336(2)	0.471(1)	0.152(2)	5.4(4)
C9	0.379(2)	0.510(1)	0.099(2)	6.7(5)
C10	0.397(2)	0.575(1)	0.158(2)	6.8(5)
C11	0.373(2)	0.612(1)	0.264(2)	6.7(5)
C12	0.331(2)	0.569(1)	0.315(2)	5.9(5)
C13	0.234(2)	0.5047(9)	0.463(1)	4.0(4)
C14	0.330(2)	0.515(1)	0.567(2)	6.1(5)
C15	0.311(2)	0.563(1)	0.667(2)	6.9(5)
C16	0.198(2)	0.598(1)	0.663(2)	7.0(5)
C17	0.101(2)	0.587(1)	0.563(2)	7.0(5)

Table 7·2. (cont'd)

atom	x	y	z	B_{eq}, Å^2
C18	0.120(2)	0.540(1)	0.460(2)	5.2(4)
C19	0.133(2)	0.422(1)	0.229(1)	4.2(4)
C20	0.048(2)	0.472(1)	0.159(2)	5.7(5)
C21	-0.062(2)	0.455(1)	0.086(2)	7.1(5)
C22	-0.078(2)	0.389(1)	0.081(2)	8.2(6)
C23	0.002(2)	0.336(1)	0.151(2)	7.3(5)
C24	0.113(2)	0.357(1)	0.230(2)	5.7(5)
C25	0.141(2)	-0.069(1)	0.242(2)	5.0(4)
C26	0.028(2)	-0.081(1)	0.188(2)	6.5(5)
C27	0.012(2)	-0.154(1)	0.132(2)	7.8(6)
C28	0.109(2)	-0.208(1)	0.131(2)	7.4(6)
C29	0.223(2)	-0.197(1)	0.179(2)	6.5(5)
C30	0.235(2)	-0.127(1)	0.235(2)	7.5(6)
C31	0.266(2)	0.004(1)	0.465(2)	4.9(4)
C32	0.242(2)	-0.042(1)	0.527(2)	6.1(5)
C33	0.313(2)	-0.051(1)	0.646(2)	6.5(5)
C34	0.403(2)	-0.016(1)	0.701(2)	7.5(6)
C35	0.423(2)	0.031(1)	0.647(2)	6.8(5)
C36	0.358(2)	0.041(1)	0.526(2)	6.5(5)
C37	0.228(2)	0.052(1)	0.228(2)	4.6(4)
C38	0.239(2)	0.124(1)	0.263(2)	6.0(5)
C39	0.282(2)	0.151(1)	0.192(2)	6.5(5)
C40	0.306(2)	0.115(1)	0.090(2)	6.0(5)
C41	0.294(2)	0.043(1)	0.055(2)	5.9(5)
C42	0.256(2)	0.012(1)	0.125(2)	5.2(4)
C43	0.034(2)	0.084(1)	0.322(2)	6.1(5)
C44	0.019(2)	0.113(1)	0.431(2)	6.4(5)
C45	-0.082(2)	0.173(1)	0.436(2)	9.2(7)
C46	-0.147(2)	0.192(1)	0.325(2)	8.4(6)

Table 7·2. (cont'd)

atom	x	y	z	B_{eq}, Å^2
C47	-0.143(2)	0.168(1)	0.219(3)	9.9(7)
C48	-0.044(2)	0.108(1)	0.210(2)	8.1(6)
C49	0.814(2)	0.737(1)	0.414(2)	5.9(5)
C50	0.929(2)	0.688(1)	0.239(2)	6.1(5)
C51	0.740(2)	0.629(1)	0.230(2)	5.6(5)
C52	0.782(2)	0.829(1)	0.244(2)	5.7(5)

a. B(iso) is defined as $4/3[a^2\beta_{11}+b^2\beta_{22}+c^2\beta_{33}+ab(\cos\gamma)\beta_{12}+ac(\cos\beta)\beta_{13}+bc(\cos\alpha)\beta_{23}]$.

Table 7·3. Positional Parameters and B_{eq} Values[a] for $(Ph_4P)_2[(CO)_4Mo(MoS_4)Mo(CO)_4]$ (7·3) (Standard Deviations in Parentheses)

atom	x	y	z	B_{eq}, Å^2
Mo1	0.10280(8)	0.26260(4)	0.04344(8)	0.90(3)
Mo2	0.35170(8)	0.25066(4)	0.01580(8)	0.95(3)
Mo3	-0.16046(8)	0.26130(4)	0.02152(8)	0.97(3)
S1	0.1599(2)	0.2309(1)	-0.1328(2)	1.3(1)
S2	0.2565(2)	0.2866(1)	0.1939(2)	1.5(1)
S3	-0.0149(2)	0.3418(1)	-0.0064(3)	1.5(4)
S4	0.0051(2)	0.1895(1)	0.1142(3)	1.6(1)
P1	0.7789(2)	0.0108(1)	0.6473(2)	1.1(1)
P2	0.2639(3)	0.4200(1)	0.5346(2)	1.7(1)
O1	0.5847(7)	0.2709(5)	0.2153(8)	3.9(4)
O2	0.4920(8)	0.2101(4)	-0.1971(8)	2.8(4)
O3	0.344(1)	0.3868(4)	-0.064(1)	4.9(5)
O4	0.3541(8)	0.1154(4)	0.0913(8)	3.3(4)
O5	-0.3214(7)	0.1580(4)	0.0763(8)	2.7(4)
O6	-0.3733(7)	0.3438(4)	-0.0980(7)	2.4(3)
O7	-0.1916(8)	0.2099(4)	-0.2563(7)	2.7(4)
O8	-0.1719(8)	0.3228(4)	0.2873(7)	2.8(4)
C1	0.9194(9)	0.0151(4)	0.7549(8)	0.9(4)
C2	0.960(1)	0.0708(5)	0.802(1)	1.6(4)
C3	1.067(1)	0.0744(5)	0.887(1)	1.9(5)
C4	1.133(1)	0.0241(5)	0.924(1)	1.7(4)
C5	1.093(1)	-0.0307(5)	0.876(1)	1.9(5)
C6	0.986(1)	-0.0350(5)	0.792(1)	1.7(4)
C7	0.655(1)	0.0143(5)	0.7287(8)	1.2(4)
C8	0.554(1)	-0.0194(4)	0.686(1)	1.4(4)
C9	0.458(1)	-0.0157(5)	0.746(1)	2.1(5)
C10	0.457(1)	0.0261(6)	0.843(1)	2.5(5)
C11	0.555(1)	0.0598(6)	0.882(1)	2.5(5)
C12	0.653(1)	0.0562(5)	0.826(1)	1.6(4)
C13	0.769(1)	0.0734(4)	0.5449(9)	1.3(4)
C14	0.865(1)	0.0872(5)	0.488(1)	2.3(5)

Table 7·3. (cont'd)

atom	x	y	z	B_{eq}, Å^2
C15	0.857(1)	0.1342(5)	0.407(1)	3.0(6)
C16	0.756(1)	0.1686(5)	0.385(1)	3.2(6)
C17	0.659(1)	0.1571(5)	0.441(1)	2.7(5)
C18	0.665(1)	0.1085(4)	0.522(1)	1.8(4)
C19	0.7714(9)	-0.0577(4)	0.5614(9)	0.9(4)
C20	0.756(1)	-0.1104(5)	0.622(1)	1.4(4)
C21	0.748(1)	-0.1640(5)	0.558(1)	2.0(5)
C22	0.756(1)	-0.1667(5)	0.432(1)	2.3(5)
C23	0.772(1)	-0.1149(5)	0.369(1)	2.1(5)
C24	0.781(1)	-0.0605(4)	0.434(1)	1.5(4)
C25	0.397(1)	0.3797(5)	0.515(1)	1.9(5)
C26	0.460(1)	0.3955(5)	0.422(1)	2.0(5)
C27	0.567(1)	0.3654(5)	0.416(1)	2.2(5)
C28	0.608(1)	0.3202(5)	0.498(1)	2.1(5)
C29	0.545(1)	0.3050(5)	0.589(1)	2.4(5)
C30	0.439(1)	0.3338(5)	0.597(1)	2.3(5)
C31	0.302(1)	0.4699(6)	0.669(1)	2.6(5)
C32	0.213(1)	0.5061(6)	0.706(1)	3.7(6)
C33	0.245(2)	0.5433(6)	0.809(1)	4.8(8)
C34	0.363(2)	0.5454(6)	0.871(1)	4.8(8)
C35	0.448(2)	0.5130(7)	0.832(1)	4.6(7)
C36	0.420(1)	0.4732(5)	0.730(1)	2.4(5)
C37	0.152(1)	0.3677(5)	0.557(1)	1.8(4)
C38	0.132(1)	0.3202(5)	0.470(1)	1.8(5)
C39	0.046(1)	0.2798(5)	0.479(1)	2.1(5)
C40	-0.020(1)	0.2855(6)	0.573(1)	2.6(5)
C41	0.001(1)	0.3306(7)	0.660(1)	2.9(6)
C42	0.087(1)	0.3713(5)	0.653(1)	2.3(5)
C43	0.216(1)	0.4643(4)	0.396(1)	1.7(4)
C44	0.255(1)	0.5215(6)	0.393(1)	3.2(6)
C45	0.230(1)	0.5554(6)	0.285(1)	3.2(6)

Table 7-3. (cont'd)

atom	x	y	z	B_{eq}, Å^2
C46	0.166(1)	0.5301(6)	0.179(1)	3.6(6)
C47	0.123(2)	0.4738(6)	0.181(1)	4.4(7)
C48	0.149(1)	0.4394(7)	0.287(1)	3.9(6)
C49	0.501(1)	0.2645(6)	0.139(1)	2.3(5)
C50	0.441(1)	0.2234(4)	-0.121(1)	1.2(4)
C51	0.346(1)	0.3382(5)	-0.037(1)	2.1(5)
C52	0.353(1)	0.1648(6)	0.066(1)	2.2(5)
C53	-0.265(1)	0.1969(4)	0.054(1)	1.1(4)
C54	-0.296(1)	0.3130(5)	-0.052(1)	1.5(4)
C55	-0.172(1)	0.2270(4)	-0.156(1)	1.4(4)
C56	-0.164(1)	0.3001(5)	0.195(1)	1.4(4)

a. B_{eq} is defined as $4/3[a^2\beta_{11}+b^2\beta_{22}+c^2\beta_{33}+ab(\cos\gamma)\beta_{12}+ac(\cos\beta)\beta_{13}+bc(\cos\alpha)\beta_{23}]$.

Table 7-4. Positional Parameters and B_{eq} Values[a] for $(Ph_4P)_2[(CO)_4W(WS_4)W(CO)_4]$ (7-4) (Standard Deviations in Parentheses)

atom	x	y	z	B_{eq}, Å^2
W1	0.1008(1)	0.26212(5)	0.0417(1)	2.94(5)
W2	0.3487(1)	0.25154(5)	0.0156(1)	2.91(6)
W3	-0.1605(1)	0.26054(5)	0.0204(1)	2.88(6)
S1	0.1594(6)	0.2328(3)	-0.1322(6)	3.1(3)
S2	0.2509(7)	0.2861(4)	0.1913(7)	4.2(4)
S3	-0.0177(7)	0.3403(3)	-0.0065(7)	3.8(4)
S4	0.0057(7)	0.1895(4)	0.1114(8)	4.4(4)
P1	0.7800(7)	0.0117(3)	0.6489(6)	3.2(4)
P2	0.2665(8)	0.4207(4)	0.5316(7)	4.2(4)
O1	0.581(2)	0.274(1)	0.208(2)	10(2)
O2	0.484(2)	0.2154(9)	-0.193(2)	5(1)
O3	0.339(3)	0.385(1)	-0.071(3)	11(2)
O4	0.356(2)	0.118(1)	0.090(2)	6(1)
O5	-0.319(2)	0.1575(9)	0.079(2)	5(1)
O6	-0.371(2)	0.346(1)	-0.095(2)	6(1)
O7	-0.190(2)	0.213(1)	-0.256(2)	6(1)
O8	-0.169(2)	0.3155(8)	0.287(2)	6(1)
C1	0.918(2)	0.017(1)	0.755(2)	2.3(5)
C2	0.963(2)	0.071(1)	0.805(3)	3.7(6)
C3	1.064(2)	0.076(1)	0.884(2)	3.6(6)
C4	1.132(3)	0.025(1)	0.917(3)	4.1(6)
C5	1.090(3)	-0.029(1)	0.866(3)	5.4(8)
C6	0.984(3)	-0.032(1)	0.786(3)	4.0(6)
C7	0.658(2)	0.016(1)	0.727(2)	3.0(6)
C8	0.561(3)	-0.017(1)	0.694(3)	4.2(7)
C9	0.462(3)	-0.012(1)	0.748(3)	4.7(7)
C10	0.462(3)	0.027(1)	0.842(3)	4.6(7)
C11	0.557(3)	0.061(1)	0.882(3)	5.0(7)
C12	0.656(2)	0.053(1)	0.824(3)	3.7(6)
C13	0.768(2)	0.074(1)	0.543(2)	3.4(6)
C14	0.856(3)	0.087(1)	0.491(3)	4.4(7)

Table 7-4. (cont'd)

atom	x	y	z	B_{eq}, Å^2
C15	0.848(4)	0.132(2)	0.408(4)	7(1)
C16	0.750(4)	0.169(2)	0.388(3)	7(1)
C17	0.654(3)	0.156(2)	0.439(3)	7(1)
C18	0.669(3)	0.102(2)	0.518(3)	6.1(8)
C19	0.771(2)	-0.055(1)	0.565(2)	2.3(5)
C20	0.756(2)	-0.108(1)	0.620(3)	3.9(6)
C21	0.745(3)	-0.160(1)	0.560(3)	4.9(7)
C22	0.754(3)	-0.163(2)	0.435(3)	5.8(8)
C23	0.771(2)	-0.113(1)	0.375(3)	4.0(6)
C24	0.777(3)	-0.058(1)	0.440(3)	4.4(7)
C25	0.399(3)	0.381(1)	0.517(3)	4.7(7)
C26	0.462(3)	0.394(2)	0.424(3)	6.1(9)
C27	0.565(3)	0.365(1)	0.417(3)	3.9(6)
C28	0.608(3)	0.321(2)	0.503(3)	6.0(8)
C29	0.539(3)	0.307(2)	0.589(3)	6.0(8)
C30	0.441(3)	0.334(1)	0.596(3)	4.5(7)
C31	0.302(3)	0.473(2)	0.670(3)	5.6(8)
C32	0.213(4)	0.507(2)	0.692(4)	9(1)
C33	0.251(4)	0.551(2)	0.799(4)	8(1)
C34	0.363(4)	0.545(2)	0.862(4)	8(1)
C35	0.450(4)	0.512(2)	0.836(4)	8(1)
C36	0.417(3)	0.473(2)	0.733(3)	6.2(9)
C37	0.156(3)	0.372(1)	0.561(3)	4.5(7)
C38	0.139(3)	0.321(1)	0.473(3)	4.1(6)
C39	0.050(3)	0.286(1)	0.483(3)	4.6(7)
C40	-0.016(3)	0.290(1)	0.575(3)	4.9(7)
C41	0.006(3)	0.337(2)	0.652(3)	5.4(8)
C42	0.093(3)	0.379(2)	0.651(3)	6.1(9)
C43	0.223(3)	0.465(1)	0.395(3)	4.3(7)
C44	0.259(3)	0.520(2)	0.394(3)	6.3(9)
C45	0.231(3)	0.555(2)	0.277(4)	7(1)

Table 7-4. (cont'd)

atom	x	y	z	B_{eq}, Å^2
C46	0.169(4)	0.532(2)	0.169(4)	10(1)
C47	0.126(4)	0.480(2)	0.178(4)	9(1)
C48	0.152(3)	0.440(2)	0.294(4)	7(1)
C49	0.484(3)	0.277(1)	0.129(3)	5.3(8)
C50	0.421(3)	0.224(2)	-0.123(3)	5.3(9)
C51	0.343(3)	0.339(2)	-0.034(3)	5.5(9)
C52	0.353(3)	0.170(1)	0.072(3)	3.8(6)
C53	-0.266(2)	0.195(1)	0.055(2)	3.3(6)
C54	-0.294(2)	0.312(1)	-0.048(2)	3.1(6)
C55	-0.173(2)	0.228(1)	-0.151(2)	2.0(5)
C56	-0.158(2)	0.300(1)	0.191(3)	3.4(6)

a. B_{eq} is defined as $4/3[a^2\beta_{11}+b^2\beta_{22}+c^2\beta_{33}+ab(\cos\gamma)\beta_{12}+ac(\cos\beta)\beta_{13}+bc(\cos\alpha)\beta_{23}]$.

Finally, all compounds were examined by X-ray powder diffraction for the purpose of phase characterization and identification. A Debye-Scherrer camera was employed to record the X-ray powder diffraction patterns. Ni-filtered Cu radiation was used. The crystals were ground to fine powder and packed into 0.5 mm glass capillaries which were sealed and mounted to the standard Debye-Scherrer powder camera which has a diameter of 114.6 mm (1 mm corresponds to 1 degree for 2θ). X-rays were generated by a Phillips Norelco XRG-5000 X-ray generator operating at 40 kV and 20 mA. Approximately, a six hour exposure time was used. Accurate d-spacings (Å) of each compound were calculated from the powder patterns recorded on a Phillips XRG-3000 computer controlled powder diffractometer[21]. To verify the homogeneities of the products, the d-spacings observed for the bulk materials were compared with the calculated d-spacings from the X-ray single-crystal structure analysis data[22]. Listings of calculated and observed d-spacings (Å) along with the observed relative diffraction intensities of these compounds are given in Tables 7·5–7·6.

Table 7·5. Calculated and Observed X-ray Powder Diffraction Patterns for $(Ph_4P)_2[(CO)_4Mo(MoS_4)]$ (7·1) and $(Ph_4P)_2[(CO)_4W(WS_4)]$ (7·2)

h k l	$d_{calc.}$ (Å)	$d_{obs.}$ (Å), I/I_{max} for (7·1)	$d_{obs.}$ (Å), I/I_{max} for (7·2)
1 0 0	11.23	11.47, 14	11.51, 22
0 0 1	10.95	10.91, 21	10.96, 26
1 1 0	10.71	10.49, 77	10.20, 45
0-1 1	9.98	9.66, 40	9.72, 32
-1 0 1	9.54	9.41, 23	9.36, 27
0 2 0	9.18	9.23, 16	9.16, 23
0 1 1	8.91	8.99, 45	8.91, 30
-1 1 0	8.74	8.77, 20	8.73, 19
1 2 0	8.05	8.06, 85	8.05, 100
-1-2 1	7.928	/	/
0-2 1	7.526	7.599, 73	7.543, 21
0 2 1	6.627	6.682, 27	6.613, 23
1 1 1	6.507	6.545, 16	6.511, 12
-2-1 1	6.109	6.216, 21	6.200, 25
-1-1 2	5.878	5.887, 83	5.865, 56
-1 0 2	5.705	5.713, 34	5.744, 31
0 3 1	5.071	5.133, 79	5.070, 52
-2-2 2	4.884	4.914, 100	4.903, 78
-2 0 2	4.770	4.781, 20	4.790, 43
1 4 0	4.630	4.653, 81	4.648, 40
0 4 0	4.588	/	4.580, 29
2 1 1	4.450	4.441, 28	4.488, 41
-1 2 2	4.380	4.309, 15	4.373, 23
-2-2 3	3.766	3.751, 23	3.778, 27
0-1 3	3.671	/	3.682, 18
-3 1 0	3.515	/	3.513, 19
2 0 2	3.405	3.423, 19	3.418, 15
-3 2 0	3.221	/	3.224, 22
-1-6 1	3.211	/	3.207, 20

Table 7·5 (cont'd)

h k l	$d_{calc.}$ (Å)	$d_{obs.}$ (Å), I/I_{max} for (7·1)	$d_{obs.}$ (Å), I/I_{max} for (7·2)
1-2 3	3.051	3.060, 11	3.057, 19
-4 0 1	2.961	2.906, 53	2.958, 12
3-2 1	2.910	/	2.914, 12
4 0 0	2.804	2.831, 53	2.815, 22
0 0 4	2.737	2.752, 26	2.726, 20
3-1 2	2.640	2.697, 9	2.648, 15
-4-2 4	2.501	2.507, 15	2.503, 15
1 1 4	2.436	2.427, 23	2.435, 12
-4 0 4	2.385	/	2.387, 17
-1-2 5	2.327	2.338, 18	2.320, 13
-1-4 5	2.219	2.221, 17	2.219, 15
-3 6 0	2.143	2.134, 13	2.147, 16
-4 1 5	2.009	2.001, 30	2.004, 22

Table 7·6. Calculated and Observed X-ray Powder Diffraction Patterns for $(Ph_4P)_2[(CO)_4Mo(MoS_4)Mo(CO)_4]$ (7·3) and $(Ph_4P)_2[(CO)_4W(WS_4)W(CO)_4]$ (7·4)

h k l	$d_{calc.}$ (Å)	$d_{obs.}$ (Å), I/I_{max} for (7·3)	$d_{obs.}$ (Å), I/I_{max} for (7·4)
0 2 0	11.30	11.61, 26	11.20, 77
0 0 1	10.67	10.90, 26	10.84, 40
0-2 1	7.80	7.92, 100	8.10, 100
0 2 1	7.71	/	7.73, 29
0 4 0	5.648	5.747, 30	5.743, 54
0 0 2	5.335	5.413, 33	5.536, 26
0-4 1	5.016	5.047, 37	5.022, 36
0 4 1	4.968	4.965, 46	4.942, 31
0-2 2	4.845	4.850, 27	/
0 2 2	4.802	/	4.796, 49
2 1 1	4.559	4.603, 23	4.601, 27
-2 3 0	4.469	4.472, 17	/
-2 1 2	4.205	4.216, 13	4.242, 10
0 6 0	3.765	3.778, 9	3.755, 13
0-6 1	3.564	3.578, 11	3.573, 10
0 2 3	3.381	3.389, 14	3.348, 12
-2 1 3	3.256	3.262, 16	3.246, 11
0-6 2	3.093	3.103, 10	3.073, 11
0 8 0	2.824	2.826, 11	2.888, 13
4 2 0	2.753	2.764, 8	2.758, 10
0-8 1	2.737	/	2.733, 9
4 0 1	2.609	2.604, 10	2.605, 9
0 2 4	2.589	2.593, 12	2.559, 13
0-8 2	2.508	/	2.484, 11
-4-1 3	2.439	2.405, 7	2.440, 13
4 4 1	2.385	/	2.379, 8
-4-6 1	2.309	2.313, 8	2.311, 10
-4 5 2	2.299	2.297, 8	2.254, 11

III. Results

1. Description of Crystal and Molecular Structures of the Compounds

(i). Structure of $(Ph_4P)_2[(CO)_4W(WS_4)]$ (7·2)

This compound is composed of non-interacting Ph_4P^+ cations and $[(CO)_4W(WS_4)]^{2-}$ cluster anions in the crystal lattice as shown in Figure 7·1. The latter has been isolated earlier as the Et_4N^+ salt and structurally characterized[9]. Figure 7·2 shows the structure of the current $[(CO)_4W(WS_4)]^{2-}$ anion that has been found as the Ph_4P^+ salt. It features a tetrahedral $[WS_4]^{2-}$ molecule acting as a bidentate ligand to another W metal which is further surrounded by four CO groups, resulting in octahedral coordination for this metal. Such a structural description naturally implies the assignment of two extreme formal oxidation states, 6+ and 0, to the same metal in two different fragments. This argument is partly supported by the tetrahedral geometry of the bridging $[WS_4]^{2-}$ ligand in the molecule. The cluster possesses C_{2v} symmetry, i.e. a C_2 running through two W atoms, a mirror containing two W metals, two bridging S atoms and two CO groups, and the second mirror being perpendicular to the first one. The bond distances of two bridging sulfur atoms to the tetrahedral metal at 2.244(5) and 2.221(5) Å are, as expected, longer than those of two terminal sulfur atoms to this metal at 2.158(5) and 2.155(5) Å. The latter are similar to that found in the parental tetrathiotungstate $(NH_4)_2[WS_4]$ (i.e. W-S=2.165 Å)[22]. The bond distances of two bridging sulfur atoms to the octahedral metal are 2.540(5) and 2.544(5) Å. The W···W distance is 3.031 Å. All these values are found comparable with those in the previously reported structure of the same anion[9]. Table 7·7 gives a comparison of some important bond distances and bond angles of the anion in two different compounds.

Table 7·7. Comparison of Geometric Data Between $(Ph_4P)_2[(CO)_4W(WS_4)]$ (7·2)[b] and $(Et_4N)_2[(CO)_4W(WS_4)]$[9][c]

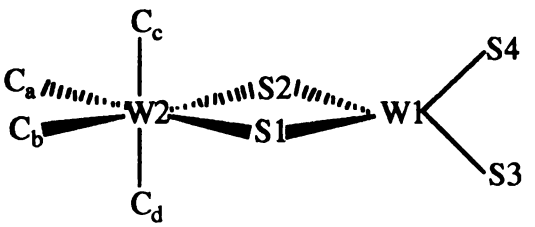
	Bond Distances (Å)	
	Ph_4P^+ salt	Et_4N^+ salt
W(1)-S(1)	2.244(5)	2.238(3)
W(1)-S(2)	2.221(5)	2.237(3)
W(1)-S(3)	2.158(5)	2.161(3)
W(1)-S(4)	2.155(5)	2.161(3)
W(2)-S(1)	2.540(5)	2.531(3)
W(2)-S(2)	2.544(5)	2.539(3)
W(2)-C_a	1.97(2)	1.91(1)
W(2)-C_b	1.99(2)	1.92(1)
W(2)-C_c	1.97(2)	2.03(1)
W(2)-C_d	2.04(2)	2.03(1)
W···W	3.031(1)	3.010(1)
	Bond Angles (deg)	
	Ph_4P^+ salt	Et_4N^+ salt
S(1)-W(1)-S(2)	110.5(2)	110.9(1)
S(1)-W(1)-S(3)	109.6(2)	108.6(1)
S(1)-W(1)-S(4)	109.6(2)	108.6(1)
S(2)-W(1)-S(3)	109.6(2)	109.2(1)
S(2)-W(1)-S(4)	108.7(2)	109.2(1)
S(3)-W(1)-S(4)	108.7(2)	110.4(2)
S(1)-W(2)-S(2)	92.4(2)	93.2(1)
S(1)-W(2)-C_c	92.5(6)	90.0(2)

Table 7·7. (cont'd)

	Bond Angles (deg)	
S(1)-W(2)-C_d	89.1(6)	90.0(2)
S(2)-W(2)-C_a	89.7(6)	90.5(5)
S(2)-W(2)-C_b	178.9(6)	177.9(3)
C_a-W(2)-C_b	89.2(8)	91.6(5)
C_a-W(2)-C_c	88.8(8)	90.0(2)
C_c-W(2)-C_d	178.3(8)	177.2(5)
W(1)-S(1)-W(2)	78.4(1)	78.4(1)
W(1)-S(2)-W(2)	78.7(1)	77.9(1)

b. The estimated standard deviations in the mean bond lengths and the mean bond angles are calculated by the equation $\sigma_l=\{\Sigma_n(l_n-l)^2/n(n-1)\}^{1/2}$, where l_n is the length (angle) of the *n*th bond, l the mean length (angle), and n the number of bonds.

c. Labeling scheme for this molecule is as following:



X-ray powder diffraction (XRD) studies of the $(Ph_4P)_2[(CO)_4Mo(MoS_4)]$ confirmed that this compound is isostructural to (7·2) (see Table 7·5).

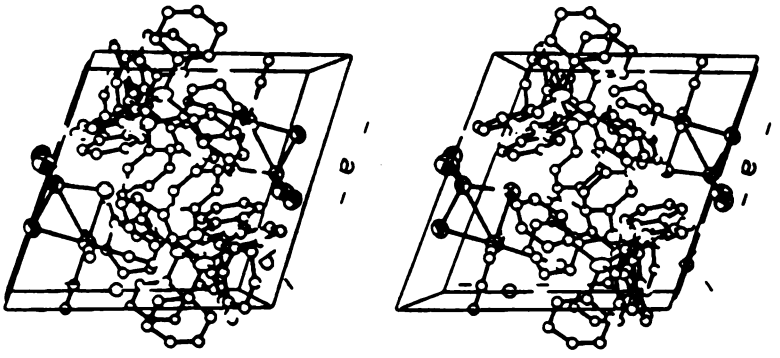


Figure 7-1. The Packing Diagram in the Unit Cell of $(Ph_4P)_2[(CO)_4W(WS_4)]$ (Stereoview)

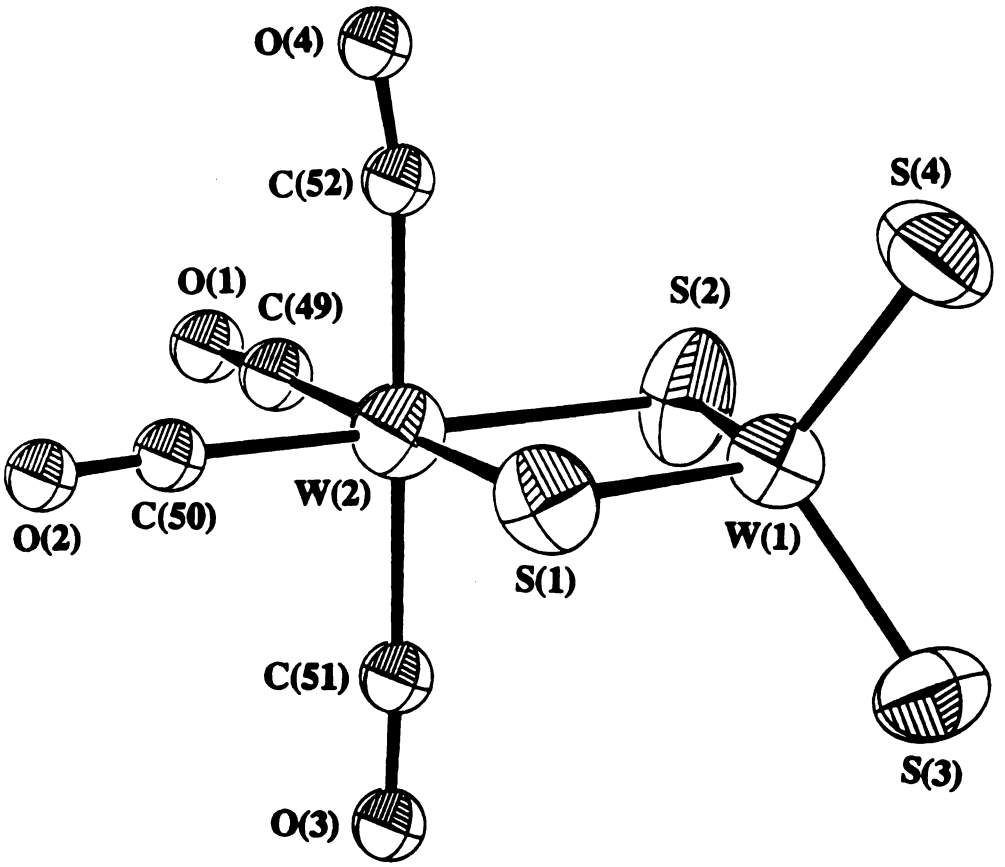


Figure 7·2. The Structure of the $[(CO)_4W(WS_4)]^{2-}$ Anion

(ii). Structure of $(Ph_4P)_2[(CO)_4Mo(MoS_4)Mo(CO)_4]$ (7·3) and $(Ph_4P)_2[(CO)_4W(WS_4)W(CO)_4]$ (7·4)

The structures of these two compounds, isotypical to each other, are hitherto unknown. The crystal lattice is made up of Ph_4P^+ cations and $[(CO)_4M(MS_4)M(CO)_4]^{2-}$ (M=Mo or W) anions as shown in Figure 7·3. The structure of the trinuclear cluster anion is depicted in Figure 7·4. This molecule contains a linear array of three metal centers, approaching an idealized D_{2d} symmetry with the principal axis running through three metal atoms. Again, if the molecule is viewed as two $M(CO)_4$ fragments bridged by a tetrathiometalate $[MS_4]^{2-}$, the two terminal M atoms would have a formal oxidation state 0, and the central M atom a formal oxidation state 6+. The bond distances of the bridging sulfur atoms to the tetrahedral tungsten average 2.211 Å in (7·4), similar to those found in the above W dimer, while their counterparts in the Mo compound average 2.228 Å, are longer than that found in $(NH_4)_2[MoS_4]$ (i.e. 2.178 Å)[23]. The M–M distances are 2.921(2) and 2.971(2) Å in the W trimer, and 2.918(2) and 2.972(2) Å in Mo trimer. The differences in bond distances and bond angles found in the Mo compound and its W analogue are very small. The important bond distances and bond angles for the two compounds are given in Table 7·8.

Table 7·8. Geometric Data of $(Ph_4P)_2[(CO)_4Mo(MoS_4)Mo(CO)_4]$ (7·3) and $(Ph_4P)_2[(CO)_4W(WS_4)W(CO)_4]$ (7·4)[b]

	Bond Distances (Å)	
	Mo compound	W compound
M(1)-S(1)	2.226(3)	2.209(7)
M(1)-S(2)	2.230(3)	2.209(8)
M(1)-S(3)	2.227(3)	2.212(7)

Table 7·8. (cont'd)

	Bond Distances (Å)	
M(1)-S(4)	2.228(3)	2.214(8)
$M_{central}$-S(mean)	2.228	2.211
M(2)-S(1)	2.509(3)	2.490(7)
M(2)-S(2)	2.496(3)	2.497(7)
M(3)-S(3)	2.540(3)	2.525(8)
M(3)-S(4)	2.539(3)	2.528(8)
$M_{terminal}$-S(mean)	2.521	2.510
M(1)···M(2)	2.918(2)	2.921(2)
M(1)···M(3)	2.972(2)	2.971(2)
M(2)-C(49)	1.99(1)	1.89(4)
M(2)-C(50)	2.03(1)	1.94(3)
M(2)-C(51)	2.06(1)	2.05(4)
M(2)-C(52)	2.02(1)	1.94(3)
M(3)-C(53)	1.97(1)	2.02(3)
M(3)-C(54)	1.98(1)	1.94(3)
M(3)-C(55)	2.03(1)	1.97(2)
M(3)-C(56)	2.07(1)	2.05(3)
	Bond Angles (deg)	
	Mo compound	W compound
S(1)-M(1)-S(2)	112.5(1)	112.2(3)
S(1)-M(1)-S(3)	106.8(1)	106.9(3)
S(1)-M(1)-S(4)	108.1(1)	109.3(3)

Table 7·8. (cont'd)

Bond Angles (deg)		
S(2)-M(1)-S(3)	110.0(1)	109.6(3)
S(2)-M(1)-S(4)	108.0(1)	108.0(3)
S(3)-M(1)-S(4)	111.4(1)	110.9(3)
S(1)-M(2)-S(2)	95.56(9)	94.6(2)
S(3)-M(3)-S(4)	92.85(9)	92.3(2)
S(1)-M(2)-C(50)	88.8(3)	84(1)
S(1)-M(2)-C(52)	87.7(3)	90.0(9)
S(2)-M(2)-C(49)	82.9(3)	81(1)
S(2)-M(2)-C(51)	85.9(3)	86(1)
S(3)-M(3)-C(54)	90.6(3)	90.7(8)
S(3)-M(3)-C(56)	86.1(3)	84.0(8)
S(4)-M(3)-C(53)	83.7(3)	84.0(8)
S(4)-M(3)-C(55)	93.3(3)	93.3(7)
M(1)-S(1)-M(2)	75.83(8)	76.6(2)
M(1)-S(2)-M(2)	76.03(8)	76.5(2)
M(1)-S(3)-M(3)	76.81(9)	77.4(2)
M(1)-S(4)-M(3)	76.84(9)	77.3(2)
M(2)-M(1)-M(3)	168.24(4)	168.81(5)

b. The estimated standard deviations in the mean bond lengths and the mean bond angles are calculated by the equation $\sigma_l=\{\Sigma_n(l_n-l)^2/n(n-1)\}^{1/2}$, where l_n is the length (angle) of the *n*th bond, l the mean length (angle), and n the number of bonds.

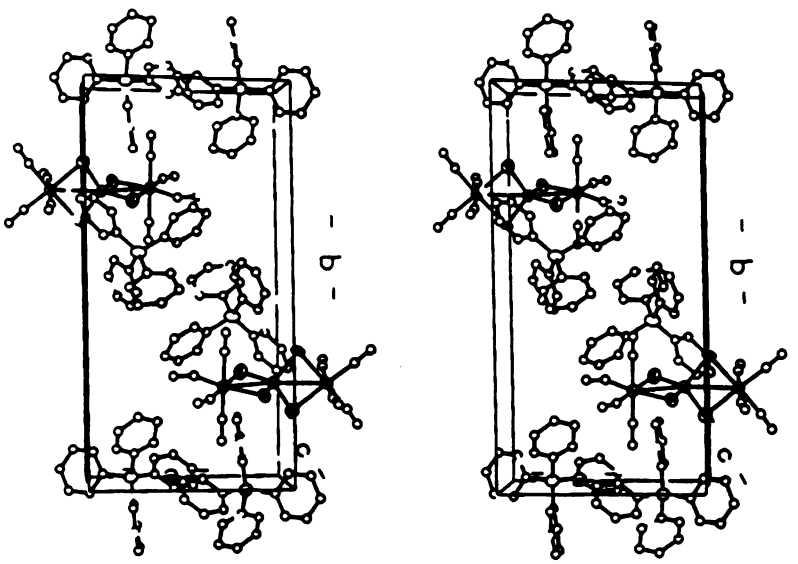


Figure 7·3. The Packing Diagram in the Unit Cell of $(Ph_4P)_2[(CO)_4M(MS_4)M(CO)_4]$ (M=Mo and W) (Stereoview)

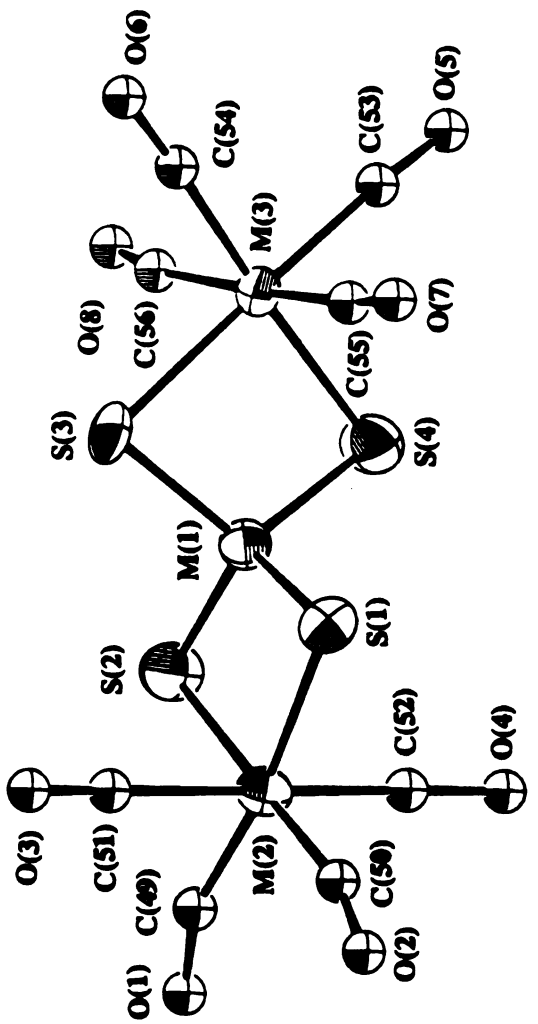


Figure 7-4. The Structure of the $[(CO)_4M(MS_4)M(CO)_4]^{2-}$ (M=Mo and W) Anions

2. Spectroscopic Studies

Figure 7·5 shows the solid-state IR spectra of the dinuclear compounds in the CO region. Each shows four well-resolved peaks as expected for a *cis*-$ML_2(CO)_4$ type molecule. The two spectra are similar, and almost superimposable. The spectra of two trinuclear compounds have a similar pattern to those of the dimers, as shown in Figure 7·6. However, three peaks in the lower energy region overlap with each other, resulting in poorly resolved absorption bands. This is because two $MS_2(CO)_4$ fragments in the trimers are crystallographically different. In the metal-sulfur stretching region, the trimers show a single absorption as to their parental $[MS_4]^{2-}$ in the same region (Figure 7·7), while the dimers have two absorptions (Figure 7·8). The latter are further split into two doublets for W compound. This is a clear indication of the reduced symmetry of the $[MS_4]^{2-}$ ligand (D_{2d} *vs.* C_{2v}) in the dimers.

The UV/vis spectra of all compounds in CH_3CN show characteristic absorptions as shown in Figures 7·9 and 7·10. Table 7·9 compares the electronic spectral data of the current four compounds with those of the previously reported compounds in this family and the free $[MS_4]^{2-}$ ligands. The two bands in the high energy region, 360 and 460 nm for Mo dimer, 340 and 408 nm for W dimer, 332(sh) and 462 nm for Mo trimer, and 330(sh) and 431 nm for W trimer, originate from ligand to metal charge transfer (LMCT) within the $[MS_4]^{2-}$ ligands. The assignment of $[MS_4]^{2-}$ absorption bands has been extensively discussed in the literature[11]. Because of the further coordination of the S atoms to the other metal centers, these bands show significant purterbation in energies. Finally, the low energy band in each spectrum, 574 nm for Mo dimer, 479 nm for W dimer, 696 nm for Mo trimer, and 566 nm for W trimer, can be tentatively assigned to the $M^0/M^{6+}\text{->}M^{1+}/M^{5+}$ valence charge transfer absorption[13].

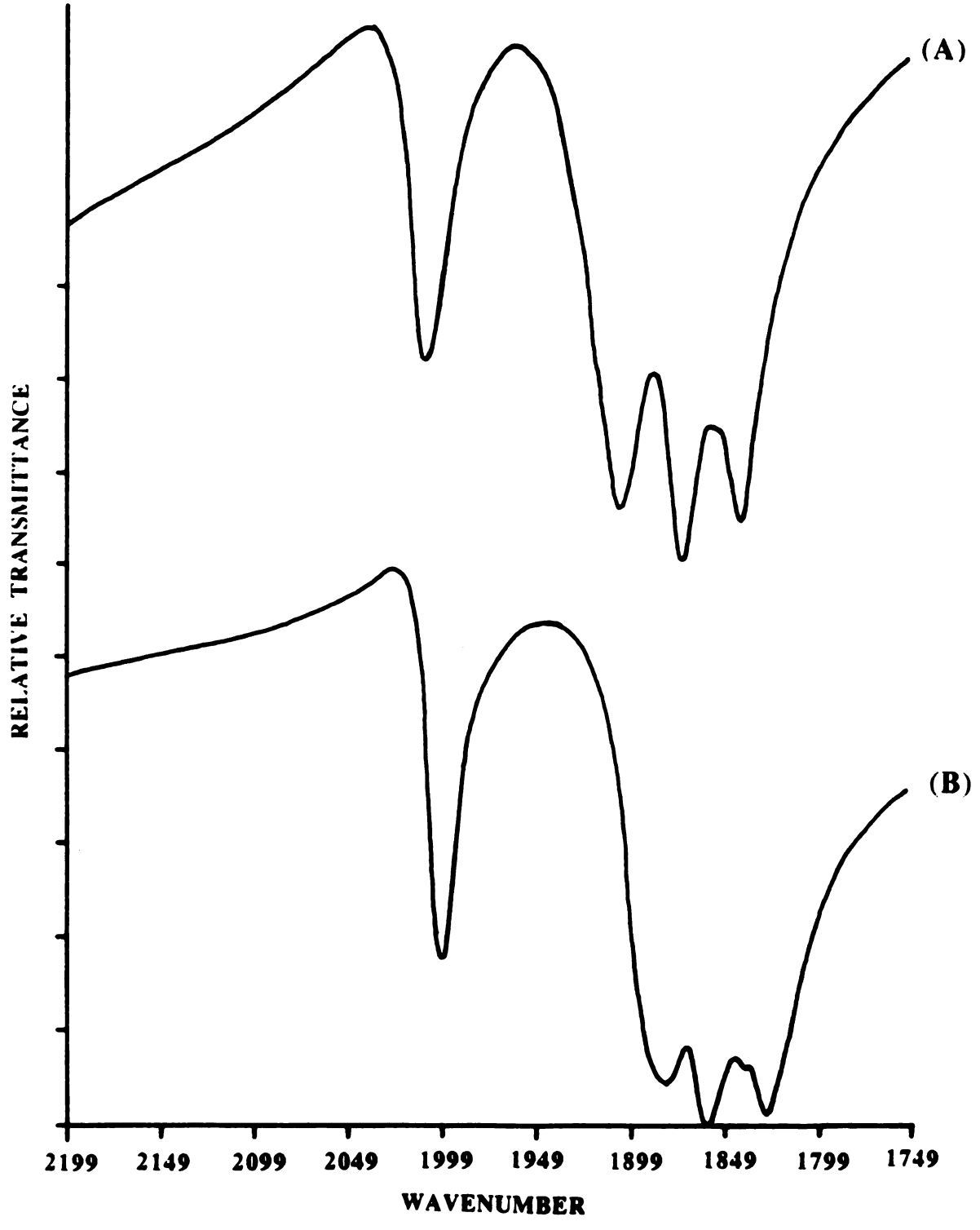


Figure 7·5. The Solid-State IR Spectra in the CO Region for (A) $(Ph_4P)_2[(CO)_4Mo(MoS_4)]$ and (B) $(Ph_4P)_2[(CO)_4W(WS_4)]$

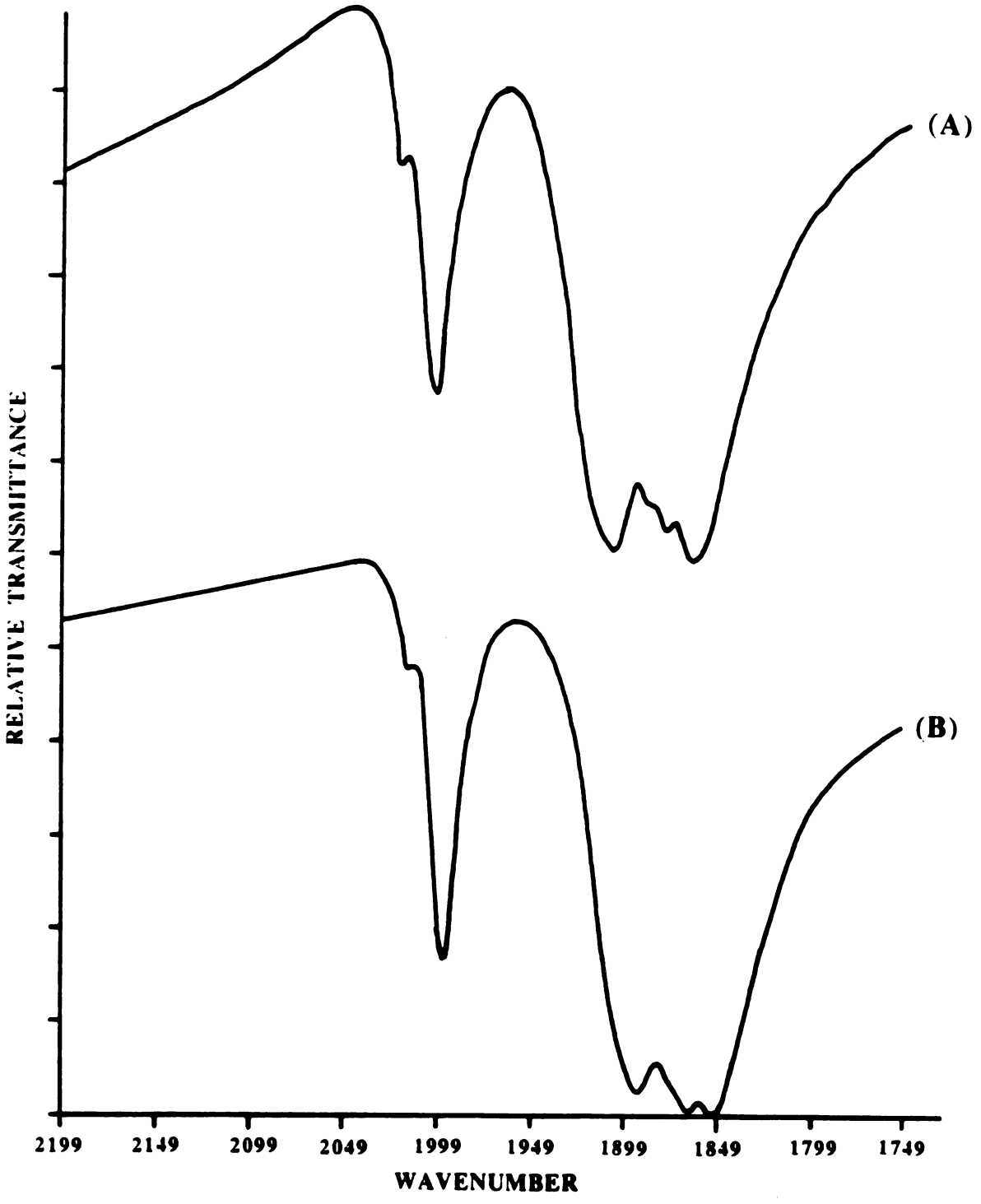


Figure 7-6. The Solid-StateIR Spectra in the CO Region for (A) $(Ph_4P)_2[(CO)_4Mo(MoS_4)Mo(CO)_4]$ and (B) $(Ph_4P)_2[(CO)_4W(WS_4)W(CO)_4]$

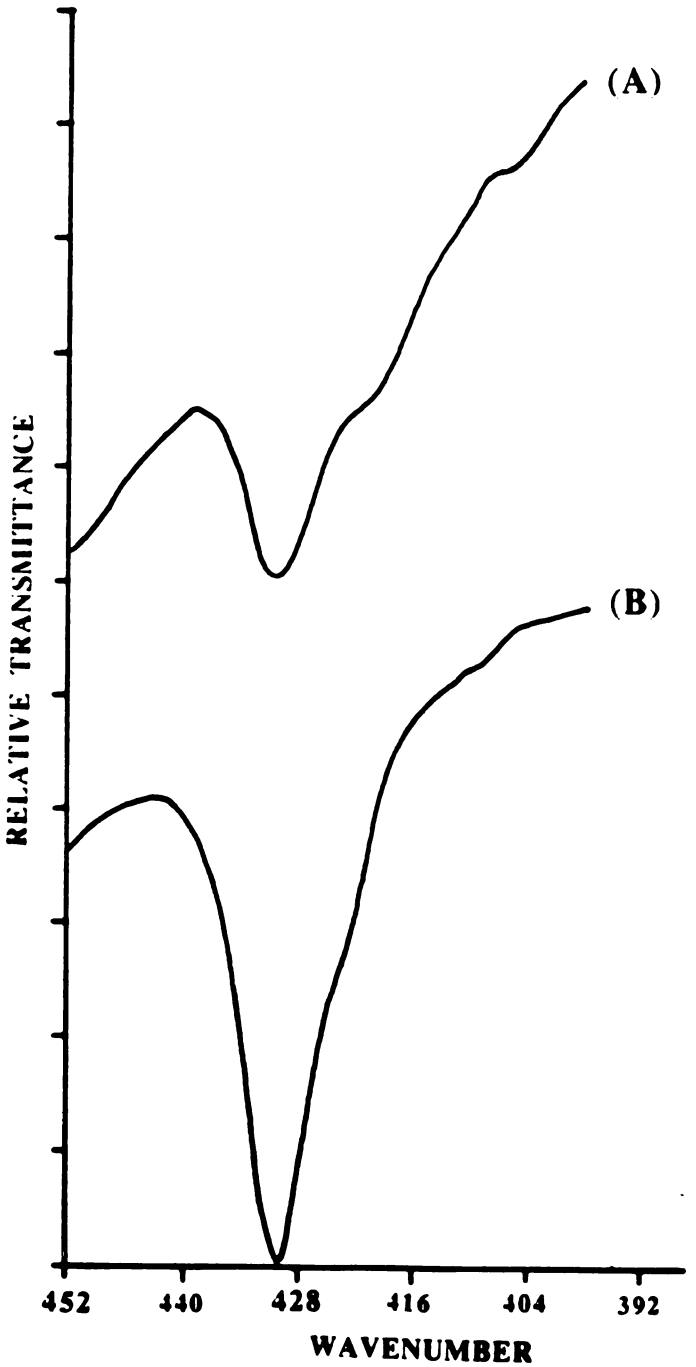


Figure 7·7. The Solid-State Far IR Spectra of (A) $(Ph_4P)_2[(CO)_4Mo(MoS_4)Mo(CO)_4]$ and (B) $(Ph_4P)_2[(CO)_4W(WS_4)W(CO)_4]$



Figure 7·8. The Solid-State Far IR Spectra of (A) $(Ph_4P)_2[(CO)_4Mo(MoS_4)]$ and (B) $(Ph_4P)_2[(CO)_4W(WS_4)]$

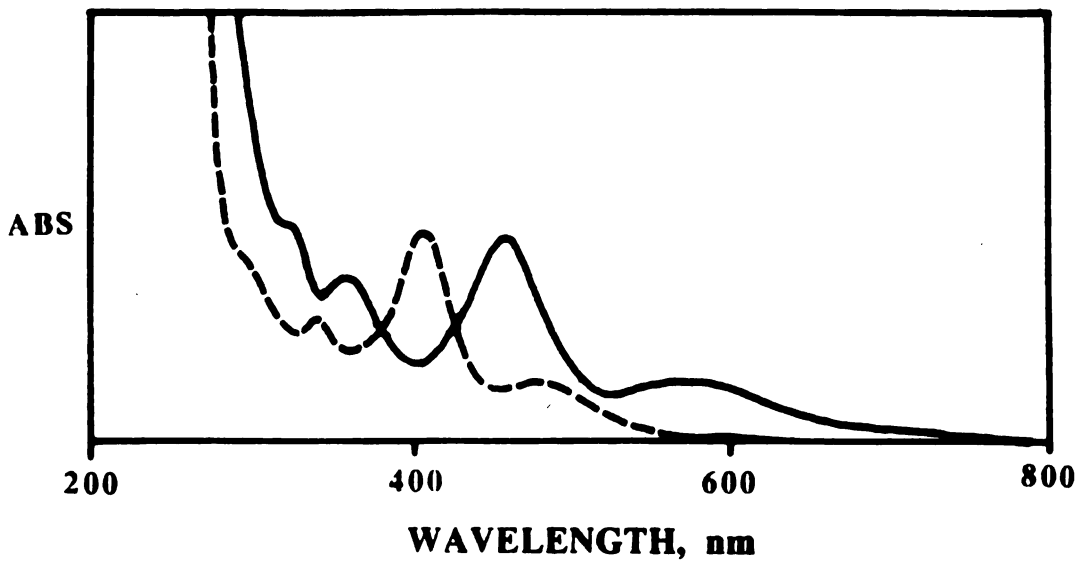


Figure 7·9. The UV/vis Spectra of (—) $(Ph_4P)_2[(CO)_4Mo(MoS_4)]$ and (---) $(Ph_4P)_2[(CO)_4W(WS_4)]$ in CH_3CN

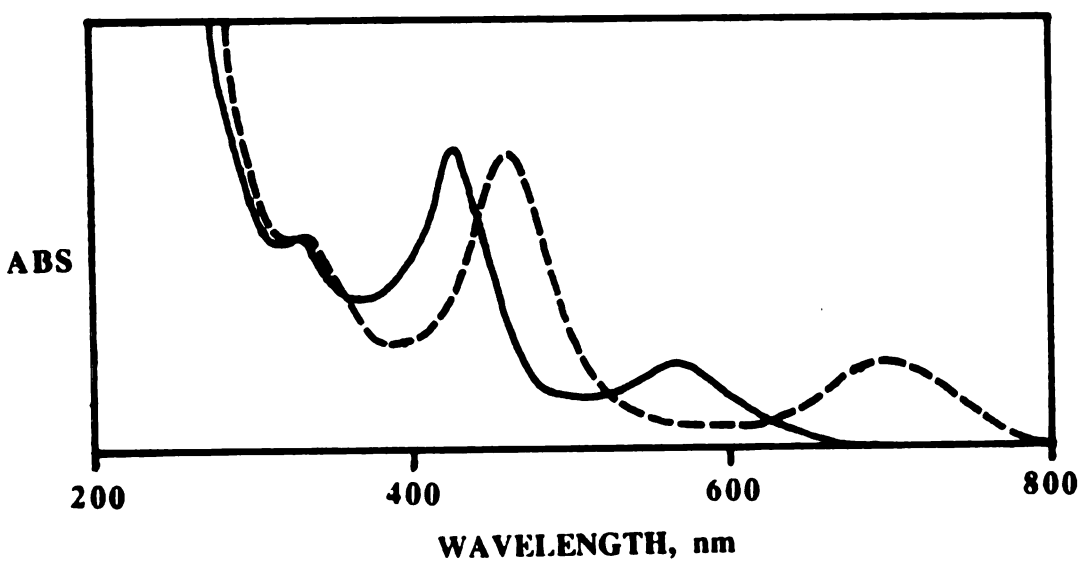


Figure 7·10. The UV/vis Spectra of (—) $(Ph_4P)_2[(CO)_4Mo(MoS_4)Mo(CO)_4]$ and (—) $(Ph_4P)_2[(CO)_4W(WS_4)W(CO)_4]$ in CH_3CN

Table 7·9 Electronic Spectral Data for $[\{M(CO)_4\}_n(MS_4)]^{2-}$ (M=Mo, W; n=0, 1, 2)[a]

compound	λ_{max}, nm (ε, $M \cdot cm^{-1}$)	reference
$(Ph_4P)_2[(CO)_4Mo(MoS_4)]$	324(sh, $11.1x10^3$), 360($8.37x10^3$), 460($10.4x10^3$), 574($3.20x10^3$)	this work
$(Ph_4P)_2[(CO)_4W(WS_4)]$	293(sh, $14.0x10^3$), 340($9.09x10^3$), 408($16.0x10^3$), 479($4.52x10^3$)	this work
$(Ph_4P)_2[(CO)_8Mo_2(MoS_4)]$	332(sh, $11.7x10^3$), 462($15.9x10^3$), 696($4.63x10^3$)	this work
$(Ph_4P)_2[(CO)_8W_2(WS_4)]$	330(sh, $14.6x10^3$), 431($20.2x10^3$), 566 ($5.70x10^3$)	this work
$(Et_4N)_2[(CO)_4Mo(MoS_4)]$	360($10.00x10^3$), 460($8.8x10^3$), 565($3.16x10^3$)	[7]
$(Et_4N)_2[(CO)_4Mo(WS_4)]$	405($8.86x10^3$), 460($3.74x10^3$)	[7]
$(Et_4N)_2[(CO)_8Mo_2(MoS_4)]$	375(sh), 455($19.0x10^3$), 675($5.38x10^3$)	[7]
$(Et_4N)_2[(CO)_8Mo_2(WS_4)]$	426($16.5x10^3$), 545($5.22x10^3$)	[7]
$(Ph_4P)_2[MoS_4]$	323($2.53x10^4$), 476($1.68x10^4$)	this work
$(Ph_4P)_2[WS_4]$	282($2.67x10^4$), 400($1.87x10^4$)	this work

a. in CH_3CN

Although the IR and UV/vis spectra of these clusters show certain similarities to each other, they are characteristic of the compound itself, namely the spectrum patterns represent the cluster structure while the peak energies depend on the metal centers. Thus, they can be used for diagnostic purposes.

3. Thermal Decomposition

Figure 7·11 shows the TGA diagrams of the four compounds in the temperature range of 25 to 800 °C. None of the compounds is found to undergo a well defined thermal decomposition that results in the loss of all the organic components. For instance, the observed weight loss of 57.2% up to 560 °C for $(Ph_4P)_2[(CO)_4Mo(MoS_4)]$ is less than that calculated for the loss of 2 Ph_4P^+ cations plus 4 CO groups (71.2%), or even less than that of 2 Ph_4P^+ cations only (61.1%). A similar behavior is exhibited by $(Ph_4P)_2[(CO)_4W(WS_4)]$. The expected weight loss for 2 Ph_4P^+ cations plus 4 CO groups, or for 2 Ph_4P^+ cations only is 61.4% and 52.7%, respectively. However, *c.a.*41.9% weight loss is observed up to 355 °C in the TGA diagram of $(Ph_4P)_2[(CO)_4W(WS_4)]$, and the compound is still losing weight beyond 800 °C. The calculated weight loss for 2 Ph_4P^+ cations plus 8 CO groups is 68.4% for $(Ph_4P)_2[(CO)_4Mo(MoS_4)Mo(CO)_4]$, and 57.0% for $(Ph_4P)_2[(CO)_4W(WS_4)W(CO)_4]$. The observed weight loss is 62% for $(Ph_4P)_2[(CO)_4Mo(MoS_4)Mo(CO)_4]$ up to 555 °C, and 44% for $(Ph_4P)_2[(CO)_4W(WS_4)W(CO)_4]$ up to 536 °C. These results indicate that carbon is retained in the residual products, perhaps forming Mo and W carbide phases.

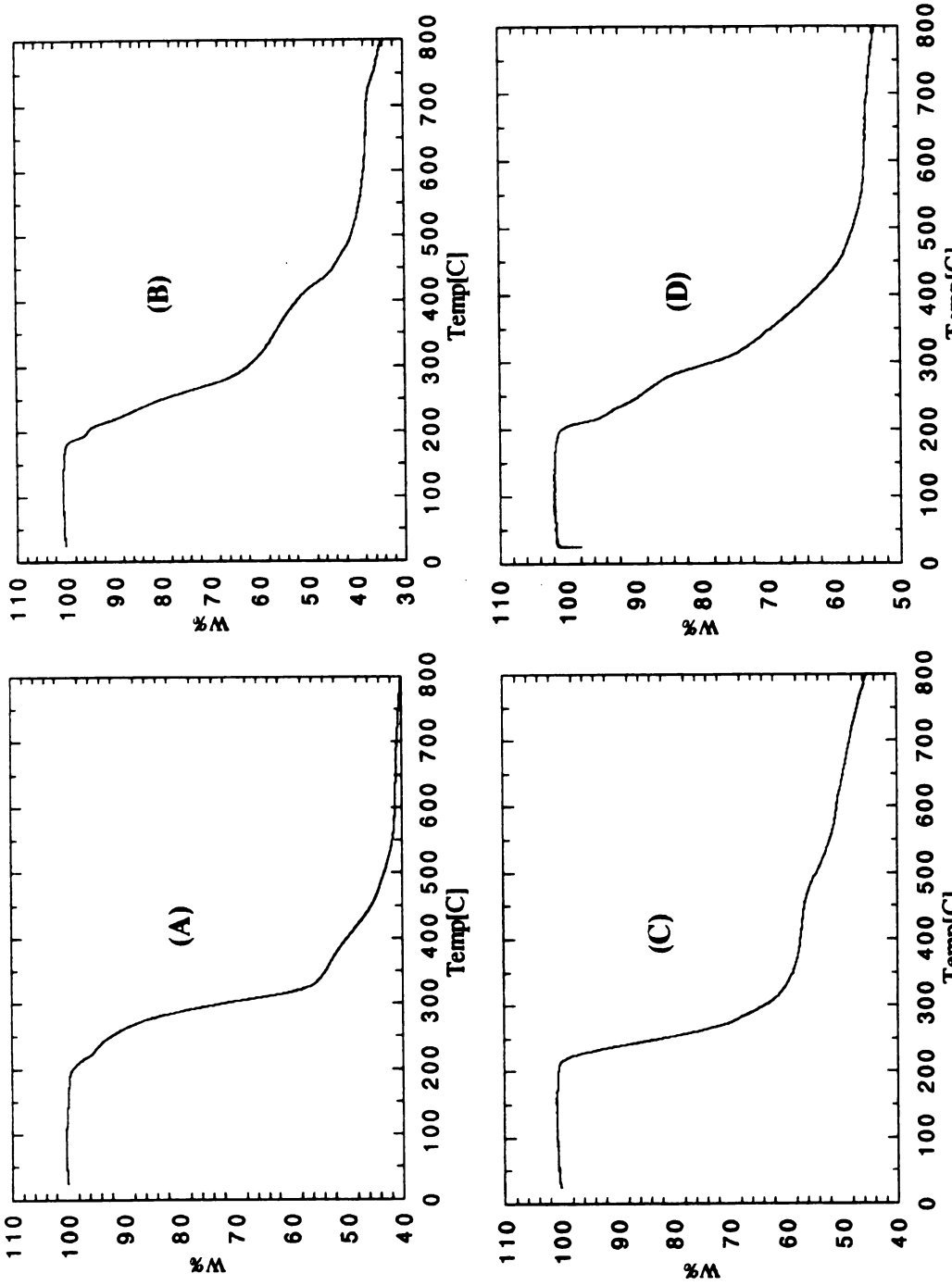


Figure 7·11. The TGA diagrams of (A) $(Ph_4P)_2[(CO)_4Mo(MoS_4)]$, (B) $(Ph_4P)_2[(CO)_4W(WS_4)]$, (C) $(Ph_4P)_2[(CO)_4Mo(MoS_4)Mo(CO)_4]$ and (D) $(Ph_4P)_2[(CO)_4W(WS_4)W(CO)_4]$

IV. Discussion

Four mixed valence clusters of the type $[\{M(CO)_4\}_n(MS_4)]^{2-}$ (M=Mo, W; n=1, 2) have been prepared from the direct reactions of $M(CO)_6$ (M=Mo, W) with Na_2S_2 in a one-step fashion under superheated MeOH conditions. Balanced equations are shown below:

$$2M(CO)_6+2Na_2S_2+2Ph_4PCl \xrightarrow[\text{sealed tube}]{\text{MeOH, 80 °C}} (Ph_4P)_2[(CO)_4M(MS_4)]+2NaCl+8CO+2Na_2S \quad \text{eq.(7·1)}$$

$$3M(CO)_6+3Na_2S_2+2Ph_4PCl \xrightarrow[\text{sealed tube}]{\text{MeOH, 80 °C}} (Ph_4P)_2[(CO)_4M(MS_4)M(CO)_4]+2NaCl+10CO+2Na_2S \quad \text{eq.(7·2)}$$

M=Mo and W

Pure single crystals of each compound can be obtained by the proper control of molar ratios of the reactants and reaction times. In the preparations of the two trimers, insufficient heating time (i.e at least 9 h for the Mo compound and 20 h for the W compound) often resulted in a mixture of dimer and trimer. Likewise, prolonged heating (up to 6 h) on the preparation of the Mo dimer according to eq (7·1) also afforded a mixture of the two. However, longer heating time seems to have lesser effect on the preparation of the W dimer. The product remained pure event after 30 h heating.

In the previously reported synthetic routes, the metal centers at the low oxidation state in the di- or trinuclear clusters were introduced by reacting $[MS_4]^{2-}$ (M=Mo or W) with diethyl dithiocarbomato carbonyl complexes $[(CO)_4M(S_2CNEt_2)]^-$[8-9], or with norbornadiene carbonyl complexes $[(CO)_4M(C_7H_8)]$[7]. In an attempt at preparing these clusters from conventional solution method, we reacted $[MS_4]^{2-}$ with $M(CO)_6$ in CH_3CN at elevated temperature (~80 °C). The reactions, monitored by UV/vis spectroscopy, gave no evidence for their formation. The products isolated from the reactions were exclusively $[MS_4]^{2-}$. This observation is consistent with the fact that reaction of $M(CO)_6$ with K_2S_4 (or K_2Se_4) in DMF solution gave clean $[MS_4]^{2-}$ in quantitative yield[1, 4]. The

stabilization of the clusters reported here is mainly due to the fact that they are removed from solution as soon as they form, since such compounds are insoluble in MeOH.

Conceptually, the above one-step synthetic reactions under solvothermal conditions requires an uneven attack of disulfide on metal carbonyl molecules in the same system: some carbonyl molecules are oxidized to its maximum oxidation state of +6 with loss of all CO groups, others remain intact in their state 0 while two CO groups from each molecule are displaced. Thus, they represent reactive intermediates in the complete oxidative decarbonylation reaction reported by Kolis and co-workers, see equation (7·3).

$$M(CO)_6 + S_x^{2-} \xrightarrow{DMF} [MS_4]^{2-} + CO \quad \text{eq.(7·3)}$$

It is worthwhile to note that replacement of K_2S_4 in place of Na_2S_2 for all preparations gave the same products, but a small amount of $(Ph_4P)_2[MS_4]$ were always present.

The X-ray diffraction studies have firmly established the identities of the compounds. All structures are based on the coordination of $[MS_4]^{2-}$ ligands to $M(CO)_4$ fragments, resulting in formally mixed valence systems. It should be noted that the metal–metal distances in both dinuclear and trinuclear clusters are approaching normal metal–metal single bonds. The M–M distances of some complexes containing $[M(\mu\text{-}S)_2M]$ (M=Mo, W) moieties with single M–M bond, or even multiple M–M bonds are in the vicinity of 2.80 Å for Mo–Mo[24-25], and 2.90 Å for W–W[26-27]. However, we believe that the metal–metal distances in the current clusters are the consequence of constraints caused by the bridging S^{2-} ligands, not necessarily imposed by bonding necessity. On the other hand, some electron back transfer from M^0 to M^{6+} may be expected from the strong acceptor properties of the $[MS_4]^{2-}$ ligands[28]. The observed low-energy transition,

attributable to the valent charge transfer, in their electronic spectra seems to support this argument[13].

In summary, despite the intensive studies of using tetrathiometalates as molecular ligands to multinuclear complexes[11-14], compounds with $[MS_4]^{2-}$ coordinated to the organometallic fragments remain relatively rare[29]. Arguments have been advanced that organometallic compounds containing metal centers in different oxidation states may display unusual catalytic properties[28b]. Given the importance of these molecular ligands in bio-inorganic chemistry, the study of tetrathiometalate coordination chemistry will remain a prominent subject. Recently, ammonium tetrathiomolybdate and ammonium tetrathiotungstate have been commercialized as reagents[30]. The relevant question to us at this stage seems to be whether hydro(solvo)thermal method can also create some synthetic excitement in this field. For example, is such a method capable of providing a new entry to novel heteronuclear metal clusters containing $[MS_4]^{2-}$ units? The answer to this question must await further exploration[31].

REFERENCES

1. J. W. Kolis, *Coord. Chem. Rev.*, 105(1990), 195-219.

2. W. A. Flomer, S. C. O'Neal, J. W. Kolis, D. Jeter and A. W. Cordes, *Inorg. Chem.*, 27(1988), 969-973.

3. L. C. Roof, W. T. Pennington and J. W. Kolis, *J. Am. Chem. Soc.*, 112(1990), 8172-8174.

4. S. C. O'Neal.and J. W. Kolis, *J. Am. Chem. Soc.*, 110(1988), 1971-1973.

5. L. A. Roof, W. T. Pennington and J. W. Kolis, *Inorg. Chem.*, 31(1992), 2056-2064.

6. S. C. O'Neal.and J. W. Kolis, *Inorg. Chem.*, 28(1989), 2780-2783.

7. L. D. Rosenhein and J. W. McDonald, *Inorg. Chem.*, 26(1987), 3414-3416.

8. B. Zhuang, P. Yu, L. Huang and J. Lu, *Inorg. Chim. Acta* , 162(1989), 121-126.

9. B. Zhuang, P. Yu, L. Huang, L. He and J. Lu, *Inorg. Chim. Acta,* 177(1990), 239-246.

10. See chapters 5 & 6.

11. (a) A. Müller, E. Diemann and C. K. Jorgensen, *Struct. Bonding,* 14(1973), 23-47. (b) E. Diemann and A. Müller, *Coord. Chem. Rev.*, 10(1973), 79-122. (c) A. Müller, E. Diemann, R. Jostes and H. Bögge, *Angew. Chem. Int. Ed. Engl.*, 20(1981), 934-955.

12. (a) A. Müller, R. Jostes, V. Flemming and R. Potthast, *Inorg. Chim. Acta*, 44(1980), L33-L35. (b) A. Müller, W. Hellmann, J. Schneider, U. Schimanski, U. Demmer, A. Trautwein and U. Bender, *Inorg. Chim. Acta*, 65(1982), L41-L42. (c) A. Müller, W. Hellmann, U. Schimanski, R. Jostes and W. E. Newton, *Z. Naturforsch.*, 38B(1983), 528-529.

13. D. Coucouvanis, *Acc. Chem. Res.*, 14(1981), 201-209.

14. (a) P. Stremple, N. C. Baenziger, D. Coucouvanis, *J. Am. Chem. Soc.*, 103(1981), 4601-4603. (b) D. Coucouvanis, E. D. Simhon, P. Stremple, M. Ryan, D. Swenson, N. C. Baenziger, A. Simopoulos, V. Papaefthymiou, A. Kostikas and V. Petrouleas, *Inorg. Chem.*, 23(1984), 741-749. (c) D. Coucouvanis and A. Hadjikyriacou, *Inorg. Chem.*, 26(1987), 1-2.

15. D. D. Perrin, W. L. F. Armarego and D. R. Perrin, *Purification of Laboratory Chemicals,* 2nd Ed., Pergamon Press, Oxford UK, 1980.

16. See chapter 2.

17. *MSC/AFC Diffractometer Control Software,* Molecular Structure Corporation, The Woodlands, Texas.

18. G. M. Sheldrick in *Crystallographic Computing,* G. M. Sheldrick, C. Kruger, and R. Doddard, Oxford University Press, 1985, p.175-189.

19. N. Walker and D. Stuart, *Acta Crystallogr.*, 39A(1983), 158-166.

20. *TEXSAN: Single Crystal Structure Analysis Software*, Version 5.0, Molecular Structure Corporation, The Woodlands, Texas.

21. H. P. Klug and L. E. Alexander, *X-ray Diffraction Procedures for Polycrystalline and Amorphous Materials,* John Wiley and Sons, New York, 1974.

22. D. K. Smith, M. C. Nichols and M. E. Zolensky, *POWD10: A Fortran IV Program for Calculating X-ray Powder Diffration Patterns,* Version 10, Pennsylvania State University, 1983.

22. K. Sasvari, *Acta Crystallogr.,* 16(1963), 719-724.

23. P. J. Lapasset, N. Chezeau and P. Belougne, *Acta Crystallogr.,* 32B(1976), 3087-3088.

24. (a) G. Bunzey, J. H. Enemark, J. K. Howie and D. T. Sawyer, *J. Am. Chem. Soc.,* 99(1977), 4168-4169. (b) G. Bunzey and J. H. Enemark, *Inorg. Chem.,* 17(1978), 682-688. (c) J. T. Huneke and J. H. Enemark, *Inorg. Chem.,* 17(1978), 3698-3699.

25. (a) A. Müller, W. O. Nolte and B. Krebs, *Angew. Chem. Int. Ed. Engl.,* 17(1978), 279-279. (b) A. Müller, W. O. Nolte and B. Krebs, *Inorg. Chem.,* 19(1980), 2835-2836. (c) W. Clegg, G. Christou, C. D. Garner and G. M. Sheldrick, *Inorg. Chem.,* 20(1981), 1562-1566. (d) W.-H. Pan, M. A. Harmer, T. R. Halbert and E. I. Stiefel, *J. Am. Chem. Soc.,* 106(1984), 459-460.

26. (a) A. Müller, M. Römer, C. Römer, U. Reinsch-Vogell, H. Bögge and U. Schimanski, *Monatsch. Chem.,* 116(1985), 711-717. (b) A. Müller, H. Bögge, E. Krickemeyer, G. Henkel and B. Krebs, *Z. Naturforsch.,* 37B(1982), 1014-1019. (c) S. A. Cohen and E. I. Stiefel, *Inorg. Chem.,* 24(1985), 4657-4662.

27. (a)S. Bhadur and J. A. Ibers, *Inorg. Chem.*, 25(1986), 3-4. (ab) R. W. M. Wardle, S. Bhaduri, C.-N. Chau and J. A. Ibers, *Inorg. Chem.*, 27(1988), 1747-1755.

28. (a) K. E. Howard, T. B. Rauchfuss and S. R. Wilson, *Inorg. Chem.*, 27(1988), 1710-1716. (b) K. E. Howard, J. R. Lockemeyer, M. A. Massa, T. B. Rauchfuss, S. R. Wilson and X. Yang, *Inorg. Chem.*, 29(1990), 4385-4390.

29. (a) K. E. Howard, T. B. Rauchfuss and S. R. Wilson, *Inorg. Chem.*, 27(1988), 3561-3567. (b) M. Kato, M. Kawano, H. Taniguchi, M. Funaki, H. Moriyama, T. Sato and K Matsumoto, *Inorg. Chem.*, 31(1992), 26-35.

30. The Strem Chemiker, Vol. XIV No. 1, Octobet, 1992.

31. See chapter 8.

CHAPTER 8

CONCLUSIONS

In this work we have developed suitable synthetic methods for making various metal polychalcogenide compounds. First, reactions of DMF extracted Zintl anions Q_x^{2-} (Q=Se, Te; n=1-5) with proper gold salts provide us with a convenient entry into the polyselenide chemistry of this coinage metal. Similarly, the synthesis of the CO-containing transition metal complexes, and the homo- and heteropolychalcogenide compounds in DMF solution is also readily achieved by the same method. Thus, we have demonstrated that in solution, alkali metal chalcogenides A_2Q_x (A=Na or K; Q=S, Se and Te) are good starting materials for making metal polychalcogenide complexes. This synthetic approach is not only rational but a far more accessible route than any previous methods. Second, our exploration in applying hydro(solvo)thermal technique to the synthesis of transition metal carbonyl chalcogenide compounds has been rewarded with discoveries of many novel clusters. Although hydro(solvo)thermal method has been known for more than a century, the current interest of using this technique to inorganic synthesis is focused on solid-state compounds[1]. Research efforts at exploring the use of this technique to synthesize organometallic compounds have not been made to any appreciable extent[2]. Our work will change the misconception that hydro(solvo)thermal chemistry is applicable only to metal oxides, silicates, etc[3].

The remarkable feature exhibited by the compounds described in this dissertation is the flexibility of the polychalcogenide ligands towards metal ions. We hope that the readers have been convinced that heavy polychalcogenide anions Se_n^{2-} and Te_n^{2-}, like

polysulfidesS_n^{2-}, are so versatile that their coordination chemistry towards metal ions is virtually inexhaustible. This can be chiefly attributed to the fact that polychalcogenide ligands are keen to respond, by adjusting their coordination modes, to the demands of the metal ions, whether these demands are of electronic or steric nature. Such versatile coordination abilities of the polychalcogenide ligands are then manifested by variety of structures exhibited by their metal complexes. For example, they can be discrete molecules, clusters or even polymeric networks[4-5]. Of course, all this also undermines our ability to predict their structures.

At this stage, at least two directions may be taken to further investigate the field. The synthesis of soluble metal polytelluride complexes seems to be a greater challenge than that of polyselenides. Under the same conditions, metal polytelluride complexes are much less stable. The reaction mixtures of M^{n+}/Te_x^{2-} in the polar solvents tend to deposite Te films on the reactor walls[6]. In order to establish the fundamentals of metal polychalcogenide chemistry, more attention must be now paid to metal polytellurides[4b, 7]. For the hydro(solvo)thermal synthesis of organometallic compounds, reactions involving other ligands such as cyclopentadienyls, phosphines, etc must be explored. Conventionally, syntheses of organometallic compounds require the selection of suitable solvents for producing homogenous solutions in which chemical reactions can take place[8]. When solvents are brought to near- or supercritical conditions, reactants need not be completely dissolved, mainly because the diffusion processes are rapid enough to extract the undissolved solids to bring about reactions. Therefore, reactants and products that are insoluble under "normal" conditions may become soluble at sub- or super-critical temperatures. The greatest advantage of using such a technique to carry out organometallic synthesis seems to be its facilitation of crystal growth for new compounds, which is not always an easy task for the organometallic chemist. Moreover, the chemistry at these conditions should be largely different from that at ambient temperatures and pressures as

the result of this different solvent behavior. Through the synthesis of yet new homonuclear and heteronuclear transition metal organometallic/polychalcogenide clusters, this method will further broaden the horizon of polychalcogenide chemistry[9].

REFERENCES

1. Several review articles dealing with different aspects of hydrothermal research are available, see (a) A. J. Ellis and W. S. Fyfe, *Rev. Pure and Appl. Chem.,* 7(1957), 261-316. (b) R. A. Laudise, *Prog. Inorg. Chem.,* 3(1962), 1-47. (c) L. M. Demianets and A. N. Lobachev in *Crystallization Process under Hydrothermal Conditions,* A. N. Lobachev Ed., Consultants Bureau, New York, 1973, p1.

2. H. K. Chae, W. G. Klemperer, D. E. P. Loyo, V. W. Day and T. A. Eberspacher, *Inorg. Chem.*, 31(1992), 3187-3189, and references therein.

3. (a) R. M. Barrer, *Hydrothermal Chemistry of Zeolites,* Academic Press, New York, 1982. (b) A. Rabenau, *Angew. Chem. Int. Ed. Engl* , 24(1985), 1026-1040. (c) R. A. Laudise, *Chem. & Engin. News,* Sept 28(1987), 30-43.

4. (a) S. Dhingra and M. G. Kanatzidis, *Science,* 1992, in press. (b) K.-W. Kim and M. G. Kanatzidis, submitted to *Inorg. Chem.* (c).S.-P. Huang and M. G. Kanatzidis, *Inorg. Chem.*, 30(1991), 1455-1466. (d) K.-W. Kim and M. G. Kanatzidis, *J. Am. Chem. Soc.*, 114(1992), 4878-4883. (e) J.-H. Liao and M. G. Kanatzidis, *Inorg. Chem.*, 31(1992), 431-439.

5. R. C. Haushalter, *Angew. Chem. Int. Ed. Engl.*, 24(1985), 433-435.

6. S.-P. Huang, S. Dhingra, K.-W. Kim and M. G. Kanatzidis, unpulished results.

7. K.-W. Kim, Group Meeting Presentation, Michigan State University, 1992.

8. Ch. Elschenbroich and A. Salzer, *Organometallics: A Concise Introduction,* 2nd Ed., VCH Publishers, Inc., New York, 1992.

9. S.-P. Huang and M. G. Kanatzidis, work in progress.

MICHIGAN STATE UNIV. LIBRARIES
31293009032164